University of Engineering and Technology, Taxila

PRESENTS

1st International Conference on Advances in Civil and Environmental Engineering

22nd - 23rd February, 2022

1ˢᵗ International Conference on Advances in

Civil and Environmental Engineering

22ⁿᵈ & 23ʳᵈ Feb, 2022

Conference Proceedings

ICACEE-2022

Department of Civil and Environmental Engineering
University of Engineering and Technology Taxila, Pakistan

Foreword

Civil and Environmental Engineering Department, University of Engineering and Technology Taxila organized two days International Conference on Advances in Civil and Environmental Engineering (ICACEE-2022) which was held on 22nd and 23rd February 2022 at UET Taxila. This was the 1st International Conference in the history of UET Taxila.

Aim of the conference was to bring together international and national researchers from the field of Civil and Environmental Engineering to share their knowledge and experience about the advances in this field of engineering with young researchers. Theme of the Conference was;

- Advance Materials for Construction, Innovative Methods and Techniques in Civil Engineering,
- Traffic and Pavement, Soil and Geoscience,
- Structure Against Extreme Loading,
- Water Environment and Health, Sustainable Water Resources,
- Renewable, Smart and Green Energy Development.

Keynote speakers from Thailand, Saudi Arabia, United Kingdom, Qatar and Japan joined the conference. Keynote speakers talked about; how to fight floods with Nature Based Solutions?, Source to tap risk assessment for intermittent water supply systems in Arid Regions, Changes in the vegetation resistance in a river at a destructive large flood event, Natural Fiber Reinforced Compresses Earth Blocks, Implementing recycled materials on Australia's Road Network.

Total 105 Papers were received from Pakistan, China, Qatar, Japan, United Kingdom, Kingdom of Saudi Arabia, Canada and Thailand. After thorough review 75 papers were accepted. Participants mainly came from university research centers and some from the industry.

Conduction of a successful conference such as ICACEE-2022 requires a lot of work by many people. We would like to thank all the members of the Organizing Committee, the session chairs and all the people who helped with the reviewing procedure of the contributed papers. Our special thanks go to the Vice Chancellor UET Taxila, Director Advanced Studies & Research and Chairman Civil and Environmental Engineering department for their support and guidance. The financial and technical support of different institutions and industries is also gratefully acknowledged.

Engr. Sadia Fida
Conference Vice-Chair

Dr Afaq Ahmad
Conference Chair

Conference Theme

- Advance Materials for Construction

- Innovative Methods and Technique in Civil Engineering

- Traffic and Pavement and Soil and Geoscience

- Structure Against Extreme Loading

- Water, Environment and Health

- Sustainable Water Resources

- Renewable, smart and green energy development

Conference Paper Details

- No of Total Submission (105)

- No of Papers Accepted (74)

- Paper Accepted with Oral Presentation (37)

- Paper Accepted with Poster Presentation (37)

- Received Papers After 5th Feb 2022 (12, Not included)

Contribution From World

18 Accepted papers are from;

- ➤ China
- ➤ Qatar
- ➤ Japan
- ➤ United Kingdom
- ➤ KSA
- ➤ Canada
- ➤ Thailand

Contribution From Pakistan

28 Accepted papers are from;

- ➤ NED, Karachi
- ➤ NUST, Islamabad
- ➤ UET Peshawar
- ➤ IIUI, Islamabad
- ➤ CUST, Islamabad
- ➤ GIKI
- ➤ MNS University
- ➤ Wali Khan University

POLITICAL MAP OF PAKISTAN UNVEILED BY PM IMRAN KHAN

Chief Guests

Engr. Imtiaz Gillani
Chairman
National Technology Council

1ˢᵗ Day

Engr. Zaheer Shah
Managing Director
Heavy Mechanical Complex, Taxila

2ⁿᵈ Day

Members of Advisory Board

Prof. Dr. Muhammad Inayatullah Khan
Patron

Prof. Dr. Qaiser-uz-Zaman Khan
Vice-Patron

Prof. Dr. Muhammad Yaqub
Principle Advisor

Engr. Dr. Mansoor Ahmad Baluch
Chief Advisor

Prof. Dr. Faisal Shabbir
Technical Advisor

Organizing Committee

Dr. Afaq Ahmad
Conference Chair

Engr. Sadia Fida
Conference Vice-Chair

Keynote Speakers

- Prof. Dr. Norio Tanaka (Saitama University, Japan)
- Prof. Dr. Vagelis Plevris (Qatar University, Qatar)
- Dr. James Grenfell (Australian Road Research Board, Australia)
- Dr. Amorn Pimanmas (Kasetsart University, Thailan)
- Dr. Muhammad Ali (University of Portsmouth, UK)
- Dr. Martina Egedusevic (University of Exeter, UK)
- Dr. Husnain Haider (Qassim University, KSA)
- Dr. Muhammad Saqib Nawaz (KAUST, KSA)
- Engr. Jawaid Malik (CPD Lecture, Major Rail Projects, Canada)

Conference Co-Chairs

- Dr. Shahzad Saleem (Assistant Prof. UET Taxila)
- Dr Naveed Ahmad (Assistant Prof. UET Taxila)
- Dr. Ghufran Ahmed Pasha (Assistant Prof. UET Taxila)
- Dr. Bilal Zaidi (Associate Prof. UET Taxila)
- Dr. Muhammad Usman Arshid (Assistant Prof. UET Taxila)
- Dr. Sadia Nasreen (Assistant Prof. UET Taxila)

Editors

- Dr. Afaq Ahmad
- Engr. Rana Ehtisham
- Engr. Waqas Qayyum

University of Engineering and Technology, Taxila

PRESENTS

1st International Conference on Advances in Civil and Environmental Engineering

Conference Date:	22nd & 23rd Feb 2022
Mode of Conference	Physical and Online

Plan of Activities

1st Day of Conference 22nd Feb 2022

1.	Conference Registration and Reception of Honourable Guests	08:30 to 09:15
2.	Opening Ceremony & Vice Chancellor's Speech	09:30 to 10:30
3.	International Key-Notes Speakers (05)	10:30 to 11:30
4.	Tea Break & Poster Presentation	11:30 to 12:00
5.	Technical Sessions in Parallel	12:00 to 13:30
6.	Prayer Break	13:30 to 14:00
7.	Lunch & Poster Presentation	14:30 to 15:30
8.	Site Seeing tour of UNESCO	15:30 to 17:00
9.	Conference Dinner	17:00 onwards

2nd Day of Conference 23rd Feb 2022

1.	CPD Lecture By Engr Jawaid Malik Project Engineer (Major Rail Projects Canada)	09:00 to 10:30
2.	International Key-Notes Speakers (04)	10:30 to 11:30
3.	Tea Break & Poster Presentation	11:30 to 12:30
4.	Technical Sessions in Parallel	12:00 to 13:30
5.	Prayer Break	13:30 to 14:00
6.	Chief Guest Speech & Prize Distribution & Closing Ceremony	14:00 to 14:30
7.	Lunch	14:30 to 15:30

https://web.uettaxila.edu.pk/1stICACEE

MDPI

icce@uettaxila.edu.pk

infrastructures

Organized By: Civil and Environmental Engineering Department

TABLE OF CONTENTS

183	Behaviour of RC Beam-Column-Slab Connection with CFRP Retrofitting Under Cyclic Loading
185	Experimental Testing & Finite Element Modeling of RCC Columns Subjected to Fire
186	Enhancement of Self-Healing Tendency of Reclaimed Asphalt using Different Additives
187	Seasonal Variation of Sun Path and its Impacts on Energy Consumption Using BIM, A Case Study of Multi-Story Educational Building
188	Estimation of Air Pollutants from vehicular emissions – A case study on Jinnah Avenue Road, Islamabad, Pakistan
189	Lateral Load Response of Full Scale Beam-Column Joints
190	Design Optimization of Precast Reinforced Box Culvert with the Application of Finite Element Modeling and Analysis
191	Evaluation of GoogLenet, Mobilenetv2, and Inceptionv3, pre-trained convolutional neural networks for detection and classification of concrete crack images
192	Prediction of steel flush end plate connection through Artificial Neural Networks (ANN)
193	Mapping Land Cover Dynamics in Chakwal District by using all Landsat Images in Google Earth Engine
194	Evaluation of Pre-trained ResNet and MobileNetV2 CNN models for the Concrete Crack Detection and Crack Orientation Classification
195	Effect of Temperature on Self-Healing of Asphalt Material
196	Application of Machine Learning to Predict the Flexural Moment Capacity of Near Surface Mounted Beam
198	Effect of non-plastic fines on hydraulic conductivity of lawrencepur sand
199	Structural Strength Evaluation and Investigating Cracking Behaviour of Newly Constructed Building
200	Finite Element Modelling and Analysis of Typical Industrial Precast Tray Slab Using ABAQUS
201	Detection of Pavement cracks of UET Taxila using pre-trained model Resnet50 of CNN
204	Review of Forensic Structural Investigations to South Champlain Tower Florida, Collapse
205	A Brief Introduction to Blockchain Technology and its Applications in Civil Engineering and Construction
206	A study on the properties of concrete aggregate replacement in rubber cement composite

PRODUCTION OF HYDROCHAR THROUGH HYDROTHERMAL CARBONIZATION

Babar Abbas, Safeerul Islam Hashmi, Sohail Akram Basra, Zainab Abbasi
Department of Environmental Engineering UET Taxila

Background

The poor sanitization perseveres challenges to the world, specifically countries with raging rates of Population growth has been evolved by the challenge. Approximately 30% - 50% food produced for human consumption purposes is laid to waste i.e. approximately 1,300 million metric tons of such consume goes all in waste. Only in a single year of 2010, approximately 34 million tons of food waste with a rate of 115 kg per person per day was wasted by the American residents.[1]

The wasted and squandered amounts of consume per year are approximately 30% for cereals, 40- 50% for fruits, vegetables and root crops, 20% for oilseeds, meat and dairy products and 35% for fish. The carbon print of consumed food is estimated at 3.3 trillion tons of CO_2 equivalent to the GHG affecting the atmosphere annually. Not only the consume waste enrages an economic loss but also very badly affects the natural resources upon which the humanitarian society relies upon to keep itself fed.[2]

Introduction

Hydrothermal Carbonization (HTC) is carried out in a self-contained environment so there is very little or no chance of environmental emission of any gases, and does not implicate any GHG emissions, then comes the moisture related problems for the biomass as biomass is naturally wet so HTC has proved itself to be very effective in case of moisturized materials too. It converts all of the feedstock material into a solid carbonaceous output which could very much be referred to 'HYDROCHAR', which in the end is a gaseous and moisturized product in an anaerobic environment at moderate temperature condition.[3]

The main products resulting after processing the biomass in an HTC apparatus are Hydrochar, some gaseous and aqueous products. Hydrochar, which we could name as the main outcome of HTC process has high calorific value and O/C ratio than that of a lower quality coal, hydrochar's H/C and O/C ratios are yet higher comparative to that of 'bio-coal' (basically referring to the pyrolysis products).[5]

When biomass is treated in an HTC apparatus, we observe an exothermic process, according the study claims, up to twenty percent of energy within biomass goes out as heat during the HTC process, and even after that the gross calorific value varying from 60-90% of feedstock shows its availability in Hydrochar.

Literature review

Hydrothermal Carbonization

1st International Conference on Advances in Civil & Environmental Engineering, University of Engineering & Technology Taxila, Pakistan

Conference date 22 &23 Feb 2022

Hydrothermal carbonization is thermochemical process that helps to convert the biomass having high moisture content, into carbonaceous solids known as Hydrochar along with the production of gaseous and aquous products within a pressured reactor or vessel at minimal temperature.[6]

A large variety of waste materials can be subjected to this process for the production of Hydrochar. Different types of feedstock can be used for HTC process including cellulose, glucose, residual agricultural waste, animal manures, food waste, municipal solid waste, sludge produced from treatment plants and aquaculture and algal residues.[8, 9]

Operational conditions

Different operational conditions are used for different types of feedstock and purposes. The hydrolysis of macromolecules starts at 180°C temperature. In practice, temperature range of 180- 250°C is maintained in HTC, during operational conditions. However, the process residence time varies from few minutes to several hours.[11]

Hydrolysis

During hydrolysis, different oligomers and glucose is produced. Hydronium ion (H_3O^+ ions) catalyze the hydrolysis process, produced as a result of dissociation of water. These oligomers and glucose produce fructose and putrefy and generate acids such as Acetic, propionic, actic, formic and levulinic acids.[14]

Dehydration

Dehydration and decarboxylation reactions result in the development of oxygen removal conditions. Dehydration reduces the molecular (O/C) and (H/C) ratios, and causes hydroxyl groups elimination same like dehydration of Glucose to HMF or 1,6-anhydroglucose during hydrothermal glucose dehydration.[17]

Polymerization

Polymerization is also one of the important routes for the formation of Hydrochar during Hydrothermal Carbonization process. The process is also called poly-condensation.[20]

Compounds are decomposed to form acids, aldehydes and phenols. They quickly combine again to make polymers that are soluble in nature, usually by polymerization or condensation reactions.[21]

Aromatization

The aromatic clusters are basic Hydrochar structural unit. Experiments with cellulose HTC show the concentration of aromatic groups in the aqueous solution reaches the critical super- saturation point by nucleation bursting of carbon-rich microspheres.[22, 23]

NMR analysis shows that the aromaticity of carbonaceous structures increases strongly with temperature and time of reaction.[24]

1st International Conference on Advances in Civil & Environmental Engineering, University of Engineering & Technology Taxila, Pakistan

Conference date 22 &23 Feb 2022

By intermolecular dehydration or aldol condensation occurs, the aromatization of soluble polymers forms when aromatic aggregates in aqueous solution reach the critical point of super-saturation, which therefore precipitates as carbon-rich microspheres.[25]

Products of HTC process

HTC process results in the production of 3 different types of components i.e. solid, aqueous solution, and small gas volume. The properties and percentages of these products is greatly affected by feedstock composition and properties as well as process conditions.[26, 27]

Solid residue i.e. Hydrochar is considered to be the main product of HTC process. It may be conveniently separated from the suspension because of its homogeneity and hydrophobicity.[28]

Experimental Setup

The major experimental setup required for this study include the feedstock material, HTC Vessel, Arduino H meter, TDS meter, COD Digester. The figure below shows the experimental setup we have developed in our laboratory for this study

Methodology

After that, HTC vessel was designed as per the standard rules (keeping in view, the safety of operators and public). The vessel was controlled using Arduino Circuit, operated through laptop. Thedesign of reactor is given in the table below

Table 1 Design information of Reactor

Sr. #	Parameter	Value
01	Material	SS (304)
02	Depth	18 in
03	Diameter	12 in
04	Max. Pressure	25 bars
05	Volume	33 L
06	Max. Temp	250 °C
07	Welded joint efficiency	0.85

Figure 1 Experimental Setup

1st International Conference on Advances in Civil & Environmental Engineering, University of Engineering & Technology Taxila, Pakistan

Conference date 22 &23 Feb 2022

08	Corrosion factor	1/8 in
09	Wall thickness	6 mm

During the experimentation phase, the feedstock was added into the vessel along with water and heated until a temperature of 200°C and pressure of 17 bars. Different residence times are providedto the raw material at these high pressure and temperature conditions.

The product obtained was dried in oven and calorific value was calculated. Apart from that the wastewater analysis was carried out for the leachate produced and results were compiled at the end.

The whole process is divided into three phases, i.e., heating phase, reaction phase and cooling phase.

- Heating Phase: Vessel was heated at high temperature i.e., 180°C and high pressure i.e., 17 bars.
- Reaction Phase: The previously achieved conditions were maintained for different time periods, i.e., 0, 15, 30, 45, 60, 90 and 120 minutes.
- Cooling Phase: Vessel was allowed to cool down to room temperature.

Figure 2 Internal view of HTC reactor

After the vessel was cooled, liquid was separated for wastewater analysis. Whereas the liquid slurry was dried in the oven at 105°C temperature to obtain hydrochar. The prepared hydrochar was then analyzed for obtaining calorific value in bomb calorimeter.

Results

Temperature and pressure were kept constant during this study, i.e., 180°C and 17 bars. Calorific value of hydrochar was calculated using bomb calorimeter and listed in the table below

Table 2 Calorific Value of Hydrochar

Sr. #	Time	Calorific value	Calorific value
	Minutes	Cal/g	kJ/kg
01	0	110	460.24
02	15	406.07	1698.99
03	30	802.6	3358.1
04	60	4504.089	18845.11
05	90	6173.74	25830.93
06	120	9129.72	38198.8
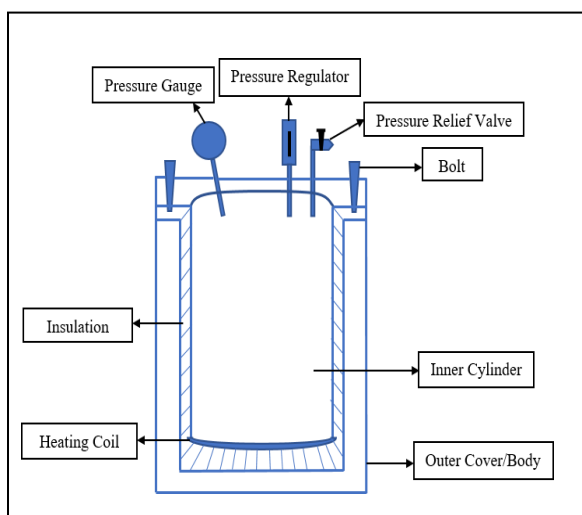
The wastewater that is produced as a result of each run was analyzed in the laboratory. Different parameters were analyzed during analysis such aspH, TSS, TDS and COD. The results of analysis are listed in the tables below

1st International Conference on Advances in Civil & Environmental Engineering, University of Engineering & Technology Taxila, Pakistan

Conference date 22 &23 Feb 2022

Table 3 pH of wastewater after each run

Serial No.	Time	pH
	Minutes	---
01	0	6.30
02	15	5.70
03	30	4.99
04	60	4.07
05	90	3.69
06	120	3.41

Table 4 TSS of wastewater after each run

Serial No.	Time	TSS
	Minutes	mg/l
01	0	121
02	15	343.15
03	30	454.04
04	60	731.88
05	90	914
06	120	937.20

Table 5 COD of wastewater after each run

Serial No.	Time	COD
	Minutes	mg/l
01	0	394.53
02	15	608.04
03	30	1001.67
04	60	1562
05	90	1489.071
06	120	2076.25

Output to Input Ratio

Energy input values were calculated using the power of heater, i.e., 2 kW and amount of feedstock taken for each run, i.e., 10 kg. The output values were calculated by the help of bomb calorimeter. Obtained values for each run are listed in the table below

1st International Conference on Advances in Civil & Environmental Engineering, University of Engineering & Technology Taxila, Pakistan

Conference date 22 &23 Feb 2022

Table 6 O/I value for each run

T	I	Yield	Calorific value	O	O/I
h	kW	kg	kJ/kg	kW	
2	4	6.5	460.24	0.42	0.11
2.25	4.5	6.01	1698.9	1.26	0.28
2.5	5	5.6	3358.1	2.1	0.2
3	6	4.37	18845.1	7.63	1.27
3.5	7	3.99	25830.9	8.18	1.17
4	8	3.4	38198.8	9.02	1.13

The graph plotted between O/I and running time is shown below

The value of O/I is maximum against the total operational time of 3 hours. 2 hours duration was required for the development of the required conditions whereas 1 hour is provided as a residence time/ reaction phase. However, when 1.5 hours residence time is provided, corresponding O/I valueis decreased.

A research study conducted in the year 2009 on the hydrothermal carbonization of organic biomass also studied the energy content and energy recovery aspects. Their results identified that the raw material used for the production of hydrochar contained total energy content of 5,700 kJ/kg. The release of energy after completion of process was identified to be 7000 kJ/kg hence resulting in the output to input ratio of 1.23.[29]

The highest value of O/I obtained in our study was 1.27. however, these studies shows that even higher values of output to input ratio can be obtainedby the optimization of various operational parameters of the process. The output energy value also has a direct relation with the type of feedstock that is being used in the process along with the operating temperature and pressure conditions. The percentages of various materials such as lignin, cellulose, carbohydrates etc. found in the feedstock also play an important role. These points must be kept in consideration before conducting the research.
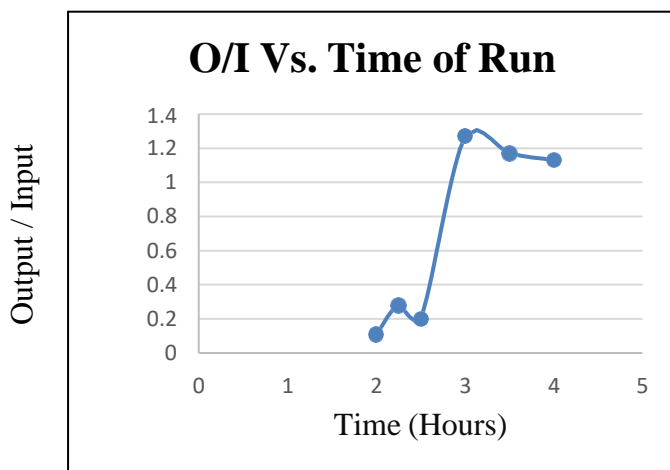
O/I Vs. Time of Run

1st International Conference on Advances in Civil & Environmental Engineering, University of Engineering & Technology Taxila, Pakistan

Conference date 22 &23 Feb 2022

Conclusions

The review of the literature has witnessed the effectiveness of hydrothermal carbonization as a purposeful and cost-effective methodology to convert biomass or other solid waste into value-added products. Based upon the conducted research work, following conclusions are drawn

- Temperature plays an important role in the process.
- Hydrochar yield decreases by increase in temperature and residence time.
- Residence time and calorific value are directly proportional to each other, i.e., "Increase inresidence time increases the calorific value of hydrochar"
- The best-fit hydrochar is produced by providing the residence time of 1 hour.
- Wastewater produced as a result of this process become acidic.
- Wastewater contains TSS and TDS in large amount.
- Wastewater can be used as a fertilizer and can also be used again in the process, after neutralizingits pH after first run.
- Output to input ratio (O/I) comes out to be 1.27 against the residence time of 1 hour.
- Hence, the hydrochar has enough potential to be used as a source of fuel in place of low-qualitycoal because of its less emissions and environmental pollution.

References

1. Baig, M.B., et al., Food waste posing a serious threat to sustainability in the Kingdom of Saudi Arabia–A systematic review. Saudi journal of biological sciences, 2019. **26**(7): p. 1743-1752.
2. Das, S., et al., Solid waste management: Scope and the challenge of sustainability.Journal of cleaner production, 2019. **228**: p. 658-678.
3. Pauline, A.L. and K. Joseph, Hydrothermal carbonization of organic wastes to carbonaceous solid fuel–A review of mechanisms and process parameters. Fuel, 2020. **279**: p. 118472.
4. Wang, L., Y. Chang, and A. Li, Hydrothermal carbonization for energy-efficient processing of sewage sludge: A review. Renewable and Sustainable Energy Reviews, 2019. **108**: p. 423-440.
5. Román, S., et al., Hydrothermal carbonization: Modeling, final properties design and applications: A review. Energies, 2018. **11**(1): p. 216.
6. Libra, J.A., et al., Hydrothermal carbonization of biomass residuals: a comparative review of the chemistry, processes and applications of wet and dry pyrolysis. Biofuels, 2011. **2**(1): p. 71-106.
7. Yoshimura, M. and J. Senthilnathan, Hydrothermal process for nano-carbons and carbonaceous materials. Nanomaterials Handbook, Second Edition, Ed: Yury Gogotsi, 2017: p. 507-533.

1st International Conference on Advances in Civil & Environmental Engineering, University of Engineering & Technology Taxila, Pakistan

Conference date 22 &23 Feb 2022

8. Erdogan, E., et al., Characterization of products from hydrothermal carbonization of orange pomace including anaerobic digestibility of process liquor. Bioresource technology, 2015. **196**: p. 35-42.

9. Parshetti, G.K., S. Chowdhury, and R. Balasubramanian, Hydrothermal conversion of urban food waste to chars for removal of textile dyes from contaminated waters. Bioresource technology, 2014. **161**: p. 310-319.

10. Savage, P.E., Organic chemical reactions in supercritical water. Chemical reviews, 1999. **99**(2): p. 603-622.

11. Funke, A. and F. Ziegler, Hydrothermal carbonization of biomass: a summary and discussion of chemical mechanisms for process engineering. Biofuels, Bioproducts and Biorefining, 2010. **4**(2): p. 160-177.

12. Behrendt, F., et al., Direct liquefaction of biomass. Chemical Engineering & Technology: Industrial Chemistry-Plant Equipment-Process Engineering-Biotechnology, 2008. **31**(5): p. 667-677.

13. Basu, P., Biomass gasification, pyrolysis and torrefaction: practical design and theory. 2018: Academic press.

14. Bobleter, O., Hydrothermal degradation of polymers derived from plants. Progress in polymer science, 1994. **19**(5): p. 797-841.

15. Shoji, D., et al., Visualized kinetic aspects of decomposition of a wood block in sub-and supercritical water. Industrial & engineering chemistry research, 2005. **44**(9): p. 2975-2981.

16. Hashaikeh, R., et al., Hydrothermal dissolution of willow in hot compressed water as a model for biomass conversion. Fuel, 2007. **86**(10-11): p. 1614-1622.

17. Kabyemela, B.M., et al., Glucose and fructose decomposition in subcritical and supercritical water: detailed reaction pathway, mechanisms, and kinetics. Industrial & Engineering Chemistry Research, 1999. **38**(8): p. 2888-2895.

18. Titirici, M.-M., A. Thomas, and M. Antonietti, Back in the black: hydrothermal carbonization of plant material as an efficient chemical process to treat the CO_2 problem? New Journal of Chemistry, 2007. **31**(6): p. 787-789.

19. Lu, X., B. Jordan, and N.D. Berge, Thermal conversion of municipal solid waste via hydrothermal carbonization: Comparison of carbonization products to products from current waste management techniques. Waste management, 2012. **32**(7): p. 1353-1365.

20. Kruse, A. and A. Gawlik, Biomass conversion in water at 330− 410 C and 30− 50 MPa. Identification of key compounds for indicating different chemical reaction pathways. Industrial & engineering chemistry research, 2003. **42**(2): p. 267-279.

21. Salak Asghari, F. and H. Yoshida, Acid-catalyzed production of 5-hydroxymethyl furfural from D-fructose in subcritical water. Industrial & Engineering Chemistry Research, 2006. **45**(7): p. 2163-2173.

22. Baccile, N., et al., Structural characterization of hydrothermal carbon spheres by advanced solid-state MAS 13C NMR investigations. The Journal of Physical Chemistry C, 2009. **113**(22): p. 9644-9654.

23. Sevilla, M. and A.B. Fuertes, The production of carbon materials by hydrothermal carbonization of cellulose. Carbon, 2009. **47**(9): p. 2281-2289.

1st International Conference on Advances in Civil & Environmental Engineering, University of Engineering & Technology Taxila, Pakistan

Conference date 22 &23 Feb 2022

24.   Falco, C., et al., Hydrothermal carbon from biomass: structural differences between hydrothermal and pyrolyzed carbons via 13C solid state NMR. Langmuir, 2011. **27**(23): p. 14460-14471.

25.   Sevilla, M. and A.B. Fuertes, Chemical and structural properties of carbonaceous products obtained by hydrothermal carbonization of saccharides. Chemistry–A European Journal, 2009. **15**(16): p. 4195-4203.

26.   Cao, X., et al., Effects of biomass types and carbonization conditions on the chemical characteristics of hydrochars. Journal of agricultural and food chemistry, 2013. **61**(39): p. 9401-9411.

BIM-based Automated Fire Hazard Assessment and Control in a Construction Facility

Usman Aftab, Muhammad Usman Hassan

Department of Construction Engineering and Management (CE&M), School of Civil and Environmental Engineering (SCEE)
National Institute of Sciences and Technology (NUST), H-12, Pakistan
uaftab.cem19@student.nust.edu.pk; usman.hassan@nice.nust.edu.pk

ABSTRACT

Hazard identification and risk assessment of a construction facility plays governing role in construction safety management. Modernization in construction designs have introduced the need of precise risk assessment against fire incidents caused by flammable materials. Prevention through Design (PtD) has been studied for automated code compliance of international safety standards, yet no studies have been found for automated risk assessment of fire hazards to assess and suggest fire prevention provisions in a construction facility. In this research, an automated framework has been developed for fire risk assessment of a building design utilizing degree of flammability of used material to suggest fire safety equipment according to international construction safety standards. This framework is integrated within Building Information Modelling (BIM) for collaborative and precise decision-making processes. The framework demonstrates effortless and accurate risk mitigation strategy against fire hazards in a building facility.

KEYWORDS: Construction Safety Management, Automated Code Compliance, Building Information Modelling (BIM), Fire Risk Assessment, Prevention through Design (PtD)

1 INTRODUCTION

Fire hazard in buildings is the likeliness of incidental or deliberate fire to jeopardize life and property in a building [1]. Construction fire safety assessment is essential for the compliance and enforcement of fire safety regulations to ensure long lasting and efficient safety of people and buildings. However, statistics show negligence of fire safety regulations in planning construction safety. All over the world, more than one million deaths have been caused by a hundred million fire incidents between 1993 and 2019 [2].

Traditional approaches such as fire sprinklers, extinguishers, and smoke detectors along with structural protection systems are developed to minimize losses. However modern construction designs, built for aesthetics and comfort, hinder the success of such approaches [1]. Modern designs are hard to comply with fire safety provisions and standards provided by dedicated organizations such as National Fire Protection Association (NFPA). Literature lacks studies on reliable tools to measure the expected level of fire through construction design and minimal work

1st International Conference on Advances in Civil & Environmental Engineering, University of Engineering & Technology Taxila, Pakistan

Conference date 22 &23 Feb 2022

has been done to suggest the automated provision of fire safety equipment based on international safety standards. This research presents an automated framework for fire hazard identification and implementation of control measures based on international construction safety byelaws. Degree of flammability of materials has been utilized for the judgement of overall expected fire hazard in a facility and NFPA regulations are integrated within Building Information Modelling (BIM) for suggesting and implementing precise provision of fire extinguishers.

2 METHODOLOGY

A framework is developed for automated assessment and provision of fire control measures by determining the fire hazard occupancy using degree of flammability of the material used in the design facility. In the developed tool, BIM-FIRE, the degree of flammability of a construction facility is determined and fire hazard occupancy is assessed using NFPA 10 standard for the provisions of fire extinguishers as a hazard control measure. As a result, automated provision of the required fire extinguishers is visualized within BIM design. The methodology of the framework is shown in Figure 1 and discussed in the following subsections.

Figure 1 Framework of the Developed Tool

2.1 Assessment of Degree of Flammability

Firstly, a construction facility is assessed for the degree of flammability of the materials used i.e. how easily something will burn or ignite, causing fire or combustion. This assessment is done using NFPA 10, clause 5.4.1, that defines the ratings of degree of flammability of various materials on a scale of 0 to 4 [3]. This was achieved by devising visual programming within Dynamo platform, where firstly all elements of a building facility and their respective materials were extracted as shown in Figure 2(a), and then a user-friendly data input user interface to assess respective degree of flammability of each material was programmed as shown in Figure 2(b).

1st International Conference on Advances in Civil & Environmental Engineering, University of Engineering & Technology Taxila, Pakistan

Conference date 22 &23 Feb 2022
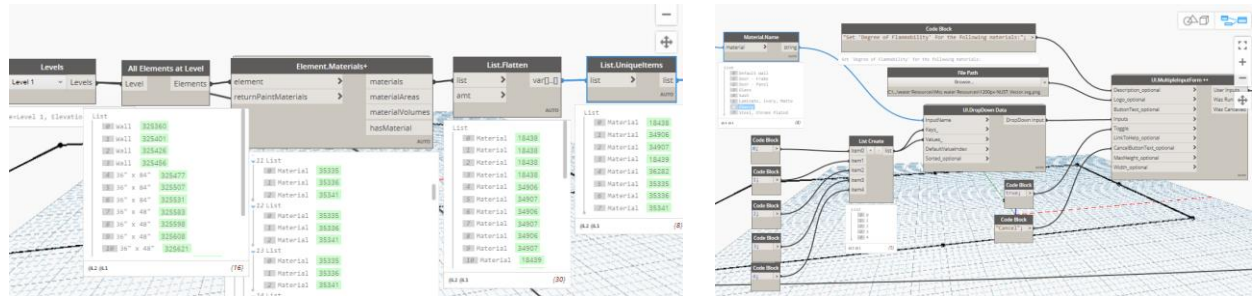
Figure 2(a) Code for Extracting Building Material List (b) Code for Data Input User Interface

2.2 Determination of Fire Hazard Occupancy

As per NFPA 10, clauses 5.4.1.1 – 5.4.1.3, fire hazard occupancy is categorized in three types based on average degree of flammability of the materials: Low, Moderate and High Hazard Occupancy. A python coded program was devised to distribute the fire hazard occupancy according to the user defined average degree of flammability in the range of 0 to 4, as shown in Figure 3.
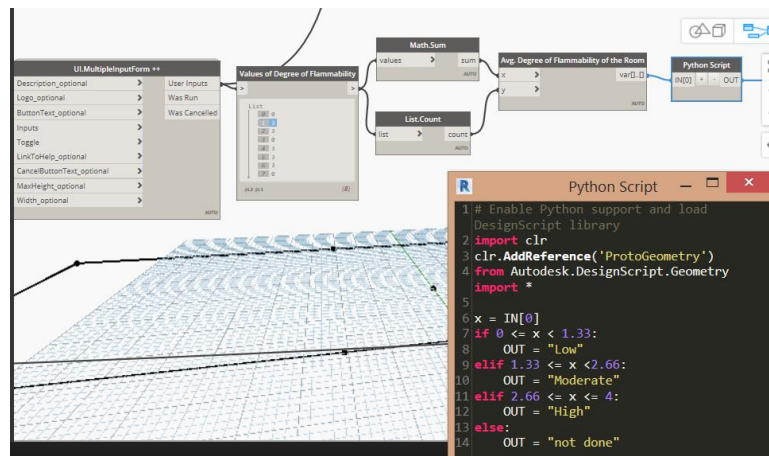
Figure 3 Distribution of Degree of Flammability into Fire Hazard Occupancy

2.3 Assessment chart for BIM-FIRE

After studying the standards for the provisions of fire extinguishers as a hazard control measure according to NFPA 10, an assessment chart is developed for BIM-FIRE tool, illustrated in Table 1. This chart defines required number of extinguishers for fire hazard control in a construction facility based on the degree of flammability, fire hazard occupancy and floor area of the facility. The programmed algorithm automatically places the required number of fire extinguishers in the BIM model as per NFPA 10 assessment chart. The sample of devised algorithm is shown in Figure 4.

1st International Conference on Advances in Civil & Environmental Engineering, University of Engineering & Technology Taxila, Pakistan

Conference date 22 &23 Feb 2022

Table 1 Assessment Chart for Required Number of Fire Extinguishers

Floor Area (sq. m)	Required number of Fire Extinguishers		
976 – 1115	6	20	40
837 – 975	4	10	30
698 – 836	3	6	20
558 – 697	2	5	10
419 – 557	2	4	6
280 – 418	1	3	4
140 – 279		2	
0 – 139			
Fire Hazard Occupancy	**Low**	**Moderate**	**High**
Degree of Flammability	**0 - 1.33**	**1.34 - 2.66**	**2.67 - 4**

```
85 elif a== "Moderate" and 3000 < b <= 4500:
86     try:
87         x = Revit.Elements.FamilyInstance.ByPoint(familytype,point1)
88     except Exception as e:
89         s = str(e)
90     OUT = x
91     try:
92         x = Revit.Elements.FamilyInstance.ByPoint(familytype,point)
93     except Exception as e:
94         s = str(e)
95     OUT = x
96     try:
97         x = Revit.Elements.FamilyInstance.ByPoint(familytype,point2)
98     except Exception as e:
99         s = str(e)
100    OUT = x
```

Figure 4 Algorithm for Automated Provision of Fire Extinguishers

3   RESULTS AND DISCUSSION

The methodology adopted for automated fire hazard assessment and control of a construction facility resulted in a BIM-based plugin, BIM-FIRE, using python programming within BIM design software Revit 2021. The tool has been evaluated on a BIM design containing various elements and materials, shown in Figure 5(a). Firstly, an automated list all the material of the design facility was extracted, and degree of flammability of each material was assigned using a user-friendly user interface, shown in Figure 5(b). Then, average degree of flammability and floor area of the bounding room was automatically extracted from the design model to be 1.875 and 399.89 sq. m respectively. In the last step, the BIM-FIRE evaluated the number of required fire extinguishers based on the degree of flammability, fire hazard occupancy and floor area of the facility using Table 1. The results lie in moderate fire hazard occupancy and require 3 fire extinguishers, that are automatically placed in the design model as per NFPA specifications, shown in Figure 5(c).

1st International Conference on Advances in Civil & Environmental Engineering, University of Engineering & Technology Taxila, Pakistan

Conference date 22 &23 Feb 2022
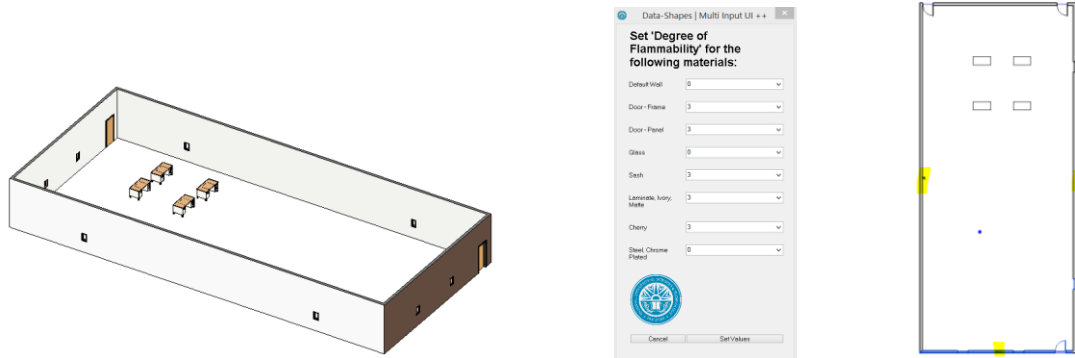
Figure 5 (a) BIM Design Model Under Study (b) Data Input User Interface (c) Placement of Fire Extinguishers as per NFPA specifications

4   CONCLUSION

It is essential to recognize the importance of precise assessment of fire prevention methods to ensure the safety of people and building facilities. With the advent of modern and automated technologies, it is becoming necessary to put an effort for developing such methods as per international standards. Therefore, this research is dedicated for providing the industry with an automated fire prevention assessment tool with the integration of BIM technology and NFPA regulations. The incorporation of the developed tool, BIM-FIRE, within BIM platform not only provides a collaborated environment for safety planning of a building design but also provides a seamless and error-free assessment for fire safety requirements. It is further programmed with NFPA standards for placing fire extinguishers based on degree of flammability and floor area of the facility. The research is targeted to provide construction managers and safety planner for an efficient and error-free implementation of NFPA standards for portable fire extinguishers in a construction facility.

5   REFERENCES

[1]   V. Kodur, P. Kumar, and M. M. Rafi, "Fire hazard in buildings: review, assessment and strategies for improving fire safety," *PSU Res. Rev.*, vol. 4, no. 1, pp. 1–23, Jan. 2020, doi: 10.1108/PRR-12-2018-0033.

[2]   N. Brushlinsky, M. Ahrens, S. Sokolov, and P. Wagner, "'World fire statistics', CTIF, International Association of Fire and Rescue Services, No. 26," 2021, [Online]. Available: https://ctif.org/sites/default/files/2021-06/CTIF_Report26_0.pdf.

[3]   D. J. Burkhart, "Nfpa 10; Standard for Portable Fire Extinguishers," 2022. [Online]. Available: https://www.nfpa.org/codes-and-standards/all-codes-and-standards/list-of-codes-and-standards/detail?code=10.

1st International Conference on Advances in Civil & Environmental Engineering, University of Engineering & Technology Taxila, Pakistan

In House Wastewater Management

Muhammad Farooq[1], Naeem Ejaz,[1] Muhammad Aleem[1]

1. University of Engineering and Technology Taxila, Punjab, Pakistan

Muhammadfarooq2459@gmail.com, naeem@uettaxila.edu.pk,engrm.aleem@gmail.com

Corresponding Author Email: Muhammadfarooq2459@gmail.com,

ABSTRACT

Water scarcity is hitting the globe along with Pakistan. Arid and semi-arid areas of the world are facing water scarcity issues. To overcome the alarming situation of water scarcity, grey water management is gaining importance to reuse it as alternative for fresh water for various purposes. This project deals with the recycling of greywater and its reuse as it is the best option to reduce water shortage in a sustainable manner. Main objective of this project is to design a sustainable and cost-efficient greywater recycling plant for a house, to treat greywater generated from a house and recommended to reuse it for the purposes of cleaning, garden watering and toilet flushing. This plant has designed with the main aim of solving water scarcity problem and increased water demand that is prevailing in Pakistan. The project will help to save the water cost significantly in areas like Karachi , Rawalpindi, and Islamabad where water requirements are being met through private water bowsers.

Keywords: wastewater, management ,design, flushing.

1 INTRODUCTION

Water is one of the greatest blessings of Allah Almighty as it is the basic component for the survival of all the life forms and their activities and plays a very essential role. Notable sources of water supply are ground and surface water. But water resources have been facing crisis across the globe and these crises are growing at significant rate (Abu-Zeid,1998). The availability of fresh water for mankind consumption and for cultural and social needs is becoming scarcer rapidly as the industrialization and urbanization have retained massive amount of pressure on water, and in some countries rising population is the cause of water scarcity (Soomro et al., 2011). Water scarcity is not only issue of Pakistan but a global issue. Arid and semi-arid areas of the world are facing water scarcity issues. Therefore, in order to overcome the alarming situation of water scarcity, it's the supreme need to take a step forward and think about the solution of it. To reduce the stress of water scarcity, grey water management is gaining international gratitude to reuse it as alternative for fresh water for various purposes, irrigation is one of them (Ghaitidak and Yadav, 2013). Recycling of greywater and its reuse is a good possibility for water management strategy in a sustainable manner. To solve the problem of increased water demand, the networks of water recycling have been evolving all over the world since last few decades (Wilcox *et al.,* 2016). Accordingly, I have designed a sustainable, eco-friendly, and cost-efficient greywater recycling

plant for a single house, to treat greywater generated from a house and recommend reusing it for the purposes of garden watering, car & floor washing and toilet flushing. This plant has designed with a main aim of solving the water scarcity problem and increased water demand that is prevailing in Pakistan.

1.1. Water Availability and Scarcity Conditions in Pakistan:

Water scarcity is hitting the globe along with Pakistan. Pakistan is already a water stressed country, with around 1200 cubic meters per capita water availability in year 2000, a drop from 5,300 cubic meters in 1951 (Ahmed, 2007). The last survey which gave the results of 1038 cubic meters was conducted almost 11 years ago in 2008.If this fresh water is replaced by recycled greywater than it would contribute effectively in lowering the demand of fresh water and water shortage problems in Pakistan. The main aim of the project is to design a grey water recycling unit to treat the grey water at household level and make it reusable. Hence the main objectives of our present study are:

- To reduce Domestic Reliance on tube wells
- To control depletion of ground water level through using recycled wastewater.
- To improve ecological of area
- To design a sustainable, eco-friendly, cost efficient and compact unit which can recycle

The greatest contest in the water resource management sector over few decades is the design and implementation of low-cost wastewater treatment that will permit reuse of treated grey water for selective residential and industrial purposes. Also recycling of grey water at household level will help the authorities to handle wastewater as very small amount of water will be collected by water authorities of Pakistan.

2   METHODOLOGY

The target area that we selected for our study on the grey water was Rawalpindi Cantt. Itis situated in Rawalpindi District of province Punjab, Pakistan. The cantonment area is mostly under the military use which includes mostly residential use of water and minimal to nonindustrial use. I selected three such houses where there was ease in collection of greywater sample. While collecting the sample adequate precautionary measures were taken. The greywater from bathroom included some water from shower drain, some from laundry drain and washbasin drain, and all were mixed. The greywater from kitchen was collected separately from the washroom and laundry greywater both the collected greywater was poured into 1.5-liter bottles and stored in a cool dry place. After the sample was collected, it was taken to the laboratory for the testing of physical and chemical parameters. Testing of sample for physicochemical and biological parameters was done.

Greywater was treated in plant by series of treatment processes and then analyzed in laboratory. Different physical and chemical parameters were obtained by laboratory testing and then results were analyzed and compared against reuse standards of water required for irrigation, garden watering, toilet flushing and cleaning purpose. To achieve the objective of our project, simple but cost effective and technically feasible scheme for greywater treatment has been selected. Main treatment is coagulation and flocculation as coagulant use for this process is readily available in market at low cost. At first, raw greywater coming from a house is stored in pre-storage tank which is also used as screening ens/mesh is installed in this tank to remove floating or coarse particles from greywater i.e. hair, solid particles etc. Main treatment selected for greywater treatment is coagulation and flocculation. After screening, greywater enters in coagulation tank (rapid mix basin) where optimum amount of coagulant (alum) is added in greywater. During coagulation

process, charges gets neutralized and heavy mass particle has formed so that it can settles easily. In flocculation tank, slow mixing for designed detention time has done and heavy mass of particles is formed and settles down at quick rate. Flocculation basin is followed by sedimentation tank where suspend solids settles down by the action of gravity and then at last, greywater make its way towards sand filtration chamber for further treatment. Flocs formed in during flocculation process settles down in sedimentation tank and they are further trapped in sand to get the maximum removal of bacteria and pathogens. Schematic flow chart for our recycling plant is shown in fi. Detail design of each tank has been discussed later in this report

3   DESIGN SUMMARY AND FINAL SKETCH OF MODEL:

3.1   Design Summary:

Table 3.1: Design Summary for Treatment Plant

Screening Chamber/ Pre-Storage Tank	Overall Dimensions	9" x 1.5' x 3' (L x W x D)
	Size of Screen (Mesh)	2 mm x 2mm
	Volume of Tank	95 liters, 3.375 ft3
Coagulation Basin	Overall Dimensions	6" x 6" x 9" (L x W x D)
	Paddle Dimensions	4" x 2"
	Volume of Basin	3.54 liters,0.125 ft^3
Flocculation Basin	Overall Dimensions	3'2" x 6" x 9" (L x W x D)
	Paddle Dimensions	4" x 2"
	Volume of Basin	22.42 liters, 0.792 ft^3
Sedimentation Tank	Overall Dimensions	3' x 1.5' x 3' (L x W x D)
	Volume of Tank	318.52 liters,11.25 ft^3
Sand Filtration Chamber	Overall Dimensions	1.5" x 1.5' x 3' (L x W x D)
	Thickness of Sand Layer	15"
	Size of Sand	600 μm
	Thickness of Aggregate Layer	4"
	Aggregate Size	1"-1.5"
	Depth of Standing Water	9"
	Volume for Standing Water	48 liters, 1.69 ft^3

3.2   Final Sketch of Model:
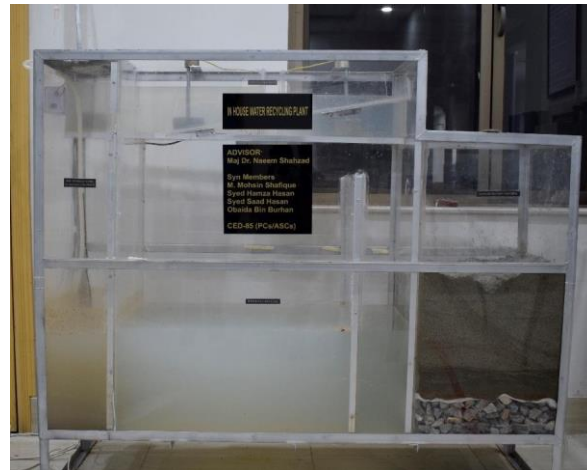
Figure 3.14: Final Sketch of Treatment Unit

4   RESULTS AND DISCUSSIONS

4.1   Parameters of Greywater:

Laboratory tests conducted on greywater gave us the value of different parameters of bathroom and kitchen greywater. The pH of bathroom greywater was 6.83 while kitchen grey water has pH of 6.79. The turbidity of bathroom greywater was high as compared to kitchen greywater. Prominent number of chlorides was present in both kitchen and bathroom greywater. The COD value for kitchen greywater was greater than greywater generated from bathroom. Bathroom greywater has BOD of 74.1 mg/l while BOD value of 60.75 mg/l was observed in Kitchen greywater. These values are the average of water collected from three different houses.

An optimum amount of coagulant was added in greywater and process of coagulation and flocculation was done in laboratory by jar test. As, in general, addition of coagulant decreases the pH of water, and it has been observed during laboratory analysis of treated samples. The turbidity removal from bathroom and kitchen greywater was 77.18 and 80.15 % respectively. The removal of nitrates from greywater was observed to be 82.79 % from bathroom and 76.92 % from kitchen greywater. A significant removal percentage of COD, BOD and TDS was also observed during testing on treated greywater.

4.2   Analysis on Treated Greywater:

Laboratory tests were conducted on both raw and treated greywater, before and after recycling of greywater As the pH has to be increased due to addition of coagulant, it can be observed in results. Turbidity of the treated greywater has decreased effectively from 125 NTU to 6.57 NTU. Significant reduction in the number of chlorides and nitrates has been observed. Sulphates in treated greywater has increased as alum was used as a coagulant. Prominent amount in the reduction of COD, TDS and TSS was observed.

After effective treatment on raw greywater, 94.74% turbidity has been removed. Treated greywater has turbidity of 6.57 NTU, which has met the reuse standard set by UK and Japan (<10 NTU) for reuse of greywater in toilet flushing, car washing, irrigation and garden watering. The observed percentage

4

removal for COD is almost 50%. Percentage removal for chlorides and nitrates are 60.12 % and 74.36%. Beside this treated greywater has no unpleasant odor and can freely be used for recommended purposes. The amount of TDS and TSS has also significantly reduced and their percentage removal of 37.8 % and 83.33 % has been observed.

Table 4.1: Removal Percentage for Different Parameters

S. no.	Parameters	Grey Water			Reuse Standard	Remarks
		Raw Greywater	Treated Greywater	Percentage Removal (%)		
1	pH	6.64	7.8	-	6 – 9	**OK**
2	EC (mS/m)	1.38	4.58	-	-	
3	Temperature (°C)	25.3	25.3	-	-	
4	Turbidity (NTU)	125	6.57	94.74%	<10	**OK**
5	Sulphates (mg/L)	36	243	-	-	
6	Nitrates (mg/L)	35.1	9	74.36%	-	
7	Chlorides (mg/L)	1179.63	470.44	60.12%	-	
8	COD (mg/L)	1766	895	49.32%	-	
9	BOD (mg/L)				<20	
10	TDS (mg/L)	1640	1020	37.80%	<1500	**OK**
11	TSS (mg/L)	300	50	83.33%	-	

4.3   Economic Analysis:

4.3.1   Cost of Installation of Plant:

4.3.1.1   Capital Cost:

Cost of Recycling Plant = Rs 42,000 (made with acrylic glass with pre-storage tank)

It is recommended to use filtration plant made up of brick masonry or concrete in order to use it in a house. The detail cost of whole assembly is shown in table 4.7. The cost was estimated by using MES schedule rates and also confirmed from 2 to 3 on field contractor. Cost of Recycling Plant = Rs 35,000 (made with acrylic glass without pre-storage tank)

4.3.1.2   Operational Cost:

Price of Coagulant (alum) = Rs 200 per kg
Amount of Coagulant used = 200 mg/l = 0.2 g/l
Amount of recycled greywater in a month = 800 liters/day x 30 days= 24000 liters
Amount of Coagulant used in a month = 4.8 kg
Power of mini pump and paddle motors = 70 Watts
Approx. time for recycling greywater = 15 hrs. /day
Consumption of Electricity = (70/1000) x 15 hrs. = 1.05 unit/day

Electricity consumed for running mini pump and paddles = 31.5 units/month
Price per Unit (IESCO) = (5.79 + 8.11)/2 = Rs 6.95
Further details are shown in table 4.8.

4.3.1.3 Cost-Benefit Analysis:

Reuse of recycled greywater in various activities will reduce the demand of freshwater and hence reduces the cost of water. Reuse of greywater can save cost of water bowsers in major cities where water requirements are being met through private water bowsers.
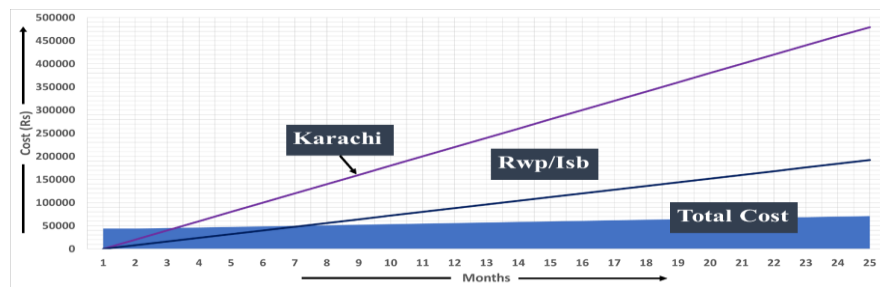
Figure 3.1 cost benefit analysis

5   CONCLUSION:

This research project concluded that greywater is a type of wastewater has a great potential for reusing it in various purposes and it will play an effective role in managing the water resources of Pakistan in a sustainable way. After analyzing the different parameters of greywater, I have designed a in house greywater recycling plant. Results and analysis of this project concluded that:

- Recycled greywater saves approximately 45 % of the freshwater in a house, making the water available for water scarcer regions of Pakistan.
- The project will help to save the water cost significantly in areas like Karachi and Islamabad where water requirements are being met through private water bowsers.
- This project is an efficient solution of all the ongoing water crisis problems of Pakistan.
- As the percentage of grey water in home wastewater is generally 50 to 80% of the total household wastewater. Therefore, recycling of greywater can efficiently reduce the quantity of wastewater produced from a house.

6   REFERNECE:

Abu-Zeid, M. A. (1998). Water and sustainable development: the vision for world water, life, and the environment. Water policy, 1(1), 9-19.

Agency-UK, E., 2011. Greywater for domestic users: an information guide. Published by environmental agency. Available at: www.enviroment-agency.gov.uk.

Ahmed, A., Iftikhar, H., & Chaudhry, G. M. (2007). Water resources and conservation strategy of Pakistan. The Pakistan development review, 997-1009.

Al-Jayyousi, O. R. (2003). Greywater reuse: towards sustainable water management. Desalination, 156(1-3), 18

1st International Conference on Advances in Civil & Environmental Engineering, University of Engineering & Technology Taxila, Pakistan

Conference date 22 &23 Feb 2022

Effect on the Mechanical Properties of Brick Masonry by Replacing the Cement Sand Mortar with Marble Waste Tile Bond Mortar

Sardar Ali, Khan Shahzada
University of Engineering & Technology Peshawar, Pakistan
13pwciv3903@uetpeshawar.edu.pk; shah_civil2003@yahoo.com

Akhtar Gul
University of Engineering & Technology Peshawar, Pakistan
akhtarwazir@uetpeshawar.edu.pk

Inayat Ullah Khan
University of Engineering & Technology Peshawar, Pakistan
16pwciv4553@uetpeshawar.edu.pk

ABSTRACT

This paper presents the effect on the mechanical properties of brick masonry by replacing the conventional mortar with a specific tile bond mortar. The key parameters evaluated contain compressive strength, stress-strain curve, direct shear strength, and diagonal shear strength. Prisms with similar dimensions were constructed in both conventional and tile bond mortar. The prisms were then tested in accordance with the required ASTM standards. The results show that the tile bond mortar effectively increases the diagonal shear strength by 8.36% although compressive strength was decreased by 13.24%. It was also concluded that the cohesion of marble waste tile bond mortar was decreased by 45%. However, its coefficient of friction was increased by 48%.

KEYWORDS: Marble waste tile bond, mechanical properties, conventional mortar

1   INTRODUCTION

Brick masonry is widely used in the construction industry in the world [1]. Brick masonry consists of brick units bonded in a specific bond pattern with the help of a paste called mortar. The mortars generally used may be Cement–Sand (CS) mortar, mud mortar, and lime mortar. The compressive strength of brick masonry depends on the strength of brick units as well as the strength of the mortar. The brick masonry has enough strength for gravity loads but has little shear strength and is vulnerable to lateral and seismic loadings [2]. Failure in a masonry wall can be classified as in-plane and out-of-plane failure [3]. Amongst the in-plane failure, shear and sliding failure needs effective bond between mortar and brick units. Recently, studies have been carried out to use lime mortar as a replacement to cement mortar [4]. But these mortars have low strength at start and required long time for hardening [5]. In this study an effort has been made to replace the conventional CS mortar with a locally available tile bond mortar. The mortar paste is just prepared by mixing the powder with water without adding any other ingredients. In addition to this, it does not require any curing of brick units

1st International Conference on Advances in Civil & Environmental Engineering, University of Engineering & Technology Taxila, Pakistan

Conference date 22 &23 Feb 2022

and assemblages. The tile bond is prepared locally, from the waste of marbles produced in marble industry hence may be called marble waste tile bond (MWTB). The waste is readily available and with a little modification, if used to replace the mortar in brick masonry, construction is expected to improve its mechanical properties [6]. It is worth mentioning that its use will also reduce the harmful environmental effects.

2 EXPERIMENTAL PROGRAM

The experimental program comprises the selection and testing of constituent materials, followed by the preparation of prism samples and their testing in accordance with required standards. Two sets of samples each with conventional CS mortar and tile bond mortar were prepared and plastered. English bond with mortar thickness of 10 mm and ratio 1:5 was used in the casting of all the CS mortar models. The use of English bond was due to its frequent use in Pakistan's brick masonry buildings, especially in the northern areas [7]. The experimental program is summarized in Figure 1.

2.1 Materials' selection

Locally available bricks brought from the kiln in a single batch were used. The marble waste tile bond was obtained from local manufacturers.
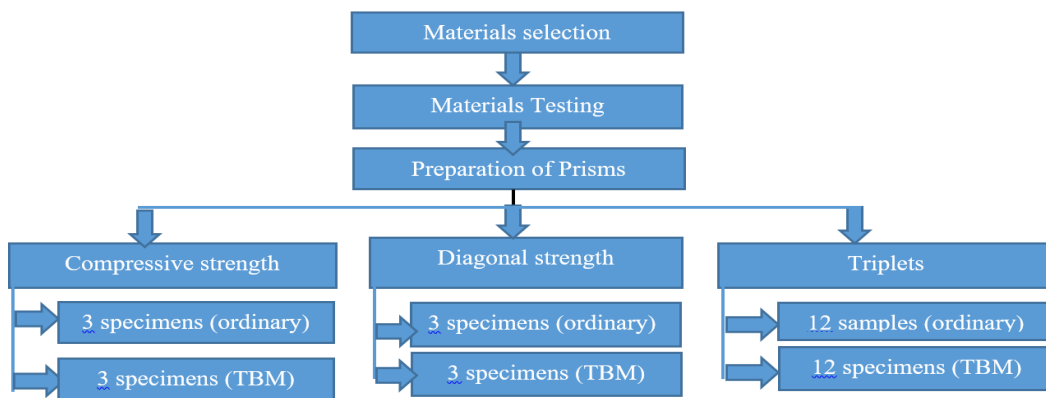
Figure 1 Summary of the experimentation process

In this study half scale down bricks were used in order to handle the sample easily and to simulate the actual field conditions by enclosing more number of mortar joints. However, scale factor was used as discussed by S. Petry and K. Beyer [8].

Table 1 Materials' Properties

Property	Mean Values	C.O.V (%)
Compressive Strength of brick units (half scale), psi (MPa), f_b	2450 (16.89)	11.2
Compressive Strength of mortar (CS mortar), psi (MPa), f_m	674.4 (4.65)	9.4
Compressive Strength of mortar (MWTBM), psi (MPa), f_m	422.1 (2.91)	14.6

1st International Conference on Advances in Civil & Environmental Engineering, University of Engineering & Technology Taxila, Pakistan

Conference date 22 &23 Feb 2022

2.2   Materials' testing

Brick units were tested for compressive strength in accordance with ASTM C-67 [9]. Mortar cubes of size 5x5x5 cm for both CS mortar (1:5) and MWTB mortar were tested in accordance with ASTM C-109. The results are presented in Table 1.

2.3   Preparation of samples

Two sets of three samples each for compressive strength and diagonal shear test were casted both in CS and MWTB mortar having the size 21.6 x 11.4 x 27.9 cm and 62.23 x 11.4 x 60.0 cm respectively [10]. The compressive strength specimens were tested under a universal testing machine (UTM) in accordance with ASTM C-1314 as shown in Figure 2(a) [11]. The diagonal strength specimens were tested in accordance with ASTM E-519 shown in Figure 2(b) [12].Triplets consisting of three bricks were prepared to find out the initial shear strength, cohesion, and coefficient of friction. Twelve samples each for conventional mortar and tile bond mortar were constructed and tested in accordance with EN 1052-3standard [13]. The testing arrangement is shown in Figure 2(c).

(a)   (b)   (c)
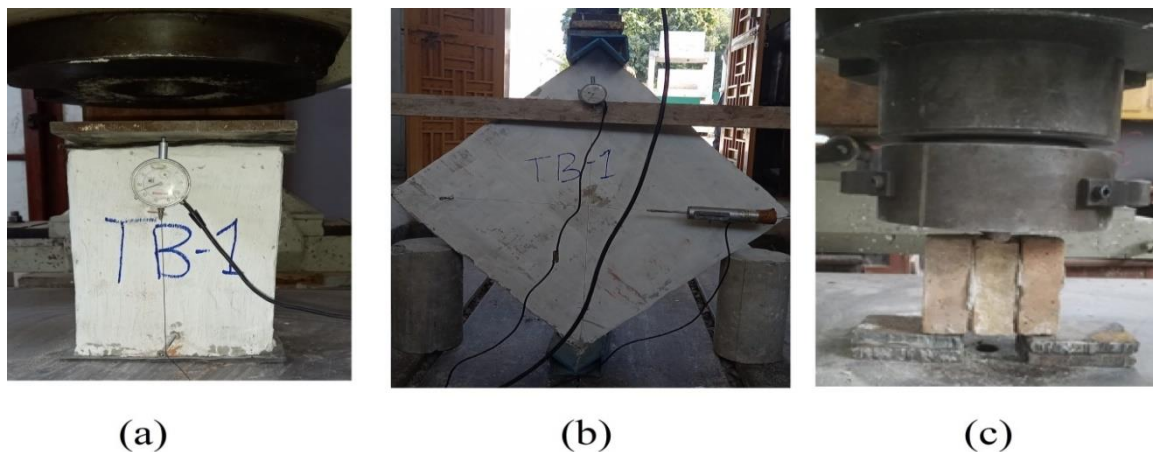
Figure 2 specimen and test set up for (a) compressive strength (b) diagonal strength

(c) Triplets testing

3   RESULTS AND DISCUSSION

3.1   Compressive strength and modulus of elasticity

The results of compressive strength and elastic modulus are presented in Table 2. The data was used to obtain the stress-strain curve shown in Figure 3(a). The elastic modulus was obtained from the plot of stress-Strain curve following the ASTM E-447 [14].

Table 2 Results of compressive strength and elastic Modulus

Specimen type	Compressive strength psi (Mpa)	C.O.V (%)	Elastic Modulus ksi (GPa)	C.O.V (%)
Control specimens	911.7 (6.286)	27.29	323.43 (2.23)	58.01
MWTB	855.72 (5.90)	33.31	219.1 (1.510)	40

1st International Conference on Advances in Civil & Environmental Engineering, University of Engineering & Technology Taxila, Pakistan

Conference date 22 &23 Feb 2022

The stress-strain curve shows that MWTB shows a mild slope compared to CS mortar thus more ductile in nature than CS mortar. The results of compressive strength lie within the normal range of compressive strength in Northern Pakistan [15].

3.2 Diagonal strength and modulus of rigidity

The results of diagonal strength are presented in Table 3. The shear stress-strain curve was obtained from the data recorded by the dial gauges. The modulus of rigidity was determined to form the plot (Figure 3b) by using the same method as used for elastic modulus. However, test results can be interpreted by different ways and by available formulas in literature [16].

Table 3 Results of shear strength and shear modulus

Specimen type	Shear strength psi (MPa)	C.O.V (%)	Shear Modulus ksi (GPa)	C.O.V (%)
Control specimens	36.55 (0.252)	13.78	129.52 (0.893)	43
MWTB mortar specimens	0.275 (39.88)	92.96	0.604 (87.60)	32.21

The results show that the MWTB mortar increases the diagonal shear strength by 8.36 % and modulus of rigidity was decreased by 32.36 %. The results of modulus of rigidity/ modulus of elasticity falls in the acceptable range, and is in close agreement with the reported results [17] and can be used for practical purposes.
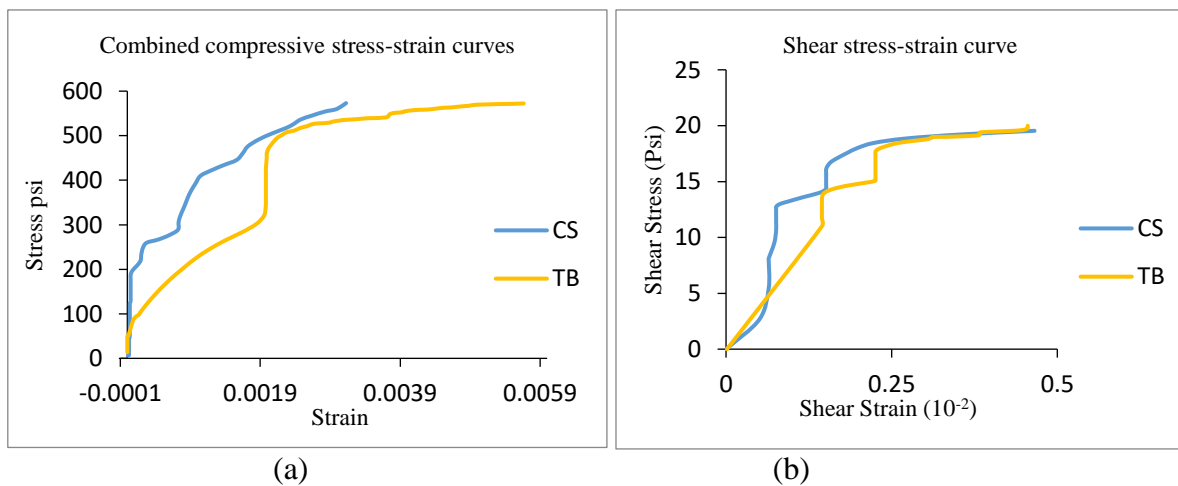
Figure 3 (a) Compressive Stress-strain Curve (b) Shear Stress-strain Curve

3.3 Direct shear strength

The data obtained from these tests were processed and analysed [18]. The normal stress and shear stress were calculated and plotted against each other as shown in Figure 4. Based on the linear regression analysis of this plot, values of cohesion and the coefficient of friction were determined. The values of initial shear strength τ_0 and coefficient of friction μ for CS mortar were recorded to be 82.67 psi (0.57 MPa) and 0.44 respectively. While for MWTB mortar, initial shear strength τ_0 and coefficient of friction μ was 44.96 psi (0.31 MPa) and 0.65, respectively.

1st International Conference on Advances in Civil & Environmental Engineering, University of Engineering & Technology Taxila, Pakistan

Conference date 22 &23 Feb 2022
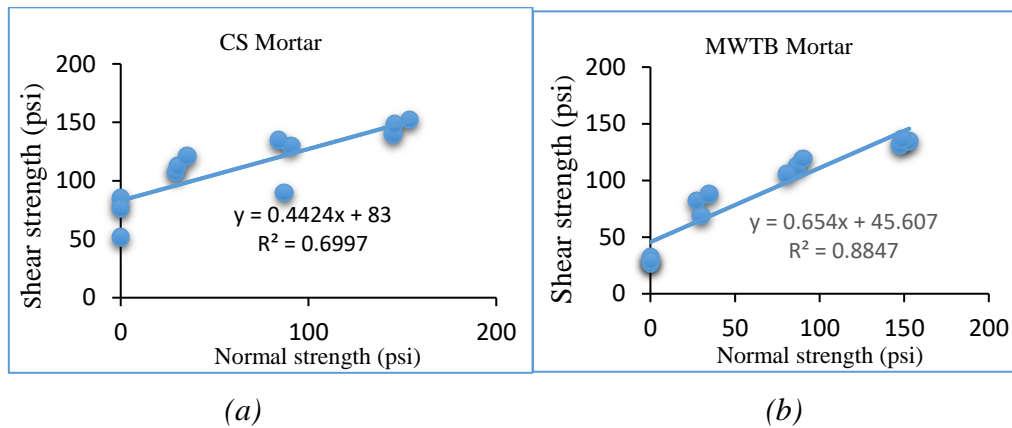
Figure 4 shear strength Vs. Normal strength (a) CS Mortar, (b) MWTB Mortar

4   CONCLUSIONS

Based on the results discussed above, following conclusions can be drawn. In the CS mortar, prisms fail along the line of action of force having one major crack along the diagonal while the behavior of MWTB mortar prisms was better and ductile under diagonal shear strength test, showing many hair line cracks before the crushing of model. Marble waste tile bond mortar models possess compressive strength nearly equal to control specimens and improved shear strength by 8.36%. Also, the coefficient of friction of marble waste tile bond mortar was increased by 48 %. However, its cohesion was decreased by 45%.

5   REFERENCES

[1]   V. Alecci, M. Fagone, T. Rotunno, and M. De Stefano, "Shear strength of brick masonry walls assembled with different types of mortar," *Constr. Build. Mater.*, vol. 40, pp. 1038–1045, 2013, doi: 10.1016/j.conbuildmat.2012.11.107.

[2]   D. Dizhur, N. Ismail, C. Knox, R. Lumantarna, and J. M. Ingham, "Performance of unreinforced and retrofitted masonry buildings during the 2010 darfield earthquake," *Bull. New Zeal. Soc. Earthq. Eng.*, vol. 43, no. 4, pp. 321–339, 2010, doi: 10.5459/bnzsee.43.4.321-339.

[3]   C. Wang, V. Sarhosis, and N. Nikitas, "Strengthening/Retrofitting Techniques on Unreinforced Masonry Structure/Element Subjected to Seismic Loads: A Literature Review," *Open Constr. Build. Technol. J.*, vol. 12, no. 1, pp. 251–268, 2018, doi: 10.2174/1874836801812010251.

[4]   Arizzi A, Viles H, Cultrone G (2012) Experimental testing of the durability of lime-based mortars used for rendering historic buildings. Constr Build Mater 28(1):807–818.

[5]   Parcesepe, Eliana & Masi, Rosa & Lima, Carmine & Mauro, Gerardo & Pecce, Marisa & Maddaloni, Giuseppe. (2021). Assessment of Mechanical and Thermal Properties of Hemp-Lime Mortar. Materials. 14. 882. 10.3390/ma14040882.

[6]   N. Bheel, K. A. Kalhoro, T. A. Memon, Z. U. Z. Lashari, M. A. Soomro, and U. A. Memon, "Use of Marble Powder and Tile Powder as Cementitious Materials in Concrete", *Eng. Technol. Appl. Sci. Res.*, vol. 10, no. 2, pp. 5448–5451, Apr. 2020.

[7]   A. Naseer (2009), "Performance Behavior of Confined Brick Masonry Buildings under Seismic Demand," PhD thesis, Department of Civil Engineering, University of Engineering & Technology, Peshawar.

[8]   S. Petry and K. Beyer, "Scaling unreinforced masonry for reduced-scale seismic testing," *Bull. Earthq. Eng.*, vol. 12, no. 6, pp. 2557–2581, 2014, doi: 10.1007/s10518-014-9605-1.

1st International Conference on Advances in Civil & Environmental Engineering, University of Engineering & Technology Taxila, Pakistan

Conference date 22 &23 Feb 2022

[9] A. C67-12, "Standard Test Methods for Sampling and Testing Brick and Structural Clay Tile," *ASTM Int. West Conshohocken, PA, USA*, vol. 04, pp. 1–12, 2009, doi: 10.1520/C0067.

[10] Borri A, Castori G, Corradi M (2015) Determination of shear strength of masonry panels through different tests. Int J Archit Herit 9(8):913–927. https://doi.org/10.1080/15583058.2013.804607

[11] ASTM C1314 - 09, "Standard Test Method for Compressive Strength of Masonry Prisms," *ASTM Int.*, pp. 1–10, 2015, doi: 10.1520/C1314-14.2.

[12] E. ASTM, "519-02: Standard test method for diagonal tension (shear) in masonry assemblages," *CD, Am. Soc. Test. Mater. Philadelphia*, 2002.

[13] EN 1052-3. Methods of test for masonry. Part 3: Determination of initial shear strength. European standard; 2007.

[14] ASTM E447, "Standard Test Methods for COMPRESSIVE STRENGTH OF MASONRY," *Astm Int.*, pp. 10–13, 1974.

[15] BCP-SP 07. Building Code of Pakistan. Ministry of Housing, Islamic Republic of Pakistan, 2007.

[16] Binda L, Cardani G, Castori G, Corradi M, Saisi A, Tedeschi C. Procedure sperimentali per la determinazione delle caratteristiche della muratura. In: Borri A, editor. Manuale delle murature storiche – vol. I. Roma: Tipografia del Genio Civile; 2011. p. 316–8.

[17] M. Javed, (2009), "Seismic Risk Assessment of Unreinforced Brick Masonry Buildings System of Northern Pakistan," PhD thesis, Department of Civil Engineering, University of Engineering & Technology, Peshawar.

[18] Andreotti, Guido & Graziotti, Francesco & Magenes, Guido. (2019). Expansion of mortar joints in direct shear tests of masonry samples: implications on shear strength and experimental characterization of dilatancy. Materials and Structures. 52. 10.1617/s11527-019-1366-5.

Prediction of Soil Compaction Parameters using Gene Expression Programming

Hasnain Ayub, Turab Jafri*
NUST Institute of Civil Engineering,
National University of Sciences and Technology, Islamabad, Pakistan.
Mkhan.ms19nice@student.nust.edu.pk; turabjafri@nice.nust.edu.pk

Syed Taseer Abbas Jaffar
Department of Civil Engineering,
University of Management & Technology, Lahore, Pakistan.
taseer.jaffar@umt.edu.pk

ABSTRACT

The determination of soil compaction parameters, maximum dry density (MDD) and optimum moisture content (OMC), in the laboratory requires considerable time and energy. Various efforts have been made to counter the issue by developing models to predict compaction parameters of soil, but they are either applicable to specific soil types or specific compaction energies. A machine learning technique, Gene Expression Programming (GEP), is used in this study to predict the compaction parameters of soil using the index properties of soils collected from literature. In terms of accuracy, the GEP models presented in this study outperformed the previously developed prediction models. The accuracy (R-squared) for training and validation of MDD was found to be 0.8945 and 0.9032, respectively, and that for training and validation of OMC was 0.9165 and 0.9251, respectively.

KEYWORDS: Soil Compaction, Maximum Dry Density, Optimum Moisture Content, Gene Expression Programming, Prediction Models

1   INTRODUCTION

Soil compaction is a dynamic process in earthwork construction in which the soil is compacted through mechanical process. The compaction process reduces the air voids by bringing the soil particle close to each other thus increasing the shear strength and reducing the permeability of soils. The compaction parameters of soils, maximum dry density and optimum moisture content, are determined in the laboratory following standard proctor compression test [1] and modified proctor compression test [2] which require significant amount of time and energy. Thus, various models have been developed in the past to predict the compaction parameters using conventional regression analysis [3],[4],[5],[6],[7],[8],[9],[10],[11]. The accuracy of simple regression analysis techniques reduces as the number of datasets increase. Therefore, machine learning approaches have been adopted to deal with large datasets. So far, the best prediction model developed for compaction parameters found in literature is by using multi expression programming (MEP) for a

1st International Conference on Advances in Civil & Environmental Engineering, University of Engineering & Technology Taxila, Pakistan

Conference date 22 &23 Feb 2022

total of 226 datasets covering both the fine-grained soil and coarse-grained soils compacted against different compaction energies [12]. Using Gene Expression Programming, this research aims at developing new prediction models with the prediction accuracy better than the conventional regression models and MEP models in the literature.

2   METHODOLOGY

For the development of the new prediction models, the data was used from the literature [12]. The dataset contained 226 records of the index and compaction properties of fine-grained and coarse-grained soils. The statistic of the index and compaction properties of soils is given in the Table 1.

Table 1 Statistics of the soil properties

Parameters	Maximum	Minimum	Standard deviation	Mean
Fine content (CF), %	100	8.6	29.9	63.1
Sand content (CS), %	89	0	23.3	29.5
Gravel content (CG), %	67.1	0	14.5	7.5
Plastic Limit (PL), %	48.3	6.1	7.4	22
Liquid Limit (LL), %	608	16	163.9	108.7
Compaction Energy (E), kj/m^3	2755	154.5	733.9	893.8
Maximum Dry Density (MDD), Mg/m^3	2.33	1.09	0.2	1.75
Optimum Moisture Content (OMC), %	43.7	5.3	6	17.5

Gene Expression Programming (GEP) was used for the development of new prediction models. GEP is an extension of Genetic programming (GP) [13]. GEP creates computer models in form of complex trees and these trees learn and adapt while changing their structure and composition. The superiority of GEP, a genetic programming-based approach, over other soft computing methods is that it produces mathematical function for the prediction, and it does not assume any prior form of existing relationship [14]. There are five components of GEP that are: the terminal set, the function set, control parameters, fitness function, and termination conditions. GEP is a genotype-phenotype evolutionary algorithm having linear chromosomes of fixed length and the computer program of GEP are encoded in these chromosomes to solve a problem. Genes are sub-programs that are created in GEP. Gene in a GEP chromosome consists of a head and a tail. The head of a gene may consist of a function or terminal symbol, but the tail consists of only terminal symbols. Expression trees (ET's) are generated as a result of these chromosomes [13]. These trees vary in size and shape. Mathematical functions are later derived from these expression trees. A typical expression tree of GEP is shown in Figure 1. In this tree D_0, D_1 and D_3 are the inputs while C_5 and C_6 are constants. The functions defined for the model are addition (+), subtraction (-), multiplication (×), and square root (sqrt). GEP is a multi-genetic programing and the genes in a chromosomes are connected via the functions defined by the user, thus creating expression trees, the complexity of which is governed by the number of genes [15]. The equation derived from the expression tree is given in Eq.   (1), where Y is the output.

1st International Conference on Advances in Civil & Environmental Engineering, University of Engineering & Technology Taxila, Pakistan

Conference date 22 &23 Feb 2022
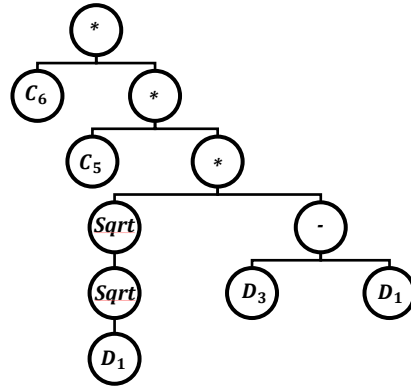
Figure 1: Expression tree (ET)

$$Y = C_6 \times C_5 [\sqrt{\sqrt{D_1}} \times (D_3 - D_0)]$$

(1)

To develop GEP prediction models for compaction parameters, GeneXproTool 5.0 was used [16]. The dataset was randomly divided into training (70%) and validation (30%). The optimal parametric setting to develop the GEP algorithm was established on the basis of hit and trial procedure and is provided in Table 2.

Table 2: Optimal parametric setting for GEP algorithm

GEP parameters	GEP settings for MDD and OMC	GEP parameters	GEP settings for MDD and OMC
General		**Genetic operators**	
Training records	158	Mutation	0.00138
Validation/Testing records	68	Inversion rate	0.00138
Number of chromosomes	100	IS transposition rate	0.00138
Head size	8	RIS transposition rate	0.00138
Number of genes	5	One-point recombination rate	0.00277
Linking function	Addition	Two-point recombination rate	0.00277
Function set	$+, -, \div, \times, \exp, x^2$	Gene recombination rate	0.00277
Numerical constants		Uniform recombination	0.00755
Constants per gene	10		
Data type	Floating point		
Ephemeral random constant	[-10,10]		

It is worth noting that Wang and Yin, 2020 [12] did not consider gravel content (CG) as an input for developing MEP model while CG is included as an input in this research.

3   RESULTS AND DISCUSSION

The expression trees ETs were developed as a result of the modelling. The expression trees were then translated to mathematical functions. The mathematical functions for ETs were then linked together via linking function. The final mathematical equations for MDD and OMC developed using GEP are given in Eq.   (2) and   (3), respectively.

1st International Conference on Advances in Civil & Environmental Engineering, University of Engineering & Technology Taxila, Pakistan

Conference date 22 &23 Feb 2022

$$\text{MDD } (Mg/m^3) = \text{CF} + 91.84 + e^{\frac{-LL}{11.69}} + (\text{CS}^2 + e^{5.46}) - 7.244 + \frac{0.146}{PL} + \text{CS} + \tag{2}$$

$$\text{CG} - (e^{-8.953} \times PL \times CF) + \frac{-0.627 \times CS \times CF}{E} - LL - 7.599 + LL - \frac{CG}{-5.5(CF)^2 + 5.07(CG)}$$

$$\text{OMC } (\%) = \frac{-34.49(PL+CS)}{-525-E} - \frac{PL}{3.57(CS+1.43)} + \frac{(7.956 \times CG + CF)(CF)(LL)}{2.06 \times E(E+CG)} + \frac{CS}{(CG+3.235)(CF)} + \tag{3}$$

$$\text{CF} + 8.4 + \frac{CF}{PL} - \frac{LL}{240.6} - CF - 4.25 + \frac{CF(PL)}{CF+PL+38.43}$$
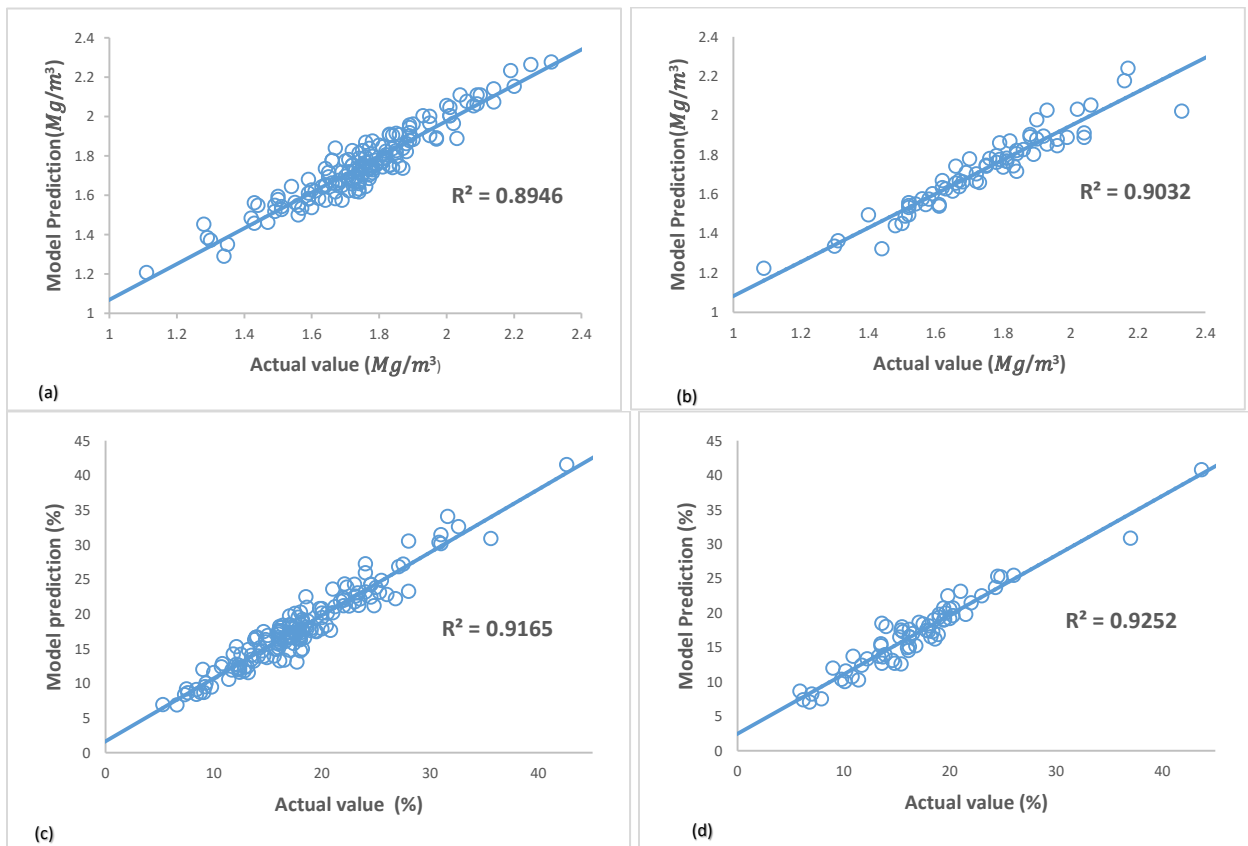
Figure 2: GEP model prediction for output vs actual output for (a) MDD Training, (b) MDD Validation, (c) OMC Training and (d) OMC Validation.

The GEP models performed better for MDD in terms of R^2 (0.8946 for training and 0.9032 for validation) while for OMC, the prediction accuracy (R^2) was almost the same as that of MEP model (0.9156 for training and 0.9252 for validation) as shown in Figure 2.

4 CONCLUSION

In this study, a comprehensive dataset of soil was used to develop prediction models for soil compaction parameters using Gene Expression Programming. Out of the 226 records, 158 were

1st International Conference on Advances in Civil & Environmental Engineering, University of Engineering & Technology Taxila, Pakistan

Conference date 22 &23 Feb 2022

used for the training of the model while 68 records were used for used for the validation of the trained models. GEP models were derived for MDD, and OMC and the accuracy of the newly developed models was evaluated. It is concluded that the presented GEP models are more accurate than both the conventional regression models and the MEP model in the literature.

5   REFERENCES

[1]   A. C. D.-18 on S. and Rock, *Standard Test Methods for Laboratory Compaction Characteristics of Soil Using Standard Effort (12 400 Ft-lbf/ft3 (600 KN-m/m3)) 1*. ASTM international, 2007.

[2]   D. Astm, "Standard Test Method for Laboratory Compaction Characteristics of Soil Using Modified Effort (D1557-12)," *ASTM, West Conshohocken, Pennsylvania, USA*, 2012.

[3]   A. N. Al-Khafaji, "Estimation of soil compaction parameters by means of Atterberg limits," *Q. J. Eng. Geol. Hydrogeol.*, vol. 26, no. 4, pp. 359–368, 1993.

[4]   L. R. Blotz, C. H. Benson, and G. P. Boutwell, "Estimating optimum water content and maximum dry unit weight for compacted clays," *J. Geotech. Geoenvironmental Eng.*, vol. 124, no. 9, pp. 907–912, 1998.

[5]   M. Omar, A. Shanableh, A. Basma, and S. Barakat, "Compaction characteristics of granular soils in United Arab Emirates," *Geotech. Geol. Eng.*, vol. 21, no. 3, pp. 283–295, 2003.

[6]   A. Sridharan and H. B. Nagaraj, "Plastic limit and compaction characteristics of finegrained soils," *Proc. Inst. Civ. Eng. Improv.*, vol. 9, no. 1, pp. 17–22, 2005.

[7]   O. Günaydın, "Estimation of soil compaction parameters by using statistical analyses and artificial neural networks," *Environ. Geol.*, vol. 57, no. 1, p. 203, 2009.

[8]   L. Di Matteo, F. Bigotti, and R. Ricco, "Best-fit models to estimate modified proctor properties of compacted soil," *J. Geotech. geoenvironmental Eng.*, vol. 135, no. 7, pp. 992–996, 2009.

[9]   C. Patra, N. Sivakugan, and B. Das, "Relative density and median grain-size correlation from laboratory compaction tests on granular soil," *Int. J. Geotech. Eng.*, vol. 4, no. 1, pp. 55–62, 2010.

[10]   H. Mujtaba, K. Farooq, N. Sivakugan, and B. M. Das, "Correlation between gradational parameters and compaction characteristics of sandy soils," *Int. J. Geotech. Eng.*, vol. 7, no. 4, pp. 395–401, 2013.

[11]   A. Saikia, D. Baruah, K. Das, H. J. Rabha, A. Dutta, and A. Saharia, "Predicting compaction characteristics of fine-grained soils in terms of Atterberg limits," *Int. J. Geosynth. Gr. Eng.*, vol. 3, no. 2, pp. 1–9, 2017.

[12]   H.-L. Wang and Z.-Y. Yin, "High performance prediction of soil compaction parameters using multi expression programming," *Eng. Geol.*, vol. 276, p. 105758, 2020.

[13]   C. Ferreira, "Gene expression programming in problem solving," in *Soft computing and industry*, Springer, 2002, pp. 635–653.

[14]   A. Johari, G. Habibagahi, and A. Ghahramani, "Prediction of soil–water characteristic curve using genetic programming," *J. Geotech. Geoenvironmental Eng.*, vol. 132, no. 5, pp. 661–665, 2006.

[15]   Z.-L. Cheng, W.-H. Zhou, and A. Garg, "Genetic programming model for estimating soil suction in shallow soil layers in the vicinity of a tree," *Eng. Geol.*, vol. 268, p. 105506, 2020.

[16]   C. Ferreira, "Gene expression programming: a new adaptive algorithm for solving problems," *arXiv Prepr. cs/0102027*, 2001.

DECLARATION

The authors declare that there is no conflict of interest.

Numerical
Investigation of Concrete Columns Reinforced with GFRP under Eccentric Loading

Arif Ahsan, Afaq Ahmad
University of Engineering & Technology Taxila, Pakistan
aarif.ahsan@students.uettaxila.edu.pk ; afaq.ahmad@uettaxila.edu.pk
Dr. Mohamed Elchalakani, Farid Abed
The University of Western Australia, American University of Sharjah
mohamed.elchalakani@uwa.edu.au ; fabed@aus.edu

ABSTRACT

Innumerable work was performed to investigate Glass Fibre Reinforced Concrete (GFRP) Columns having stainless steel stirrups under Eccentric Loading. Gleaned from the Author's Actual Experimental results of the dissected models. Six Eccentric Columns finite element analysis (FEA) models for specimens were prepared with the help of the commercial software ABAQUS Standard together with MATLAB, and Calibration to the FEM was performed for the various geometric variables such as dilation angle, viscosity parameter, mesh size, and element types. The study included the actual behavior of materials and the concrete damage-plasticity model. The simulation study of the GFRP RC finite element model validated in Agreement with respect to the experimental results and Concrete damaged plasticity Model.

KEYWORDS: FEA, Abaqus, Concrete damaged plasticity, GFRP, Eccentric

1   INTRODUCTION

From the last few decades, Several experiments have been carried out in order to increase the strength and durability of Reinforced Concrete Structures. Concrete having steel is more vulnerable to corrosion results the loss of strength and spalling. As a result, the Concrete structure life reduces. To improve the service life of the concrete structures, an alternative to conventional materials was required. Replacement of the ordinary steel with the Fibre Reinforced Polymer (FRP) has many advantages like enhanced strength, more strength, lightness, and low corrodibility[1]. The most suited substitute for steel bars is glass fiber-reinforced polymer (GFRP), which is very lightweight, low density has More strength, less thermal conductivity, higher electromagnetic resistance, and significantly hinders corrosion effectively.[2].

A substantial amount of work is being performed to comprehend and understand the behavior of the Fiber-reinforced Polymer Concrete (FRPC).[3] Investigated that the behavior of the GFRP Reinforced column is much similar with the normally reinforced concrete column having 1% reinforcement of cross-section.[2],[4]

When subjected to eccentric loading, the Axial Capacity of a GFRP column with different reinforcement ratios is significantly affected and reduced when particularly in comparison to a steel-reinforced column. It was reported, GFRP RC column under eccentric loading exhibited

1st International Conference on Advances in Civil & Environmental Engineering, University of Engineering & Technology Taxila, Pakistan

Conference date 22 &23 Feb 2022

Large lateral displacement resulting in a Reduction in axial capacity. [5] depicted that, HSC Circular columns having GFRP Reinforcement, failure under small eccentricity was because of the crushing failure of concrete on compression face. At large eccentricity, HSC Circular GFRP concrete Column showed flexure tension failure.

Finite element simulations were done to evaluate the behavior of GFRP RC columns with varying slenderness ratios, findings of the finite element analysis (FEA) and testing results of failure mechanisms and post-buckling performance were found to be in close agreement.[6]

2   FINITE ELEMENT MODELING & SIMULATION

2.1   Methodology

Numerical investigation of Eccentrically Loaded Glass Fiber Reinforced Polymer Reincoref Concrete (GFRP-RC) Columns Specimen was done with the help of Commercially used Software ABAQUS Standard 6.14. A total of 06 Controlled Model of GFRP Reinforced columns were Modelled. While performing the modeling of Columns Specimen, the Base of the. GFRP Reinforced Columns simulations were carried out as a 3D solid stress section model. And 3D deformable truss components were adopted to simulate the reinforcing bars. For Studying the Damaged Concrete Behavior of GFRP-RC Column, Characteristics of the modified Concrete Damaged Plasity Model was used.

2.2   Model Characteristics

For modeling specimen in the Abaqus, Fixity was assigned at the Base of all the GFRP RC columns to apply the Axial force, and there was no restraints at the top of the columns. Static loading with minimal Fluctuations was exerted on top of reinforced concrete columns using a displacement control approach to estimate the axial load-deflection history up to failure. At various eccentricities from the top center of the columns, Loading was applied in the form of displacement which was 20 mm. To uniformly distribute the load the Steel bearing plate was used of 50 mm thickness at Top and Bottom of the Column. These induced plates have the Modulus of Elasticity value of 210 Gaga Pascal having the Steel Density of 7.83e-9 tonne/mm3.

2.3   Equations

Majewski [7] presented the relationship between the ultimate strain ε_{cu1} and average compressive strength of concrete ε_{c1} Shown in Eq. (1) and Eq. (2)

$$\varepsilon_{c1} = 0.0014\left[2 - e^{-0.024f_{cm}} - e^{-0.140f_{cm}}\right] \quad (1)$$

$$\varepsilon_{cu1} = 0.004 - 0.0011\left[1 - e^{-0.0215f_{cm}}\right] \quad (2)$$

1st International Conference on Advances in Civil & Environmental Engineering, University of Engineering & Technology Taxila, Pakistan

Conference date 22 &23 Feb 2022
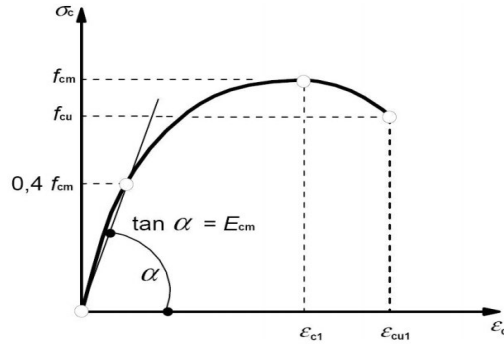
Figure 2. Stress-strain diagram for analysis of structures

At the initial, phase the concrete stress-strain relationship in the elastic range will be linear. The Eq. (3)

$$\sigma_c{}^1 = E_o \varepsilon_c \qquad (3)$$

Based on the secant Modulus of concrete the linear relationship is given as given by Eq. (4)

$$E_o = \left(0.8 + 0.2 \frac{f_{cm}}{88}\right) E_{ci} \quad (4)$$

$$E_{ci} = 1000 \, f_{cm}{}^{1/3}$$

The limit at which concrete reaches its compressing crushing is given by Eq. (5),

$$\sigma^2{}_c = \frac{E_{ci}\frac{\varepsilon_c}{f_{cm}} - \left(\frac{\varepsilon_c}{\varepsilon_{cm}}\right)}{1 + \left(E_{ci}\frac{\varepsilon_c}{f_{cm}} - 2\right)\frac{\varepsilon_c}{\varepsilon_{cm}}} \qquad (5)$$

3   TABLES AND FIGURES

Six models were prepared to have a Transverse Reinforcement spacing of 50 mm and 100 mm. And the eccentricities applied to loading were 25mm, 50mm, and 75mm. The reinforcement ratio was 1.35% of the cross-sectional area of the specimen columns. Table 1 presents the main concrete material parameters, loading increments, and sizes in the ABAQUS Standard Step Module.

Table 1: Material characteristics

Parameter	Value
Concrete ρ (ton/mm^3)	2.4 x 10^{-9}

1st International Conference on Advances in Civil & Environmental Engineering, University of Engineering & Technology Taxila, Pakistan

Conference date 22 &23 Feb 2022

Poisson's ratio, ν	0.2
E_c Concrete Elasticity Modulus (N/mm^2)	26587
Loading Incretement interval	0.01
Minimum Increment interval	10^{-10}
Total increments	1000

For Numerical Simulation of GFRP RC columns, Suporrt Restraints and general arrangements are shown in Figure 1.
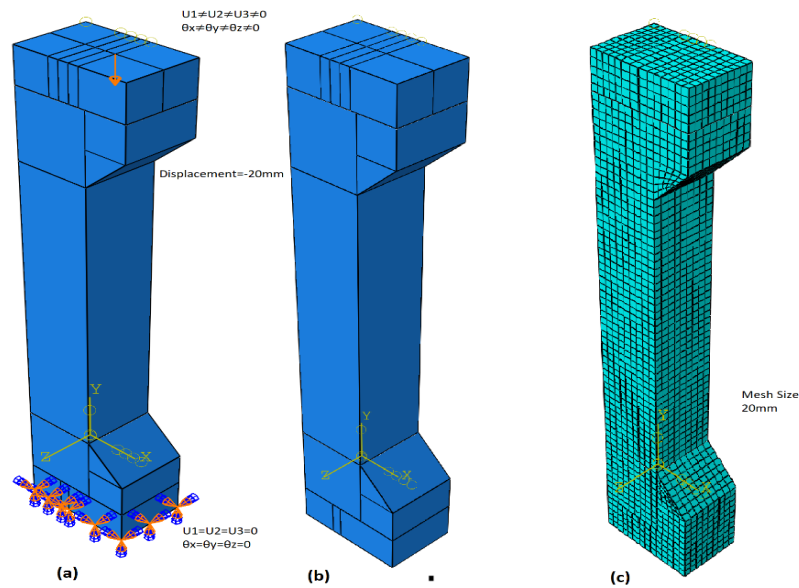
Figure 1. GFRP RC Column (1) Constraints, (2) Geometry (3) finite element meshing

3.1   FEA Result Curves

1st International Conference on Advances in Civil & Environmental Engineering, University of Engineering & Technology Taxila, Pakistan

Conference date 22 &23 Feb 2022
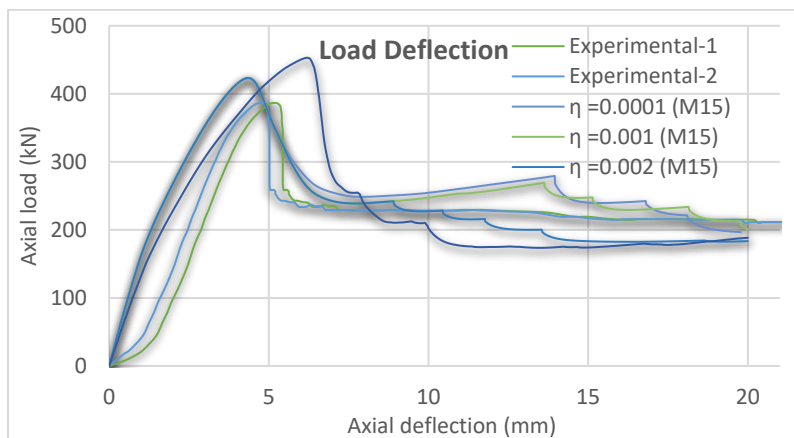
4   CONCLUSION

In this Study, the CDP model, when compared to other models, the CDP model deals with the plastic behavior, compressive behavior, tensile behavior, confinement, and damage mechanism of concrete and can converge the findings to precision, was used for stimulation of FEM of GFRP RC columns in a Commercial Software Abaqus under the Eccentric Loading. It was observed that with the variation of viscosity and mesh size of specimen results also fluctuates. All the results of the FEA stress-strain curve and Eccentric load-deflection curve are in correlation. A slight deviation of results was observed in the elastic phase of deflection curves,

5   ACKNOWLEDGEMENTS

REFERENCES

1.   Nunes, F., et al., *Experimental and numerical study on the structural behavior of eccentrically loaded GFRP columns.* 2013. **72**: p. 175-187.
2.   Hadi, M.N. and I.B.R.J.J.o.C.f.C. Widiarsa, *Axial and flexural performance of square RC columns wrapped with CFRP under eccentric loading.* 2012. **16**(6): p. 640-649.
3.   De Luca, A., F. Matta, and A.J.A.s.j. Nanni, *Behavior of full-scale glass fiber-reinforced polymer reinforced concrete columns under axial load.* 2010. **107**(5): p. 589.
4.   Bakouregui, A.S., et al., *Axial load–moment interaction diagram of full-scale circular LWSCC columns reinforced with BFRP and GFRP bars and spirals: Experimental and theoretical investigations.* 2021. **242**: p. 112538.
5.   Hadhood, A., H.M. Mohamed, and B.J.J.o.C.f.C. Benmokrane, *Experimental study of circular high-strength concrete columns reinforced with GFRP bars and spirals under concentric and eccentric loading.* 2017. **21**(2): p. 04016078.
6.   Turvey, G., Y.J.C. Zhang, and Structures, *A computational and experimental analysis of the buckling, postbuckling and initial failure of pultruded GRP columns.* 2006. **84**(22-23): p. 1527-1537.
7.   Raza, A. and A.J.A.i.C.E. Ahmad, *Numerical investigation of load-carrying capacity of GFRP-reinforced rectangular concrete members using CDP model in ABAQUS.* 2019. **2019**.

1st International Conference on Advances in Civil & Environmental Engineering, University of Engineering & Technology Taxila, Pakistan

Conference date 22 &23 Feb 2022

Experimental Investigation of Local Scouring around the Round Nose Bridge Pier using Different Vegetation Conditions.

Hafiz Ubaid-Ur-Rehman[1], Naeem Ejaz[1]
University of Engineering & Technology Taxila, Pakistan
Ubaidsiddiqui1964@gmail.com, naeem@uettaxila.edu.pk

Muhammad Aleem[1]
University of Engineering & Technology Taxila, Pakistan
engrm.aleem@gmail.com

ABSTRACT

Various methods and techniques have been used to study the scouring around bridge piers. In this investigation, round nose bridge pier was integrated into a uniform graded sand bed with median diameter 'd50' = 0.57 mm and geometric standard deviation of grain sizes was σ_g = 1.22 < 1.30 when σ_g <1.30 the bed particle is regarded as uniform, of the laboratory channel with three discharges of 0.023 m3/s, 0.027 m3/s and 0.032 m3/s in each test. Flexible and rigid vegetation is to be used at 0D,4D and 6D distances form the round Nose Bridge Pier against each discharge, whereas 'D' is the diameter of round nose of Pier. Vegetation was used on the upstream side. The duration of each test was maintained for 3 hours. The local scour of pier was measured around the diagonal upstream, downstream, left, right, upstream, and diagonal downstream with the point gauge. Experimental results shows that the scouring around the round nose bridges pier using flexible vegetation reduced up to 50.0% at 0D and 38.11% and 30.15% at 4D and 6D distance respectively. While reduction in scouring is 33.44%, 30.92% and 27.38% in case of rigid vegetation at 0D,4D and 6D distances respectively. It was noted that the scouring around the round nose bridges pier using flexible vegetation was minimum as compared to rigid vegetation. By increasing the distance between the pier and the vegetation, the effect of flexible and rigid vegetation on the scouring around the pier decreased.

KEYWORDS: Round Nose bridge pier; Scour depth; Flexible vegetation; Rigid Vegetation; Flow intensity.

1   INTRODUCTION

The formation of local scour holes around bridge piers is almost an unavoidable problem in alluvial channel beds subjected to the erosive action of oncoming river flows. The design and construction of bridges spanning across alluvial channels requires the knowledge or at least as

1st International Conference on Advances in Civil & Environmental Engineering, University of Engineering & Technology Taxila, Pakistan

Conference date 22 &23 Feb 2022

accurate an estimate as possible of maximum scour depth which might occur during the anticipated life of the bridge near the piers [1].

A unifying theory for estimating scour depth at piers is still in an embryonic stage, mainly due to the complex nature of the scour problems. Major scouring usually occurs during floods which are unsteady flows and may even have different flow directions from normal flows. Scour is caused by three-dimensional boundary-layer separation at the pier, resulting in erosion of bed material by the local flow structure, which is characterized by a high level of turbulence and vorticity. The investigation of scour at bridge piers has been on-going for several decades.

Numerous experimental and analytical investigations of local pier scour were conducted in alluvial channels and series of prediction equations were developed by researchers to estimate the maximum scour depth at bridge piers under different approach flow, sediment size and gradation, pier type and size conditions [2].

The local scour at bridge pier continues for a sufficiently long time until the hydrodynamic forces in the scour hole are no longer able to remove particles from the hole. At this condition, the scour hole reaches an equilibrium condition, and the scour depth does not change appreciably unless the flow conditions or bed material changes change.

2   METHODOLOGY

The experimental materials and methodology are discussed in the following section. All the experimental trials were carried out on rectangular channel made of concrete having dimensions 20.0 m long, with depth of 0.75 m and 1.0 m wide, situated in Water Resources Lab, Department of Civil Engineering, University of Engineering and Technology Taxila, Pakistan. A river model is built in the centre of the rectangular channel. The main channel was filled with the fine sand. Bed was levelled after each trial and length of sand bed was kept 8m and depth was kept 15cm. This segment is used to perform for all scour experiments. The bridge pier positioned in centre of channel width at 4m from start of sand bed. During each trial, the discharge was kept constant.
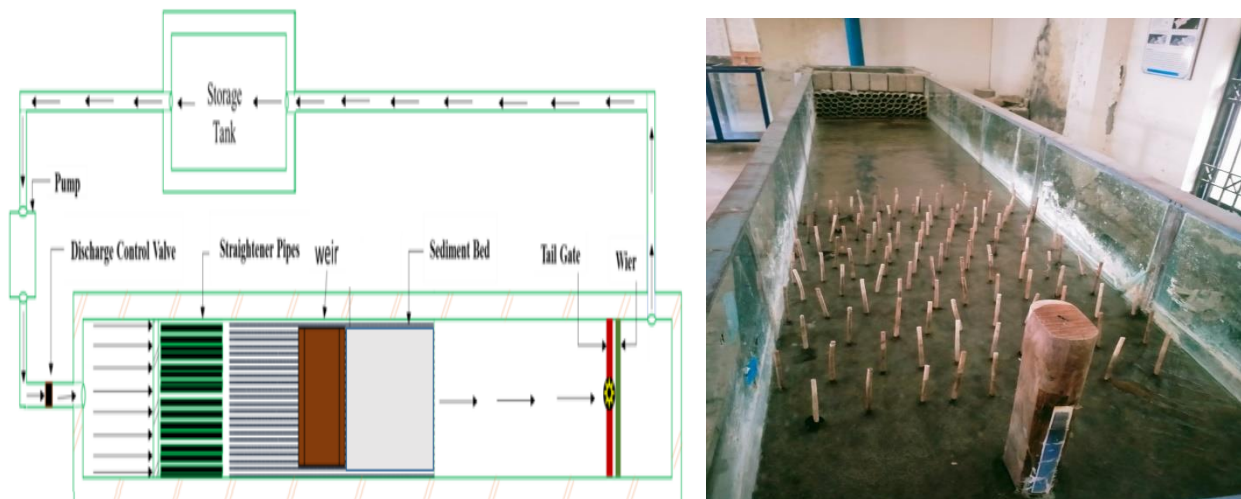
Fig 2.1: Top View of Laboratory Channel

1st International Conference on Advances in Civil & Environmental Engineering, University of Engineering & Technology Taxila, Pakistan

Conference date 22 &23 Feb 2022

This research carried out in different phases.

1. Firstly, experiments performed to investigate scouring around the round nose pier by using regular sand bed material at three different discharges of 0.023m³/s, 0.027 m³/s and 0.032 m³/s.
2. Secondly, experiments performed by using sand bed material with flexible vegetation at 3 different distances 0D,4D and 6D on each discharge.
3. Thirdly, experiments performed by using sand bed material with rigid vegetation at 3 different distances 0D,4D and 6D on each discharge.

2.1 Material.

A round nose bridge pier having nose diameter 6 cm was inserted in the centre of the testing section of the channel. The length of the channel gives sufficient distance downstream of the pile to guarantee that the turbulent flow does not interfere with the downstream border. B/D values larger than 10 are required for the tested pier diameters, where B is the flume width and D is the pier nose diameter (i.e., D=6cm). According to Chiew and Melville (1987)., this eliminates the side wall and pier obstruction effects The average width of the featured pier is less than one-sixth the width of the flume. To mitigate the negative consequences of side walls, as Frostick recommends, McClelland, and Mercer (2011) [4].

For rigid vegetated channel experiments, the plants were simulated by means of wood cylinders of 3 mm diameter, while the flexible model array was constructed from commercial broom head. Both kinds of artificial vegetation were embedded in the sand bed separately perforated uniformly with holes of 3 mm, that is the diameter of the rigid elements, D, whereas, in the case of flexible vegetation, 8 single elements of the broom head with a diameter 0.4 mm each one was stacked.

2.2 Equations

Compound rectangular-trapezoidal sharp-crested weir were used to measure the discharges. In present discharge of 0.023 m³/s, 0.027m³/s & 0.032m³/s were used. The discharge can be changed by using valve and can be adjusted by head over weir. The values of discharges were calculated by CRTSC (compound rectangular-trapezoidal sharp-crested) equation (1.1).

$$Q = \left(\tfrac{2}{3}\right)C_{rd2}\sqrt{2g}\,b_2 h_2^{3/2} + \left(\tfrac{2}{3}\right)C_{rd1}\sqrt{2g}\,(2b_1)\,h_1^{3/2} + \left(\tfrac{8}{15}\right)C_{td}\sqrt{2g}\,\tan\left(\tfrac{\theta}{2}\right) h_{1e}^{5/2} \qquad (1.1)$$

Where
b = weir length, g = gravitational acceleration, θ = notch angle, h = water head on the weir crest
C_{rd} = discharge coefficient of the rectangular sharp-crested weir, he = effective head,
C_{td} = discharge coefficient for triangular sharp-crested weir

1st International Conference on Advances in Civil & Environmental Engineering, University of Engineering & Technology Taxila, Pakistan

Conference date 22 &23 Feb 2022

3   RESULTS & DISCUSSION:

Scouring depth around the pier increases as the discharge increases keeping all other parameters constant. Fig (2.2) shows maximum scour depth without vegetation at Q_1(0.023 m3/s) discharge was 2.90 cm, when we use rigid vegetation at 0D,4D and 6D (0,24cm and 36cm), scouring depth reduces from 2.90cm to 1.93cm, 2.29cm and 2.43cm respectively. When we use flexible vegetation at 0D,4D and 6D (0,24cm and 36cm), scouring depth reduces from 2.90 to 1.45cm, 1.93cm and 2.30cm respectively. Hence scour depth reduces maximum in case of flexible vegetation.

Similarly, maximum scour depth without vegetation at Q_2(0.027 m3/s) discharge was 3.0 cm, when we use rigid vegetation at 0D,4D and 6D (0,24cm and 36cm), scouring depth reduces from 3.0cm to 2.09cm, 2.38cm and 2.61cm respectively while using flexible vegetation at 0D,4D and 6D (0,24cm and 36cm), scouring depth reduces from 3.0 to 1.90cm, 2.36cm and 2.72cm respectively. Similarly, in case of Q_3(0.032 m3/s) discharge scour depth was 3.25 cm, when we use rigid vegetation at 0D,4D and 6D (0,24cm and 36cm), scouring depth reduces from 3.0cm to 2.36cm, 2.57cm and 2.84cm respectively while using flexible vegetation at 0D,4D and 6D (0,24cm and 36cm), scouring depth reduces from 3.25cm to 2.27cm, 2.62cm and 3.08cm respectively.
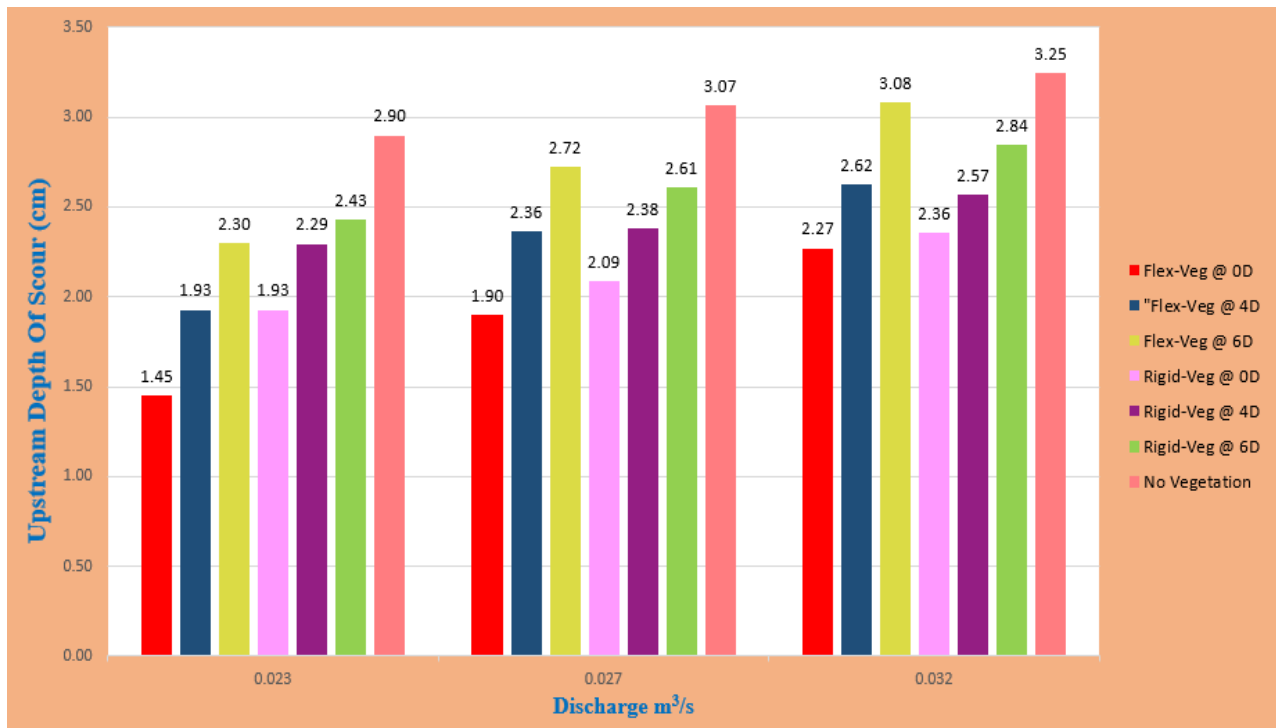
Fig.2.2: Relationship between scour depth (ds) and discharges

Figure (2.3) shows that ds/D ratio reduces as the distance between the pier and the vegetation reduces. In case of Q_1 (0.023 m3/s) discharge having flexible vegetation, ds/D ratio was 0.38, 0.32

1st International Conference on Advances in Civil & Environmental Engineering, University of Engineering & Technology Taxila, Pakistan

Conference date 22 &23 Feb 2022

and 0.24 when the distance between pier and flexible vegetation was 6D,4D and 0D(36cm,24cm,0) respectively while in case of Q_2(0.027 m3/s) and Q_3 (0.032 m3/s) discharge ds/D ratio was 0.45, 0.39, 0.31 and 0.51, 0.43, 0.37 respectively. Similarly, In case of Q_1 (0.023 m3/s) discharge having rigid vegetation, ds/D ratio was o.41,0.38 and 0.32 when the distance between pier and flexible vegetation was 6D,4D and 0D(36cm,24cm,0) respectively while in case of Q_2(0.027 m3/s) and Q_3(0.032 m3/s) discharge ds/D ratio was 0.43, 0.40, 0.35 and 0.47, 0.43, 0.39 respectively.
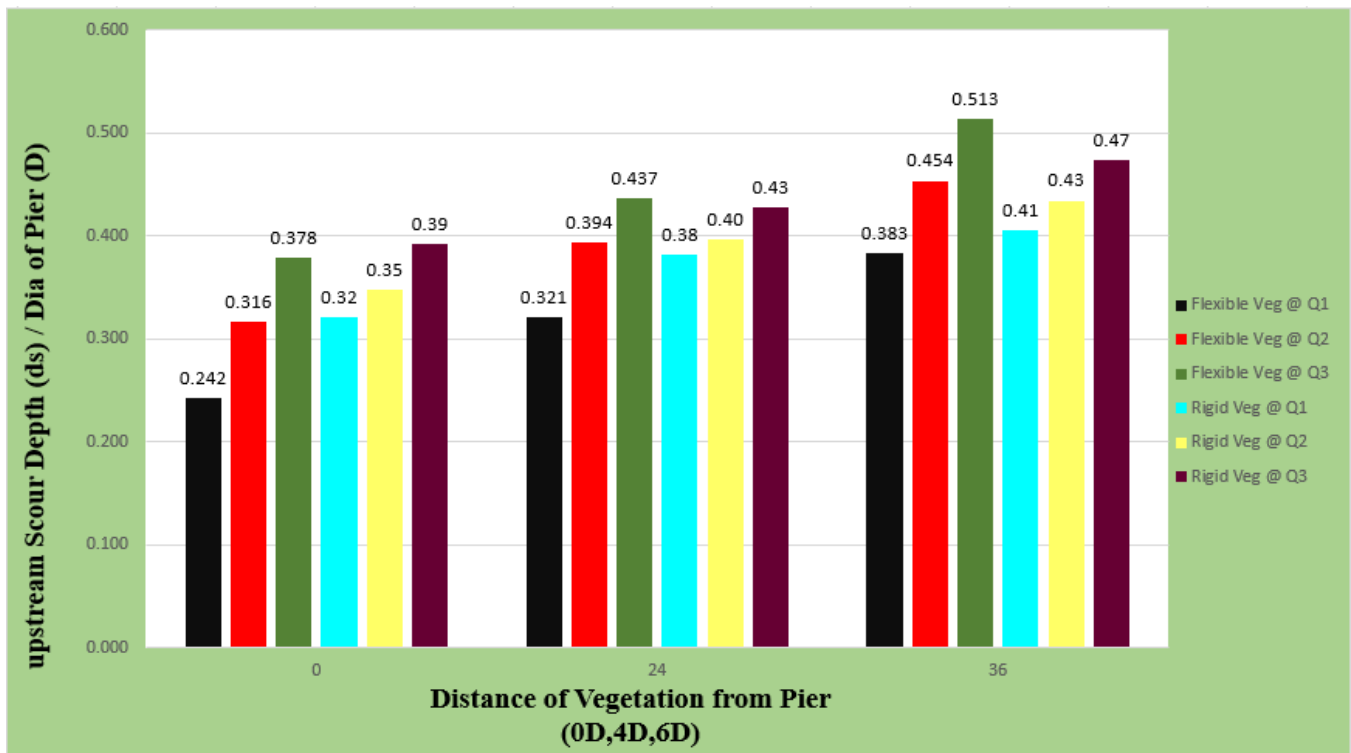
Fig.2.3: The ds/D versus Distance b/w vegetation and the round nose bridge pier installed at upstream side.

4   CONCLUSION

Detail experiments were performed to investigate the scouring pattern around a single round nose bridge pier with or without the vegetation and different trends were drawn on the graph using different parameters. The following conclusions drawn after experimental results.

1. The Scouring depth around the pier increases by increasing the flow discharge in clear water condition.
2. After installation of flexible and rigid vegetation individually, maximum scouring reduction around the pier was observed at minimum or zero separation distance between the pier and vegetation.

1st International Conference on Advances in Civil & Environmental Engineering, University of Engineering & Technology Taxila, Pakistan

Conference date 22 &23 Feb 2022

3. Maximum reduction in scouring around the pier was observed in case of flexible vegetation when the distance between pier and flexible vegetation is minimum or 0D which is up to 50.0%. Similarly, 38.11% and 30.15% reduction in scouring in case case of flexible vegetation at 4D and 6D distance respectively. While in case of rigid vegetation, reduction in scouring is 33.44%, 30.92% and 27.38% at 0D,4D and 6D respectively.

4. Ds/d ratio in case of flexible vegetation reduced maximum as compared to that of rigid vegetation.

5   ACKNOWLEDGEMENTS

6   REFERENCES

[1] T. K. T. Tsujimoto, " Velocity profile of flow in vegetated-bed channels," Kazavava University, KHL Progressive Report 1, 1990.

[2] B. Barkdoll, "Time scale for local scour at bridge piers," *Journal of Hydraulic Engineering,* vol. 10, no. 126, pp. 793 - 794, 2000.

[3] H. W. S. Y.-J. C. Fu-Chun Wu, "Variation of roughness coefficients for unsubmerged and submerged vegetation," *Journal of Hydraulic Engineering,* vol. 125, no. 9, pp. 934-942., 1999.

[4] Y. Chiew, "Scour Protection at Bridge Piers," *Journal of Hydraulic Engineering,* vol. 9, no. 118, pp. 1260-1269, 1992.

[5] A. G. R. &. C. Tafarojnoruz, "Bridge pier scour mitigation under steady and unsteady flow conditions.," in *Acta Geophysica, 60(4), 1076–1097.*, 2012.

[6] N. E. A. A. Muhammad Aleem, "Experimental Investigation of double bridge pier scouring after installation of broad crested trapezoidal weir at upstream.," in *International Conference on Hydrology and Water Resources*, Lahore, 2021.

Evaluation of existing models for PET FRPs confined square RC specimens

Muhammad Hamza

University of Engineering & Technology Taxila, Pakistan

muhammadhamza1601@gmail.com;

Shahzad Saleem

University of Engineering & Technology Taxila, Pakistan

shahzad.saleem@uettaxila.edu.pk

ABSTRACT

Many stress-strain models have been presented previously for investigating compressive behavior of fiber-reinforced polymer (FRP) confined concrete; however, many of these models apply to conventional FRPs (e.g., carbon FRP (CFRP), glass FRP (GFRP), aramid FRP (AFRP)). Recently, polyethylene terephthalate (PET) FRP, which is a new type of FRP having a large rupture strain (LRS), has been introduced and successfully used for increasing the strength of concrete structures. Few models exist for PET FRP confined concrete, however, in these models, the influence of internal steel confinement is missing. The applicability of present stress-strain models that evaluates the influence of ties and longitudinal steel reinforcement on the compressive response of PET FRP confined concrete remains a question. The main goal of this paper is to check the efficiency of existing models developed for columns confined by conventional FRPs in evaluating the stress-strain behavior of PET FRP confined square columns. Experimental results show that all the models that have been considered underestimate the ultimate conditions.

KEYWORDS: steel jackets, polymers, PET FRPs.

1   INTRODUCTION

Providing the external confinement of a suitable material to concrete can increase its compressive strength considerably [1]. For this purpose from the previous two decades, fibre-reinforced polymers (FRPs) have been extensively used. Among these FRPs, carbon FRP (CFRP), glass FRP (GFRP), and aramid FRP (AFRP) were mostly considered. These FRPs usually possess high elastic modulus and strength, however, their rupture strain is low (in the range from 0.15 to 3.0%) [2]. Because of their low rupture strain, these FRPs can be categorized as conventional FRPs. Various models have been introduced for stress-strain behavior of concrete confined by these conventional FRPs.

  In real structures, the majority of concrete columns are of square or rectangular shape having steel reinforcement inside. Strengthening/retrofitting of RC columns with conventional FRPs not only leads to significant increase in strength and ductility but it also delays the initiation of longitudinal bars buckling. Comparatively, few models have considered the effect of internally

1st International Conference on Advances in Civil & Environmental Engineering, University of Engineering & Technology Taxila, Pakistan

Conference date 22 &23 Feb 2022

provided steel reinforcement on the stress-strain response of CFRP, GFRP, or AFRP confined concrete.

Most recently, a new type of FRP i.e., polyethylene terephthalate FRP (PET FRP) having low elastic modulus and a large rupture strain (more than 5%), has emerged which is more environmentally friendly, as it is obtained by recycling waste plastic bottles. Because of low stiffness, PET FRP does not provide high restraint to bar buckling compared to conventional FRPs [3]. Nevertheless, due to its large rupture strain (LRS), PET FRP-confined RC columns experienced high deformation despite the excessive bar buckling.

It is to be noted that only handful of studies considered the modeling of stress-strain behavior of PET FRP confined plain concrete. To the best of the authors' knowledge, no study considered the effect of the internal transverse and the longitudinal steel reinforcement provided on the compressive response of PET FRP confined conlumn. As a first step, in this paper, the efficency of current stress-strain models established for conventional FRPs to predict the response of PET FRP confined square RC column specimens is evaluated.

Existing stress-strain models

Harajli et al. [4] presented an analytical study based upon the area and the material characteristics of FRP, aspect ratio of cross-section, the corner radius of specimens, and the configuration of ties used. A model was developed for both the CFRP and GFRP confined concrete. The specimens had a corner radius of 15mm, 22.5mm, and 30mm respectively. The aspect ratios for the specimen were 1, 1.7, 2.3, and 3.7. The model presented a two-stage relationship for stress-strain response. Later, Julian et al. [5] modified this model for square and low-strength concrete specimens confined with CFRPs.

Eid et al. [6] represented a model for the combined effect of internal and external confinement in which two and four layers of CFRPs were wrapped around the specimens. Transverse reinforcement having 6 mm diameter and an average yield strength of 258 MPa was used.

Carlo et al. [11] presented a model for both the rectangular and circular specimens with or without internal confinement. The model presented two conditions; first when the column has 2r/b< 0.3, decreasing branch occurs after the peak stress, and second when 2r/b>0.3, no decreasing branch occurs after peak stress. Table 1 displays the expressions of these models discussed.

Table 1:Existing analytical models.

Model	Expressions
Harajli et al. [4]	$f_1 = f_{c'} + k_1 \varepsilon_{lo} \left(\frac{k_{ef} p_f E_f}{2} + \frac{k_{es} k_v p_{st} E_s}{2} \left(\frac{A_{cc}}{A_g} \right) \right), f_2 = \sqrt{K_o^2 - K} - K_0$ $\varepsilon_{co} = \varepsilon_o [1 + (310.57\varepsilon_{lo} + 1.9) \left(\frac{f_1}{f_{c'}} - 1 \right)]$

1st International Conference on Advances in Civil & Environmental Engineering, University of Engineering & Technology Taxila, Pakistan

Conference date 22 &23 Feb 2022

Eid et al. [6]	$f_1 = \frac{a\varepsilon_c}{1+b\varepsilon_c+z\varepsilon_c^2}, \varepsilon_c < \varepsilon_{cc\prime}$ $f_2 = f_{cc\prime}\exp(k(\varepsilon_c - \varepsilon_{cc\prime})^{k_2} + E_{cu}(\varepsilon_c - \varepsilon_{cc\prime})$, $\varepsilon_{cu} > \varepsilon_c > \varepsilon_{cc\prime}$ $f_2 = f_{cc\prime}\exp(k(\varepsilon_c - \varepsilon_{cc\prime})^{k_2}, \varepsilon_c > \varepsilon_{cu}$
Julian et al. [5]	$f_1 = \left[f_{co}\left(\frac{2\varepsilon_c}{\varepsilon_{co}} - \left(\frac{\varepsilon_c}{\varepsilon_{co}}\right)^2\right)\right] \times C_{FRP}, 0 < \varepsilon_c < \varepsilon_{co}$ $f_2 = \sqrt{K_o^2 - K} - K_0 \times C_{FRP}, \varepsilon_{co} < \varepsilon_c < \varepsilon_{cu}$ $\varepsilon_{cu} = \varepsilon_o\left[1 + (310.57\varepsilon_{lo} + 1.9)\left(\frac{f_1}{f_{c\prime}} - 1\right)\right]x\beta$
Carlo et al. [11]	$f_1 = f_{co}\left(1 + k_1.\frac{P_u}{f_{co}}\right), \varepsilon_c = \varepsilon_{co}$ $f_2 = 0.55 + 1.5\left(\frac{2r}{b}\right), \varepsilon_c = \varepsilon_{cu}$ $\frac{\varepsilon_{cu}}{\varepsilon_{co}} = 2 + B(\frac{P_u}{f_{co}})$ $\frac{\varepsilon_{cc}}{\varepsilon_{cu}} = 0.55 + 1.5\left(\frac{2r}{b}\right), \frac{2r}{b} < 0.3$

2   EXPERIMENTAL DATA

In this paper, sixteen small-sized square RC column specimens were considered that were tested in compression by Saleem et al. [13]. Eight specimens had an internal stirrup spacing of 85 mm, whereas, in the remaining eight specimens, a spacing of 155 mm was used. In each group, there were two controlled, two single layer, two double layers, and two triple layers confined concrete specimens. The cross-section and height of all the specimens were the same i.e., 150 x 150 mm and 325 mm respectively. To avoid stress concentrations, the corners of specimens were made round to radius of 26 mm.

3   RESULTS

The comparison between the theoretical stress-strain curves that were obtained from existing models and experimental stress-strain results of this study is presented in Figure 1. In general, it can be observed that all the models underpredict the complete stress-strain behavior, especially the ultimate strain. The model of Eid et al. [6] and Carlo et al. [11] performed relatively better in predicting the ultimate conditions. However, there is a need to modify these models to consider the large rupture strain and low elastic modulus of PET FRP for a better prediction of LRS FRP-confined concrete response.

1st International Conference on Advances in Civil & Environmental Engineering, University of Engineering & Technology Taxila, Pakistan

Conference date 22 &23 Feb 2022
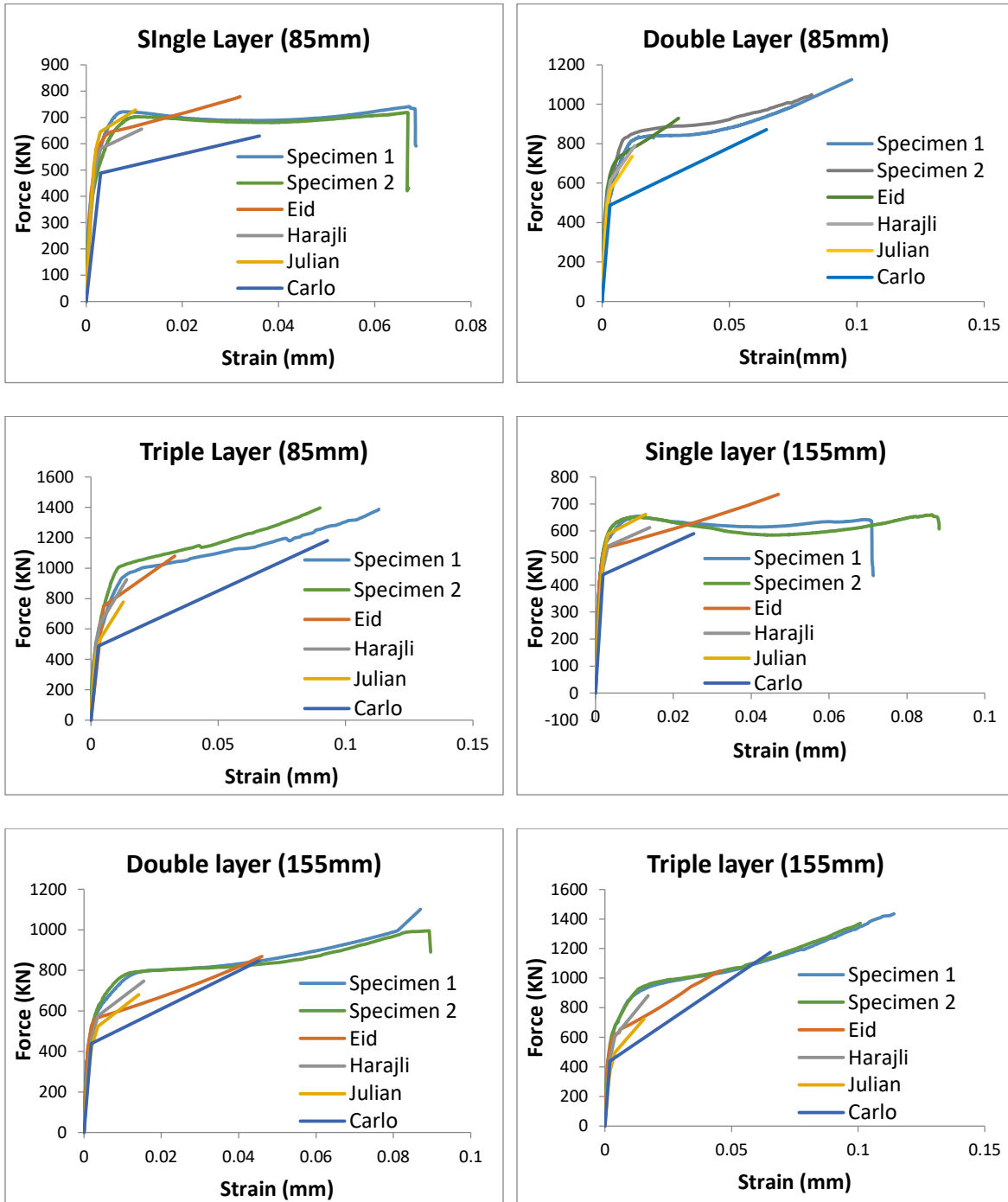
Figure 1: Existing models results (Where 85mm and 155mm represent the spacing between ties).

4   CONCLUSIONS

The conclusions drawn from this study are as follow:

   i.   CFRP and GFRP models are not suitable in prediction of stress-strain behavior of PET FRP non-circular confined RC.

  ii.   The ultimate strains produced in PET FRPs are considerably higher as compared to the predicted strains from the models. In other words, PET FRPs-confined concrete undergoes greater strain as compared to GFRP and CFRP confined concrete.

 iii.   The results obtained from models considered in case of PET FRP confined concrete are not satisfactory. Therefore, a separate model should be developed for aforesaid confinement that can accurately predict stress-strain behavior.

REFERENCES

1.   Saadatmanesh H, Ehsani MR, Li MW. Strength and ductility of concrete columns externally confined with fiber composite straps.ACI Struct J 1994;94(1):434-471.

2.   Mirmiran A, Shahawy M Behavior of concrete columns confined by fiber composites. J Struct Engrg, ASCE 1997;123(5):583-90.

3.   Pimanmas,A. and Saleem, S. (2018).Evaluation of existing stress-strain models and modeling of PET FRP confined concrete.J. Compos.Construct. 22(3),1-41.

4.   Harajli,M. N.(2006).Axial stress-strain relationship for FRP confined circular and rectangular concrete columns.Cem.Concr.Compos.,28(10), 938-948.

5.   Carrillo, J.; Valencia-Mina, W.; Bojórquez, E. Compressive performance of square and low-strength concrete columns retrofitted with externally-bonded CFRP. Mater. Today Commun. 2020, 23, 100874.

6.   Eid R, Paultre P. Plasticity-based model for circular concrete columns confined with fibre composite sheets.Eng Struct 2007;29(12):3301-11.

7.   Lam L,Teng JG. Design-oriented stress-strain model for FRP-confined concrete in rectangular column. J Reinf Plast Compos 2003;22(13):1149-86.

8.   Wu Y-F, Wei Y-Y. Effect of cross sectional aspect ratio on the strength of CFRP confined rectangular concrete columns. Eng Struct 2010;32:32-45.

9.   Wang L-M, Wu Y-F, Effect of corner radius on the performance of cfrp-confined square concrete column:Test.Eng Struct:2008;30:493-505.

10.   Ozbakkaloglue T.Axial compressive behaviour of square and rectangular high-strength concrete-filled FRP tubes. ASCE J Compos Construct 2013;17(1):151-61.

11.   Pellegrino C. and Modena C.. Analytical model for FRP confinement of concrete columns with and withod internal steel reinforcement.J Compos.Constr, 14(6),693-705.

12.   Ilki,A,Peker,O.,Karamuk,E.,Demir,C., and Kumbasar,N.(2008).FRP retrofit of low and medium strength circular and rectangular reinforced concrete column.J. Mater. Civ.Eng.,20(2),169-188.

13.   Saleem S, Pimanmas A, Qureshi MI, Rattanapitikon W. Axial behavior of PET FRP confined reinforced concrete. J Compos Constr ASCE 2021;25(1):04020079.

A Numerical Approach for Predicting Optimum Length of a Protective dike

Sohail Iqbal, Ghufran Ahmed Pasha, Usman Ghani, Afzal Ahmed
Department of Civil Engineering, University of Engineering
and Technology, Taxila 47080, Pakistan
sohailsakhani147@gmail.com; ghufran.ahmed@uettaxila.edu.pk;
usman.ghani@uettaxila.edu.pk; afzal.ahmed@uettaxila.edu.pk

ABSTRACT

Rigid structures, including groins or dikes, are built around riverbanks for multiple reasons. Scoring around the dike is one of the most critical parameters in dike design. This paper discusses the depth averaged velocity and turbulent kinetic energy (*TKE*)across a series of dikes with and without protective dike (PD) , placed upstream of the main dikes. The studied PD with different lengths were numerically investigated by applying the Reynolds stress turbulence model (RSM). For the post-processing code, FLUENT (ANSYS) was utilized. The depth averaged velocity and *TKE* was captured at the upstream and downstream of the main dike. The findings revealed that minimizing these flow characteristics (depth averaged velocity and *TKE*) by adding a suaitable length of PD helps reduction in scouring. Hence, a PD with length of 0.5 L' to 0.6L'(where L' is the length of existing dike length) is suggested to protect existing spur dike from failure due to scouring.

KEYWORDS: Protective dike, turbulence modelling, open channel flow.

1   INTRODUCTION

The scour around the dike is one of the major problems that cause partly or fully failure of the hydraulic structure. Therefore, the scour hole in terms of depth and volume is an important parameter that should be addressed. However, compared with previous studies related to scour around bridge piers [1] and abutments [2], scour phenomena around dikes have not been addressed as they involve different dikes arrangements and flow complexities[3].
To minimize the scouring, Zhang et al. [4]. suggested different design parameters (size, shapes, and the distance between two dikes) of dikes Despite numerous suggestions, many existing dikes in the whole world face scouring problems. The scouring problem is mostly observed at the nose of dikes. To protect the dikes from scouring, two solutions were suggested by Li et al [5]. In the first method, different revetments were provided around the edge of the dike. While in the second method, flow direction was changed by providing an extra dike PD. Moreover, different shapes of collars (circular and rectangular) around the edge of dikes were used by Atarodi et al., [6] to protect from scouring.
Previous researchers used an open channel to investigate different flow characteristics [7,8] by applying the Reynolds stress model. Iqbal et al. [9] also used RSM to investigate the flow behavior around the dikes in an open channel. The main goal of the present study is to investigate the flow

1st International Conference on Advances in Civil & Environmental Engineering, University of Engineering & Technology Taxila, Pakistan

Conference date 22 &23 Feb 2022

characteristics in the presence of a PD in the rectangular open channel using Reynolds stress modeling (RSM)..

2   MATERIALS AND METHOD
2.1   Numerical model Validation

For the validation of the numerical model, experimental data of Weitbrecht [10] was used. The experimental domain was 260 cm in length, 180 cm in width, and 4.6 cm in height. The top view of the experimental domain is shown in Figure 1. The same geometry was used in the numerical model as the experimental domain for validation. All the other components of dikes and channel height were kept the same. The adopted mesh used for the present validation was tri-pave with almost 6 million nodes.Depth averged flow velocity and water depth were 0.0160 m/s and 4.6 cm, respectively. Periodic boundary conditions were provided at the inlet and outlet of the channel, while slip conditions were given out the outer wall. A good agreement between the validated numerical and experimental data of Weitbrecht [10] can be observed in Figure 2.

| (a) | (b) |
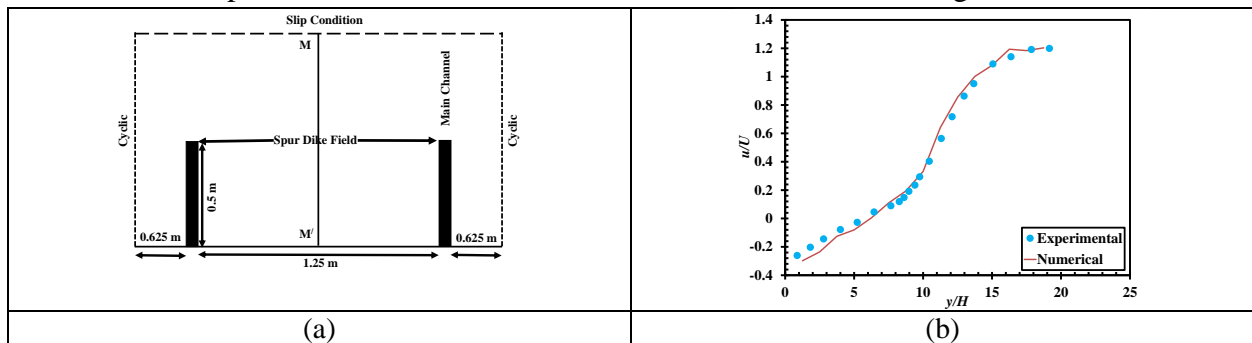
Figure 1 (a)Detailed view of the experimental domain of Weitbrecht [10], where MM$^/$is the location of depth averaged streamwise velocity measurement (b) Comparison of experimental and numerical averaged streamwise velocity at MM$^/$

2.2   Numerical modal simulation

For the numerical simulation, the computational domain was extended in length, and the new dimensions are 390 ×180 ×4.6 cm. In addition, a protective rectangular dike was placed upstream of the main dikes (Figure 3), with three different lengths. Different parameters used for numerical simulation are enlisted in Table 1.

Table 1 Hydraulic Conditions for Numerical Simulation

Cases	Discharge (L/s)	Protective dike (PD) length 'L' (cm)	Dike width (cm) 'w'	Dike length (cm) 'L$^/$'	Dike height (cm) 'h'	Velocity 'U' (m/s)

1st International Conference on Advances in Civil & Environmental Engineering, University of Engineering & Technology Taxila, Pakistan

Conference date 22 &23 Feb 2022

A	1.324	without PSD	5	50	4.6	0.0160
B	1.324	17	5	50	4.6	0.0160
C	1.324	29	5	50	4.6	0.0160
D	1.324	50	5	50	4.6	0.0160

Other hydraulic conditions, including discharge, water depth, and initial velocity, were kept the same as used for numerical validaiorn (see section 2.1) in the numerical simulation process. To achieve the pressure velocity coupling SIMPLE scheme, the Reynolds stress model (RSM) was applied.
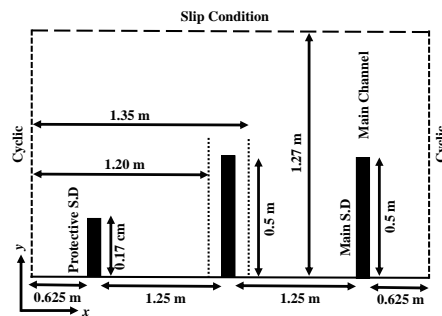
Figure 3 Boundary conditions of the computational domain for the numerical simulation

3   RESULTS AND DISCUSSION

3.1 Flow Velocity

Figure 4 (a and b) shows the calculated depth averaged velocity. The upstream and downstream measuring positions are located at 1.20 m and 1.35 m, respectively, from the inlet (Figure 3). In Figure 4a, the values of depth averaged velocity showed higher values for case A near the bank and the mainstream flow. In case C, the velocity showed the lowest velocity from the bank to the mainstream, but after the dike location (mainstream), it increased. Therefore, for riverbank protection, low-velocity flow can be obtained by providing small length PD (Case C).

(a)   (b)
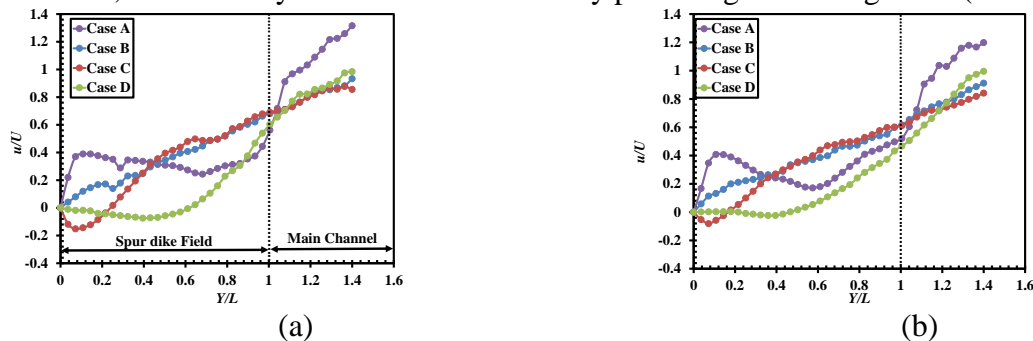
Figure 4 Streamwise depth averged *velocity distribution at (a) upstream and (b) downstream side of initial dike for three different PD lengths 17cm, 29 cm, and 50cm.*

1st International Conference on Advances in Civil & Environmental Engineering, University of Engineering & Technology Taxila, Pakistan

Conference date 22 &23 Feb 2022

The same velocity behavior was observed at the downstream (Figure 4b) side, as shown in Figure 4a. The depth averged velocity reduction for case D within the spur dike field was higher at the upstream side compared to the downstream side. Case C showed intermediate behavior in between Case B and Case D.

3.2 Velocity and *TKE* distribution

Figure 5 represents the depth averged velocity and *TKE* distribution for different lengths of PD. From Figure 5a, it is obvious that the velocity values were maximum for case A than case B, case C, and case D. The main objective of a PD is to reduce the value of depth averged velocity, which is reduced near the bank as well as in the near the nose of dike after providing the PD. The highest value can be observed for case A when no PD was provided. However, case C is suitable, which generated less velocity at the upstream (Figure 5a) and downstream (Figure 5b) of initial dike within spur dike field and in the mainstream.
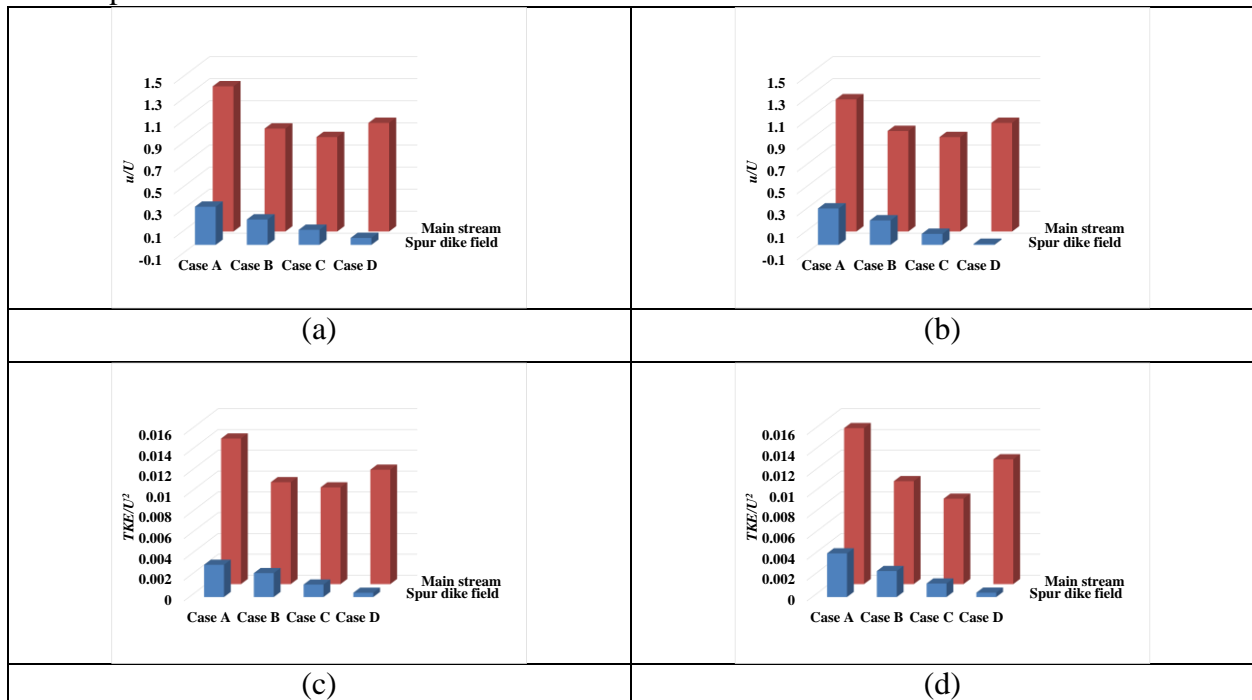
Figure 5 Depth averged Velocity (a and b) and TKE (c and d) distribution for all the cases (case 1-4)

The *TKE* behavior in the presence of different PD showed similar behavior as it was observed in the velocity profiles. From Figures 5c and 5d, maximum turbulence was observed in case A, where the PSD was not provided. After providing PSD, *TKE* was minimum in spur dike field at the upstream and downstream of the initial dike for case D compared to all other cases. However, the opposite trend was obsereved for case D in the mainstream because the larger dike length generated larger turbulence near the nose of the dike (main field). Hence it is suggested that case C performed better in both locations (within spur dike field and mainstream) compared to case B and Case D.

1st International Conference on Advances in Civil & Environmental Engineering, University of Engineering & Technology Taxila, Pakistan

Conference date 22 &23 Feb 2022

4   CONCLUSION

In present numerical study, the optimum length of PD was proposed to protect the existing dike from scour. The findings indicated a PD length of 0.5 to 0.6 L performed better compared to other lengths of dikes. It is concluded that the proper design of a PD greatly reduces the extent of deflected flow caused by the main dikes and widens the longitudinal flow constriction in front of the main dikes. From the present study following results are concluded.

1. When compared to no protective dike case (case A), the depth averged velocity reduction within the spur dike field was 82 % and 95 % for case D, and 61 % and 70 % for case C, respectively, measured at the upstream and downstream of the initial dike. Furthermore, the mainstream depth averged velocity reduction was 25% and 18% for case D, and 34% and 29% for case C, measured at *u/s* and *d/s* of the initial dike.
2. *TKE* reduction for the spur dike field for case D was 87% and 90%, while 61% and 69% for case C at the *u/s* and *d/s* of the dike. Similarly, in the mainstream, reduction in *TKE* was 21% and 20% for case D while it was 34% and 45% for case C at the *u/s* and *d/s* of the dike, respectively.

It is suggested that in future reports, the economic investigation of the cost of repairing the spur and shoreline disruption needs to be taken into consideration in certain real scenarios.

REFERENCES

[1]   Li, J., et al., *CFD investigations of tsunami-induced scour around bridge piers*. Ocean Eng*, 2022.* **244** 110373

[2]   Sharp, J.A. and McAlpin, T.O. *Case Study: Experimental Investigation into the Feasibility of Pier Nose Extensions to Reduce Local Scour around Bridge Piers*. J. Hydraul. Eng*, 2022.* **148** 5021010

[3]   Ahmed, H., Tanaka, N. and Tamai, N. *Flow modeling and analysis of compound channel in river network with complex floodplains and groynes*. J. Hydroinformatics, 2011. **13** 474–88

[4]   Zhang H., et al., *Experiment and simulation of turbulent flow in local scour around a spur dyke*. Int. J. Sediment Res*, 2009.* **24** 33–45

[5]   Li, H., et al., *Parallel walls as an abutment scour countermeasure* J. Hydraul. Eng., 2006. **132**

[6]   Atarodi, A., et al., *Experimental Investigation of Scour Reduction Around Spur Dikes by Collar Using Taguchi Method*. Iran. J. Sci. Technol. - Trans. Civ. Eng., 2021. **45** 971–83

[7]   Tariq, K., et al., *Development of ecosystem-based flood mitigation approach – investigations by experiments and numerical simulation. Water Environ. J,* 2021. **35** 685–703

[8]   Pasha, G.A. and Tanaka, N. Un*dular hydraulic jump formation and energy loss in a fl ow through emergent vegetation of varying thickness and density. Ocean Eng,* 2017. **141** 308–25

[9]   Iqbal, S., et al., *Flow Dynamics Around Permeable Spur Dike in a Rectangular Channel*. *Arab. J. Sci. Eng,* 2021.

[10]   Weitbrecht, V. *Influence of dead-water zones on the dispersive mass transport in rivers* (KIT Scientific Publishing), 2004.

Experimental Investigation of Local Scouring Reduction Using Double Hooked Collar

Ghulam Dastgeer[1], Naeem Ejaz[1]
University of Engineering & Technology Taxila, Pakistan
dastageer070@gmail.com, naeem@uettaxila.edu.pk

Muhammad Aleem[1]
University of Engineering & Technology Taxila, Pakistan
engrm.aleem@gmail.com

ABSTRACT

The major threat responsible for bridge impairment is the local scour around the bridge pier. To reduce scouring by applying different countermeasures is one of the major concerns in the design of piers. To reduce scouring due to the formation of vortex and rise of flow different techniques are adopted. In this work, the experimental reduction of scouring is studied by using single hooked and double hooked collars around a rectangular bridge pier. To reduce the scouring, single and double hooked collars are placed at different depths below and above the streambed level, so that we can conclude optimal depth for maximum scour reduction. We got the best results by placing a double hooked collar, one at streambed and another hooked collar at a depth of 0.5B below the streambed. Adapting this arrangement, the lower collar was not subverted even after 48 hours of experiment, showing a maximum of 58% reduction in scouring compared with pier without any protection. By using a single hooked collar at 0.5B above the streambed level and the bed level, scouring was reduced by 21% and 34% respectively. On the other hand, by using a double hooked collar at a depth of 0.5B above the bed, it is reduced by 50%.

KEYWORDS: Scouring; Double Hooked Collar; Rectangular Bridge Pier; Single Hooked Collar

1 INTRODUCTION

Scouring is caused at the foundations of the hydraulic bridge by the flow deflected by sediment-embedded bridge piers, and it can even challenge the stability of the bridge structure. This happens because the bearing capacity of the surrounding bed material is reduced due to the local scouring. The total scouring at a river crossing is the sum of the general scouring, contraction scouring, and the local scouring[1],[2]. The local scouring is caused by the formation of vortices at the bases of bridge piers and abutments. The vortex tends to reduce the bed material from the pier base [2].

Two main procedures can scale down the scour depth. The first process includes reinforcing the potential of bed material to stand up to erosion. This is generally done by installing an armoring

1st International Conference on Advances in Civil & Environmental Engineering, University of Engineering & Technology Taxila, Pakistan

Conference date 22 &23 Feb 2022

tool at the bed, like a riprap. The riprap presents a physical barrier that withstands the erosive potential of the flow. The second process works to limit the downflow facing the pier and the horseshoe vortex, scouring the bed material[3],[4]. This is usually achieved by installing a collar around the pier. The efficiency of the collar depends upon its size and its location relative to the streambed [5, 6]. However, it is not possible to install a big size collar in practical engineering. So, considering all these aspects, including ease of construction and finances, the width of the collar is reduced.[7] The main focus of this study is new types of collars, Single and Double Hooked collars, along with varying relative depths above or below the streambed.

2   METHODOLOGY

The experimental study was performed at the Hydraulics Laboratory, The Civil Engineering Department, University of Engineering and Technology, Taxila. An open channel of the rectangular dimensions, that is, 96cm wide, 75cm deep, and 20 m long with glass sidewalls and the concrete bottom was used for the experimental setup.

2.1   Laboratory Channel

The flow was supplied to the channel from an underground tank through a pump. The channel flow was measured by using a compound rectangular trapezoidal sharp-crested weir provided at the end of the channel. The experimental flume has five components
1. Inflow pipe
2. Turbulence Control
3. Weir
4. Settling pool
5. Outflow Pipe
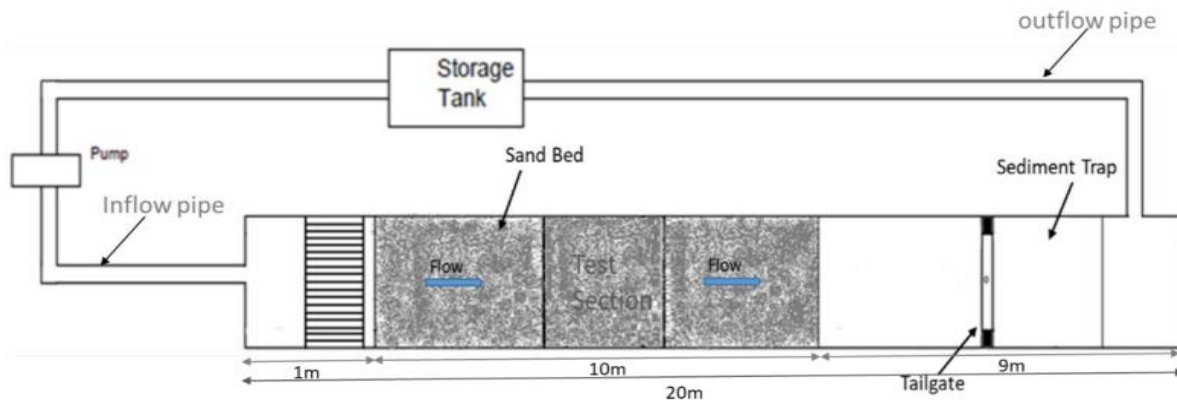
2.2 Material

A rectangular bridge pier having a cross-section of 6cm on each side is inserted in the center of the testing section of the channel. The length of the channel gives sufficient distance downstream of the pier to guarantee that the turbulent flow does not interfere with the downstream border.

1st International Conference on Advances in Civil & Environmental Engineering, University of Engineering & Technology Taxila, Pakistan

Conference date 22 &23 Feb 2022

Single and Double Hooked collars are required for this experimental work. The width of both collars used is two times the width of the rectangular pier with a hook-on upstream face to resist the effect of vortices on the upstream face.

This research was carried out in different phases:

1. In the first phase, the experimental setup was made in the laboratory, and experiments were performed at five different discharges of
   $0.024\text{m}^3/\text{s}, 0.029\text{m}^3/\text{s}, 0.034\text{m}^3/\text{s}, 0.039\text{m}^3/\text{s}$, and $0.044\text{m}^3/\text{s}$ on each case.
   Firstly, experiments were performed on a simple rectangular bridge pier without any countermeasure at five different discharges to note down scour depths.
2. Secondly, experiments were performed by using a single hooked collar at 0.5B above the streambed level at five different discharges.
3. Thirdly, experiments were done by using a single hooked collar at the streambed on each discharge of $0.024\text{m}^3/\text{s}$, $0.029 \text{ m}^3/\text{s}$, $0.034 \text{ m}^3/\text{s}, 0.039\text{m}^3/\text{s}$, and $0.044\text{m}^3/\text{s}$.
4. Fourthly, experiments were performed by installing double hooked collars, one at the bed and the other at 0.5B above the streambed level.
5. Finally, experiments were performed by using double hooked collars, one at the bed and the other buried 0.5B below the streambed at each discharge to get scour depth.

2.3 Equations

All the experiments were carried out on clear water conditions. To measure the value of discharges following equation is to be used.

$$Q_t = 2/3 C_{rd2}\sqrt{2g}\ (b_2 h_{23/2}) + 2/3 C_{rd1}\ \sqrt{2g}\ (2b_1)\ h_{13/2} + 8/15 C_{td}\ \sqrt{2g}\ (\tan(\theta/2))\ h_{1\ e5/2}$$

Where

θ = Notch angle, b = Width of weir, C_{rd}= Coefficient of discharge of the rectangular sharp-crested weir, C_{td}= Coefficient of discharge for triangular sharp-crested weir, g = gravitational acceleration, h = Water head on the weir crest, h_e = Effective head

1st International Conference on Advances in Civil & Environmental Engineering, University of Engineering & Technology Taxila, Pakistan

Conference date 22 &23 Feb 2022

3 TABLES AND FIGURE
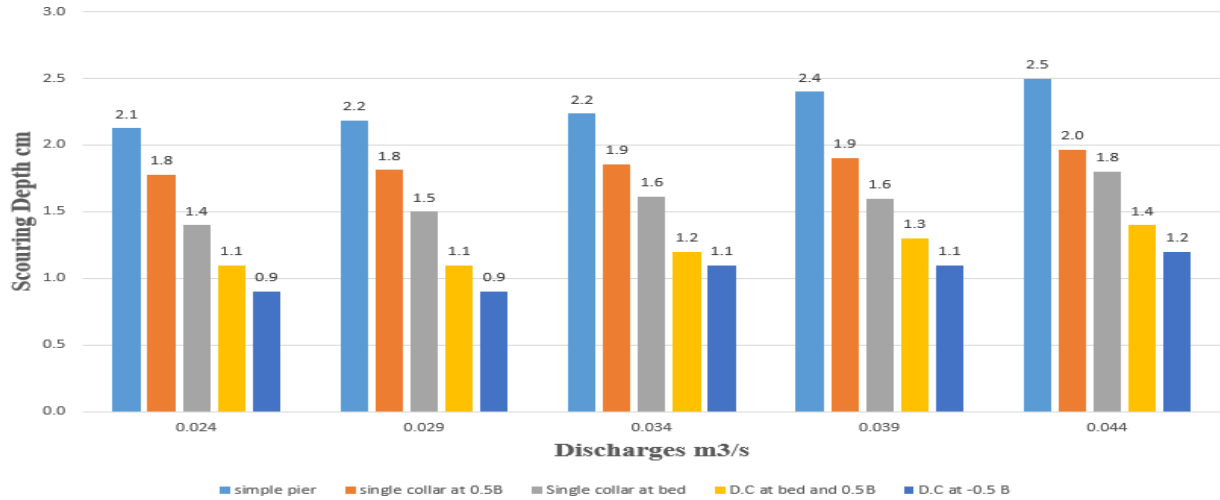
Fig.3.1: Relation between depth of scouring and discharges
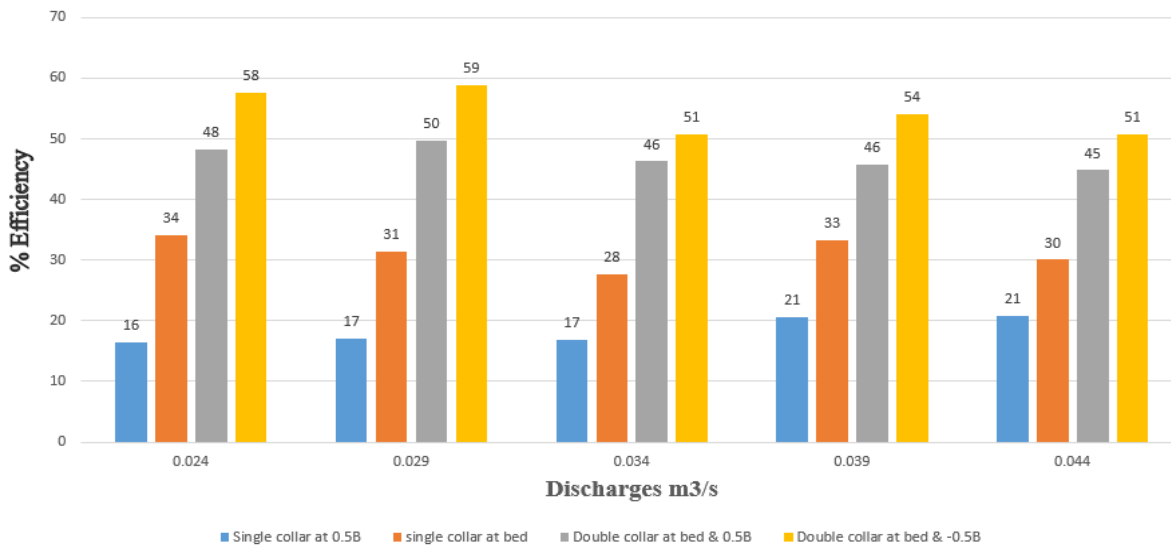
Fig.3.2: Relation between scour reduction %age efficiency and discharges w.r.t unprotected pier

4   CONCLUSION

In this work, the efficiency of single as well as the double hooked collar was studied experimentally on rectangular piers placed in an open channel.
The following conclusions were drawn from this experimental work

1st International Conference on Advances in Civil & Environmental Engineering, University of Engineering & Technology Taxila, Pakistan

Conference date 22 &23 Feb 2022

1. Scouring depth decreases with the use of single and double hooked collars. The efficiency of these collars depends upon their location.
2. The most proficient arrangement was when one collar was set at the streambed level, and one more was introduced half a pier below the bed level. In this arrangement, the lower collar was not subverted after 48 hours of experiment, and scouring was diminished to around 58 % compared to an unprotected pier.
3. The efficiency of a single hooked collar at the bed level and 0.5B above the bed level was 34 % and 21 % respectively. The double hooked collar at the bed and 0.5B above the bed, reduced scouring up to 50% as compared to the unprotected pier.

5   ACKNOWLEDGEMENTS

6   REFERENCES

1.   Tafarojnoruz, A., R. Gaudio, and F.J.J.o.h.e. Calomino, *Evaluation of flow-altering countermeasures against bridge pier scour.* 2012. **138**(3): p. 297-305.
2.   Chen, S.-C., et al., *A hooked-collar for bridge piers protection: flow fields and scour.* 2018. **10**(9): p. 1251.
3.   Zarrati, A., M. Nazariha, and M.J.J.o.H.E. Mashahir, *Reduction of local scour in the vicinity of bridge pier groups using collars and riprap.* 2006. **132**(2): p. 154-162.
4.   Hamidifar, H., M.H. Omid, and M. Nasrabadi. *Reduction of scour using a combination of riprap and bed sill.* in *Proceedings of the Institution of Civil Engineers-Water Management.* 2018. Thomas Telford Ltd.
5.   Mashahir, M., et al., *Effect of collars and bars in reducing the local scour around cylindrical bridge piers.* 2009.
6.   Zarrati, A.R., et al., *Scour countermeasures for cylindrical piers using riprap and combination of collar and riprap.* 2010. **25**(3): p. 313-322.
7.   Abdel-Aal, G., Y. Mohamed, and E.-D.J.C.E. Waheed, *O. and El-folly, M.,(2008), Local scour mitigation around bridge piles using protective plate (collar), Scientific bulletin. Faculty of engineering. Ain Shames University. Faculty of engineering.*

1st International Conference on Advances in Civil & Environmental Engineering, University of Engineering & Technology Taxila, Pakistan

Conference date 22 &23 Feb 2022

Compressive Behavior of Square and Rectangular Column Specimens Confined by Natural Fiber Rope

Owais Hassan Shah[1], Muhammad Salman[2], Muhammad Noman[3], Shahzad Saleem[4]

Department of Civil Engineering, University of Engineering and Technology, Taxila, Pakistan

owais.hassan@students.uettaxila.edu.pk[1]; 17-CE-96@students.uettaxila.edu.pk[2]; 17-CE-108@students.uettaxila.edu.pk[3];shahzad.saleem@uettaxila.edu.pk[4]

ABSTRACT

It is well known that the external confinement can considerably enhance the ductility and strength of confined concrete. However, the effectiveness of confinement reduces as the cross-section of concrete member changes from circular to rectangular shape. Furthermore, the fiber-reinforced polymers (FRPs) that are being used for the confining purpose are synthetic in nature and are costly in developing countries. The major goal of this research study is to examine compressive behavior of square and rectangular concrete columns confined by natural fiber rope (NFR) which is cheap and more environmentally friendly. For this purpose, a total of 18 specimens were prepared and tested in uniaxial compression. The considered parameters were cross-sectional shape (i.e., square, and rectangular) and number of NFR layers. The test results indicated that both the peak and post-peak behaviors were found significantly influenced by the considered parameters. Furthermore, both square and rectangular specimens showed highly ductile behavior. Due to knife action at the sharp corners, all specimens failed by the rupture of ropes at one of the corners.

KEYWORDS: Compression, Rope, Square, Rectangular, Stress-strain response

1   INTRODUCTION

The use of FRP (Fiber-reinforced polymer) composites for reinforcement of concrete (RC) structures is becoming one of the more appealing options in construction sector for the retrofitting of reinforced concrete structures [1]. In the case of concrete jacketing, a reinforced concrete shell is added around the structural member to improve the strength and ductileness of member [2].

During last few years, diverse types of FRPs have been effectively used for improvement of strength and ductileness of brickwork and Reinforced concrete structures [3]. These FRPs are collectively known as synthetic FRPs [4], as these FRPs are generally produced using synthetic chemicals and incorporate uni-directional or bi-directional fabrics like aramid, carbon and glass etc. The past researches have revealed that FRPs reinforcing is extremely successful to modify the functioning of concrete members. A few studies have shown skin issues, for example, aggravation and hypersensitive interaction dermatitis for laborers through synthetic FRP assembling and application methodology [5]. The principal disadvantages are identified with their high material expense and accessibility. Studies were led on the utilization of conservative and harmless to the ecosystem strands including hemp [6], jute [7] and sisal [7]. Natural fibers are lighter in weight, low to medium tensile properties, cheaper, non-abrasive in nature and easily accessible when compared to conventional FRPs. Another study conducted by Reddy and Sen [8] revealed that incorporated sisal and jute fiber improved axial strength and ductility of concrete columns.

1st International Conference on Advances in Civil & Environmental Engineering, University of Engineering & Technology Taxila, Pakistan

Conference date 22 &23 Feb 2022

This research study was conducted to explore the compressive behavior of square and rectangular concrete columns by natural fiber rope (NFR) which is cheap and more environment friendly. For this purpose, a total of 18 specimens were prepared and tested in uniaxial compression. Cross sectional shape (i.e., square and rectangular) and number of NFR layers were the considered parameters.

2   EXPERIMENTAL PROGRAM

Overview of the test specimens summarized in Table 1. A total of 18 rectangular concrete specimens were tested. The total experimental program was divided into three groups. Group A, B and C contains 6 square specimens, 6 rectangular specimens with (L/W) ratio of 1.5 and 6 rectangular specimens with (L/W) ratio of 2, respectively. All the specimens have the same 28MPa cylindrical compressive strength on 28 days. Specimen designation is given to represent cross-sectional shape (S for square and R for Rectangular), corner radius (R0 for zero corner radius and R21 for 21mm corner radius) and the number of layers (L0 for zero layer, L1 for one layer and L2 for two layers). For example, in the designation of specimen R1.5 R21 L2, the first letter denotes rectangular specimen with (L/W) ratio of 1.5, the second letter denotes corner radius of 21mm and the last one represents 2 number layers of NFR. In each case, two similar specimens were tested to obtain the average results.

2.1   SPECIMENS PREPARATION

A total of 18 small sized square and rectangular specimens with a size of 150 x 150, 184 x 122, and 212 x 106 mm were prepared using plywood molds. The height of all specimens was 300 mm. The specimens are shown in Figure 1. Specimens wrapped in NFR were rounded off at corner by 21 mm radius to avoid premature failure of NFR.
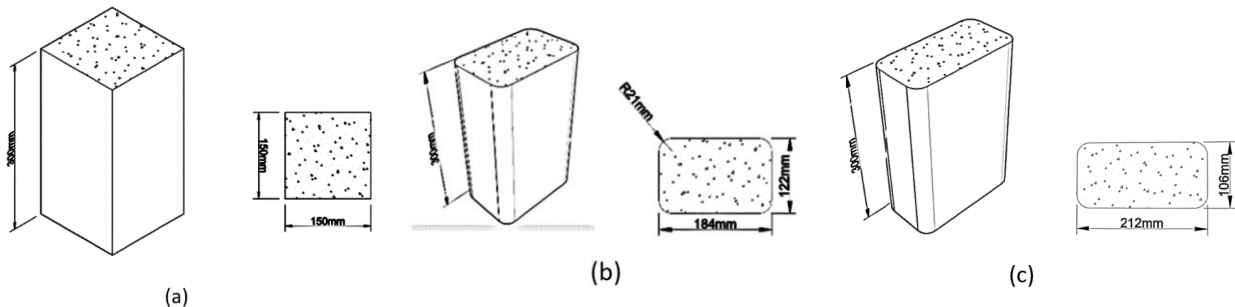
Figure 1: Details of test specimens: (a) square specimen; (b) rectangular specimen (L/W=1.5); (c) rectangular specimen (L/W=2)

2.2   NATURAL FIBER ROPE

Cotton fiber ropes were used in the NFR composite, that were obtained from a local manufacturer. The cotton rope was approximately 2.5mm in diameter.

2.3   RESIN

A high-performance epoxy resin that comes in two parts was used to bond NFR with concrete

1st International Conference on Advances in Civil & Environmental Engineering, University of Engineering & Technology Taxila, Pakistan

Conference date 22 &23 Feb 2022

surface in the experimental program. The epoxy resin is part A, while the hardener is part B. By weight, both parts were mixed together at a 2:1 ratio (i.e., part A: part B = 2:1).

Table 1. Test Matrix – Experimental Program

S. No.	Group	Specimens Designation	Shape of Specimens	L/W Ratio	Strength of Concrete MPa	Numbers NFR Layers	Number of Similar Specimens
1.	A	SR0L0	Square	1	28	0	2
2.		SR21L1	Square	1	28	1	2
3.		SR21L2	Square	1	28	2	2
4.	B	R1.5R0L0	Rectangular	1.5	28	0	2
5.		R1.5R21L1	Rectangular	1.5	28	1	2
6.		R1.5R21L2	Rectangular	1.5	28	2	2
7.	C	R2R0L0	Rectangular	2	28	0	2
8.		R2R21L1	Rectangular	2	28	1	2
9.		R2R21L2	Rectangular	2	28	2	2

2.4 NFR WRAPPING

NFR was directly applied to the specimen's surface by using common hand lay-up technique after 28 days of curing. Wrapping of specimen started from one end to the other. First of all, the rope was applied at the start point of the specimen with the application of epoxy and left for hardening of rope over the specimen for 6 hours. After 6 hours, epoxy was applied over the specimen and rope was wrapped continuously around the entire specimen. A 25 mm wide layer of rope was also applied at both ends of specimens to prevent specimens ends from premature failure.

2.5 INSTRUMENTATION AND TESTING PROCEDURE

Uni-axial compression testing machine was used for testing of specimens. Both square and rectangular specimens were instrumented with one vertical linear variable displacement transducers (LVDTs) for determination of axial deformation. All specimens (square and rectangular) were axially compressed in a displacement-controlled manner to failure in a 2000 KN capacity uni-axial compression testing machine.

3. TESTING RESULTS AND DISCUSSIONS

3.1 STRESS-STRAIN RESPONSE

In all control specimens irrespective of their cross-sectional shape, axial-stress increased linearly up to peak stress value and then a sudden drop was observed. After that the load was sustained until the specimen's failure.

3.2 EFFECTS OF NFR LAYERS

The effect of number of NFR layers on peak axial stress of both types of specimens is shown in Figure 2. The peak strength increases with increasing NFR thickness in NFR-confined square specimens. When compared to the control specimen, the square specimen with one layer of NFR

1st International Conference on Advances in Civil & Environmental Engineering, University of Engineering & Technology Taxila, Pakistan

Conference date 22 &23 Feb 2022

failed at a compressive strength of 26% higher. When the number of NFR layers were increased to two, the compressive strength increased by 51%. When compared to the unconfined specimen, the compressive strength of the rectangular specimen with a (L/W) ratio of 1.5 and one layer of NFR increased by 15%, while the compressive strength of the rectangular specimen with a (L/W) ratio of 1.5 and two layers of NFR increased by 37%. When compared to the control specimen, the rectangular specimen with a (L/W) ratio of 2- and one-layer NFR failed at 24% higher compressive strength. Similarly, the highest compressive strength increase was 51% in rectangular specimen with (L/W) ratio of 2 and two layers of NFR.
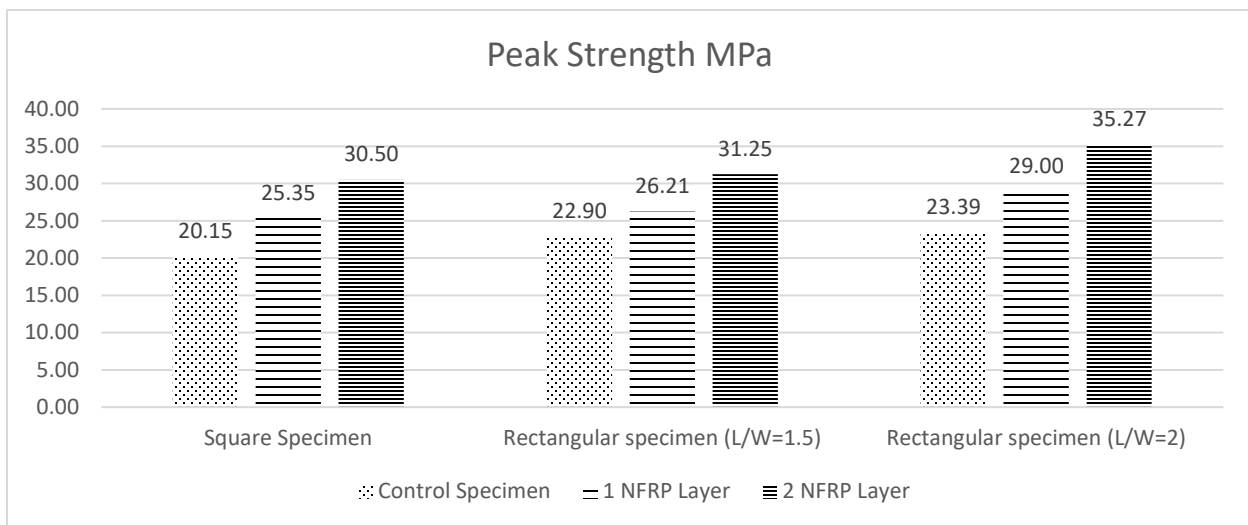
Figure 2. Bar chart showing peak strength

3.3 EFFECT OF CROSS-SECTIONAL SHAPE

For one layer of NFR Wrapping, the rectangular specimen with a length to width ratio of 1.5 exhibits 3.40% higher compressive strength as compared to the square specimen wrapped with one layer of NFR. While rectangular specimen with (L/W) ratio of 2 exhibits 14.40% higher compressive strength as compared to the same. When wrapped with two layers of NFR rapping, rectangular specimens with (L/W) ratio of 1.5 have a 2.46% higher compressive strength than square specimens wrapped with two layers of NFR. When compared to the same, rectangular specimen with a (L/W) ratio of 2 has 15.64 % higher compressive strength. In the case of two NFR layers, the increase in compressive strength is relatively lesser as compared to one-layer NFR.

3.4 FAILURE MODE

The typical failure of NFR confined specimens (square and rectangular) caused by NFR shell rapture is illustrated in Figure 3. The failure of both square and rectangular specimens was gradual and quiet. Some snapping sounds could also be heard as the final failure approached. Stress concentration on specimen's corners resulted in rupture of NFR shell in almost all the specimens.

1st International Conference on Advances in Civil & Environmental Engineering, University of Engineering & Technology Taxila, Pakistan

Conference date 22 &23 Feb 2022

(a)   (b)   (c)

Figure 3. Failure modes of specimens; (a) S R21 L1; (b) R1.5 R21 L1; (c) R2 R21 L2

4 CONCLUSIONS

The purpose of this research is to determine the compressive behavior of square and rectangular specimens confined with natural cotton rope. A total of 18 specimens were tested for this purpose using a monotonic axial compression testing machine. The number of NFR layers and the cross-sectional shape were the parameters used. Conclusions are as under:

- Natural cotton fibers rope can improve the strength and deformability of concrete in both square and rectangular specimens. Compressive strength and deformability increase as NFR shell thickness increases for both square and rectangular specimens.
- Natural fiber rope reinforced polymer composite can be effectively developed by applying epoxy resin to the cotton rope.
- For all specimens, NFR failure always occurred at or near one of the corners due to stress concentrations.

5 REFERENCES

1. Al-Zaid RZ, Al-Negheimish AI, Al-Saawani MA and El-Sayed AK (2012) Analytical study on RC beams strengthened for flexure with externally bonded FRP reinforcement. Composites Part B: Engineering 43(2): 129–141.
2. T.C. Triantafillou, E. Choutopoulou, E. Fotaki, M. Skorda, M.Stathopoulou, and K. Karlos, "FRP confinement of wall-like reinforced concrete columns". Mater. Struct. vol. 49, no. 1-2, pp. 651-664, 2016.
3. Antonopoulos CP and Triantafillou TC (2003) Experimental investigation of FRP-strengthened RC beam-column joints. Journal of Composites for Construction 7(1): 39–49.
4. T. Norris, H. Saadatmanesh, and M.R. Ehsani, "Shear and flexural strengthening of R/C beams with carbon fiber sheets", J. Struct. Eng. vol. 123, pp. 903-911, 1997.
5. K. Tarvainen, R. Jolanki, L. Forsman-Grönholm, T. Estlander, P. Pfäffli, J. Juntunen, et al., "Exposure, skin protection and occupational skin diseases in the glass fibre reinforced plastics industry", Cont. Dermat. vol. 29, pp. 119-127, 1993.
6. Siriluk, S. Behaviours of Rc Deep Beams Strengthened in Shear Using Hemp Fiber Reinforced Polymer Composites. Int. J. Geomate 2018, 15, 89–94.
7. Pimanmas, A.; Hussain, Q.; Panyasirikhunawut, A.; Rattanapitikon, W. Axial strength and deformability of concrete confined with natural fibre-reinforced polymers. Mag. Concr. Res. 2019, 71, 55–70.
8. Sen, T.; Paul, A. Confining concrete with sisal and jute FRP as alternatives for CFRP and GFRP. Int. J. Sustain. Built Environ. 2015, 4, 248–264.

Effects of bidding on the success of construction project

Muhammad Salman
University of Engineering & Technology Taxila, Pakistan
MMSalman02@gmail.com

Muhammad Noman
University of Engineering & Technology Taxila, Pakistan
2016n5608@gmail.com

ABSTRACT

Construction bidding is the procedure of submitting a tender (proposal) to undertake or manage the undertaking of a construction project. From project management perspective, it is very important component for proper project performance. Success of any construction project is mainly based on the following three factors: Schedule, Quality and Cost. Bidding process is the project early-stage success evaluating factor which has direct impact on cost and indirect impact schedule and quality of construction project. Bidding process needs a lot of attention not only by contractors to secure the construction project but also by clients for the success of construction project. The research is basically divided into two parts first is to investigate the factor causing flaws in bidding process for successful bid and second is to investigate the effects of wrong bid on construction projects. The result shows that proper management and estimation is very important factor in evaluating the successful bid.

KEYWORDS: Project bidding process, successful construction project, project performance

1   INTRODUCTION

Pakistan is considered as one of the developing countries of world. Construction sector is one of the most important sectors which is striving to get Pakistan out of this label. The construction industry influences the GDP rate and jobs in almost all countries and thus due to this construction sector is considered very important for a country's economic progress. Moreover, Pakistani construction industry just not performs the above listed functions for the betterment but also makes its crucial contribution in the economic industries like Power and energy, Development of water resources and dam technology, Planning and architecture, Engineering in Public Health, communication, Gas, oil and petrochemical. Almost 40-50 other businesses and sectors in the country are directly and indirectly influenced by the accomplishments of construction sector [1]
In any project under any constructing firm has almost the same steps of completion. Bidding is the very initial step in the development phase of the project life cycle that decides the progress of the business. Therefore, this phase is therefore an initial important step. [2] Hence Bidding serves as the foundation of construction project life cycle if anything goes wrong with it, that will surely affect the contracting firm and the construction industry as a whole. It is therefore Effective

1st International Conference on Advances in Civil & Environmental Engineering, University of Engineering & Technology Taxila, Pakistan

Conference date 22 &23 Feb 2022

construction expenses control and cost computation during the bidding phase of customers building projects is of considerable importance.

2   RESEARCH OBJECTIVES AND METHODOLOGY

In addition, with highlighting the importance bidding system in Pakistan, there are mainly three objectives of our research. first one is to find the flaws in our bidding system, second one is to find the factors on which our bidding system relies and third one is to guess the improvement afterword's. this research has given us the basic factors which must be taken in consideration while undergoing the bidding process.

Major factors that will be involved in bidding process will be identified through review of related literature, discussion with practitioners and from the data collected through survey forms filled by different clients, consultant as well as contractors. Final report and bid cost of different construction project will be collected and analysed to evaluate the effect of bidding process on construction project.

3   LITERATURE REVIEW

When a construction project is finished in time and within a decided budget and all the stakeholders are satisfied and happy with the performance of contractor, Then the building project is seen as successful [1]. It must also be remembered that Completing construction contracts within the specified time is a used as a measure of performance and efficiency of the contractor or the contracting firm [2]. Hence to make any construction project successful economy and resources estimation is very crucial which is done in the bidding process of the project, so any wrong bid will cause damage to just not only the project but the contracting firm and hence as whole it will affect the construction sector to some extent.

The completion of a construction project on schedule is very rare [3-6]. In many countries, though, the building industry especially, the contracting firms are criticized for the inefficiencies due to outcomes like time and expense overruns, low profitability, bad quality and consumer dissatisfaction [7, 8]. Cost overrun in construction projects is a global problem and the these cost overruns usually results in conflict between owners, project managers and contractors [9, 10].

Cost overruns due to wrong bids is one of the biggest challenges faced by the contracting firms in both developed and developing countries that trigger delays in building industry. [11]. Flyvbjerg [12] analysis found that 9 out of 10 projects in a survey of 258 organizations in 20 countries and five continents worldwide had the problem of cost overruns. In reality, almost every building project takes delays and the severity of such delays varies considerably across projects and countries [13]

According to A. Bagies and C. Fortune inaccurate bid details and cost estimation is considered to be one of the main problems being faced by the contractors [14] The client takes a huge risks by choosing a bid unrealistic low estimate which may be submitted by mistake or unintentionally. [15] and by doing so he just only take a risk of damaging the reputation of his own firm but also the wellbeing of construction industry. Hence, it is essential to recognize the factors that cause overruns in costs to prevent and mitigate problems Because normally the first step in resolving an

1st International Conference on Advances in Civil & Environmental Engineering, University of Engineering & Technology Taxila, Pakistan

Conference date 22 &23 Feb 2022

issue is to identify the root causes and then after that remedial step can be taken. Since the perennial dilemma of building costs overruns is not sorted out yet so the there is still a need of debate and further research to reach a conclusion [16]

In this research paper we have develop a relationship between the wrong bids and project failures. Moreover, we will also investigate about the fundamental causes of cost overruns and then their potential effects on the development of project. Because bids are serving as the very first step to the completion of project so any wrong bid will impact the project adversely and damaging the project means damaging the construction industry.

4   RESULTS AND DESCUSSION

As discussed in methodology, A questionnaire was distributed among contractors, and they were ought to mark the possible factors involved in wrong bids with 5 being the highest involved in causing wrong bids and 1 being the least. In the presented study different factors causing wrong bids and effects of wrong bids are analysed through statistical analysis technique and results are shown below

4.1   Factors involved in wrong bids

In Table 1 average score of different factors is shown with 5 being the highest and 1 being the lowest. It has clearly been concluded that "**Wrong Estimation of Bill of quantities (BOQ)**" with average score of 4.37 is found out to be the highest factor that results in wrong bid of most of the projects. Moreover "**Competition between Contractors for getting bid**" with average score of 1.37 is the lowest contributing factor for wrong bids by the contractors.

Table 1 Scale of different factors causing wrong bids

FACTORS	Scale
Political Monopoly	3.87
Improper Feasibility Report	4
Rushed Bids/inaccurate takeoffs	3.37
less Experience of firm in related engineering project	1.87
Wrong Estimation of Bill of quantities (BOQ)	4.37
Competition between Contractors for getting bid	1.37
Lack of information flow between parties	3.25
Incomplete design at the time of tender	2.87
fluctuation of prices of materials	2.37

After the Statistical excel analysis of survey data, all scores of factors are summed up as total and then the percent of different factors is calculated. As shown below it can be concluded that 17% of wrong bids occur due to "**Wrong Estimation of Bill of quantities (BOQ)**". Similarly, from the Graphical presentation it can also be concluded that 5% of the wrong bids are caused due to

1st International Conference on Advances in Civil & Environmental Engineering, University of Engineering & Technology Taxila, Pakistan

Conference date 22 &23 Feb 2022

"**Competition between Contractors for getting bid**". Moreover, from the presented pie chart it can also predicted that how many wrong bids are caused by other factors
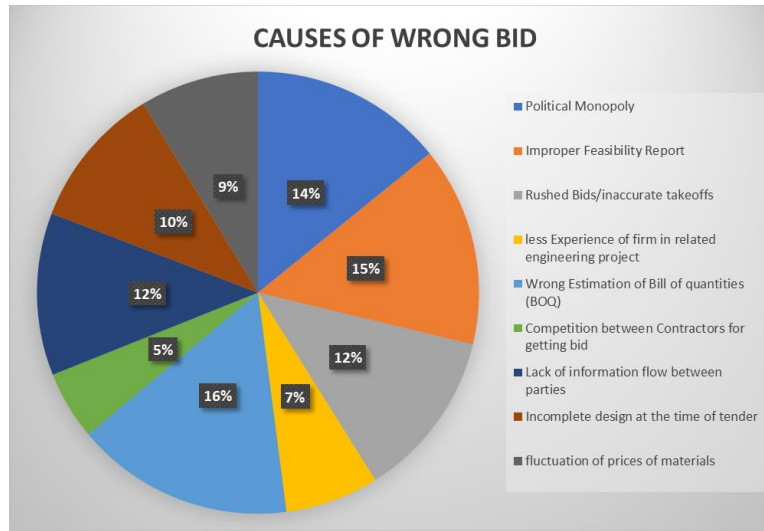
Figure 1: Graphical representation of Factors involved in wrong bids

4.2   Effects of wrong bids

In Table 2 average score of different effects that are caused by wrong bids are shown. It has clearly been concluded that "**Poor quality of work**" with average score of 4.75 is found out to be the most abundant effect that is caused by the wrong bids hence it can be said that the quality of work is highly dependent on Bidding if projects and wrong bid will highly be affected in negative manner. Moreover **"Economic un stability of client"** with average score of 1.5 is the least effect that is caused by wrong bids according to different contractors.

Table 2 Scale of different Effects of wrong bids

EFFECTS	SCALE
Delays in project	4.12
Poor quality of work	4.75
Economic un stability of client	1.5
Creates stress to the client	3.87
Total project abandonment	2.12
Bad reputation with client	3.37
Loss of profit to contractor	3.62
Lack of Risk Management	4.37
Litigation	2.25

1st International Conference on Advances in Civil & Environmental Engineering, University of Engineering & Technology Taxila, Pakistan

Conference date 22 &23 Feb 2022

Below is the graphical representation of percentage of effects resulted in due to wrong bids. After the Statistical excel analysis of the survey data, all scores of effects are summed up as total and then the percent of different effects is calculated.

As shown below it can be concluded that 16% of wrong bids effects "quality of work". Hence Poor quality of work is the highest effected parameter due to wrong bids. Similarly, from the Graphical presentation it can also be concluded that "Economic un stability of client" with 5% effected rate is being the least parament effected by wrong bids. Moreover, From the given chart it can also be concluded that wrong bids effect the schedule of projects and causes delays. In addition to that, from the presented pie chart, we can also predict how wrong bids effects other parameters
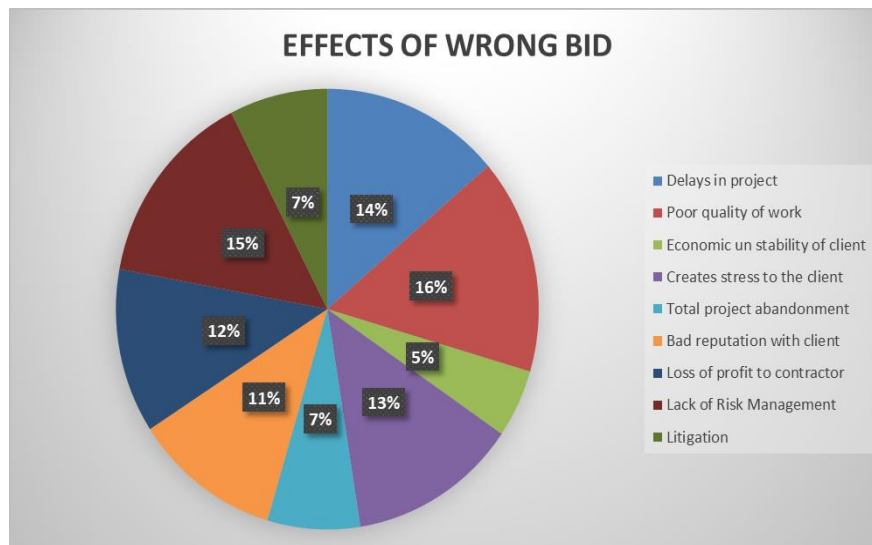
Figure 2: Graphical representation of Effects of wrong bids

5   RECOMMENDATIONS

Construction companies must be able to handle a variety of bidding scenarios in today's highly competitive market. The first decision they had to make was whether or not to submit a bid after receiving a tender invitation. Several elements and factors have a role in the final decision of the contractors. This selection relies heavily on the specific project and the overall macro environment. Recognition that only the lowest bidder will provide an adequate service has resulted in an increasing desire to transition from "lowest-price wins" to "multi-criteria selection" in the selection process for contractors. hence, the construction industry's competitive bidding process and bid strategy need to be studied.

6   CONCLUSION

Statistical analysis of data collected by questionnaire survey reveals that different factors are involved in bidding process for success of construction projects. Consultants should check the project site and made an estimate according to market prices and then tender the project.

1st International Conference on Advances in Civil & Environmental Engineering, University of Engineering & Technology Taxila, Pakistan

Conference date 22 &23 Feb 2022

Consultants should not give projects to bids which are lower than their own estimated costs. On the other hand, Contractors should also be regulated under proper authority, so their past performance record is always in front of consultants.

REFERENCES

1. Gündüz, M., Y. Nielsen, and M.J.J.o.m.i.e. Özdemir, *Quantification of delay factors using the relative importance index method for construction projects in Turkey.* 2013. **29**(2): p. 133-139.
2. Chan, D.W. and M.M.J.I.J.o.p.m. Kumaraswamy, *A comparative study of causes of time overruns in Hong Kong construction projects.* 1997. **15**(1): p. 55-63.
3. Arditi, D., et al., *Reasons for delays in public projects in Turkey.* 1985. **3**(2): p. 171-181.
4. Assaf, S.A., M. Al-Khalil, and M.J.J.o.m.i.e. Al-Hazmi, *Causes of delay in large building construction projects.* 1995. **11**(2): p. 45-50.
5. Baldwin, J.R., et al., *Causes of delay in the construction industry.* 1971. **97**(2): p. 177-187.
6. Vidogah, W. and I.J.J.o.m.i.e. Ndekugri, *Improving management of claims: contractors' perspective.* 1997. **13**(5): p. 37-44.
7. Chan, A.P. and A.P.J.B.a.i.j. Chan, *Key performance indicators for measuring construction success.* 2004.
8. Yasamis, F., et al., *Assessing contractor quality performance.* 2002. **20**(3): p. 211-223.
9. Azhar, N., R.U. Farooqui, and S.M. Ahmed. *Cost overrun factors in construction industry of Pakistan*. in *First International Conference on Construction in Developing Countries (ICCIDC–I), Advancing and Integrating Construction Education, Research & Practice*. 2008.
10. Creedy, G.D., et al., *Evaluation of risk factors leading to cost overrun in delivery of highway construction projects.* 2010. **136**(5): p. 528-537.
11. Enshassi, A., et al., *Delays and cost overruns in the construction projects in the Gaza Strip.* 2009.
12. Flyvbjerg, B., M.K. Skamris Holm, and S.L.J.T.r. Buhl, *How common and how large are cost overruns in transport infrastructure projects?* 2003. **23**(1): p. 71-88.
13. Alaghbari, W.e., et al., *The significant factors causing delay of building construction projects in Malaysia.* 2007.
14. Bagies, A. and C. Fortune. *Bid/no-bid decision modelling for construction projects*. in *Procs 22nd Annual ARCOM Conference*. 2006. Citeseer.
15. Ioannou, P.G., R.E.J.J.o.C.E. Awwad, and Management, *Below-average bidding method.* 2010. **136**(9): p. 936-946.
16. Kasimu, M.J.I.j.o.c.r.i.b., *Significant factors that causes cost overruns in building construction project in Nigeria.* 2012. **3**(11): p. 775-780.

1st International Conference on Advances in Civil & Environmental Engineering, University of Engineering & Technology Taxila, Pakistan

Conference date 22 &23 Feb 2022

Mechanical and Physical Properties of Cellular Lightweight Concrete (CLC) Blocks

Khalid Khan, Inayat Ullah Khan
University of Engineering & Technology Peshawar, Pakistan
16pwciv4552@uetpeshawar.edu.pk: 16pwciv4553@uetpeshawar.edu.pk

Majid Khan
University of Engineering & Technology Peshawar, Pakistan
majidayubbi@gmail.com

Muhammad Shakeel
University of Engineering & Technology Peshawar, Pakistan
18pwciv5186@uetpeshawar.edu.pk

Adil Khan
University of Engineering & Technology Peshawar, Pakistan
18pwciv5027@uetpeshawar.edu.pk

ABSTRACT

Foam concrete has excellent physical properties such as thermal and acoustic insulation, fire poof and light-weight. In the past, FC application was only limited to non-structural uses. However, in near past the application of FC has been extended to structural application as well. As, the design and assessment of masonry structures need mechanical and physical properties of masonry units. Thus, series of experiments has been carried out on CLC blocks. In addition, compressive strength and flexural strength was found very small as compared to conventional blocks. However, the thermal insulation was very small and water absorption was high compared to normal blocks. Therefore, CLC blocks with low density can be found very useful to use as an infill material.
KEYWORDS: Foam Concrete, Mechanical and Physical Properties, Compressive and Flexural Strength, Thermal Conductivity and Water Absorption.

1   INTRODUCTION

Foam Concrete (FC) can be known by other academic names as light-weight, reduce density and cellular light-weight concrete [1]. FC comprises of cement-based slurry having cement, water, fly ash, sand and foaming agents. FC is very versatile in nature due to its unique physical properties such as light-weight, thermal insulation, fire proof, acoustic and eco-friendly[2]. By proper mix proportion and ingredient selection wide range density FC can be produced, which can be used for various purposes such as insulation, filling applications and as a structural material [3].
FC was patented by Axel Eriksson, dated back in 1923. First comprehensive review was conducted by Valore on FC (Valore, 1954). As FC is a novel material, therefore further research was continued on various aspects such as composition, applications and some specific properties [5].

1st International Conference on Advances in Civil & Environmental Engineering, University of Engineering & Technology Taxila, Pakistan

Conference date 22 &23 Feb 2022

Furthermore, new methods and techniques were developed in 1970s and 1980s, which helps in the commercialization and application of FC in construction industries [6].

In the very past, the application of FC was only limited to non-structural purposes such as backfilling, retaining walls, heat insulations and sound insulations [6]. Nevertheless, in the past decades, effort has been made to extend the application of FC as a structural materials [7]. As, the application of foam concrete increases with advancement in material technology, Asia continent only accounted for the 50% production of FC throughout the world [8]. Currently, in Pakistan Foam concrete or CLC blocks use in construction industry also seems as one of the attractive materials in very future.

CLC blocks are light-weight compared to conventional concrete blocks, due to which the compressive strength and other mechanical properties are lower than conventional blocks. Due to light-weight and low compressive strength CLC blocks are mainly use as a infill material in buildings [9]. The mechanical and physical properties of infill material affect the performance and behavior of frame structures up to great extent. The design and assessment of new constructed or existing building, the mechanical and physical properties of masonry units play an important role. Therefore, evaluation of these properties such as compressive strength, flexural strength, water absorption, thermal conductivity and dry density is the need of the day for construction industry in Pakistan.

2 MATERIAL AND METHODS

In the production of CLC blocks, cement, sand, fly ash, water and foaming agents are used. The only imported material used in these blocks are foaming agents and the rest of material is locally available.

2.1 Preparation of CLC Blocks

The only factor which controls other parameters is density of FC. According to ASTM C796-97 the required density and water to binder ratio was selected. Therefore, keeping in mind the target dry density of 770 Kg/m^3 the material proportions as given in Table 1 was selected.

Table 1 *CLC Blocks Basic Ingredients*

Foam Concrete Ingredients			
Ingredients	Density	Weight (kg)	Unit weight (KN/m^3)
Cement	1440 (kg/m^3)	100	3.15
Fly ash	1350 (kg/m^3)	200	2.5
Fine aggregate	1500 (kg/m^3)	50	3.2
Water	1000 (kg/m^3)	180	1
Foaming agent	70 (g/cm^3)	240	1.45

1st International Conference on Advances in Civil & Environmental Engineering, University of Engineering & Technology Taxila, Pakistan

Conference date 22 &23 Feb 2022

CLC Blocks were prepared as shown in Figure 1 (a), following typical procedure as practicing in market were used for production. Pre-forming Method for FC manufacturing was used. At the end, all these materials were mixed through mixture. In the start oil was poured at the internal side of the moulds.

As FC is relatively a novel material, and there is no proper guidelines and methods available to assess the mechanical and physical properties. Thus, for the preparation and tests of CLC blocks conventional concrete standards were followed in this study. All tests have been performed at University of Engineering and Technology Peshawar.

a   b   c   d   e
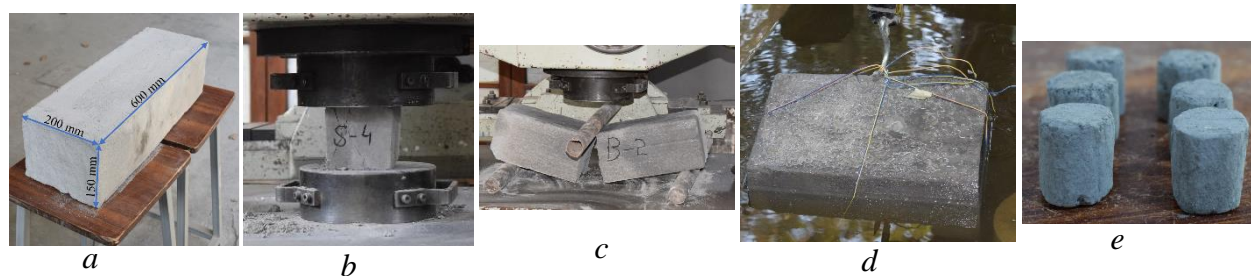
Figure 1: (a) CLC block (b) Compression test sample (c) Flexural Strength sample (d)Water absorption sample (e) Thermal conductivity sample

Compressive strength was measured with 100 x 100 x 100 mm standard cubes as shown in Figure 1 (b), as per the ASTM C 513-89. The load rate was selected as stated in relevant standard.

Flexural strength test was performed as shown in Figure 1 (c), as per the ASTM C 293, three points bending with beam dimension 500 x 200 x 150 mm, distance between support was 300 mm. as shown in Figure 1 (c), support and other specifications were selected as per the aforementioned standard.

Water absorption of CLC blocks were determined on five blocks as shown in Figure 1 (d) as stated in ASTM C 140. Immersed, wet and dry weight were measured as per the standard.

Thermal conductivity was performed on four samples of dimensions 25 mm diameter and 30 mm in length as per Helton Heat Conductance Apparatus manual. Figure 1 (e) shows the samples used for thermal conductance.

3   RESULTS AND DISCUSSION

3.1   Compressive strength

FC cubes tested under compression as shown in Figure 1 (a), the failure mechanism is same as conventional concrete. All samples were failed as a conical post breakage failure patterns. There is no significant variation observed because of almost same density cubes were tested. The compressive strength of FC is primarily function of density, as present study used low density of FC therefore compressive strength was also not observed to much as shown in Figure 2 (a).

1st International Conference on Advances in Civil & Environmental Engineering, University of Engineering & Technology Taxila, Pakistan

Conference date 22 &23 Feb 2022

3.2 Flexural Strength

Specimens were tested as per the requirements of ASTM C 293. Beams were failed in tension as ordinary concrete due to high tensile stresses developed at the bottom fibers. Previous research shows that the flexure strength of FC also decreases as with density decreases. Figure 2 (b) shows the flexural strength of CLC blocks.

3.3 Water Absorption

Specimens were tested as per the ASTM C 67. Figure 2 (c) shows that the water absorption o FC is very high as compared to conventional concrete due to high pores and low density. All specimens show approximately same water absorption capacity due to uniform density.

3.4 Thermal Conductivity

Therma conductance of FC depends on density and material properties. Moreover, the density of FC is low in present study, thus the thermal conductance is very low compared to normal concrete. Figure 2 (d) shows the value of thermal conductance and variation although no significant variation observed due to uniform density.
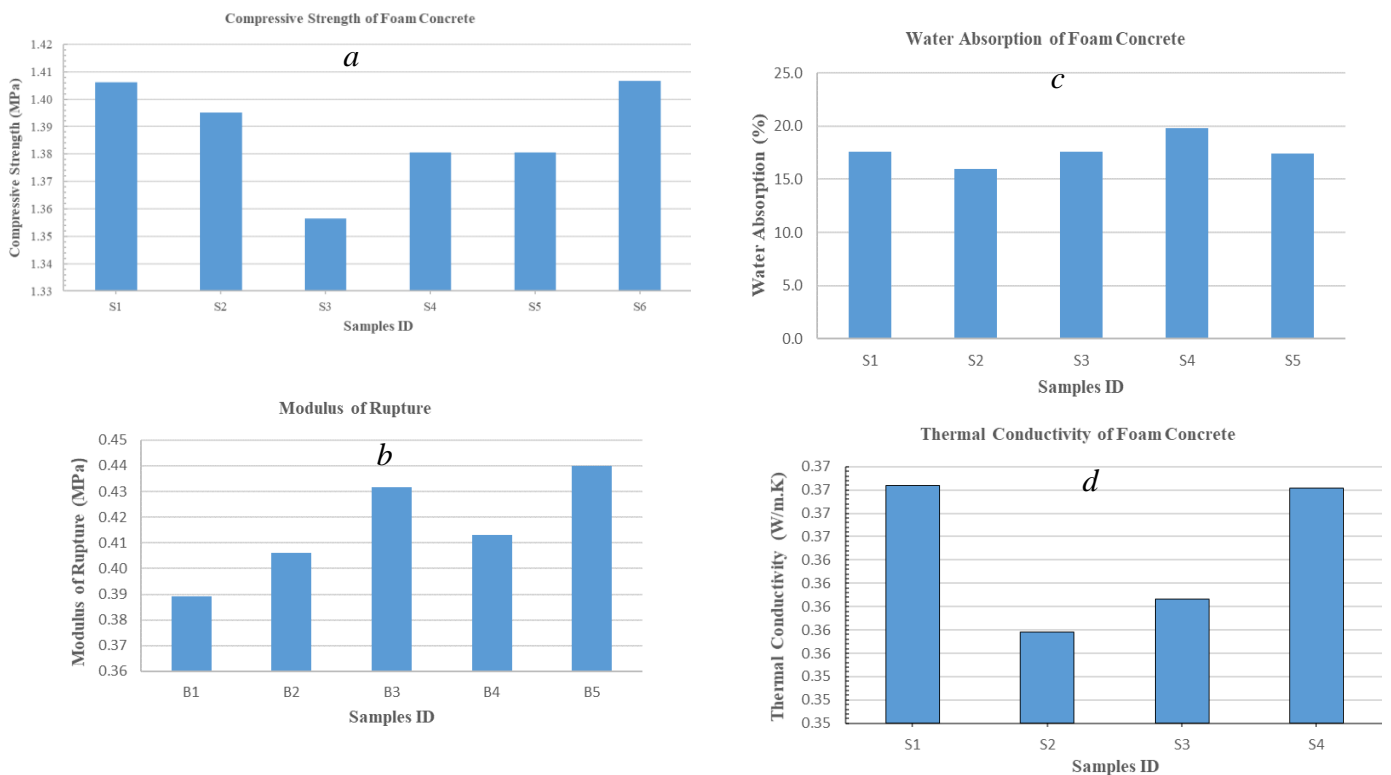
Figure 2: *(a) Compressive Strength, (b) Flexural Strength, (c) Water Absorption (d) Thermal Conductivity*

1st International Conference on Advances in Civil & Environmental Engineering, University of Engineering & Technology Taxila, Pakistan

Conference date 22 &23 Feb 2022

4   CONCLUSIONS

Foam concrete is a novel material in construction industry. FC has very superb physical properties due to which its application has been extended to structural purposes as well. Structural performance of masonry structures basically depends on material properties. Therefore, experimental study has been concluded and following conclusions can be drawn;

- Compressive strength and flexural strength are decreases with decrease in density of FC.
- High foam content also causes drastically reduction in strength of FC.
- Water absorption increases with more foaming agents and low density.
- Thermal conductance is very low due to low density of FC.

Based on experimental results, CLC blocks with very low density is recommended for infill walls and non-structural purposes. However, for load bearing purpose high density FC is recommended. Furthermore, study will be needed to find out CLC blocks masonry behavior under diagonal, shear and compression loading.

5   REFERENCES

[1]   S. van Dijk, *Foamed concrete: a Dutch view*. Slough: British Cement Association, 1991.

[2]   M. Saidani, U. Ogbulogugo, E. Coakley, and G. Sam, "Lightweight cementetious (GEM-TECH) structural material," *Proc Int Congr Technol Concr Durab*, pp. 186–95, 2016.

[3]   K. Ramamurthy, E. K. Nambiar, and G. I. S. Ranjani, "A classification of studies on properties of foam concrete," *Cem. Concr. Compos.*, vol. 31, no. 6, pp. 388–396, 2009, doi: 10.1016/j.cemconcomp.2009.04.006.

[4]   R. Valore, "Cellular Concretes Part 1 Composition and Methods of Preparation," 1954. doi: 10.14359/11794.

[5]   Rudnai, "Lightweight Concretes," 1963.

[6]   D. Aldridge, "Introduction to foamed concrete: What, why, how?," *Proc. Int. Conf. Use Foam. Concr. Constr.*, pp. 1–14, Jan. 2005.

[7]   R. Dhir, M. Newlands, and A. McCarthy, *Use of Foamed Concrete in Construction*. 2005.

[8]   F. A. Oginni, "Continental Application of Foamed Concrete Technology: Lessons for Civil Engineering Infrastructures Development for Africa," *Adv. Appl. Sci. Technol. Vol 2*, vol. 5, no. 4, pp. 15–24, 2015, doi: 10.9734/BJAST/2015/13063.

[9]   C. R. Cook, *FIP manual of lightweight aggregate concrete, second edition: Published by The Surrey University Press, Bishopriggs, Glasgow G64 2NZ, Scotland,*. 1983.

1st International Conference on Advances in Civil & Environmental Engineering, University of Engineering & Technology Taxila, Pakistan

Conference date 22 &23 Feb 2022

Mechanical Properties of Dry Stack Masonry using Hydraform Blocks

Inayat Ullah Khan, Khan Shahzada
University of Engineering & Technology Peshawar, Pakistan
16pwciv4553@uetpeshawar.edu.pk; khanshahzada@uetpeshawar.edu.pk

Akhtar Gul
University of Engineering & Technology Peshawar, Pakistan
akhtarwazir@ uetpeshawar.edu.pk

Khalid Khan
University of Engineering & Technology Peshawar, Pakistan
16pwciv4552@uetpeshawar.edu.pk

Abdul Rahim Khan
University of Engineering & Technology Peshawar, Pakistan
18pwciv5057@uetpeshawar.edu.pk

ABSTRACT

Dry Stack Block Masonry (DSBM) is a surface bonded material, whose entire properties depends on the surface characteristics. In this paper, the basic mechanical properties of DSBM has been evaluated, through direct compression and diagonal tension test, performed according to the guidelines of ASTM. The compressive strength and elastic modulus of DSBM is comparable with that of the brick masonry. Moreover, the ratio of shear and elastic modulus is in close agreement, with the range reported in previous research. The stress and strain curve, obtained from direct compression test, is analogous to mortared masonry. The sliding of dry stack masonry units, limits the diagonal tensile and shear strength of DSBM system. Some recommendations are given at the last, for improvement of parameters, obtained from diagonal tension test.

KEYWORDS: Mechanical Properties, Dry stack block masonry, diagonal tension test

1 INTRODUCTION

Dry Stack Block Masonry (DSBM), is a new emerging building material, commercialized during the material revolution era of 20th century [1]. Existing DSBM is a mortarless material, which is similar to ancient dry stack stone masonry (DSSM) [2]. Though, the existence of dry stack stone masonry (DSSM) is found thousand years ago in the form of Zimbabwe ruins, Shona Kingdom and Egyptian Pyramids etc. [1], but ancient DSSM was having large and huge sections, whose handling and construction was time consuming and challenging [1]. Having these issues, the interest in use of DSSM was lost at that time.

Keeping in view, the beneficial construction and structural behaviour, the ancient DSSM has been mechanized and transformed into concrete blocks or Stabilized Compressed Earth Blocks (SCEB), having thin sections and self-interlocking mechanism [3]. The self-interlocking mechanism is

provided in SCEB, in the form of grooves and depressions, at head and bed faces [4]. Hydraform block is one the simple type of self-interlocking SCEB, industrialized by Hydraform Africa (pty) Ltd in 1988 and now available in more than forty (40) different countries of the world [1]. Due to the presence of self-interlocking mechanism, the productivity of DSBM is 71 % more than the conventional masonry [3]. It is 27% economical compare to conventional masonry, due to absence of mortar and speedy construction [1]. DSBM has space for reinforcement, conduit and electrical wire placing [5]. Like different developing countries, DSBM is also getting popularity in Pakistan, due to eco-friendly, economical and faster construction features. It is expected, that DSBM will replace passable volume of conventional masonry construction in nearby future [6].

Earthquake occurred in different parts of the world, triggered the attention of the researchers toward the mechanical properties evaluation of various materials [7]. The seismic performance of full scale structure, depends on the basic properties of a material [8]. Keeping in view, the weak performance of masonry in recent past earthquakes, the introduction of any novel masonry materials, need proper laboratory testing before commercialisation [4]. Moreover, mechanical properties of any masonry material, plays a key role in the design and analysis of a particular structural system [9]. Some of the researchers, worked on the coefficient of friction [10], water absorbance and rain penetration intensity of DSBM [5]. But no research has been performed on the compressive strength, elastic modulus, shear modulus, diagonal tensile and shear strength of this novel masonry typology. So purpose of this research, is to evaluate these mechanical properties of DSBM, built with Hydraform blocks.

2 MATERIAL AND METHOD

2.1 Hydraform Block

The tests are performed on Hydraform block, introduced by ECO Brick Enterprise Islamabad, Pakistan. The dimension and interlocking of Hydraform block are shown in Figure 1.
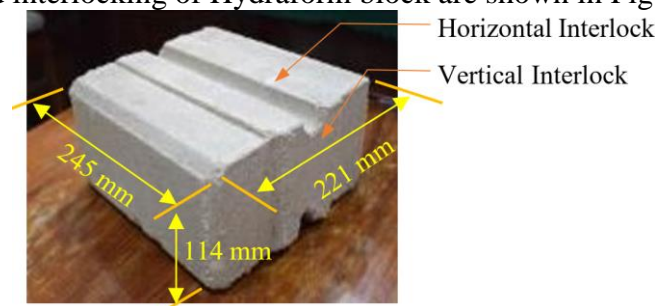
Figure 1: Hydraform Block

2.2 Direct Compression Test

The average value of compressive strength f_{dm} and elastic modulus E_{dm} of DSBM has been found through direct compression test, performed according to requirements of ASTM C1314 [11]. The test is performed on DSBM wallet, having dimension of 456 mm $\times$ 596 mm $\times$ 221 mm (18" $\times$ 24" $\times$ 8.7"), as shown in Figure 2b. The elastic modulus is found from stress and strain curve, in the range of 1/20 to 1/3 times of maximum compressive stress and corresponding strain [10].

1st International Conference on Advances in Civil & Environmental Engineering, University of Engineering & Technology Taxila, Pakistan

Conference date 22 &23 Feb 2022

2.3 Diagonal Tension Test

The shear modulus, diagonal tensile and shear strength has been evaluated through diagonal tension test, performed according to requirements of ASTM E519 [12]. The size of the wall is 1200 mm × 1200 mm (4' × 4'), as shown in Figure 2a, constructed according to ASTM E519. The wall is loaded along one of the diagonal and corresponding displacement was recorded through linear variable displacement transducers (LVDTs). Two LVDTs are attached to the wall along the diagonals, to recorded the diagonal distortion produced in the wall. The diagonal load (P) is applied through hydraulic jack system, having capacity of 50 tons, which were further connected with static data acquisition system having maximum scanning speed of 20 channels per second.
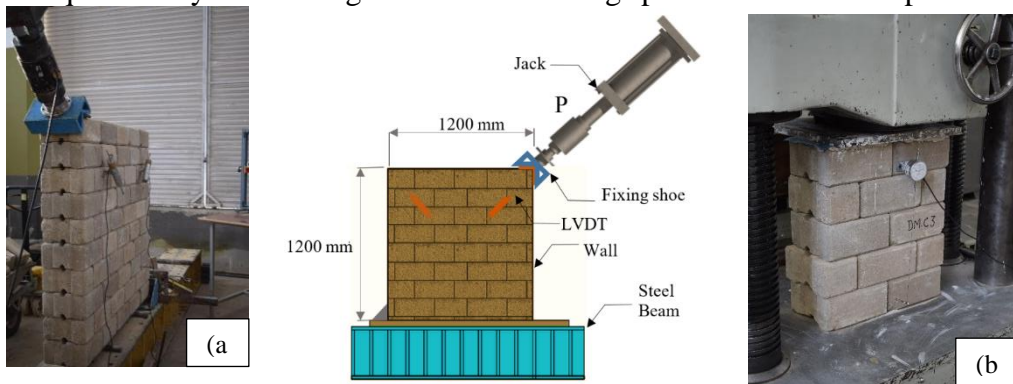
Figure 2: (a) Diagonal Tension Test (b) Direct compression test

The parameters from diagonal tension test is calculated according to the equations, given by ASTM E519, given as under;

$$Shear\ stress = \ \tau_d\ = \frac{0.707P}{Area\ of\ specimen} \tag{1}$$

$$A\ = \frac{width + height\ of\ specimen}{2} \tag{2}$$

$$shearing\ strain = \in_s = \frac{Diagonal\ shortening + Diagonal\ extension}{gage\ length} \tag{3}$$

$$Shear\ modulus = G_d = \frac{\tau_d}{\in_s} \tag{4}$$

The shear modulus is found at different stress level. Generally the value of G, was selected corresponding to $\frac{\tau_{max}}{3}$ [13].

3 RESULT AND DISCUSSION

3.1 Compressive strength and elastic modulus

Three specimen were tested, according to ASTM C1314, to find average compressive strength and elastic modulus. The average value of elastic modulus and compressive strength is given in Table 1 and 2, respectively. The stress curve for one specimen is shown in Figure 3.

1st International Conference on Advances in Civil & Environmental Engineering, University of Engineering & Technology Taxila, Pakistan

Conference date 22 &23 Feb 2022

Table 1 Elastic modulus of DSBM

Specimen	Elastic modulus E_{dm}, MPa (psi)	Average E_{dm}, MPa (psi)
Specimen 01	493 (71500)	
Specimen 02	486 (70453)	486 (70567)
Specimen 03	481 (69745)	

Table 2 Compressive strength of DSBM

Specimen	Compressive strength f_{dm}, MPa (psi)	Average f_{dm}, MPa (psi)
Specimen 01	2.40 (348)	
Specimen 02	2.45 (355)	2.40 (348)
Specimen 03	2.36 (342)	

The stress-strain curve (Figure 3) for DSBM presents that yielding starts at stress and strain of 2.14 MPa (310 psi) and 0.053 mm/mm, respectively. The compressive strength of DSBM is almost equal to the mortared masonry, reported by researcher [14]. The ultimate strength of DSBM, occurred at the strain of 0.081 mm/mm. The stress strain curve for DSBM is analogues to conventional mortared masonry.
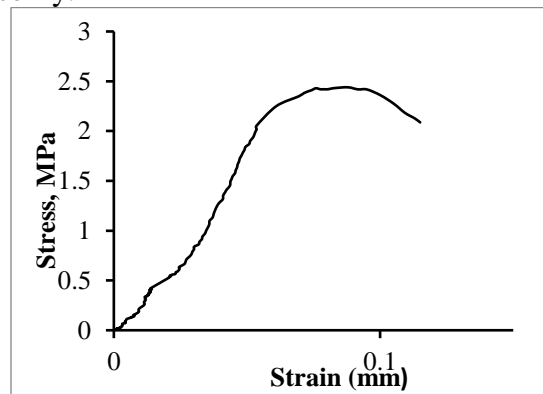
Figure 3: Stress and strain curve for DSBM wallet

3.2 Parameters from diagonal tension test

Three specimen were tested, according to ASTM E519. The values of diagonal tensile, shear strength and shear modulus is given in Table 3.

Table 3 Parameters from diagonal tension test

Specimen	Diagonal tensile strength MPa (psi)	Shear strength MPa (psi)	Shear Modulus, G_{dm}, MPa (psi)
Specimen 01	0.034 (4.93)	0.037 (5.365)	127 (18430)
Specimen 02	0.034 (4.97)	0.027 (3.915)	120 (17435)
Specimen 03	0.033 (4.76)	0.025 (3.625)	114 (16456)

The average shear stress and strain curve is shown in Figure 4, drawn from the data of diagonal tension test, recorded through diagonally attached LVDTs. The right and left side of graph,

1st International Conference on Advances in Civil & Environmental Engineering, University of Engineering & Technology Taxila, Pakistan

Conference date 22 &23 Feb 2022

indicates shortening and elongating diagonal strain, respectively. The maximum shear stress, occurs at the strain of 0.051 mm/mm, both in compression and tension. Moreover, it is cleared from the stress and strain curve, that diagonal tension failure is brittle one, causing abrupt shear stress degradation. The reason is that, since DSBM is mortarless, so all the shear forces is resisted by surface friction and when get equal to shear strength of the masonry, sudden sliding of blocks occurs which decreases shear strength suddenly. Moreover, the ratio of G/E is equal to 0.27, which is in close agreement with the range, reported by Tomaževič (1999) [15].
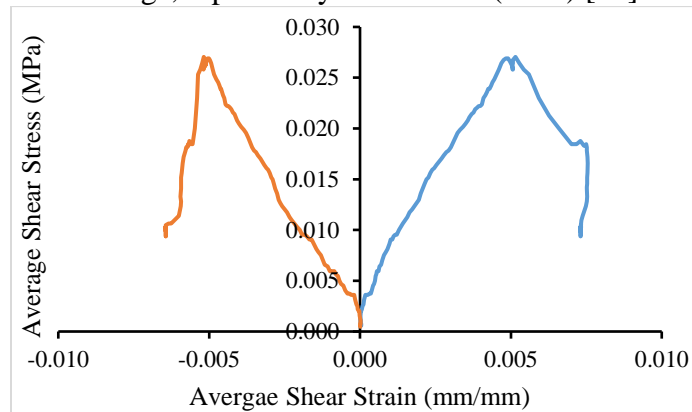
Figure 4: Average shear stress and strain curve

4   CONCLUSION

In this paper, mechanical properties of DSBM has been discoursed. The tensile and shear strength of DSBM is low, due to free sliding and rotation of masonry units, which limits these parameters. Moreover, the compressive strength and elastic modulus of DSBM is comparable with that of the mortared masonry. The stress and strain curve of DSBM, drawn from the data of direct compression test, is analogues to mortared masonry.

5   RECOMMENDATIONS

The tensile and shear strength of DSBM is low, due to free motion of units. These parameters can be improved, through the application of axial compression load, which will ensure the tight contact of interlocking blocks. The application of axial compressive load in diagonal tension test, will represent a real scenario, existed in a typical building. These load may result from dead load of wall itself, or combined load transformed from top stories. Furthermore, DSBM should be confined, to avoid the free sliding of masonry units, which will improve the properties of masonry.

REFERENCES

1.   Pave R, Uzoegbo H (2010) Structural Behaviour of Dry Stack Masonry Construction. Proc, SB10 Portugal: Sustainable Building Affordable to All: Low Cost Sustainable Solutions, Algarve, Portugal 4:45–89

1st International Conference on Advances in Civil & Environmental Engineering, University of Engineering & Technology Taxila, Pakistan

Conference date 22 &23 Feb 2022

2. Uzoegbo HC (2001) Lateral Loading Tests on Dry-Stack Interlocking Block Walls. In: Structural Engineering, Mechanics and Computation. Elsevier, pp 427–436
3. Ramamurthy K, Kunhanandan Nambiar E (2004) Accelerated masonry construction review and future prospects. Progress in Structural Engineering and Materials 6:1–9
4. Ali M, Gultom RJ, Chouw N (2012) Capacity of innovative interlocking blocks under monotonic loading. Construction and Building Materials 812–821. https://doi.org/10.1016/j.conbuildmat.2012.08.002
5. Deepak B (2010) Interlocking dry stacked masonry. p 10
6. Saari S, Bakar BHA, Surip NA (2017) Flexural Strength of Interlocking Compressed Earth Brick (ICEB) Unit. IJPS 3:. https://doi.org/10.12962/j23546026.y2017i6.3232
7. Khan I, Gul A, Shahzada K, et al (2021) Computational Seismic Analysis of Dry-Stack Block Masonry Wall. Civil Engineering Journal 7:488–501
8. Khan I, Gul A, Shahzada K, et al (2021) Computational Seismic Analysis of Dry-Stack Block Masonry Wall. Civ Eng J 7:488–501. https://doi.org/10.28991/cej-2021-03091668
9. Calderini C, Cattari S, Lagomarsino S (2010) The use of the diagonal compression test to identify the shear mechanical parameters of masonry. Construction and building materials 24:677–685
10. Hafeez J, Ali SM, Shahzada K (2018) EVALUATION OF SHEAR STRENGTH OF HYDRAFORM DRY STACK MASONRY - Google Search. https://www.google.com/search. Accessed 27 Oct 2021
11. ASTM C1314 (2014) Standard Test Method for Compressive Strength of Masonry Prisms. https://www.astm.org/c1314-12.html. Accessed 31 Dec 2021
12. ASTM E (2002) 519-02. Standard test method for diagonal tension (shear) in masonry assemblages. ASTM International, West Conshohocken, PA
13. Magenes G, Penna A, Galasco A, Rota M (2010) Experimental characterisation of stone masonry mechanical properties. pp 247–256
14. Shahzada K, Khan AN, Elnashai AS, et al (2012) Experimental Seismic Performance Evaluation of Unreinforced Brick Masonry Buildings. Earthquake Spectra 28:1269–1290. https://doi.org/10.1193/1.4000073
15. Tomazevic M (1999) Earthquake-resistant design of masonry buildings. Imperial College Press, London

Solar Roof Tiles: An Experimental Approach Towards the Thermal Energy Analysis for Application in Domestic Buildings

Nadeem Abbas, Muhammad Bin Zubaid Ramay
Civil Engineering Department / Electrical Engineering Department
University of Engineering & Technology Taxila, Pakistan
Nadeem.Abbas@students.uettaxila.edu.pk; mbzubaid.ramay@students.uettaxila.edu.pk

Ehtisham Rana, Mudassar Habib
University of Engineering & Technology Taxila, Pakistan
Rana.Ehtisham@students.uettaxila.edu.pk; Mudassar.Habib@students.uettaxila.edu.pk

ABSTRACT

Sustainable electricity generation is one of the significant problems, and photovoltaics have enormous potential in solving this problem for the domestic market. This paper comprises the detailed design of photovoltaic roof tiles, which can be effectively integrated into the domestic roof structure. Factors affecting the consumption of solar roof tiles in the domestic market are also evaluated. The aesthetics of integrating solar roof tiles, pricing for the domestic users and regulatory problems are the most critical factor that created a problem for the increasing consumption of solar roof tiles. Without understanding the current practices of the materials used in roofing, it is not entirely possible to maximize the integration of solar roof tiles for domestic use. They are attached firmly to the roof by using specially designed clips on wooden battens. Rafters of roof structure can help connect battens firmly to the rope, and in this way, the solar tiles can promote domestic energy savings. Sarking felt can also be provided between the battens and rafters, which can help to provide the secondary production against the environmental agents. Waterproofing is one of the significant features of this layer, and therefore, it is effectively recommended for the construction of roofing with solar roof tiles. Solid Works was used to stimulate the photovoltaic roof tiles, and electro-mechanical modelling is also done by using MATLAB, which help in protecting the stability of the system. The study recommends improving the regulatory policies and reducing the price per square foot as both of these factors can effectively increase the consumption of solar roof tiles in the domestic market.

KEYWORDS: Solar roof tiles, thermal energy analysis and energy in domestic buildings

1   INTRODUCTION

There are a variety of roofing materials available, and they have their function and aesthetic requirements for domestic users. Shingles having the solar energy generation future is one of the best products available in the market for domestic honours that can help to reduce energy demand significantly. It comes in the category of the solar energy solution that is commonly known as the building-integrated photovoltaics [5]. Different combinations of solar shingles are used in limited quantity because there are commercial constraints that do not allow the scaling up of technology. However, the maximum power generation capability of the single solar roof tile can reach around a hundred watts. In the areas where the climate is hot, the potential of photovoltaic roof tiles

1st International Conference on Advances in Civil & Environmental Engineering, University of Engineering & Technology Taxila, Pakistan

Conference date 22 &23 Feb 2022

increases because they can help increase energy generation and contribute to the reasonable satisfaction of domestic customers [8]. However, the installation needs to be carried out at a 45-degree angle to the solar rays to maximize energy production. The supporting structure also needs to be constructed under the roof tiles as it can significantly reduce environmental damage and contribute effectively in firmly joining the solar roof tiles together.

Table 1 Comparison of photovoltaic cell parameters

Parameter	Mono (156 mm)	Poly	Mono (125 mm)	Back contact
Efficiency (%)	19	18	19	23
Open Circuit Voltage (V)	0.65	0.61	0.60	0.69
Short Circuit Current (A)	8.74	8.46	5.63	6.01
Maximum Power Point Power (W)	4.30	4.03	2.10	3.49
Maximum Power Point Voltage (V)	0.51	0.52	0.51	0.60
Maximum Power Point Current (A)	8.21	7.91	5.31	5.81

Different semiconductor technologies are also present concerning where energy efficiency ratings can provide significant leverage to domestic customers in reducing energy consumption as shown in Table 1. Crystalline silicon wafer, CdTe and dye-sensitized solar cells are the common examples of different solar cells available in the market with various sizes and life spans. However, the availability issues significantly damage the solar roof tiles' sustainability [6]. The regulation of solar roof tiles is also not aligned with the interest of the consumers, which create problems in sustainable installation of the tiles on the roofs, and ultimately, it can create significant problems for the industry to be scaled up.

Previous studies have shown significant information regarding the possible outcome of using solar photovoltaic cells [9]. However, they are unclear because of using conventional empirical methods and not having significant induction of new methodology by which the customer trust could build up. It is the reason that despite having significant advantages, the cost of solar roof tiles is not in the affordable range for domestic customers [10]. The latest research combined with no regulation in the market negatively impacts the consumption of solar roof tiles, and even customers can reject the solar roof tiles because of their aesthetics. There is a need for practical evaluation of the efficiency of the solar roof tiles so that the factors affecting the buying decision of the consumers should be addressed from the regulatory, pricing, and aesthetic perspectives.

2   LITERATURE REVIEW

Previous studies have shown significant information regarding the commercial viability of photovoltaic solar tiles, but comprehensive information is still lacking to ensure sustainable use. In a study done by the Zalamea León & Cuevas Barraza (2019), it is evident that solar tiles can work efficiently in the cold climate, but it was also one of the limitations of this study that did not provide satisfactory outcomes that could be applied in the hot regions [11]. In another study done

1st International Conference on Advances in Civil & Environmental Engineering, University of Engineering & Technology Taxila, Pakistan

Conference date 22 &23 Feb 2022

by the Carvalho et al. (2019), it is evident that the natural conditions influence the energy generation capacity of solar roof tiles, and ultimately it can directly affect the satisfaction of consumers [3]. The study is limited in the context of only considering the environmental factors that vary significantly all around the globe, and therefore, the study does not provide practical implications for the scaling up of Technology.
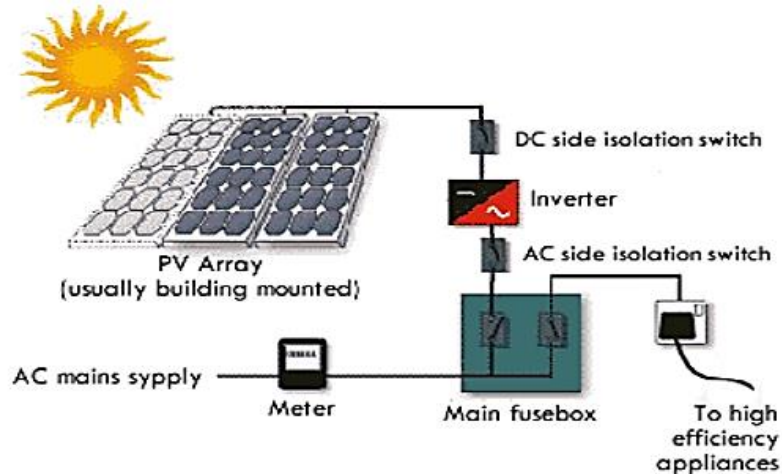
Figure 1: Working of Building integrated photovoltaic array

Reviews of sophisticated models of analysis like the simulation tools are not effectively demonstrated by Alim et al. (2020), resulting in the proper implementation of photovoltaic solar roof tiles commercially [1]. Working solar roof tiles in the lab environment is effectively provided in the previous studies done by authors. However, it is not significant enough to provide long-term implications that could be used to maximize the design suitability to domestic consumption. As pointed out by the Balali et al (2020), difficulties exist, which can contribute to less regulation of the product in the market and create difficulties for the industries to reduce the prices [2].

The lifetime of the solar tiles is estimated to be at least 25 years, but different technologies used to build up the semiconductor layer can degrade over time because of environmental factors. However, the energy generation capacity and the environmental influence are also the matter constants that contribute to decreasing the commercial sustainability of solar roof tiles [7]. The typical design orientation of the solar roof tiles demonstrated by previous studies can be infinite, but the potential dimensions that create more aesthetics and efficiency are limited concerning the semiconductor technologies.

The energy density cannot be expressed within the single solar roof tile, which can contribute negatively to the suitability of solar roof tiles for domestic customers. There are indeed highly sophisticated methods available from the research text that can provide important information regarding the efficiency of solar roof tiles, but they have their limitations and may not provide for understanding to consumers [4]. However, the progress in the development of solar roof tiles is significantly increasing as more industries are considering new methods of manufacturing that can contribute to minimal layer thickness. That can contribute to the reduction of the prices of the solar tiles are the outcomes from the future perspective are blurry and create more problems in the path

1st International Conference on Advances in Civil & Environmental Engineering, University of Engineering & Technology Taxila, Pakistan

Conference date 22 &23 Feb 2022

of sustainable manufacturing of the solar roof tiles and maximizing their practical application on the roofs. The lack of contextual analysis and the significant gaps in the researchers propose the need to address the contemporary issues that can create method problems for the Solar roof tile industries to affect domestic consumers positively.

3   METHODOLOGY

The design of the model of roof tiles is carried out using Solid Works software as shown in Figure 2. The model is effectively stimulated to determine the energy generation that can provide sustainable development to the consumption of solar roof tiles in the domestic market. Individual roof tile model is made using the solid work software, and then the piezoelectric material is attached to the solar tile and a valuable energy source to determine the response when it is stimulated to measure energy consumption. The tides are integrated into the proper pattern so that they can represent the solar roof tiles installed on the house, and from there, the measurements are recorded in the context of effectively building the aesthetic experience as well as providing more excellent reliability in the measurement of solar efficiency in the context of domestic consumption.

Figure 2: Modeling in Solid Works

The life cycle cost analysis is done using ANSYS software as it is a part of primary quantitative research analysis in which temperature measurement concerning the various environmental conditions is carried out to stimulate energy generation. MATLAB Simulink is a practical module used to research parameters contributing to the sustainable development of solar roof tiles. A customized code is developed to analyze voltage, current, sun position, and temperature.
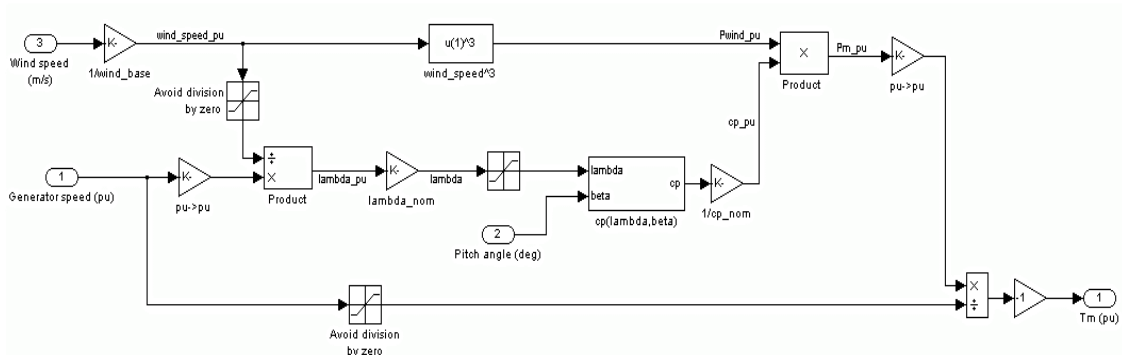
Figure 2: MATLAB Simulink model for solar energy generation from roof tiles

The detailed statistical analysis is carried out by using five different cases:
1. Modified Siemens roof tile (ceramic)
2. Modified Siemens roof tile (concrete)
3. Elkem process with roof tile (ceramic)
4. Elkem process with roof tile (concrete)
5. Monocrystalline solar panel

The combined impact of the different orientations of the solar roof tiles is calculated using the life cycle impact theory, in which all the cases are evaluated to determine the net energy performance. The measurements are carried out using the effective combination of cases, and the cycle inventory is also calculated to determine the possible applications of photovoltaic roof tiles in the domestic market. Cost analysis is also part of this study conducted to determine the life cycle assessment and the possible applications of increasing the solar roof tile consumption.

4   RESULTS AND DISCUSSION

According to findings, it is evident that photovoltaics was not implemented in the market concerning the current growth; however, they were present for some years in integrated photovoltaics. The production of solar roof tiles indeed requires the roof first, but at the same time, their efficiency needs to be maximized further as the high potential exists in improving the domestic energy savings.
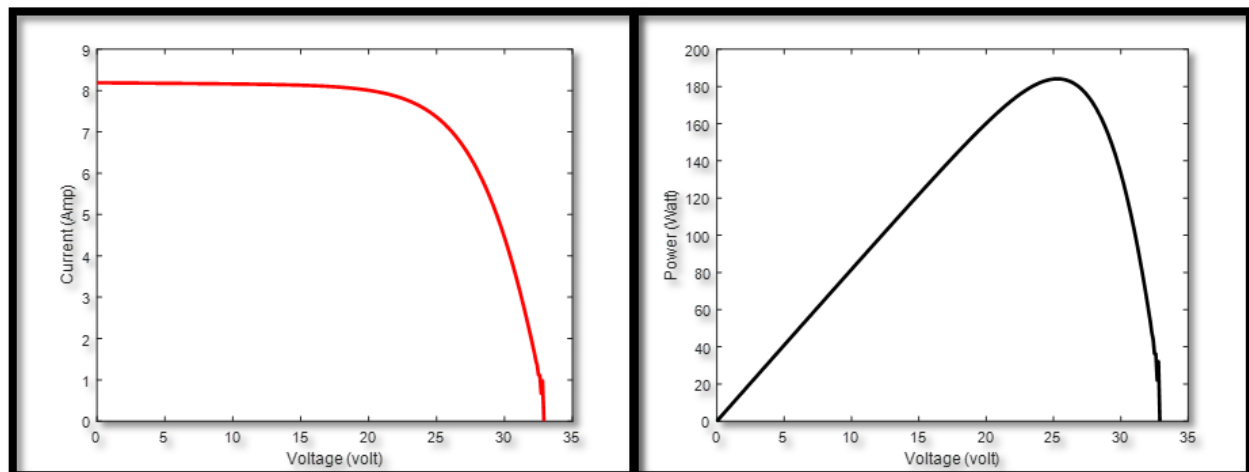
Figure 3: Current, Power and Voltage behavior observed from MATLAB

For the consumers, the price and solar efficiency are the most critical factors that can help them make their buying decisions. However, it is always categorized as one of the premium products

1st International Conference on Advances in Civil & Environmental Engineering, University of Engineering & Technology Taxila, Pakistan

Conference date 22 &23 Feb 2022

for domestic users because it is made up of quartz, and still, the estimates are not precise in terms of the total demand from the perspective of domestic consumers and overall sustainable price. It is found from the study that nearly the cost of installation of photocatalytic roof tiles is 21.85 USD per square foot. Cost is high compared to the other forms of construction on the roof, and therefore it can directly affect the buying decision of the consumers and may not help in maximizing the competitive value of solar roof tiles as they are not being produced widely.
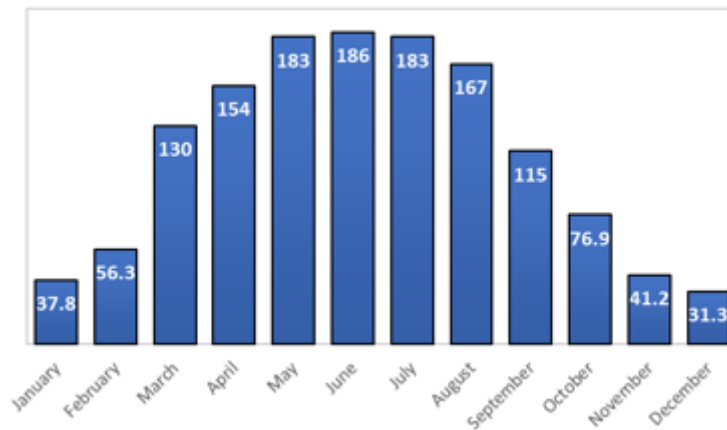
Figure 4: Power generation behavior observed for a year

5 CONCLUSION

Continual improvement is needed in increasing the cell efficiencies of photovoltaics, and in this way, their production could be increased according to the requirements of urban areas. The energy-generating efficiency of photovoltaic roof tiles is highly significant, making them essential for the domestic energy market. However, it is crucial to integrate the photovoltaics in an aesthetically pleasing manner. It can significantly increase the demand for products in domestic consumption and make the product fully sustainable for consumers looking for green energy. The product has a high value in terms of increasing green energy consumption for domestic purposes, and also it can let the consumers save the environment effectively. Installing the photovoltaic roof tiles does not require exceptional technicians, and it is one of the significant benefits for domestic consumers as they can get the product installed on their homes without having extra expenses. It is a highly developing industry that needs to be adopted on a wide scale because it has enormous potential in maximizing energy saving in the domestic scenario, and it can quickly help reduce the environmental footprint of buildings.

REFERENCES

[1]   Mohammad A. Alim, Zhong Tao, Md Jaynul Abden, Ataur Rahman, and Bijan Samali. 2020. Improving performance of solar roof tiles by incorporating phase change material. *Sol. Energy* (2020). DOI:https://doi.org/10.1016/j.solener.2020.07.053

1st International Conference on Advances in Civil & Environmental Engineering, University of Engineering & Technology Taxila, Pakistan

Conference date 22 &23 Feb 2022

[2]   Amirhossein Balali, Alireza Valipour, Edmundas Kazimieras Zavadskas, and Zenonas Turskis. 2020. Multi-Criteria Ranking of Green Materials According to the Goals of Sustainable Development. *Sustainability* 12, 22 (November 2020), 9482. DOI:https://doi.org/10.3390/su12229482

[3]   Monica Carvalho, Valeska L. Menezes, Kelly C. Gomes, and Raoni Pinheiro. 2019. Carbon footprint associated with a mono- Si cell photovoltaic ceramic roof tile system. *Environ. Prog. Sustain. Energy* 38, 4 (July 2019), 13120. DOI:https://doi.org/10.1002/ep.13120

[4]   Syed Ahmad Farhan, Fouad Ismail Ismail, Osamah Kiwan, Nasir Shafiq, Azni Zain-Ahmed, Nadzhratul Husna, and Afif Izwan Abd Hamid. 2021. Effect of Roof Tile Colour on Heat Conduction Transfer, Roof-Top Surface Temperature and Cooling Load in Modern Residential Buildings under the Tropical Climate of Malaysia. *Sustainability* 13, 9 (April 2021), 4665. DOI:https://doi.org/10.3390/su13094665

[5]   Chiara Ferrari, Ali Gholizadeh Touchaei, Mohamad Sleiman, Antonio Libbra, Alberto Muscio, Cristina Siligardi, and Hashem Akbari. 2014. Effect of aging processes on solar reflectivity of clay roof tiles. *Adv. Build. Energy Res.* 8, 1 (January 2014), 28–40. DOI:https://doi.org/10.1080/17512549.2014.890535

[6]   Chiara Ferrari, Antonio Libbra, Federico Maria Cernuschi, Letizia De Maria, Stefano Marchionna, Matteo Barozzi, Cristina Siligardi, and Alberto Muscio. 2016. A composite cool colored tile for sloped roofs with high 'equivalent' solar reflectance. *Energy Build.* 114, (February 2016), 221–226. DOI:https://doi.org/10.1016/j.enbuild.2015.06.062

[7]   Dr. Mohammad Monirujjaman Khan. 2020. An Eco-friendly and Cost Effective Building for Future Smart Cities. In *Proceedings of 1st International Electronic Conference on Applied Sciences*, MDPI, Basel, Switzerland, 8572. DOI:https://doi.org/10.3390/ASEC2020-08572

[8]   Guillaume Doudart de la Gree, Argyrios Papadopoulos, Michael Debije, Mark Cox, Zachar Krumer, Angele Reinders, and Alexander Rosemann. 2015. A new design for luminescent solar concentrating PV roof tiles. In *2015 IEEE 42nd Photovoltaic Specialist Conference (PVSC)*, IEEE, 1–5. DOI:https://doi.org/10.1109/PVSC.2015.7355832

[9]   Luciana M. Schabbach, Deivis L. Marinoski, Saulo Güths, Adriano M. Bernardin, and Márcio C. Fredel. 2018. Pigmented glazed ceramic roof tiles in Brazil: Thermal and optical properties related to solar reflectance index. *Sol. Energy* 159, (January 2018), 113–124. DOI:https://doi.org/10.1016/j.solener.2017.10.076

[10]   Esteban Zalamea-León, Juan Mena-Campos, Antonio Barragán-Escandón, Diego Parra-González, and Pablo Méndez-Santos. 2018. URBAN PHOTOVOLTAIC POTENTIAL OF INCLINED ROOFING FOR BUILDINGS IN HERITAGE CENTERS IN EQUATORIAL AREAS. *J. Green Build.* 13, 3 (June 2018), 45–69. DOI:https://doi.org/10.3992/1943-4618.13.3.45

[11]   Esteban Zalamea León and Cristian Cuevas Barraza. 2019. Adaptability of photovoltaic mono-polycrystalline solar panels and photovoltaic roof tiles on dwelling roofs of real estate developments. *Rev. la construcción* 18, 1 (April 2019), 42–53. DOI:https://doi.org/10.7764/RDLC.1.1.42

PAPER ID: 127

1st International Conference on Advances in Civil & Environmental Engineering, University of Engineering & Technology Taxila, Pakistan

Conference date 22 &23 Feb 2022

Numerical Investigation of Typical Scale Down Bridge Pier Retrofitted with CFRP under Seismic Loading

Mustahsan Iqbal, Muhammad Khalid Hafeez
University of Engineering & Technology Taxila, Pakistan
mustahsaniqbal@rocketmail.com; raokhalidhafeez@gmail.com

Dr. Qaiser-Uz-Zaman
University of Engineering & Technology Taxila, Pakistan
dr.qaiser@uettaxila.edu.pk

ABSTRACT:
On 8 October, 2005, an earthquake with a magnitude of Mw 7.6 rocked the Pakistan-controlled sector of Kashmir. As a result, many bridges suffered varied degrees of earthquake-related damage. It was important to enhance their strength and endurance. Retrofitting of bridge piers using Fiber Reinforced Polymers is one of the modern approaches for rehabilitating structures. This restricts the concrete, resulting in a significant increase in column strength. In order to explore the effectiveness of Carbon Fiber Reinforced Polymers (CFRP), current research used state-of-the-art engineering simulation software "Seismostruct" to simulate scaled down (1:4) High Strength Concrete (HSC) circular bridge pier models. To determine improvements in strength, ductility and stiffness, the model was submitted to Quasi-Static Cyclic Tests (QSCT) and Pushover Analysis. The model was refitted with CFRP wraps and the failures at their susceptible plastic zones were investigated. The goal of this simulation was to see how bridge piers would react in a seismic event. The results reveal that retrofitting R.C columns with CFRP increases their strength and allows them to disperse more energy.

KEYWORDS: CFRP, Quasi static cyclic Tests, Pushover Analysis, Retrofitting.

1 INTRODUCTION

Earthquakes are one of nature's deadliest forces, capable of shaking structures to their breaking point Bridges are particularly prone to damage during earthquakes, and if they are damaged, the entire transportation system is disrupted. As a result of the earthquake of 2005 in Pakistan, there was a pressing need to amend the seismic zone, and a new Building Code of Pakistan (2007), known as BCP-2007, was created. Almost every city in Pakistan has been upgraded to a greater seismic prone zone as a result of the revised building code. Many bridges were built before October 2005, and they all followed the West Pakistan Highway Code (1967). As a result, bridges were vulnerable to damage and required retrofitting to meet the needs for strength and ductility.

A research study was carried out in which columns were continuously reinforced by CFRP and were tested under constant compression load combined with a horizontal quasi static cyclic load test. The results concluded that CFRP confinement completely changed the failure mode of the columns[1]. An investigation was carried out to study the effect of retrofitting on change in dynamic properties of scale down bridge piers. Piers were tested twice, first in damaged state, and then retrofitted with single layer of CFRP. Results showed that energy dissipation and ductility of retrofitted column increases as compared to control model[2]. A low strength scale down concrete bridge pier model was simulated and analysed using analytical techniques. Results show that retrofitting of undamaged

1st International Conference on Advances in Civil & Environmental Engineering, University of Engineering & Technology Taxila, Pakistan

Conference date 22 &23 Feb 2022

state improves their ductility and made them capable to dissipate the energy more efficiently[3]. In another study, externally bonded Carbon Fiber Reinforced Polymer (CFRP) retrofit technique was implemented to improve the behaviour of RC columns tested under constant axial load and cyclic lateral load. It was found that (i) With CFRP lateral confinement, behaviour of slender RC columns tested under low and moderate axial load was improved in terms of ductility, energy dissipation and failure mechanism (ii) Using longitudinal CFRP retrofitting with the lateral CFRP confinement increased both the effective stiffness and lateral strength of column[4]. An investigation was carried out in which plastic hinge region of FRP-confined RC Columns was studied by finite element model. The results of investigation were (i)The plastic hinge length of FRP-confined columns is very different from that of normal RC Column. Lengths of both the rebar yielding zone and curvature localization zone increases first and then decrease as the confinement ratio increases (ii) For flexural retrofitting of the RC Columns, FRP jacket needs to cover at least the length of concrete crushing zone, which is significantly affected by FRP confinement[5]. Bridges built according to the criteria of ancient design codes have generally performed poorly during seismic events and have been deemed insufficient in strength and ductility, necessitating retrofitting to improve their strength and ductility. The subject research deals with numerical evaluation and modelling of High Strength Concrete Bridge Pier retrofitted with CFRP to determine its efficiency in boosting the pier's strength.

2   METHODOLOGY OF WORK

The current study employs finite element modelling to examine the dynamic properties of High Strength bridge pier columns. For the columns encased with CFRP Layers, the hysteretic performance and energy dissipation capacity were evaluated. The effectiveness of CFRP was measured in terms of increased lateral load capacity using high-strength circular columns. The model geometry, various dimensions, as well as the type and degree of applied loading, are identical to those used in experimental studies. The control specimen was first modelled and evaluated using "Seismostruct" through Finite Element Method (FEM). The model was then retrofitted by encapsulating it in layers of Carbon Fiber Reinforced Polymer (CFRP) and re-analysed with the same software. Before being damaged, the model was retrofitted with CFRP, implying that the methodology used was pre-retrofitted.

The original measurements of the bridge pier were scaled down to 1:4. After scaling down, the pier reached a height of 6 ft and 3 in (75 in) with a diameter of 1 ft (12 in).The pier was reinforced with 16#3 longitudinal steel bars and #1@6 in c/c spacing lateral reinforcement with a concrete cover of 1.25 in. Following that, the same scenario is recreated in Seismostruct to evaluate the effectiveness and performance of confined concrete. Seismostruct version 2020 was used to simulate a 3D solid model of a bridge pier. Pier elements are inelastic force-based (FB) frame elements. The pier is divided into five sections and 400 fibers are used to represent it. The concrete used has a modulus of elasticity of 4453.95 ksi, mean compressive strength of 6.192 ksi, mean tensile strength of 0.382 ksi. For longitudinal reinforcement, the steel employed has yield strength of 83 ksi, modulus of elasticity of 29000 ksi and mean strength of 19.5 ksi. CFRP used have fiber thickness of 0.04 in, tensile strength 153 ksi, tensile modulus of 9400 ksi. Static pushover analysis was used to stimulate Quasi Static Cyclic Load. The column was subjected to a gravity load of 42.2 kips in the form of concrete blocks put at the top of the column in addition to the lateral load. For each cycle, the lateral load simulated on the circular column is applied in terms of varying drift levels in one direction, followed by a restoring force in the opposite direction, forming the hysteresis loop. The lateral force is applied 75 inches (1905 mm) from the base.

1st International Conference on Advances in Civil & Environmental Engineering, University of Engineering & Technology Taxila, Pakistan

Conference date 22 &23 Feb 2022
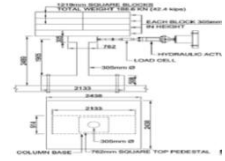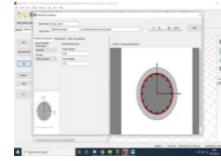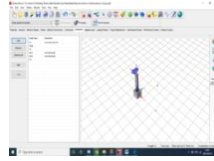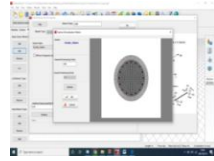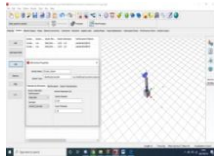
| Figure 1: Numerical Modelling | Figure 2: Meshing Arrangement | Figure 3: Boundary Conditions | Figure 4: Cross-Section | Figure 5: Plan and Elevation |

Drift levels applied are 0.1%, 0.25%, 0.5%,1%.2%,3%,4%,5% of height of pier. Displacements are determined based on these drift values, for example, 0.1% of 1905mm equals 1.9mm up to 5%.

3   SEISMOSTRUCT RESULTS

At various drift levels, simulations of quasi-static cyclic load tests were performed. Following the Quasi-Static Cyclic Load Testing simulation, the following steps were taken:

a) The output data from Seismostruct model analysis was exported to Excel spreadsheets.
b) Hysteresis loop curve at various drift level were plotted individually. The hysteresis curves for Control Model, Undamaged Retrofitted Models (Single and Double Layer) for High Strength columns of 6192 psi have been shown from Figure 6 to Figure 8.
c) For quantifying the energy dissipation at various drift levels, the area under the loops was calculated; graphs were plotted for peak energy dissipation against different drift value, named as energy dissipation curves shown from figure 9 to figure 11.

It was discovered that as the drift levels increase, energy dissipation increases as well. It's also worth noting that energy dissipation was insignificant before 1% drift level, indicating that there was very little or no energy dissipation. These energy dissipation of Control Model (CM), Undamaged Retrofitted Model- Single Layer (UDRM-SL) and Undamaged Retrofitted Model- Double Layer (UDRM-DL) of High Strength Concrete Bridge Pier (6192 psi) were then compare with energy dissipation of Control Model (CM), Undamaged Retrofitted Model- Single Layer (UDRM-SL) and Undamaged Retrofitted Model- Double Layer (UDRM-DL) of Low Strength Concrete Bridge Pier Columns (1800 psi and 2400 psi) are shown in Figure 14 to Figure 17.
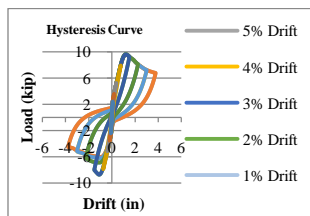
| Figure 6: Control Model (6192 psi) | Figure 7: Single Layer Models (6192 psi) | Figure 8: Double Layer Models (6192 psi) | Figure 9:- Control Models |

| Figure 10: Single Layer Model | Figure 11: - Double Layer Model | Figure 12: CM Comparison | Figure 13: CM Comparison |
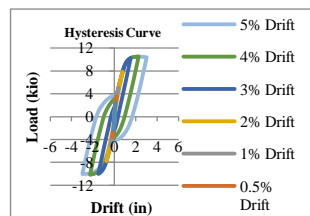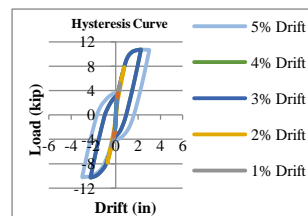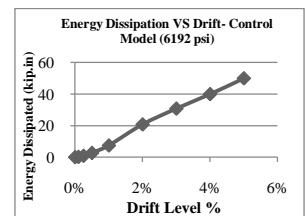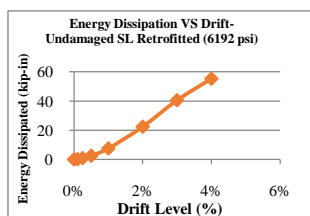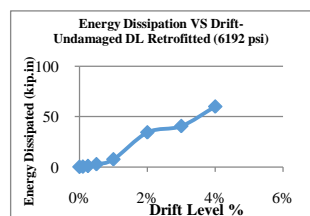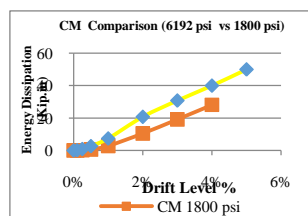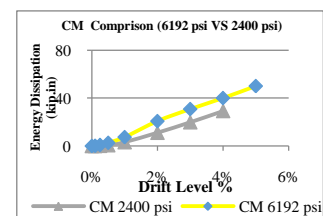
1st International Conference on Advances in Civil & Environmental Engineering, University of Engineering & Technology Taxila, Pakistan

Conference date 22 &23 Feb 2022
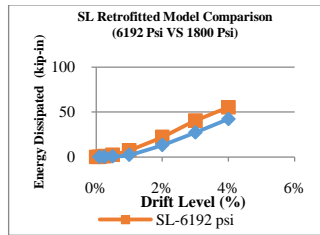
| Figure 14: UDRM-SL Comparison | Figure 15: UDRM-SL Comparison) | Figure 16: UDRM-DL Comparison | Figure 17: UDRM-DL Comparison |
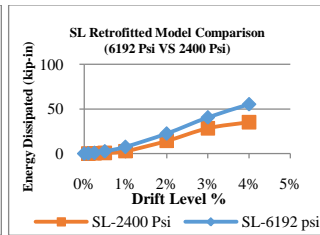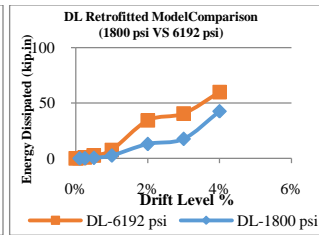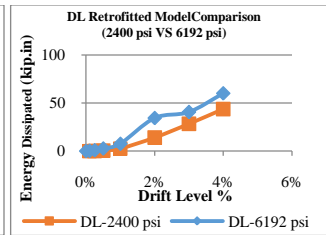
4   DISCUSSION ON RESULTS

It was observed that energy dissipation goes on increasing with the increase in drift level and also pier is capable to dissipate significantly large amount of energy when retrofitted with CFRP as compare to control state. It was also worth noting that as number of layers of CFRP increases, energy dissipation also increases. Concrete strength also plays a key role. Energy dissipation in case of High Strength Concrete (HSC) is very huge as compare to energy dissipated in case of Low Strength Concrete (LSC). A comparison was done between energy dissipation curves for Control Models (CM), Undamaged Retrofitted Models- Single Layer (UDRM-SL), Undamaged Retrofitted Models- Double Layer (UDRM-DL) of High strength concrete (6192 psi) and Control Model (CM), Undamaged Retrofitted Models- Single Layer (UDRM-SL) and Undamaged Retrofitted Models- Double Layer (UDRM-DL) of Low Strength Concrete (1800 psi and 2400 psi).

Following are the results of comparisons:

Table 1:   Single Layered CFRP Model Results - Percentage Increase in Energy Dissipation

	COMPARISON BETWEEN CONTROL AND UNDAMAGED MODELS OF 6192 Psi			
	Model Name	Model Type	Energy Dissipation (Kip. In)	Percentage Increase
	Undamage Models	CM-6192 Psi	20.0781	**38.04%**
		UDRM-SL 6192 Psi	27.7155	
		CM-6192 Psi	20.0781	**49.87%**
		UDRM-DL 6192 Psi	30.0920	
	COMPARISON BETWEEN CONTROL MODELS OF 6192 Psi, 1800 & 2400 Psi			
	Model Name	Model Type	Energy Dissipation (Kip. In)	Percentage Increase
SINGLE LAYERED MODELS RESULTS	Control Models	CM-1800 Psi	14.0600	**42.80%**
		CM-6192 Psi	20.0781	
		CM - 2400 Psi	14.6200	**37.33%**
		CM-6192 Psi	20.0781	
	COMPARISON BETWEEN UNDAMAGED RETROFITTED MODELS - SINGLE LAYER CFRP OF 6192 Psi,1800 Psi & 2400 Psi			
	Model Name	Model Type	Energy Dissipation (Kip. In)	Percentage Increase
	UDRM-SL	UDRM-SL 1800 Psi	21.1061	**31.32%**
		UDRM-SL 6192 Psi	27.7155	
		UDRM-SL 2400 Psi	17.6060	**57.42%**
		UDRM-SL 6192 Psi	27.7155	

1st International Conference on Advances in Civil & Environmental Engineering, University of Engineering & Technology Taxila, Pakistan

Conference date 22 &23 Feb 2022

Table 2: Double Layered CFRP Model Results - Percentage Increase in Energy Dissipation

Double Layer Models Results		COMPARISON BETWEEN UNDAMAGED RETROFITTED MODELS - DOUBLE LAYER CFRP OF 6192 Psi, 1800 & 2400 Psi			
		Model Name	Model Type	Energy Dissipation (Kip. In)	Percentage Increase
	UDRM-DL		UDRM-DL 1800 Psi	21.2408	**41.67%**
			UDRM-DL 6192 Psi	30.0920	
			UDRM-DL 2400 Psi	21.9058	**37.37%**
			UDRM-DL 6192 Psi	30.0920	

4   CONCLUSION

This clearly shows that energy dissipation is increased by increasing strength of Concrete as well as wrapping of a layer of CFRP. The difference between finite element model results and experimental results depends upon factors like human error, instrumental error and realistic environmental conditions.

5   Acknowledgement:

REFERENCES:

1.   Colomb, F., et al., *Seismic retrofit of reinforced concrete short columns by CFRP materials.* Composite Structures, 2008. **82**(4): p. 475-487.
2.   Khan, Q.-U.-Z., et al., *Seismic Evaluation of Repaired and Retrofitted Circular Bridge Piers of Low-Strength Concrete.* Arabian Journal for Science and Engineering, 2015. **40**(11): p. 3057-3066.
3.   Saeed, H.Z., et al., *Experimental and finite element investigation of strengthened LSC bridge piers under Quasi-Static Cyclic Load Test.* Composite Structures, 2015. **131**: p. 556-564.
4.   Aules, W.A., *Behavior of Non-Ductile Slender Reinforced Concrete Columns Retrofit by CFRP Under Cyclic Loading*. 2019, Portland State University.
5.   Yuan, F., Y.-F. Wu, and C.-Q. Li, *Modelling plastic hinge of FRP-confined RC columns.* Engineering Structures, 2017. **131**: p. 651-668.

Investigation of High Strength Concrete Bridge Piers Retrofitted with CFRP under Seismic Loading

Obaid Shahid Mir, Muhammad Khalid Hafeez
University of Engineering & Technology Taxila, Pakistan
mirobaid937@gmail.com; raokhalidhafeez@gmail.com

Dr. Qaiser-Uz-Zaman
University of Engineering & Technology Taxila, Pakistan
dr.qaiser@uettaxila.edu.pk

ABSTRACT

8th October 2005 marks a dark day in the history of Pakistan as a massive nature Earthquake struck Country's Northern regions due to which many bridges were damaged. It is imperative to increase their strength and soundness which can be accomplished through the use of Carbon Fiber Reinforced Polymers (CFRP) retrofitting. High-strength concrete (HSC) is now often used in bridge construction. The behaviour of HSC before and after retrofitting is the focus of this study. Quasi static cyclic loadings (QSCT) with axial load is applied to scaled down (1:4) RC bridge piers under various drift levels in an experimental research. Carbon fibre reinforced polymer (CFRP) sheets were applied to the scaled-down pier models. The Energy Dissipation capability of retrofitted bridge piers was increased as a result of the exterior confinement by CFRP sheets which also improved the vulnerability/failure zones of the structures. The modified model was able to carry higher loading than the original or un-retrofitted model. Based on the findings of this study, it is expected that following retrofitting, these bridges will be able to withstand significantly larger weights, as required by the new Building Code.

KEYWORDS: CFRP, Energy dissipation, Quasi-static cyclic Loading (QSCT), Retrofitting

1 INTRODUCTION

The jugular vein of the transportation system is the bridge. Bridges are most vulnerable to damages after an earthquake, resulting in halting of the entire transportation network of the affected area. The majority of bridges built in Pakistan were not structurally designed to meet current seismic requirements. Following the earthquake in Pakistan on 8 October 2005, seismic zoning were changed, resulting in new Building Code of Pakistan BCP-2007. Four low strength concrete (LSC) pier column models (1800 & 2400 Psi) scaled at 1:4 were subjected to QSCT. It was concluded that energy dissipation capacity of 1800 & 2400 Psi columns is almost same. Thus strength of concrete in this range does not affect the total energy absorption[1].

The columns which were damaged during the experimentation under reference [1] were retrofitted and also further models were casted and retrofitted in undamaged state to examine the effects of retrofitting on Energy Dissipation capability of LSC (1800 Psi & 2400 Psi) RC piers.

1st International Conference on Advances in Civil & Environmental Engineering, University of Engineering & Technology Taxila, Pakistan

Conference date 22 &23 Feb 2022

Comparison indicated that Energy Dissipation capability of Damaged but retrofitted models was enhanced along with their strength and ductility to withstand even larger potential earthquakes[2]. A study was conducted on strengthening RC columns with a longitudinal CFRP sheet anchored to the column base. Results concluded that the use of a CFRP sheet improved both the effective stiffness and the lateral strength of the RC columns [3]. The behaviour of Non-Ductile slender reinforced concrete columns retrofitted with CFRP subjected to cyclic loading revealed significant improvement in terms of displacement ductility, load level, energy dissipation and failure mechanism[4]. Experimental work was conducted to evaluate the effectiveness of application of CFRP sheets to retrofit beams columns non-ductile joints. The Energy Dissipation capability and number of cycles were increased. Applying two layers of CFRP sheets seemed less effective than one layer[5].

Previously, LSC was used to construct bridges in accordance with the old design code, which has performed poorly and their strength and ductility was not sufficient. There is an unrelenting need to reinforce existing bridge piers. The purpose of this study is to examine and calculate the Energy Dissipation capacity of HSC bridge piers after they have been wrapped with CFRP. The performance of bridge piers composed of LSC (1800 & 2400 Psi) and HSC (6192 Psi) in terms of Energy Dissipation capability is also compared in this study. References [4] and [5] show that research on LSC has already been done. Test results of both studies are compiled for comparison with the test findings of the current study. The results show a considerable increase in Energy Dissipation capability in HSC models, which is discussed in detail in section 3 of this study.

2   EXPERIMENTAL SETUP

The test was held at the Earthquake Engineering Center (EEC) of the Department of Civil Engineering at UET Peshawar. The Following tests were performed on the Models:
i)   Quasi-Static Cyclic loading tests (QSCT)   ii) Compressive strength tests

The research comprises of QSC testing of Six (6) bridge pier models. RC Piers are scaled down to 1:4 scale having concrete strength of 6.192 ksi. CFRP HEX 103-C is used for retrofitting with a fabric thickness of 1.016 mm, tensile strength of 153 ksi and tensile modulus of 9400 ksi. Steel with a yield strength of 83 ksi & modulus of elasticity 29000 ksi. The whole pier model assembly is loaded with a physical load of 42.4 kips. The models which are subjected to QSCT include two models in each of the category i-e. Control Models (CM), Damaged retrofitted columns (DRM) and Undamaged retrofitted columns (UDRM). The model testing was carried out according to the following plan:

a) Two test models of high-strength concrete (6192 psi) were casted and both were subjected to QSCT without any retrofitting up to failure referred as Control Models (CM).

b) These two damaged models were rehabilitated using crack filling & CFRP retrofitting. One model was retrofitted with a single layer of CFRP and named as Damaged Retrofitted Model – Single Layer (DRM-SL) whereas the other model was retrofitted with a double layer of CFRP

1st International Conference on Advances in Civil & Environmental Engineering, University of Engineering & Technology Taxila, Pakistan

Conference date 22 &23 Feb 2022

and named as Damaged Retrofitted Model –Double Layer (DRM-DL). QSCT was applied to these two units until they failed.

c) Two other models of HSC (6192 psi) were casted and retrofitted in their undamaged state before being exposed to QSCT. One model was retrofitted with a single layer of CFRP (UDRM-SL) while the other model was retrofitted with double layer of CFRP (UDRM-DL). Also, HSC (6192 psi) Cylinders were prepared and compressive strength was tested.

e) QSCT was carried out at various drift levels, ranging from 0% to 4% and up to 5% in some situations. The cause for the 5% drift in a few cases was due to either failure requirements specified for the models or safety concerns of the Lab equipment. Subsequent to QSCT, the following steps were taken:

➢ The data from the data logger was reorganised in IGOR Pro's spread sheets. Figures 5, 6 & 7 show the hysteresis curves that were created for each drift level separately. All of the models have hysteresis curves as a result of QSCT for lateral load with changes in drift levels. From these hysteresis curves, Energy dissipation as calculated using area under the Curve method.

Fig.1 Loading Mechanism   Fig.2 Damaged Pier   Fig. 3 Prepared Surface   Fig. 4 CFRP Application

3   DISCUSSION ON EXPERIMENTAL RESULTS

The data acquired from the experimental results by the data logger was analysed by using IGOR Pro in which data is arranged in the form of sheets. A total of 6 Pier models were tested. Every model was subjected to QSCL. These graphs depict the Energy dissipated by the models. When these graphs are combined, they form a hysteresis curve as shown in Figure 4, 5 & 6. The areas under these curves were calculated and energy dissipation curves were made from these values. The energy dissipation curves for Control Models, Damaged Retrofitted Models and Undamaged Retrofitted Models of Low strength concrete (1.8 & 2.4 ksi) obtained from doctoral research of Ali S. M. (2009) and M. Iqbal (2012) under reference [1] and [2] were compared with corresponding models of High Strength Concrete i-e. 6.192 ksi.
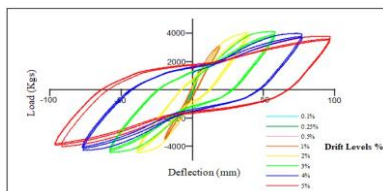
Fig. 5 Hysteresis Curves – CM 6.192 ksi   Fig. 6 Hysteresis Curves - DRM 6.192 ksi   Fig. 7 Hysteresis Curves - UDRM 6.192 ksi
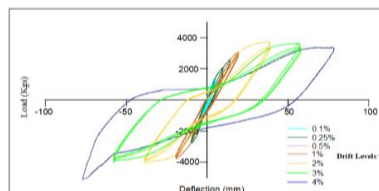
1st International Conference on Advances in Civil & Environmental Engineering, University of Engineering & Technology Taxila, Pakistan

Conference date 22 &23 Feb 2022
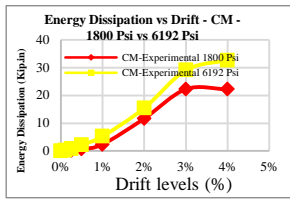
Fig. 8 CM 1.8 vs 6.192 ksi
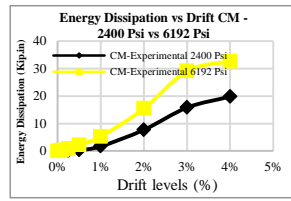
Fig. 9 CM 2.4 vs 6.192 ksi
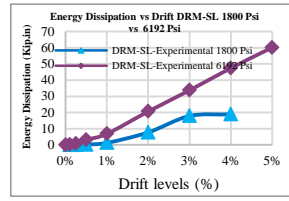
Fig. 10 DRM-SL 1.8 vs 6.192 ksi
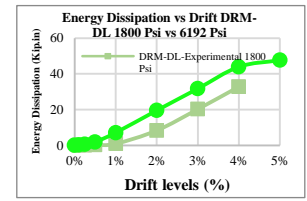
Fig. 11 DRM-DL 1.8 vs 6.192 ksi
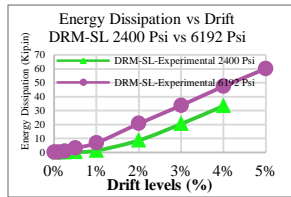
Fig. 12 DRM-SL 2.4 vs 6.192 ksi
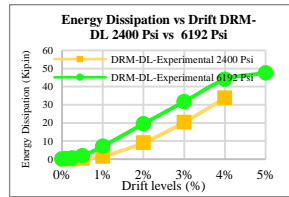
Fig. 13 DRM-SL 2.4 vs 6.192 ksi
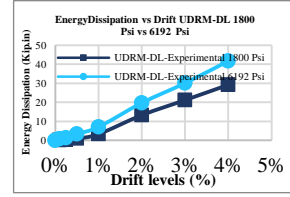
Fig. 14 UDRM-SL 1.8 vs 6.192 ksi
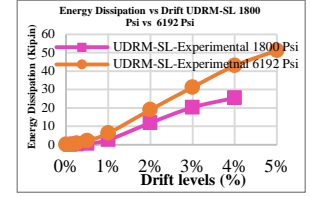
Fig. 15 UDRM-SL 1.8 vs 6.192 ksi
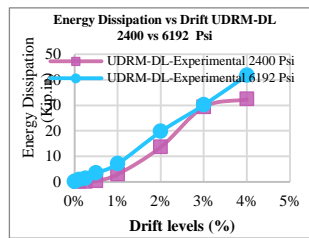
Fig. 16 UDRM-DL 2.4 vs 6.192 ksi
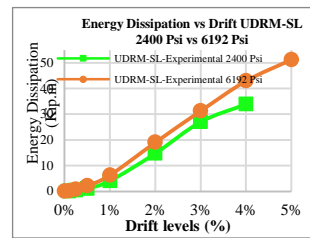
Fig. 17 UDRM-SL 2.4 vs 6.192 ksi

COMPARISON BETWEEN CONTROL, DAMAGED AND UNDAMAGED MODELS OF HSC 6192 Psi			
Model Type	Model Nomenclature	Energy Dissipation (Kip. In)	Percentage Increase
Damaged Models	CM-6192	85.5258	31.68%
	DRM-SL 6192	112.6180	
	CM-6192	85.5258	22.70%
	DRM-DL 6192	104.9360	
Undamaged Models	CM-6192	85.5258	19.59%
	UDRM-SL 6192	102.2828	
	CM-6192	85.5258	21.61%
	UDRM-DL 6192	104.0117	

COMPARISON BETWEEN CONTROL MODELS OF HSC 6192 Psi & LSC 1800 & 2400 Psi			
Model Type	Model Nomenclature	Energy Dissipation (Kip. In)	Percentage Increase
Control Models	CM-1800 Psi	59.7150	43.22%
	CM-6192	85.5258	
	CM - 2400 Psi	53.8000	58.97%
	CM-6192	85.5258	

COMPARISON BETWEEN CONTROL MODELS OF HSC 6192 Psi & LSC 1800 & 2400 Psi			
Model Type	Model Nomenclature	Energy Dissipation (Kip. In)	Percentage Increase
Control Models	CM-1800 Psi	59.7150	43.22%
	CM-6192	85.5258	
	CM - 2400 Psi	53.8000	58.97%
	CM-6192	85.5258	

COMPARISON BETWEEN DAMAGED RETROFITTED MODELS - SINGLE LAYER CFRP OF HSC 6192 Psi & LSC 1800 & 2400 Psi			
Model Type	Model Nomenclature	Energy Dissipation (Kip. In)	Percentage Increase
DRM-SL	DRM-SL 1800 Psi	55.4096	103.25%
	DRM-SL 6192 Psi	112.6180	
	DRM-SL 2400 Psi	64.0110	75.94%
	DRM-SL 6192 Psi	112.6180	

COMPARISON BETWEEN DAMAGED RETROFITTED MODELS - DOUBLE LAYER CFRP OF HSC 6192 Psi & LSC 1800 & 2400 Psi			
Model Type	Model Nomenclature	Energy Dissipation (Kip. In)	Percentage Increase
DRM-DL	DRM-DL 1800 Psi	62.4800	67.95%
	DRM-DL 6192 Psi	104.9360	
	DRM-DL 2400 Psi	65.0800	61.24%
	DRM-DL 6192 Psi	104.9360	

COMPARISON BETWEEN UNDAMAGED RETROFITTED MODELS - SINGLE LAYER CFRP OF HSC 6192 Psi & LSC 1800 & 2400 Psi			
Model Type	Model Nomenclature	Energy Dissipation (Kip. In)	Percentage Increase
UDRM-SL	UDRM-SL 1800 Psi	74.9416	36.48%
	UDRM-SL 6192 Psi	102.2828	
	UDRM-SL 2400 Psi	81.0805	26.15%
	UDRM-SL 6192 Psi	102.2828	

COMPARISON BETWEEN UNDAMAGED RETROFITTED MODELS - SINGLE LAYER CFRP OF HSC 6192 Psi & LSC 1800 & 2400 Psi			
Model Type	Model Nomenclature	Energy Dissipation (Kip. In)	Percentage Increase
UDRM-DL	UDRM-DL 1800 Psi	79.6007	30.67%
	UDRM-DL 6192 Psi	104.0117	
	UDRM-DL 2400 Psi	91.6367	13.50%
	UDRM-DL 6192 Psi	104.0117	

Fig. 18 Percentage increase in Energy Dissipation of CM, DRMs & UDRMs (1.8, 2.4 & 6.192 ksi)

1st International Conference on Advances in Civil & Environmental Engineering, University of Engineering & Technology Taxila, Pakistan

Conference date 22 &23 Feb 2022

The figures above (8 to 17) represent the behaviour of Energy Dissipation Capacity of Control Models (CM), Damaged retrofitted columns (DRM) and Undamaged retrofitted columns (UDRM) in a graphical comparison between the HSC models (6.192 Ksi) & LSC models (1.8 & 2.4 ksi). It is obvious from these figures that by increasing the strength of concrete, significant increases in Energy Dissipation capacity are observed.

4 CONCLUSION

The tabulated results in Fig. 18 clearly show that there is a significant increase in Energy Dissipation capability of the HSC models as compared to the LSC models as well as in the Energy Dissipation capability of the HSC retrofitted models as compared to the HSC unretrofitted/control models. The existing bridges made of High strength concrete after revision of Building code need structural improvements in order to comply with the safe provisions of revised building code. The existing bridge piers when retrofitted with CFRP will show a considerable increase in Energy Dissipation capability as it is evident from the results of this research. Hence, it is recommended that the existing bridge piers of HSC be retrofitted with Single or Double layer of CFRP to meet the present codal requirements instead of demolishing a whole bridge. This will increase its Energy Dissipation capability and also it will fulfill the criteria of revised building codes provisions.

5 ACKNOWLEDGMENT

6 REFERENCES

1. ALI, S.M., *Study of energy dissipation capacity of RC bridge columns under seismic demand*. 2009, University of Engineering and Technology, Peshawar, Pakistan.
2. Tahir, M.F., A. Ahmad, and M. Iqbal, *Seismic evaluation of repaired and retrofitted circular bridge piers of low-strength concrete.* Arabian Journal for Science and Engineering, 2015. **40**(11): p. 3057-3066.
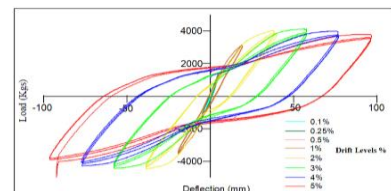3. del Rey Castillo, E., J. Ingham, and M. Griffith. *Seismic strengthening of RC columns with straight FRP anchors*. in *Proceedings of the 13th conference on Fiber Reinforced Polymers in Reinforced Concrete Structures (FRPRCS-13), American Concrete Institute (ACI), Anaheim, California, USA*. 2017.
4. Aules, W.A., *Behavior of Non-Ductile Slender Reinforced Concrete Columns Retrofit by CFRP Under Cyclic Loading*. 2019, Portland State University.
5. Zerkane, A.S., Y.M. Saeed, and F.N. Rad, *Cyclic loading behavior of CFRP-wrapped non-ductile beam-column joints.* Special Publication, 2019. **331**: p. 34-54.

1st International Conference on Advances in Civil & Environmental Engineering, University of Engineering & Technology Taxila, Pakistan

Conference date 22 &23 Feb 2022

RECYCLING PAPER WASTE INTO PLASTER COMPOSITE MIXTURE

Minahil Fatima, Ayesha Ejaz, Gulshan sikandar

University of Engineering & Technology Taxila, Pakistan

17-ENV-17@students.uettaxila.edu.pk ; 17-ENV-42@students.uettaxila.edu.pk ; 17-ENV-71@students.uettaxila.edu.pk

Engr. Babar Abbas

University of Engineering & Technology Taxila, Pakistan
babar.abbas@uettaxila.edu.pk

ABSTRACT

The sole purpose of this study is to recycle the paper wastes into plaster mortar that can be used for construction purposes, decoration pieces. The waste paper was collected from the block of an institution UET Taxila**.** Waste generation of the waste paper was calculated the paper waste was then characterized and the components present in the block was mainly A4 paper. This waste paper was generally collected to make plaster mortar. This was done by different methods that includes the mixing of cement, sand and waste paper by hand mixing and hand shredding, and machine mixing and machine shredding. Different blocks was formed by both methods and tests were performed that shows machine mixing and machine shredding method is better than manual shredding and mixing. The compressive strength of the waste paper plaster mortar was greater than that of the conventional mortar. Along with that, waste paper plaster mortar proves to be more cost efficient too.

KEYWORDS: Paper waste, recycling need, waste management, plaster mortar by paper wastes, conventional plaster mortar.

1. INTRODUCTION

Waste is defined as any product that is left over and have no value to the owner. (Alam & Ahmade, 2013; Sasikumar & Krishna, 2009). Solid waste is generated from different sources like industries, residential activities, institutes, commercial activities. (Jerry, 2015). Most common diseases that arise from improper   dumped solid waste are; Cancer, Congenital malformations, Neurological disease, Nausea and vomiting and Fever. (Alam & Ahmade, 2013). As the population is increasing

1st International Conference on Advances in Civil & Environmental Engineering, University of Engineering & Technology Taxila, Pakistan

Conference date 22 &23 Feb 2022

day by day so demand for the construction of building is also increasing and due to this reason severe shortage in the materials for the buildings is occurring regionally. That's why the conversion of solid waste to the materials that is useful for construction and buildings is challenge for civil engineers. Bricks made of paper fibers agglomerated with cement are an inexpensive material, with good thermal insulating properties, with remarkable resistance, produced through the recovery of paper waste. The technology for the manufacture of the material is non-polluting and does not involve high energy consumption. One of the recipes for obtaining this material consists of a mixture of: 60% paper. (Byström & Lönnstedt, 1997)

2. METHODOLGY

In the first step, paper waste was collected from the block of Ibn-e-Sina in UET Taxila. Then characterization of this waste in A4 paper, cardboard and newspaper. After following the required procedure, we made the plaster mortars. At the end, we performed the tests, for determining the strength of this mortar and compared it with the original mortar.

Waste paper Generation Rate

Waste paper (A4, Newspaper, cardboard) collection

Study the fundamental Mortar Making

Identify mortar

Manual, Machine Mortar making

Testing

Results

3. TABLES AND FIGURES

1st International Conference on Advances in Civil & Environmental Engineering, University of Engineering & Technology Taxila, Pakistan

Conference date 22 &23 Feb 2022
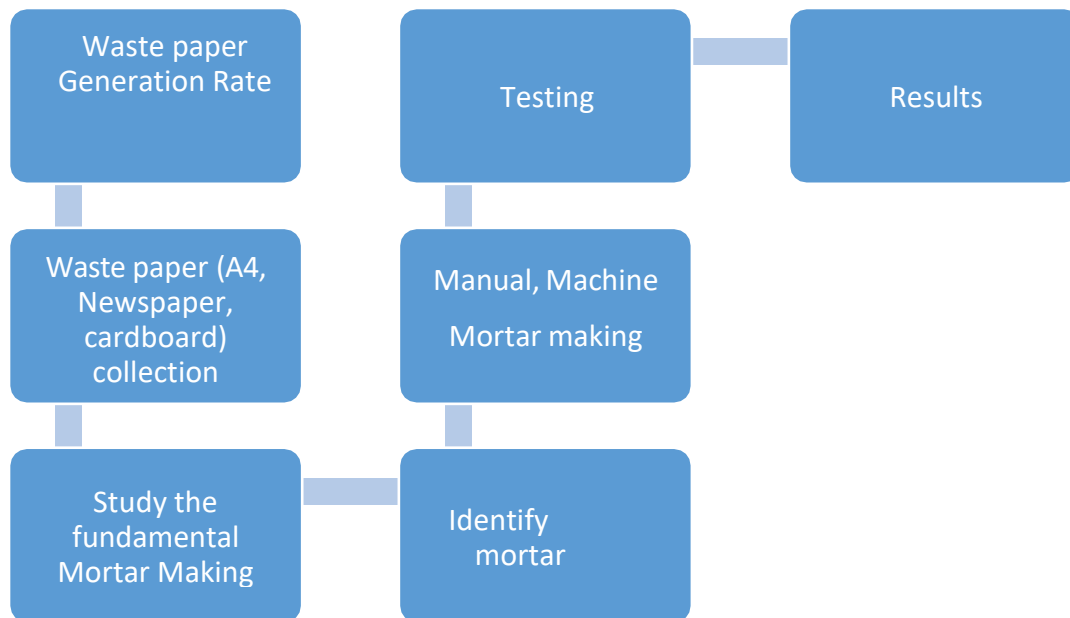
3.1. Shredding and mixing by hand

Table 1: Result for Compressive Strength of mold prepared

by shredding and mixing by hands

After 7 day				
Sample dimension 70mm x 70mm				
Sample 1	A1	A2	Average	Pressure $PSi = \dfrac{224.82}{Area} \times KN$
1	13	14	13.5	401.33
After 14 days				
Sample dimension 70mm x 70mm				
Sample 2	A3	A4	Average	Pressure $PSi = \dfrac{224.82}{Area} \times KN$
2	18	21	19.5	579.89
After 21 days				
Sample dimension 70mm x 70mm				
Sample 3	A5	A6	Average	Pressure $PSi = \dfrac{224.82}{Area} \times KN$
3	21	24	22.5	669.10
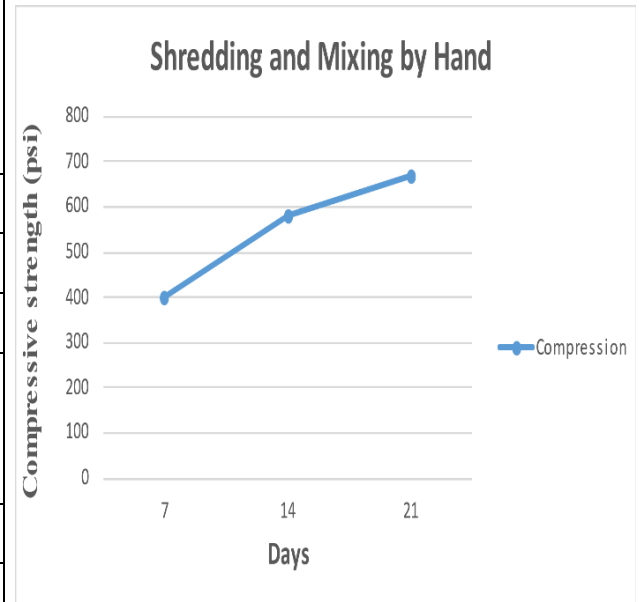
Figure 1 Graph for plaster mortar by shredding by hand and mixing by machine

1st International Conference on Advances in Civil & Environmental Engineering, University of Engineering & Technology Taxila, Pakistan

Conference date 22 &23 Feb 2022

3.2. Shredding by machine and mixing by hand

Table 2: Result for Compressive Strength of molds Prepared by

Shredding by machine and mixing by hands

After 7 days				
Sample dimension 4inch x 4 inch				
Sample 1	H1	H2	Average	$PSi = \dfrac{Pressure}{Area} \times KN$ (with 224.82)
1	63	70	66.5	934.40
After 14 days				
Sample dimension 70mm x 70mm				
Sample 2	H3	H4	Average	$PSi = \dfrac{Pressure}{Area} \times KN$ (with 224.82)
2	88	85	86.5	1215.43
After 21 days				
Sample dimension 70mm x 70mm				
Sample 3	H5	H6	Average	$PSi = \dfrac{Pressure}{Area} \times KN$ (with 224.82)
3	88	90	89	1250.56
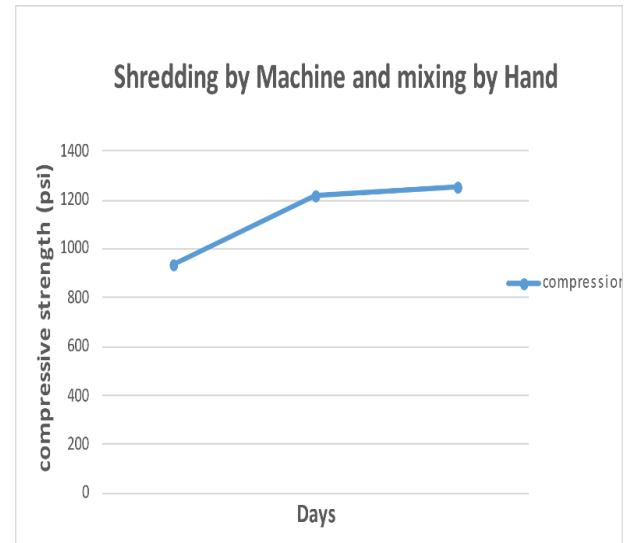
Figure 2:Graph for plaster mortar by shredding by machine and mixing by hand

1st International Conference on Advances in Civil & Environmental Engineering, University of Engineering & Technology Taxila, Pakistan

Conference date 22 &23 Feb 2022

4. CONCLUSION

It has been witnessed that using paper waste into making plaster mortar is not only useful for the environment by helping to reduce the pollution, but is also cost effective and light weight. The prepared plaster mortar is then undergrown different tests, to ensure its properties Based on the results, the paper fibers had a significant effect on the mechanical and physical properties of the compounds as the paper fiber content increased and the water absorption increased significantly. Measurements of mechanical strength obtained in compressive strength and flexural strength tests have revealed that paper mud sludge add-on mortars have potential for application in building construction. In cold regions plaster mortar containing paper waste is much beneficial because paper contain fiber and that is good for heating the buildings. Another comparison is among the shredding of paper waste. So, the use of paper waste in making plaster mortar is beneficial in many aspects so its use should be encouraged as it saves environment too by utilizing the paper waste.

REFERENCES

1. Aciu, C., Ilutiu-Varvara, D., Cobirzan, N., & Balog, A. (2014). Recycling of paper waste in the composition of plastering mortars. *Procedia Technology, 12*, 295-300.

2. Agulló, L., Aguado, A., & Garcia, T. (2006). Study of the use of paper manufacturing waste in plaster composite mixtures. *Building and environment, 41*(6), 821-827.

3. Ahmadi, B., & Al-Khaja, W. (2001). Utilization of paper waste sludge in the building construction industry. *Resources, conservation and recycling, 32*(2), 105-113.

4. Alam, P., & Ahmade, K. (2013). Impact of solid waste on health and the environment. *International Journal of Sustainable Development and Green Economics (IJSDGE), 2*(1), 165-168.

Compressive Behavior of Natural Fiber Rope Confined RC Circular Columns

Wajahat Ali, Shahzad Saleem
Department of Civil Engineering
University of Engineering & Technology Taxila, Pakistan
engr.wajahat@hotmail.com; shahzad.saleem@uettaxila.edu.pk

ABSTRACT

The strength and deformation capacity of old reinforced concrete (RC) columns can be improved significantly by using the external confinement of suitable materials. Most of the fiber reinforced polymers (FRPs) used for this purpose are costly, synthetic in nature, and usually imported from abroad. By using the locally available natural materials that are more environmentally friendly, the self-reliance of developing countries like Pakistan can be increased. The focus of this study is on the compressive behavior of natural fiber rope (NFR) confined circular RC columns in which differently spaced transverse steel reinforcement is used. The columns were subjected to compressive load, gradually increasing up to failure. A total of 12 specimens were tested. The parameters considered were transverse steel reinforcement spacing and number of NFR layers. The results show a bi-linear stress-strain response of confined specimens in which the post-peak strength and deformation were increased with an increase in number of NFR layers or with a decrease in spacing of stirrups. All confined specimen exhibited high axial deformation compared to the control specimens.

KEYWORDS: Circular, Compression, Concrete, Stress-strain response, Rope confinement.

1 INTRODUCTION

To rehabilitate reinforced concrete (RC) structures, there is an increasing amount of work on strengthening methods [1]. During the recent two decades, a significant amount of research has been done on the use of various fibre reinforced polymers (FRPs) to enhance the ductility and strength of poorly detailed RC column [2]. To strengthen the concrete structures by FRP composites is very demanding and popular [3]. The FRPs displays two main roles. First, it increases strength and ductility of RC columns, and the other is it restrain the buckling of main longitudinal rebars [4].

In developing countries, it is advantageous to use local available materials to strengthen the RC structures. The ability of a natural fibre ropes (NFR) to restrain longitudinal rebars in column from buckling, depends on their stiffness [5]. The Cotton and Nylon ropes possess high deformability. These fibre ropes (NFR) provide a uniform confinement to concrete core under concentric axial compression. By using the locally available natural materials that are more environmentally friendly, the self-reliance of developing countries like Pakistan can be increased.

1st International Conference on Advances in Civil & Environmental Engineering, University of Engineering & Technology Taxila, Pakistan

Conference date 22 &23 Feb 2022

The focus of this study is on the compressive behaviour of natural fibre rope (NFR) confined circular RC columns in which differently spaced transverse steel reinforcement is used.

2   EXPERIMENTAL PROGRAMME

A total of 12 RC specimens were prepared. All specimens were circular in cross section. For each column, two similar samples were prepared. The variables considered were the number of NFR layers and spacing of lateral confining reinforcement. The height and diameter of specimen are kept 300 and 150 mm, respectively. The steel cages were prepared and put inside the steel moulds by maintaining the cover distance. Concrete mix proportion was kept same for all batches. For 28 days, the specimens were cured in water. The specimen's details are given in Table 1.

2.1   NFR Wrapping

After curing for 28 days, a coat of two-part epoxy was applied on the surface of RC column specimen. The NFR were chosen having approximately 3 mm diameter. Cotton and Nylon ropes were confined around specimens carefully soon after application of epoxy. It strengthened the bond between the NFR and RC column surface. For two layered specimens, epoxy was also applied on surface of specimens after each layer of confinement. To avoid failure at top and bottom, specimens were confined with extra layers of NFR over the 25 mm width at top and bottom of each specimen. The top surface of specimens was capped with high strength gypsum for uniform loading.

2.2   Materials Properties

The specimens were prepared in two batches. The target compressive strength of concrete was 20 MPA for all specimens. The maximum size of coarse aggregates was kept less than 20mm.

Table 1: Detail of Test Matrix

Serial.	Specimen Label	Confining Material	No. of Layers	No. of specimens
I.	CL_O	-	-	2
II.	CCL1	COTTON	1	2
III.	CCL2	COTTON	2	2
IV.	CNL1	NYLON	1	2
V.	CNL2	NYLON	2	2

2.3   Test Setup

For this experimental study, all the RC column specimens were tested to failure under compression with the help of a universal testing machine (UTM) of 5000 kN capacity. Due to lack of instrumentation, only axial deformation was recorded using linear variable differential transducers

1st International Conference on Advances in Civil & Environmental Engineering, University of Engineering & Technology Taxila, Pakistan

Conference date 22 &23 Feb 2022

(LVDT). The specimens were tested under deformation control until final rupture of NFR occurred.

3   TEST RESULTS

The test results showed a bi-linear stress–strain response of confined specimen in which the post-peak strength and deformation capacity was increased with an increase in number of NFR layers. All confined specimens exhibited high axial deformation compared to control specimen, as shown in Figure 1. The buckling behavior of longitudinal reinforcement was also influenced with the number of layers. After reaching maximum axial stress, a small drop in strength was observed which shows strength softening. The curve then showed a relative stable line for specimens confined with cotton ropes, whereas in nylon rope confined specimens, the curve ascended again until failure. Nylon rope confined specimen showed a large deformation (strain) before its final rupture as compared to cotton rope confined specimen.

3.1   Effects of NFR Layers

The stress-strain curve for both nylon and cotton NFR is shown in Figure 1. It is to be noted that the stress in this figure is normalized with respect to control specimens. The specimen confined with single and double layers showed ductile behavior after the peak load as compared to unconfined RC specimens. With an increase in number of NFR layers, the strength and deformation capacity of RC columns also increased. Similarly, the axial strain capacity of NFR confined RC column enhanced with NFR layers for both cotton and nylon ropes, as shown in Figure 1.

| (a) | (b) |
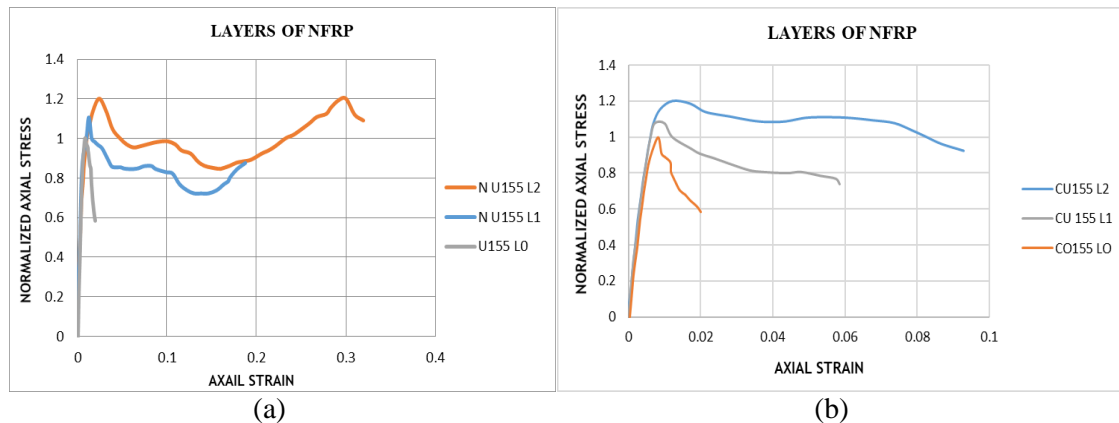
Figure 1: Effect of NFR Layers on stress-strain response (a) nylon ropes (b) cotton ropes

A comparison between Nylon and Cotton ropes (NFR) confined specimens is shown in Figure 2. The Nylon rope confined specimen showed a better ductile behavior before its final rupture. The

1st International Conference on Advances in Civil & Environmental Engineering, University of Engineering & Technology Taxila, Pakistan

Conference date 22 &23 Feb 2022

axial strain of nylon rope confined specimen is much better than that of cotton rope confined specimen.
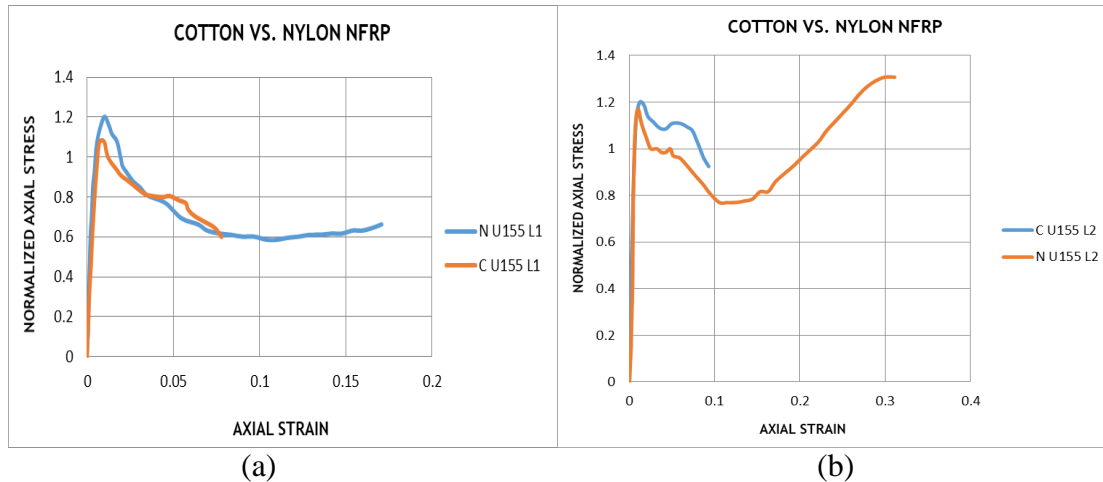
Figure 2: Stress-Strain curves for cotton vs. nylon ropes (a) single layer (2) double layer

3.2 Failure Mode

The failure modes of the NFR confined RC circular column are shown in Figures 3. All the specimens failed by tensile rupture of NFR (nylon and cotton ropes). The tensile rupture of cotton and nylon ropes are approximately at the center of specimen. The failure was very distinguished for both single- and double-layer epoxy bonded Cotton and nylon ropes (NFR). Higher axial deformation can be clearly seen for nylon confined specimens.

Figure 3: Typical failure mode of 1- & 2-layer NFRP confined specimens.

1st International Conference on Advances in Civil & Environmental Engineering, University of Engineering & Technology Taxila, Pakistan

Conference date 22 &23 Feb 2022

4   CONCLUSIONS

This paper presents test results to observe the compressive response of RC column specimens confined by epoxy bonded Cotton and Nylon ropes (NFR). Based on the results, the following conclusions can be summarized:

1. Epoxy bonded cotton and nylon ropes (NFR) were highly effective in increasing the compressive strength and deformation of RC circular column specimens.

2. Stress –strain behavior of NFR confined RC circular column can be defined with two linear parts in which the slope of lines improves as the number of NFR layers increases.

3. Nylon ropes confined specimen showed higher deformation as compared to cotton rope confined specimens.

5   REFERENCES

[1]   S. Suon, S. Saleem, and A. Pimanmas, "Compressive behavior of circular concrete columns confined by basalt fiber reinforced polymer (BFRP)," *Key Eng. Mater.*, vol. 765 KEM, pp. 355–360, 2018, doi: 10.4028/www.scientific.net/KEM.765.355.

[2]   S. Saleem, Q. Hussain, and A. Pimanmas, "Compressive Behavior of PET FRP–Confined Circular, Square, and Rectangular Concrete Columns," *J. Compos. Constr.*, vol. 21, no. 3, p. 04016097, 2017, doi: 10.1061/(asce)cc.1943-5614.0000754.

[3]   M. W. Khan, M. Hamza, I. Khader, and S. Saleem, "AXIAL BEHAVIOR OF NON-BONDED

[4]   Y. L. Bai, J. G. Dai, and J. G. Teng, "Buckling of steel reinforcing bars in FRP-confined RC columns: An experimental study," *Constr. Build. Mater.*, vol. 140, pp. 403–415, 2017, doi: 10.1016/j.conbuildmat.2017.02.149.

[5]   Y.-L. Bai, J.-G. Dai, and J.-G. Teng, "Monotonic Stress–Strain Behavior of Steel Rebars Embedded in FRP-Cnfined Concrete Including Buckling," *J. Compos. Constr.*, vol. 21, no. 5, p. 04017043, 2017, doi: 10.1061/(asce)cc.1943-5614.0000823.

1st International Conference on Advances in Civil & Environmental Engineering, University of Engineering & Technology Taxila, Pakistan

Conference date 22 &23 Feb 2022

Economization of Stiffeners Considering Near- Fault Ground Motion Effects on Confined Brick Masonry Structures

Sami Ullah, Iqbal Ahmad, Majid Ali

Department of Civil Engineering

Capital University of Science and Technology, Islamabad, Pakistan

samiullahktk426@gmail.com; ahmad.ce9@gmail.com; professor.drmajid@gmail.com

ABSTRACT

Confined brick masonry structures (masonry walls without reinforcement and confined with horizontal and vertical lightly reinforced concrete elements) are preferred in earthquake prone regions due to their good performance against seismic loading. In a previous work, horizontal and vertical stiffeners are quantified using a diagonal approach with the help of static analysis for a typical house design. However, there is a need to check with the help of dynamic analysis whether it can be further economized or not. In this paper, the effects of near-fault ground motion on the seismic response of the same masonry structure are compared using nonlinear method. Inelastic time history analysis has been used to predict the seismic displacement demands of the studied building. It has been observed that near-fault earthquakes as per dynamic analysis are not as much severe as predicted by the static analysis. Therefore, the outcome of this study will help to further economize the horizontal and vertical stiffeners.

KEYWORDS: Confined brick masonry, earthquake, nonlinear, stiffeners.

1   INTRODUCTION

Masonry structures are mostly used in the world for residential purposes as it is economical as compared to other type of structures and still have historical buildings of masonry construction around the world [1]. The unreinforced masonry (URM) structures are vulnerable to failure in seismic zones as these structures do not have enough capability to resist lateral forces of the earthquake [2]. The masonry structures are basically the rigid skeleton of solid element which transmit the stresses through the structure and provide continuity to the structure [3]. In 2005 earthquake occurred in Kashmir, Pakistan, which completely paralyzed Pakistan and known is the deadliest earthquake. In this earthquake a lot of economic and human losses occurred due to the failure of unreinforced brick masonry construction and non-engineering practices which caused collapse of the structures [4].

The URM construction failed due to its incapability to resist the lateral loads due to earthquake. These structures later confined by French structural engineer Paul Cottancin by proposing reinforced concrete stiffeners vertical as well as horizontal which improved its resistance against lateral loading [5]. The confined masonry (CM) structures are the structures in which reinforced concrete vertical stiffeners or tie-columns are construction at all the columns and connect with reinforced concrete horizontal stiffeners or bond beam to avoid the disintegration of the masonry walls and increase the ductility of the structure [6]. The CM construction now used in the world

1st International Conference on Advances in Civil & Environmental Engineering, University of Engineering & Technology Taxila, Pakistan

Conference date 22 &23 Feb 2022

for low rise building in which the masonry walls are constructed before casting of reinforced concrete vertical and horizontal stiffeners [7].

In this paper a confined brick masonry two storey building including mumty is selected for seismic zone 4 with soil profile type SD. Nonlinear dynamic/time-history analysis is performed for near-fault ground motion records to determine the seismic demand of the structure. These analysis results will help in designing the buildings in seismic zone 4 where severe earthquakes occurred and badly effect the buildings which ultimately causes economic and human lives losses. This analysis also helps in making the construction work economical so that the structure should not be under-designed or over-designed.

2   CONCEPT OF CONFINED BRICK MASONRY CONSTRUCTION

Confined brick masonry structure is basically the structure/building with reinforced concrete vertical and horizontal stiffeners in which tie-columns is mostly provided at the corners or intersection of the walls as well as around the opening and the reinforcement provided upon the height and size of the building [8]. The CM buildings can be seen throughout the world constructing now a days due to its enhancement in seismic performance of the masonry buildings by incorporating reinforced concrete stiffeners [9]. As the reinforced concrete vertical and horizontal stiffeners/ties provided at the corner of the building and walls intersection as well as around the opening were found most effective technique for strengthen the masonry buildings [10]. In confined brick masonry construction, the masonry walls are constructed first then the reinforced concrete vertical and horizontal stiffeners are constructed and the stiffeners are properly connected [11]. The confinement elements of the building like reinforced concrete vertical and horizontal stiffeners not only enhance the strength of the building but also increase the ductility of the structures which helps in resisting the lateral load due to earthquakes [12]. The confined brick masonry construction consists of the foundation, plinth beam, masonry walls, vertical and horizontal reinforced concrete stiffeners, floor(s) and roof slabs [13].

3   SELECTION OF CASE STUDY STRUCTURE

A simple house is selected for modelling and analysis of the confined brick masonry structure. The ground floor framing plan of the selected house is shown in figure 1 with 25 reinforced concrete vertical stiffeners locations. The selection of these reinforced concrete vertical stiffener's is based on three categories. The red colour showing the most necessary locations of the stiffeners, the cyan colour showing second most important locations, while the green colour showing the third important locations for the stiffeners provision [5]. These locations for reinforced concrete vertical stiffeners are selected to properly hold the masonry walls and resist efficiently the lateral forces due to earthquake.

1st International Conference on Advances in Civil & Environmental Engineering, University of Engineering & Technology Taxila, Pakistan

Conference date 22 &23 Feb 2022
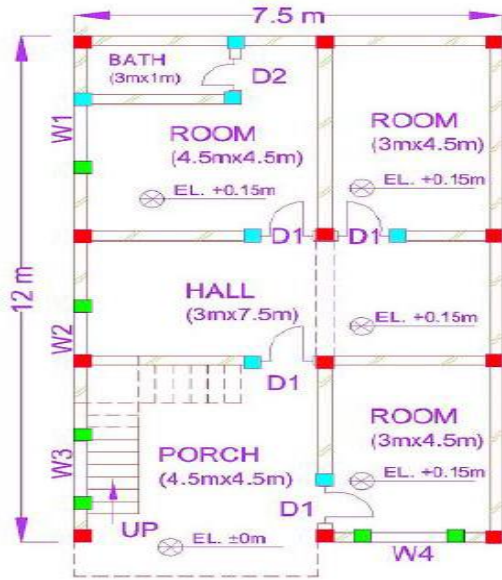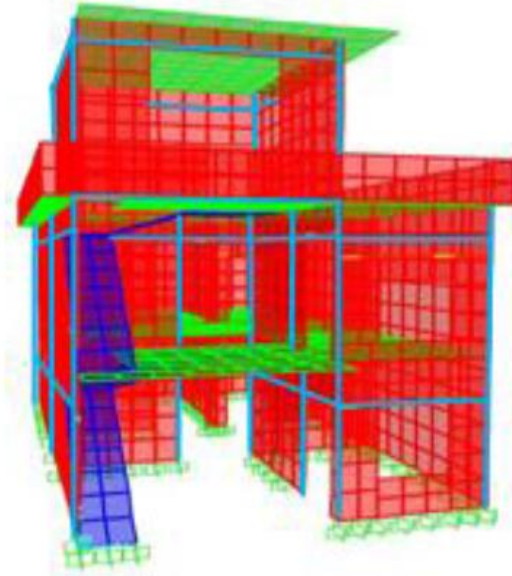
(a)   (b)

Figure 1: Selection of house (a) framing plan of the house (b) 3D view of the house

The house selected for the modelling and analysis with first and second most important locations of the reinforced concrete vertical stiffeners as shown with red and cyan colour while the green colour (third category) stiffeners are avoided to construct the economic structure. The sections selected for reinforced concrete vertical and horizontal stiffeners are shown in table 1 which include 4-φ13 longitudinal reinforcement for vertical stiffeners and φ6-90mm/180mm stirrups while 4-φ13 longitudinal reinforcement and φ6-100mm stirrups for horizontal stiffeners.

Table 1: Cross-section details of vertical and horizontal reinforced concrete stiffeners

Descriptions	Size	Fc' (MPa)	Longitudinal Reinforcement	Transverse/Stirrup Reinforcement
Vertical Stiffeners	230mm×230mm	20	4-φ13	φ6-90mm/180mm
Horizontal Stiffeners	230mm×150mm	20	4-φ13	φ6-100mm

4   NONLINEAR DYNAMIC ANALYSIS

The nonlinear dynamic analysis is performed on the model shown above in figure 1 which helps in to investigate the seismic demand of the confined brick masonry structure for vertical stiffeners at 19 location provided and sections of vertical and horizontal stiffeners used in construction as shown in table 1 for seismic zone 4 and soil profile type SD. The results obtained from the nonlinear time-history analysis with near fault ground motion records are shown in table 2 where seismic demand is shown in mm for ground, first floor and mumty of the house shown in figure 1.

1st International Conference on Advances in Civil & Environmental Engineering, University of Engineering & Technology Taxila, Pakistan

Conference date 22 &23 Feb 2022

Table 2: Seismic Demand of Confined Brick Masonry Structure

S. No	PEER Record No	Locations	Year	Magnitude M_w	Closest Distance (Km)	Demand x-axis (mm)	Demand y-axis (mm)
1	2114	Denali, Alaska	2002	7.9	2.74	22.3	6.61
2	1605	Duzce, Turkey	1999	7.14	6.58	22.23	8.47
3	159	Imperial Valley-06	1979	6.53	0.65	22.29	8.63
4	1141	Dinar, Turkey	1995	6.4	3.36	22.13	7.88

It can be seen from the above results that the seismic demand in x-axis is higher than the seismic demand in y-axis of the confined masonry structure. The seismic demand of the confined brick masonry structure is also less than the target displacement of the structure which is much higher than the seismic demand. Therefore, the vertical and horizontal reinforced concrete stiffeners proposed for confining brick masonry structures are sufficient to be used for seismic zone 4 and soil type SD of low-rise buildings.

5   CONCLUSION

The following conclusions have been drawn from the results of this research work:
1. The reinforced concrete vertical stiffeners should be provided at the corners of the walls and around opening where necessary.
2. The horizontal reinforced concrete stiffeners should be provided above the openings of the doors and windows.
3. The vertical and horizontal reinforced concrete will be better to use as proposed as its seismic demand is less than the target displacement for such high magnitude of near-fault ground motion records.

The confined brick masonry structure constructed with proposed section of reinforced concrete stiffeners gives better performance and the seismic demand is lower than expected from nonlinear time-history analysis for near fault ground motion records. The number of locations of reinforced concrete stiffeners selected is 19 instead of 12 and 31 to get the efficient strength of the structure and also to get economic structure to avoid over-strengthening of the structure. The confined brick masonry structure with vertical reinforced concrete stiffeners provided at corners or intersection of the walls and horizontal stiffeners above the opening can efficiently improve the behaviour of the masonry structure under seismic loading. These stiffeners basically improve the capacity of the masonry structure against lateral loadings as well as enhance the ductility of the structure but the loads of the structure are transferred by the masonry walls of the structure.

1st International Conference on Advances in Civil & Environmental Engineering, University of Engineering & Technology Taxila, Pakistan

Conference date 22 &23 Feb 2022

6   ACKNOWLEDGEMENTS

The authors would like to acknowledge all organizations/persons who have helped in this research.

REFERENCES

[1]   Y. Wu, S. Gu, G. Zhao, and S. Li, "Damage assessment of the in-service brick masonry structure using acoustic emission technique," *Mater. Struct. Constr.*, vol. 53, no. 2, 2020, doi: 10.1617/s11527-020-01475-y.

[2]   "Calvi Testing Masonry.Pdf." .

[3]   R. S. Olivito and P. Stumpo, "Fracture mechanics in the characterisation of brick masonry structures," *Mater. Struct. Constr.*, vol. 34, no. 4, pp. 217–223, 2001, doi: 10.1007/bf02480591.

[4]   K. Shahzada *et al.*, "Experimental seismic performance evaluation of unreinforced brick masonry buildings," *Earthq. Spectra*, vol. 28, no. 3, pp. 1269–1290, 2012, doi: 10.1193/1.4000073.

[5]   M. Khan and M. Ali, "Optimization of concrete stiffeners for confined brick masonry structures," *J. Build. Eng.*, vol. 32, no. February, p. 101689, 2020, doi: 10.1016/j.jobe.2020.101689.

[6]   M. Tomaževič and I. Klemenc, "Seismic behaviour of confined masonry walls," *Earthq. Eng. Struct. Dyn.*, vol. 26, no. 10, pp. 1059–1071, 1997, doi: 10.1002/(SICI)1096-9845(199710)26:10<1059::AID-EQE694>3.0.CO;2-M.

[7]   H. Okail, A. Abdelrahman, A. Abdelkhalik, and M. Metwaly, "Experimental and analytical investigation of the lateral load response of confined masonry walls," *HBRC J.*, vol. 12, no. 1, pp. 33–46, 2016, doi: 10.1016/j.hbrcj.2014.09.004.

[8]   M. Tomaževič and I. Klemenc, "Verification of seismic resistance of confined masonry buildings," *Earthq. Eng. Struct. Dyn.*, vol. 26, no. 10, pp. 1073–1088, 1997, doi: 10.1002/(SICI)1096-9845(199710)26:10<1073::AID-EQE695>3.0.CO;2-Z.

[9]   I. Koutromanos, A. Stavridis, P. B. Shing, and K. Willam, "Numerical modeling of masonry-infilled RC frames subjected to seismic loads," *Comput. Struct.*, vol. 89, no. 11–12, pp. 1026–1037, 2011, doi: 10.1016/j.compstruc.2011.01.006.

[10]   A. Chourasia, S. Singhal, and J. Parashar, "Experimental investigation of seismic strengthening technique for confined masonry buildings," *J. Build. Eng.*, vol. 25, no. June, p. 100834, 2019, doi: 10.1016/j.jobe.2019.100834.

[11]   A. Naseer, "Performance Behavior of Confined Brick Masonry Buildings under Seismic Demand," 2009.

[12]   A. Darbhanzi, M. S. Marefat, and M. Khanmohammadi, "Investigation of in-plane seismic retrofit of unreinforced masonry walls by means of vertical steel ties," *Constr. Build. Mater.*, vol. 52, pp. 122–129, 2014, doi: 10.1016/j.conbuildmat.2013.11.020.

[13]   R. Marques and P. B. Lourenço, "Unreinforced and confined masonry buildings in seismic regions: Validation of macro-element models and cost analysis," *Eng. Struct.*, vol. 64, pp. 52–67, 2014, doi: 10.1016/j.engstruct.2014.01.014.

Practical application of structural health monitoring in civil engineering structures: A review

Muhammad Sohaib, Qaiser-uz-Zaman Khan

University of Engineering & Technology Taxila, Pakistan

muhammad.sohaib2@students.uettaxila.edu.pk, dr.qaiser@uettaxila.edu.pk

Syed Saqib Mehboob

University of Engineering & Technology Taxila, Pakistan

syed.saqib@uettaxila.edu.pk

ABSTRACT

This study explores structural health monitoring (SHM) technique and damage valuation of civil engineering structures including buildings, bridges, and structural elements. From this approach, data acquisition methods and SHM sensors can monitor scaled models and real-life structures to predict the damage and to investigate the response of structures. This paper presents the implementation of different SHM systems (vibration-based methods, vision-based methods, and strain-based fiber optics) by deploying sensors (accelerometers, fiber optic sensors, and piezoelectric sensors) to examine the static and dynamic response of structures.

KEYWORDS: structural health monitoring; accelerometers; monitoring; frequency; sensors

1   INTRODUCTION

Structural Health Monitoring is a technology that is used to monitor the condition of structures while they are being built and while they are in use. Due to advances in the technology of sensors, the Structural Health Monitoring approach has been in constant modification for decades because numerous sensors give extensive information related to structural behavior [1]. The strength of structures reduces due to consistent loads and fatigue specially in the high seismic region so, there came a need for the monitoring system to be able to determine the structure's health status [2]. Considering safety and performance It is important to monitor the extent of deterioration and the location. There has been an evolution in the execution of the monitoring approach which includes vibration-based structural health monitoring to represent the dynamic response of structure including modal characteristics [3]. These modal parameters include frequency, damping ratio, and mode shapes. Structures are also subjected to static loading conditions and these parameters involve temperature, displacement, and strain.

2   LITERATURE REVIEW

2.1   Procedure of SHM

Bernagozzi et al. [4] used an output-only modal recognition technique for the identification of frequencies and mode shapes of a four-story frame of steel model structure under ambient shaking. Capozucca [5] used a vibration monitoring technique for assessing the dynamic response of reinforced concrete beams by considering three beams with different diameters and

1st International Conference on Advances in Civil & Environmental Engineering, University of Engineering & Technology Taxila, Pakistan

Conference date 22 &23 Feb 2022

using the fast Fourier Transform (FFT) technique to evaluate frequency. Chang et al. [6] proposed structural monitoring using artificial intelligence on single and many damaged columns in a seven-story building. They implemented stochastic subspace system identification to derive frequency and mode shapes. Khuc and Catbas [7] used regular cameras and computer vision techniques to get the displacement and structural vibrations. Park et al. and Pierdicca et al. [8-9] performed an ambient vibration test on under-construction the Lotte World Korea's tallest building and school building for one year respectively, to find the dynamic response of a structure. Barsocchi et al. [10] used automated modal identification on Matilde Tower in Livorno (Italy) by using sensors of low cost and an improved grid of sensors to detect the tower's dynamic response.

2.2 Different Sensors used in SHM

Yazdizadeh et al. [11] carried out monitoring on three different grades of concrete by using electrical resistance strain gauge sensors and fiber Bragg grating sensors (type of fiber optics) to investigate creep and shrinkage. Zhao et al. [12] implemented multi-agent and system-based structural health monitoring using strain gauges, fiber optic, and piezoelectric sensors to determine states of structure. Ghosh et al. [13] utilized cost-effective and non-destructive technology approach to detect localized cracks on beams.

3 PROCESS OF DAMAGE DETECTION IN STRUCTURES USING SHM

Pešic et al., Chen et al., and Nayeri et al. [14-16] carried out dynamic monitoring on five concrete beams, eleven spans of Nelson St. off-ramp bridge, and a 17-story building located in Los Angeles California using finite element analysis software ABAQUS, N4SID algorithm and NExT/ERA method respectively. Lorenzoni et al. [17] implemented structural health monitoring on cultural heritage structure Roman Arena of Verona in Italy by installing accelerometer sensors, displacement, and acceleration transducers by implementing frequency domain decomposition (FDD) and using ARTeMIS software. Michel et al. and Brincker et al. [18-19] used the frequency domain decomposition (FDD) method for analysis of the nine-story reinforced concrete building in Grenoble and a 2-story building model respectively. Lee et al. [20] implemented vibration-based monitoring on the bridge deck by attaching accelerometers and using time-domain decomposition (TDD).

Ubertini and García-Macías [21] recorded ambient vibrations for one month of sciri tower which is located in Italy by deploying twelve accelerometers on towers. Rahmani et al., Kaya et al., and García-Macías et al. [22-24] presented an algorithm using MATLAB software for analysis of 12-story reinforced concrete Sherman oak building, tall buildings in UAE, and Consoli Palace in Gubbio for detection of modal parameters. Oh et al. [25] carried out Model Updating Method using the modal replies derived from the dynamic response of a four-story shear-type test frame.

4 STATIC ANALYSIS OF STRUCTURES IN SHM

Li et al. [26] developed Fiber Bragg Grating (FBG) displacement sensor to measure vertical displacement. Ni and Chen [27] applied strain gauges on Hong Kong's Tsing Ma suspension

1st International Conference on Advances in Civil & Environmental Engineering, University of Engineering & Technology Taxila, Pakistan

Conference date 22 &23 Feb 2022

bridge having the main length of 1377 m. Saisi et al. [28] performed static monitoring on the bell tower of Church Santa Maria del Carrobiolo in Italy. An ambient vibration test was carried out under ten displacement transducers and five temperature sensors showing there is no exact solution to find unusual cracks. Ayyildiz et al. [29] experimented on carbon fiber reinforced polymer concrete column to detect fracture using piezoelectric sensors (PZTs). Koo et al. [30] implemented a static monitoring system using strain gauges, temperature, and wind sensors on the Tamar suspension bridge to observe the performance of a structure. Burud and Kishen [31] experimented on three notched plain concrete beams having different lengths using piezoelectric acoustic emission sensors, linear variable transformer sensors, and displacement opening gauge to find the change in volume of the zone of a fracture process while applying load.

5   DYNAMIC ANALYSIS OF STRUCTURES IN SHM

Stiros et al. [32] used GPS and RTS (robotic total stations) combining accelerometers and monitored Evripos cable-stayed bridge to measure dynamic displacement. Lorenzoni et al. [33] installed displacement transducers and piezoelectric accelerometers on Verona's Roman Arena and Conegliano Cathedral then monitored It for three years to study the behavior of buildings. Asadollahi et al. and Lofrano et al. [34-35] captured vibration responses of twin cable-stayed Jindo bridges in Korea for one year and beams respectively.

Pakzad and Fenves [36] deployed dense wireless accelerometer sensors on Golden Gate Bridge to collect vibration data for three months performing Statistical analysis to measure frequencies, mode shapes, and damping ratio. Ubertini et al. [37] discussed the results of a structural health monitoring system based on vibration. using accelerometers and temperature sensors installed in the bell tower of San Pietro for one year. Results show that this is a low-cost and vibration-based system for damage detection. Kuddus et al. [38] experimented on a reinforced concrete column using a target-free and vision-based approach to get acceleration and dynamic displacement. Hapsari et al. [39] employed accelerometers on the bridge prototype. They applied the fast Fourier transform technique to know the value of frequency and used software Arduino IDE.

5.1   Structural health monitoring using accelerometers

Many researchers [40-44] have employed accelerometers to find dynamic properties of structure such as mode shapes and frequency on University of Aveiro Campus, bridge model, four-story shear frame, support beams, and Erqi Yangtze River Bridge in Wuhan respectively.

6   CONCLUSION

This paper discusses structural health monitoring review of civil engineering structures such as bridges, buildings, and structural elements by using various damage detection approaches under different algorithms and sensors to predict the reduction of stiffness, the extent of damage, existence, and the origin of damage in structures for saving cost and improving safety. Laboratory specimens and real-life structures were monitored to find the structure's static and dynamic properties along with finite element analysis. Different sensors were used for

1st International Conference on Advances in Civil & Environmental Engineering, University of Engineering & Technology Taxila, Pakistan

Conference date 22 &23 Feb 2022

monitoring but accelerometers were very effective in collecting acceleration response and extracting modal details such as mode shapes and frequency. Future work is required on damping ratios as they are variable, sensitive to time-varying, less consistent, and difficult to find.

REFERENCES

[1] Bas, S., N. M. Apaydin, A. Ilki, and F. N. Catbas, *Structural health monitoring system of the long-span bridges in Turkey*, Structure and Infrastructure Engineering, 2018. **14**(4): p. 425-444.

[2] Venanzi, I., A. Kita, N. Cavalagli, L. Ierimonti, and F. Ubertini, *Earthquake-induced damage localization in a historic masonry tower through long-term dynamic monitoring and FE model calibration*, Bulletin of Earthquake Engineering, 2020. **18**(5): p. 2247-2274.

[3] Deraemaeker, A., E. Reynders, G. De Roeck, and J. Kullaa, *Vibration-based structural health monitoring using output-only measurements under changing environment*, Mechanical systems and signal processing, 2008. **22**(1): p. 34-56.

[4] Bernagozzi, G., C. E. Ventura, S. Allahdadian, Y. Kaya, L. Landi, and P. P. Diotallevi, *Output-only damage diagnosis for plan-symmetric buildings with asymmetric damage using modal flexibility-based deflections*, Engineering Structures, 2020. **207**: p. 110015.

[5] Capozucca, R., *A reflection on the application of vibration tests for the assessment of cracking in PRC/RC beams*, Engineering structures, 2013. **48**: p. 508-518.

[6] Chang, C.-M., T.-K. Lin, and C.-W. Chang, *Applications of neural network models for structural health monitoring based on derived modal properties*," Measurement, 2018. **129**: p. 457-470.

[7] Khuc, T. and F. N. Catbas, *Completely contactless structural health monitoring of real-life structures using cameras and computer vision*, Structural Control and Health Monitoring, 2017. **24**(1): p. 1852.

[8] Park, H.S. and B. K. Oh, *Real-time structural health monitoring of a supertall building under construction based on visual modal identification strategy*, Automation in Construction, 2018. **85**: p. 273-289.

[9] Pierdicca, A., F. Clementi, P. Mezzapelle, A. Fortunati, and S. Lenci, *One-year monitoring of a reinforced concrete school building: Evolution of dynamic behavior during retrofitting works*, Procedia Engineering, 2017. **199**: p. 2238-2243.

[10] Barsocchi, P., *et al.*, *Wireless sensor networks for continuous structural health monitoring of historic masonry towers*, International Journal of Architectural Heritage, 2021. **15**(1): p. 22-44.

[11] Yazdizadeh, Z., H. Marzouk, and M. A. Hadianfard, *Monitoring of concrete shrinkage and creep using Fiber Bragg Grating sensors,* Construction and Building Materials, 2017. **137**: p. 505-512.

[12] Zhao, X., S. Yuan, H. Zhou, H. Sun, and L. Qiu, *An evaluation on the multi-agent system based structural health monitoring for large scale structures*, Expert Systems with applications, 2009. **36**(3): p. 4900-4914.

[13] Ghosh, A., D. J. Edwards, M. R. Hosseini, R. Al-Ameri, J. Abawajy, and W. D. Thwala, *Real-time structural health monitoring for concrete beams: a cost-effective 'Industry 4.0'solution using piezo sensors*, International Journal of Building Pathology and Adaptation, 2020.

[14] N. Pešić, N., S. Živanović, J. Dennis, and J. Hargreaves, *Experimental and finite element dynamic analysis of incrementally loaded reinforced concrete structures*," Engineering structures, 2015. **103**: p. 15-27.

[15] Chen, G.-W., P. Omenzetter, and S. Beskhyroun, *Modal systems identification of an eleven-span concrete motorway off-ramp bridge using various excitations*, Engineering structures, 2021. **229**: p. 111604.

1st International Conference on Advances in Civil & Environmental Engineering, University of Engineering & Technology Taxila, Pakistan

Conference date 22 &23 Feb 2022

[16]   Nayeri, R.D., S. F. Masri, R. G. Ghanem, and R. L. Nigbor, *A novel approach for the structural identification and monitoring of a full-scale 17-story building based on ambient vibration measurements*, Smart Materials and Structures, 2008. 17(2): p. 025006.

[17]   Lorenzoni, F., F. Casarin, C. Modena, M. Caldon, K. Islami, and F. da Porto, *Structural health monitoring of the Roman Arena of Verona, Italy*, Journal of Civil Structural Health Monitoring, 2013. **3**(4): p. 227-246.

[18]   Michel, C., P. Guéguen, and P.-Y. Bard, *Dynamic parameters of structures extracted from ambient vibration measurements: An aid for the seismic vulnerability assessment of existing buildings in moderate seismic hazard regions*, Soil dynamics and earthquake engineering, 2008. **28**(8): p. 593-604.

[19]   Brincker, R., L. Zhang, and P. Andersen, *Modal identification of output-only systems using frequency domain decomposition*, Smart materials and structures, 2001. **10**(3): p. 441.

[20]   Lee, L.S., V. M. Karbhari, and C. Sikorsky, *Structural health monitoring of CFRP strengthened bridge decks using ambient vibrations*, Structural Health Monitoring, 2007. **6**(3): p. 199-214.

[21]   García-Macías, E. and F. Ubertini, *Automated operational modal analysis and ambient noise deconvolution interferometry for the full structural identification of historic towers: A case study of the Sciri Tower in Perugia, Italy*, Engineering Structures, 2020. **215**: p. 110615.

[22]   Rahmani, M., M. Ebrahimian, and M. I. Todorovska, *Time-wave velocity analysis for early earthquake damage detection in buildings: Application to a damaged full-scale RC building*," Earthquake Engineering & Structural Dynamics, 2015. **44**(4): p. 619-636.

[23]   Kaya, Y. and E. Safak, *Real-time analysis and interpretation of continuous data from structural health monitoring (SHM) systems*, Bulletin of Earthquake Engineering, 2015. **13**(3): p. 917-934.

[24]   García-Macías, E. and F. Ubertini, *MOVA/MOSS: Two integrated software solutions for comprehensive Structural Health Monitoring of Structures*, Mechanical Systems and Signal Processing, 2020. **143**:p. 106830.

[25]   Oh, B.K., D. Kim, and H. S. Park, *Modal response-based visual system identification and model updating methods for building structures*, Computer-Aided Civil and Infrastructure Engineering, 2017. **32**(1): p. 34-56.

[26]   Li, C., L. Sun, Z. Xu, X. Wu, T. Liang, and W. Shi, *Experimental investigation and error analysis of high precision FBG displacement sensor for structural health monitoring*, International Journal of Structural Stability and Dynamics, 2020. **20**(6): p. 2040011.

[27]   Ni, Y. and R. Chen, *Strain monitoring based bridge reliability assessment using parametric Bayesian mixture model*, Engineering Structures, 2021. **226**: p. 111406.

[28]   Saisi, A., C. Gentile, and A. Ruccolo, *Pre-diagnostic prompt investigation and static monitoring of a historic bell-tower*, Construction and Building Materials, 2016. **122**: p. 833-844.

[29]   Ayyildiz, C. *et al.*, *Structure health monitoring using wireless sensor networks on structural elements*, Ad Hoc Networks, 2019. **82**: p. 68-76.

[30]   Koo, K.-Y., J. Brownjohn, D. List, and R. Cole, *Structural health monitoring of the Tamar suspension bridge*, Structural Control and Health Monitoring, 2013. **20**(4): p. 609-625.

[31]   Burud, N. B. and J. C. Kishen, *Response based damage assessment using acoustic emission energy for plain concrete,* Construction and Building Materials, 2021. **269**: p. 121241.

[32]   Stiros, S., P. Psimoulis, F. Moschas, V. Saltogianni, E. Tsantopoulos, and P. Triantafyllidis, *Multi-sensor measurement of dynamic deflections and structural health monitoring of flexible and stiff bridges*, Bridge Structures, 2019. **15**(1-2): p. 43-51.

[33]   Lorenzoni, F., F. Casarin, M. Caldon, K. Islami, and C. Modena, *Uncertainty quantification in structural health monitoring: Applications on cultural heritage buildings*, Mechanical Systems and Signal Processing, 2016. **66**: p. 268-281.

1st International Conference on Advances in Civil & Environmental Engineering, University of Engineering & Technology Taxila, Pakistan

Conference date 22 &23 Feb 2022

[34] Asadollahi, P. and J. Li, *Statistical analysis of modal properties of a cable-stayed bridge through long-term wireless structural health monitoring*, Journal of Bridge Engineering, 2017. **22**(9): p. 04017051.

[35] Lofrano, E., A. Paolone, and M. Vasta, *Identification of uncertain vibrating beams through a perturbation approach*, ASCE-ASME Journal of Risk and Uncertainty in Engineering Systems, Part A: Civil Engineering, 2016. **2**(2): p. 4015006.

[36] Pakzad, S.N. and G. L. Fenves, *Statistical analysis of vibration modes of a suspension bridge using spatially dense wireless sensor network*, Journal of structural engineering, 2009. **135**(7): p. 863-872.

[37] Ubertini, F., G. Comanducci, and N. Cavalagli, *Vibration-based structural health monitoring of a historic bell-tower using output-only measurements and multivariate statistical analysis,* Structural Health Monitoring, 2016. **15**(4): p. 438-457.

[38] Kuddus, M.A., J. Li, H. Hao, C. Li, and K. Bi, *Target-free vision-based technique for vibration measurements of structures subjected to out-of-plane movements*, Engineering Structures, 2019. **190**: p. 210-222.

[39] Hapsari, A., E. Supriyanto, A. Hasan, and A. Suharjono, *Accelerometer sensor data analysis of bridge structural health monitoring system*, IOP Conference Series: Materials Science and Engineering, 2021. **1108**(1): p. 012026.

[40] Antunes, P.C., J. M. Dias, H. Varum, and P. André, *Dynamic structural health monitoring of a civil engineering structure with a POF accelerometer*, Sensor Review, 2014.

[41] Cantero, D., P. McGetrick, C.-W. Kim, and E. OBrien, *Experimental monitoring of bridge frequency evolution during the passage of vehicles with different suspension properties*, Engineering Structures, 2019. **187**: p. 209-219.

[42] Lofrano, E., A. Paolone, and M. Vasta, *A perturbation approach for the identification of uncertain structures*, International Journal of Dynamics and Control, 2016. **4**(2): p. 204-212.

[43] Yang, X., A. Swamidas, and R. Seshadri, *Crack identification in vibrating beams using the energy method*, Journal of sound and vibration, 2001. **244**(2): p. 339-357.

[44] Han, H., J. Wang, X. Meng, and H. Liu, *Analysis of the dynamic response of a long span bridge using GPS/accelerometer/anemometer under typhoon loading*, Engineering Structures, 2016. **122**: p. 238-250.

1st International Conference on Advances in Civil & Environmental Engineering, University of Engineering & Technology Taxila, Pakistan

Conference date 22 &23 Feb 2022

Traffic Optimization of Five-Legged Roundabout Using Synchro Software

Engr. Hafiz Muhammad Usman Azeem

MNS University of Engineering & Technology Multan, Pakistan

University of Engineering & Technology Taxila, Pakistan

hafizusmanazeem@gmail.com

Prof. Dr. Naveed Ahmed

University of Engineering & Technology Taxila, Pakistan

n.ahmad@uettaxila.edu.pk

Muhammad Abou Bakar Farooq

MNS University of Engineering & Technology Multan, Pakistan

engr.mabf@yahoo.com

ABSTRACT

Transportation from the beginning has always been very integral to the growth and development of any society all around the world. One of the most common challenges and difficulties of transportation for most countries are the issue of congestion and this is mainly because of population growth and transportation planning. This study appraises an un-convectional method of traffic management by using synchro software to analyze a prominent roundabout (Vehari chowk) within the city and to proffer the possible solutions accordingly. This roundabout plays a key role as it connects other cities and important facilities within the city. In this study, the five legs of the roundabout are analyzed using synchro software to determine the degree of congestion, fuel consumption and other future forecasts necessary to make appropriate decision to ensure a sustainable transportation system. The data for peak hour is collected in the said location by using manual countdown method. Analysis of the roundabout is done by developing the geometry, by adding the counted traffic volume and considering the necessary parameters of the software. Results have shown that there is 45% reduction in number of stops, preventconsumable fuel by about 58% by considering best possible solution out of all. The results of study can then be utilized and adopted by any five-legged intersection for best accommodation and fluent of traffic.

Keywords: Transportation, Congestion, Synchro, Peak hours data and Consumable fuel.

1st International Conference on Advances in Civil & Environmental Engineering, University of Engineering & Technology Taxila, Pakistan

Conference date 22 &23 Feb 2022

1 INTRODUCTION

Due to increase in constant growth, development of global economy and population which has been a major factor contributing towards traffic congestion thus, leaving traffic engineers with the responsibility of finding appropriate solutions to enhance general network conditions and operations. It has negative impact related to wastage of fuel resulting in emission of carbon

1st International Conference on Advances in Civil & Environmental Engineering, University of Engineering & Technology Taxila, Pakistan

Conference date 22 &23 Feb 2022

dioxide and many other dangerous gases. The U.S. Travel Association released a survey finding that Americans avoided an estimated 47.5 million auto trips due to highway congestion in 2018 costing the economy $30 billion in travel spending and 248,000 American jobs, according to the organization's economists. Research was conducted in the city of Doha to check the safety and operational performance of a signalized roundabout through simulation approach and by applying the surrogate safety assessment model. The results indicated that the signal timings and phasing schemes are associated with the level of safety at the signalized roundabout by reducing or increasing the potential traffic conflicts. Moreover, it was found that high traffic demand at signalized roundabouts is not necessarily related to the high traffic conflicts or high conflict severity.[1] The aim of the research was to analyze real time situation of two congested roundabout in Sibiu and to propose the solution to improve the traffic speed at concerned location by using Synchro software. The geometry of roundabout was changed in this study fromreal one. It was concluded that with the change of geometry, traffic speed increased withenhancement of level of service.[2] The problem in the city of Multan which a state in Republic of Pakistan is as common to most developing countries is that of congestion at peak hours. In tackling this problem, traffic organization is key through signalized junctions and roundabout using smart software and, in this case, I have studied it through Synchro software. Due to the traffic congestion issues at roundabout named as Vehari chowk, this study is an effort tominimize the congestion at that point by reducing the number of stops, to make roundabout eco- friendly by diminishing the consumption of fuel which will directly or indirectly helpful for road user to save their money and to propose the alternate traffic flow plan to reduce the traffic congestion at Vehari chowk, Multan by adopting the best suitable method, so that traffic flow can be smoothened.

2 METHODOLOGY AND SOFTWARE

2.1 Methodology

2.1.1 Data Collection

First, a survey is conducted to know the peak hour time by visually observing of approaches of the Vehari chowk roundabout, through google maps and by questioning related to congestion from public to get the highest possible traffic volume which is always a best in conducting research to design for worst scenario. Data is obtained by manual count method and is recorded into the sheets that have been labelled according to the necessary parameters. Different manual count devices are used for different kind of traffic i.e., heavy traffic, light traffic, motorcyclist, pedestrian etc. Past data of the roundabout is collected from concerned department to know the trend of traffic. Data related to geometry of the roundabout and approaches are obtained by usingdifferent measuring instruments and plot by using software AutoCAD.

2.1.2 Analysis method

The analysis for this data is done based on traffic volume, types of vehicles, direction of vehicle, movement of motorcyclists and pedestrians, geometric properties related to diameter of

1st International Conference on Advances in Civil & Environmental Engineering, University of Engineering & Technology Taxila, Pakistan

Conference date 22 &23 Feb 2022

roundabout, number of lanes, lane width and distribution. The data as stated earlier is obtained for the five arms of the roundabout, labeled Arm A, B, C, D and E as 6:00pm to 7:00pm peak hours data. It is then recorded into the sheet for every 15 minutes interval respectively, taking note of the type of car and other relevant details which are sorted afterwards during the data appropriation process.

2.2 Software

Synchro software is a complete package for analyzing, modeling, optimizing, managing and simulation traffic systems. The software covers the parameters like capacity analysis, coordinate and optimize, actuated signals, unsignalized intersections, time space diagram, traffic impact analysis, simulations, 3D animations and controller interface to perform its working. The synchro ribbon is divided into different tabs to perform according to requirements. Tabs include home tabs, options tab, transfer tab, optimize tab, reports tab and help tab. It consists of the groups and commands that is used accordingly to optimize the roundabout in this study. Realtime geometry of the roundabout including approaches are created in the software and all the extracted data added by calculating peak hour factors. After adding all the necessary information to the software, analysis report is generated by the software.

3 DATA ANALYSIS & RESULTS

Vehari chowk roundabout connecting five major legs, N5 Northward side Kumharanwala chowk (leg A), Makhdoom Rasheed road Westward side (leg B), Vehari road West-Southward side BCG chowk (leg C), N5 Southward side Bahawalpur bypass chowk (leg D) and Vehari road Eastward side (leg E).
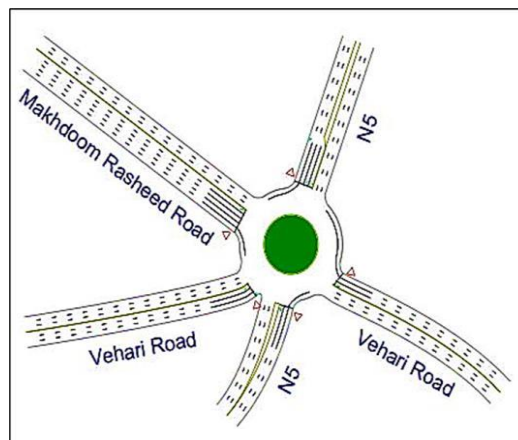
Fig 3.1: Synchro generated image of roundabout

1st International Conference on Advances in Civil & Environmental Engineering, University of Engineering & Technology Taxila, Pakistan

Conference date 22 &23 Feb 2022
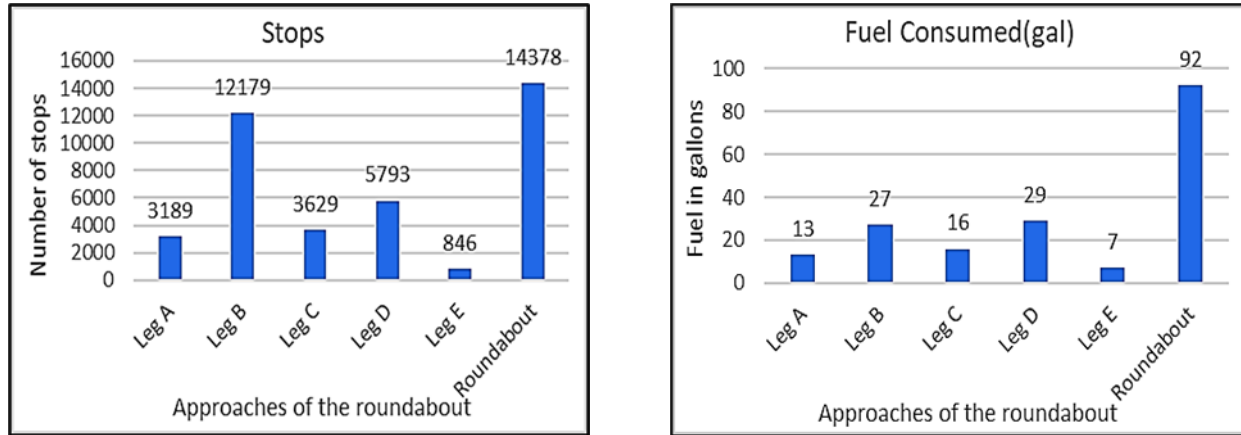
Fig 3.2: Graphical representation of number of stops and consumable fuel

Analysis have shown that there is a lot of congestion in terms of number of stops on the roundabout especially traffic coming from leg A, B, C and D that causes major disaster in the said area. Due to the congestion in the roundabout, there is a long dense line of vehicle generated,92 gallon of fuel is consumed in one hour duration of time. This directly effects the economy of people in terms of fuel consumption.

4 DISCUSSION

There are three options deduced as a means of solving the problem about the roundabout. The first methodology is to alter the geometric shape of the roundabout intersection with provision of signals, second is to replace the roundabout with signalized intersection and third one is provision of channelized and signalized roundabout with underpass for main approaches as well as fifth approach (leg B) having high density of traffic encounter.

4.1 Signalized Roundabout & Intersection

After Implementing signalized roundabout and signalized intersection, the effectiveness, congestion and longevity of this option is tested and analyzed to get a deeper information as the roundabout is sustainable or not. Based on analysis it is not sustainable and suitable for traffic to flow smoothly in near future. Congestions related issues will remain there and this model will not sort out the consumption related issues in current as well as in future.

4.2 Underpasses with Channelized & signalized Roundabout

This solution will help to reduce the volume of traffic currently experienced in this location. However, it is important to note that this option is a lot more expensive than first two option. Although when the cost is considered holistically, i.e., the life cycle cost of this option, it shows

1st International Conference on Advances in Civil & Environmental Engineering, University of Engineering & Technology Taxila, Pakistan

Conference date 22 &23 Feb 2022

advantage of long-term user benefit. This option also has an advantage in terms of environmental impact over the first and second option. The underpass option is about adding an extra lane on north-south and west approaches. The parameters for example delays, queues, level of service, fuel consumption, CO, CO_2, NOx gases, and Capacity will be sorted out by choosing this model.
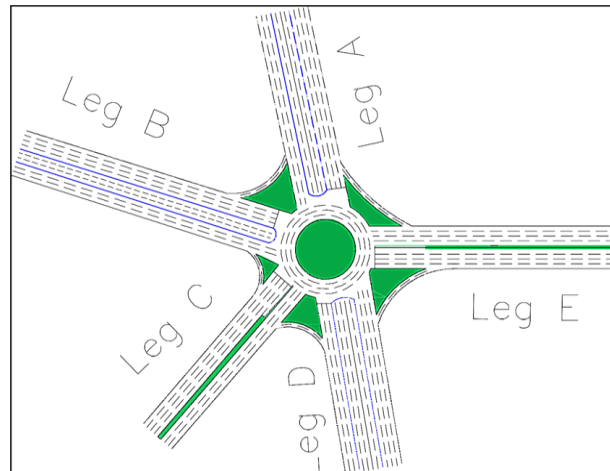
Fig 4.1: Geometry of roundabout created by AutoCAD
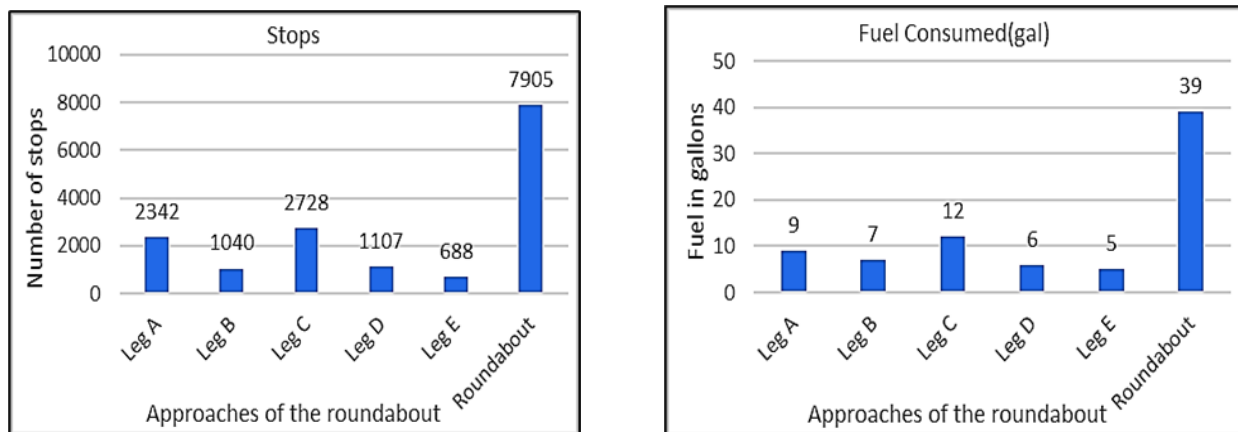
Fig 4.2: Graphical representation of different gases as an emission

After implementing the model, number of stops for roundabout is reduced about 45% and file consumption is reduced to about 58%. Also, there is reduction in number of stops and in the consumption of fuel to all the approaches which helps to make eco-friendly environment.

1st International Conference on Advances in Civil & Environmental Engineering, University of Engineering & Technology Taxila, Pakistan

Conference date 22 &23 Feb 2022

5 CONCLUSION

The following conclusions can be drawn from this study:

➢ The first solution is about providing an extra lane to each leg with signalized roundabout, there is a little bit control over the stops but not at that level that fulfill our requirements and not seeing the significance reduction in congestion.
➢ The second solution is about providing an extra lane to each leg with signalized intersection, there is a little bit reduction in number of stops but not at that level that fulfill our requirements and not seeing the significance reduction in congestion and other parameters.
➢ Third solution is provision of channelized and signalized underpass having roundabout for remaining approaches with the increment in the lanes, which is more suitable because it will give the better level of service even after 10 years and have less negative environmental impacts, but it needs more cost as compared to solution one and two but more affective and reduce the issue of congestion at that point with great extent. Results have shown that there is 45% reduction in number of stops, prevent consumable fuel by about 58%.

6 RECOMMENDATION

Third option (Underpass with channelized and signalized roundabout) is strongly recommended as the most suitable option to tackle the issue of the roundabout traffic congestion because it will manage to meet with all the conditions we are looking for.

7 REFERENCES

1.   Ghanim, M., et al., *Safety and Operational Performance of Signalized Roundabouts: A Case Study in Doha.* Procedia Computer Science, 2020. **170**: p. 427-433.
2.   Ind , M. *Improving performance of roundabout intersections by optimizing traffic-flow speed.* 2017.

1st International Conference on Advances in Civil & Environmental Engineering, University of Engineering & Technology Taxila, Pakistan

Conference date 22 &23 Feb 2022

Experimental study of hydraulic characteristics in an open channel flow with Vegetation and Dyke.

Muhammad Imran, Dr. Naeem Ejaz
University of Engineering & Technology Taxila, Pakistan
Imransamtia989@gmail.com; naeem.ejaz@ uettaxila.edu.pk

ABSTRACT

During extreme floods, structures (homes and buildings) that are directly exposed to flood waves may experience large hydrodynamic forces which could lead to substantial structural damage. To mitigate the damage, vegetation and dyke can act as a barrier to dissipate the energy of flood. This study involves laboratory experiments to determine energy loss of a steady sub-critical flow through vegetation and dyke by changing the distance between vegetation and dyke. Dyke of three different height and width were used, while vegetation thickness was kept constant. The distance between dyke and vegetation greatly affects the energy dissipation. For smaller distance between dyke and vegetation the energy loss is maximum as compared to the larger distance between the dyke and vegetation. By increasing the distance from 10 cm to 20 cm, the energy loss decreases from 4-6 %.

The height of dyke and dyke width have greater effects on the energy dissipation. The energy loss is maximum in the case of large dyke as compared to the smaller dyke. By increasing height of Dyke from 4 cm to 5 cm (Large dyke have height and width of 5cm and 43cm while small dyke has height and width of 4cm and 21.5cm), the energy loss is increased from 30% to 43 %

KEYWORDS: Flood, Vegetation, Energy Dissipation (ED), Backwater Rise profile (BWRP), Relative Backwater Rise Profile (RBWRP), Small Dyke (SD), Intermediate Dyke (ID), Large Dyke (LD),

1 INTRODUCTION

Beyond normal limit overflow of large amount of water on dry land is called flood[1]. Flood is potential force of nature that has power to generate great causes to human life, agricultural land, crops, livestock's, structures etc. Mostly flood occurs near a river or a stream. Flood can occur due to heavy rainfall over the catchment area[2]. From 1973 Pakistan has faced seven major flood disaster and it affected almost 40 million people while a drought in 1999 affected 3 million people and earthquake in 2005 and 2008 affected 7 million people[3]. The 2010 flood is called super flood. It affected 78 districts out of 141 districts and 1.8 million homes were damaged or destroyed by this severe flood in KPK, Punjab and Sindh provinces. Almost collateral damage was estimated $9.7 billion. From 1950-2018, Pakistan has faced 35 flood events causing a lot of destructions.

1st International Conference on Advances in Civil & Environmental Engineering, University of Engineering & Technology Taxila, Pakistan

Conference date 22 &23 Feb 2022

In Pakistan construction of dames, barrages, bunds etc. are flood mitigation practices. They fail during heavy rainfall and during high flood. The technique of vegetation can also be used as flood disaster mitigation which is more economical and effective. It does not involve so much capital. This technique is being used effectively in Japan. The main idea of this technique is to decrease the energy of flow to minimize the losses of flood[4]

Floods affect all over the world because they are natural disaster. It destroys lands, structures such as dams, barrages, bunds, and livestock. The conventional methods to decrease the losses of floods are time consuming or time taking and requires a lot of capital. Also, they are not friendly to environment. The best solution to decrease the losses due to floods with economical and friendly to environment is use of soft as well as hard solution. Here in Pakistan the main reason of flood is monsoon rainfall and vegetation are very good for mitigation the losses of flood due to monsoon rainfall[5].

By use of dyke and vegetation the following objectives are obtained.
- To evaluate the energy loss with the help of vegetation and dyke by changing distance between vegetation and dyke[6].
- To investigate the effect of height and width of different types of dyke on energy loss[7].
- To study the water surface profiles and relative backwater rise profiles using different types of dyke[8].

2   RESEARCH METHODOLOGY

A glass-walled flume which is 10m in length, 0.305m in width and 0.5m in height present at Civil Engineering Department, UET Taxila was used. Almost 33 percent of the canal length (i.e., 3m) was installed with horizontal wooden bed over which the dyke can be moved at required distance. Vegetation was fix on the bed. The horizontal slope of the bed was set to zero.

The trees chosen for this research are eucalyptus (locally known as Sufaida) that are found abundantly in Punjab and does require much water for its growth, so it will be more suitable for the areas near water body. It has an average height of 20m and average diameter at breast height of 20 to 30cm at maturity. For a scale of 1/100, wooden cylinders were used which had the diameter of 0.3cm (3mm) and were fixed in a wooden plank in a staggered manner. For the experiments, vegetation model with vegetation density value of G/d-1.09 was made. Where G/d-1.09 represents intermediate vegetation.

Another vegetation parameter used in these experiments is known as vegetation thickness (dn) which is defined as a product of a diameter of a tree (d) at breast height and the number of trees (n) in a rectangle with a frontage of unit length along the shoreline and depth equal to the width (W) of the forest. Value of dn used was 185.04 (No.cm). It is calculated as

$$dn = \frac{2}{\sqrt{3}D^2}Wd \qquad\qquad\qquad Equation\ 1$$

G/d = 1.09 (For intermediate vegetation G/d = 1.09)
G = 1.09 x 3 = 3.27mm (As d = 3mm = 0.3cm)
D = 1.5 + 1.5 +3 + 3.27 +3.27 = 12.54mm = 1.254cm

1st International Conference on Advances in Civil & Environmental Engineering, University of Engineering & Technology Taxila, Pakistan

Conference date 22 &23 Feb 2022

$dn = \frac{2}{2.17} 8.4 \; x \; 0.3 \; x \; 100 \; = 185.04$

This study defines the energy reduction rate [%] as

Energy reduction rate [%] $= \frac{E1-E2}{E1} \; X100$ *Equation 2*

Froud number is calculated as.

$Fr = \frac{V}{\sqrt{gy}}$ *Equation 3*

Specific Energy

$E = Y + \frac{V2}{2g}$ *Equation 4*

Table 1. Experimental Conditions

Case	Dyke Height(cm)	Dyke Width(cm)	Vegetation Width(cm)	Spacing dyke and vegetation (cm)	Frequency
Large Dyke	5	43	8	10,15,20	12,14,16,18,20,22,24
Intermediate Dyke	4.5	22	8	10,15,20	12,14,16,18,20,22,24
Small Dyke	4	21.5	8	10,15,20	12,14,16,18,20,22,24

Locate the point of the formation of the hydraulic jump by finding the Froude number along the length of water surface profile and study the effects of distance and type of dyke on the formation of the hydraulic jump. Classify the jumps into 3 different types, Type A, Type B, Type C depending upon the distance of the formation of the jump from the top width of the dyke.

3   RESULTS

Since the vegetation density is constant and the results are based on the distance between the dyke and vegetation. The energy loss is maximum when the height of the dyke is more and decreases with the decrease in dyke height. The loss of energy decreases while increasing the Froude number. The maximum loss of the energy is at the minimum Froude number 0.4 as compared to the energy loss at Froude number 0.65

The energy loss is directly proportional to the height of the dyke, as the energy loss is maximum in the case of the large dyke and minimum in the case of the small dyke. In the case of

1st International Conference on Advances in Civil & Environmental Engineering, University of Engineering & Technology Taxila, Pakistan

Conference date 22 &23 Feb 2022

one dyke, the energy loss is maximum when the distance between the dyke and vegetation is minimum (as 10 cm) and minimum energy loss at larger distance (as 20cm).

Figure 1 shows that energy dissipation for small dyke at 10 cm, 15 cm and 20 cm distance at Froude number ranging 0.4 to 0.65. Energy loss is maximum at 10 cm distance and Froude number of 0.4(43%). Similarly figures 2 and 3 for intermediate and large dykes show energy loss is maximum at 10 cm distance and Froude number of 0.4 which is 50% and 54% respectively. While figure 4 shows comparison of energy loss in all three types of dykes. It shows maximum energy loss in case of large dyke and less in small dyke.
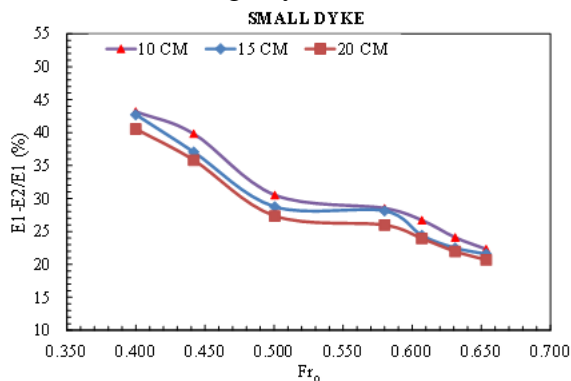
Figure 1. ED for SD
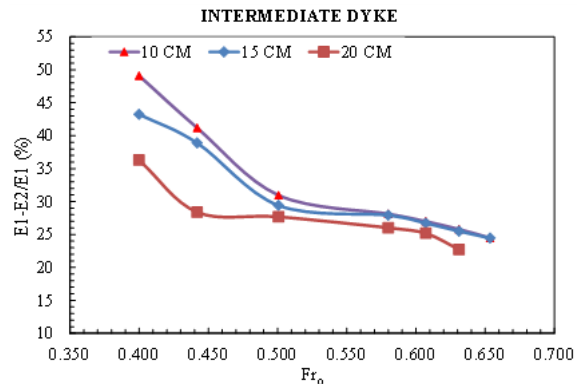
Figure 2. ED for ID
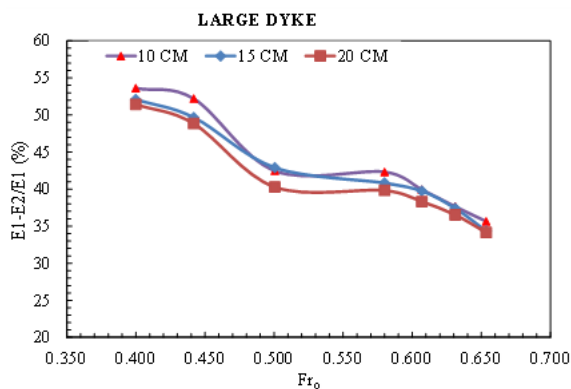
Figure 3. ED for LD
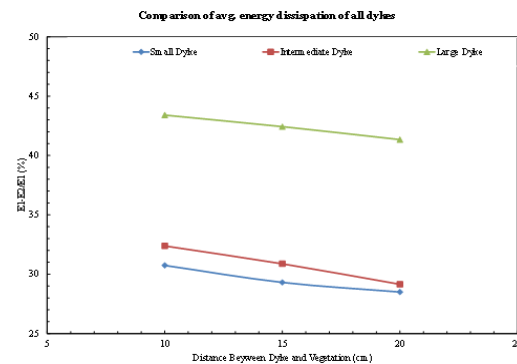
Figure 4. Comparison of avg ED

4   CONCLUSION

Conclusions based on the experiments are below listed.

1. The height of dyke and dyke dimensions have greater effects on the energy dissipation. The energy loss is maximum in the case of large dyke as compared to smaller dyke. By increasing Height of dyke from 4 cm to 6.5 cm the effect of the energy loss is increased from 30 to 43 %

1st International Conference on Advances in Civil & Environmental Engineering, University of Engineering & Technology Taxila, Pakistan

Conference date 22 &23 Feb 2022

2. By increasing the distance from 10 cm to 20 cm the energy loss decreases to 4 % to 6 %.
3. In the case of the constant or same dyke the energy loss is maximum at the 10 cm (smaller distance) as compared to 20 cm (larger distance) distance between the dyke and vegetation.
4. At the upstream side of the vegetation, keeping the vegetation thickness constant, the increase in backwater rise profile is more when the Froude number is increased
5. By increasing the distance between dyke and vegetation the type of jump changes.

5   ACKNOWLEDGEMENTS

REFERENCES

[1]   S. Deen, "Pakistan 2010 floods. Policy gaps in disaster preparedness and response," *International Journal of Disaster Risk Reduction*, vol. 12, pp. 341–349, Jun. 2015, doi: 10.1016/j.ijdrr.2015.03.007.

[2]   A. Parsaie, H. Yonesi, and S. Najafian, "Prediction of flow discharge in compound open channels using adaptive neuro fuzzy inference system method," *Flow Measurement and Instrumentation*, vol. 54, pp. 288–297, Apr. 2017, doi: 10.1016/j.flowmeasinst.2016.08.013.

[3]   A. Adhikari, K. C. Patra, and N. Adhikari, "Prediction of Discharge in Straight Compound Channels using Conventional and Soft Computing Tools," *Int. Journal of Engineering Research and Application www.ijera.com*, vol. 7, no. 2, pp. 42–51, 2017, doi: 10.9790/9622-0708024251.

[4]   H. Gotoh, Y. Yasuda, and I. Ohtsu, "Effect of channel slope on flow characteristics of undular hydraulic jumps," 2005. [Online]. Available: www.witpress.com,

[5]   Z. Fuat Toprak, "Flow discharge modeling in open canals using a new fuzzy modeling technique (SMRGT)," *Clean - Soil, Air, Water*, vol. 37, no. 9, pp. 742–752, Sep. 2009, doi: 10.1002/clen.200900146.

[6]   N. Tanaka and Y. Igarashi, "MULTIPLE DEFENSE FOR TSUNAMI INUNDATION BY TWO EMBANKMENT SYSTEM AND PREVENTION OF OSCILALTION BY TREES ON EMBANKMENT."

[7]   R. A. H. Muhammad and N. Tanaka, "Energy reduction of a tsunami current through a hybrid defense system comprising a sea embankment followed by a coastal forest," *Geosciences (Switzerland)*, vol. 9, no. 6, Jun. 2019, doi: 10.3390/geosciences9060247.

[8]   G. A. Pasha and N. Tanaka, "Undular hydraulic jump formation and energy loss in a flow through emergent vegetation of varying thickness and density," *Ocean Engineering*, vol. 141, pp. 308–325, 2017, doi: 10.1016/j.oceaneng.2017.06.049.

Effect of pH on the Degradation of Nitrobenzene in Wastewater

Muhammad Imran Nawaz, Chengwu Yi, Chundu Wu

School of the Environment and Safety Engineering

Jiangsu University, Zhenjiang 212013, P.R. China

imrannawaz43@live.com; yichengwu0943@163.com; wucd@ujs.edu.cn

ABSTRACT

The aim of this study is to use dielectric barrier discharge technique to examine the effect of pH on the nitrobenzene degradation efficiency in wastewater. The water pollution is universal concern because of diversity of the pollutants and their reactions at different conditions. This article outlines the diverse effect of pH values and how it affects the treatment process using a dielectric barrier discharge. DBD generates a huge number of active species which act as strong oxidizing agents and start the pollutant's degradation present in wastewater. A number of distinct tests were conducted to attain the optimum pH levels for the highest NB degradation efficiency. The results of this research demonstrated that the neutral pH levels can give the highest degradation efficiencies of NB. This study could result greater removal of nitrobenzene in wastewaters by providing optimum pH levels for its degradation at lowest price and greater efficiency, it can also be used to diminish other wastewater pollutants by suggesting a favourable solution for their treatment.

KEYWORDS: Dielectric Barrier Discharge, Nitrobenzene, pH, Degradation efficiency

1   INTRODUCTION

Environmental pollution influencing water quality has become more common and life-threatening in recent decades. The discharge of industrial wastewaters into surface and subsurface water bodies is one of the most serious sources of water pollution.

Toxifying the natural waterbodies with different pollutants has become a core concern in the current years due to their high environmental toxicity, permanence, and abundance [1, 2]. Polluted waters, particularly those containing toxic and dangerous substances such as Nitrobenzene, are extremely detrimental to both humans and animals. These pollutants also pose a significant threat to aquatic life and the ecosystem. A multitude of physical, chemical, and biological technologies, as well as combinations of such techniques have been devised for wastewater treatment with the intention to address the water pollution issues. However, such old methods are either obsolete or inefficient, and have negative consequences such as secondary pollution and higher operational and maintenance cost. To reduce various types of pollutants from wastewater, some environmentally pleasant, economically satisfactory, and physically fit methods and techniques should be utilised, after which the water could be applied for other uses or safely discharged into streams, rivers or oceans.

1st International Conference on Advances in Civil & Environmental Engineering, University of Engineering & Technology Taxila, Pakistan

Conference date 22 &23 Feb 2022

Advanced oxidation processes (AOPs) are revolutionary treatment procedures that supply energy to a system in the form of chemical, electrical, or radiative energy to generate powerful oxidizing species [3]. Electrical plasma technology is one of the AOPs that have sparked a lot of interest in the elimination of organic contaminants. The primary generation of oxidising species in the form of molecules (H_2O_2, O_3, etc.), radicals (H•, O•, OH•), ultraviolet light, shockwaves, and electrohydraulic cavitation are all part of this technique, which is extremely efficient and environmentally compatible [4-6]. Whenever these procedures are utilised for wastewater treatment, the active species operate as strong oxidising agents, causing contaminants in the wastewater to degrade. The hazardous and damaging pollutants could be degraded into less toxic and harmless byproducts as a result of this destruction. Consequently, these techniques show up to be crucial for treating wastewater [7].

Dielectric barrier discharge (DBD) plasma is a modern technique having special benefits. Therefore from the last few decades, it has attained consideration of professionals and researchers [8, 9]. These days it is largely applied in several fields such as; for surface water treatment [10, 11], for catalyst treatment [12], for the decomposition of volatile organic compound (VOC) [13] and for many other research areas. The application of DBD technology to wastewater treatment is an innovative approach [14]. DBD plasma has evolved into the most effective approach, generating a lot of attention in the area of treatment and environmental safety. It is stable and easy to create at normal conditions, resulting in a uniform discharge throughout the entire electrode area [15, 16]. The use of a DBD reactor for wastewater treatment is said to induce a variety of chemical and physical reactions that are directly or indirectly liable for the breakdown of chemical compounds present in wastewater [17].

The goal of this study is to explore the effect of pH on nitrobenzene degradation efficiency in wastewater by means of the dielectric barrier discharge technique. This research could lead to better nitrobenzene removal in wastewaters by recommending optimal pH levels for its degradation at the lowest cost and with the greatest efficiency. It could also be used to reduce other wastewater pollutants as a suitable treatment solution.

2   METHODOLOGY

In this study we checked the effect of pH on the treatment of nitrobenzene in wastewater. A novel Dielectric Barrier Discharge reactor was used for this purpose. Several experiments were performed by varying the pH for each treatment and its effect on the degradation of NB was checked. The experimental setup is shown in the Figure 1. It mainly consists of a wastewater barrel, an oxygen supply, the DBD reactor, and the water circulation system. Wastewater was filled into the WW barrel and pH of the sample was adjusted by 0.1 N NaOH and 0.1 N HCL solutions.

The concentration of NB was calculated with the help of a UV-visible spectrophotometer (UV-9600 Rayleigh, China) at a wavelength of 262 nm [18, 19] while the pH of the solution was measured by the pH meter (FE20, Mettler Toledo Corporation, China). The system was initiated by applying oxygen and a high voltage to the DBD reactor which in return produced an enormous amount of active species that caused the degradation process. The reactor was operated for 60 minutes and the samples were drawn after each 5 minute's duration to check the

1st International Conference on Advances in Civil & Environmental Engineering, University of Engineering & Technology Taxila, Pakistan

Conference date 22 &23 Feb 2022

degradation efficiency. Several experiments at different pH levels were performed to get the optimum pH which gives the highest NB degradation efficiency.
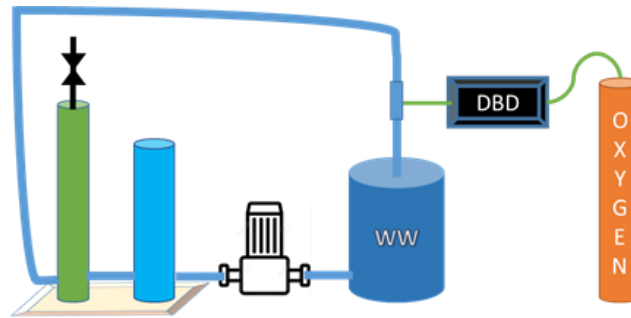
Figure 1: Experimental system flowchart

3   RESUTS

Processing units at different industries use varying pH level for their operations and to get their required purposes. The pH plays an important role in each process. Therefore, we have selected several pH levels to check the degradation of nitrobenzene with DBD. In separate experiments we have treated the NB having the pH levels of 2.6, 4.5, 7.4, 9.5, and 12.4. The results of these experiments are represented in Figure 2. These results show that the efficiency was highest at a pH level of 7.4, while it was lowest at 2.6 and 12.4. It revealed that the degradation efficiency was improved as we move from acidic to neutral or basic to neutral conditions. In other words it can be said that the degradation efficiencies are higher at neutral pH levels and are also reasonable at slightly acidic or slightly basic conditions.
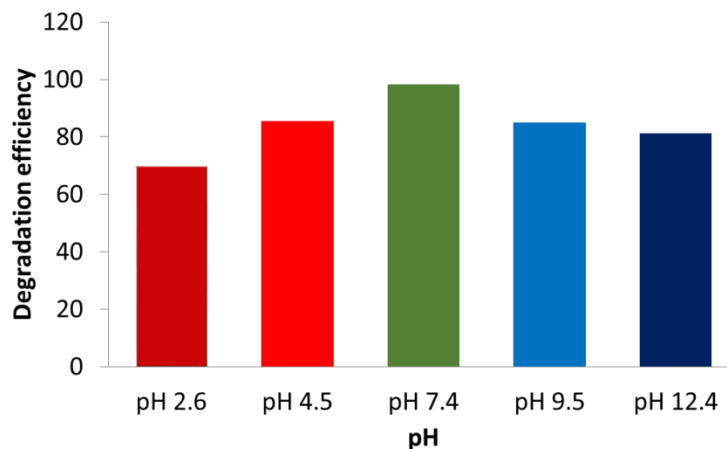
Figure 2: Effect of pH on the degradation efficiency of NB

1st International Conference on Advances in Civil & Environmental Engineering, University of Engineering & Technology Taxila, Pakistan

Conference date 22 &23 Feb 2022

Similar results were presented by several other studies [20, 21]. This research gives a clear guide for the pH values for the degradation of NB in wastewaters. Furthermore, this technique can also be implemented for the degradation of several other types of organic pollutants.

4   CONCLUSION

The treatment of pollutants from industrial wastewaters requires specific pH levels for their efficient degradation. In this research the effect of pH on the degradation of NB in wastewater was evaluated by using a DBD reactor. The findings of this research conclude that the neutral pH levels are the most favourable conditions for the treatment of NB in wastewater. The findings of this research would help the researchers, the industrialists and the treatment organizations to treat the NB and also other organic pollutants at a specific and optimum pH levels.

5   ACKNOWLEDGEMENTS

REFERENCES

1.   Chen, H., et al., *Contamination characteristics, ecological risk and source identification of trace metals in sediments of the Le'an River (China).* Ecotoxicology and Environmental Safety, 2016. **125**: p. 85-92.
2.   Kiguchi, O., G. Sato, and T. Kobayashi, *Source-specific sewage pollution detection in urban river waters using pharmaceuticals and personal care products as molecular indicators.* Environmental Science and Pollution Research, 2016. **23**(22): p. 22513-22529.
3.   Andreozzi, R., et al., *Advanced oxidation processes (AOP) for water purification and recovery.* Catalysis Today, 1999. **53**(1): p. 51-59.
4.   Bogaerts, A., et al., *Gas discharge plasmas and their applications.* Spectrochimica Acta Part B: Atomic Spectroscopy, 2002. **57**(4): p. 609-658.
5.   Locke, B., et al., *Electrohydraulic discharge and nonthermal plasma for water treatment.* Industrial & engineering chemistry research, 2006. **45**(3): p. 882-905.
6.   Tscharntke, T., et al., *Landscape perspectives on agricultural intensification and biodiversity–ecosystem service management.* Ecology letters, 2005. **8**(8): p. 857-874.
7.   Deng, Y. and R. Zhao, *Advanced Oxidation Processes (AOPs) in Wastewater Treatment.* Current Pollution Reports, 2015. **1**(3): p. 167-176.
8.   Xu, G.-M., Y. Ma, and G.-J. Zhang, *DBD plasma jet in atmospheric pressure argon.* IEEE Transactions on Plasma Science, 2008. **36**(4): p. 1352-1353.

1st International Conference on Advances in Civil & Environmental Engineering, University of Engineering & Technology Taxila, Pakistan

Conference date 22 &23 Feb 2022

9. Nawaz, M.I., et al., *A study of the Performance of dielectric barrier discharge under different conditions for nitrobenzene degradation.* 2019. **11**(4): p. 842.
10. Liu, C., et al., *Comparative study on the effect of RF and DBD plasma treatment on PTFE surface modification.* Materials Chemistry and Physics, 2004. **85**(2): p. 340-346.
11. Ren, C.-S., et al., *Surface modification of PE film by DBD plasma in air.* Applied surface science, 2008. **255**(5): p. 3421-3425.
12. Kuai, P.-y., C.-j. Liu, and P.-p. Huo, *Characterization of CuO-ZnO catalyst prepared by decomposition of carbonates using dielectric-barrier discharge plasma.* Catalysis letters, 2009. **129**(3-4): p. 493-498.
13. Hopkins, A. and B. Holz, *Grassland for agriculture and nature conservation: production, quality and multi-functionality.* Agronomy research, 2006. **4**(1): p. 3-20.
14. Mok, Y.S. and J.-O. Jo, *Degradation of organic contaminant by using dielectric barrier discharge reactor immersed in wastewater.* IEEE Transactions on Plasma Science, 2006. **34**(6): p. 2624-2629.
15. Hu, Y., et al., *Application of dielectric barrier discharge plasma for degradation and pathways of dimethoate in aqueous solution.* Separation and Purification Technology, 2013. **120**: p. 191-197.
16. Liu, Y., et al., *Treatment of aniline contaminated water by a self-designed dielectric barrier discharge reactor coupling with micro-bubbles: optimization of the system and effects of water matrix.* Journal of Chemical Technology & Biotechnology. **0**(0).
17. Nawaz, M.I., et al., *Experimental study of nitrobenzene degradation in water by strong ionization dielectric barrier discharge.* 2021. **42**(5): p. 789-800.
18. Cui, S., et al., *Adsorption properties of nitrobenzene in wastewater with silica aerogels.* Science China Technological Sciences, 2010. **53**(9): p. 2367-2371.
19. Xia, K., F. Xie, and Y. Ma, *Degradation of nitrobenzene in aqueous solution by dual-pulse ultrasound enhanced electrochemical process.* Ultrasonics sonochemistry, 2014. **21**(2): p. 549-553.
20. Yin, W., et al., *Experimental study of zero-valent iron induced nitrobenzene reduction in groundwater: The effects of pH, iron dosage, oxygen and common dissolved anions.* Chemical engineering journal, 2012. **184**: p. 198-204.
21. Wu, C.-Q., D.-T. Fu, and X. Chen, *Nitrobenzene degradation by micro-sized iron and electron efficiency evaluation.* Chemical Papers, 2014. **68**(10): p. 1350-1357.

1st International Conference on Advances in Civil & Environmental Engineering, University of Engineering & Technology Taxila, Pakistan

Conference date 22 &23 Feb 2022

Comparative Analysis of Inflows calculated from Remote Gauging Station and Gridded Precipitation data sets with Observed Inflow

(A Case Study of Pindiali Small Dam District Mohamad, Khyber Pakhtunkhwa, Pakistan)

Zafar Ullah Khan, Mujahid Khan, Salah Ud Din
University of Engineering & Technology Peshawar, Pakistan
cezafar1@gmail.com; mujahidkhan@uetpeshawar.edu.pk

ABSTRACT

Hydrology plays a key role in the design of any hydraulic structures. Hydraulic structures are usually designed for certain return period. If a recorded gauged flow/discharge data is available for a certain area, flood can be estimated for various return periods. However, if the discharge data is missing/not available then the inflow is estimated from the rainfall data. In this research study an effort has been made to compare onsite observed inflows, with the inflows estimated from Peshawar gauging station (being the nearest) and from gridded precipitation data set for Pindiali small reservoir catchment. Pindiali Small Dam site, located in District Mohmand, Khyber Pakhtunkhwa, Pakistan was selected for the case study because of low density of meteorological station gauge in Pakistan. Soil Conservation Service -Curve Number method is used for gauged rainfall data. SCS Curve number method is simple and many researchers prefer this model for small watersheds [1]. Inflows from gridded precipitation data were estimated using Soil and Water Assessment Tool (SWAT). Average observed inflow at the dam site was 35.97 AF, whereas the calculated values were 619.50 AF and 34.02 AF using SCS method and gridded precipitation data, respectively. It is concluded that the average observed inflow is closely estimated by the gridded data set.

KEYWORDS: Gauged inflow, SCS curve number, gridded data, arc SWAT

1   INTRODUCTION

Data gauges for recording runoff flows is always a limiting factor especially in developing countries like Pakistan. There are many basins in the country where measuring gauges not installed. In the absence of recording inflow gauge stations, alternative methods are used to estimate runoffs. The objective of this research was to compare recorded inflows, inflows estimated from recorded rainfall and inflows from gridded precipitation data set. The most widely used method by the design consultants and hydrologists in the Province of KP for calculating runoff from recorded rainfall is Soil Conservation Service -Curve Number method. In this method the initial abstraction ratio (λ) is usually assumed to be 0.2 [2]. However, the initial abstraction

1st International Conference on Advances in Civil & Environmental Engineering, University of Engineering & Technology Taxila, Pakistan

Conference date 22 &23 Feb 2022

ratio must be calibrated for a watershed having rainfall-runoff data because this value varies from watershed to watershed [3].

2   METHODOLOGY

Pindiali Small Dam is located towards North-West at a distance of 64 km from the provincial capital Peshawar, Khyber Pakhtunkhwa, Pakistan. Coordinates of the dam site are 34°23'13.09"N and 71°27'24.78"E and catchment area is 17.00 sq. miles (44.00 sq.km). The catchment area is generally barren and hilly. The catchment area is having two distinct streams namely Nao khwar running from North and China Nao khwar running from West side. The Nao khwar is the main stream having longer path. The streams originate from barren hills at an elevation of about 1530 and 1500 meters. The length of main stream in the catchment is 9.90 km. The bed slope of the stream is 1 in 43 (2.32 %). Daily rainfall data for Peshawar was collected from Pakistan Meteorological Department Peshawar for a period covering August, 2017 to December, 2018. Era-Interim gridded data was used for this period which was downloaded from European Centre for Medium-Range Weather Forecasts [4]. Soil data of Pindiali small dam was downloaded from Food and Agriculture Organization (FAO) Website [5]. Global Cover land use data was downloaded from the European Space Agency [6]. Digital elevation Model was downloaded from the CGIAR Consortium for Spatial Information (CGIAR-CSI) [7]. Digital elevation model, land use map, soil data and gridded data set has been used in the Arc SWAT model and is shown in figure 1. Arc SWAT developed by Dr. Jeff Arnold for the USDA Agricultural Research Service (ARS).
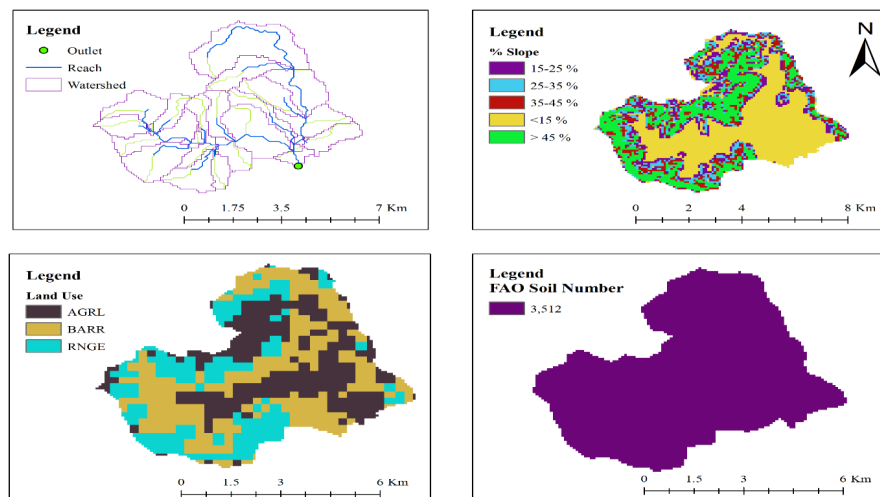
Figure 1. Land use soil and slope map of catchment

1st International Conference on Advances in Civil & Environmental Engineering, University of Engineering & Technology Taxila, Pakistan

Conference date 22 &23 Feb 2022

3   RESULT AND DISCUSSIONS

Inflow at the reservoir were recorded by noting level of reservoir on daily basis. Based on the levels, inflows were calculated using area capacity curve. During the period from August 2017 to December 2018, ten events of flood took place. The maximum inflow was recorded in the month of July, 2018 having inflows of 191.20 AF. The inflows corresponding to these events are shown in Figure 2.
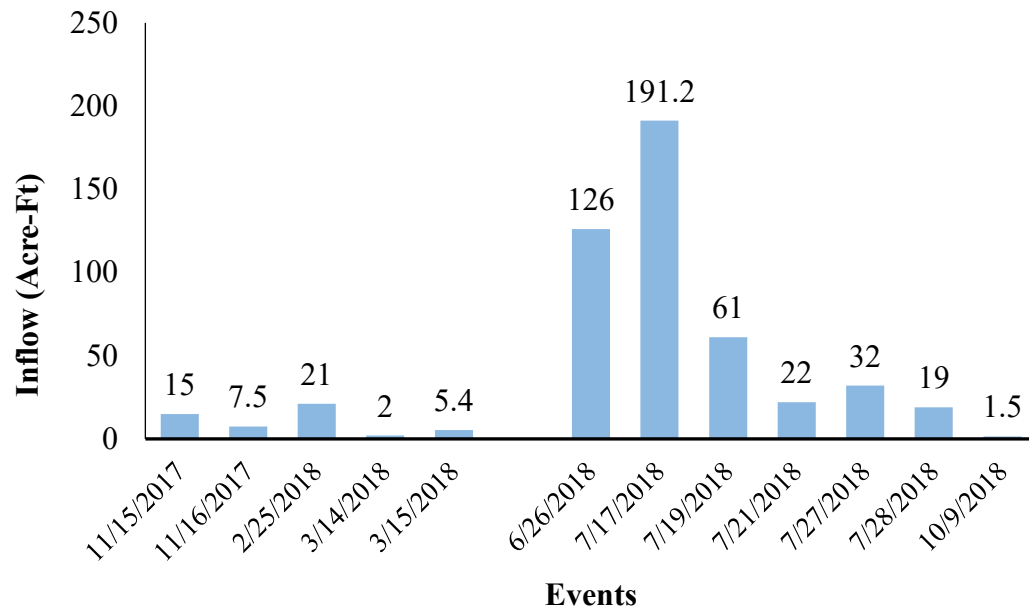
Figure 2:   Inflow at the dam site from observed data

In the SCS curve number method, daily rainfall data (peshawar station) was used to estimate inlfows to the reservoir. Only four events of rainfall created runoff. The results are shown in Figure 3. The maximum inflow was calculated in the month of November, 2017 and July, 2018, having inflows of 1026 AF.

1st International Conference on Advances in Civil & Environmental Engineering, University of Engineering & Technology Taxila, Pakistan

Conference date 22 &23 Feb 2022
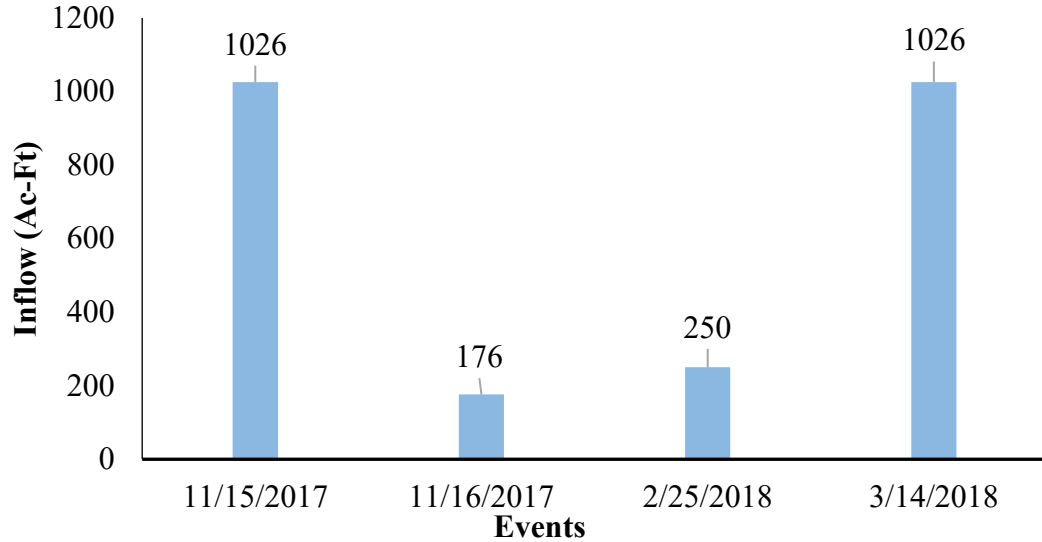
Figure 3: Inflow at some particular days corresponding to the rain event from climate station

The inflow was also calculated from the gridded data using arc SWAT tool which is an extension of ArcMap. The results of these flows are shown in Figure 4. The maximum inflow was noted in the month of May, 2018, having inflows of 107.31 AF.
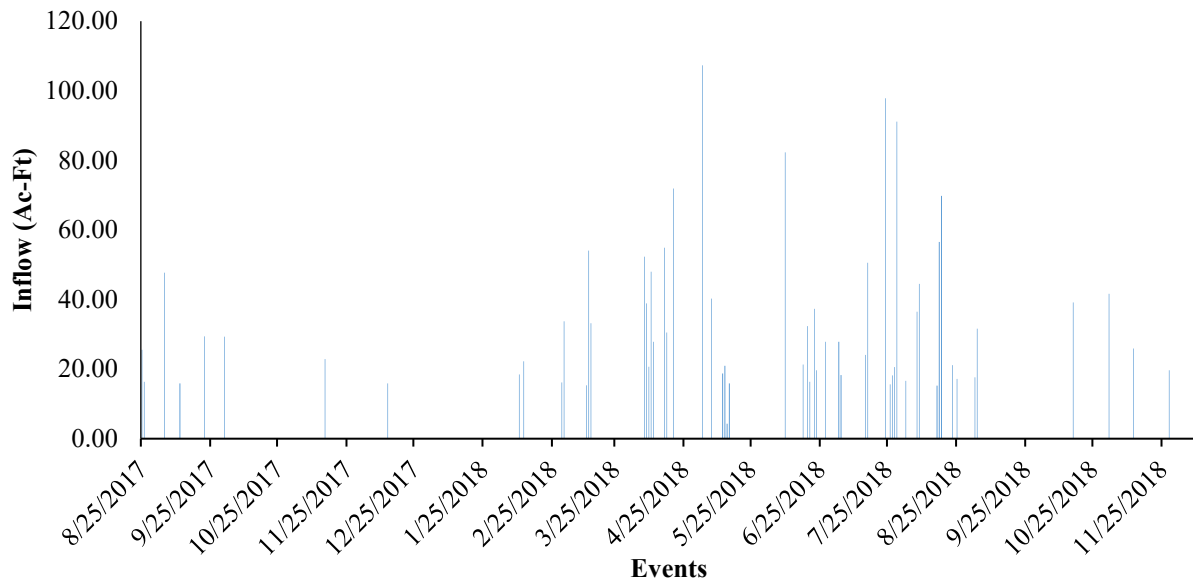
Figure 4:   Daily Inflow at Dam Site from Gridded Data

1st International Conference on Advances in Civil & Environmental Engineering, University of Engineering & Technology Taxila, Pakistan

Conference date 22 &23 Feb 2022

3.1 Comparison of Monthly Inflows, Calculated from Observed on Site, Gauging station data and Estimated from Gridded precipitation Data Set

Monthly inflow generated for Pindiali small dam for the above three methods are shown in Figure 5. Average inflows at the dam site was 35.97 AF whereas the estimated values using gauged and gridded precipitation data were 619.50 AF and 34.02 AF respectively.
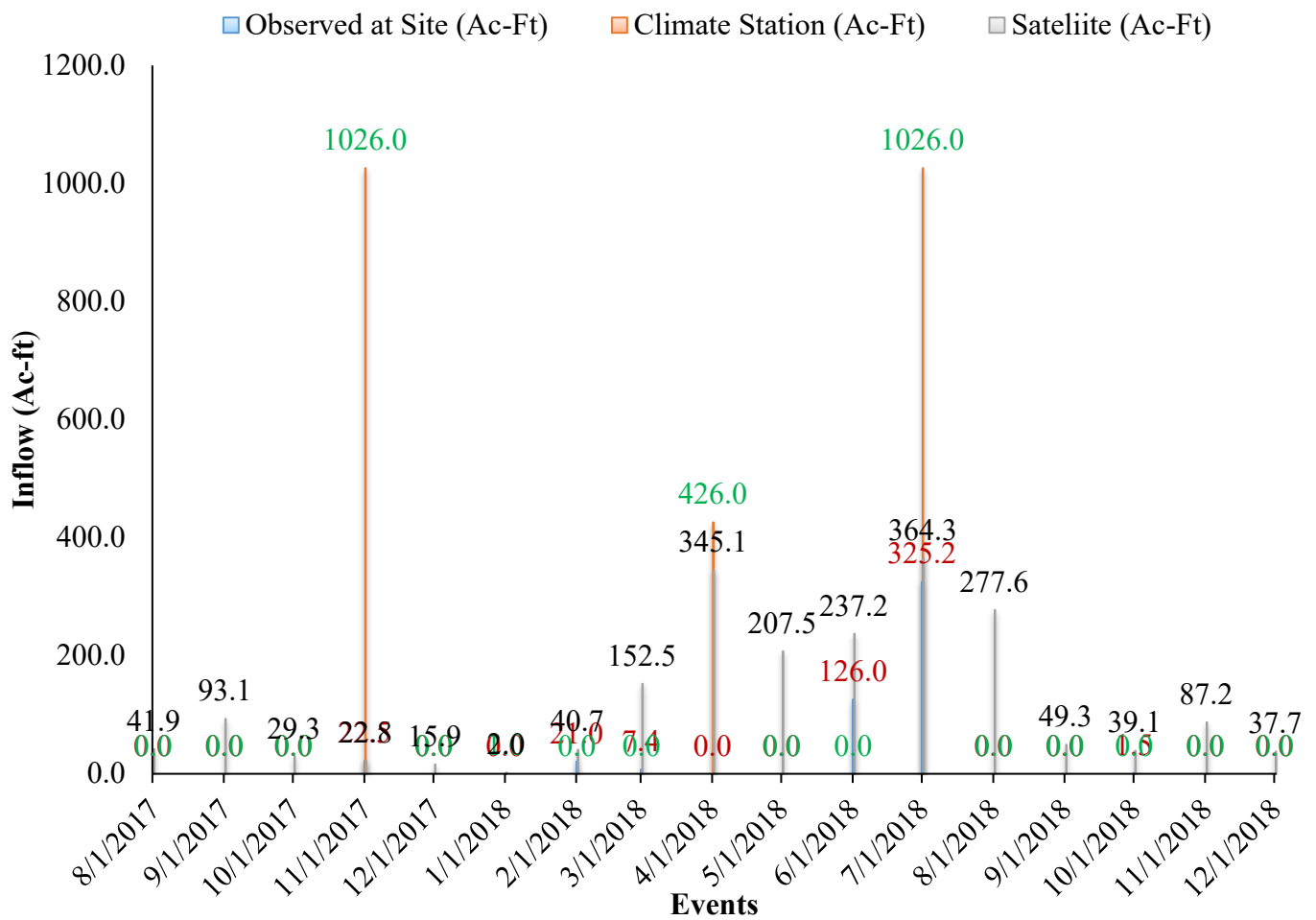
Figure 5:   Monthly Flow at Pindiali Dam site

1st International Conference on Advances in Civil & Environmental Engineering, University of Engineering & Technology Taxila, Pakistan

Conference date 22 &23 Feb 2022

4   CONCLUSIONS

Monthly recorded average inflows at the dam site was 35.97 AF and the estimated values using gauged and gridded precipitation data were 619.50 AF and 34.02AF respectively. Hence, the flow calculated from gridded data source is in close agreement with the observed value.

5   ACKNOWLEDGEMENTS

Web-1: http://apps.ecmwf.int/datasets/data/interim-full-daily
Web-2: http://www.fao.org/soils-portal/soil-survey/soil-maps-and-databases/faounesco-soil-map-of-the-world/en/
Web-3: http://due.esrin.esa.int/page_globcover.php
Web-4: http://srtm.csi.cgiar.org

6   REFERENCES

1. V. P. S. Surendra Kumar Mishra, "Another look at SCS-CN Method," Journal of Hydrologic Engineering, no. 4, pp. 257-264, 1999.
2. A. T. H. Victor Mockus, National Engineering Handbook, Washington, DC: Natural Resources Conservation Services, 2004.
3. V. P. S. Surendra Kumar Mishra, "A re-look at NEH-4 curve number data and antecedent moisture condition criteria," Hydrol. Processes, vol. 20, no. 13, pp. 2755-2768, 2006.

On Field Regulation and Optimization of Irrigation Water for Kharif Crops

Ali Raza, Afzal Ahmed
University of Engineering & Technology Taxila, Pakistan
University of Engineering & Technology Taxila, Pakistan
ali.raza3@students.uettaxila.edu.pk; afzal.ahmed@uettaxila.edu.pk

Ghufran Ahmed Pasha
University of Engineering & Technology Taxila, Pakistan
ghufran.ahmed@uettaxila.edu.pk

ABSTRACT

The prudential utilization of surface water remains one of the most vital contributions made to society by civil engineers that is imparting a crucial and extensive role in crop growth. The optimization of existing water resources is of prime importance, by keeping in view the water scarcity issue, to enhance the agricultural yield of a country, especially at canal tails. In this study, it is discussed that how a prudent and effective use of existing irrigation system will optimize the agriculture yield. The study was carried out to check the effects of water levels, at head reaches of canal, at crop yield. It was analysed that as discharge value increases difference between average crop yield of overall canal reach and crop yield at tails decreases. The efficiency of canals will be enhanced by using emendated irrigation schedule for better and ameliorated outcomes at canal tails. The emended irrigation schedule as well as the consideration of cropping pattern will impart its role to enhance the efficiency of canals, ultimately resulting into more productivity.

KEYWORDS: Tail Running Distance, Crop Yield, Irrigation Schedule, Kharif Season

1   INTRODUCTION

The population of the world is increasing day by day that requires an additional demand of water will also be required creating stress on water resources [1]. A study, conducted by the International Food Policy Research Institute (IFPRI), on water productivity summarized that cereals production increases due to the basin efficiency. The major contribution to enhance the crop yield was due to the improvement of the efficiency [2]. Quantitating the region wise demand of irrigation water and consideration of temporal and spatial characteristics, are of great importance to embellish substantial use of existing irrigation resources [3]. The optimum application of irrigation water has direct contrast with the well-established fact that different regions have different needs and conditions [4]. The key problem and obstacle among the selection of the right strategy is the requirement of crop yield quality vis-à-vis quantity in the existing cropping pattern [5]. It is also required to grow crops which produce enough yield in response to the available water using sustainable irrigation management [6]. In 2000, Kofi Annan, then the UN Secretary General, declared that the world needs a Blue Revolution to generate approximately 40-45% share of the

1st International Conference on Advances in Civil & Environmental Engineering, University of Engineering & Technology Taxila, Pakistan

Conference date 22 &23 Feb 2022

food around the globe [7]. Cotton yield can be significantly enhanced by effective irrigation supply at regular intervals [8]. In the Indo-Pak region, almost all canals are 'supply controlled' rather than to be 'demand controlled'. The difference was determined between adequate irrigation and inadequate irrigation [9]. Crop yield is low at tails as irrigators get low discharge. This can be improved by adopting proper irrigation scheduling, cropping pattern, and embellishing water productivity [10].

In this study, effect of authorized supply of irrigation water on agricultural yield specifically for Kharif Crops i.e., Cotton, Rice, and Sugarcane is analysed. A suitable strategy is developed to overcome the problems of irrigation scheduling and to drive methodology to overcome tail water shortage. Command area of Dajal Branch was selected for this purpose that takes off from D.G. Khan Canal at Tail Running Distance (TRD) 345230 ft. DG Khan canal originates from Taunsa Barrage which regulates the flow of Indus River and feeds the culturable command area (CCA) of 2.1 million acres.

2 METHODOLOGY

The key concern of this study is to achieve a sustainable irrigation approach. This study was adopted to monitor the effects of water levels on crop yield in the South region of Punjab, Pakistan.

2.1 Data Collection

The daily discharge data of Dajal Branch was collected. The annual average discharge data (Kharif Season) was determined by gauging stations installed at head reaches of canals.

2.2 Cropping Pattern in D.G Khan

The region observes arid climate having low rainfall (below 200 mm annual) and high solar radiation over most parts of the land. Irrigation is essential as the crops in the region cannot be grown with the available rainfall. There are different variety of crops grown in D.G Khan area; however, Kharif Season Crops (Cotton, Rice, and Sugarcane) were discussed in this study.

2.3 Development of Correlation

Climate change and consistent population growth have over-stressed the existing irrigation schedule. In this regard, a correlation was developed between average yield of Kharif Crops and the yields of the same crops at the Canal Tails versus Head Discharge. The seasonal discharge data was compared with the crop yield data. The data is comprised of 10 years from 2011 to 2020.

3 RESULTS AND DISCUSSION

3.1 Tail Shortage

The farmers, having agricultural land at tails of canals, do not get sufficient share of water; it causes a significant impact on crop production. Dajal branch was fed with maximum discharge in 2019

1st International Conference on Advances in Civil & Environmental Engineering, University of Engineering & Technology Taxila, Pakistan

Conference date 22 &23 Feb 2022

i.e., 1229.25 cusec while minimum discharge occurred in 2015 i.e., 988.82 cusec. Figure 1 represents the sugarcane yield versus the average discharge. It is evident that minimum discharge occurred in 2015, during 2011 to 2020, that resulted into the lowest yield i.e., 710 mds/acre (1 mds = 40 kg) while at tails it was 675 mds/acre, leaving a difference of 35 mds/acre. On the other hand, highest discharge occurred in 2019 that resulted in highest yield i.e., 1035 mds/acre while yield at tails was 1025 mds/acre, leaving a difference of 10 mds/acre. A similar fate was shared by the cotton crop as maximum cotton yield was 26.95 mds/acre (2019) while the yield at tails was 25.25 mds/acre for the same year. It is evident from figure 2 that difference between average yield and yield at tails fell from 3.7 mds/acre (2015) to 1.7 mds/acre (2019) for cotton. Figure 3 entails the same for Rice crop as difference between average yield and yield at tails fell from 3.25 mds/acre (2015) to 1.2 mds/acre (2019). Hence, it was observed that the yield at tails approaches to average yield value as average discharge value increases. The difference between the average crop yield (throughout the canal reach) and yield at tails (at the last RD's of far-off minors) decreases as discharge distribution is ensured throughout the canal reach uniformly.
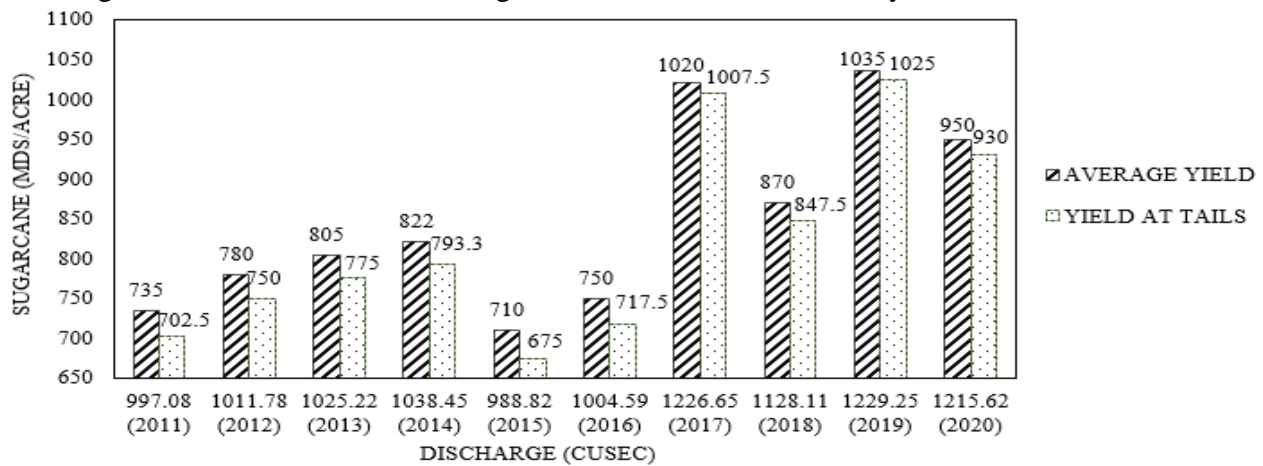
Fig. 1: Sugarcane Average Yield and Yield at Tails Vs Average Head Discharge at Dajal Branch
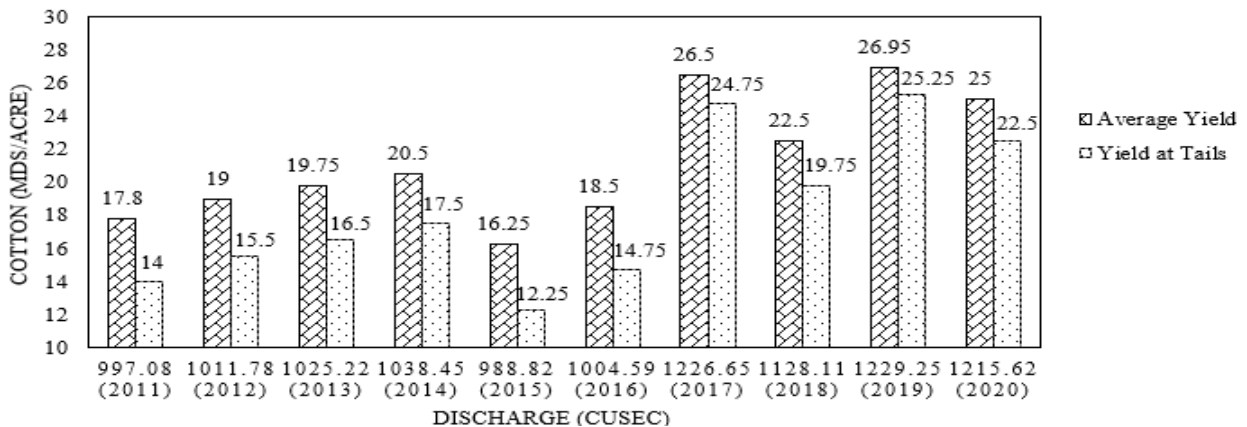
Fig. 2: Cotton Average Yield and Yield at Tails Vs Average Head Discharge at Dajal Branch

1st International Conference on Advances in Civil & Environmental Engineering, University of Engineering & Technology Taxila, Pakistan

Conference date 22 &23 Feb 2022
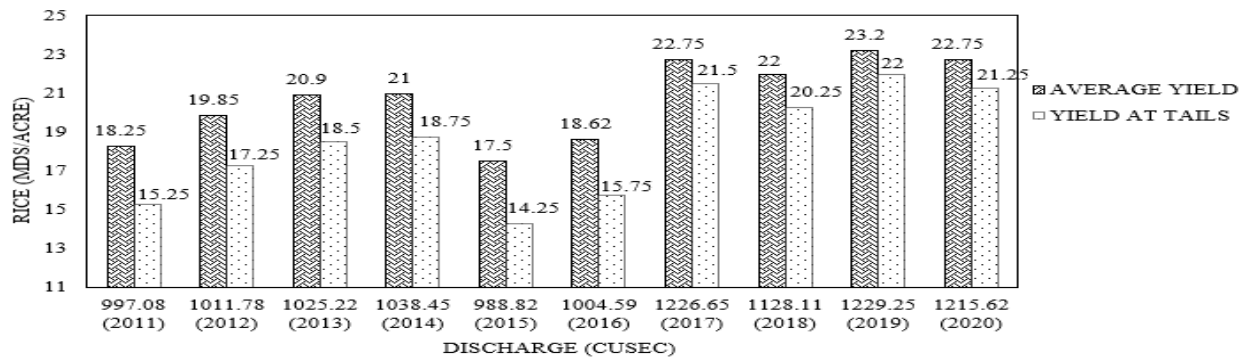
Fig. 3: Rice Average Yield and Yield at Tails Vs Average Head Discharge at Dajal Branch

3.2 Optimization of Irrigation System

The purpose of the study was to identify the sections of the command area that is getting lower number of waterings than proportioned. It was observed that thoroughly distribution of irrigation minors will result in higher productivity as evident from figure 1, figure 2, and figure 3. It shows that indicates that minors that takes off from canal tails were able to withdraw adequate water supply to nourish the crop plants as they were able to get more no of waterings which ultimately improved efficiency of irrigation system. The yield will be further enhanced and optimized through proper rotation and fully transferring water to the tail ends of minors.
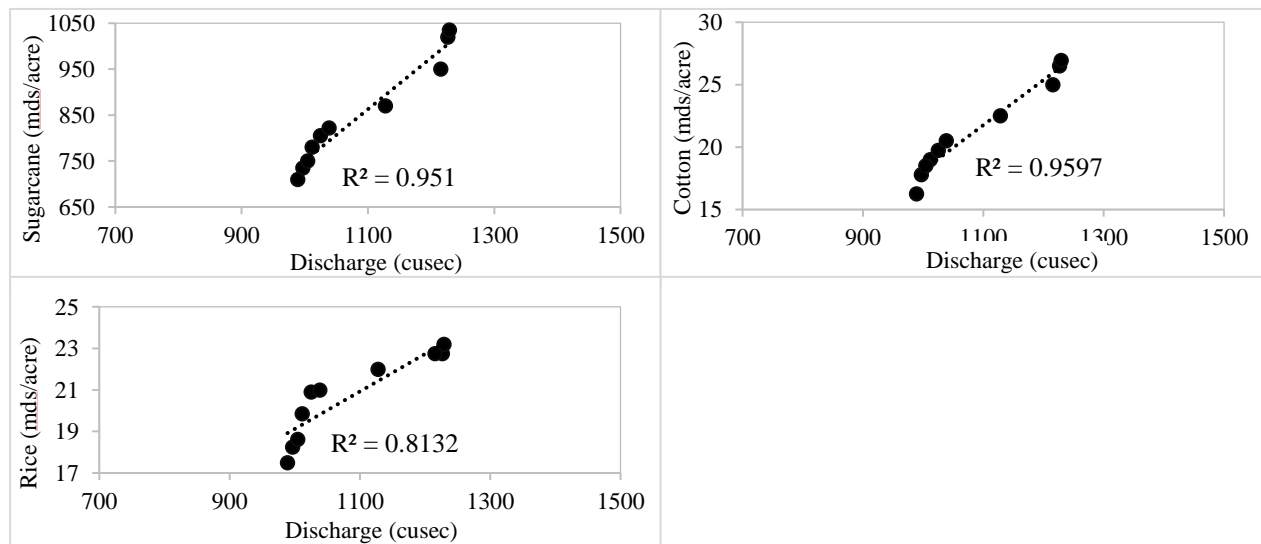
Fig 4: Linear Regression Analysis: Sugarcane, Cotton, and Rice

$$Ys = \mathbf{1.1182}\, Q - 367.2 \quad ; R^2 = 0.951 \tag{1}$$

$$Yc = \mathbf{0.0361}\, Q - 17.939 \quad ; R^2 = 0.9597 \tag{2}$$

1st International Conference on Advances in Civil & Environmental Engineering, University of Engineering & Technology Taxila, Pakistan

Conference date 22 &23 Feb 2022

$$Yr = \mathbf{0.018\ Q} + 1.0761\ ;\ R^2 = 0.8132 \tag{3}$$

Here Ys represents average Sugarcane yield, Yc indicates average cotton yield, and Yr represents average Rice yield while Q represents discharge that is constant for all cases due to same canal i.e., Dajal Branch. The above equations were derived using linear regression analysis as shown in figure 4.

4   CONCLUSION

The available crop data was analysed with respect to the discharge in the canal. It was revealed by the figures that the difference among average crop yield and crop yield at the tail of the same canal was less as discharge was increased. The regression analysis was performed between discharge and average yield of Sugarcane, cotton, and rice which resulted into higher values of R^2 that indicated that the relation between average yield and discharge supplied though out the Kharif season is very close. Hence, the upgradation of irrigation schedule as well as adequate discharge supply will result in higher productivity.

REFERENCES

1. Zahra, M. B., Aftab, Z. E. H., & Haider, M. S. (2021), *Water productivity, yield and agronomic attributes of maize crop in response to varied irrigation levels and biochar–compost application*. Journal of the Science of Food and Agriculture.
2. Yazar, A., Sezen, S. M., Gencel, B., & Bozkurt-Colak, Y. (2006), Country Report: *Water use efficiency of major crops in Turkey*.
3. Vogeler, I., Thomas, S., & Van Der Weerden, T. (2019). *Effect of irrigation management on pasture yield and nitrogen losses*. Agricultural Water Management, **216**, 60-69.
4. Knox, J. W., Kay, M. G., & Weatherhead, E. K. (2012). *Water regulation, crop production, and agricultural water management — Understanding farmer perspectives on irrigation efficiency.* Agricultural water management, **108**, 3-8.
5. Padilla-Díaz, C. M., Rodriguez-Dominguez, C. M., Hernandez-Santana, V., Perez-Martin, A., Fernandes, R. D. M., Montero, A., ... & Fernández, J. E. (2018). *Water status, gas exchange and crop performance in a super high density olive orchard under deficit irrigation scheduled from leaf turgor measurements.* Agricultural Water Management, **202**, 241-252.
6. Parry, M. A. J., Flexas, J., & Medrano, H. (2005). *Prospects for crop production under drought: research priorities and future directions.* Annals of Applied Biology, **147**(3), 211-226.
7. Döll, P., & Siebert, S. (2002). *Global modeling of irrigation water requirements*. Water resources research, **38**(4), 8-1.
8. Onder, D., Akiscan, Y., Onder, S., & Mert, M. (2009). *Effect of different irrigation water level on cotton yield and yield components.* African Journal of Biotechnology, **8**(8).
9. C. Taylor. (1980). *Economic analysis to support irrigation investment and management decesions*. Report of a Planning Workshop on Irrigation Management.
10. Wade, R. (1980). *Access to the irrigation department: the tail-end problem under South Indian irrigation canals*. Indian Journal of Public Administration, **26**(2), 359-377.

1st International Conference on Advances in Civil & Environmental Engineering, University of Engineering & Technology Taxila, Pakistan

Conference date 22 &23 Feb 2022

Estimation of passenger car unit on undivided roads in Pakistan

Syed Muhammad Muzammil Zia, Dr. Jawad Hussain
University of Engineering & Technology Taxila, Pakistan
engrmuzammilzia@gmail.com; jawad.hussain@uettaxila.edu.pk

ABSTRACT

The maximum numbers of roads in Pakistan are undivided (two-way roads). Due to the poor economic situation and increase in poverty, the government of Pakistan is fewer funds to construct one-way roads. There are many vehicles (small cars, large cars, rickshaws, motorbikes, buses, multi-axle trucks, and tractor-trailers) moving on these roads at the same time. So it is a big problem for a traffic engineer to analyze these mixed traffic compositions. Passenger car unit (PCU) is a common approach to convert the different traffic compositions into similar traffic compositions. When we do analysis of PCU value on different road widths, this study attempts to convert all types of vehicles into equal numbers of vehicles. Data are collected at different national, provincial and districts highways in Pakistan. The output proves that PCU for a vehicle changes with change in traffic volume, traffic composition, traffic moves in one or two-way direction, and the road width. In this study, we use a speed-based method to determine the PCU values. By this method, the value of PCU is largely affected by the speed of the vehicle and the area covered by the vehicle. This paper explains how the volume of traffic, traffic composition on a road, road width, and movement of traffic in one or two ways can affect the average PCU value for different vehicles. For example the average PCU value for bus changes from 7.67 to 4.24. All these effects are summarized in this document.

KEYWORDS: Passenger car unit, Traffic composition, Traffic volume, Road width

1 INTRODUCTION

Roads in Pakistan are classified as motorways, national highways, provincial highways, and district roads. The motorway is a network of roads that consist of multiple lanes, one-way and high speed roads. The total length of functional motorways in Pakistan is 2570 km. According to the ministry of communication total length of national highways in Pakistan is 12130 km [7]. According to the ministry of communication of Punjab province total length of provincial highways is more than 40000 km. Maximum national, provincial, and districts roads in Pakistan are undivided roads. Due to lack of funds, the government is not eligible to construct one-way roads (divided roads) [8]. On two-way roads, the driver is highly disturbed by the opposite side of the vehicle. This disturbance is increased at night time due to opposite side vehicle lights [5]. And another basic issue in the analysis of traffic flow on highways in Pakistan is the different sizes of vehicles moving on the road at the same time. The operating situation on a highway becomes difficult when all these vehicles of different categories move on the same highway without any separation [2]. Motorbikes enter into the gaps between heavy traffic vehicles (HTV)

1st International Conference on Advances in Civil & Environmental Engineering, University of Engineering & Technology Taxila, Pakistan

Conference date 22 &23 Feb 2022

and become the operating condition poor [4]. Passenger car unit (PCU) is an approach to convert the different traffic compositions into similar traffic compositions [6]. This paper explains how the value of PCU for the same vehicle changes when it travels on motorways (one-way road), national highways, provincial highways (two-way road), or district road (two-way road).

2 RESEARCH METHODOLOGY

The present study used a speed-based method for calculating the PCU value of different vehicle. This method is very effective for heterogeneous traffic [6]. According to this method equation, the PCU value is higher when the velocity of the vehicle is low and the area of vehicle is large. In this study, we take Suzuki Meharan as a standard passenger car. To calculate the value of passenger car unit for vehicle 'r' in terms of per hour equation is given below.

$$PCU_r = \frac{Vs}{Vr} \times \frac{Ar}{As}$$

Vr = mean speed of vehicle 'r' ; Vs = mean speed of the standard car
Ar = rectangular area of vehicle type 'r' ; As = rectangular area of the standard car

3 DATA COLLECTION AND EXTRACTION

Data for this research was collected at one motorways section (divided roads), two national highways sections (one section is divided and other is undivided roads), five provincial highways sections (undivided roads), and two district roads (undivided roads). The width shown in table excludes the shoulder width. The details of the selected section are given in table 1.

Table 1 displays ten sections of highways

Section Number	Highway Section Detail	Road Width (m)
1	Multan to Sukkur motorway (M-5) near to Shujaabad (one-way) one side	11.35
2	Torkham to Karachi national highway (N-5) near to Multan (one-way) one side	8.25
3	Peshawar to Hyderabad national highway (N-55) near to DG khan (two-way)	8.5
4	Muzaffargarh to Mianwali road (MM Road) near to Chowk azam (two-way)	8.25
5	Multan to Layyah provincial highway near to head Muhammad wala (two-way)	8.15
6	Muzaffargarh to Jhang road Provincial highway near to Muzaffargarh (two-way)	8
7	Layyah to DG khan road near to Kot sultan (two-way)	7.85
8	Multan to Vehari road near to 14 kassi (two-way)	7.75
9	Shujaabad to Jalalpur road near to Peer gaib (two-way)	7.5
10	Gailywal to Jalal pur road near to baloch mor (two-way)	4.5

We observed the different types of vehicles (Meharan cars, xli cars, rickshaws, motorbikes, vans, buses, multi-axle trucks and tractor-trailers etc) on these ten sections. All of these vehicles can be divided into eight different categories. So values of PCU for all other vehicles are derived from this car. For the determination of PCU value, we calculate the projected area of each vehicle.

1st International Conference on Advances in Civil & Environmental Engineering, University of Engineering & Technology Taxila, Pakistan

Conference date 22 &23 Feb 2022

This is average vehicle area which calculated here. The detail of these vehicle categories and vehicle area ratio to standard car are given in table 2.

Table 2 displays vehicle categories and area ratio to standard car to vehicle type

Vehicle category	Vehicle included	L (m)	W (m)	Area (sq.m)	Area ratio to Standard car to vehicle type (As/Ar)
Standard car (SC)	Meharan, alto	3.3	1.41	4.653	1
Large car (LC)	XLI, GLI, Sportage	4.53	1.7	7.701	0.604207246
Motorbike (MB)	Motorcycle	1.88	0.81	1.5228	3.055555556
Rickshaw (RS)	Rickshaw	3	1.2	3.624	1.283940397
Light traffic vehicle (LTV)	Mini trucks and vans	4.84	1.88	9.0992	0.511363636
Heavy traffic vehicle (HTV)	Multi axle trucks	11.5	2.45	28.175	0.165146406
Bus	Bus and mini Buses	10.65	2.5	26.625	0.174760563
Tractor Trailers (TT)	Tractor and trailers	9.362	2.43	22.7497	0.204530529

We calculate the speed of the vehicle, composition of traffic, and volume of traffic from ten sections of highways. Speed of vehicle calculated with the help of digital speed meter. All other parameters like traffic composition and traffic volume are calculated manually. This data collection process had done in three days at each highway section from 8:30 AM to 6:30 PM. After calculation of speed of vehicle it divided with the speed of standard car then we get its ratio. This ratio of Vs/Vr is divided by the area ratio As/Ar to the standard car to vehicle type and gets the PCU value of the required vehicle. PCU value, average speed Vs/Vr values of different categories of vehicle, and traffic volume per hour are given in table 3.

Table 3 displays average speed ratio, PCU values of different vehicles and traffic volume

Section Number	Average speed values Vs/Vr								Traffic volume per hour	PCU VALUES							
	SC	LC	MB	RS	LTV	HTV	BUS	TT		SC	LC	MB	RS	LTV	HTV	BUS	TT
1	1	0.78			1.06	1.29	0.9		740	1	1.3			2.07	7.79	5.14	
2	1	0.78	1.4	1.75	1.08	1.37	0.88	2.33	610	1	1.29	0.46	1.36	2.11	8.32	5	11.4
3	1	0.82	1.38	1.86	1.07	1.44	0.96	2.6	570	1	1.36	0.45	1.45	2.09	8.75	5.46	12.7
4	1	0.79	1.27	1.82	1.09	1.41	0.9	2.58	490	1	1.32	0.41	1.42	2.13	8.54	5.13	12.7
5	1	0.78	1.24	1.84	1.1	1.36	0.86	2.19	458	1	1.29	0.41	1.43	2.15	8.23	4.94	10.7
6	1	0.73	1.31	1.67	1.12	1.22	0.81	1.96	410	1	1.21	0.43	1.3	2.2	7.41	4.62	9.63
7	1	0.72	1.18	1.68	1.13	1.18	0.74	1.93	401	1	1.2	0.39	1.31	2.21	7.16	4.24	9.44
8	1	0.71	1.06	1.56	1.11	1.22	0.79	2	416	1	1.18	0.35	1.22	2.17	7.39	4.54	9.8
9	1	0.69	1.2	1.58	1.07	1.32	0.8	1.75	327	1	1.14	0.39	1.23	2.08	8.03	4.59	8.58
10	1	0.77	1.18	1.74	1.15	1.74	1.34	2.35	291	1	1.28	0.38	1.36	2.24	10.5	7.67	11.5

1st International Conference on Advances in Civil & Environmental Engineering, University of Engineering & Technology Taxila, Pakistan

Conference date 22 &23 Feb 2022

4   DATA ANALYSIS AND DISCUSSION OF RESULTS

Figure 01 explains multi axel trucks (HTV), due to their large size compared to the standard cars, their PCU value is more than LC, LTV, and BUS. Another factor that effects on PCU value of the vehicle is road width. As many times road width increased value of PCU for LC, LTV, HTV, and BUS are also increased for two-way sections. But section number 10 (two-way section) for all vehicles LC, RS, LTV, HTV, BUS, TT and one way section only for LTV and HTV, this trend is opposite. For one way section the value of PCU for LC (1.29-1.3) and BUS (5-5.14) increase by increase of road width. If the traffic volume, road width and traffic composition will be the same for one-way and two-way traffic. The value of PCU for all vehicle categories will be greater for two way section as compared to one way section but only for BUS, this trend is the opposite. Because of BUS speed is more at motorway (one-way section) as compared to two-way section. Here its speed is dominating.
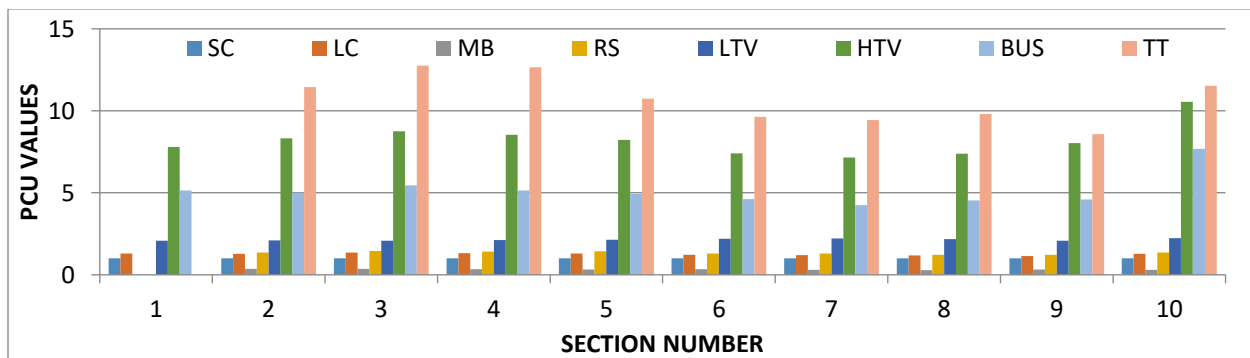
Figure 01 displays comparison of different categories of vehicle with different highways section.

PCU value is largely affected by traffic composition. In this study, section 10 (4.5 m road width) has a maximum number of motorbikes, here the PCU value of BUS(7.67), LTV(2.24), TT(11.5), and HTV(10.5) are maximum as compared to remaining all other sections. Because of different traffic composition (motorbikes are 41.2 % here) smaller the road width but the maximum value of PCU for almost all types of vehicles.
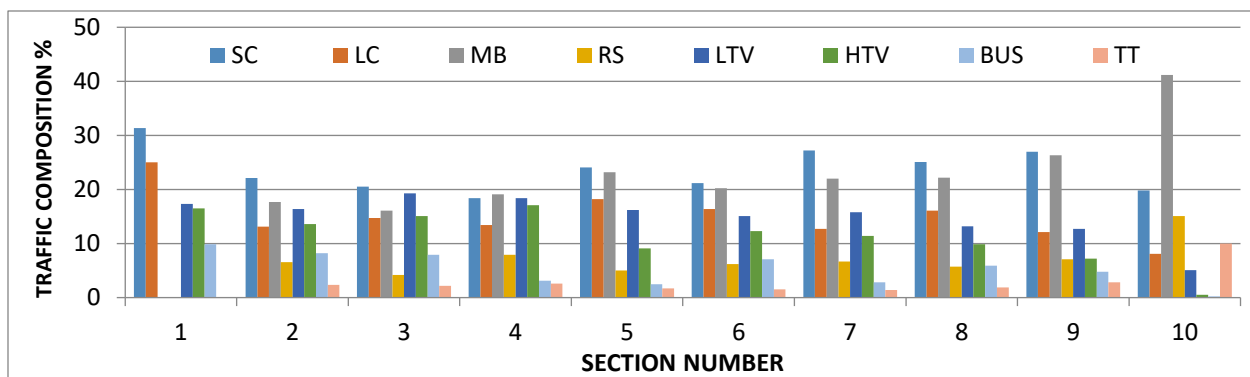
Figure 02 displays traffic composition on all ten sections of highways.

1st International Conference on Advances in Civil & Environmental Engineering, University of Engineering & Technology Taxila, Pakistan

Conference date 22 &23 Feb 2022

5   CONCLUSION

The results show that the PCU of a vehicle changes with change in traffic volume, traffic composition, traffic flow is one or two-way and road width. On two ways roads, driver is highly disturbed by the opposite side of the vehicle. This disturbance is increased at night time due to opposite side vehicle lights. The value of PCU for all vehicle categories will be greater for two way section as compared to one way section but only for BUS, this trend is the opposite. Because of BUS speed is more at motorway (one-way section) as compared to two-way section. Here its speed is dominating. PCU value of LC for one way section (1.3, 1.29) is decreased when road width decreased, and also for two way section this trend will be the same for LC (1.36, 1.32). It also depends upon the traffic composition. PCU value for LC on section 6 to 9 is less due to different traffic compositions. Here the size of the vehicle is dominating. Road width also affects the PCU value of all types of vehicles. We can say that if wider the road, the more congested freedom will be and extra space for vehicles to maintain their maximum velocity. Values of PCU for LC, HTV, and BUS are increased by increasing the road width. But this trend becomes opposite for smaller congested roads of the village. Because, in section number 10 PCU value of all these vehicles is maximum but the road width is small (4.5 m). Due to different traffic composition percentages and big size vehicles are not able to achieve their required speed here. So we can say that the velocity ratio of heavy vehicles increased here. Due to increase in velocity ratio the PCU value of heavy vehicles increased here.

The results of this research paper will be helpful for NHA and the Provincial highway department of Punjab. In the future departments can be used these results for traffic flow and highway capacity study.

REFERENCES

[1] Al-kaisy, A., Jung, Y., Rakha, H., 2005. Developing passenger car equivalency factors for heavy vehicles during congestion. J. Transp. Eng., ASCE 131 (7), 514–523.

[2] Geistefeldt, J., 2009. Estimation of passenger car equivalents based on capacity variability. Transportation Research Record: Journal of the Transportation Research Board 2130, 1–6.

[3] DeLuca M DellAcqua, G, 2014. Calibrating the passenger car equivalent on Italian two line highways: A case study. Transport 29 (4), 449–456.

[4] Mondal, S. et al, 2017. Estimation of passenger car unit for heterogeneous traffic stream of urban arterials: case study of Kolkata. Transp. Lett. Taylor &Francis 7867, 1–13.

[5] Ballari, S.O., 2019. Estimation of passenger car equivalents for heterogeneous traffic stream. Int. J. Innov. Technol. Explor. Eng. 8 (6), 1026–1031.

[6] Estimation of passenger car unit on urban roads (2020) by Manjul sharma and Subhdip biswas civil engineering department, national institute of technology Hamirpur India.

[7] National Highway Authority Government of Pakistan (www.nha.gov.pk).

[8] Communication and works department Government of Punjab (www.punjab.gov.pk).

Effect of Addition of Crumb Rubber on Bitumen Performance Grade (PG) and Rutting Resistance

Engr. Muhammad Gohar, Dr. Naveed Ahmad
M.Sc. Research Scholar, Professor
University of Engineering & Technology Taxila, Pakistan
goharmalik_civil59@yahoo.com; n.ahmad@uettaxila.edu.pk

Engr. Waqas Haroon
PhD Research Scholar, University of Engineering & Technology Taxila, Pakistan
Lecturer, Department of Civil Engineering and Technology, FET, Islamabad, Pakistan
waqas.haroon@iiu.edu.pk

ABSTRACT

Crumb rubber was introduced in asphalt a few years ago as a measure to help dispose this waste through its utilisation in construction of new pavements. The current research work focuses on the use of the local recycled tire rubber (crumb rubber) to study its effects on the resulting bitumen. This research has ben carried out on materials that are being used on one of the Pakistan Motorways (M-2 Islamabad to Lahore 355 km approximately) for rehabilitation purposes. The modified rubber bitumen was produced by using the wet process and four samples of mixtures were compared. Comparison was based on three concentrations of crumb rubber. The influences of temperature on complex shear modulus, phase angle and rut factor are studied at a frequency of 10 Hz using Dynamic Shear Rheometer. The analysis of results confirms that the use of asphalt rubber considerably increases the resistance to permanent deformation. Modified Bitumen with 15% Crumb Rubber is more effective in increasing rut resistance.

KEYWORDS: Bitumen, Crumb rubber, Dynamic Shear Rheometer, Rutting Resistance

1. INTRODUCTION

Over the last few decades, rubber has used in asphalt as an additive due to its elastic properties. Literature reveals that two methods have been employed for the modification of asphalt by using rubber i.e., wet, and dry process[1], [2]. According to Kamal et al.[3], based on a field study conducted in Pakistan, performance of asphaltic base and wearing course under the same environmental and trafficking conditions built from Crumb Rubber modified bitumen (CRMB) was comparable with that of the conventional asphalt. Experimental study conducted by researcher Celauro and his fellows[4] found improvement in viscosity of

1st International Conference on Advances in Civil &
Environmental Engineering, University of Engineering & Technology
Taxila, Pakistan

Conference date 22 &23 Feb 2022

CRMB. Researcher Cao and Liu[5] used Sasobit, Evotherm, and chemical welfare agent (CWA) additives in asphalt-rubber stone mastic asphalt to reduce the mixing and compaction temperatures of AR-SMA mixtures. The research concluded that Sasobit improved high temperature performance, whereas the other additives yield no significant differences. According to scientist Cong et al.[6] the properties of Crumb Rubbers modified asphalt made with 80/100pen binder showed better results than the one made with 60/80pen binder at low and high temperatures. Researcher Lopez-Moro [7] illustrated the modification of asphalt by Crumb Rubber using dry process and concluded that there was improvement in binder's resistance to rutting and increment in bitumen's stiffness. Researcher F. Moreno [8] tested a set of bitumen mixes produced by adding different percentage of rubber modifier and proved that the performance of Crumb Rubber modifier mixes was superior. Researcher H.Wang[9] studied the fatigue cracking property by employing the notched semi-circular bending (SCB) test on Crumb Rubber modified asphalt mixture and found similar results. Researcher A.Cetin [10]investigated the effect of concentration of Crumb Rubber on the performance characteristics of porous asphalt mixture. This research showed that crumb rubber size and content plays a significant role, and bigger sizes may compromise the performance characteristics. Researcher G. Shafabakhsh[11] concluded that the use of CR powder results in a considerable decrease in the rate of rutting depth of rubber asphalt mixtures compared to the conventional asphalt mixtures. Researcher H.Liu[12] concluded that with shear temperature of 180 °C, shear time of 45 minutes, and shear rate of 5000 rpm are the best preparation process parameters for the rubber modified asphalt.

This study aims to evaluate the effects of CRMB prepared in field with lab prepared CRMB samples based on rutting resistance and PG value. Field samples were prepared by blending the modifier (Crumb Rubber) in bitumen in the Plant used on Pakistan Motorway (M2).The first objective is to determine and evaluate the physical properties of the conventional and modified field and lab (0% CR, 9.5% CR lab, 9.5% CR field and 15% lab) bitumen samples. The main objective is to compare the rutting performance of all the modified samples through DSR. Finally, the physical and rutting resistance results of modified bitumen samples are compared.

2. EXPERIMENTAL PROGRAM

In this study, base bitumen 60/70 was procured from Attock Oil Refinery limited (ARL), Morgah, Pakistan. The four qualitative tests were performed on neat and modified bitumen samples i.e., penetration, softening, specific gravity and ductility according to ASTM D5, ASTM D36, ASTM D 70, and ASTM D 113, respectively. Crumb rubber powder was mixed with bitumen at a rate of 9.5% and 15 % by mass of total bitumen by wet process at a low speed for about five minutes in the lab. The blend was then heated and stirred at a speed of 3000 rpm with a high-speed mechanical stirrer for about 45 minutes at a temperature between 175 °C and 185 °C. Optimum dosage of crumb rubber was calculated based on maximum rutting resistance parameter.

*1st International Conference on Advances in Civil &
Environmental Engineering, University of Engineering & Technology
Taxila, Pakistan*

Conference date 22 &23 Feb 2022

2.1. Dynamic Shear Rheometer (DSR)

The DSR is a device that tests the bitumen stress/strain properties considering both elastic and viscous behaviour. It measures the complex shear modulus (G*) and phase angle (δ) (known as rheological properties) at different temperatures. Bitumen of required quantity is placed between two parallel plates and tested at desired oscillation speed.

3. Results and Discussions

3.1. Effect of CRMB on Physical Properties of Bitumen

The effect of CR on bitumen physical properties is presented in table 1. The penetration test results indicate that incorporation of crumb rubber into the neat bitumen has increased the stiffness of resultant bitumen. Almost 34% reduction in the penetration value was recorded at 15% CR dosage as compared to that of base bitumen. The possibility of this prominent reduction is due to the greater concentration of crumb rubber. 15% CRMB improved the softening, flash point, and fire point by 24%, 4%, and 8% respectively. Thus, in simple words the addition of crumb rubber in bitumen increases its viscosity, hardness, and deformation resistance capability.

Table 1: Properties of Different Types of Bitumen Test Results

Sr. No	Description	ARL 60/70	CRMB in Field (9.5%)	CRMB in Lab (9.5%)	CRMB in Lab (15%)
1	Specific Gravity	1.029	1.08	1.082	1.1
2	Flash Point (°C)	302	306	308	315
3	Fire Point (°C)	305	316	319	331
4	Softening Point (°C)	50	56	58	62
5	Penetration (1/10th of mm)	62	48	46	41
6	Ductility @ 25 °C (cm)	100 above	100 above	100 above	100 above

3.2. Effect of CRMB on Rheological Properties of Bitumen

Frequency sweep test was run on DSR machine to determine the rheological properties and rut resistance (G*/sinδ) properties of bitumen and its modifications at temperature ranges from 10 to 80 °C and a strain of 12% with an angular frequency range from 0.1 to 10 rad/s. Master curves were drawn by using Rheoplus Software to determine the influence of modification of bitumen at different temperatures. G*/sinδ is determined at each frequency level and at various temperatures by calculating Complex modulus (G*) and phase angle (δ). Master curves of Rut resistance (G*/sinδ) shows that at 10 rad/s and at low frequency, neat

*1st International Conference on Advances in Civil &
Environmental Engineering, University of Engineering & Technology
Taxila, Pakistan*

Conference date 22 &23 Feb 2022

bitumen has the least value of G*/Sin δ among all the four types of mixes. Results shownin figure 1 presents that 15% CRMB prepared in lab has provided significant rut resistance amongst all the samples. Figure 2 illustrates Influence of temperature on G*/Sin δ and shows that 15% CRMB prepared in lab has given better results among all samples. It is concluded that at 10 rad/s ARL 60/70 bitumen has the least value of G*/Sin δ while 9.5% CRMB prepared in lab shows better results than 9.5% CRMB prepared in field and base ARL 60/70. CRMB with 15%crumb rubber prepared in Lab has given the best results for resistance (rut factor) against rutting among all the other specimen.
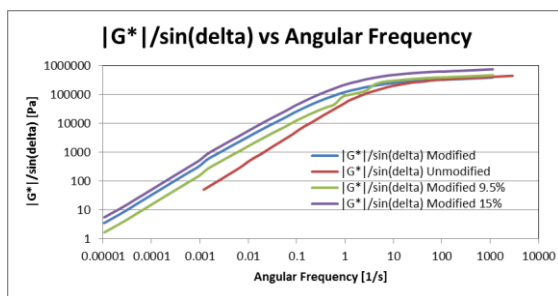
Figure 1: Master curves for Rutting Resistance
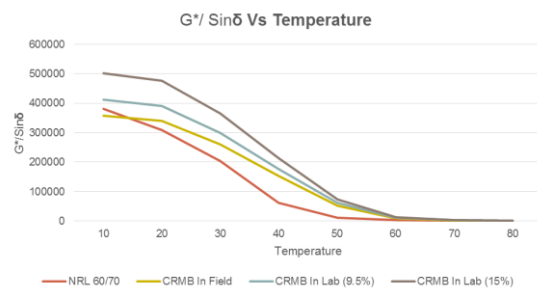
Figure 2: Influence of Temperature on Rutting Resistance

3.3. Temperature Zoning

To check the feasibility of PG 70 to be implemented in Pakistan, the G*/sinδ at 10 Hz frequency and at different temperatures was computed. Temperature at which rut factor is close to 1 kPa is selected as Performance Grade (PG) and from the table 3 at 70°C, rut factor value is close to 1 kPa so PG 70 has been achieved by CRMB in laboratory and it can be used for 70% regions of Pakistan as per temperature zoning done by Mirza et al. [13],.

Table 2: Tabular View of Temperature Zoning

Temperature (°C)	Storage Modulus (Pa)	Loss Modulus (Pa)	Complex Shear Modulus (kPa)	Phase Shift Angle (°)	G*/Sinδ (kPa)	High PG
58	1505.8	6582.9	6.75	77.1	6.93	
64	504.22	2926	2.97	80.2	3.01	PG 70
70	168.13	1336.3	1.35	82.8	1.36	

The ranking indicates that CRMB being prepared by adding 15%crumb rubber by weight in lab has shown the best results during DSR analysis among all four types.

*1st International Conference on Advances in Civil &
Environmental Engineering, University of Engineering & Technology
Taxila, Pakistan*

Conference date 22 &23 Feb 2022

4.   Conclusions

Following conclusions are drawn from this work:

- The crumb rubber assimilation affects the properties of the conventional bitumen. Penetration test results revealed that the penetration values of CRMB at 15% dosage of crumb rubber are 34% lesser than that of the conventional bitumen. This means that the incorporation of additives results in the increase in stiffness and viscosity of the conventional bitumen.

- CRMB has greater rutting resistance as compared to conventional bitumen. The results show that at higher temperatures, modified bitumen with 15%CR has higher value of G* and G*/sin (δ) and lower value of Phase angles (δ) as compared to all samples at a frequency of 10rad/s.

- Overall rutting performance of 15% CR with penetration grade "60/70" bitumen shows satisfactory performance based on lower penetration and phase angle, high G*, PG, and softening point values among all the modified bitumen.

REFERENCES

[1]   F. Moreno, M. C. Rubio, and M. J. Martinez-Echevarria, "The mechanical performance of dry-process crumb rubber modified hot bituminous mixes: The influence of digestion time and crumb rubber percentage," *Construction and Building Materials*, vol. 26, no. 1, pp. 466–474, 2012.

[2]   F. Moreno, M. Rubio, and M. Martinez-Echevarria, "Analysis of digestion time and the crumb rubber percentage in dry-process crumb rubber modified hot bituminous mixes," *Construction and Building Materials*, vol. 25, no. 5, pp. 2323–2334, May 2011.

[3]   M. Kamal, K. Khan, I. Hafeez, and K. Kumar, "Comparison of CRMB Test Sections with Conventional Pavement Section Under the Same Trafficking and Environmental Conditions," *Arabian Journal for Science and*, 2009.

[4]   B. Celauro, C. Celauro, and D. Presti, "Definition of a laboratory optimization protocol for road bitumen improved with recycled tire rubber," *Construction and Building*, 2012.

[5]   W. Cao and S. Liu, "Performance Evaluation of Asphalt-Rubber Stone Matrix Asphalt Mixtures with Warm Mix Asphalt Additives," *Journal of Testing and Evaluation*, 2012.

[6]   P. Cong, P. Xun, M. Xing, and S. Chen, "Investigation of asphalt binder containing various crumb rubbers and asphalts," *Construction and Building Materials*, 2013.

[7]   F. López-Moro, M. Moro, and F. Hernández-Olivares, "Microscopic analysis of the interaction between crumb rubber and bitumen in asphalt mixtures using the dry process," *and Building Materials*, 2013.

[8]   F. Moreno, M. Sol, J. Martín, M. Pérez, and M. C. Rubio, "The effect of crumb rubber modifier on the resistance of asphalt mixes to plastic deformation," *Materials and Design*, vol. 47, pp. 274–280, 2013.

[9]   H. Wang, Z. Dang, L. Li, and Z. You, "Analysis on fatigue crack growth laws for crumb rubber modified (CRM) asphalt mixture," *Construction and Building Materials*, 2013.

1st International Conference on Advances in Civil & Environmental Engineering, University of Engineering & Technology Taxila, Pakistan

Conference date 22 &23 Feb 2022

[10]   A. Cetin, "Effects of crumb rubber size and concentration on performance of porous asphalt mixtures," *International Journal of Polymer Science*, 2013.

[11]   G. Shafabakhsh, M. Sadeghnejad, and Y. Sajed, "Case study of rutting performance of HMA modified with waste rubber powder," *Case Studies in Construction*, 2014.

[12]   H. Liu, G. Luo, X. Wang, and Y. Jiao, "Effects of preparation process on performance of rubber modified asphalt," *IOP Conference Series: Materials*, 2015.

[13]   Mirza, M.W.; Abbas, Z.; Rizvi, M.A. Temperature Zoning of Pakistan for Asphalt Mix Design. Pak. J. Eng. Appl. Sci. **2011**, 8, 49–60.

1st International Conference on Advances in Civil & Environmental Engineering, University of Engineering & Technology Taxila, Pakistan

Conference date 22 &23 Feb 2022

Improvement in Mechanical Characteristics of E-waste Plastic Concrete by Surface Modification of Aggregates

A. Khursheed, M. Irshad Qureshi

Department of Civil Engineering

University of Engineering & Technology Taxila, Pakistan

Ahsan.khursheed@students.uettaxila.edu.pk; Irshad.qureshi@uettaxila.edu.pk

ABSTRACT

Production of Electronic Waste is increasing promptly in the world on account of its vast applications in various fields of life, but it is also adversely affecting the natural environment and brings detrimental effects on human health. On one hand, the application of plastic aggregates in the preparation of concrete helped in the reduction of environmental pollution, production of lightweight, economical, and more durable concrete but on another hand low bonding strength between cement matrix and aggregates surface leads towards reduction in concrete strength. This research study is intended to partially replace the natural coarse aggregates with untreated as well as physically and chemically treated E-waste aggregates to observe the effects on concrete properties and compare the results with control mix. In the physical treatment technique, aggregates were subjected to surface coating of a mixture of Silica Fume and Cement having a ratio of 30:70 while in the chemical treatment technique, aggregates were treated by using Sulphuric acid (H_2SO_4). The properties of plastic aggregates concrete were examined for 10%, 20%, and 30% replacement level with w/c ratio of 0.5 and mix ratio as 1: 1.5: 3. Both adopted surface modification techniques have improved the compressive and split tensile strength of concrete. Physical treatment of aggregates increased 25% compressive and 15% split tensile strength while chemical treatment increased 19% compressive and 13% split tensile strength against 30% replacement level. Similarly, for both techniques and all replacement levels, the slump value has been reduced. The bond improvement is indirectly indicated by the betterment of concrete strength.

KEYWORDS: E-Waste, Surface Treatment, Compressive Strength, Split Tensile Strength

1   INTRODUCTION

The Concrete is second most-consumed material after water on earth and the first most consumed material in the construction industry. Its nature is heterogeneous and composite, and it possess several desirable qualities that make it the first choice in the field of construction. Some of these qualities include strength, durability, fire resistance, formality, and cost-effectiveness as compared to the other materials. Almost 70 - 80% volume of concrete is occupied by aggregates and these aggregates greatly affect the properties of fresh and hard concrete [1]. Mostly these aggregates are obtained from the quarries of different rocks and are crushed to the required size to enable them to use in concrete. With an ever-increasing population, the demand for new buildings and infrastructure is increasing. To fulfil this demand, the requirement of construction materials

1st International Conference on Advances in Civil & Environmental Engineering, University of Engineering & Technology Taxila, Pakistan

Conference date 22 &23 Feb 2022

especially aggregates is becoming challenging. Large production of coarse aggregates results in depletion of natural resources and causes several environmental issues [2]. Research is being conducted in the world to find alternate materials that can be used partially to replace natural aggregates in concrete without compromising its major attributes.

Among these substitution materials, electronic waste or E-waste is the one that has a large-scale production and poses quite serious environmental concerns [2]. This waste in the form of aggregates in concrete helps in the production of lightweight, economical, and environment-friendly concrete in addition to the reduction in landfills and other costs associated with waste management [3]. Day to day technological advancements propels towards the increase in production and consumption of electrical and electronic equipment. Owing to this advancement, people throw away the old products and buy the newer ones with the latest technology resulting in the production of a huge amount of electrical and electronic scrap. E-waste consists of discarded electronic and electrical appliances such as computers, printers, laptops, television, mobile phones, personal stereo, air conditioner, refrigerators, washing machines, and other household appliances that have become dysfunctional [3]. However, the partial usage of plastic in concrete to replace the natural aggregates results in a reduction in concrete strength. The possible reason stated behind this reduction in strength was the weak surface bonding between cement matrix and plastic aggregates because plastic aggregates fail to form a strong bond with cementations matrix due to their flat shape and smooth surface [4,5]. Presently, studies are being conducted to explore the effect of surface-treated aggregates on physical properties and compressive strength of concrete and it is suggested that altering the surface of plastic aggregates will play an important role in developing a stronger bond and improving the concrete properties [6].

Subsequently, this experimental investigation is an effort to overcome this negative aspect of E-waste plastic aggregates through their surface modification. Although there exist many plastics Surface Treatment Techniques, many of them are expensive, difficult to adopt on large scale, and somewhat complex [7]. Therefore, one chemical surface treatment technique which includes surface modification using the Sulphuric acid solution and other was physical treatment technique that includes the coating of aggregates together with Cement and silica Fume composite, were adopted for this research work. Consequently, the testing results show that the treatment of aggregates has a good impact on concrete compressive and split tensile strength hence, bond improvement is indirectly indicated by the betterment of concrete strength [8].

2   EXPERIMENTAL PROGRAM

2.1   MATERIALS

Materials required for the preparation of E-waste plastic aggregates concrete include OPC as the binder, natural sand as fine, natural crushed rocks, and E-waste crushed to the required size as coarse aggregates. Ordinary Portland cement locally manufactured, Lawrencepur sand as fine aggregate, Margalla crush as natural coarse aggregates, and common tap water were used in this research work. Similarly, crushed E-waste was used as plastic aggregates with different percentages to replace natural coarse aggregates. Sieve analysis results are shown in Figure 1. The detailed process of E-waste aggregates manufacturing is schematically illustrated in Figure 2.

1st International Conference on Advances in Civil & Environmental Engineering, University of Engineering & Technology Taxila, Pakistan

Conference date 22 &23 Feb 2022
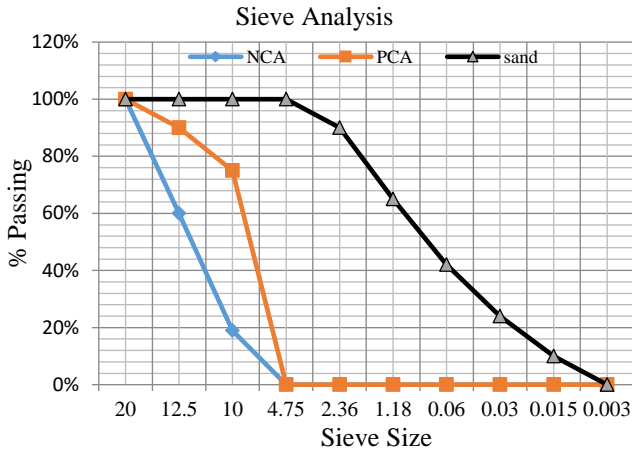
Figure 1: Gradation curve of materials
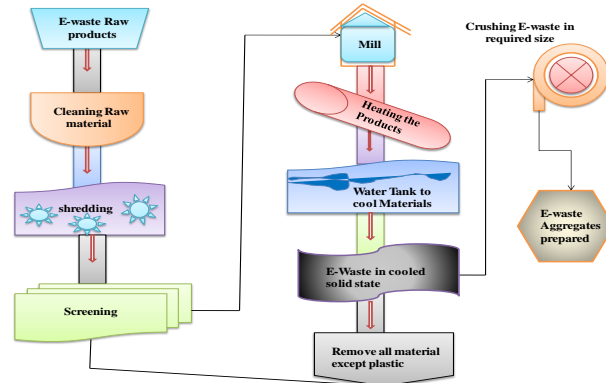
Figure 2: Diagram of E-Waste Aggregates preparation

2.2 TREATMENT

Two different surface treatment techniques including chemical and physical were adopted with the intention to increase the bond between incorporated plastic aggregates surface and cement matrix [8]. In chemical treatment, the manufactured plastic aggregates were treated by soaking them into diluted solutions of sulphuric acid 2.5%wt for a 24-hour time duration. Similarly, during physical treatment aggregates were surface coated by using silica fume slurry prepared by mixing cement and silica fume together with a ratio of 70:30. Aggregates were dipped into it to get the surface coating and later excess slurry was drained out and aggregates were cured for 7 days [6,8].

2.3 EXPERIMENTAL PROGRAM AND METHODS

Table-1 shows the detail of the experimental program and methods followed in this research study.

Table 1: Summary of Properties determined, Experiments performed, standard adopted specimen type, and No. of Specimens

Concrete Properties	Test	Standards	Specimen Shape	Age (Days)	Mix ID			
					CM(N)	CM(U)	SA-T	SF-T
Fresh properties	slump test	ASTM C143/C 143M-20	Cone	After Mixing	3	3	3	3
Mechanical properties	Compressive Strength Test	ASTM C39/C39M-21	Cylindrical	7	3	9	9	9
				28	3	9	9	9
	Split Tensile Strength Test	ASTM C496/C496M-17	Cylindrical	7	3	9	9	9
					3	9	9	9

1st International Conference on Advances in Civil & Environmental Engineering, University of Engineering & Technology Taxila, Pakistan

Conference date 22 &23 Feb 2022

Total	28	12	36	36	36
G. Total		**120**			

3 RESULTS AND DISCUSSION

3.1 WORKABILITY

The slump value of concrete has increased with an increasing percentage of E-waste aggregates [5,8] as shown in figure 3. This rise can be attributed to low water absorption and smoother surface texture of plastic aggregates which resulted in less friction between aggregates particles with
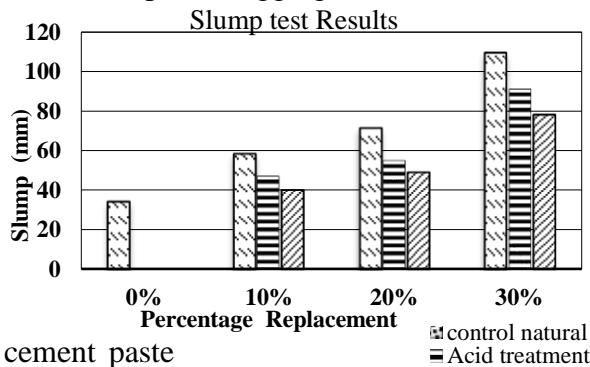
cement paste [6–8]. Amongst treatment techniques, the lowest value of slump was observed for mix prepared with silica fume coated aggregates.

Figure 3: Slump Test Results   *Figure 4(a): 07 days compressive strength Results*
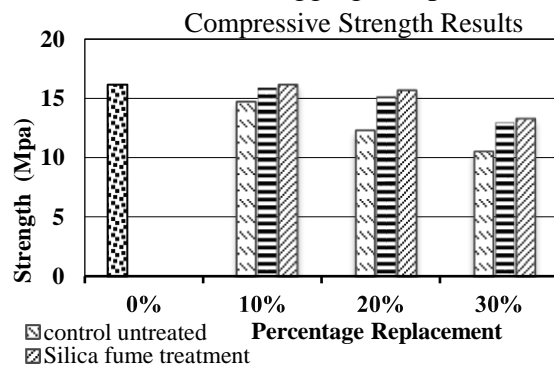
3.2 COMPRESSIVE STRENGTH

Substitution of plastic aggregates in concrete results in the decrease in compressive strength on account of low bonding characteristics [3,4]. But, through aggregate surface treatments adopted in this research work, the testing results are somehow satisfactory. The maximum increase in
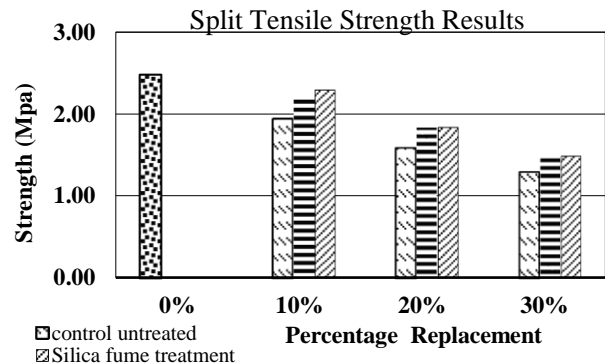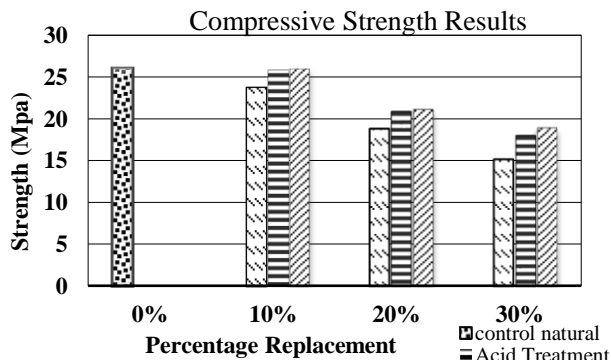
compressive strength was noticed for aggregates coated with silica fume by 9%, 12%, and 25% against 10%, 20%, and 30% replacement levels. The compressive strength of concrete after 7 and 28-days of testing are shown in figures 4(a) and 4(b).

1st International Conference on Advances in Civil & Environmental Engineering, University of Engineering & Technology Taxila, Pakistan

Conference date 22 &23 Feb 2022

Figure 4(b): 28 days Compressive Strength   *Figure 5: 28 days split tensile strength*

3.3   SPLIT TENSILE STRENGTH

The maximum increment in the split tensile strength after 28 days of testing was noticed for silica fume coated aggregates as 18%,16%, and 15% against 10%, 20%, and 30% replacement levels as compared to controlled untreated mix as shown in figure 5.

4   CONCLUSIONS

Following are the main conclusions that are drawn from this research work.

- The substitution of (E-waste) electronic waste aggregates in the concrete has greatly affected the workability of concrete. The values of slump have increased from 50% - 100% against 20 and 30% replacement ratio. This increase in workability pertains to less water absorption capacity and the smoother surface of plastic aggregates which resulted in less friction among particles ensuring greater workability.
- But after incorporating surface-treated aggregates in concrete, the decrease in concrete workability was observed because the treatment has changed the initially smoother surface to rougher causing more contact and greater surface friction between the particles resulting in a low slump and workability.
- The compressive and split tensile strength of plastic (E-waste) aggregates concrete reduced as percentage replacement of aggregates is increased. So, between both the techniques used, silica fume coating displayed the highest improvement of strength which is an indirect representation of bond improvement. It has enhanced the compressive strength up to 25% and the split tensile strength up to 15% against 30% replacement level when compared with untreated control mix strength. Therefore, a replacement level of 30% after treatment with silica fume coating can be used as the strength achievement is more than the minimum requirement i.e.,17 Mpa.

5.   REFERENCES

1.   O. v O and A. E. Emmanuel, "A Study of the Effect of Aggregate Proportioning On Concrete Properties," *American Journal of Engineering Research (AJER*, no. 7, pp. 61–67, 2018, [Online]. Available: www.ajer.org
2.   F. K. Alqahtani *et al.*, "Lightweight Concrete Containing Recycled Plastic Aggregates," 2015.
3.   B. T. A. Manjunath, "Partial Replacement of E-plastic Waste as Coarse-Aggregate in Concrete," *Procedia Environmental Sciences*, vol. 35, pp. 731–739, 2016, doi: 10.1016/j.proenv.2016.07.079.
4.   B. T. A. Manjunath, "Partial Replacement of E-plastic Waste as Coarse-Aggregate in Concrete," *Procedia Environmental Sciences*, vol. 35, pp. 731–739, 2016, doi: 10.1016/j.proenv.2016.07.079.
5.   Z. Ullah, M. I. Qureshi, A. Ahmad, S. U. Khan, and M. F. Javaid, "An experimental study on the mechanical and durability properties assessment of E-waste concrete," *Journal of Building Engineering*, vol. 38, p. 102177, Jun. 2021, doi: 10.1016/J.JOBE.2021.102177.

1st International Conference on Advances in Civil & Environmental Engineering, University of Engineering & Technology Taxila, Pakistan

Conference date 22 &23 Feb 2022

6. Ľ. Bágeľ and P. Matiašovský, "Central Europe towards Sustainable Building CESB10 Prague Material Efficiency SURFACE PRETREATMENT-A WAY TO EFFECTIVE UTILIZATION OF WASTE PLASTICS AS CONCRETE AGGREGATE. REVIEW AND FIRST EXPERIENCES."
7. S. Popovics, "Attempts to improve the bond between cement paste and aggregate."
8. Z. H. Lee, S. C. Paul, S. Y. Kong, S. Susilawati, and X. Yang, "Modification of Waste Aggregate PET for Improving the Concrete Properties," *Advances in Civil Engineering*, vol. 2019, 2019, doi: 10.1155/2019/6942052.

Review of Different Approaches Used for Resource Levelling

Muhammad Nasir Aziz, Sarah Usman

National University of Science and Technology, Pakistan

maziz.mscem21nit@student.nust.edu.pk, susman.mscem21nit@student.nust.edu.pk

ABSTRACT

Scheduling is a crucial task for the efficient management of construction projects. Different scheduling techniques are used to schedule the project in temporal dimensions. The resource levelling problem (RLP) occurs in project scheduling where the goal is to minimize the fluctuations of the resource demand. RLP refers to the difficulty of minimizing the fluctuation of daily resource usage without violating logical relationships between the activities and the original duration of the project. Different methods have been introduced for solving this problem, some of which are discussed in this paper. Float consumption method can incorporate resource levelling in the schedule by giving float consumption rate to each activity to keep all the activities from becoming critical. If all the available floats are consumed for levelling the resources it will result in a non-flexible and rigid schedule. To make the consumption of total float optimal, float loss and resource levelling is assigned a cost, and the function of cost is kept as the objective function which in turn optimizes schedule flexibility too. Most resource levelling methods use traditional finish to start (FS) relationship only. This problem is addressed by running a genetic algorithm which uses four dependence relationships between activities. This method levels resource fluctuations far better than only using traditional finish to start relationship. But this method can produce some impractical solutions which could not be implemented in real projects. Different methods for resource levelling have their benefits and limitations and still have many more shut doors to open.
KEYWORDS: Scheduling, Resource Levelling Problem, Float loss, Precedence Relationship

1 INTRODUCTION

Successful execution of a construction project depends on the extent of impeccability of its planning process. Ensuring that a project will be completed on schedule, with the allocated budget and uncompromised quality requires the development of a reliable schedule. Therefore, researchers have focused on creating different scheduling techniques like CPM, LOB, PERT etc. Although these methods are excellent for scheduling, one common problem in all the scheduling techniques is that the resources are considered unlimited, and hence the effects of resource availability on the schedule is not accounted for. After it was established that resource constraints can cause delays in projects which could be avoided by utilizing resources ingeniously, resource management techniques were discovered. Resource management is addressed by dividing it into two major categories resource allocation and resource levelling [1].

Resource allocation is the assignment of available resources and scheduling of the project activities based on these resources. In a situation where the required resources are not available, related activities face delays. If critical activities delay by such reason, the duration of the project also gets

1st International Conference on Advances in Civil & Environmental Engineering, University of Engineering & Technology Taxila, Pakistan

Conference date 22 &23 Feb 2022

affected. Resource levelling deals with the efficient utilization of resources under a fixed project duration [2].

The resource levelling problem emerges when the fluctuations in the resource demand are to be reduced. Major Variations in the resource demands can cause cost and time over runs, crew being idle, and rehiring of the crew. The solution for this problem is achieved through the reorganizing of the project activities in temporal dimension without changing their precedence relationships [3]. Different methods and techniques have been used in the past for minimizing resource fluctuations without changing the project's completion schedule. Each one has its benefits and limitations. The methods applied in studies on resource management can be classified into three broad categories: (1) Analytical Methods, (2) Heuristic Methods [4], (3) Meta-Heuristic Methods [5], Particle Swarm Optimization (PSO) [6] among many others.

2   RESOURCE LEVELLING BY USING FLOAT CONSUMPTION RATE

Float is an important factor for resource levelling, but utilizing all the floats in a project can result in severe delays. A study was conducted which considers the schedule flexibility while levelling the resources. A float consumption rate is assigned to each activity and then the levelling process is performed. It also demonstrates the impacts of assigning different consumption rates to floats, on schedule flexibility and resource levelling.

An excel model is developed for network-based schedules, which enables the scheduler to allot float consumption rates to each activity for achieving balance between resource utilization and schedule flexibility.

Float consumption rate is the percentage that determines the maximum amount of float a certain activity can consume to shift its start time. Different criteria can be used for choosing the float consumption rate. It can be chosen on the basis of complexity of each activity or any other factor that the scheduler considers. A network based schedule with 11 activities is taken as an example. An objective function is defined for the model. And then the float consumption rates are assigned to each activity. First the calculations are done by taking the consumption rate as 90% for first half activities and 50% for the second half.

The results showed an improvement percentage of 49% percent when the float consumption rate of 50% and 90% were used, and an improvement percentage of 64% when 100% consumption rate was used. Although the improvement factor with complete consumption is better, but that schedule gives no flexibility and may result in the project failing to meet its objectives. The other schedule with consumption rates less than 100% are more flexible [7].

3   RESOURCE LEVELLING OPTIMIZATION BY INCORPORATING FLOAT LOSS IMPACT

Successful completion of construction projects depends on reliable scheduling which requires efficient utilization of numerous resources. The schedule is dependent on resources as it dictates the requirement of resources at a particular time. Scheduling without taking resource limits into account gives unreliable schedules. Resource management is vital in a well-organized schedule.

1st International Conference on Advances in Civil & Environmental Engineering, University of Engineering & Technology Taxila, Pakistan

Conference date 22 &23 Feb 2022

Traditionally CPM is used to schedule project activities based on logic after that resource management techniques, resource allocation and resource levelling, are used. Most of the resource levelling methods used focus on relocating noncritical activities within their available float. This is how the impact of float loss is ignored. The total float provides flexibility to the schedule in which activity could be delayed without delaying the project completion date. It is an attribute of a network path and does not correspond to a certain activity. Similarly, there is also a debate on either client is the owner of this float or the contractor. De La Garza et al. said that the float is dealt with as a commodity between contractors and owners. Therefore, the total float is given a cost as Float Loss Cost (FLC) and incorporated into the proposed model.

In this paper, a Non-Linear Integer Programming (NLIP) model is developed to optimize the resource levelling considering the Float loss cost. CPM calculations of forwarding and backward passes are done and total floats are calculated. Float cost and resource fluctuations are assigned a value as FLC and resource fluctuation cost (RFC). The objective function is to minimize the total cost of the project.

The model application was done on 'What's best solver 14.0' for Excel. A project with 11 activities was taken as an example. Each activity was given minimum, most likely, and the maximum duration was given to calculate probabilities afterward. Further, each activity float was given a float loss value. Simple CPM calculations were done first and a base schedule was developed. Then traditional resource levelling was performed and after that, this model was run which provided resource fluctuation cost and float loss cost (FLC).

The results found out that there were more resource fluctuations in the proposed model schedule but the total cost was lesser than traditional levelling and it was more flexible in terms of total floats of activities. Moreover, the probability of completing the project on scheduled time was more than traditional resource-levelling.

Resource levelling is achieved by consuming the total float of activities. The proposed model gives more realistic solutions for project managers who want to reduce cost impact and increase schedule flexibility. This model acts more like a traditional method if float loss is given lesser value as compared to resource fluctuations and vice versa. Therefore, its schedulers choose how productively one uses it. [8]

4 RESOURCE LEVELLING OPTIMIZATION BY USING PRECEDENCE RELATIONSHIP OPTIONS

Projects are scheduled using different techniques to arrange activities according to their temporal dimensions and precedence relationships. This seems good to schedule activities by traditional methods but without resource optimization and resource levelling, it could cause a lot more cost and become impractical due to resource constraints if they are not considered. Mainly in resource levelling problems reduction of undulations in resource utilization levels is an objective function and resources are supposed unlimited. Previous studies focus on resource levelling by using only basic finish-to-start (FS) precedence relationships and moving activities with allocated resources in their free float. This research goals to form a new model for Resource Levelling Problem which handles different precedence relationships between activities. The proposed model is an

1st International Conference on Advances in Civil & Environmental Engineering, University of Engineering & Technology Taxila, Pakistan

Conference date 22 &23 Feb 2022

optimization model for the Resource levelling problem (RLP). It comprises three elements decision variables, objective function, and constrain functions. The model also performs CPM calculations to determine the scheduled time of activities according to their assigned relationships. There are two decision variables these are the shifting of activity from its earliest start towards late dates and the second is the precedence relationship options. The project manager fixes some of the dependencies between activities and the remaining activities have non-mandatory dependencies. The relationship of   Activities with non-mandatory dependence with the predecessor can be illustrated by four cases with the assumption that one relationship is limited to two options and FS relationship is default among them (1) have default (FS) relationship without option (2) have default relationship (FS) or no relationship (3) have default (FS) relationship or SS relationship (4) Default FS or FF.

The objective function of the model is an optimization of fluctuations of resource utilization levels. It is done by reducing the resource fluctuation moment about the time axis of the project. Like traditional RLP problems total prescribed duration of the project is set as the constraint. Further the author proves in case studies that this model also provides better resource levelling solutions with reduced project durations. A Genetic Algorithm is used to run this model and the stopping criteria are being set to 50 generations. The GA-based optimization of this proposed model is run with VBA on Excel.

To test this model two different projects were taken from previous researches [13 -14]. Two scenarios are taken to compare their results in a test run. one is by having all the relationships as traditional FS relationships for all activities and optimizing that for the best resource levelled solution. The second scenario is according to the proposed model some activities are set with fixed dependencies and others have options for the four cases illustrated above. GA optimization Results show that this proposed RLP model gives far better results than the model without relationship options. The improvement percentage value of an objective function (M_x) is 76.8% and 90.8% for the proposed RLP model and GA resource optimization is 43.5% and 41.8% for the traditional model.

However, the proposed model takes a long time to find an optimal solution due to an increase in feasible options. Moreover, this model can generate such solutions for non-mandatory dependent activities which may be difficult to manage in real life, can have complicated network paths and overlapping activities [3].

5   CONCLUSION

Resource Levelling Problem (RLP) is a typical nondeterministic polynomial time (NP) hard problem. For large projects, the difficulty of solving the problem is increased. Finding an exact solution for this type of problem is impossible. To find a favourable solution for NP-hard problems a computationally complex, exhaustive analysis is needed in which all possible outcomes are tested. Researchers have designed new techniques and methods to solve the modern encountered issues in scheduling resource-dependent projects. These issues are majorly related to the large computing time for finding the optimum solution, applications of a method for different types of

1st International Conference on Advances in Civil & Environmental Engineering, University of Engineering & Technology Taxila, Pakistan

Conference date 22 &23 Feb 2022

projects, integration of resources, and several resources are taken into account while performing. The solution is achieved by,

- Using different methods for each type of schedule
- Modifications in the traditional scheduling techniques, like changing the precedence relationships or specifying the float consumption rates
- Different objective functions are created and analyzed
- Comparing which method performs better under different types of constraints i.e. heuristic versus meta-heuristic method

6   RECOMMENDATIONS

- Although many different methods are used for levelling a single resource, research involving multiple resources is still scarce. Because real projects almost always involve multi-resources, so for the researches to be useful for the industry it should involve multi-resources.
- Usually, the algorithms are run using excel, researchers in the construction industry need to consider using programming languages for running different algorithms.
- The research to date mostly involves basic precedence relationships like SS, FF, FS, and SF. Different relationships between the activities should be explored.

REFERENCES

[1]   Hariga, M. and El-Sayegh, S. , "Cost optimization model for the multiresource leveling problem with allowed activity splitting", Journal of Construction Engineering and Management, Vol. 137 No. 1, pp. 56-64.

[2]   Hinze, J.W., Construction Planning and Scheduling, Pearson Prentice Hall, Upper Saddle River, NJ.

[3]   V. Benjaoran, W. Tabyang, and N. Sooksil, "Precedence relationship options for the resource levelling problem using a genetic algorithm," *Constr. Manag. Econ.*, vol. 33, no. 9, pp. 711–723, 2015, doi: 10.1080/01446193.2015.1100317.

[4]   Harris, R.B., Precedence and Arrow Networking Techniques for Construction, Wiley, New York, NY.

[5]   Hegazy, T., "Optimization of resource allocation and leveling using genetic algorithms", Journal of Construction Engineering and Management, Vol. 125 No. 3, pp. 167-175.

[6]   Alsayegh, H. and Hariga, M., "Hybrid meta-heuristic methods for the multi-resource leveling problem with activity splitting", Automation in Construction, Vol. 27 No. 1, pp. 89-98

[7]   A. Damci, D. Arditi, and G. Polat, "Use of float consumption rate in resource leveling of construction projects," 2020.

[8]   S. El-Sayegh, "Resource levelling optimization model considering float loss impact," *Eng. Constr. Archit. Manag.*, vol. 25, no. 5, pp. 639–653, 2018, doi: 10.1108/ECAM-10-2016-0229.

Low price instrumentations for structural health monitoring – A review

Haider Ilyas and Majid Ali

Capital University of Science and Technology, Islamabad, Pakistan.
haiderilyasidm585@gmail.com; professor.drmajid@gmail.com

ABSTRACT

Structural health monitoring is an advanced and multi-disciplinary technology that is used to monitor structures with the help of different techniques, sensors, management of data acquisition, and algorithms. In recent times, SHM is gaining popularity in developed countries. It is important for the safety and sustainability of structures as it detects damages and changes when a structure is under considerable force. But for developing countries, accepting it is an unreliable task due to economic reasons. The majority of the world's population lives in developing and underdeveloped countries. To implement SHM, we strongly need a setup of low-price instruments and techniques. The primary objective of this research paper is to build a low-price setup and technique for SHM so that it can lead to avoiding financial and human loss. A critical review was made keeping in mind the previous research and the high-end deployed SHM on various structures. The low-priced reliable accelerometers were marked out to select the best possible instrument for SHM. Their working phenomenon was thoroughly analyzed in detail. Finally, a vibration-based method which is a reliable technique is picked out for the deployment of SHM for structures in developing countries.

KEYWORDS: Structural health monitoring; low-price instrument; simple technique, sensor

1   INTRODUCTION

Structural health monitoring (SHM) is the advanced technology that is used for health monitoring with the help of sensors, data acquisitions, data processing, data management, and response system based upon damage pattern evaluation [1]. Different techniques are discussed that could be used to monitor different structures depending upon price, instrumentation, and precision. In those techniques, the simplified one was the Vibration-based damage detection technique that could be used for SHM. It consists of a process that involved data acquisition, data compression, feature selection, and statistical model development [2]. The price of an instrumentational setup that mainly consists of sensors depends upon their functionality, characteristics, and precision. To detect damage in the structure with low price aspect, electromechanical-based techniques are widely used due to their simplicity such as piezoelectric sensor which is accelerometer was a major part of the instrumentation. These are low price, thin, lightweight, and require low power [3]. The process of data acquisition is discussed where its precision and procedure of acquiring data highly

1st International Conference on Advances in Civil & Environmental Engineering, University of Engineering & Technology Taxila, Pakistan

Conference date 22 &23 Feb 2022

depends on the numbers and types of sensors to be used, their key locations areas that recorded generated responses by an automated monitoring system [4].

2   BASIC CONCEPT OF SIMPLIFIED STRUCTURAL HEALTH MONITORING TECHNIQUE

Structural health monitoring techniques comprising from simple to advance depend upon different types of technologies but their core principle is the same, to detect a change in structure and give early warning. In the perspective of it, electromechanical impedance-based techniques were an efficient technique. It excited the lead zirconate titanate (PZT) sensors linked to the structure and measured the resultant electrical impedance. As for the simplified SHM technique, the PZT sensors were inexpensive, small, lightweight, and required low power [3]. Computer vision technology was another technique used for SHM. At a local level, it was used to sense cracks in concrete, roadways, and steel structures. Also, it did crack transmission monitoring, loose bolt, and rust detection in steel structures. At a global level, it did exterior load evaluation [5]. The other technique was the vibration method and finite element model updating. It was used for steel structures for estimation of fatigue damage. In this method, a finite element model was developed that was further checked with dynamic characteristics that were measured in real operational conditions [6].

In recent times, non-contact monitoring methods had been used for SHM because of advancements in instrumentation. Target-tracking digital image correlation was one of these methods which focus on the displacement and deformation measurements in structure [7]. Other than that, in the vibration-based method, a modal analysis approach determines modal parameters. The frequency-based damage techniques lie in this domain, it is a simple technique that achieves damage detection based on changes in natural frequencies, these changes occur due to changes in mass and stiffness, etc. of the structural properties [8]. As we wanted to opt for a basic and simplified technique with economic priorities, we would consider a vibration-based technique for its simplicity, economical and reliable results.

3   INSTRUMENTATION SETUP, WORKING PHILOSOPHY, AND PRICING ASPECT

To monitor the health of the structure, sensors are the main instruments that played an important part in it. Several sensors are used for several purposes considering their price and characteristics. Optical fiber-based was used for structural health monitoring of concrete-based structures [9]. Fiber-optic sensors were used with additional strategies to detect strain in structures [10]. While for other purposes like corrosion, corrosion sensors were there for it that monitors corrosion in structures [11]. As we are discussing different types of sensors where each one has unique characteristics and principles. Typical sensing methods are shown in Table 1 [12].

Prioritizing an aspect of pricing, the strategy of using the accelerometers comes first. Piezoelectric sensors apart from buildings were also widely used in bridges, gas pipelines, and wind turbine blades were used to monitor damages in structure. There were piezoelectric actuators where signals from a Phased Array instrument based on ultrasonic waves passed through it and were then

1st International Conference on Advances in Civil & Environmental Engineering, University of Engineering & Technology Taxila, Pakistan

Conference date 22 &23 Feb 2022

received in the piezoelectric sensors that check the health of structures [13]. Considering the pricing aspect with precision where 90% accuracy can be predicted by using accelerometers [4], we would go for accelerometers. Their accuracy is high as discussed but considering implementing it in a building where due to complexities, its result accuracy may fall a little bit still, it would give a much indication to take precaution at right time to avoid human and financial loss.

Table 1. Typical sensing methods for structural health monitoring [12]

Group of Sensor	Types of Sensor	Types of Measurement	Physical principle	Reliability issue
Ceramics	Piezoelectric	Strain ultrasound, vibration	Electromechanical	Brittle rupture
	Piezoelectric	Temperature	Thermoelectric	Brittle rupture
	Ferroelectric	Vibration, RFIDs temperature	Dipole moment	Brittle rupture
Electromagnetic	MWM, Foil EC	Fatigue, crack, corrosion	Eddy currents, dielectric	Power fault
Thick/thin film	Strain/crack gauges	Crack growth, strain	Electrical resistance	Power fault
	Thermocouples	Temperature	Electrical resistance	Oxidation
	Electrochemical	Chemical	Electrical resistance	Power fault
Fiber-optic	Bragg grating	Strain, temperature, chemical	Optical reflectance	Brittle rupture
Wireless	Active sensor, Passive sensor	Vibration, strain, force	Sensing interface	Electrical short, power fault

4 DATA ACQUISITION AND SHM PRECISION

Data acquisition is a major part of SHM to identify damages i.e. to monitor changes on a global level in the structure. The data could be combined and transformed into graphs via seismosignal. And, from seismosignal to digital devices where the results could give an early warning system. Its illustration of said process is shown in Figure 1. In the aspect of it, a vibration-based method was a tool that could be used for damage detection in SHM. Data acquisition was one process of the vibration-based method where it involved the numbers and types of sensors to be used, their locations, and data-acquisition hardware [2]. Data transmission was the next step in SHM to transmit data, so it could be used for different purposes. The data could be transmitted by wired and wireless transmission systems. In the wireless transmission system, the permanent wireless devices in the structure could be deployed which can automatically transmit data to supplier software and other analysis tools [14]. The next step that was data processing was critical for extracting information about undamaged and damage identification in structures. Data storage was used for managing huge data from sensors which provides data collecting techniques to provide

1st International Conference on Advances in Civil & Environmental Engineering, University of Engineering & Technology Taxila, Pakistan

Conference date 22 &23 Feb 2022

information and evaluation about structure [15]. In this way, a whole process is required through which structural health monitoring occurs.
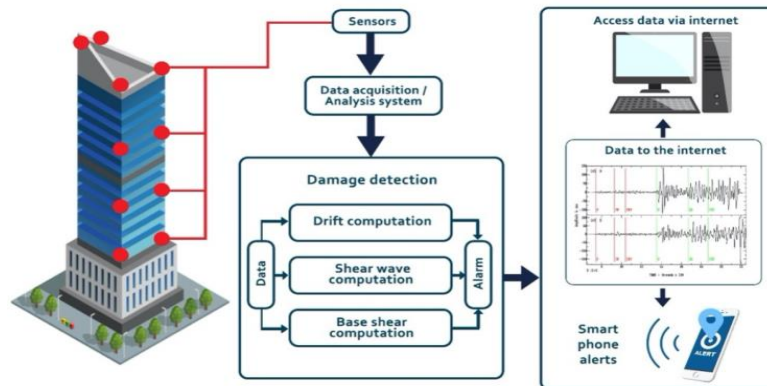
Figure 1. The process of SHM from data acquision to final result [4]

5   CONCLUSION

Structural health monitoring is the technology that with the help of sensors, data acquisitions, and data processing is used to monitor structures. The conclusion made is as follow :

- The Vibration-based method is considered a convenient method to identify damage based upon changes in vibration characteristics in a structure.
- One of the most common sensors employed in SHM instrumentational systems is the accelerometer. So far it has been the most simple for data acquisition, economical and reliable for results.
- The cost-effectiveness of SHM deployment depends on the placement of sensors in critical locations in a structure, which would undoubtedly require prior structural heuristic assessments.

For the simplified SHM technique, the vibration-based method is considered for its ability to monitor structural health with the help of accelerometers. The basic purpose is to present a low-price technique so that structures in developing countries could be kept safe from damages in a way to stop losses of lives.

6   ACKNOWLEDGEMENTS

The authors would like to thank every person who helped them in their literature work.

REFERENCES

[1]   B. K. Nuhu, I. A. M. A. Adegboye, J. Kyeong, O. M. Olaniyi and C. G. Lim, "Distributed network-based structural health monitoring expert system," *Building Research & Information,* vol. 49, no. 1, pp. 144-159, 2021.

1st International Conference on Advances in Civil & Environmental Engineering, University of Engineering & Technology Taxila, Pakistan

Conference date 22 &23 Feb 2022

[2] C. R. Farrar, S. W. Doebling and D. A. Nix, "Vibration-based structural damage identification," *Philosophical transactions. Series A, Mathematical, physical, and engineering sciences,* vol. 359, no. 1778, pp. 131-149 , 2001.

[3] F. G. Baptista and J. V. Filho, "A New Impedance Measurement System for PZT-Based Structural Health Monitoring," *IEEE Transactions on Instrumentation and Measurement,* vol. 58, no. 10, pp. 3602 - 3608, 2009.

[4] A. Sivasuriyan, D. S. Vijayan, W. Górski, Ł. W. nski, M. D. Vaverková and E. Koda, "Practical Implementation of Structural Health Monitoring in Multi-Story Buildings," *Buildings,* vol. 11, no. 6, p. 263, 2021.

[5] C.-Z. Dong and F. N. Catbas, "A review of computer vision–based structural health monitoring at local and Global levels," *Structural Health Monitoring,* vol. 20, no. 2, p. 52, 2021.

[6] D. Giagopoulos, A. Arailopoulos, V. Dertimanis, C. Papadimitriou, E. Chatzi and K. Grompanopoulos, "Structural health monitoring and fatigue damage estimation using vibration measurements and finite element model updating," *Structural Health Monitoring,* vol. 18, no. 4, p. 1189–1206, 2019.

[7] L. Ngeljaratan and M. A. Moustafa, "Structural health monitoring and seismic response assessment of bridge structures using target-tracking digital image correlation," *Engineering Structures,* vol. 213, no. 8, p. 110551, 2020.

[8] S. Das, P. Saha and S. K. Patro, "Vibration-based damage detection techniques used for health monitoring of structures: a review," *Journal of Civil Structural Health Monitoring,* vol. 6, no. 3, p. 477–507, 2016.

[9] K. Bremer, F. Weigand, Y. Zheng, L. S. Alwis, R. Helbig and B. Roth, "Structural Health Monitoring Using Textile Reinforcement Structures with Integrated Optical Fiber Sensors," *Sensors,* vol. 17, no. 2, p. 345, 2017.

[10] A. Güemes, A. Fernández-López, P. F. Díaz-Maroto, A. Lozano and J. Sierra-Perez, "Structural Health Monitoring in Composite Structures by Fiber-Optic Sensors," *Sensors,* pp. 18, 1094, 2018.

[11] R. F. Wright, P. Lu, J. Devkota, F. Lu, M. Ziomek-Moroz and P. R. O. Jr., "Corrosion Sensors for Structural Health Monitoring of Oil and Natural Gas Infrastructure: A Review," *Sensors,* vol. 19, no. 18, p. 3964, 2019.

[12] H. Chen and Y.-Q. Ni, Structural Health Monitoring of Large Civil Engineering Structures, John Wiley & Sons Ltd, 2018.

[13] G. Aranguren, P. M. Monje, V. Cokonaj, E. Barrera and M. Ruiz, "Ultrasonic wave-based structural health monitoring embedded instrument," *AIP Review of Scientific Instrument,* vol. 84, no. 12, p. 125106, 2013.

[14] E. J. Baas, M. Riggio and A. R. Barbosa, "A methodological approach for structural health monitoring of mass-timber buildings under construction," *Construction and Building Materials,* vol. 268, pp. 121153-121164, 2021.

[15] C. J. A. Tokognon, B. Gao, G. Y. Tian and Y. Yan, "Structural Health Monitoring Framework Based on Internet of Things: A Survey," *IEEE Internet of Things Journal,* vol. 4, no. 3, pp. 619 - 635, 2017.

1st International Conference on Advances in Civil & Environmental Engineering, University of Engineering & Technology Taxila, Pakistan

PHYSICOCHEMICAL TREATMENT OF MARBLE INDUSTRY WASTEWATER USING NATURAL COAGULANTS AND SUSTAINABLE SLUDGE REUSE

Tayyaba Kanwal[1]; Tayyaba Aslam Khan[1]; Zain ul Abaideen[2]

Engr. Sadia Fida[1]

University of Engineering & Technology Taxila, Pakistan
tayyabakanwal468@gmail.com; tabby.14khan@yahoo.com; zainulabaideen30@gmail.com;
Sadia.fida@uettaxila.edu.pk

ABSTRACT

Untreated marble wastewater discharge in water bodies causes a lot of environmental impacts since it has lot of total solids, Turbidity and Total dissolved solids(TDS). This study employs four natural coagulants (chickpea, tamarind seeds, rice starch, and moringa olifiera), and by using these coagulants physicochemical treatment adopted for treating marble industry wastewater. Chickpea displayed the maximum removal efficiency of 99.4% for turbidity at optimum coagulant dose of 500 ppm. Moringa Olifera reduced pH from 8.3 to 7.1, and showed the maximum removal efficiency of 92.5 % for TDS at an optimum coagulant dose of 500 ppm. Rice starch expose the least favorable results. Tamarind seeds exhibit the maximum removal efficiency of 73.4 % for TSS at an optimum coagulant dose of 500 ppm. Marble sludge was utilized to produce green concrete blocks. The block with 40% marble powder, and 60% proportion of sand, natural aggregate, and cement was desirable as based on high compressive strength.

KEYWORDS: Marble Wastewater, Coagulants, Sludge, Concrete, Turbidity, Total Dissolved Solids, Total Suspended Solids.

1. INTRODUCTION

The marble factories create a large amount of leftovers, polluting natural sources of water. Marble industry effluents have turbidity, TDS and TSS [8]. Ferric Chloride and alum are the typical coagulants used for wastewater treatment [2]. Natural coagulants are effective and produce lesser sludge as compared to chemical coagulants. Figure 1 displays the methodology flow diagram. In this study, wastewater samples were collected from Unique Marble Industry which is situated in I-9 Islamabad. Unique Marble
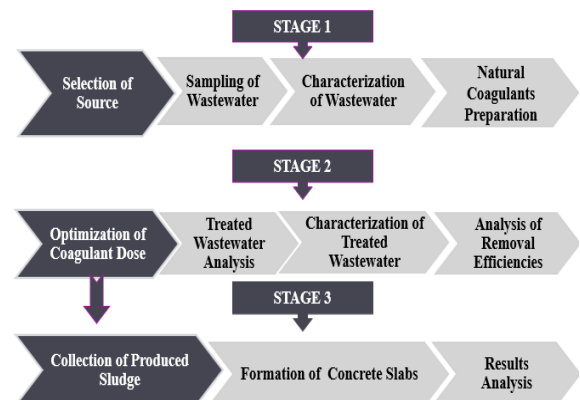
Figure 1:Methodology Flow Diagram

Industry generates a lot of wastewater, without any proper wastewater treatment, and has no proper recovery of sludge. Time-based composite sampling in plastic bottles, carrying 24 liters of water was performed [1].

2. MATERIALS AND METHODS

2.1.Analytical Methods

Diverse analytical methods were utilized for monitoring the parameters i.e. pH was measured by pH meter, Total dissolved solids(TDS) and Total suspended solids(TSS) were detected by Gravimetric method, [5] Chemical oxygen demand(COD) was detected by COD meter, Turbidity was detected by turbidity meter, and Hardness was detected by Titration with EDTA solution [2].

2.2.Coagulants and Stock Solution Preparation

Chickpea seeds were dried in sun for 2 days, grinded, sieved through No. 200 sieve, and then 10 g of coagulant was added in 1000 ml of water to gain 10,000 mg/L of coagulant. Tamarind seeds were dried in sun and dissolved in water to obtain the stock solution. Rice washed, and 6 g of rice starch is dissolved in 200 mL of water in glass bottle, then it was autoclaved at $1210^{o}C$ and 117 KPa for 20 minutes. It is then stirred at $800^{O}C$, and 400 rpm in hotplate stirrer. Moringa Olifiera seeds are taken out from pods and sieved through 600 micrometer sieve, and mixed with ethanol to eliminate alcohol. It is blended at hot plate stirrer for 45 minutes, and centrifuged for 10 minutes at 4000 rpm [10]. The solution is dried for 24 hours for gaining a glue like consistency, and dissolved in water to gain 10,000, 20,000 and 30,000 mg/L of solution.

2.3.Jar Test

Sample was poured in 12 containers (Paochin, 1985). During the jar test trials, 4 trials were performed. During coagulation process, the time was kept for 1 minute, and speed was kept 120 rpm [7]. During flocculation process, during trial 1 the time was kept for 20 minutes, and speed was kept 20 rpm. During trial 2 the time was kept for 30 minutes, and speed was kept 20 rpm. During trial 3 the time was kept for 20 minutes, and speed was kept 30 rpm. During trial 4 the time was kept 40 minutes, and speed was kept 30 rpm. Same trials were used for all the coagulants [3]. The apparatus used for conducting jar test is shown below in figure 2 (Haghiri, Daghighi, & Moharramzadeh, 2018) [6].

Figure 2: Jar Test Apparatus

For chickpea, Tamarind, olifiera and rice starch 210 ml, 240 ml, 270 ml and 260 ml of sludge was collected respectively [4] .The resulting marble sludge from the jar test was utilized to make green concrete blocks named as MP10, MP20, MP30, MP40, and MP50. The mixture proportions of green concrete blocks by resultant marble sludge are provided in table 1 [4].

Figure 3: Sludge Dispensation.

Table 1: Mixture Proportions of Green Concrete Blocks

Sr. No	Mixtures	MP10	MP20	MP30	MP40	MP50	Ratio Calculations
1	Water/Cement ratio	0.6 kg/m^3	0.6	0.6	0.6	0.6	0.6
2	Water	192 kg/m^3	192	192	192	192	0.0473/100 x 0.6= 0.000028 kg
3	Cement	320 kg/m^3	320	320	320	320	1/6.774 x 9.5=1.40kg
4	Coarse aggregate	771 kg/m^3	771	771	771	771	2.4009/6.774 x 9.5= 3.37 kg
5	Sand	969 kg/m^3	861	753	645	537	4.71/100 x 0.9=0.00473 kg
6	Marble powder	10% (0.049 kg)	20% (0.993 kg)	30% (0.149 kg)	40% (0.198 kg)	50% (0.248 kg)	----
7	Marble powder	108 kg/m^3	216	324	432	540	----

3. RESULTS AND DISCUSSIONS

Raw wastewater which was collected from Unique Marble Industry was characterized and compared with the National Environmental Quality Standards (NEQS) as shown below in table 2 [5].

Table 2: Final Characterization

Sr. No	Parameters	NEQS	Marble Sample Wastewater	Values Obtained by Using Natural Coagulants			
				Moringa Olifiera	Chickpea	Tamarind Seeds	Rice Starch
1	Hardness (mg/L)	250	>180 as hard water	140	60	140	110
2	Turbidity (NTU)	----	>1000 mostly	52	35	39	138
3	pH	6.5-10	5-10	7.1	7.3	7.6	7.5
4	TSS (mg/L)	150	50-500	105	95	93	113
5	TDS (mg/L)	3500	<10000	450	2700	700	1400
6	COD (mg/L)	150	100-300	135	150	144	146

3.1.Graphical Comparison

After applying jar test for treating marble industry wastewater graphs were generated for diverse parameters. The effective graphs of all parameters against natural coagulants are given below. In case of moringa olifiera when dose is 400 ppm, it has reduced pH drastically from 8.3 to 7.1. In case of chick pea when dose is 500 ppm it has reduced the pH to 7.3. In case of tamarind seeds when dose is 450 ppm it has reduced the pH to 7.5. In case of rice starch when dose is 500 ppm it has reduced the pH to 7.6. Figure 4 shows graph b/w removal efficiency of pH and effective coagulant dose. In case of moringa olifiera when dose is 500 ppm it has achieved the highest removal efficiency which is 99.25%. In case of chick pea when dose is 500 ppm it has achieved the highest removal efficiency which is 99.44%. In case of tamarind seeds when dose is 500 ppm it has achieved the highest removal efficiency which is 99.25%. In case of rice starch when dose is 500 ppm it has achieved the highest removal efficiency which is 98%. Figure 5 shows graph b/w removal efficiency of turbidity and effective coagulant dose [1].

In case of moringa olifiera when dose is 500 it has achieved the highest removal efficiency which is 67.71%. In case of chick pea when dose is 500 it has achieved the highest removal efficiency which is 73%. In case of tamarind seeds when dose is 500 it has achieved the highest removal efficiency which is 73.42%. In case of rice starch when dose is 500 it has achieved the highest removal efficiency which is 67.61% [2]. Figure 6 shows graph b/w removal efficiency of TSS and effective coagulant dose [7].

In case of moringa olifiera when dose is 500 ppm it has achieved the highest removal efficiency which is 92.5%. In case of chick pea when dose is 500 ppm it has achieved the highest removal efficiency which is 55%. In case of tamarind seeds when dose is 500 ppm it has achieved the highest removal efficiency which is 88.33%. In case of rice starch when dose is 500 ppm it has achieved the highest removal efficiency which is 76.6%. Figure 7 shows graph b/w removal efficiency of TDS and effective coagulant dose.
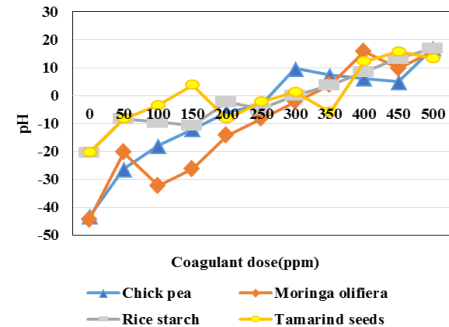
Figure 4: Graph of pH
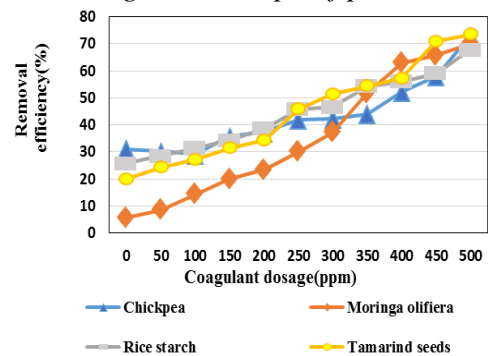
Figure 5: Graph of Turbidity
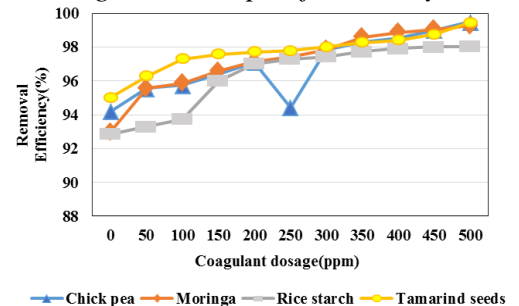
Figure 6: Graph of TSS
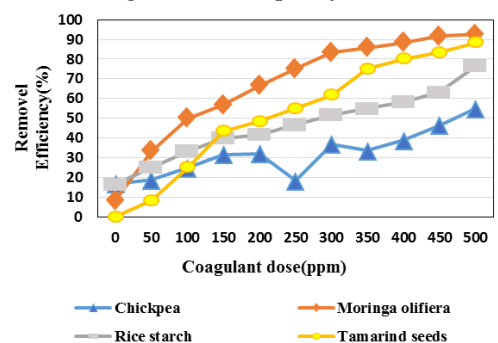
Figure 7: Graph of TDS

3.2. Formation of Concrete Slabs by Sludge

The solid was formed by supplanting sand with marble powder at 10%, 20 %, 30%, 40 %, 50% and 90% by volume [9]. This cluster of tests was named using the MP (marble powder) prefix in the MP material mix used in the examples [10]. An example is referred to as MP10 if sand is replaced by 10% of the volume of marble powder [8]. The proportion of water / cement (W / C) was kept constant during this test. Blocks of concrete mold is shown below in figure 8 [10].

Figure 8: Blocks of concrete mold

4. CONCLUSION

The initial turbidity of the water was 7000 NTU. Chickpea displayed the maximum removal efficiency of 99.4% for turbidity at optimum coagulant dose of 500 ppm. Moringa Olifera reduced pH from 8.3 to 7.1, and displayed maximum removal efficiency of 92.5 % for TDS at an optimum coagulant dose of 500 ppm. Rice starch gave least favorable results. Tamarind seeds displayed maximum removal efficiency of 73.4 % for TSS at an optimum coagulant dose of 500 ppm. As removal of turbidity is the priority, so chickpea is the desirable coagulant. Marble sludge was utilized to produce green concrete blocks, and concrete block with 40% marble powder, and 60% proportion of sand, natural aggregate, and cement was the desirable block based on high compressive strength.

5. RECOMMENDATIONS

Chick pea can be used as a natural coagulant as it gave the most effective results. Concrete arranged with 60 % (sand, natural aggregate, cement) and 40% Marble sludge powder was the best based on the highest compressive strength.

6. ACKNOWLEDGEMENTS

All acclaim is for Allah, and to Holy Prophet Muhammad (P.B.U.H) and special thanks to our supervisor Engr. Sadia Fida, Assistant Professor Dr Sadia Nasreen, and Prof. Dr. Qaisar uz Zaman for guiding us in the research.

7. REFERENCES

1. Abdelkader, S., El-Gendy, A., & El-Haggar, S. (2021). Removal of trivalent chromium from tannery wastewater using solid wastes.
2. Pollution indicandum and marble waste polluted ecosystem; role of selected indicator plants in phytoremediation and determination of pollution zones Ali, S. (2019).
3. Selection of coagulant using jar test and analytic hierarchy process: A case study of Mazandaran textile wastewater Davoodi, M. (2018).

4. Process standardization for preparation of green chickpea (Cicer arietinum L.) Burfi. The Pharma Innovation Journal, 8(11), 201-206(2019).
5. Preparation and characterization of a novel adsorbent from Moringa oleifera leaf. Applied Water Science, 7(3), 1295-1305 (2017).
6. Çınar, M. E., & Kar, F. (2018). Characterization of composite produced from waste PET and marble dust.
7. Crini, G., & Lichtfouse, E. (2019). Advantages and disadvantages of techniques used for wastewater treatment.
8. Mechanical, environmental and economic performance of structural concrete containing silica fume and marble industry waste powder (2018).
9. Marras, G., & Careddu, N. (2018). Sustainable reuse of marble sludge in tyre mixtures. Resources Policy, 59, 77-84.
10. Mohite, A. M., Mishra, A., & Sharma, N. (2020). Effect of different grinding processes on powder characteristics of tamarind seeds.

Development of Unheated Bricks Using Bacteria

Ammar Ahmad, Hassan Mehmood Subhani
Department of Civil Engineering, International Islamic University Islamabad, Pakistan
engrammar43@gmail.com, hhms6677@gmail.com

Farhan Younas
Faculty of Basic and Applied Sciences, International Islamic University Islamabad, Pakistan
farhan.younas@iiu.edu.pk

Muhammad Noman, Khanzaib Jadoon
Department of Civil Engineering, International Islamic University Islamabad, Pakistan
muhammad.noman@iiu.edu.pk, khanzaib.jadoon@iiu.edu.pk

ABSTRACT

Conventional fired clay brick-making process involves wood, coal, and other fuels responsible for gigantic CO_2 emissions in the atmosphere. This research aims to produce biologically cemented, environmentally friendly sandstone bricks by employing a microbially induced calcite precipitation (MICP) technique that requires no fire in its manufacturing process. The bacteria were extracted from manure for making bricks. The bricks samples were made using different quantities of bacterial solution with varying pH values. The performance of these bio-bricks was then assessed using the compressive strength test. The maximum compressive strength of 800 psi could be achieved. Calcite precipitation induced by microbial activity following urea hydrolysis proved a novel technique for bricks cementation processes with the potential to replace the conventional fire clay bricks.

KEYWORDS: MICP, Bio-bricks, Sand-bricks, Sporosarcina Pasterurii, Bacteria, Cementation

1   INTRODUCTION

Bricks are the basic unit for the construction of the structure. Man has used it for thousands of years, and it is one of the oldest building units. The use of clay bricks dates to Mesopotamian, Egyptian and Roman periods [1]. Conventional bricks are made by firing clay at a high temperature of 1200 °C for 2 to 3 days [2]. The configuration of earthen-based components such as shale clay sand in brick making consequently caused depletion of resources, energy consumption, and environmental. Although clay is the most abundant natural material on earth, its use on such a huge scale has also reduced good quality agricultural soil that can be alternately used for crop production. Also, the traditional brick-making process involves consuming tons of energy in the form of various fuels, leading to large economical expenditures and creating air pollution.

1st International Conference on Advances in Civil & Environmental Engineering, University of Engineering & Technology Taxila, Pakistan

Conference date 22 &23 Feb 2022

The current brick-making process must be modified, or a new methodology should be introduced to make bricks production pollution-free, environmentally friendly, economical, and sustainable. This research focuses on a novel Microbial Induced Calcite Precipitation (MICP) method for manufacturing the targeted bricks. The concept of MICP is to pour a bacterial solution into the molds, strengthening the sand particles by bonding them together to form a brick of equal strength to normally fired clay bricks. Microbially induced calcite precipitation (MICP) is a natural biochemical process that results in the formation of calcium carbonate ($CaCO_3$) crystals due to the presence of the Microorganism (Bacteria) from a supersaturated solution [3].

This research work also analyses the performance of desert sand as an alternative material for bricks that can replace clay because desert sand is in abundance and has not been used in the construction industry in any capacity. Although the sand is completely cohesionless and difficult to bind sand particles together, we see sandstones exist in nature. Bernardi et al. [4] performed a detailed investigation on the cementation of sand through microbial activity by precipitating calcium carbonate in the sand bulk and producing a solid unit of brick. The bacteria in the presence of urea $CO(NH_2)_2$ produces the Urease enzyme. The Urease enzyme acts as a catalyst to speed up urea's hydrolysis reaction (see Figure 01). This hydrolysed ammonium and carbamic acid spontaneously give ammonia (NH_3) and carbonic acid mole. (H_2CO_3).

$$Urea + H_2O \rightarrow NH_2COOH + NH_3$$
$$NH_2COOH + H_2O \rightarrow NH_3 + H_2CO_3$$
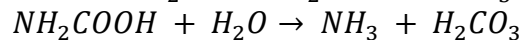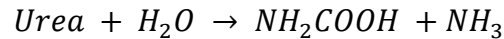
Carbonic acid ionises in water to give bicarbonate ions, while Ammonia (NH_3) in the presence of water forms ammonium ion to form ammonium and hydroxide ion. The hydroxide ions increase the pH, which results in carbonate ions (CO_2^{-3}) [5]. The formation of (NH_4^+) ions increases the pH, and the reaction continues spontaneously, precipitating calcium carbonate at the end.

$$H_2CO_3 \rightarrow HCO^{-3} + H^+$$
$$2NH_3 + 2H_2O \rightarrow 2NH^{+4} + 2OH^-$$
$$HCO^{-3} + H^+ + 2OH \rightarrow CO_2^{-3} + 2H_2O$$
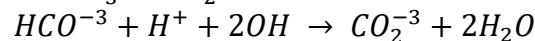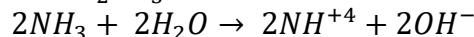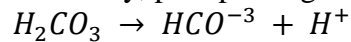
The formation of $CaCO_3$ occurs at the surface of the bacterial cell if enough concentration of Ca_2^+ is present in the solution.

$$Ca^{+2} + Bacterial\ cell \rightarrow Cell - Ca^{+2}$$
$$Cell - Ca^{+2} + CO_2^{-3} \rightarrow Cell - CaCO_3$$
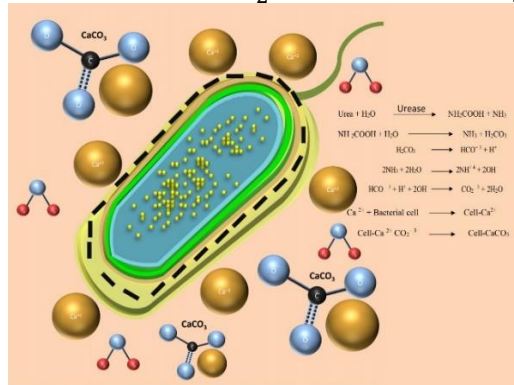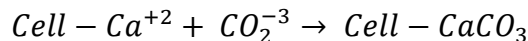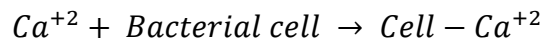
Figure 1: Cementation process of sand through microbial activity

1st International Conference on Advances in Civil & Environmental Engineering, University of Engineering & Technology Taxila, Pakistan

Conference date 22 &23 Feb 2022

The MICP process is a controllable mechanism that can produce high concentrations of CaCO3 [6]. The bacterial cell surface carries a negative charge that attracts the calcium and magnesium ions towards itself and binds them on the cell [7]. However, calcium ions tend to attract the negatively charged bacterial cell more than magnesium ions [3]. These cations at the cell surface react with anions to form calcium carbonate crystals. Bacteria serve as nucleation sites, so they are very important for calcite precipitation, and they can also influence the type of mineral being formed at the cell surface.

2   EXPERIMENTAL WORK

The bacteria must be able to produce urease enzymes to produce calcium carbonate. For this research project, two different bacteria were extracted from the manure and imported from Germany named Sporosarcina Pasterurii DSMZ 33. The bacterial pellet was suspended in sterile Nutrient broth containing 0.2% urea and was incubated at 30 °C and 150 rpm for 4-5 hours. For testing the cementing properties of bacteria, $5x10^6$ CFU/ml of Sporosarcina Pasterurii was used. The nutrient solution or the cementing solution was prepared using 0.28% of Soy Broth composed of Scharlau, 118-334 mM of urea, 131-188 mM of ammonium chloride NH_4Cl, 26 mM sodium hydrogen carbonate, 55 mM of calcium chloride $CaCl_2$, 1L of purified water. Media were pasteurised to stop uncleanness. An aqueous solution of $CaCl_2$ dihydrate as a source of Calcium ions was prepared.

A specific wooden mould with inside glass plates and scaled-down sizes was used compared to conventional brick moulds (4.5" x 2.25" x 1.5") (See Figure 02). Three types of sand were used, i.e., Ravi sand, Ghazi sand, Desert sand (Rohi, Bahawalpur). Sieve analysis was performed according to ASTM C136-05 to determine the particle size distribution of the sands (see Figure 03). The fineness modulus of Ravi, Ghazi, and Desert sand was 2.73, 2.85, and 2.43, respectively.

Figure 2: Casting of the brick
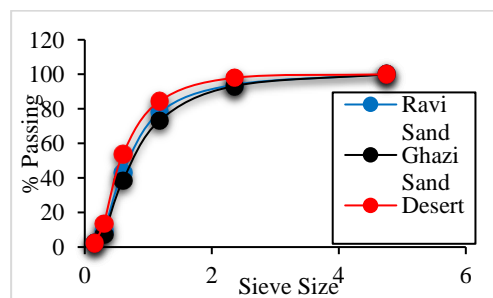
Figure 3: Particle size distribution of the sands
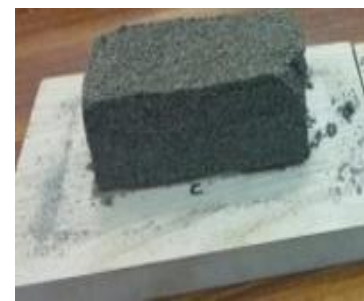
Figure 4: Bio-brick after the curing process

To make the sample brick, a cementation solution of varying pH was set from 7.25 up to 8 pH prepared using nutrient media. The solution was added to the sand and mixed thoroughly with a mixer. 15.0 ml of 55.0 mM $CaCl_2$ was added to 750 ml of the prepared cementing solution. The solutions were injected into the sample with an enormous flow using a drip. 750 ml of the bacterial solution with live cells were then injected into the sample via gravity flow through the injection or drip. The solutions were let on to set in the sample for 4-10 hours. One more stack of cementing

1st International Conference on Advances in Civil & Environmental Engineering, University of Engineering & Technology Taxila, Pakistan

Conference date 22 &23 Feb 2022

solution with urea $(CONH_2)_2$ and calcium chloride $(CaCl_2)$ was prepped and injected into the sample via gravity flow using a drip. This mechanism was repeated 5-8 times. The sample was then turned 180 degrees upside-down, with the underside of the sample becoming the upper side and the upper side would become the underside. This mechanism was repeated 5-8 times. Figure 04 shows the post-cured bio-brick.

3   RESULTS & DISCUSSION

The compressive strength was found to be 384 psi, 782 psi, and 817 psi for Ravi, Ghazi, and desert sand, respectively, at 40 ml. The quantity of cementing solution was increased in increment of 10 ml from 40 to 80 ml. The samples with 60 ml solution showed a compressive strength of 432 psi for Ravi, 819 psi for Ghazi, and 852 psi for desert sand. It was found that increasing the solution quantity increased the compressive strength of bricks. However, after 60 ml, the compressive strength declined (see Figure 05). In all these samples pH of the solution is kept constant at 8 while all the samples were cured 7 times.

In order to find the optimum value of pH for cementing solution, the solution was prepared at 5 different pH values from 7.5 to 8.25 with an increment of 0.25, but the quantity of solution was kept constant at 60 ml. Maximum strength was achieved at a pH of 8 for all the types of sands. It was also revealed that a pH value greater than 8 reduced the compressive strength of bricks (see Figure 06). Ravi sand showed the least compressive strength whereas, desert and Gazi sand bricks have higher compressive strength values.
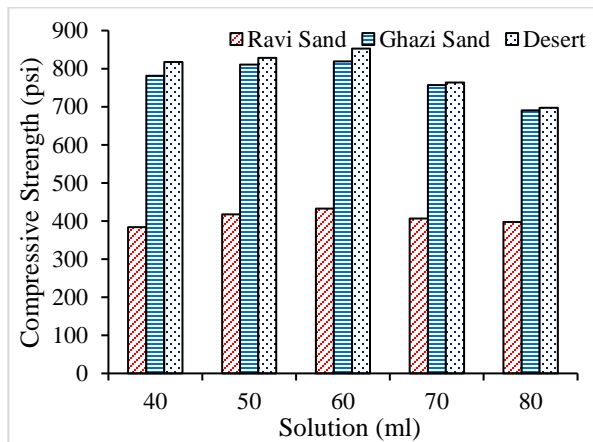
Figure 5: Compressive Strength for Different Quantities of Solution
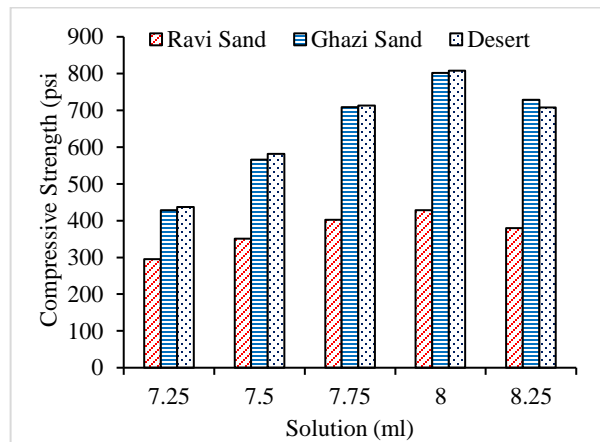
Figure 6: Compressive Strength for Different Values of pH

4   CONCLUSION

The following conclusions can be drawn from the study:

1st International Conference on Advances in Civil & Environmental Engineering, University of Engineering & Technology Taxila, Pakistan

Conference date 22 &23 Feb 2022

1. Calcite precipitation induced by microbial activity following urea hydrolysis has been proved as a novel technology with a broad range of possible applications.
2. Bio bricks are environmentally friendly as no environmental and health hazards are associated with their production.
3. This process of bio-bricks manufacturing eliminates carbon dioxide emissions related to burring of bricks and saves the agricultural land.
4. A higher compressive strength value for all types of sand was achieved at an optimum solution quantity of 60 ml.
5. Bio bricks give good results when treated at a pH of 8.
6. The compressive strength of bricks was observed to be 800 psi.
7. The bricks utilising the natural cementation process can replace traditional fired clay because they can be made as strong as tradition fired clay brick by controlling the conditions and factors influencing the mineral precipitation.

5   ACKNOWLEDGEMENTS

REFERENCES

[1] Fernandes F.M. , Lourenço P.B. , Castro F., Ancient clay bricks: manufacture and properties Mater. Technol. Pract. Hist. Herit. Struct. (2010), pp. 29-48
[2] Pariyar, S. K., Das, T. and Ferdous, T. (2013) 'Environment And Health Impact For Brick   Kilns In Kathmandu Valley', International Journal of Scientific & Technology Research, 2(5), pp. 184–187.
[3] Anbu P., Kang C.-H., Shin Y.-J., So S.-S., Formation of calcium carbonate minerals by bacteria and its multiple applications SpringerPlus, 5 (2016), p. 250
[4] Bernardi D., Dejong J.T., Montoya B.M., Martinez B.C., Bio-bricks: biologically cemented sandstone bricks Constr. Build. Mater., 55 (2014), pp. 462-469
[5] Fujita Y., Ferris F.G., Lawson R.D., Colwell F.S., Smith R.W., Calcium carbonate precipitation by ureolytic subsurface bacteria Geomicrobiol J, 17 (2000), pp. 305-318
[6] Dhami, N. K., Reddy, M. S. and Mukherjee, A. (2012) 'Improvement in strength properties of ash bricks by bacterial calcite', Ecological Engineering. Elsevier B.V., 39, pp. 31–35. doi: 10.1016/j.ecoleng.2011.11.011.
[7] Santosh K., Ramachandran S.K., Ramakrishnan V., Bang S.S., Remediation of concrete using microorganisms J. Am. Concr. Inst., 98 (4) (2001), pp. 3-9.

PAPER ID: 153

1st International Conference on Advances in Civil & Environmental Engineering, University of Engineering & Technology Taxila, Pakistan

Conference date 22 &23 Feb 2022

Synthesis of biodiesel from waste cooking oil using LiO/WO₃ catalyst

Hamza Sajjad [a, *]

[a] Department of Mechanical and Aeronautical Engineering, University of Engineering & Technology (UET) Taxila, Rawalpindi, Pakistan
Hamza.sajjad@students.uettaxila.edu.pk, Hamza.sajjad.858@gmail.com

Haris Maroof [b]

[b] Department of Thermal System Energy Engineering, US-Pak Center for Advanced Studies in Energy (USPCAS-E), University of Engineering & Technology (UET) Peshawar, Pakistan

Syed Nasir Shah [c]

[c] Department of Energy Engineering, Faculty of Mechanical and Aeronautical Engineering, University of Engineering & Technology (UET) Taxila, Rawalpindi, Pakistan

Sadia Nasreen [d]

[d] Department of Environmental Engineering, University of Engineering & Technology (UET) Taxila, Rawalpindi, Pakistan

Ammar Maroof [e]

[e] Department of Agriculture, Abdul Wali Khan University Mardan (AWKUM), Pakistan

ABSTRACT

The scarcity of the globe's fossil reserves, coupled with elevated ecological anxieties and surging petroleum oil prices, worries over energy safety have compelled scientific community to take action and seek alternate energy sources. Biodiesel (alkyl esters of long-chain fatty acids) is a prominent biofuel substitute for petrodiesel. This work focuses on the synthesis of hybrid heterogenous lithium doped tungsten oxide catalyst using wet impregnation method and its implementation in synthesis of biodiesel from economical waste cooking oil (WCO). The several biodiesel production parameters such as LiO/WO₃ catalyst concentration, WCO/methanol molar ratio, and temperature were optimized to investigate their influence on biodiesel yield. The optimum LiO/WO₃ catalyst concentration of 3 wt.%, WCO/methanol molar ratio of 1:11, temperature of 90 °C, and residence duration of 4 hrs produced a maximal yield of 92%.

Keywords: lithium, tungsten, biodiesel, transesterification, waste cooking oil

1. INTRODUCTION

Fatty acid methyl ester (FAME), generally known as biodiesel, is identified as an optimistic alternate to petrodiesel. The mostly employed process for the synthesis of FAME is the transesterification/esterification, in which oil triglycerides (TAGs)/free fatty acids (FFA) and alcohol are utilized as reactants and driven by suitable catalyst presence. The waste cooking oil (WCO), which is quite feasible as a raw material for production of FAME, as it is economically viable, its high availableness for commercial-scale production, and its utilization in transesterification will also help in minimizing the environmental concerns, regarding dumping of these waste oils. However, its only limitation is that it has higher FFA than edible vegetable oils

1st International Conference on Advances in Civil & Environmental Engineering, University of Engineering & Technology Taxila, Pakistan

Conference date 22 &23 Feb 2022

[1], [2]. Traditional homogenous catalysts were used to drive the transesterification and they had many drawbacks like formation of soap during transesterification by their reaction with FFA, non-reusable, their segregation from transesterification products through neutralization causing generation of salts. The large quantity of wastewater formation during purification of produced products made the process quite environmental unfriendly and long. These drawbacks can be prevented by utilizing heterogeneous solid catalysts. As they are in solid form and can be segregated from the products by filtration with no requirement of lengthy purification and can provide high reusability, therefore making the process ecological friendly and economical. Heterogeneous catalysts have the ability to perform simultaneous transesterification and esterification for conversion of both TAGs and FFA from oil into biodiesel with-out any prior treatment of oil [2]–[4]. This study focuses on the production of FAME by transesterification of methanol and WCO using hybrid heterogenous lithium doped tungsten oxide catalyst. The optimization for the influence of several transesterification method parameters on waste cooking oil biodiesel (WCOBD) yield such as concentration of catalyst, WCO/methanol molar ratio, and temperature of process was analyzed.

2. EXPERIMENTAL ANALYSES

2.1 Materials

The WCO was obtained from the local market and domestic households. The analytical grade $LiCO_3$ (> 97%), ammonium metatungstate, and methanol (99%) were acquired from Sigma-Aldrich Pvt Ltd. The impurities from WCO were eliminated by filtration, as depicted in Figure 1.

Figure 1: Filtration of waste cooking oil (a,b), methanol (c), paraffin oil (d)

2.2 Preparation of catalyst

The solid catalyst, LiO/WO_3 was synthesized by wet impregnation method. The determined concentrations (1:1 molar ratio) of metallic precursors were dissolved and stirred in 200 millimeters of solvent at room temperature. The water was then evaporated by slowly heating at 60 °C and left overnight. This is followed by the drying at 50 °C of wet mixture in oven. Finally, the resultant mixture was calcinated at 700 °C for 2 hr.

1st International Conference on Advances in Civil & Environmental Engineering, University of Engineering & Technology Taxila, Pakistan

Conference date 22 &23 Feb 2022

2.3   Transesterification procedure

The experimental setup displayed in Figure 2 was compromising of hotplate (MS300HS) with agitation and temperature regulator over which silver bowl was placed. The silver bowl was filled with paraffin oil, in which two neck round bottom flask was partially immersed. The condenser was linked to the flask and its function was to condense the methanol back to the glass flask. The experiments for FAME production to assess the catalytic performance of lithium doped tungsten oxide catalyst was conducted under the following conditions: concentration of LiO/WO_3 catalyst (1.0 – 4.0 wt.%, based on WCO wt), WCO to methanol molar ratio (1:3 – 1:20), temperature (50 – 120 °C) and fixed process duration of 4 hrs. The determined quantity of LiO/WO_3 catalyst, methanol, and WCO were added into the flask to start the transesterification reaction. Residence time was measured from the point when the temperature of the paraffin oil reached the desired temperature. The temperature of the paraffin oil was measured using thermometer. A small submersible pump was also placed in bucket, and it was employed for the regulating of water through the condenser. Following the end of the reaction, the WCOBD and the byproduct glycerin were poured into the funnel with filter paper to segregate the LiO/WO_3 catalyst. Then, WCOBD was segregated from glycerin by centrifugation (80-2 Electronic centrifuge). The transesterification products are shown in Figure 3. The yield of WCOBD was calculated by the following equation 1.

$$\text{Yield (\%) of WCOBD} = \frac{\text{WCOBD produced}}{\text{WCO used for reaction}} \times 100 \qquad (1)$$
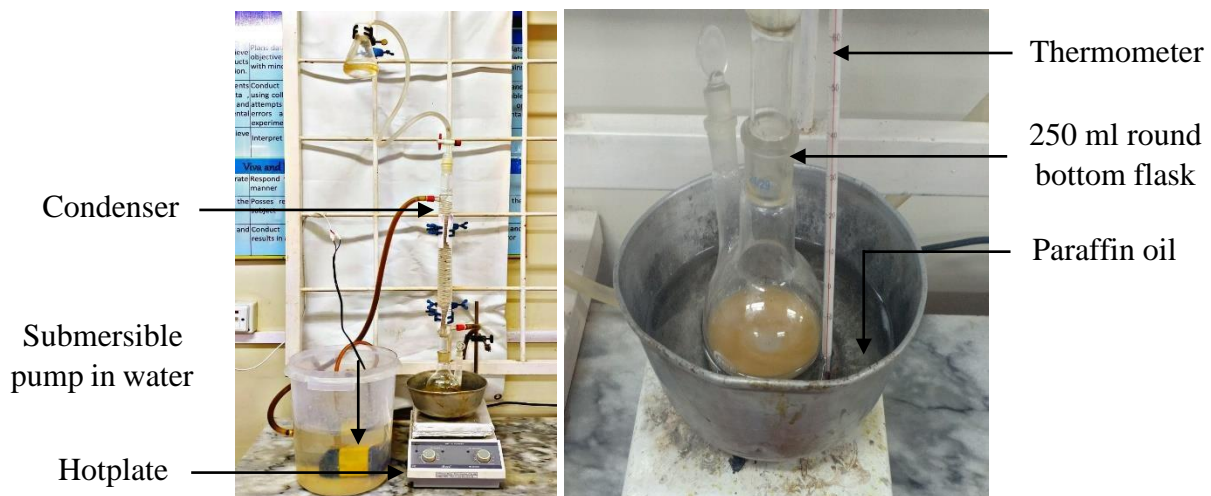
Figure 2: Experimental setup for WCOBD production

1st International Conference on Advances in Civil & Environmental Engineering, University of Engineering & Technology Taxila, Pakistan

Conference date 22 &23 Feb 2022

Figure 3: Product samples (a), biodiesel and byproduct glycerin from transesterification (b)

3. RESULTS AND DISCUSSIONS

3.1 Optimization of WCOBD production parameters

3.1.1 Influence of LiO/WO$_3$ catalyst concentration on WCOBD yield

The concentration of LiO/WO$_3$ catalyst is a quite critical factor for WCOBD productivity using transesterification method. To investigate the catalyst performance by transesterifying methanol and WCO, the LiO/WO$_3$ catalyst concentration was varied from 1.0 to 4.0 wt%, with the difference of 0.5 wt%, while other variables were kept constant during these experiments like WCO/methanol molar ratio (1:17) and temperature (100 °C). Figure 4 illustrates the outcomes in terms of WCOBD yield versus concentration of catalyst. WCOBD formation improved from 62 to 92% as the concentration of LiO/WO$_3$ catalyst increased. The improvement in yield can be described by the rise in the number of active centers on the LiO/WO$_3$ catalyst surface with the increase in concentration [5]. The 3.0 wt% was chosen as optimal due to the minimum development in WCOBD yield beyond that.

1st International Conference on Advances in Civil & Environmental Engineering, University of Engineering & Technology Taxila, Pakistan

Conference date 22 &23 Feb 2022
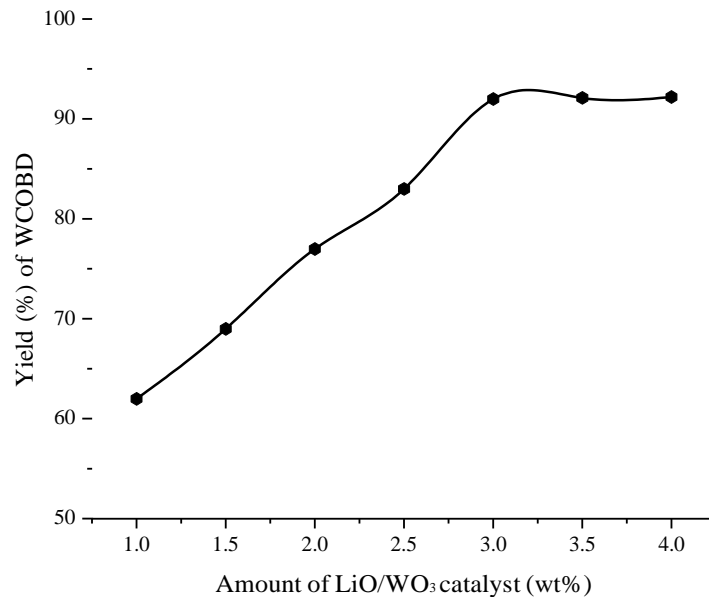
Figure 4: Influence of LiO/WO₃ catalyst concentration on WCOBD yield

3.1.2 Influence of WCO to methanol molar ratio on WCOBD yield

In this investigation, the quantity of methanol was varied (1:3, 1:5, 1:8, 1:11, 1:14, 1:17, 1:20) to evaluate its effect on the oil transformation efficiency at constant conditions (3.0 wt.% concentration of LiO/WO₃ catalyst and 100 °C process temperature). The stoichiometric molar ratio to drive the transesterification reaction is 1:3, however, owing to the reversibility of the reaction, a surplus quantity of methanol is mostly employed to compel the reaction to forward direction (FAME generation) and the higher ratios improve the solubility by minimizing the immiscibility of oil and alcohol, which enhances the biodiesel yield [6], [7]. It can be observed from Figure 5, the WCOBD yield increased with the rise in methanol concentration from 1:3 to 1:20. When the higher ratios were utilized for WCOBD production, there was surplus methanol left at the end of experiment and its recovery can raise the production cost [8]. Therefore, 1:11 was selected as optimum for further production processes.

1st International Conference on Advances in Civil & Environmental Engineering, University of Engineering & Technology Taxila, Pakistan

Conference date 22 &23 Feb 2022
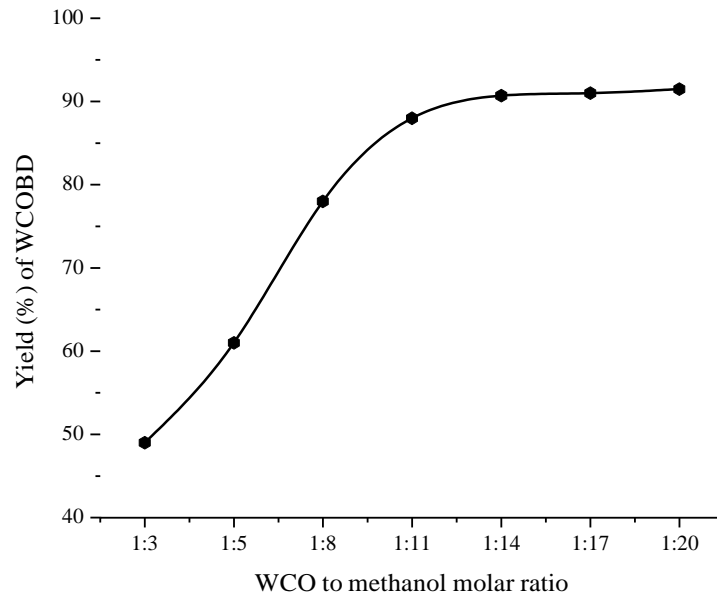
Figure 5: Influence of WCO to methanol molar ratio on WCOBD yield

3.1.3   Influence of process temperature on WCOBD yield

One of the major factors in transesterification is temperature of process, which has a dominant impact on the outcomes. Elevated temperatures, for instance, enhance the process kinetics, which
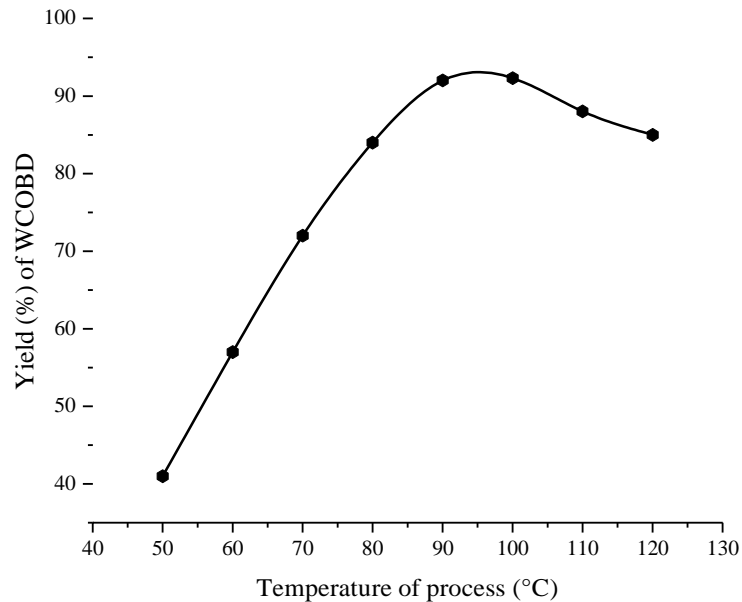
Figure 6: Influence of process temperature on WCOBD yield

leads to a shorter process duration [8]. In order to study the impact of process temperature for production of WCOBD from WCO in LiO/WO$_3$ catalyst presence, the temperature was varied in

1st International Conference on Advances in Civil & Environmental Engineering, University of Engineering & Technology Taxila, Pakistan

Conference date 22 &23 Feb 2022

the vicinity of 50 to 120 °C at the constant conditions (3.0 wt.% concentration of LiO/WO$_3$ catalyst and WCO/methanol molar ratio of 1:11), as displayed in Figure 6. The process temperature was quite influential on WCOBD yield from 50 to 90 °C, then during 90 to 100°C rise the conversion became steady, beyond from 100 °C, the yield declined to 85%. The fall in WCO conversion efficiency at higher temperatures was owing to less presence of alcohol in the reaction medium and its higher presence in the vapor phase, although during the process the alcohol was continuously recovered by condensation, still alcohol presence remained low [9]. Hence, keeping in mind the energy considerations for WFOBD production, 90 °C was indicated as optimum.

CONCLUSION

The lithium doped tungsten oxide hybrid heterogeneous catalyst was effectively deployed in WCOBD production via transesterification and demonstrated excellent catalytic activity, despite the use of low-grade raw material in this study. The optimization of several biodiesel production parameters reached a maximal yield of 92 % at optimal LiO/WO$_3$ catalyst concentration of 3 wt.%, WCO/methanol molar ratio of 1:11, temperature of 90 °C, and residence duration of 4 hrs. The aspect of the economically viable and ecological friendly process was guaranteed by the utilization of inexpensive waste cooking oil and hybrid solid catalysis in biodiesel production.

REFERENCES

[1]   M. M. K. Bhuiya, M. G. Rasul, M. M. K. Khan, N. Ashwath, A. K. Azad, and M. A. Hazrat, *Second generation biodiesel: Potential alternative to-edible oil-derived biodiesel.* Energy Procedia, vol. 61, no. 14, pp. 1969–1972, 2014, doi: 10.1016/j.egypro.2014.12.054.

[2]   B. Changmai, C. Vanlalveni, A. P. Ingle, R. Bhagat, and L. Rokhum, *Widely used catalysts in biodiesel production: A review*. RSC Adv., vol. 10, no. 68, pp. 41625–41679, 2020, doi: 10.1039/d0ra07931f.

[3]   E. Rashtizadeh, F. Farzaneh, and Z. Talebpour, *Synthesis and characterization of Sr3Al2O6 nanocomposite as catalyst for biodiesel production*. Bioresour. Technol., vol. 154, no. 14, pp. 32–37, 2014, doi: 10.1016/j.biortech.2013.12.014.

[4]   A. L. De Lima, C. M. Ronconi, and C. J. A. Mota., *Heterogeneous basic catalysts for biodiesel production*. Catal. Sci. Technol., vol. 6, no. 9, pp. 2877–2891, 2016, doi: 10.1039/c5cy01989c.

[5]   M. Feyzi and G. Khajavi, *Investigation of biodiesel production using modified strontium nanocatalysts supported on the ZSM-5 zeolite*. Ind. Crops Prod., vol. 58, pp. 298–304, 2014, doi: 10.1016/j.indcrop.2014.04.014.

[6]   Z. Ullah *et al., Phosphonium-based hydrophobic ionic liquids with fluorous anions for biodiesel production from waste cooking oil*. Int. J. Environ. Sci. Technol., vol. 16, no. 3, pp. 1269–1276, 2019, doi: 10.1007/s13762-018-1735-6.

[7]   V. K. Booramurthy, R. Kasimani, and S. Pandian, *Biodiesel Production from Tannery Waste using a Nano Catalyst (Ferric-Manganese Doped Sulphated Zirconia)*. Energy Sources, Part A Recover. Util. Environ. Eff., vol. 0, no. 0, pp. 1–13, 2019, doi: 10.1080/15567036.2019.1639849.

[8]   S. Nasreen, H. Liu, D. Skala, A. Waseem, and L. Wan., *Preparation of biodiesel from soybean oil using La/Mn oxide catalyst*. Fuel Process. Technol., vol. 131, no. March 2019, pp. 290–296, 2015,

1st International Conference on Advances in Civil & Environmental Engineering, University of Engineering & Technology Taxila, Pakistan

Conference date 22 &23 Feb 2022

doi: 10.1016/j.fuproc.2014.11.029.

[9]   F. Jamil *et al., Biodiesel production by valorizing waste Phoenix dactylifera L. Kernel oil in the presence of synthesized heterogeneous metallic oxide catalyst (Mn@MgO-ZrO2)*. Energy Convers. Manag., vol. 155, no. August 2017, pp. 128–137, 2018, doi: 10.1016/j.enconman.2017.10.064.

1st International Conference on Advances in Civil & Environmental Engineering, University of Engineering & Technology Taxila, Pakistan

Conference date 22 &23 Feb 2022

COMPARATIVE STUDY AND NUMERICAL INVESTIGATION OF REINFORCED CONCRETE JOINTS

Tufail Mabood

University of Engineering and Technology Peshawar, Pakistan

13bnciv0557@uetpeshawar.edu.pk

Muhammad Fahim

University of Engineering and Technology Peshawar Pakistan.

drmfahim@uetpeshawar.edu.pk

ABSTRACT

Pakistan is located in an earthquake-prone region [1], [2]. Most of structures damaged in the 2005 Kashmir earthquake lacked conventional material strength characteristics & joint details [2]. Structures failed to resist the earthquake in Kashmir, lack material strength characteristics and joint details [3]. Beam column joints are key components to consider when modelling and monitoring structural performance to avoid catastrophic failure during natural disasters such as earthquakes. As a result, identifying the damage with high precision is essential [4]. This paper offers a parametric investigation using intermediate and special moment resistance frame guidelines for frames with code compliance, non-code compliant, and partially code compliant models for cyclic loading. The materials used in the Abaqus models are based on Pakistani construction practices. The materials used in the Abaqus models are based on the construction practises used in Pakistan. Concrete and reinforced steel are rated at 14 and 306 Mega Pascal, respectively. Mesh sensitivity analysis was performed, and the results were associated with important of the updated mesh. The parametric investigation's findings demonstrated that the study's performance revealed a significant evidence of the need for code compliance models. The obtained findings are provided to show the evolution of the plastic hinge as well as the hysteresis performance.

KEYWORDS: Beam-column joints, ABAQUS, Finite Element Analyses, Earthquake.

1   INTRODUCTION

Many structures built across Pakistan have serious problems in terms of seismic resistance [5]. The absence of earthquake resilience in pre-2005 reinforced-concrete structures is one such flaw. Shear reinforcement provided in these structures were weak, and their efficacy is questionable [6]. Since the Quetta and Kashmir earthquakes, the earthquake department at university of engineering and technology Peshawar, has been analysing and improving the seismic capability of structures in preparation for future earthquakes [5]. The analysis presented here on existing joints constructed with having no standard code regulations. Because many of the structures built during the relevant time period include flexural reinforcement bar cut-off in plastic hinges locations in beam and column connections [7], the focus of this study was on how seismic detailing in the hinging zones improved behaviour. Two suggestions were seismic hooks and moving the lap splices away from

1st International Conference on Advances in Civil & Environmental Engineering, University of Engineering & Technology Taxila, Pakistan

Conference date 22 &23 Feb 2022

the joint outsides of the columns as per special moment resistance frame guidelines [8]. This shear reinforcement was to keep longitudinal reinforcement combine. This strategy's effectiveness was evaluated using two beam column joints, based on several studies performed in the past [9], [10]. All were vertically cycled to replicate seismic deformations after being axially loaded to represent the dead load. The lateral cycles were quasi-static and continued until the strength was significantly reduced. The seismic durability of the connection was determined by the number of cycles necessary to induce this degradation. Seismic durability, in this sense, refers to a column's capacity to survive huge inelastic cyclic deformations without losing significant strength, hence maintaining lateral resistance, stiffness, and energy dissipation. This seismic confinement with seismic hooks was proven to significantly improve seismic performance.

2   RESEARCH APPROACH

2.1   Model details, Setup and specifications

The experimental work cited here is performed at university of engineering at technology Peshawar laboratory. This research looks at the behaviour of probable locations of plastic hinges with splices. As a result, the span-to-depth ratios of the test members had to be efficient for flexural stiffness and failure responsible for flexural modes to take precedence comparatively to shear failure modes; the test specimen column and beam were 2.743 and 2.438 metres long, respectively. The applied axial load was designed to keep the force from the top storey constant across the research study, In 5 to 20 percent of range for load limit [11] on column as an axial regime from top of the story to bottom of the story. Because larger values give the most brittle behaviour, the concrete stresses responsible for compression failure, 15% is considered. Dead load on column was applied, but the base of the column was held on a plate with a pin connection. Cyclic loading applied at the end of cantilever to perform the cyclic loading study. Number 19 and 16 longitudinal bars were used in the beam and columns for Models 1 and 2, respectively, while number 10 was used for the shear reinforcement. All of the details are included in the Figure 1& Figure 2. Based on the experimental configuration, 14 and 308 Megapascal concrete and reinforcing steel are employed in the simulation. Axial an axial load of 190 kilo newton and 159 kilo newtons was applied for model 1 and model 2 respectively. Until failure, cyclic lateral loading was used in the tests.

1st International Conference on Advances in Civil & Environmental Engineering, University of Engineering & Technology Taxila, Pakistan

Conference date 22 &23 Feb 2022
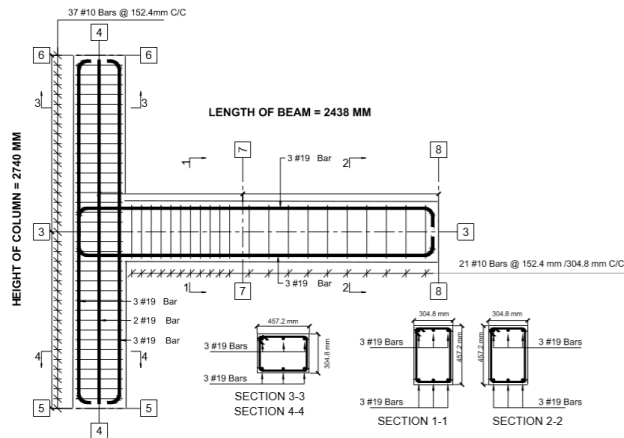
Figure 1: Model 1 incorporated in the study with Special moment resistance guidelines.
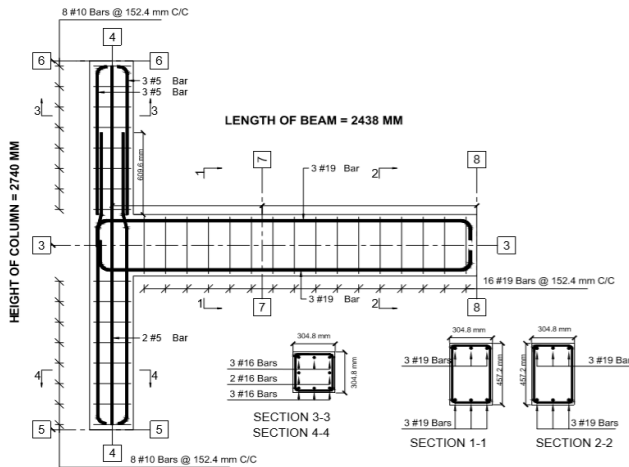
Figure 2: Model 2 incorporated in the study with Special moment resistance guidelines.

To cause initial yield, the model 1 and model 2 required a tip lateral displacement of 25.4 mm coupled with the cyclic protocol shown in Figure 3. Using cyclic displacement, all subsequent displacements of all specimens were defined as shown in Figure 3.

1st International Conference on Advances in Civil & Environmental Engineering, University of Engineering & Technology Taxila, Pakistan

Conference date 22 &23 Feb 2022
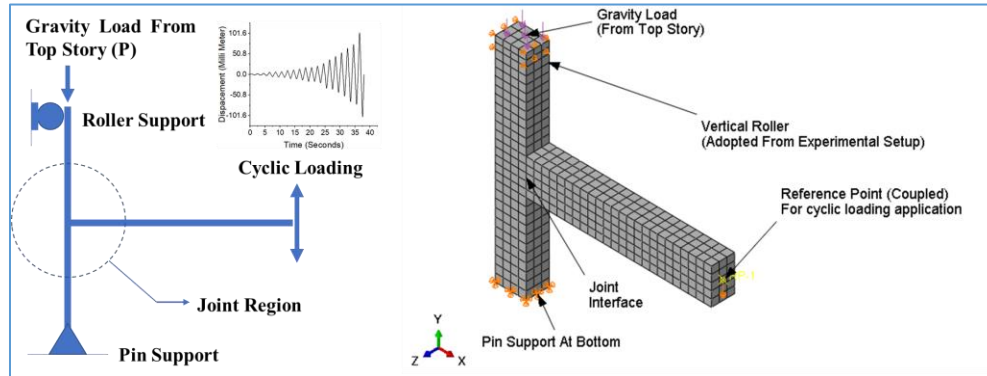
Figure 3: The Modeling Idealization incorporated in the cyclic protocol and models end conditions.

2.2 Numerical Approach.

A numerical model was created using ABAQUS/CAE, and the advanced formulations available in ABAQUS were used to evaluate the models' performance and to post-process the data. Concrete damage plasticity was used to represent the concrete, as this approach is suitable for simulation of such kind of studies [12]. Elastoplastic steel was used to model the reinforcing steel. Models are generated in part modules in ABAQUS, and properties are assigned in the property's module with the appropriate sections as per ABAQUS documentation [13]–[17] All of the models were afterwards put together in assembly module. Steps are specified as a dead load for monotonic pressure from the top storey, while cyclic loading is applied to the model's cantilever end as many researchers have adopted this approach [18]. The source files are meshed after assembling. After meshing, the input files are prepared and submitted to ABAQUS for analysis using the python interpreter instead of the graphical user interface.

2.3 Results

After successful simulation the results obtained are shown in the Figure 4 & Figure 5 respectively. The results obtained presents the cyclic degradation in the Figure 4 while the compression damage and misses stresses in Figure 5 respectively.

1st International Conference on Advances in Civil & Environmental Engineering, University of Engineering & Technology Taxila, Pakistan

Conference date 22 &23 Feb 2022
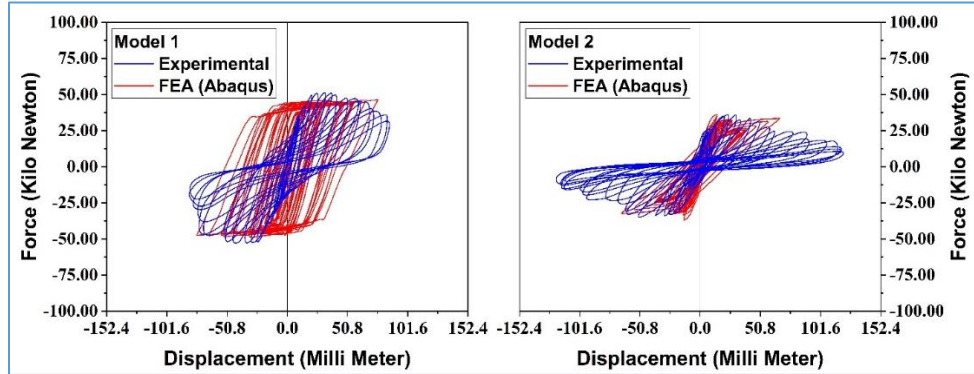
Figure 4: hysteresis curve obtained for Model 1 and Model 2
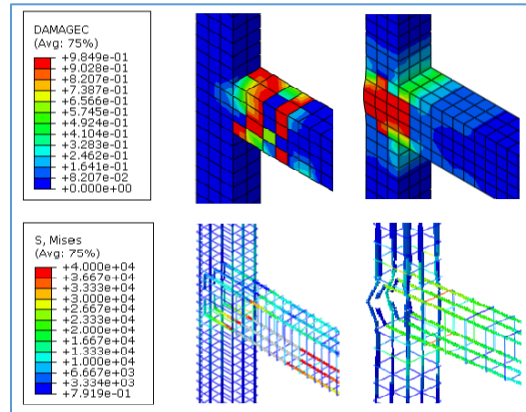
Figure 5: Compression damage and Misses stresses observed in the models. Left model presents model 1 while right represents model 2.

After post processing the results, the energy absorption for both of the models is evaluated with respect to drift of 0.82, 1.60 & 2.48% tabulated in Table 1.

Table 1: Energy Absorption observed during simulation for both models

Model	Drift	Energy Absorption (Kilo joule)	
		Experimental	Numerical
Model 1	0.82	0.57283	0.59093
Model 2		0.42119	0.54758
Model 1	1.60	1.46350	1.46961
Model 2		1.07901	1.09938
Model 1	2.46	2.34157	2.29792
Model 2		1.66849	1.66657

1st International Conference on Advances in Civil & Environmental Engineering, University of Engineering & Technology Taxila, Pakistan

Conference date 22 &23 Feb 2022

3 CONCLUSION AND RECOMMENDATIONS

Some major findings based on the data obtained (Figure 4 & Figure 5) are presented in the points below at the conclusion of this study, that are;

- The column of the model 2 has a plastic hinge that indicates a strong beam weak column connection and should be avoided in construction. Model 1 depicts the benefit, whereas Model 2 illustrates the opposite scenario.
- Because the lack of confining action in the joint zone causes more plastic deformation in the Model 2 than in the Model 1, it is advisable to keep the lap splices away from the joints. This was one of the primary causes of failure during the 2005 earthquake in Pakistan-administered Kashmir.
- When compared to Model 1, the joint's initial stiffness is lower, resulting in a decrease in the joint's capacity to endure further deformation, and the joints deform quickly as a result.
- •The energy absorptions for model 1 and model 2 reveal 5.17 percent, 37.03 percent, and 63.13 percent improvement, respectively, for 0.82, 1.60, and 2.46 drift. As a result, it demonstrates how the stirrup spacing given with no overlap in the joint improved the joint's energy absorption. To increase ductility, it is advised that shear reinforcement be provided in accordance with the standard moment resistance frame requirements.

REFERENCES

[1] M. S. Siddique and J. Schwarz, "Elaboration of multi-hazard zoning and qualitative risk maps of Pakistan," *Earthq. Spectra*, vol. 31, no. 3, pp. 1371–1395, 2015, doi: 10.1193/042913EQS114M.

[2] Pakistan Metrological Department and NOSAR, *Seismic Hazard Analysis and Zonation for Pakistan, AJK*, 1st ed. Azad and Jammu Kashmir: NORSAR, PMD, 2007.

[3] "Seismic Fragility of Reinforced Concrete Moment Resisting Frame Structures In Pakistan | Request PDF," *Conference: 4th International Conference on Sustainability in Process IndustryAt: Peshawar, Pakistan*, 2019. https://www.researchgate.net/publication/334288271_Seismic_Fragility_of_Reinforced_Concrete _Moment_Resisting_Frame_Structures_In_Pakistan (accessed Jan. 13, 2022).

[4] Seismic Provisions, "Building Code of Pakistan (Seismic Provisions 2007)," p. 303, 2007, doi: 10.1193/042913EQS114M.

[5] G. D. Dellow, Q. Ali, S. M. Ali, S. Hussain, B. Khazai, and A. Nisar, "Preliminary reconnaissance report for the Kashmir earthquake of 8 October 2005," *Bull. New Zeal. Soc. Earthq. Eng.*, vol. 40, no. 1, pp. 1–8, 2007, doi: 10.5459/bnzsee.40.1.18-24.

[6] M. Rizwan, "Performance – based seismic assessment of rc smrf compliant & noncompliant structures," 2019.

[7] Dr. A. Naeem, "A Summary Report on Muzaffarabad Earthquake," 2005. [Online]. Available: https://reliefweb.int/report/pakistan/pakistan-summary-report-muzaffarabad-earthquake.

[8] J. P. Moehle, J. D. Hooper, and C. D. Lubke, *Seismic design of reinforced concrete special moment frames: a guide for practicing engineers*, 2nd ed., vol. 2, no. 1. National Institude of Standards and Technology, 2008.

[9] A. K. Kaliluthin, S. Kothandaraman, T. S. Suhail Ahamed, and A. Professor, "A Review on Behavior of Reinforced Concrete Beam-Column Joint," *Int. J. Innov. Res. Sci. Eng. Technol. (An ISO Certif. Organ.*, vol. 3297, no. 4, pp. 11299–11312, 2014, [Online]. Available: www.ijirset.com.

1st International Conference on Advances in Civil & Environmental Engineering, University of Engineering & Technology Taxila, Pakistan

Conference date 22 &23 Feb 2022

[10] T. Supaviriyakit, A. Pimanmas, and P. Warnitchai, "Nonlinear finite element analysis of non-seismically detailed interior reinforced concrete beam-column connection under reversed cyclic load," *ScienceAsia*, vol. 34, no. 1, pp. 49–58, 2008, doi: 10.2306/scienceasia1513-1874.2008.34.049.

[11] B. H. L. Coffman, M. L. Marsh, and C. B. Brown, "REINFORCED-CONCRETE COLUMNS Experimental Specification Earthquakes in the western Washington region may produce moderately Test Arrangement Control Column (Column t)," vol. 119, no. 5, pp. 1643–1661, 1993.

[12] C. Le Thanh, H.-L. Minh, and T. Sang-To, "A nonlinear concrete damaged plasticity model for simulation reinforced concrete structures using ABAQUS," *Frat. ed Integrità Strutt.*, vol. 16, no. 59, pp. 232–242, Dec. 2021, doi: 10.3221/IGF-ESIS.59.17.

[13] "The Part module." https://abaqus-docs.mit.edu/2017/English/SIMACAECAERefMap/simacae-m-Prt-sb.htm (accessed Jun. 30, 2020).

[14] "Creating a mesh." https://abaqus-docs.mit.edu/2017/English/SIMACAECAERefMap/simacae-t-mgncreatemesh.htm (accessed Jun. 30, 2020).

[15] "Amplitude Curves." https://abaqus-docs.mit.edu/2017/English/SIMACAEPRCRefMap/simaprc-c-amplitude.htm (accessed Jun. 30, 2020).

[16] "The Interaction module." https://abaqus-docs.mit.edu/2017/English/SIMACAECAERefMap/simacae-m-Itn-sb.htm (accessed Jun. 30, 2020).

[17] "Preprocessing, simulation, and postprocessing." https://abaqus-docs.mit.edu/2017/English/SIMACAEGSARefMap/simagsa-c-abspresimulationpost.htm (accessed Mar. 12, 2021).

[18] M. Omidi and F. Behnamfar, "A numerical model for simulation of RC beam-column connections," *Eng. Struct.*, vol. 88, pp. 51–73, 2015, doi: 10.1016/j.engstruct.2015.01.025.

Parametric Study of Group Helical piles under Axial loading: A Numerical Study

Hamza Ahmad Qureshi, Muhammad Safdar
Earthquake Engineering Center, Department of Civil Engineering, University of Engineering and Technology, Peshawar, Pakistan.
18pwciv4995@uetpeshawar.edu.pk ; drsafdar@uetpeshawar.edu.pk

Muhammad Haseeb
Department of Civil Engineering, University of Engineering and Technology, Peshawar, Pakistan.
19pwciv5328@uetpeshawar.edu.pk

ABSTRACT

Helical pile is an emerging deep foundation technique used in advanced countries. The compressive capacity of helical pile is greater than conventional piles. Its capacity depends on the number of helix, inter helix spacing, pile group spacing, helix diameter, helix diameter configuration, embedment depth, shaft diameter etc. In this paper, parametric study of group helical piles under axial (compressive) loading have been done using Plaxis 3D software. Only three parameters, number of helix, inter helix spacing, pile group spacing are studied in this paper. It was found that the settlement reduced upto 29.73 % with the addition of helix to conventional piles. The capacity of group helical piles increases with the increase in number of helix, inter helix spacing and pile group spacing.

1. INTRODUCTION

Helical pile is an innovative technique, of deep foundation that offers high structural stability and resistance by transferring the structure's load to the earth [1]. The fundamental components of a helical pile, include lead (main shaft), extensions, a helical bearing plate, and a pile cap. The first part into the ground is the lead section which usually contains one or more helical bearing plates and a tapered pilot. The lead section is pushed deeper into the ground by extension sections until it reaches the required bearing level [2]. A hydraulic drive head delivers torque and axial force to install helical piles into the ground [3]. During the 1830s. Alexander Mitchell, a blind brickmaker and civil engineer from Ireland, was the first to create helical piles made of wrought iron to sustain structures erected on mud and sand [2]. Because soil displacement around the helices was limited, it was discovered that the capacity of helical pile group was greater than conventional pile groups [3]. Helical piles provide a number of advantages over conventional piles, like high axial capacity, light-weight and mobile installation equipment, minimal soil disturbance, low noise and vibration during installation, and its re-usability are just a few of these benefits [4].

Several researchers [5, 6, 7] studied that the bearing capacity increases as the number of helixes increases, whereas the bearing capacity also increase as the distance between helix increases. Ahmed *et al.* [7] did numerical modelling using Plaxis 3D and found the maximum pile capacity with the three-helix case rose by 115.4% when compared to the case without helix. When comparing the case of spacing 3.5D (diameter of helix) to the case of spacing 0.5D, the pile capacity increased by 130.7%. The compressive [6, 8, 9, 10] and tensile capacity [9, 11] of helical piles increase as the helix diameter increases. The ultimate axial compressive capacity is increased by 43.13% to 60% when the helix diameter is doubled. As the helix size grows, the axial compressive capacity increases as well. The axial compressive capacity of a helical pile with decreasing helix diameter from top to bottom is greater than the reverse configuration of helixes and consistent helixes sizes [6].

2. NUMERICAL MODELING

Several researchers [12, 13] use Plaxis-2D program for numerically analyzing helical piles, but in this study, we use Plaxis-3D to find the parametric behavior of group helical piles under axial loading. In our model we created raft, pile and helix as plate elements. The dimension of raft was 1ft by 1ft, 2 in above from soil surface. Helical pile of length 1.5 ft, having shaft diameter (d) of 0.75 in and helix diameter (D) 1.5 in. Soil hardening model was used in the analysis. Other properties of the soil and plate elements are shown in table 1.

Table 1 Properties of the soil and plate elements

Properties	Soil	Plate (Raft, shaft, helix)
Unit weight (lb/ft^3)	95	168
Young's modulus (lbf/ft^2)	200599	1441000000
Poisson's ratio	0.3	0.31
Cohesion	0	-
Angle of internal friction (degree)	34	-
Reduction factor	0.71	-
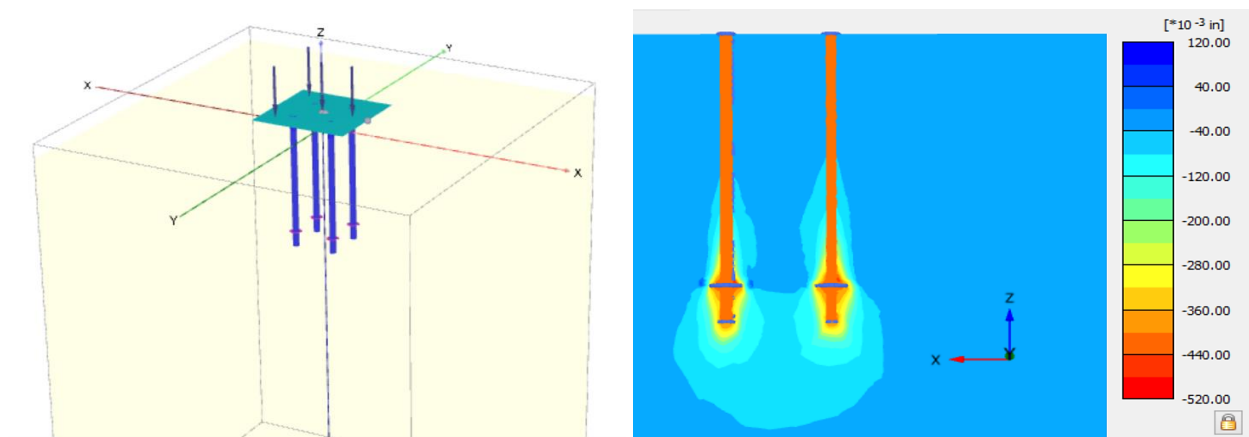
Figure 1: Group of 4 Helical Piles with Single Helix (Left), Vertical Cross Section of Helical Pile with Single Helix after Numerical Analysis.

3. RESULT AND DISCUSSION

In this study we only discuss the effect of number of helix, inter helix spacing and pile group spacing, on the axial compressive capacity of helical piles. A load of 2000 N was applied on raft and settlement was recorded for each condition.

3.1 Number of helix:

We found that introducing helix to conventional piles reduce the settlement upto 29.73 %. It was also noted that with the increase in helix number, the pile group settlement is further reduced as shown in figure 2. Spacing between the helix was kept 2D.
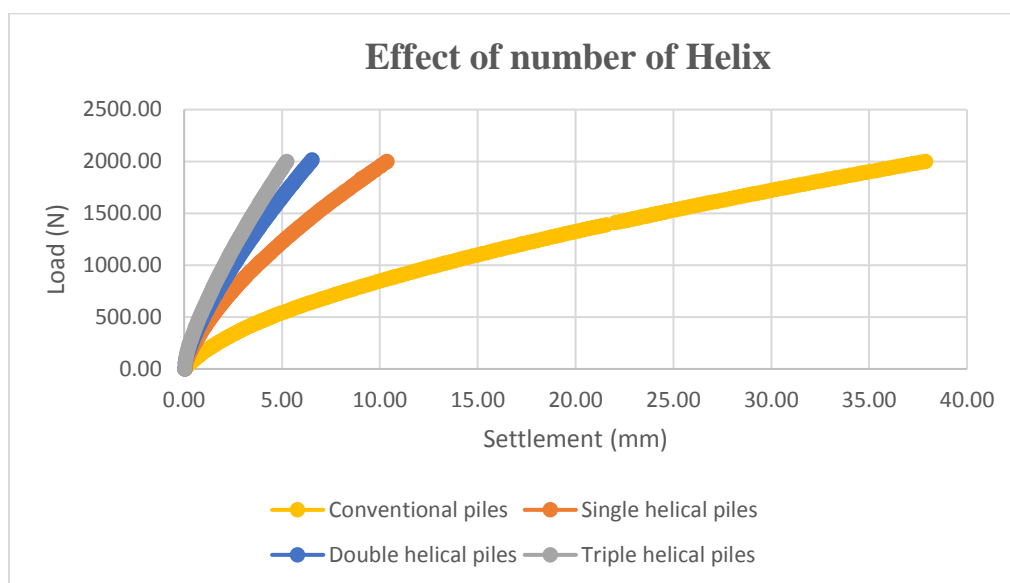
Figure 2: Effect of Helix Number on the Axial Capacity of Helical Piles

3.2 Inter helix spacing:

To find the effect of inter helix spacing, numerical modelling of double helical pile group with a spacing of 2D, 3D, 4D between the helix was done. It was noted that the settlement reduced due to increase in the spacing between the helix (as shown in figure 3), but the effect observed in our analysis was very low because of the small dimension of our model.
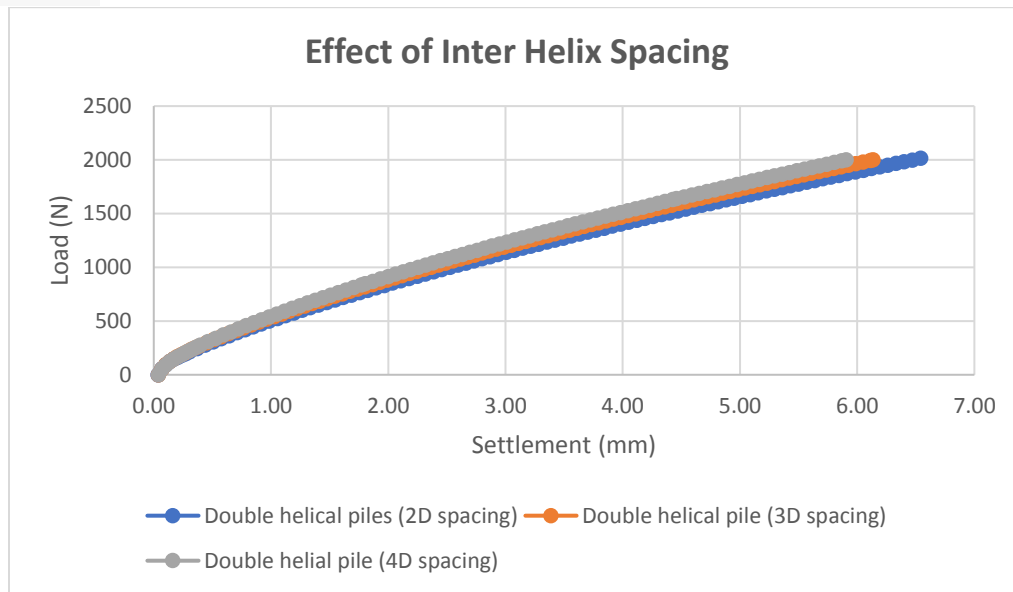
Figure 3: Effect of Inter Helix Spacing on the Axial Capacity of Helical Piles

3.3 Pile group spacing

The effect of pile group spacing was also evaluated, it was found that as the spacing between the piles increases, settlement also reduces as shown in figure 4. It's because the interaction between the group pile decreases.
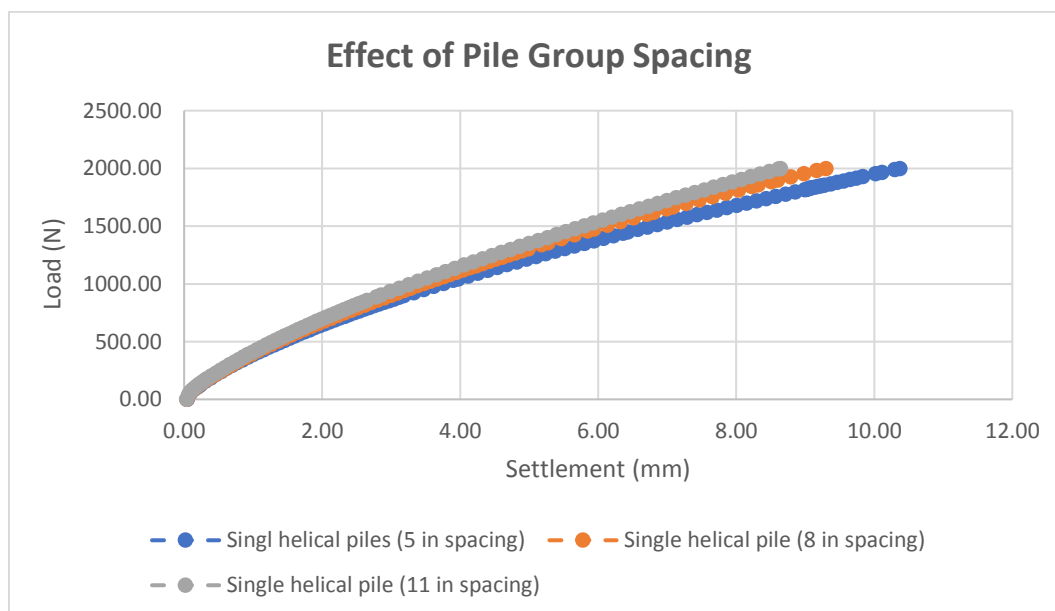
Figure 4: Effect of Pile Group Spacing on the Axial Capacity of Helical Piles

4. CONCLUSION

- Introducing helix to conventional piles reduce the settlement upto 29.73 %.
- With the increase in helix number, pile group settlement is further reduced.
- It was noted that the settlement reduced due to increase in the spacing between the helix.
- It was found that as the spacing between the piles increases, settlement also reduces.
- In general, we can say that the capacity of group helical piles increases with the increase in number of helix, inter helix spacing and pile group spacing.

5. REFRENCES

1. Weidong, Li., *Axial load tests and numerical modeling of single-helix piles in cohesive and cohesionless soils*, Acta Geotechnica. 2018
2. Howard, A., Perko, *Helical Piles: A Practical Guide to Design and Installation*. 2009, p.2-3,5-11.
3. Elsherbiny, Z., *Axial and lateral performance of helical pile groups.* The University of Western Ontario. 2011: London, Canada.
4. Lanyi, Stephen, A., *Behavior of Helical Pile Groups and Individual Piles under Compressive Loading in cohesive soil.* 2017: Edmonton. Alberta.
5. Stephen, A., L. Bennett and L. Deng*, Axial load testing of helical pile groups in glaciolacustrine clay.* 2018: Canada.
6. Dewi, R., *Effect of Helical Geometry on the Axial Compressive Capacity.* International Journal of Innovative Science and Research Technology. 2020.
7. Ahmed. S. Ali, Nahla. M. Salim, and Husam. H. Baqir., *Numerical Modelling of Axially Loaded Helical Piles: Compressive Resistance.* Civil Engineering Department. University of Technology. 2021: Baghdad, Iraq.
8. Safdar, M. and H. A. Qureshi, *Parametric Study and Design Method for Axial Capacity of Helical piles: A Literature Review*, Journal of Applied and Emerging Sciences*,* vol. 11, no. 2, 2021.
9. Gandhi, S.R., *Numerical analysis of helical piles in cohesionless soil.* International Journal of Geotechnical Engineering. 2017: India.
10. Abbas, *Parameters Affecting Screw Pile Capacity Embedded in Soft Clay Overlaying Dense Sandy Soil.* Materials Science and Engineering. **745**: 2020.
11. Gavin, *In situ and laboratory tests in dense sand investigating the helix-to-shaft ratio of helical piles as a novel offshore foundation system*. Frontiers in Offshore Geotechnics. 643–648. 2015.

1st International Conference on Advances in Civil & Environmental Engineering, University of Engineering & Technology Taxila, Pakistan

Conference date 22 &23 Feb 2022

Suitability of Flood Frequency Method for Kabul River and Swat River Near Charsadda

Kamil Ahmad
M.Sc Scholar/Civil Engineering Department
University of Engineering & Technology Taxila, Pakistan
kamipak11@gmail.com

Usman Ali Naeem
University of Engineering & Technology Taxila, Pakistan
usman.naeem@ uettaxila.edu.pk

Sayed Suliman
Deputy Director/Irrigation Department KPK
engrsayed.suliman@gmail.com

ABSTRACT

The importance of frequency analysis cannot be denied while estimating the magnitude of a flood for certain return period. The reliability of results in this case depends on the data length and data quality. In this study flood frequency analysis has been performed for Swat River and Kabul River near district Charsadda. Three methods of flood frequency analysis Gumbel's Extreme Value Distribution, Log-Pearson Type III Distribution (LP3), and Log-Normal Distribution (LN) were used to calculate maximum flood peaks for different return periods. The annual peak discharge data, from 1965 to 2018 (54 years flood data) was collected from Irrigation Department KPK. The data was segmented into different data sets A, B, C, D and E, after which frequency analysis was performed. For sufficient data, it was concluded for both the rivers that LN method is the most suitable approach for predicting the peaks against return periods of more than 25 years.

KEYWORDS: Flood Frequency, Log Normal, Kabul River, Swat River, Annual Peaks

1   INTRODUCTION

Due to climate change the occurrence of natural disasters is increasing which results in increase of sea level [1]. When a natural disaster such as flood occurs the water due to its high velocity can wash away the belongings and can cause human causalities [2]. Floods may occur anywhere having different sizes and durations. In year 1931 the world's deadliest flood occurred and it caused the deaths of between 2 to 4 million residents living in China [3]. Pakistan suffered the most devastating floods of its entire history during the year 2010 which caused a great loss of human life as well as losses to the economy and infrastructure [4].The design and building of certain structures, hence, depends on the magnitude of flood. In Pakistan, the floodplains are transforming into permanent habitant [5].Mainly the floods in district Charsadda are due to heavy rainfalls of monsoon and occur often both in Swat River and Kabul River. As a result it brings

1st International Conference on Advances in Civil & Environmental
Engineering, University of Engineering & Technology Taxila, Pakistan
Conference date 22 &23 Feb 2022

considerable damage to the people, and economy of the area [6]. To mitigate such impacts, it is required to predict the future floods against certain return periods. Certain methods are available to perform frequency analysis. In this study an effort has been made to determine the most suitable frequency analysis method for the two rivers in district Charsadda.

2 STUDY AREA AND DATA COLLECTION

Kabul River is one of the main rivers in Pakistan which originates from Hindu Kush Mountains in Afghanistan. In Pakistan the Kabul River passes through Charsadda, Nowshera and Peshawar [7].
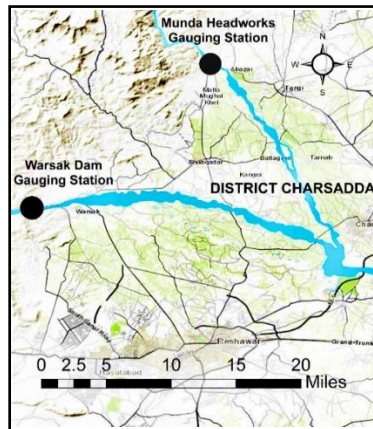
Figure 1: Location Map of the Study Area

The Swat River also originates from Hindu Kush mountains and is a perennial river. The main source of Swat River is Usho River, Gabral River and high glacial valleys. The Swat River joins the Kabul River near Charsadda [8]. River Swat is gauged at Munda headworks whereas River Kabul is gauged at Warsak Dam as shown in Figure 1.

3 METHODOLOGY

The annual peak discharge (m³/s) of Kabul River and Swat River from 1965 to 2018 (54 years flood data) was collected from Irrigation Department Khyber Pakhtunkhwa. The acquired data was then segmented into five data sets (broadly distinguished as limited and sufficient data) as shown in Table 1. After that the flood frequency analysis, by using Log Normal distribution (LN), Log Pearson Type III distribution (LP3) and Gumbel's Extreme Value distribution was performed.

Table 1 Segmented Data for both Kabul and Swat Rivers

Sr. No	Data Set	Duration in Years	Period Considered
1	A	10 (limited data)	1965 to 1974
2	B	20 (limited data)	1965 to 1984
3	C	30 (Sufficient data)	1965 to 1994
4	D	40 (Sufficient data)	1965 to 2004

1st International Conference on Advances in Civil & Environmental Engineering, University of Engineering & Technology Taxila, Pakistan

Conference date 22 &23 Feb 2022

5	E	54 (Sufficient data)	1965 to 2018

The idea of segmentation was to evaluate the performance of the above three mentioned methods under limited to sufficient data conditions for both Kabul and Swat Rivers. The flood peaks having return periods of 10, 15, 25, 50 and 100 years were estimated against each data set through Gumbel's, LP3 and LN approach. The estimated peaks were then compared with respective annual actual flows. In case of Gumbel's approach, a series of annual peak data having N observations is required to be assembled in descending order from where the annual mean of the peak flow data $\bar{x}$ is calculated and standard deviation σ_x is further computed which is given as in Equation (01).

$$\sigma_x = \sqrt{\frac{1}{(N-1)}\sum_{i=1}^{n}(x-\bar{x})^2} \tag{01}$$

By using Gumbel's distribution Table [9], the respective values of $\overline{y_n}$ and S_n are then noted against the N data observations. The values of $\overline{y_n}$ and S_n are then used to calculate the flood frequency factor K as given in Equation (02).

$$K = \frac{y_t - \overline{y_n}}{Sn} \tag{02}$$

y_t can be calculated by the following Equation (03), in which T is the desired return period value e.g. 25, 50 or 100 etc.

$$y_t = -[ln.ln.(\frac{T}{T-1})] \tag{03}$$

Finally, the above calculated values are put in Equation (04) to estimate the probable flood magnitude x_T of the desired return period (say 25, 50 or 100 years etc).

$$x_T = \bar{x} + K.\sigma_x \tag{04}$$

In case of LP3 method the random hydrologic series X is transformed into Z variates logarithmic form (base 10) which is given in Equation (05).

$$Z = logx \tag{05}$$

From where the mean $\bar{Z}$ and standard deviation σ_z is computed for the sample size N and is given in Equation (06).

$$\sigma_Z = \frac{\sum(Z-\bar{Z})^2}{(N-1)} \tag{06}$$

In LP3 the coefficient of skew C_S is calculated by using Equation (07).

$$C_S = \frac{N\sum(Z-\bar{Z})^3}{(N-1)(N-2)\sigma_Z{}^3} \tag{07}$$

While using LN the value of the coefficient of skew C_S is taken 0.

1st International Conference on Advances in Civil & Environmental Engineering, University of Engineering & Technology Taxila, Pakistan

Conference date 22 &23 Feb 2022

With the help of coefficient of skew C_S the Frequency Factor K_Z is selected from Table [10]. The recurrence interval Z_T against Z series is calculated by using Equation (08)

$$Z_T = \bar{Z} + K_Z\sigma_Z \qquad (08)$$

Finally the magnitude of maximum flood X_T for return period T is computed by using the following Equation (09).

$$X_T = antilog\ (Z_T) \qquad (09)$$

4   RESULTS AND DISCUSSION

For the whole data set E, the frequency analysis was carried out by using the three approaches against return periods of 15, 25, 50 and 100 years as shown in Figure 2 (Swat River) and Figure 3 (Kabul River). In case of Swat River, it was found that the peaks computed by Gumbel's method were much higher as compared to other two methods. But in case of Kabul River the maximum flood computed by LN was found higher than the other two methods.
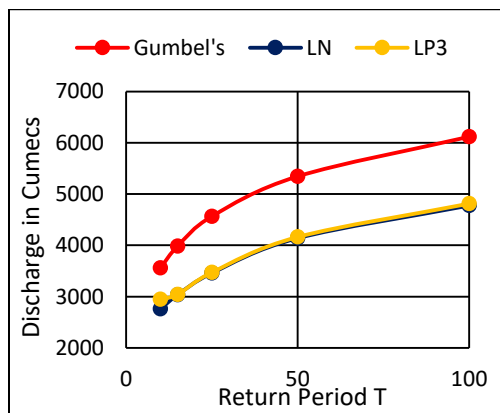
Figure 2: River Swat at Munda Headwork's   *Figure 3: River Kabul at Warsak Dam*
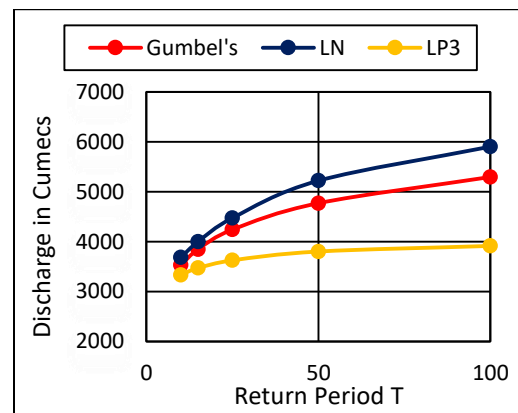
Maximum flood peaks against the return periods of 10, 15, 25, 50 and 100 years were computed by considering each data set of both rivers as given in Table 1. After estimation of respective flood peaks, a comparison was established between the estimated and actual peaks which helped to determine the most suitable technique. For Swat River the results of first two data sets A and B show that the maximum flood for return period 10, 15 and 25 year computed by LP3 method was found close to the actual annual peak discharge. Whereas, for the return periods of 50 and 100 years, the maximum flood computed by LN method was found near to gauged values as shown in Table 2 and Table 3.

Table 2 Maximum flood peaks compared and computed against different return periods for Swat River using Data Set A

Return Period	Estimated Flood in cumecs			Observed Flows in cumecs
	Gumbel's	**LP3**	**LN**	
10	2271	**2043**	2252	1871

1st International Conference on Advances in Civil & Environmental Engineering, University of Engineering & Technology Taxila, Pakistan

Conference date 22 &23 Feb 2022

15	2499	**2119**	2458	2011
25	2781	**2222**	2770	2011
50	3160	2342	**3266**	3629
100	3535	2418	**3723**	3629

Table 3 Maximum flood peaks compared and computed against different return periods for Swat River using Data Set B

Return Period	Estimated Flood in cumecs			Observed Flows in cumecs
	Gumbel's	**LP3**	**LN**	
10	2155	**2081**	2268	2011
15	2360	**2172**	2482	2011
25	2613	**2298**	2809	2406
50	2953	2454	**3331**	3629
100	3290	2559	**3814**	3629

In case of data set C and D, the result shows that peaks computed by LN was found near to gauged values as compared to other two methods which is shown in Table 4 and 5.

Table 4 Maximum flood peaks compared and computed against different return periods for Swat River using Data Set C

Return Period	Estimated Flood in cumecs			Observed Flows in cumecs
	Gumbel's	**LP3**	**LN**	
10	2231	**2177**	2396	2011
15	**2428**	2255	2609	2406
25	2672	2378	**2931**	3629
50	2999	2482	**3441**	3629
100	3323	2559	**3908**	3629

Table 5 Maximum flood peaks compared and computed against different return periods for Swat River using Data Set D

Return Period	Estimated Flood in cumecs			Observed Flows in cumecs
	Gumbel's	**LP3**	**LN**	
10	2173	2125	**2394**	3629
15	2360	2187	**2610**	3629
25	2591	2268	**2938**	3629
50	2901	2356	**3457**	3629
100	3209	2407	**3935**	3629

For Kabul River the peaks estimated by LP3 against the return periods of 10, 15, 25, 50 and 100 years were found close to respective actual annual peaks for data sets A and B. The results are tabulated in Table 6 and Table 7.

Table 6 Maximum flood peaks compared and computed against different return periods for Kabul River using Data Set A

1st International Conference on Advances in Civil & Environmental Engineering, University of Engineering & Technology Taxila, Pakistan

Conference date 22 &23 Feb 2022

Return Period	Estimated Flood in cumecs			Observed Flows in cumecs
	Gumbel's	LP3	LN	
10	4422	**4019**	4072	3279
15	4838	**4260**	4350	3524
25	5352	**4597**	4763	4021
50	6042	**5093**	5396	4324
100	6727	**5511**	5959	4324

Table 7 Maximum flood peaks compared and computed against different return periods for Kabul River using Data Set B

Return Period	Estimated Flood in cumecs			Observed Flows in cumecs
	Gumbel's	LP3	LN	
10	4074	**3838**	3848	3414
15	4426	**4072**	4089	4021
25	4862	**4416**	4444	4021
50	5446	**4930**	4984	4324
100	6027	**5380**	5460	4324

In case of data sets C and D, the flood peaks computed by Gumbel's against the return periods of 10, 15 and 25 years were found closest to measured discharge. Whereas, for the return periods of 50 and 100 years, LN method ensures the closest results. The respective values are tabulated in Table 8 and Table 9.

Table 8 Maximum flood peaks compared and computed against different return periods for Kabul River using Data Set C

Return Period	Estimated Flood in cumecs			Observed Flows in cumecs
	Gumbel's	LP3	LN	
10	**3742**	3578	3562	4021
15	**4050**	3803	3772	4021
25	4431	**4335**	4079	4324
50	4943	4649	**4542**	4324
100	5450	5111	**4984**	4324

Table 9 Maximum flood peaks compared and computed against different return periods for Kabul River using Data Set D

Return Period	Estimated Flood in cumecs			Observed Flows in cumecs
	Gumbel's	LP3	LN	
10	**3507**	3373	3371	4324
15	**3801**	3584	3580	4324
25	**4164**	3896	3887	4324
50	4651	4368	**4353**	4324
100	5134	4786	**4763**	4324

1st International Conference on Advances in Civil & Environmental Engineering, University of Engineering & Technology Taxila, Pakistan

Conference date 22 &23 Feb 2022

5   CONCLUSIONS

Following are the conclusions.

Swat River

- ✓ For the prediction of flood magnitude against the return periods of more than 25 years, LN method was found best and does not depend on the data length.
- ✓ In case when the length of data is compromised, LP3 method can be helpful in predicting more realistic flood magnitudes against the return periods up to 25 years.

River Kabul

- ✓ LP3 method was found best against all the considered return periods where the provided data length limits up to 20 years.
- ✓ For the data length of more than 20 years, LN method proves best for predicting flood magnitudes against the return periods of more than 25 years.

REFERENCES

1. Adger, W.N., *Vulnerability.* Global environmental change, 2006. **16**(3): p. 268-281.
2. Marvi, M.T., *A review of flood damage analysis for a building structure and contents.* Natural Hazards, 2020. **102**(3): p. 967-995.
3. Uddin, K., et al., *Application of remote sensing and GIS for flood hazard management: a case study from Sindh Province, Pakistan.* American Journal of Geographic Information System, 2013. **2**(1): p. 1-5.
4. Khan, A.N., *Analysis of 2010-flood causes, nature and magnitude in the Khyber Pakhtunkhwa, Pakistan.* Natural hazards, 2013. **66**(2): p. 887-904.
5. Hashmi, H.N., et al., *A critical analysis of 2010 floods in Pakistan.* African Journal of Agricultural Research, 2012. **7**(7): p. 1054-1067.
6. Khan, A.N., et al., *Causes, Effects and Remedies: A Case Study of Rural Flooding in District Charsadda, Pakistan.* Journal of Managerial Sciences, 2013. **7**(1).
7. Khattak, M.S., et al., *Floodplain mapping using HEC-RAS and ArcGIS: a case study of Kabul River.* Arabian Journal for Science and Engineering, 2016. **41**(4): p. 1375-1390.
8. Farooq, M., M. Shafique, and M.S. Khattak, *Flood frequency analysis of river swat using Log Pearson type 3, Generalized Extreme Value, Normal, and Gumbel Max distribution methods.* Arabian Journal of Geosciences, 2018. **11**(9): p. 1-10.
9. Selaman, O.S., S. Said, and F. Putuhena, *Flood frequency analysis for Sarawak using Weibull, Gringorten and L-moments formula.* J. Inst. Eng, 2007. **68**: p. 43-52.
10. Benson, M.A., *Uniform flood‑frequency estimating methods for federal agencies.* Water resources research, 1968. **4**(5): p. 891-908.

Impact of Accessibility and Traffic Heterogeneity on Mobility of Multilane Open Access Highway

Jamal Ahmed Khan, Dr M. Bilal Khurshid

PGWing SCEE, National University of Sciences and Technology (NUST), Islamabad, Pakistan, Director Transportation, Frontier Works Organization (FWO), Rawalpindi, Pakistan

jahmed.tnphd15nit@student.nust.edu.pk , Khurshid90@gmail.com

Dr Arshad Hussain

PGWing SCEE, National University of Sciences and Technology (NUST), Islamabad, Pakistan,

drarshad@nit.nust.edu.pk

ABSTRACT

Rapid urbanization and open accessibility along national highways have impacted their mobility to a great deal in Pakistan. This study intends to explore the effect of traffic heterogeneity and accessibility on mobility of open access multilane highway. It was observed that the average speed of vehicles was considerably lower than the posted speed limit that confirms the decrease in overall mobility of the highway. Detail analysis of license plate matching data confirmed that the highway is providing access to the surrounding area reasonably well, but at the same time, it is also a major reason for the decrease in mobility of same highway. Another finding of the research is that the travel time of cars, vans, and heavy vehicles is significantly associated with the volume of heavy vehicles in the traffic flow. However, no significant relationship is found between the proportion of slow-moving vehicles and the travel time of cars, vans, and heavy vehicles.

KEYWORDS: Mobility, Accessibility, Multi-Lane highway, Traffic Heterogeneity

1. INTRODUCTION AND LITERATURE REVIEW

Mobility refers to the through portion of trips and is most affected by supply and demand, land use, and other factors on the road. In highway systems, mobility is provided by high-type facilities, such as freeways, expressways, and other multilane-divided highways. However, due to rapid urbanization, change in land-use patterns, and open accessibility along highways, the mobility of multilane highways has been explicitly reduced in developing countries like Pakistan. These open access highways are different from partial or complete controlled access highways because, in these highways, vehicles can directly access to and from the adjacent properties without any ramps or designated access points.

According to the highway capacity manual, multilane highways are divided highways with a minimum of two lanes in each direction. Their speed limits usually range from 60-100 Kph with zero or partial access control [1]. These roadway facilities usually provide through service that ranges from 60 to 100 percent depending upon either it is a freeway or arterial [2].

Several studies have been carried out in developing countries like India, Egypt to analyse the impact of traffic composition on the capacity as well as mobility of multilane highways and found that it decreases when the percentage of heavy vehicles (H.V.) in traffic stream [3-5]. Similar trends were observed even in developed countries as well like America and China [6, 7]. There are many mobility performance measures for highways that are currently in use all over the world. Travel Time is a relatively new and modern method used in more developed

1st International Conference on Advances in Civil & Environmental Engineering, University of Engineering & Technology Taxila, Pakistan

Conference date 22 &23 Feb 2022

countries that cater for both user and travel agency requirements [8]. Furthermore, measures such as travel speed, and travel delay can also be used as they are easy to understand for road users. Travel time reliability is also of great concern for road travellers and transportation planners. Federal Highway Administration has specified measures that describe time reliability in slightly different ways, including Travel Time Index, Buffer Index, Planning Time, and Planning Time Index [9].

Synthesis of past literature confirmed that multilane highways are usually designed to provide greater mobility and less accessibility. This condition is achievable on fully controlled or partial controlled access highways, but the situation differs in open access highways. Therefore, this study explored how open access (no access control) along with traffic composition impacted mobility on such highways.

2. METHODOLOGY AND SITE SELECTION

The video photographic survey method was adopted for the collection of field data using three teams. Three observation points were established for installing the video cameras: start of section, end of section, and mid-block. Data comprised twelve sessions for which the data was recorded on six working days in morning and afternoon peak hours. All the vehicles are classified into six categories: Car, Van, Bus, Truck, Trailer, and other slow vehicles (O.V.) (Motorbikes, Rickshaw, Tractor Trollies, and Animal driven carts).

The study section of 9km was selected in the northern region of national highway N-5 (Four lane divided highway) between two major cities of Islamabad and Taxila. The study section was selected away from any intersection with no significant horizontal and vertical grade. The posted speed limit was 100kph and 90kph for LTV and HTV respectively. The selected section had a sub urban roadside characteristic with a high density of commercial properties (12.22 property per km), access points (Major Road access density =1/km, Street access density =3.88/km) and U-turn (1.11/km).

License Plate Matching Technique data was used to measure travel time based on guidelines suggested by the travel time data collection handbook that was afterward used to calculate the average speed of each category of vehicle [10]. The baseline condition i.e. free flow speed (FFS) for the analysis was identified as posted speed [11]. So, by using (1), the free flow T.T. can be calculated as:

$$TT = \frac{s}{v} \tag{1}$$

For LTV
$$Free\ Flow\ TT = \frac{9}{100} * 60$$
$$Free\ Flow\ TT = 5\ mins\ 15\ sec$$

Whereas for HTV
$$Free\ Flow\ TT = \frac{9}{90} * 60$$
$$Free\ Flow\ TT = 6\ mins$$

3. RESULTS AND ANALYSIS

Figure. 1 illustrates the traffic composition for all twelve sessions. The presence of cars and vans in the traffic stream was substantial as they share about 65–70 percent of total traffic. At the same time, the proportion of trucks and trailers were around 9-16 and 1-2.5 percent,

1st International Conference on Advances in Civil & Environmental Engineering, University of Engineering & Technology Taxila, Pakistan

Conference date 22 &23 Feb 2022

respectively. It was also observed that a substantial number of slow-moving vehicles like rikshaw, motorbikes and tractor trollies were also present in the traffic stream. However, very few buses were observed during the study period.
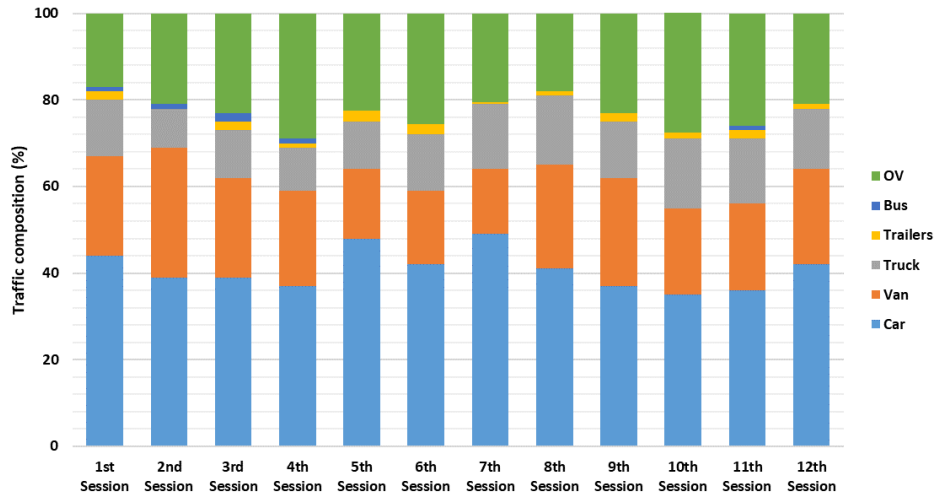
Figure 1. Composition of Traffic for all Sessions

3.1 Speed and Travel Time Analysis

Speed limits are usually decided based on 85th percentile speed; therefore, 85th percentile speed and travel time were considered for analysis[12]. According to Fitzpatrick [12], multilane-divided highways passing through an urban area having level terrain (as in the case of this study) have anticipated operating, posted, and design speeds as 80-100,70-90 and 70-100 kph, respectively. However, the analysis (Table 1) shows a significant speed reduction for all the vehicle categories. Moreover, speed reduction can also be verified by equating the actual posted speed with the observed values in the field. These evaluations strengthen the supposition that the overall mobility of the highway has been significantly reduced. The major speed reduction was observed in the case of trailers, whereas least in the case of cars when compared with the free flow speed (Posted speed) (Table 1).

As expected longest average travel time was for the trailer (Table 1). On the other hand, the buses have the shortest travel time of 9.7 mins. But as the buses are only 1% of total traffic so they are not truly representative of the actual condition of travel on the highway. However, more important is the travel time of cars and vans since they constitute approximately 65 % of the total traffic. Travel time for these two categories is double the free-flow travel time, i.e., approximately 12 mins compared to 5.4 mins to traverse the section. This increase in travel time could be due to several reasons, however, a few apparent reasons were density of adjacent commercial properties, major road access density, street access density and density of U-turn to access the opposite side of the road. The other major reason is the presence of a large number of heavy vehicles in the traffic stream that is discussed in successive sections. The delay computed for the corridor is 8.42 mins indicating that the average travel time (14.18 mins) is more than double the free-flow travel time (5.7 mins). At the same time planning time index (PTI) values revealed that the average travel time in the study section is 2.66 times more than

1st International Conference on Advances in Civil & Environmental Engineering, University of Engineering & Technology Taxila, Pakistan

Conference date 22 &23 Feb 2022

free-flow travel time, which means for a 15-minute trip, 40 minutes should be planned. A study conducted under similar conditions in India by Bharti, Sekhar [13] also observed a higher value of 3.2 for interrupting flow urban corridors.

Table 1. Classified Travel Time and Speed Data

Vehicle Type	Free Flow T.T.	Max. T.T. (mins)	Min. T.T. (mins)	Avg. T.T. (mins)	85th Percentile TT	Average Speed (km/h)	85th Percentile TT	Variance (%)	T.T. Delay (mins)	Planning Time Index
Car	5.4	16.0	7.3	10.1	11.9	54.8	65.1	2.9	6.5	2.37
Van	5.4	22.0	6.5	10.4	12.0	53.6	61.9	4.0	6.6	2.44
Truck	6	27.7	9.0	14.6	19.8	40.7	53.4	24.6	13.8	3.96
Trailer	6	17.6	11.0	15.0	17.2	37.6	44.3	12.2	11.2	2.91
Bus	6	10.0	9.2	9.7	10.0	55.6	57.0	0.2	4	1.66
Average	5.7	-	-	11.96	14.18	48.46	-	-	8.42	2.66

Mehran and Nakamura [14] during their study on Tokyo Expressway found that a trip may take 30 % and 100 % more time than free-flow travel time during the morning and afternoon peak periods, respectively. That study was conducted in a limited-access environment with the same speed limit as in the case of this study, i.e., 100 km/h. However, in case of this study travel time was observed to be more than 1.5 times than free-flow travel time. The above comparisons showed that open access along the road and direct access to adjacent properties surely results in highway mobility reduction.

3.2 Mobility vs. Open Accessibility

A detailed analysis of travel time and accessibility was carried out to study the impact of open access on highway mobility. The percentage of undetected LTV and HTV at both the start and endpoint of the study section ranges from 71-83 % of total LTV traffic and 72-89 percent of total HTV traffic respectively. A possible reason for the large number of undetected HTV was the existence of aggregate crushing plants in the study section that were major attraction area for HTV traffic. Whereas LTV vehicles dispersed in the study section and used highway to access nearby or connected areas Figure 2 shows that as the number of vehicles accessed from and to the adjacent area increased, it reduced the speed of vehicles (relative to FFS). Regression analysis was carried out to explore the relationship between the percentage of undetected vehicles and the percentage speed reduction of vehicles relative to FFS, as shown in Figure 2. A strong relationship (R^2 =0.68) is found between the speed reduction of LTV relative to FFS and the percentage of undetected LTV. However relatively weak relationship has been found between the percentage of undetected LTV on the speed reduction of HTV relative to FFS (R^2 =0.20) and the percentage of undetected HTV on speed reduction of HTV relative to FFS (R^2 =0.31). In comparison, no significant relationship has been observed between the percentage of undetected HTV and the speed reduction of LTV relative to FFS. According to Figure 2, every 1 % increase in LTV using the highway for accessing adjacent land, highway mobility in terms of % speed reduction of LTV (relative to FFS) is reduced by 1.05 %.

4

1st International Conference on Advances in Civil & Environmental Engineering, University of Engineering & Technology Taxila, Pakistan

Conference date 22 &23 Feb 2022
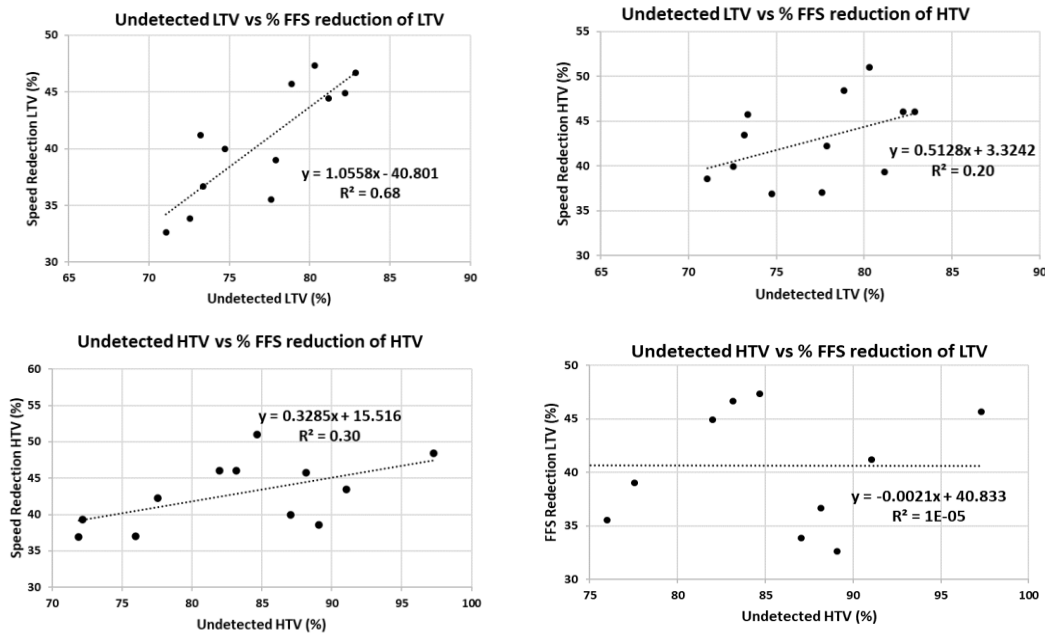
Figure 2. Relationship Between Highway Mobility and Open Access

3.3 Mobility vs. Traffic Composition

To better understand the influence of traffic composition on surrounding traffic, reduction in vehicular speed relative to FFS was investigated. Regression analysis of the relationship between percentage of HTV in the traffic stream and percentage speed reduction of LTV and HTV (relative to FFS) is presented in Figure 3. It is revealed that percentage of heavy vehicles has a strong positive relationship with the percentage speed reduction of LTV relative to FFS ($R^2 = 0.65$). However, a very weak relation has been observed between %HTV and % speed reduction of HTV relative to FFS ($R^2 = 0.20$).
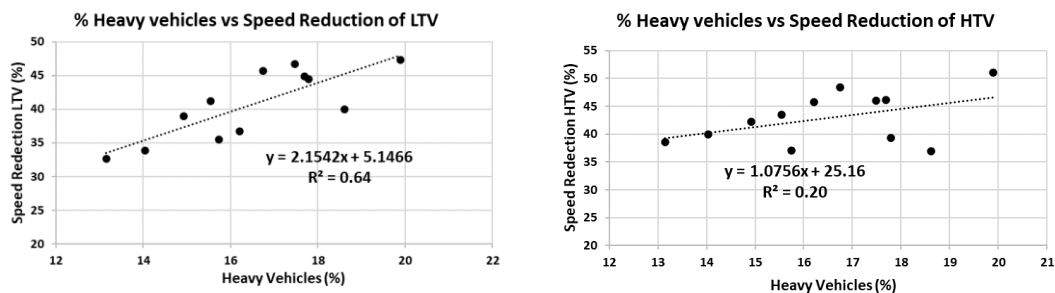
Figure 3. Relationship Between Heavy Vehicle % and Speed Reduction of Vehicles

According to Figure 3, the beta coefficient (β) of the independent variable (% heavy vehicles in this case) confirmed that for every 1% increase in the percentage of heavy vehicles, the mobility of highway in terms of speed reduction of LTV is reduced by 2.1%. It might be because trucks have limited manoeuvrability, and it takes a lot of time for a truck to accelerate after braking or overtake another truck, making a platoon of vehicles behind it, impacting the speed of surrounding traffic. On the other hand, the presence of a substantial amount of other

1st International Conference on Advances in Civil & Environmental Engineering, University of Engineering & Technology Taxila, Pakistan

Conference date 22 &23 Feb 2022

slow-moving vehicles in the traffic stream has no significant impact on the travel time of LTV and HTV. It could be supported by the fact that they do not occupy much space on the road, particularly two and three-wheelers, not impacting the overall travel flow.

4. CONCLUSIONS

The investigation of results revealed that highway is performing its function of providing accessibility reasonably well but at the same time it is significantly impacting the overall mobility. Comparison of results of this study with other studies also confirmed that open access has a substantial impact on the mobility of multilane-divided highways compared to limited or controlled access. Therefore, to improve mobility on open access highways, it is necessary to provide frontage roads that permit access to abutting land and at the same time allow high-speed travel on the main highway. The regression analysis also revealed that the percentage of heavy vehicles in the traffic stream is another significant factor associated with a speed reduction of highway mobility. However, other slow-moving vehicles (Two, three-wheelers, non-motorized vehicles) do not significantly impact the mobility of any of the vehicles.

REFERENCES

1. HCM, *HIGHWAY CAPACITY MANUAL 2010*. Transportation Research Board, National Research Council, Washington, DC. 2010. 1207.
2. Roess, R.P., E.S. Prassas, and W.R. McShane, *Traffic engineering*. 2011.
3. Semeida, A.M., *New models to evaluate the level of service and capacity for rural multi-lane highways in Egypt*. Alexandria Engineering Journal, 2013. **52**(3): p. 455-466.
4. Chandra, S., A. Mehar, and S. Velmurugan, *Effect of traffic composition on capacity of multilane highways*. Ksce journal of civil engineering, 2016. **20**(5): p. 2033-2040.
5. Azeem, S., W. Imran, and G. Amin, *Mix Use Traffic and Added Impedance Affecting Traffic Flow Variables*. SSRG International Journal of Civil Engineering, 2019. **6**: p. 48-50.
6. Moridpour, S., E. Mazloumi, and M. Mesbah, *Impact of heavy vehicles on surrounding traffic characteristics*. Journal of advanced transportation, 2015. **49**(4): p. 535-552.
7. Gao, C., et al., *Influence of Large Vehicles on the Speed of Expressway Traffic Flow*. Advances in Civil Engineering, 2020. **2020**.
8. Lasley, P., et al., *Developing a total peak period travel time performance measure: An updated concept paper*. Transportation research record, 2014. **2420**(1): p. 15-22.
9. FHWA, *Travel time reliability: Making it there on time, all the time. FHWA Report, Federal Highway Administration, US Department of Transportation, http://www.ops.fhwa.dot.gov/publications/tt /index. htm.* 2017.
10. Turner, S.M., et al., *Travel time data collection handbook*. 1998, United States. Federal Highway Administration.
11. Deardoff, M.D., B.N. Wiesner, and J. Fazio, *Estimating free-flow speed from posted speed limit signs*. Procedia-social and behavioral sciences, 2011. **16**: p. 306-316.
12. Fitzpatrick, K., et al. *Design speed, operating speed, and posted speed limit practices*. in *82nd Annual Meeting of the Transportation Research Board, Washington, DC*. 2003.
13. Bharti, A.K., C.R. Sekhar, and S. Chandra, *Travel time reliability as a level of service measure for urban and inter-urban corridors in India*. CURRENT SCIENCE, 2018. **114**(9): p. 1913.
14. Mehran, B. and H. Nakamura. *Performance Evaluation of Highway Segments Using Travel Time Based Performance Measures*. in *Proceedings of the Eastern Asia Society for Transportation Studies Vol. 6 (The 7th International Conference of Eastern Asia Society for Transportation Studies, 2007)*. 2007. Eastern Asia Society for Transportation Studies.

1st International Conference on Advances in Civil & Environmental Engineering, University of Engineering & Technology Taxila, Pakistan

Conference date 22 &23 Feb 2022

Climatic Condition of Pakistan and the Prospect of Geothermal Energy

Muhammad Tayyab Naqash, Qazi Umar Farooq, Ouahid Harireche
Department of Civil Engineering,
Faculty of Engineering, Islamic University of Madinah, Kingdom of Saudi Arabia
tayyab@iu.edu.sa, umar@iu,edu.sa, ouahid.harireche@iu.edu.sa

ABSTRACT

To augment Pakistan's long-term energy needs, it is imperative to develop renewable energy technologies such as geothermal. The country has a lot of potential in terms of renewable energy. Despite this, it remains an energy-deficient country that relies on crude imports to meet its demands. This study examines Pakistan's meteorological conditions by providing climate data collected over the last 36 years using the RET-screen program. Based on the literature, the country's geothermal energy potential has been discussed. For authorities and potential investors, the study emphasized the country's substantial geothermal energy resources.

KEYWORDS: Geothermal energy, thermal contours, precipitation, renewable energy, earth temperature, temperature profile, climatic conditions.

1   INTRODUCTION

With rising global energy consumption, a substantial transition from conventional energy to renewable energy sources is required to avoid global warming. Summers in Pakistan are long, especially in the country's central and southern regions. Due to a lack of supplies, regular power outages are common in rural and urban areas, including megacities like Karachi, Lahore, Peshawar, and Rawalpindi. Furthermore, most geothermal hot springs and mud volcanoes are found inside Pakistan's seismic belt, which serves as a source of sustainable geothermal energy. However, no one or organization has comprehensively assessed their full potential [1], [2].

Central South-Eastern Asia is made up of China, Pakistan, and India, and it is a developing region in search of energy supplies to meet its expanding economic demands. These countries have tremendous potential for regional prosperity and socioeconomic growth. Pakistan's energy consumption is comparable to that of its neighbours; nonetheless, it may play a critical role in the region by facilitating energy sharing. Pakistan's electricity demand increases at an annual rate of 11%, while generation is comparatively low. It's worth noting that geothermal energy is one of the most ancient, adaptable, and widely used renewable energy sources. However, due to a lack of understanding, confidence, and management, researchers and practitioners in this field in the country have paid less attention.

The impact of solar radiation, rainfall, the seasonal cycle in the atmosphere, air temperature, local vegetation, soil type, and depth, among other factors, causes monthly variations in soil temperature. Pakistan has sunny weather throughout the country, resulting in shallow geothermal

1st International Conference on Advances in Civil & Environmental Engineering, University of Engineering & Technology Taxila, Pakistan

Conference date 22 &23 Feb 2022

energy supplies in nearly all of the country's provinces [3] [4]. These could be used for cooling & heating buildings and supplying hot water during the winters [5] [6] [7] [8].

2   EXISTING STUDIES ON GEOTHERMAL ENERGY

Tauqir and Shuja [9] used surface indications of geothermal activity in different regions, such as the Chagai volcanic arc and its extension to Iran, to link tectonic and geologic aspects. Khan and Raza [10] observed geothermal gradients' function in Pakistan's hydrocarbon exploration. Tauqir and Shuja [11] concluded that the geotectonic environment in Pakistan and surface manifestations show the possibility of recovering geothermal fluids in sufficient quantities to warrant commercial exploitation. Bakht [12] conducted a similar study by providing an overview of the geothermal resources after examining the geologic and tectonic features related to the surface manifestation of geothermal activity in Pakistan. Alam et al. [13] found that the indications of geothermal energy are present in geotectonic or geothermal environments. Zaigham and Nayyar [3], [13] studied the renewable hot, dry rock geothermal energy source and its potential. Ahmad and Rashid [14] studied the geothermal energy resources of Pakistan for electric power generation. Abbas et al. [15] highlighted the national-level issues and challenges from a geothermal energy perspective by investigating geothermal energy sources, technologies, and potential. Ahmad [4] provided a general overview on the potential of geothermal energy in Pakistan, whereas Ahmad et al. [16] presented a comparative review of the renewable energy sectors and sharing opportunities. Younas et al. [17] provided a survey on the geothermal energy potential for electric power generation by discussing the current energy crisis in Pakistan. Gondal et al. [5] conducted an assessment of geothermal energy and discovered that, while hydrothermal resources have significant potential for geothermal energy, no significant practical measures have been made.

Mehmood et al. [18] studied the geothermal energy potential of Pakistan, based on abandoned oil and gas wells, to efficaciously reutilize them by incorporating subsurface data of thermal characteristics of rock sequence. Moreover, Aftab et al. in [19] also studied the exploration prospects of geothermal energy in Pakistan for implementation in different areas. Kazmi and Sheikh [20] They investigated a hybrid geothermal–photovoltaic–wind system for a village in Azad Jammu and Kashmir, Tattapani, having adequate geothermal energy accessible from hot springs to meet the village's perennial baseloadload requirements. They presented a design with the lowest net possible cost. Shah [21] used Fuzzy Delphi, Fuzzy Analytical Hierarchy Process, and environmental Data Envelopment Analysis to investigate the feasibility of six renewable energy sources for hydrogen generation in Pakistan: wind, solar, biomass, municipal solid waste, geothermal, and micro-hydro. Zeb et al. [22] used the Transient Plane Source technique to investigate the heat transport parameters of porous igneous basalt rocks in pore spaces under ambient air conditions.

3   CLIMATIC DATA FOR MAJOR CITIES

It is worth mentioning that Pakistan imports fossil fuel in petroleum and hardly accomplishes the domestic energy demand [15]. It has an extensive range of variability and is located between (240–

1st International Conference on Advances in Civil & Environmental Engineering, University of Engineering & Technology Taxila, Pakistan

Conference date 22 &23 Feb 2022

370 °) North latitudes and (620–750 °) East longitudes. The north is dominated by mountains, which have wet to arid climates; higher altitudes receive winter precipitation in snow. To determine the viability of harvesting any renewable energy within the specified location, accurate values of climatic data are required. The RET-screen provides climate data based on mean average annual values over 36 years. This is beneficial for researchers and investors to use in their evaluation of any renewable energy project. Because of its geographical location (between 25° and 36° N), Pakistan has a continental climate with extreme seasonal and daily temperature changes [20].

Table 1: Climatic data for major cities of Pakistan

City	Lat	Lon	min__air_temp	max_air_temp	Precipitation	earth_Temp
Karachi	24.9	67.1	7.1	45.8	244.4	29.6
Gawader	25.1	62.3	10.2	41.1	84.3	28.5
Hyderabad	25.4	68.4	12.5	39.9	89.2	28.3
Sukkur	27.7	68.8	4.6	49.0	135.6	29.5
Sibi	29.5	67.9	-5.3	39.3	58.9	19.9
Dera Ghazi Khan	30	70.7	3.3	48.1	214.4	28.0
Multan	30.2	71.5	-4.3	38.9	191.3	18.5
Quetta	30.3	66.9	3.5	49.2	197.6	28.2
Lahore	31.5	74.4	2.7	48.7	302.7	27.2
Bannu	33	70.6	1.1	46.9	443.9	24.5
Kohat	33.6	71.4	1.4	46.2	392.2	24.0
Islamabad	33.7	73.1	3.6	47.0	743.7	24.6
Taxila	33.8	74.1	-0.1	42.6	889.8	19.9
Peshawar	34	71.5	1.7	45.2	791.7	22.1
Abbottabad	34.1	73.2	-7.3	34.6	791.0	13.5
Gilgit	35.9	74.3	-14.2	32.0	464.7	9.3
Chitral	36	71.7	-15.2	29.3	485.0	7.1

4   ISOTHERMS AND CONTOURS

From the climatic assessments, it can be observed that the minimum temperature in winter reaches around -30 °C (**Figure 1 left**). In contrast, the country's maximum temperature during summer reaches about 50°C (Figure 1 right) [7]. On the other hand, the annual average maximum temperature reaches about 50° C in summer in the country's southern region.

1st International Conference on Advances in Civil & Environmental Engineering, University of Engineering & Technology Taxila, Pakistan

Conference date 22 &23 Feb 2022
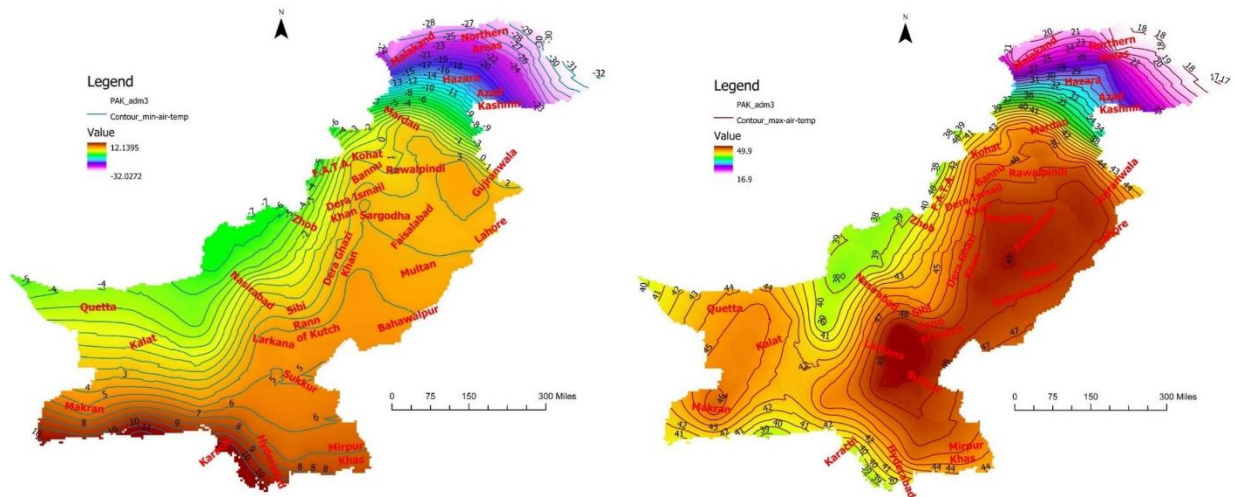
Figure 1: Yearly earth temperature Isotherms minimum (left) and maximum (right)

The middle Indus River basin has a tropical and continental climate, but the lower Indus River basin has an arid environment. Baluchistan has an arid environment with the least precipitation throughout the year, making it vulnerable to desertification [23].
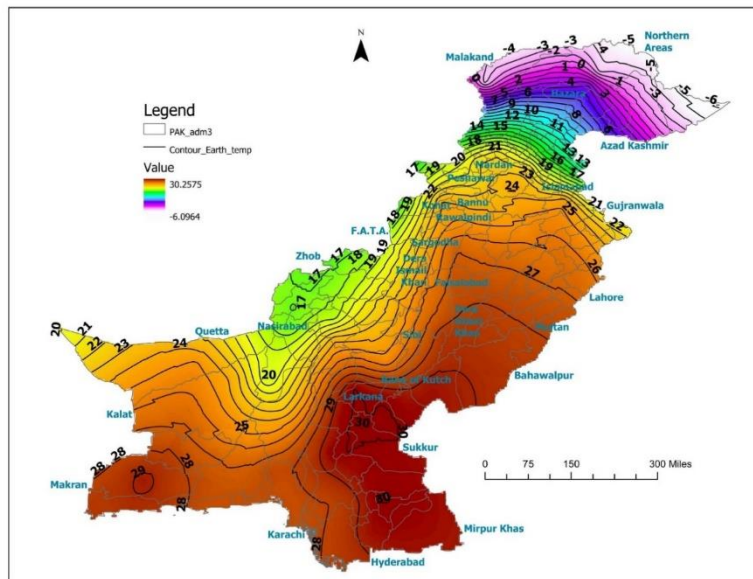
Figure 2: Isotherms of average yearly earth temperature

The climate in Islamabad, the capital city, ranges from a daily low of 2 °C in January to a daily high of 38 °C in June. According to the data, most of the annual precipitation falls between July and August, with the rest of the year seeing substantially less rain. The isotherms of earth

1st International Conference on Advances in Civil & Environmental Engineering, University of Engineering & Technology Taxila, Pakistan

Conference date 22 &23 Feb 2022

temperature for Pakistan are shown in Figure 2. For a general overview and assessment, these are believed to be useful for technicians involved in geothermal system design. These are based on daily statistics from the RET-screen database for 36 years (1983 to 2020).

5   CONCLUSIONS

- Geothermal energy is now regarded as one of the most promising alternative energy sources. It is renewable, dependable, clean, and environmentally friendly.
- Pakistan offers a diverse range of conventional and non-conventional renewable energy sources with considerable potential. Many of them haven't been thoroughly investigated, exploited, or developed. Government support could be critical in exploiting the country's geothermal resources.
- Many rural communities lack electrification because they are too far from the national grid to be connected. As a result, shallow geothermal is required, which may provide the need for indoor cooling in the summer and heating in the winter while using relatively less electric energy.
- The isotherm shows that the maximum temperature in the summer in most parts of the country is around $50\,^{o}$ C. In some regions of the country, however, the minimum temperature in the winter is approximate -30° C. These contours are beneficial to technicians who are assessing and designing geothermal systems.
- Geothermal resources in Pakistan's northern regions have been recognized for a long time, but no real attempt has been made to tap this potential for electric power generation.

6   REFERENCES

[1]   J. Hirunlabh, S. Thiebrat, and J. Khedari, "Chilli and garlic drying by using waste heat recovery from geothermal power plant," *RERIC Int. Energy J.*, 1999.
[2]   Y. He and G. Wang, "Assessing high temperature geothermal resource - An economic and environmental perspective," *Int. Energy J.*, 2018.
[3]   N. A. Zaigham and Z. A. Nayyar, "Renewable hot dry rock geothermal energy source and its potential in Pakistan," *Renewable and Sustainable Energy Reviews*, vol. 14, no. 3. pp. 1124–1129, Apr. 2010, doi: 10.1016/j.rser.2009.10.002.
[4]   J. Ahmad, "The geothermal energy potential of Pakistan clean sustainable solution for our energy future," 2014.
[5]   I. A. Gondal, S. A. Masood, and M. Amjad, "Review of geothermal energy development efforts in Pakistan and way forward," *Renewable and Sustainable Energy Reviews*. 2017, doi: 10.1016/j.rser.2016.12.097.
[6]   M. T. Naqash, Q. U. Farooq, and O. Harireche, "Assessment of Ground to Air Heat Transfer System for Local Soil Conditions," in *3rd Conference on Sustainability in Civil Engineering (CSCE'21)*, 2021, no. 21, pp. 2–7.
[7]   M. T. Naqash, Q. U. Farooq, and O. Harireche, "Assessment and feasibility of shallow geothermal for heating and cooling systems under local climatic and soil conditions," *Int. J. Energy, Environ. Econ.*, vol. 27 (4), pp. 235–255, 2021.
[8]   M. T. Naqash, M. H. Aburamadan, O. Harireche, A. AlKassem, and Q. U. Farooq, "The Potential of Wind Energy and Design Implications on Wind Farms in Saudi Arabia," *Int. J. Renew. Energy Dev.*, vol. 10, no. 4, pp. 839–856, Nov. 2021, doi: 10.14710/ijred.2021.38238.

1st International Conference on Advances in Civil & Environmental Engineering, University of Engineering & Technology Taxila, Pakistan

Conference date 22 &23 Feb 2022

[9]   T. A. Shuja, "Geothermal areas in Pakistan," *Geothermics*, 1986, doi: 10.1016/0375-6505(86)90083-0.

[10]   M. A. Khan and H. A. Raza, "The Role of Geothermal Gradients in Hydrocarbon Exploration in Pakistan," *J. Pet. Geol.*, 1986, doi: 10.1111/j.1747-5457.1986.tb00388.x.

[11]   T. A. Shuja, "Small geothermal resources in Pakistan," *Geothermics*, 1988, doi: 10.1016/0375-6505(88)90075-2.

[12]   M. S. Bakht, "An Overview of Geothermal Resources of Pakistan," *World Geotherm. Congr. Khyushu-Tohoku, Japan, May 28-June 10*, 2000.

[13]   N. Alam Zaigham, Z. Alam Nayyar, and N. Hisamuddin, "Review of geothermal energy resources in Pakistan," *Renewable and Sustainable Energy Reviews*. 2009, doi: 10.1016/j.rser.2007.07.010.

[14]   I. Ahmad and A. Rashid, "Study of geothermal energy resources of Pakistan for electric power generation," *Energy Sources, Part A Recover. Util. Environ. Eff.*, 2010, doi: 10.1080/15567030802606210.

[15]   T. Abbas, A. Ahmed Bazmi, A. Waheed Bhutto, and G. Zahedi, "Greener energy: Issues and challenges for Pakistan-geothermal energy prospective," *Renewable and Sustainable Energy Reviews*. 2014, doi: 10.1016/j.rser.2013.11.043.

[16]   S. Ahmed, A. Mahmood, A. Hasan, G. A. S. Sidhu, and M. F. U. Butt, "A comparative review of China, India and Pakistan renewable energy sectors and sharing opportunities," *Renewable and Sustainable Energy Reviews*. 2016, doi: 10.1016/j.rser.2015.12.191.

[17]   U. Younas *et al.*, "Pakistan geothermal renewable energy potential for electric power generation: A survey," *Renewable and Sustainable Energy Reviews*. 2016, doi: 10.1016/j.rser.2016.04.038.

[18]   A. Mehmood, J. Yao, D. Yan Fun, and A. Zafar, "Geothermal Energy Potential of Pakistan on the Basis of Abandoned Oil and Gas wells," *J. Pet. Environ. Biotechnol.*, 2017, doi: 10.4172/2157-7463.1000332.

[19]   S. M. Aftab, M. A. Farooqui, and T. Maqsood, "Exploration Prospects of Geothermal Energy in Pakistan," 2019, doi: 10.1130/abs/2019am-338378.

[20]   S. W. S. Kazmi and M. I. Sheikh, "Hybrid geothermal–PV–wind system for a village in Pakistan," *SN Appl. Sci.*, 2019, doi: 10.1007/s42452-019-0643-9.

[21]   S. A. A. Shah, "Feasibility study of renewable energy sources for developing the hydrogen economy in Pakistan," *Int. J. Hydrogen Energy*, 2020, doi: 10.1016/j.ijhydene.2019.09.153.

[22]   A. Zeb, M. Abid, M. A. Zeb, M. O. Qureshi, U. Younas, and I. Batool, "Measurement and prediction of thermal conductivity of volcanic basalt rocks from Warsak area," *Adv. Mater. Sci. Eng.*, 2020, doi: 10.1155/2020/4756806.

[23]   R. Anjum, X. He, J. I. Tanoli, and S. T. Raza, "Contemporary temperature fluctuation in urban areas of pakistan," *Atmosphere (Basel).*, 2017, doi: 10.3390/atmos8010012.

1st International Conference on Advances in Civil & Environmental Engineering, University of Engineering & Technology Taxila, Pakistan

Conference date 22 &23 Feb 2022

Premature Pavement Failures; Diagnosis & Remedies

Muhammad Abubakar, Prof. Dr. Naveed Ahmad
University of Engineering & Technology Taxila, Pakistan
mabubakar030@gmail.com; n.ahmad@uettaxila.edu.pk

ABSTRACT

This paper will visually examine, evaluate and provide remedial measures for premature failures in flexible pavements. It is quite important to examine and identify the causes that lead to premature failures in flexible pavement in order to save economy, repetition of efforts/manpower and permanent inconvenience for plying traffic. Premature failures is not only a dilemma of developing countries but even in country like United States premature failures can be seen i.e. early rutting in HMA. This work is consisted of three tasks: first covered the visual inspection and identification of the pavement failures, second investigated the actual causes of these failures while in third remedial measures are described after thorough investigation, experimental work and physically examining the response of remedial measures after executing them in field.

KEYWORDS: pavement failures, inspection, maintenance, remedies, early rutting

1. INTRODUCTION

Pavement distresses continue to happen despite significant advancements in pavement technology. Pavement deterioration process usually starts at very slow pace so that it may not usually noticeable while in some cases it accelerates at faster rate due to deficiencies and mishandling during construction. We are here considering the Premature Failures i.e. Failures that develop or establish before the completion of design life and expected no. of axles on which the pavement has been destined.

In Pakistan some of the roads constructed in remote areas have inappropriate design approach lacks proper check / supervision and usage of unspecified material during construction results in the premature and early failures. Indus Highway (N-55) from KM 940 to KM 970 ACW / ECW was selected for this study. An intensive field work was carried out on the existing pavement condition of this road. It was found out that most of the damaged pavement sections suffered from severe cracking in ACW while extensive rutting failures occurred in ECW. These failures in both sections emerged in early stages or immediately after construction.

In our research we are taking this part of **Indus Highway** also known as **National Highway 55 (N-55)**. Indus Highway is 1264 km long two to four-lane national highway that runs along the Indus River in Pakistan connecting the port city of Karachi with the North Western city of Peshawar via Dera Ismail Khan.

1st International Conference on Advances in Civil & Environmental Engineering, University of Engineering & Technology Taxila, Pakistan

Conference date 22 &23 Feb 2022

Fig: 1 (Indus Highway N-55)

2. PAVEMENT EVALUATION PROCEDURE

The objective of this study is to establish guidelines and find out the premature pavement failures, their causes, early diagnosis and remedial measures. This proposed method has some basic steps as follows:

i. Collection of Literature & Review
ii. Site Visit / Inspection
iii. Experimental work / Testing
iv. Determine the Causes of Failures
v. Revised JMF / Field execution
vi. Selection of best Maintenance option
vii. Final Report

3. CASE STUDY

The highway section of N-55 in this research is from KM 940 to KM 970 ACW / ECW. Dualization of this road has been done as a foreign funded project (Post Flood Rehabilitation) in 2010 while the construction was too hap hazard in this remote location the quality of work lags far behind the quality standards. The road fails to comply with moving traffic even before the DLC period. Large number of maintenance projects also fails before completion of their design life making situation worse. In this section of ECW pavement fails due to severe early rutting in newly laid HMA while main failure in ACW section is excessive alligator cracks. It is to be noted that alligator cracks and rutting phenomenon is so adverse in this whole region while not a single research or design review have been initiated by any concerned department while authorities blame that only over loading is the cause of early failure.

To-date there have been number of maintenance works accomplished i.e Structural/Functional overlay along with Crack Relief Layer, DST/TST, Bitmac and Seal Coat on Existing Road but after movement of heavy traffic both section fails to comply. This research will cover all aspects i.e. Failures their Causes, early Diagnosis and Remedial measures. Most of the maintenance solutions are already executed at Site near Karak and responded extraordinary well, thus giving us the best maintenance option.

1st International Conference on Advances in Civil & Environmental Engineering, University of Engineering & Technology Taxila, Pakistan

Conference date 22 &23 Feb 2022

4. FIELD SURVEY OF FAILURES
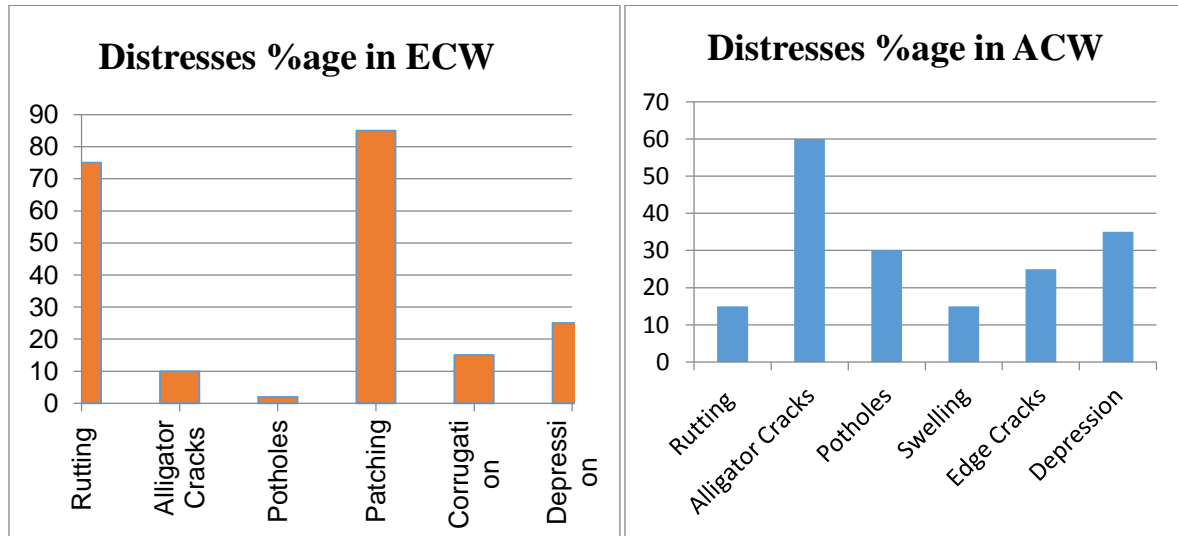
Graph1 (Distresses in newly laid Asphalt of ECW) Graph2 (Distresses in existing carriageway ACW)

During detailed inspection it is to be noted that under same traffic conditions the road portion beneath the CPEC Bridge which avoids direct sun light is still in perfect condition as shown in **fig 2** while as soon as we pass the bridge the rutting got more and more intense shown in **fig 3**. This phenomenon clearly depicts that overloading is not only the cause of extensive rutting but softening point of 60/70 bitumen in this harsh weather of DI Khan also plays an important part.

| *Fig: 2 No sign of Rutting underneath bridge (N-55)* | *Fig: 3 Severe Rutting after Bridge due to elevated pavement temperature (N-55)* |

Apart from softening point many factors of HMA are directly contributing in the formation of rutting i.e. gradation, aggregate blend, class of Asphalt, optimum binder content and flexible

1st International Conference on Advances in Civil & Environmental Engineering, University of Engineering & Technology Taxila, Pakistan

Conference date 22 &23 Feb 2022

pavement layers thickness. The more thickness and OBC of Asphalt the more it will prone to rutting especially in elevated temperatures. Finer gradation of ABC is more likely to rut earlier **fig 4**. Single layer of ABC of courser gradation (NHA Class A) is highly recommended in such areas **fig 5**.

| *Fig: 4 Excessive rutting in newly laid HMA having 1 Layer of AWC (5cm) Class B & 2 layers of ABC (16cm) Class B N-55* | *Fig: 5 Condition of road after 6 months (Revised JMF this Research) 1 layer of ABC (8cm) class A & 1 layer of AWC (5cm) class B* |

5. CAUSES OF FAILURES, DIAGNOSIS AND REMEDIAL MEASURES

Rutting

Causes:

- Extensive over loading
- Softening point of bitumen
- Dense graded asphalt
- Improper Mix Design (JMF)
    1. Filler Bitumen Ratio
    2. Grade of Bitumen
- Improper initial compaction of Hot Mix Asphalt
- Excess depth of flexible pavement thickness also leads to rutting

Early Diagnosis:

- Dense channels start to emerge under axles at early stage when road is opened to heavy traffic.
- Pavement starts to get stiffed and in-service compaction starts when opened to traffic due to lack of initial compaction during construction.

1st International Conference on Advances in Civil & Environmental Engineering, University of Engineering & Technology Taxila, Pakistan

Conference date 22 &23 Feb 2022

Remedial Measures:

- Controlled loading and heavy fines to over loaded vehicles.
- Comprehensive JMF.
  1. Filler bitumen ratio preferably between 1 & 1.5 (closer to 1.5 in hot areas is preferred).
  2. Aggregate blend curve preferably not be located exactly on mid-point (maximum density curve) a zig zag pattern is ideal.
  3. Aggregate blend needed to be on courser side of JMF limits in heavy traffic areas.
- VMA Curve (optimum binder content should preferably on dry side in hot climate)
- Using PMB (Polymer Modified Bitumen) in extreme climatic conditions.

Alligator Cracks

Causes:
- Ground / Sub surface movement of underlying layers.
- Inadequate pavement thickness
- Improper surface / sub surface drainage.
- Week or unspecified subgrade (A6/ A7 or black cotton soil).
- Insufficient embankment height as compared to N.S.L in water logged areas.
- Premature hardening of bitumen / inappropriate bitumen grade and quality.

Early Diagnosis:
- Pavement starts to deflect abnormally under axle of heavy duty vehicles.
- Subsurface ground movement.
- Ponding of water in creeks due to open texture Asphalt layer.
- If subgrade is opened for some time as a trial for heavy traffic before applying granular layers it will predict the response of sub structure and will easily be tackled accordingly.

Remedial Measures:
- Removal of unspecified and weak subbase or subgrade and to completely replace it with good quality material preferably non-plastic material in marshy and water prone areas.
- Sufficient embankment height in water logged or areas prone to floods.
- Adequate pavement thickness and proper surface / sub surface drainage.
- Planting trees near the embankment where water level is continuously rising.

1st International Conference on Advances in Civil & Environmental Engineering, University of Engineering & Technology Taxila, Pakistan

Conference date 22 &23 Feb 2022

6.   CONCLUSION

1. A-6 / A-7 embankment material to be removed completely and replaced before applying granular layers in specified and water prone areas.
2. Embankment height need to be increased where there is continuous dripping of water or crops like Rice and Sugarcane are in vicinity while N.S.L and F.R.L are adjoining.
3. Aggregate Base used in ACW is unspecified and do not comply with specifications, its CBR value coincides with Sub Base instead of aggregate base. It also has elevated PI values and sand equivalent is also lags far behind the specification limits. An additional layer of WBM or Aggregate Base can be laid in order to increase the structural capacity
4. Excessive over loading is not the only reason of extensive rutting in newly laid Asphalt of ECW as portrayed by local authorities, it just act as a catalyst and magnifying factor i.e. road is almost in perfect condition where there is not a direct sun light or hot weather.
5. Asphaltic base course layer is a governing factor and mainly contributes in rutting.
6. To avoid extreme early rutting in HMA layers, polymer modified bitumen (PMB) can be used to stabilizing the layer and to increase the softening point upto (10 - 15 degrees).
7. The Asphaltic base, class A of NHA specification with JMF on courser side responds 60 to 80 % better against rutting as compared to Class B.
8. The Asphaltic Base Class A resist well against rutting while it is open textured as compared to Class B. The probability of interconnection of voids is also greater, so urgent over lay of Asphaltic Wearing Class B (finer gradation) is highly recommended to seal off the surface in order to avoid penetration of rain or surface water.
9. The more thickness of flexible pavement the more it will prone to rutting. (Some CPEC Projects on N-55 are already facing this issue in their very early stages)

7.   ACKNOWLEDGEMENTS

8.   REFERENCES

1.   Todd V. Scholz, Sathyanarayanan Rajendran "Investigating premature pavement failure due to moisture" Oregon Department of Transportation Research Section & Federal Highway Administration Washington, DC.
2.   Magdi M.E. Zumrawi "Survey and Evaluation of flexible Pavement Failures" University of Khartoum, Department of Civil Engineering, Khartoum, Sudan.
3.   Eva Remišová1, Michal Holý "Changes of Properties of Bitumen Binders by Additives Application'' 2017.

Producing Lightweight Concrete With Pumice Coarse Aggregates

Imtiaz Ali, Anass Khan, Zainab Akbar
BS student, Department of Civil Engineering,
University of Engineering & Technology Peshawar, Pakistan
imtiazanjum.pk@gmail.com; anasskhan143@gmail.com; zain.mir195@gmail.com;

Fayyaz Rahman, Waqas Adil
Lecturer, Department of Civil Engineering,
University of Engineering & Technology Peshawar, Pakistan
waqasadil1991@gmail.com

ABSTRACT

The use of lightweight concrete is growing rapidly in the construction industry in recent years due to its advantages over ordinary concrete. In this research work, pumice is utilized as a coarse aggregate for the production of lightweight aggregate concrete. Six samples are prepared with 5%, 10%, 20%, 30%, 50%, and 100% replacement of ordinary coarse aggregate replacement with pumice. Physical and mechanical tests are performed on all the samples and the results are compared with normal aggregate concrete. The test results suggest that pumice concrete can be used in seismic zones, lightweight structures, and pavement. In comparison to normal concrete pumice concrete have lower strength, so it can be used for manufacturing concrete blocks.

KEYWORDS: Coarse aggregate, Concrete, Lightweight, Pumice.

1   INTRODUCTION

Lightweight aggregate concrete (LWAC) is available in many parts of the world [1]. Lightweight aggregate can be classified into two types: Natural lightweight aggregate and artificial lightweight aggregate. Examples of Natural lightweight aggregates are Pumice, sawdust, Rice husk, dolomite, scoria, volcanic cinders, etc. Artificial lightweight aggregates are expanded slate, shale, artificial cinders, coke breeze, foamed slag, bloated clay, sintered fly ash, and exfoliated vermiculate [2]. LWAC is commonly produced by replacing normal weight aggregate partially or wholly with lightweight aggregate [3]. Pumice is one of the natural lightweight aggregates produced at the time of volcanic eruption when the gases are released during the solidification process of molten lava [4].

 Pumice has a density of 0.25 g/cm3 so it flows on the surface of the water and is an expanding agent that increases the volume of the mixture. Pumice has a high melting point and low specific gravity, therefore it can be used in concrete for fire resistance purposes. It also has excellent strength and insulation properties [2]. LWAC has a higher strength to weight ratio, heat insulation, reduced dead load properties so, it has got too many applications such as the construction of

1st International Conference on Advances in Civil & Environmental Engineering, University of Engineering & Technology Taxila, Pakistan

Conference date 22 &23 Feb 2022

different building parts, especially in seismic zones [1], [3], construction of roof deck, pavement, precast concrete, wall panels, masonry bricks or blocks [1].

The presence of voids in pumice makes its use favorable in pervious concrete (PC). According to the Environmental Protection Agency (EPA) of United States, the use of PC is one of the best materials for the reduction of stormwater runoff because it provides more free drainage in pavement and can reduce the stormwater runoff in the storm event by providing rapid drainage, and thus reducing the occurrence of flooding scenario. It also helps in improving the quality of stormwater by removing the suspended particles. This is why PC can be used as eco-friendly material in pavements like walkways, parking areas, tennis courts, slope stabilization systems, shoulders, alleys, light traffic roads, and low-grade roads [5]. Thus the use of pumice is a good approach for the production of lightweight, economic, and environmentalist concrete [4].

2   RESEARCH METHODOLOGY:

In this research work, natural coarse aggregate is replaced by lightweight pumice aggregate to obtained lightweight aggregate concrete. Used pumice aggregate is obtained from a textile company. Pumice aggregate is incorporated in concrete by various percentages (5, 10, 20, 30, 50 & 100) % by replacing the natural coarse aggregate and six different mixes are produced. The concrete cylinders have a height of 12 inches and a diameter of 6 inches. Different test results of all these mixes were compared with the control mix (NC).

The material used in this research includes Natural coarse aggregate (NA), used pumice coarse aggregate (PA), natural river sand, and cement. Ordinary Portland cement is used as a binder. Locally available sand is used as fine aggregate, which has a specific gravity of 2.68. The coarse aggregate used are NA and PA, which have bulk densities of 1474 kg/m^3 and 705 kg/m^3 respectively.
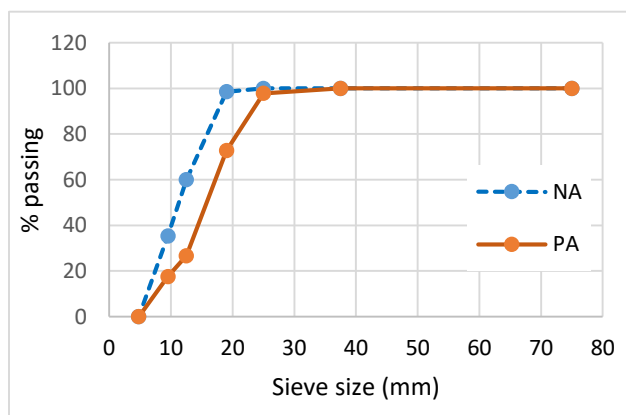
Fig. 1: Gradation curve of PA and NA

Fig.2: Mixing of concrete ingredients

1st International Conference on Advances in Civil & Environmental Engineering, University of Engineering & Technology Taxila, Pakistan

Conference date 22 &23 Feb 2022

2.1 Material Test

The specific gravity of fine aggregate is determined as per ASTM C128 [6]. The bulk density of both PA and NA coarse aggregates is determined as per ASTM C29/C29M-07 [7]. Sieve analysis of coarse aggregate is conducted according to ASTM C136 / C136M – 19 [8]. The particle size distribution of NA and PA can be seen from the gradation curve in Fig. 1.

2.2 Mix design ratio's

The mix design for all mixes is based on the ACI 318 standard with a constant W/C ratio of 0.5. The quantities of all ingredients are shown in Table.1. NC, P5, P10, P20, P30, P50 and P100 shows normal concrete,5% ,10%, 20%,30%, 50% and 100% replacement of normal aggregate with pumice aggregate respectively. Hand mixing is used for all batches. The fresh and hardened state properties are then determined. The specimens are cured in water for 28 days after casting.

Table 1: Mix proportion of ingredients per m3

Specimen ID	Cement (kg/m3)	Coarse Aggregate		Fine Aggregate (kg/m3)	Water (kg/m3)
		Normal Aggregates (kg/m3)	Normal Aggregates (kg/m3)		
NC	350	1280	0	756	175
P5	350	1216	64	756	175
P10	350	1152	128	756	175
P20	350	1024	256	756	175
P30	350	896	384	756	175
P50	350	640	640	756	175
P100	350	0	1280	756	175

3 RESULTS AND DISCUSSIONS

Various tests are performed on all concrete samples in both fresh, and hardened states, and then the results are compared with Normal aggregate concrete. Fresh state tests include: (i). Slump test (ii). Bulk density. Hardened state tests include: (i). Bulk density and (ii). Compressive test.

3.1 Fresh Concrete

3.1.1 Slump Test

The workability of all mixes of fresh LWGCs is determined by conducting slump tests as per ASTM C143/C143M-15a [9]. The test is performed to check the consistency of freshly made concrete. The results of the slump tests are shown in Fig. 3. The slump values decrease as the replacement of PA increases.

1st International Conference on Advances in Civil & Environmental Engineering, University of Engineering & Technology Taxila, Pakistan

Conference date 22 &23 Feb 2022

3.1.2   Bulk density

The bulk density of all concrete mixes in the fresh state is determined as per ASTM C1688M-14a [10]. The result of fresh bulk densities for all mixes is shown in Fig. 4. Bulk density in fresh state decreases as the PA replacement increases and is minimum at 100% replacement.
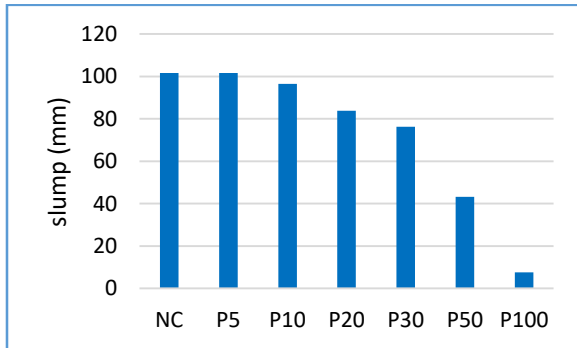
Fig. 3: Slump test results
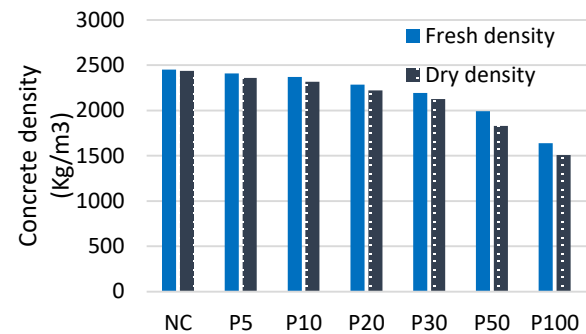
Fig. 4: Fresh and dry densities of concrete

3.2   Harden concrete

3.2.1   Bulk Density

The bulk density of all concrete samples in the hardened state is determined as per ASTM C642 − 13 after 28 days [11]. The result of bulk densities for all mixes is shown in Fig. 4. Bulk density decreases as the % replacement of PA increases.

3.2.2   Compressive strength

The compressive strength of all the samples is determined after 28 days of casting. The tests are conducted via a compression testing machine as per ASTM C39/C39M [12]. The compressive strength decreases as the percentage of Pumice increases as clear from the result in Fig. 6.

Fig. 5: Concrete Cylinder in compression test
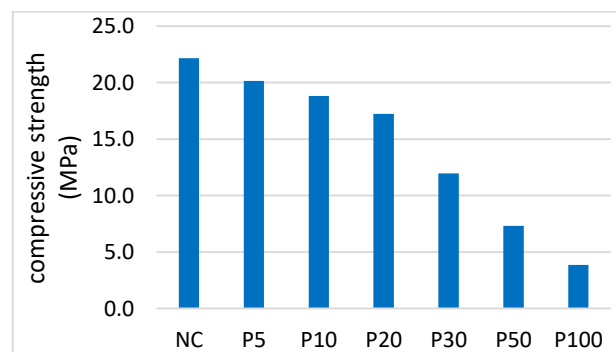
Fig. 6: Compression test result

1st International Conference on Advances in Civil & Environmental Engineering, University of Engineering & Technology Taxila, Pakistan

Conference date 22 &23 Feb 2022

4   CONCLUSIONS

From the above results the following conclusion can be drawn:
- Slump is reduced with increased content of pumice aggregates. This is because of the porous nature of pumice which retains water from the mix.
- Compressive strength is reduced with increase in pumice aggregates content. The strength decrement is due to the porous nature of pumice, which traps water from the mix, and thus the availability of water content for hydration reaction decreases.
- Reduction in density implies that pumice-based lightweight aggregate can be used in lightweight structures as well as in the earthquake-resisting structure.

5   REFERENCES:

[1] Ampol Wongsa, Vanchai Sata a, Peem Nuaklong, Prinya Chindaprasirt, "Use of crushed clay brick and pumice aggregates in lightweight," *Construction and Building Materials,* p. 1025–1034, 2018.

[2] R S MURALITHARAN and V RAMASAMY, "Basic Properties of Pumice Aggregate," *International Journal of Earth Sciences and Engineering,* vol. 08, pp. 256-258, 2015.

[3] Mustafa Sarıdemir, Serhat Çelikten, "Investigation of fire and chemical effects on the properties of alkali-activated lightweight concretes produced with basaltic pumice aggregate," *Construction and Building Materials,* 2020.

[4] Murat Kurt a, Muhammed Said Gül, Rüstem Gül, Abdulkadir Cüneyt Aydin, Türkay Kotan, "The effect of pumice powder on the self-compactibility of pumice," *Construction and Building Materials,* p. 36–46, 2016.

[5] Hatice Öznur Öz, "Properties of pervious concretes partially incorporating acidic pumice," *Construction and Building Materials,* p. 601–609, 2018.

[6] A. C128, "Specific Gravity and Absorption of Fine Aggregate".

[7] A. C29/C29M-07, "Standard Test Method for Bulk Density ("Unit Weight") and Voids in Aggregate".

[8] A. C136, "To determination of particle size distribution of coarse aggregates by sieving.".

[9] A. C. −. 15, "Standard Test Method for Slump of Hydraulic-Cement Concrete".

[10] A. C1688M-14a, "Standard Test Method for Density and Void Content of Freshly Mixed Pervious Concrete density".

[11] A. C. −. 13, "C Standard Test Method for Density, Absorption, and Voids in Hardened Concrete".

[12] A. C39/C39M-21, "Standard Test Method for Compressive Strength of Cylindrical Concrete Specimens".

Evaluation of Water Quality Suitability for Drinking purpose in Pakistan: A Case Study of Taxila City; (I) **Physicochemical Analysis**

NAYAB ZAHRA

Department of Environmental Engineering
University of Engineering & Technology Taxila, Pakistan
nayab.zahra@ uettaxila.edu.pk

BILAL ASIF

Department of Environmental Engineering
University of Engineering & Technology Taxila, Pakistan
bilal.asif@uettaxila.edu.pk

ABSTRACT

This present study is an investigation and evaluation of water quality for citizens of Taxila, Pakistan. Water samples were collected from five different tube wells, attached filtration plants, and two-house connections from each tube well that make a total of twenty sampling sites. Four physical parameters (pH, turbidity, hardness, and total dissolved solids) and two chemical parameters (chlorides and sulfates) were investigated and compared with Punjab Environmental Quality Standards for Drinking Water (PEQSDW). The results confirmed that physicochemical were within the prescribed limits of PEQSDW. However, a minor problem of hardness was found in some samples. It is suggested to practice regular water quality testing and lying of sewerage and water pipes on opposite sides of roads.

KEYWORDS*:* Physicochemical parameters, Chlorination, Water quality

1. INTRODUCTION

Safe drinking water supply and adequate sanitation are essential for every individual. Supply of good quality drinking water at the door of every user and proper disposal of wastewater generated is required [1, 2]. Clean potable water should be free from organic substances, disease-causing microorganisms and some minerals because these factors are harmful to human health [3]. In developing countries, people are facing serious health issues due to the unavailability of clean drinking water. About 783 million people in the world lack safe drinking water [4]. While in Pakistan 38.5 million people have no access to safe drinking water which is expected to be 52.8 million by 2015 [5]. In Pakistan, clean water is supplied through hand pumps and piped networks. If the supplied drinking water is unsafe then it causes serious diseases and even death. Water-borne diseases, gastroenteritis and diarrhea are due to the supply of polluted water which leads to death while every fifth citizen is facing this problem [6]. The aim of this research is the evaluation of water quality in Taxila city by analyzing physiochemical parameters. To the best of the author's knowledge, this type of study has never been conducted and hopefully, it will provide useful insight for the various stakeholders involved.

EXPERIMENTAL METHODS

2.1 Study Area

The Taxila city was selected as a test case for this study. Samples were collected from tube wells, house connections and filtration plants from each area. Traditionally, water quality experts

1st International Conference on Advances in Civil & Environmental Engineering, University of Engineering & Technology Taxila, Pakistan

Conference date 22 &23 Feb 2022

communicate their decision on drinking water quality by comparing the individual parameters with certain guideline values, so the results of our samples were compared with PEQSDW [7]. Three times sampling was done from each location to confirm the statistical importance of the results. For this study, a total of 60 samples was tested. Locations of samples are given in Table 1.

Table 1 Description of the sampling points

Sampling Points	Description	Sampling Points	Description
T-1	Tubewell installed at HIT	T3HC-1	House connection no. 1 of T-3
F-1	Filtration plant at HIT	T3HC-2	House connection no. 2 of T-3
T1HC-1	House connection no. 1 of T-1	T-4	Tubewell installed at Wah cantt
T1HC-2	House connection no. 2 of T-1	F-4	Filtration plant at Wah cantt
T-2	Tubewell installed at UET Taxila	T4HC-1	House connection no. 1 of T-4
F-2	Filtration plant at UET Taxila	T4HC-2	House connection no. 2 of T-4
T2HC-1	House connection no. 1 of T-2	T-5	Tubewell installed at Green Gardens
T2HC-2	House connection no. 2 of T-2	F-5	Filtration plant at Green Gardens
T-3	Tubewell installed at HMC	T5HC-1	House connection no. 1 of T-5
F-3	Filtration plant at HMC	T5HC-2	House connection no. 2 of T-5

2.2. Parameters Tested

Six water quality parameters; four physical parameters (pH, turbidity, total dissolved solids (TDS) and hardness), two chemical parameters (sulphates and chlorides) were analyzed by using procedures written in standard methods [8].

2. RESULTS AND DISCUSSION

3.1 pH

The mean pH values are presented at different sampling locations in Figure 1. The allowable limit according to PEQSDW for pH lies between 6.5 and 8.5 [7]. pH values below 6.5 increase corrosion in a household piping system and above 8.5, it is unsuitable for proper disinfection. The values of pH of different sampling locations of this city vary from 6.98 to 8.53. These results show that pH values at house connections and other sources were under recommended limits.

1st International Conference on Advances in Civil & Environmental Engineering, University of Engineering & Technology Taxila, Pakistan

Conference date 22 &23 Feb 2022
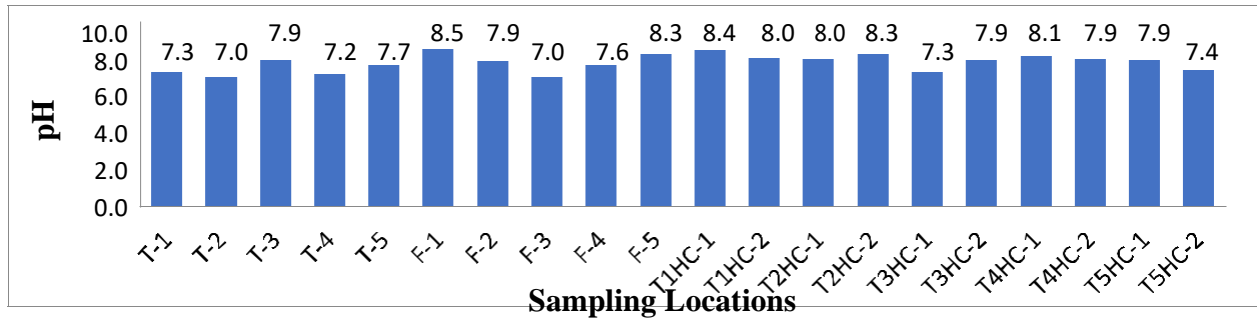
Figure 1 Comparison of Mean values of pH at various sampling locations

3.2 Turbidity

The mean values of turbidity are presented at different sampling locations including tube wells, filtration plants and house connections in Figure 2. The allowable limit according to PEQSDW for turbidity is <5 NTU [7]. The values of turbidity at all points were under permissible limits of water quality standards that lie between 3.1 NTU and 1.28 NTU. At T-1 and its adjacent house connections T1HC-1 and T1HC-2, values of turbidity were 2.04 NTU, 2.78 NTU and 3.1 NTU respectively were slightly higher than other values. Moreover, at filtration plants, values of turbidity were lesser than the turbidity at respective tube wells due to water filtration.
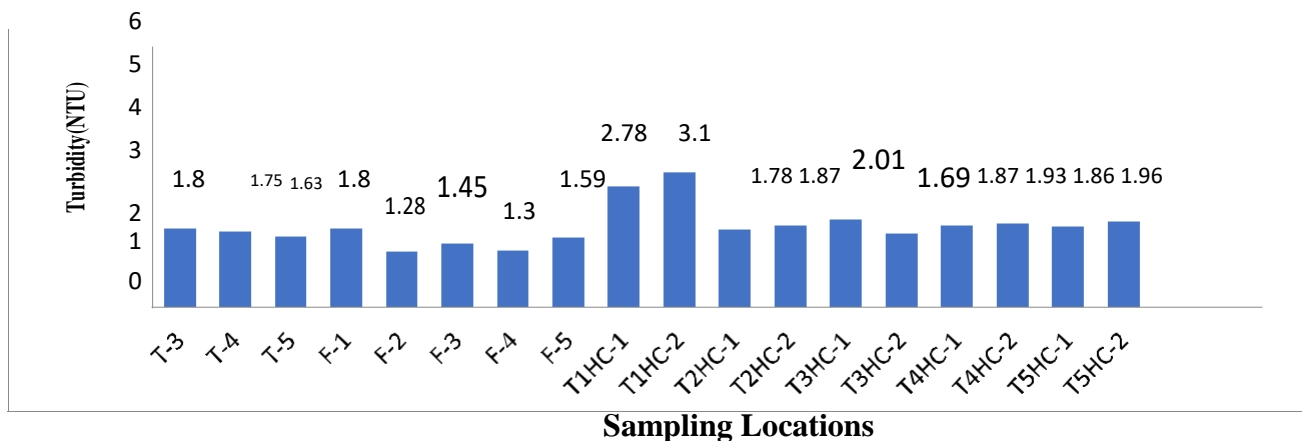
Figure 2 Comparison of mean values of turbidity at various sampling locations

1st International Conference on Advances in Civil & Environmental Engineering, University of Engineering & Technology Taxila, Pakistan

Conference date 22 &23 Feb 2022

3.3 Total Dissolved Solids (TDS)

The mean values of TDS are presented at different sampling locations including tube wells, filtration plants and house connections in Figure 3. The allowable limit according to PEQSDW Water for TDS is <1000 mg/L [7] because the value of TDS >1000 mg/L can cause a taste to the water. Moreover, it can also lead to the production of large amounts of scales in boilers, water pipes, household appliances and heaters [9] Fig. 4 shows that all the values of TDS were below 1000 mg/L ensuring that the quality of water was good for TDS.
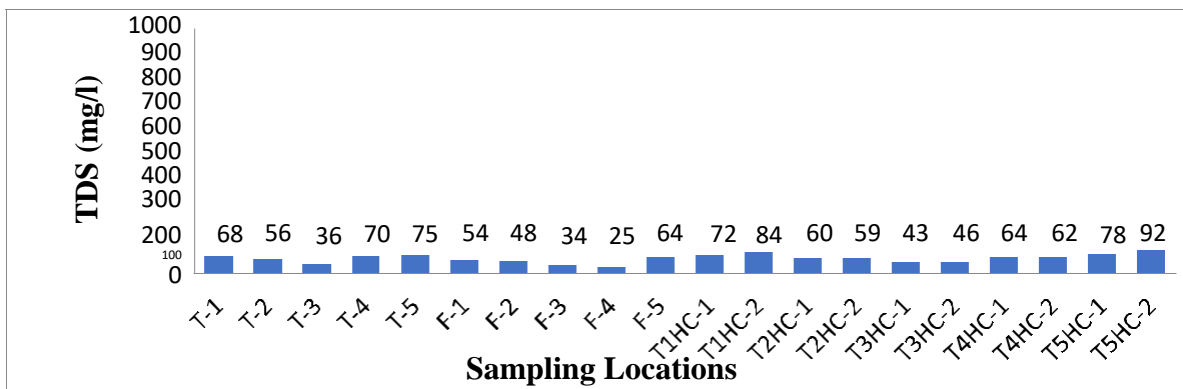
Figure 3 Comparison of mean values of TDS at various sampling locations

1st International Conference on Advances in Civil & Environmental Engineering, University of Engineering & Technology Taxila, Pakistan

Conference date 22 &23 Feb 2022

3.4 Hardness

The mean values of hardness are presented at different sampling locations including tube wells, filtration plants and house connections in Figure 4. The allowable limit according to PEQSDW for hardness is <500 mg/L as $CaCO_3$ [7]. Hard water consumes more soap for washing and it also causes excessive scaling in boilers leading to enormous loss of fuel as compared to soft water. The values of hardness at T-3, F-3 and its adjacent house connection T3HC-1 and T3HC-2 are 580,546, 586 and 610 mg/L as $CaCO_3$ respectively which are slightly higher than the standards conforming the extensive deposits of limestone and dolomite rocks in Taxila [10].
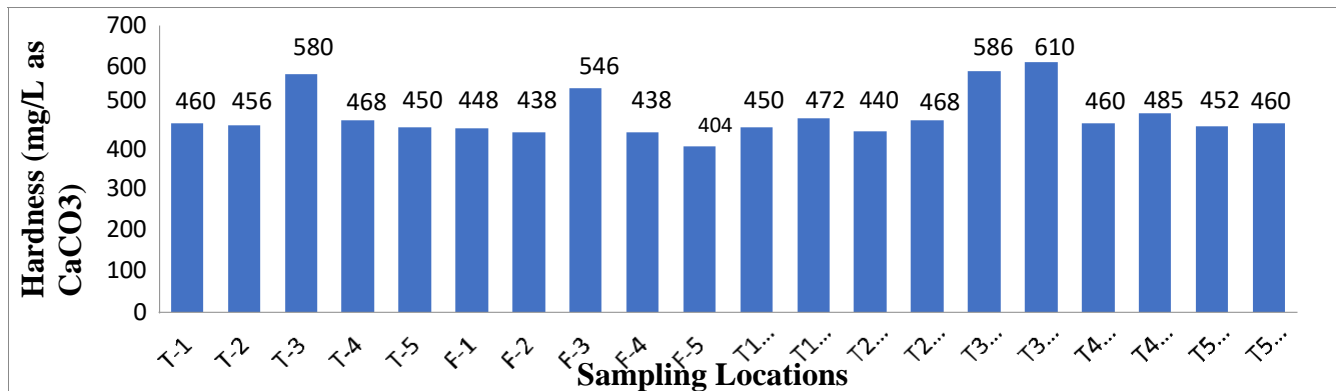
Figure 4 Comparison of mean values of hardness at the various sampling locations

3.5 Chlorides

The mean values of chlorides are presented at different sampling locations including tube wells, filtration plants and house connections in Figure 5. The allowable limit according to PEQSDW for chlorides is <250 mg/L [7]. The values of chlorides were high at T5HC-1 (57.49 mg/L) and T5HC-2 (60.38 mg/L) among all sampling sites, but these values also lie within permissible limits.
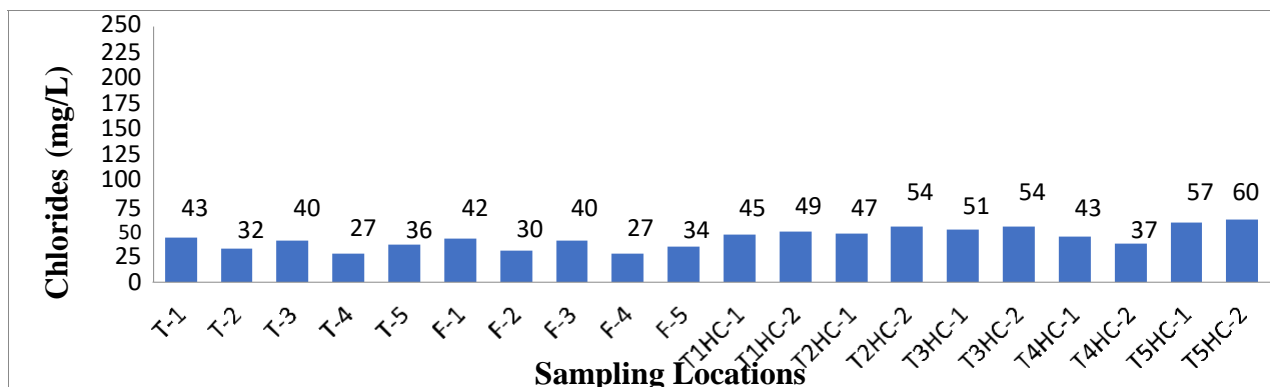
Figure 5 Comparison of mean values of Chlorides at various sampling locations

1st International Conference on Advances in Civil & Environmental Engineering, University of Engineering & Technology Taxila, Pakistan

Conference date 22 &23 Feb 2022

3.6 Sulphates

The mean values of sulphates are presented at different sampling locations including tube wells, filtration plants and house connections in Figure 6. The allowable limit according to PEQSDW for sulphates is <250 mg/L [7]. Maximum sulfates values were found at T-3 and its adjacent house connection but still lie under allowable limits of water quality standards.
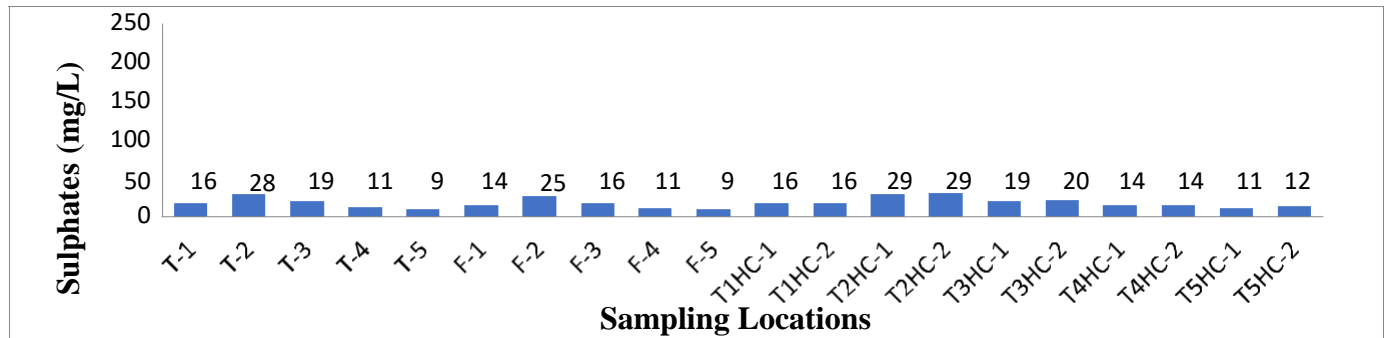
Figure 6 Comparison of mean values of sulphates at various sampling locations

3. CONCLUSION

Physicochemical parameters at all tube wells and filtration plants were under the prescribed limits of PEQSDW. Therefore, it can be said the source of drinking water in Taxila, Tehsil is acceptable for drinking concerning physicochemical parameters. Water supply lines and sewer pipes must be on the opposite side of the road, pipe joints must be sealed efficiently, and old pipes should be replaced after an appropriate time.

References:

1. Azizullah, A., et al., *Water pollution in Pakistan and its impact on public health—a review.* Environment international, 2011. **37**(2): p. 479-497.
2. Pakistan, G.o.t.I.R.o., National Sanitation Policy, M.o. Environment, Editor. September 2006, Government of the Islamic Republic of Pakistan: Islamabad, Pakistan., *National Sanitation Policy*. 2006: Islamabad.
3. Van Leeuwen, F., *Safe drinking water: the toxicologist's approach.* Food and Chemical Toxicology, 2000. **38**: p. S51-S58.
4. UNICEF, *Children dying daily because of unsafe water supplies and poor sanitation and hygiene, UNICEF says*. 2013, UNICEF: NEW YORK.
5. Hamid, A., et al., *Intensive report on total analysis of drinking water quality in Lahore.* International Journal of Environmental Sciences, 2013. **3**(6): p. 2161-2171.
6. Kahlown, M., et al., *Water quality status, national water quality monitoring program.* Fourth Technical ReportPCRWR, 2006. **5**.
7. Department, E.P., *Punjab Environmental Quality Standards for Drinking Water*. 2016, Government of Punjab: Lahore: Lahore.

1st International Conference on Advances in Civil & Environmental Engineering, University of Engineering & Technology Taxila, Pakistan

Conference date 22 &23 Feb 2022

8. APHA, *Standard Methods for the Examination of Water and Wastewater. 21st Edition,*. 2005, Washington DC: American Public Health Association.
9. Organization., W.H., *Guidelines for drinking-water quality. Vol. 1, Recommendations, 3rd ed.* . 2004: World Health Organization. https://apps.who.int/iris/handle/10665/42852.
10. Sheikh, I.M., et al., *Environmental geology of the Islamabad-Rawalpindi area, northern Pakistan.* Regional Studies of the Potwar-Plateau Area, Northern Pakistan. Bull. G, 2008.

Evaluating the Performance of Hot Mix Asphalt Reinforced with fibres from Natural, Synthetic & Semi-Synthetic sources

Syed Bilal Shah[1] , Dr. Syed Bilal Ahmed Zaidi[2]

1MSc. Scholar, Department of Civil Engineering, University of Engineering and Technology Taxila, Pakistan. bilalshah120@gmail.com

[2]Associate Professor, Department of Civil Engineering, University of Engineering and Technology Taxila, Pakistan. bilal.zaidi@uettaxila.edu.pk

ABSTRACT

The application of fibres as a modifier in the asphalt binder has been extensively increased due to their improved performance. This research aims to find the best combination of fibre type and content required to enhance the stability and mechanical properties of hot mixed asphalt. Three different types of fibres are used from three different sources (natural, synthetic and semi-synthetic sources). Silk fibre, polyester fibre and viscose rayon fibre with a length of 6-8mm were used with fibre contents of 0.3%, 0.5% and 0.7% by weight of the asphalt mixture. The experimental outcomes showed that all the fibre-reinforced asphalt concrete enhances the stability and mechanical performance of HMA compared to the control sample. 0.5% silk fibre showed better performance compared to the other two fibre types and dosages.

KEYWORDS : Asphalt binder, asphalt mixture, Marshall stability, rutting, semi circular bend specimen

1. INTRODUCTION

Asphalt concrete (AC) consists of aggregates, air voids and Asphalt binder mostly bitumen of specified grade to form flexible pavement, due to the strong adhesion properties of bitumen with aggregates it provides high stability and excellent mechanical properties [1, 2] However, pavements are repetitively exposed to heavy traffic loads that cause different types of distresses and damages, and the effect of these distresses and damages are intensified under the influence of moisture and temperature. This causes severe defects to the pavement that leads to fatigue cracking, asphalt draining down and rutting (permanent deformation) [3-7]. To enhance these properties of asphalt mix while the pavements are exposed to the same or more severe conditions researchers have conducted different types of studies, in which one of the most effective methods is to add fibres in asphalt mixture [8-12]. With the addition of fibres in the asphalt mix, the draining down and leakage properties of the Asphalt mixture has been significantly improved[8, 9]. The fibres tend to improve other properties of asphalt mixture such as static and dynamic stabilities, permanent deformation such as rutting and fatigue cracking [10-12]. As the high strength required for today's traffic density which is not affordable by normal paved surfaces. So, this research intends to increase the strength of HMA which ultimately increase the service life of the paved surface.

1st International Conference on Advances in Civil & Environmental Engineering, University of Engineering & Technology Taxila, Pakistan

Conference date 22 &23 Feb 2022

Qinglin Guo et al investigated low temperature cracking properties of HMA reinforced with basalt, glass and steel fibres by 0.5% weight of the total mix. His results showed that FRAC has better ductility at lower temperatures than plain Asphalt mixtures [13]. Qinwu Xu et al used polyester, polyacrylonitrile, lignin and asbestos fibres of 0.3% by mass of mix in HMA. His results showed that FRAC reduced rutting depth by 19.57%, 32.56%, 8.43% and 11.40% for 2500 cycles while the SITS (split indirect tensile strength) was improved by 6.8%, 8.3%, 1.11% and 3.4% also toughness was improved by 41%, 71%, 15.4% and 26.6% respectively [14]. F. Moreno et al investigated the effect of acrylic fibre on HMA with a fibre percentage of 0.3% by weight of the mixture. In his investigation, he found that Marshall stability, stress stability at low temperature increases with the inclusion of acrylic fibre. Also the final deformation (rut depth) decreases from 6.025mm to 2.025 [15]. Min-Jae Kim et al used polypropylene, Polyester Nylon and Carbon fibres in HMA that showed an increase in Marshall stability, Indirect Tensile strength and toughness with an increase in fibre percentage from 0.5% to 1%. While dynamic stability showed good results at 0.5% fibre content [16]. Pawan Kumar et al used jute fibres in Stone mastic asphalt and showed that with an increase in fibre content from 0 to 0.3% drain down values decrease. Also, rutting depth and accumulated strain against cycling loading were reduced for both natural and synthetic fibres [17].

The fibres used in this research are natural, synthetic and semi-synthetic fibres. In natural fibres, silk fibres have been used as it is the strongest natural fibre available. In synthetic fibres, polyester fibres have been selected as this fibre form a 3D network in HMA due to which improved mechanical properties are achieved in HMA. Viscose Rayon is a semi-synthetic cellulose regenerated fibre, selected as the third type to study the stability and mechanical properties of HMA in this research.

2. MATERIALS

2.1 Asphalt binder

The asphalt binder of grades 60-70 produced by Attock oil refinery was used for the preparation of all mixture types. The basic physical properties of the asphalt binder were quantified following ASTM standards listed in Table 1.

Table 1

Tests	Unit	Value	Specifications
Penetration	0.1mm	65	ASTM D5
Softening point	^{o}C	48	ASTM D36
Ductility	Cm	102	ASTM D13

2.2 Fibres

Three different types of fibres used in this research are collected from the local textile industry. The silk fibre is the strongest natural fibre obtained from animals. Polyester fibre is synthetic fibre while viscose rayon is a semi-synthetic fibre.

1st International Conference on Advances in Civil & Environmental Engineering, University of Engineering & Technology Taxila, Pakistan

Conference date 22 &23 Feb 2022

2.3 Aggregates

The aggregates used in this research work are collected from Margalla source. National Highway Authority (NHA) gradation Class B was followed for the preparation of asphalt mixtures as shown in Table 2.

Table 2

Sieves	Size in mm	Min	Max	In this work
3/4	19	100	100	100
½	12.5	75	100	90
3/8	9.5	60	80	70
No. 4	4.75	40	60	50
No. 8	2.36	20	40	30
No. 50	0.300	5	15	10
No. 200	0.075	3	8	5
Pan	filler			5

3. METHODOLOGY

Silk fibre, polyester fibre and viscose rayon fibre with a length of 6-8mm were used with fibre contents of 0.3%, 0.5% and 0.7% by weight of the asphalt mixture. Samples were prepared for Marshall stability test, wheel tracker test and semi-circular three-point bend test. Figure 1.
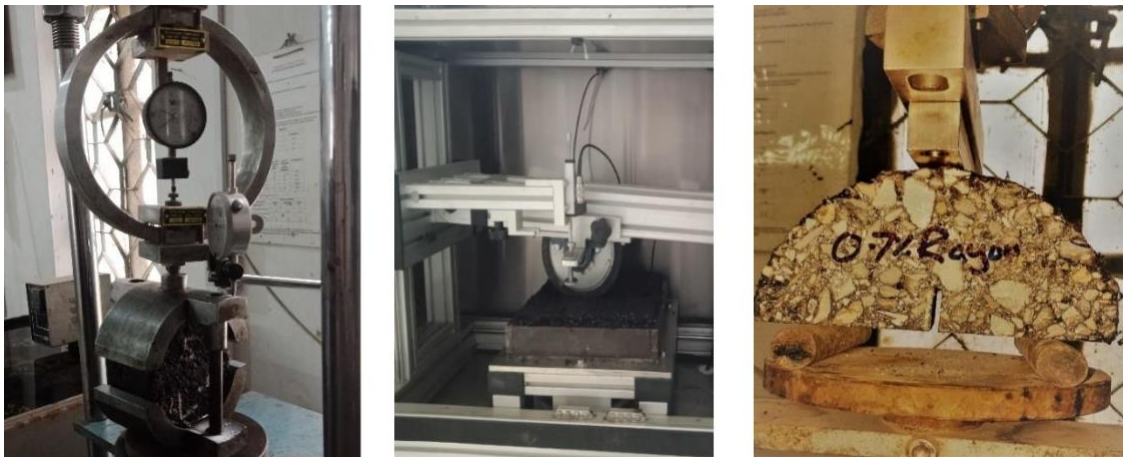
Figure 1. Marshall Stability, Wheel tracker and Semicircular bend test setup

4. RESULTS AND DISCUSSION

4.1 Marshall Stability

The Marshall stability followed an improving trend when the fibre percentage was increased from 0 to 0.5% fibre content. Silk and viscose rayon showed maximum stability value at 0.5% fibre content (Exception for polyester that showed maximum stability at 0.3% fibre content). Overall, 0.5% silk fibre showed the best result for the Marshall stability that was improved 35.6% from the

1st International Conference on Advances in Civil & Environmental Engineering, University of Engineering & Technology Taxila, Pakistan

Conference date 22 &23 Feb 2022

control specimen followed by 0.5% rayon fibre that showed 26% improvement while 0.3% polyester showed 12% improvement than the control sample, the results are shown in figure 2.
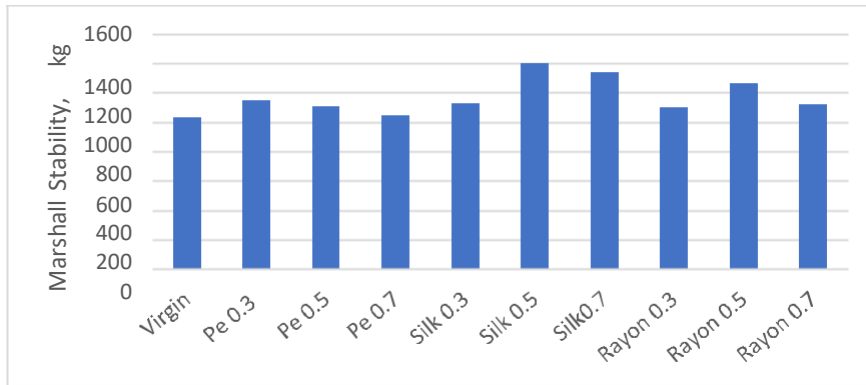
Figure 2. Marshall stability of Asphalt mix with and without fibres

4.2 Wheel tracker Test

Wheel tracker test was performed at 60 ^{O}C for 10000 cycles with 15mm maximum allowable rutting depth. The test temperature was maintained throughout the test. From the test data dynamic stability, rate of deformation and maximum rut depth was obtained. Dynamic stability was calculated through equation (1).

$$DS = \frac{15}{60-45} \qquad (1)$$

Here DS is Dynamic Stability, N is the number of cycles per minute,, D_{60} is the rutting depth at 60 minutes, D_{45} is the rutting depth at 45 minute.

The control sample failed at 9700 cycles as the maximum rut depth of 15mm was reached. Overall Silk fibres showed better rut resistance than all other fibres as shown in figure 3. Silk and viscose rayon fibre showed maximum resistance to rutting at 0.5% fibre content (Exception for Polyester fibre that showed better resistance to rutting at 0.7% fibre content). The dynamic stability was maximum for all those fibre and contents that showed better rut resistance. Similarly, the rate of deformation was minimum for all those fibres and contents that showed minimum rut depth. Shown in figure 4.
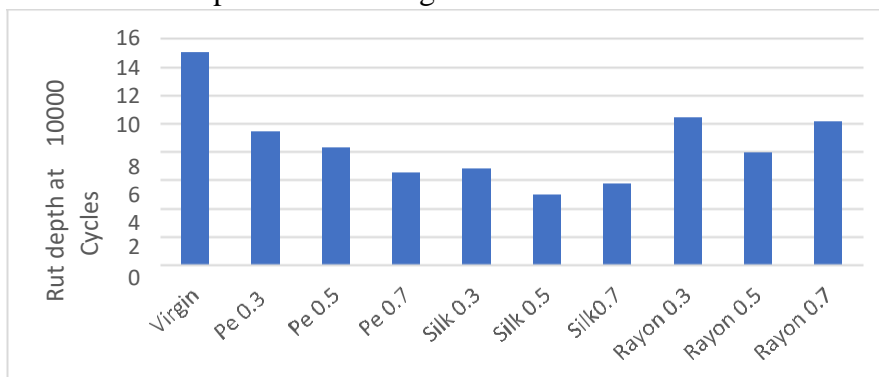
Figure 3. Maximum rut depth for asphalt concrete with and without fibres

1st International Conference on Advances in Civil & Environmental Engineering, University of Engineering & Technology Taxila, Pakistan

Conference date 22 &23 Feb 2022
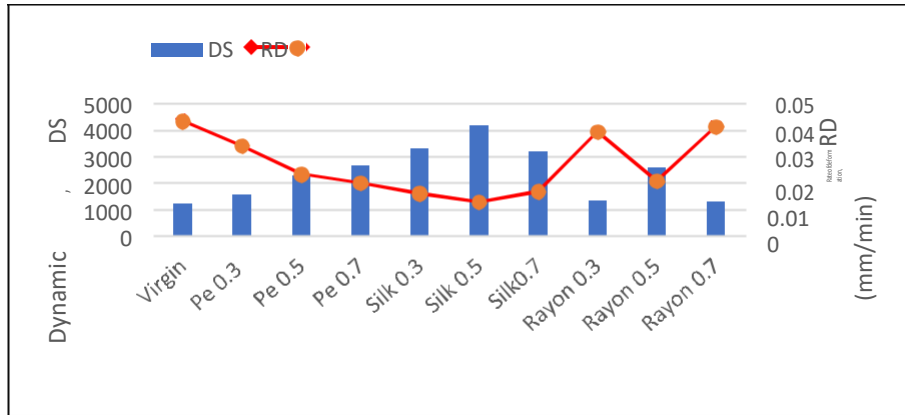
Figure 4. Dynamic stability and rate of deformation for asphalt mix with and without fibres.

4.3 Semi Circular bend test

All the fibre reinforced asphalt concrete shows better resistance to cracking than the control sample. Results are shown in figure 5. Polyester and silk fibre showed maximum resistance to cracking at 0.5% fibre content while viscose rayon fibre showed maximum cracking resistance at 0.3% fibre content.
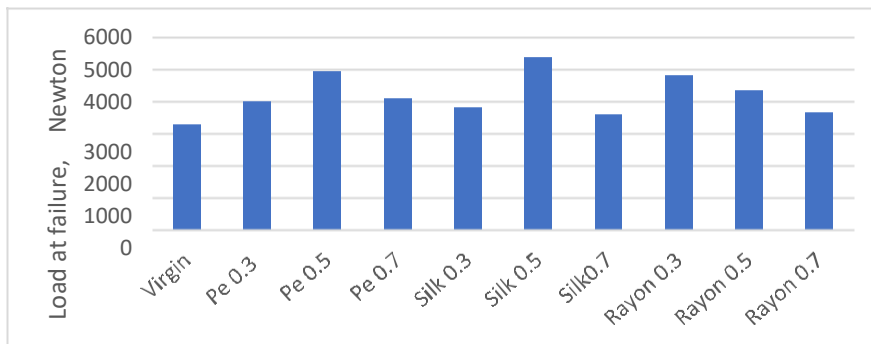
Figure 5. Load at failure of asphalt concrete with and without fibres

5. CONCLUSION

Three types of mechanical tests were performed i.e., Marshall stability, Wheel tracker and semicircular bend test to investigate the influence of three types of fibres from three different sources and three percentage fractions of fibres. Following are the conclusion of this research work.

1st International Conference on Advances in Civil & Environmental Engineering, University of Engineering & Technology Taxila, Pakistan

Conference date 22 &23 Feb 2022

1. Silk fibre, the strongest natural fibre has shown the best performance for all the test parameters in comparison to the other two fibres. The optimum performance was observed at a dosage of 0.5%.

2. Polyester fibre gave different results for each of the studies parameters. In Marshall stability, 0.3% dosage was found better performing while the optimum dosage for wheel tracker and semicircular bend test were reported as 0.7% and 0.5% respectively.

3. Overall silk fibre showed the best performance in all of the studies parameters, followed by polyester and then viscose rayon fibre.

1st International Conference on Advances in Civil & Environmental Engineering, University of Engineering & Technology Taxila, Pakistan

Conference date 22 &23 Feb 2022

REFERENCES

1. Akmal, N. and A.M. Usmani, *Applications of Asphalt-Containing Materials.* Polymer News, 1999. **24**(4): p. 136-140.
2. Murali Krishnan and, J. and K. Rajagopal, *Review of the uses and modeling of bitumen from ancient to modern times.* Appl. Mech. Rev., 2003. **56**(2): p. 149-214.
3. Xu, Q., H. Chen, and J.A. Prozzi, *Performance of fiber reinforced asphalt concrete under environmental temperature and water effects.* Construction and Building materials, 2010. **24**(10): p. 2003-2010.
4. Kennedy, T.W., F.L. Roberts, and K.W. Lee, *Evaluation of moisture effects on asphalt concrete mixtures*. 1983.
5. Airey, G., et al., *The influence of aggregate, filler and bitumen on asphalt mixture moisture damage.* Construction and building materials, 2008. **22**(9): p. 2015-2024.
6. Wu, S., Q. Ye, and N. Li, *Investigation of rheological and fatigue properties of asphalt mixtures containing polyester fibers.* Construction and Building Materials, 2008. **22**(10): p. 2111-2115.
7. Gorkem, C. and B. Sengoz, *Predicting stripping and moisture induced damage of asphalt concrete prepared with polymer modified bitumen and hydrated lime.* Construction and Building Materials, 2009. **23**(6): p. 2227-2236.
8. Fitzgerald, R.L., *Novel applications of caron fiber hot mix asphalt reinforcement and carbon-carbon pre-forms*. 2000, Michigan Technological University Michigan.
9. Hassan, H.F., S. Al-Oraimi, and R. Taha, *Evaluation of open-graded friction course mixtures containing cellulose fibers and styrene butadiene rubber polymer.* Journal of materials in civil engineering, 2005. **17**(4): p. 416-422.
10. Goel, A. and A. Das. *Emerging road materials and innovative applications*. in *National conference on materials and their application in Civil Engg*. 2004.
11. Peltonen, P., *Wear and deformation characteristics of fibre reinforced asphalt pavements.* Construction and building Materials, 1991. **5**(1): p. 18-22.
12. Tapkın, S., *The effect of polypropylene fibers on asphalt performance.* Building and environment, 2008. **43**(6): p. 1065-1071.
13. Guo, Q., et al., *Investigation of the low-temperature properties and cracking resistance of fiber-reinforced asphalt concrete using the DIC technique.* Engineering Fracture Mechanics, 2020. **229**: p. 106951.
14. Chen, H., et al., *Evaluation and design of fiber-reinforced asphalt mixtures.* Materials & Design, 2009. **30**(7): p. 2595-2603.
15. Moreno-Navarro, F., et al., *High-modulus asphalt mixtures modified with acrylic fibers for their use in pavements under severe climate conditions.* Journal of Cold Regions Engineering, 2016. **30**(4): p. 04016003.
16. Kim, M.-J., et al., *Enhancing mechanical properties of asphalt concrete using synthetic fibers.* Construction and Building Materials, 2018. **178**: p. 233-243.
17. Kumar, P., et al., *Use of jute fibre in stone matrix asphalt.* Road materials and pavement design, 2004. **5**(2): p. 239-249.

1st International Conference on Advances in Civil & Environmental Engineering, University of Engineering & Technology Taxila, Pakistan

Conference date 22 &23 Feb 2022

Effect Of Bentonite And Lime Powder On Durability Properties Of Self-Compacting Concrete

Shahzad Ahmed, Asst. Prof. Muhammad Saad

University of Engineering & Technology Taxila, Pakistan

Shahzad.Ahmad@uettaxila.edu.pk, Muhammad.saad@uettaxila.edu.pk

ABSTRACT

Common problems which occur during service life of reinforced concrete structure (RCC) includes corrosion of steel, sulphate attack and alkali aggregate reaction. As a result of these problems service life, strength and durability structures is compromises. This results in excessive maintenance and repairs that ultimately increases the cost. This huge economic impact urge researchers to find ways for searching a cost-effective and durable product. Self-compacted concrete (SCC) is one of the advancements and its application involves exposure to water absorption and chemical attack. This study explores the behaviour and durability properties of SCC by partially replacing bentonite with pozzolana and also compares the bentonite replacement with the control mix. The research also investigates the effect of compositional parameters on durability properties such as coarse aggregate volume and w/c ratio for same design strength. It also examines the impact of pozzolana for rheological improvement in comparison to control mix. The durability properties assessed were the water absorption and acid attack. From test results it can be concluded that bentonite modification in SCC is not beneficial in reducing water absorption but has been found effective in reducing sulphate attack.

KEYWORDS: Durability; Acid Attack; Sorptivity; Self-compacted concrete

1   INTRODUCTION

The category of concrete which has the capability to cast in a formwork and the ability to fill it under its own weight is called self-compacted Concrete (SCC). This filling of the formwork does not need any compaction or external vibration. SCC has been used in many structures around the world, concluding in the creation of international guidelines. It was developed in mid 80s, and many investigations have been made to improve its properties [1].

SCC has numerous benefits and advantages as compared to conventional concrete. Such advantages contain an enhanced concrete quality, fast construction and less total cost. The hardened properties of SCC and conventional concrete are mostly the same, and also the structural design requirements were the same as reported in the literature [2].

As compared to conventional concrete, SCC is stronger, durable and has the less permeability. These properties are because of low water cement ratio in SCC mixes. These features make SCC to be capable of producing durable structures apart from its tendency of on-site conditions regarding labor quality and the availability of casting and compacting system [3].

1st International Conference on Advances in Civil & Environmental Engineering, University of Engineering & Technology Taxila, Pakistan

Conference date 22 &23 Feb 2022

Sulphate attack is a major factor that causes expansion and result in high deterioration of concrete structure. Expansion occurs due to reaction of sulphate ions with some hydration products in concrete structure [4]. Solution of sodium or magnesium sulphate, or a mixture of the two is used while testing the RCC structure as specimen is inserted in the solution [5]. The impact of sulphate attack is frequently evaluated through numerous indicators such as change in length, loss or increase of mass, differing surface rigidity [6], reduction in strength and elastic modulus.

In our research work we used two different mix designs; each mix design consists of Six different types of samples 30A, 30B, 30C,60A,60B & 60C. These 6 samples having compressive strength of 30 and 60 MPa with different percentage of coarse aggregate. The coarse aggregate decreases from A to C; more percentage of course aggregate is in A sample and less in C type samples.[7]

2   GENTERAL METHODOLOGY

Durability properties of SCC checked in this Research work. For this purpose, two different mix designs of SCC prepared and different test done to check durability properties.

2.1   Control Mixture

SCC consist of lime powder used as a control mix prepared and cured. After curing Sorptivity and acid attack tests were carried out.

2.2   SCC (15% Replacement with Bentonite)

In this Mixture design of SCC, Cement replaced with 15% bentonite. Literature shows that the 15% replacement of Cement with bentonite has very less effect on fresh properties without Compromising strength which also proves in this study as well.[8] After curing Sorptivity and acid attack were carried out. Then comparing these mix design test results to check the durability properties of self-compacted concrete.

3   TABLES AND FIGURES

Table 1 Mix Design compositing of Control Mix

MIX DESIGN	CEMENT	BENTO	GGBS	WATER	SP (Super Plasticizer)	LP (Lime Powder)	FA (1) (Fine Agg.)	FA(2) (Fine Agg.)	CA (Coarse Agg.)
30 A	240	0	80	201.6	1.4	109	164	579	924
30 B	240	0	80	201.6	1.6	156	234	530	840
30 C	240	0	80	201.6	2.3	194	291	504	756
60 A	315	0	105	197.5	2.3	94	141	536	924
60 B	315	0	105	197.5	2.4	125	188	528	840
60 C	315	0	105	197.5	2.8	172	258	477	756

Table 2 Mix Design compositing 15% Replacement with Bentonite

1st International Conference on Advances in Civil & Environmental Engineering, University of Engineering & Technology Taxila, Pakistan

Conference date 22 &23 Feb 2022

MIX DESIGN	CEMENT	BENTO	GGBS	WATER	SP (Super Plasticizer)	LP (Lime Powder)	FA (1) (Fine Agg.)	FA(2) (Fine Agg.)	CA (Coarse Agg.)
30 A	204	36	80	201.6	1.4	109	164	579	924
30 B	204	36	80	201.6	1.6	156	234	530	840
30 C	204	36	80	201.6	2.3	194	291	504	756
60 A	267.75	47.25	105	197.5	2.3	94	141	536	924
60 B	267.75	47.25	105	197.5	2.4	125	188	528	840
60 C	267.75	47.25	105	197.5	2.8	172	258	477	756

3.1 Final Results
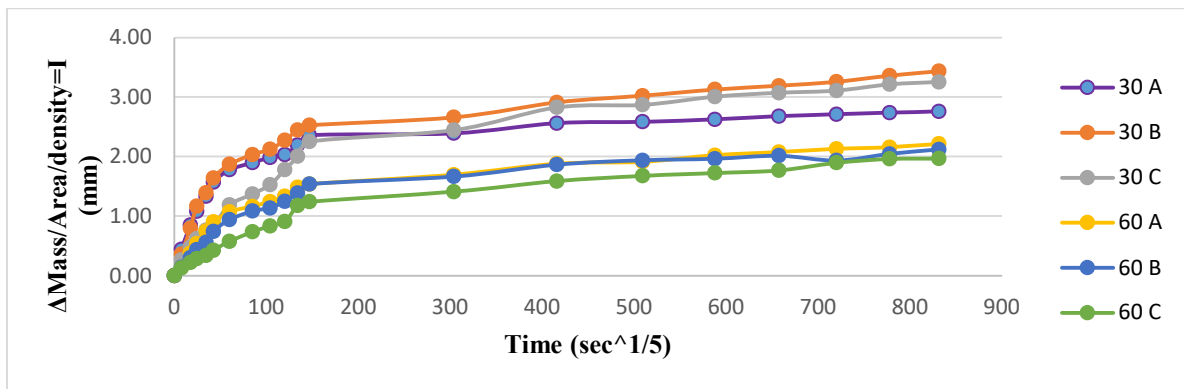
Figure 3: Sorptivity Results of different strength control mix SCC
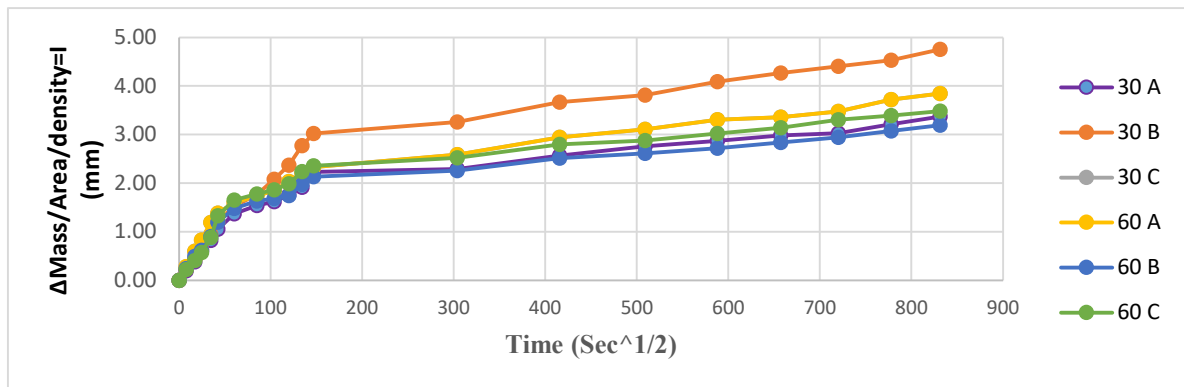
Figure 4: Sorptivity Results of different strength 15% replacement of bentonite mix SCC

1st International Conference on Advances in Civil & Environmental Engineering, University of Engineering & Technology Taxila, Pakistan

Conference date 22 &23 Feb 2022
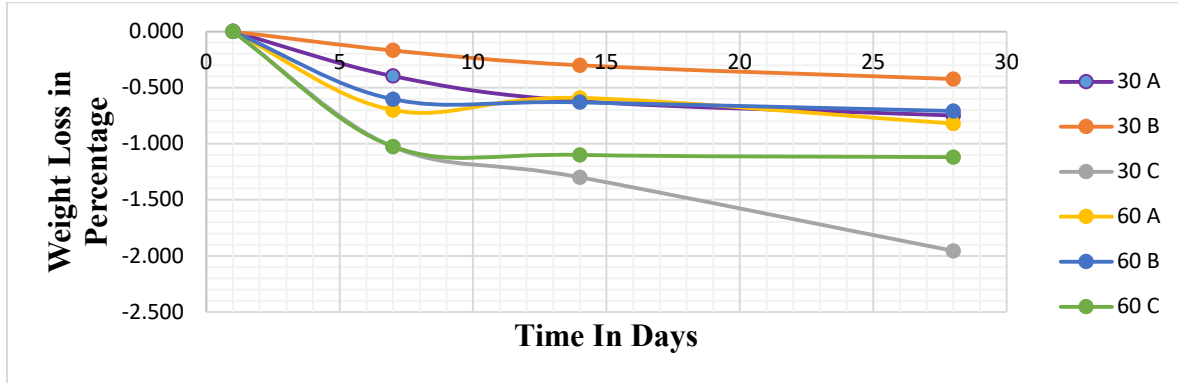
Figure 5: Acid Test Results of different strength control mix SCC
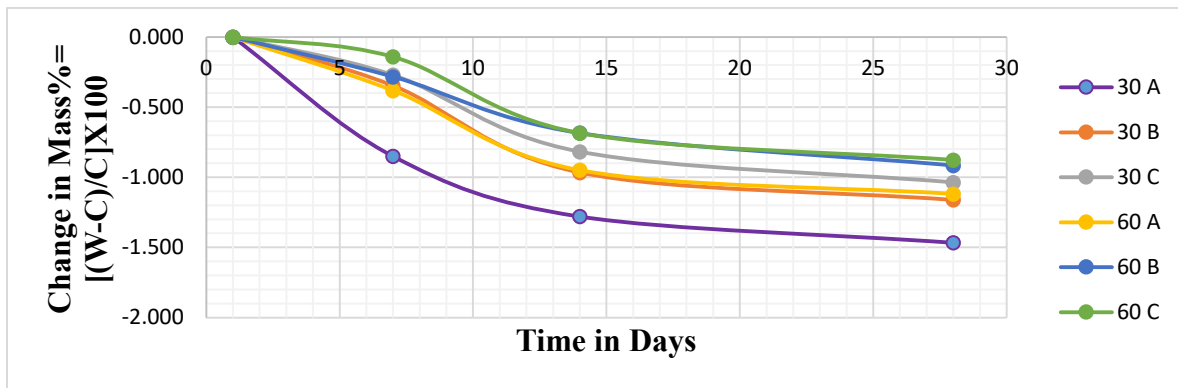
Figure 5: Acid Test of different strength 15% replacement of bentonite mix SCC

4 CONCLUSION

- The test results have shown significant improvements in durability properties of self-compacted concrete.
- The results of control and bentonite modified mix show that the water absorption is more in modified mix as compared to control mix of same strength. Moreover, water absorption is more in mix having less coarse aggregate contents than that of the mix having more aggregate contents for same design strength.
- In the acid attack test results, more weight loss observed for the control mix as compared to modified bentonite mix under same condition. The percentage loss between these two mixes is in range of 15 to 20%.
- From test results it can be concluded that bentonite modification in SCC is not beneficial in reducing water absorption but has been found effective in reducing sulphate attack.

1st International Conference on Advances in Civil & Environmental Engineering, University of Engineering & Technology Taxila, Pakistan

Conference date 22 &23 Feb 2022

5   ACKNOWLEDGEMENTS

This research is in collaboration and under supervision of Assistant Professor Muhammad Saad. I am thankful to my supervisor Assistant Professor Muhammad Saad for his guidance and support during this research work. All the data presented in this paper is unique and authentic.

REFERENCES

1.   Okamura, H. and M.J.J.o.a.c.t. Ouchi, *Self-compacting concrete.* 2003. **1**(1): p. 5-15.
2.   Kim, J. and S. Han. *Mechanical properties of self-flowing concrete. High-performance concrete: Design and materials and recent advances in concrete technology.* in *Proc., 3rd CANMET/ACI International Conf., Advances in Concrete Technology, edited by VM Malhotra. Farmington Hills, MI: American Concrete Institute.* 1997.
3.   El-Dieb, A., M.R.J.C. Taha, and B. materials, *Flow characteristics and acceptance criteria of fiber-reinforced self-compacted concrete (FR-SCC).* 2012. **27**(1): p. 585-596.
4.   Chen, E. and C.K.J.E.F.M. Leung, *Finite element modeling of concrete cover cracking due to non-uniform steel corrosion.* 2015. **134**: p. 61-78.
5.   Li, Z., *Advanced Concrete Technology, Hoboken.* 2009, NJ: John Wiley & Sons Inc. Lombardo, TG, Giovambattista, N. & Debenedetti, PG.
6.   Ouyang, W.-y., et al., *Evolution of surface hardness of concrete under sulfate attack.* 2014. **53**: p. 419-424.
7.   M.S. Abo Dhaheer, M.M. Al-Rubaye, W.S. Alyhya, B.L. Karihaloo & S. Kulasegaram (2015): Proportioning of self–compacting concrete mixes based on target plastic viscosity and compressive strength: mix design procedure, Journal of Sustainable Cement-Based Materials, DOI: 10.1080/21650373.2015.1039625.
8.   Zine el-abidinelaidani , bencha benabeda ,raja babousninab, m. kamal gueddouda & el-hadjkadri experimental investigation on effects of calcined bentonite on fresh, strength and durability properties of sustainable self-compacting concrete, Construction and Building Materials Volume 230, 10 January 2020, 117062.

1st International Conference on Advances in Civil & Environmental Engineering, University of Engineering & Technology Taxila, Pakistan

Conference date 22 &23 Feb 2022

Sustainable concrete: A Review

Wasif Ali
BS Student
Capital University of Science and Technology, Pakistan
h.wasifali@gmail.com

Saqib Khalid
BS Student
Capital University of Science and Technology, Pakistan
saqibskkhalid@gmail.com

Muhammad Saad Hassan
BS Student
Capital University of Science and Technology, Pakistan
saadrajapeace@gmail.com

Mehran Sudheer
Lecturer
Capital University and Science and Technology, Pakistan
mehran.sudheer@cust.edu.pk

Majid Ali
Professor
Capital University and Science and Technology, Pakistan
majid.ali@cust.edu.pk

ABSTRACT

This paper reviews the sustainable concrete aspects. It is known that cement in the entirety of its various kinds and structures is a fundamental item that, when joined with different fixings in the right proportion of, makes it a significant structure material. Concrete is a magnificent illustration of cement based building material. The construction enterprise has an instantaneous and seen to have an effect on international resources, power consumption, and carbon dioxide emissions. Many advantages of using waste material in production have usually been mentioned in preceding literature, including shortened production time, decrease normal production cost, progressed quality, improved durability, higher architectural appearance, worked on word related wellness and security, significantly less creation web site online waste, considerably less natural discharges, and markdown of solidarity and water utilization. The supportable cement (SC) includes a decrease of the measure of contaminating and carbon dioxide (CO_2) gases radiated during the making of concrete, more productive utilization of waste materials, advancement of low-energy, durable, adaptable structures and constructions taking advantage of the warm mass of cement in a design to decrease energy interest.

KEYWORDS: cement, CO_2, production cost

1st International Conference on Advances in Civil & Environmental Engineering, University of Engineering & Technology Taxila, Pakistan

Conference date 22 &23 Feb 2022

1 INTRODUCTION

The world's yearly cement creation of 1.6 billion tons represents around 7% of the worldwide stacking of carbon dioxide into the environment. They add to respiratory issues brought about by exhaust cloud and air contamination, as well as adding to environmental change by catching hotness. Different ramifications of environmental change delivered by ozone depleting substances incorporate outrageous climate, food supply deficiencies, and expanding out of control fires [1]. The dwindling supply of limestone in certain geographical areas is one of the most severe risks to the cement industry's long-term viability. Limestone is required to produce cement. As limestone becomes a scarce resource, so will employment and construction in the concrete industry. As a result, those involved in such industries must build new techniques for producing concrete that uses as little limestone as possible.[2] Hence there is a need of sustainable concrete. With the help of sustainable concrete not only the concrete industry continues to evolve to meet the changing needs and exceptions of society, but it must also continue to employ people like batch plant operators, truck drivers, steel workers, labourers, carpenters, finishers, machine operators, and testing technicians, as well as experts like engineers, architects, site supervisors, and inspector The use of sustainable concrete results in numerous benefits .The studies reported herein suggest unique concrete combinations that are cost-effective and ecologically beneficial alternatives to the environment. The advantages are classified as follows: (1) Energy conservation and Greenhouse gases reduction, (2) Natural resource and land conservation, and (3) Reduced landfill expenses [3]. However, with inclusion of sustainability in concrete there are some challenges too. The studies indicate a list of several barriers' factors categorised as social, economic, and technical barriers factors [6,7].

2 SUSTAINABLE CONCRETE

2.1 Inclusion of sustainability aspect in concrete

Sustainability means "meeting the requirements of the current generation without endangering future generations' ability to fulfil their own necessities" [7,8]. The long-term viability of the cement concrete substantial enterprises is basic to the wellbeing of our planet and human turn of events. Other than that, the creation of concrete, a basic component of cement, brings about huge carbon dioxide and other ozone harming substances (GHGs) outflows. The ecological issues related with carbon dioxide will assume a vital part in the cement concrete industries' long-term development in the twenty-first century [6]. Production of cement is not only a useful source of societal development; it is also a significant source of employment. [8]

These waste materials come primarily from domestic wastes, factory and commercial waste, and disposal of waste [11]. In spite of the chance of reusing these waste materials, by far most are discarded in landfills, which hurts the climate as well as has social and financial results. A built system is liable for huge energy use and fossil fuel by-products all through its whole life cycle, from material procurement to end-of-life [11,12,13]. A significant piece of this is because of the utilization of virgin materials during development. As indicated by studies, materials represent over 15% of a structure's energy use and fossil fuel by-products [6]. Moreover, the utilization of unreasonable virgin unrefined components in development materials consumes regular assets and adds to the natural weight [13].

1st International Conference on Advances in Civil & Environmental Engineering, University of Engineering & Technology Taxila, Pakistan

Conference date 22 &23 Feb 2022

Many advantages of using waste material in production have been mentioned in preceding literature [3,4,5], including shortened production time, decrease normal production cost, progressed quality, improved durability, higher architectural appearance, improved occupational fitness and safety [12]. As a result, not only the concrete industry continues to evolve to meet the changing needs and exceptions of society, but it must also continue to employ people like batch plant operators, truck drivers, steel workers, labourers, carpenters, finishers, machine operators, and testing technicians, as well as experts like engineers, architects, site supervisors, and inspectors.

2.2   Benefits of sustainable concrete

Sustainable concrete has the potential to perform as well as or better than conventional concrete in structural applications [6]. Sustainable concrete has the following goals: reduce the quantity of pollutants and carbon dioxide (CO_2) emissions released during the concrete manufacturing process [7]. The studies reported herein suggest unique concrete combinations that are cost-effective and ecologically beneficial alternatives to the environment [8,9]. The concrete industry will be relied upon to service two pressing demands of human society: environmental preservation and satisfying the infrastructure requirements for rising global industrialization and urbanisation [11]. lowering the cost of building by minimising cement use. The use of industrial effluents helps to safeguard the environment and natural resources. Reduces The Power consumption: If you mix concrete with a little less Portland cement, it consumes less energy. These advantages are classified as follows: (1) Energy conservation and Greenhouse gases reduction, (2) Natural resource and land conservation, and (3) Reduced landfill expenses. These advantages are described below:

1. Energy conservation and Greenhouse gases: Extensive usage of sustainable concrete in the structure business will bring about energy reserve funds and, therefore, long haul decreases in ozone harming substances outflows. In light of energy requests for delivering concrete, the decrease in the energy utilization and GHG emanations by utilizing practical substantial will come from two sources: (1) diminished concrete utilization because of supplanting of concrete with fly-debris and slag, (2) diminished transportation distance of natural stone/stone from quarries to the handling plants.

2. Natural resource and land conservation: The ground's water storage capacity is reduced by excavating the aggregate. Increased use of sustainable concrete in the construction sector will reduce demand for these resources, allowing water resources to be conserved and natural habitats to be protected.

3. Reduced landfill expenses: Development and destruction squander dump costs proceed to climb, and landfills are by and large more seriously controlled. Therefore, it checks out to search for elective techniques for discarding concrete from C&D tasks. Total processors are beginning to recognize this reality and are thinking about getting recovered cement for a "tipping fee" that is significantly not exactly the expense of landfilling the material and supplying recycled concrete aggregate of adequate quality for many purposes [10]. This figure shows the cycle of sustainability depends on environment, social and economic aspects. Green

1st International Conference on Advances in Civil & Environmental Engineering, University of Engineering & Technology Taxila, Pakistan

Conference date 22 &23 Feb 2022

concrete offers a higher strength-to-weight ratio and a lower shrinkage rate than Portland cement-only concrete [11].
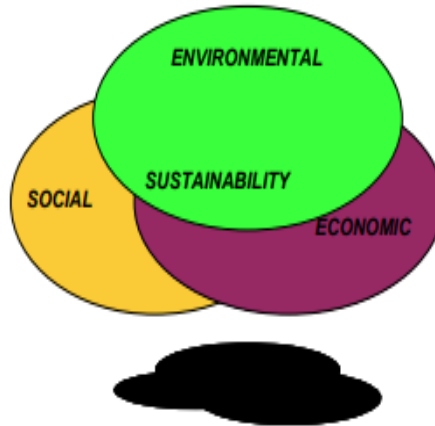
Figure 1: The triple bottom line of sustainability

2.3 Challenges for adoption of sustainable concrete in practical applications

Green structure execution in enormous scope is a major test [12]. The customary idea of correspondence in view of media and message configuration isn't adequate to manage the current difficulties of the arising improvement structure. Table 1 shows uses of different waste material used in the production of concrete and their sources [13]. Heterogeneous designing can help the improvement of new materials by comprehension the boundaries to execution [14].

Table 1 Recycled materials used in green building construction

Product name	Sources and uses
Newspaper wood	Every year in Norway, 1 million tons of paper and card wood are recycled [13].
Nappy roofing	Polymers are extracted from the thrown away nappies and sanitary products and used for manufacturing different construction materials [13].
Wine cork panels	Granulated cork combined with wine bottle cork form this kind of panels, which can be used as floor tiles [13].

The significant hindrances for sustainable concrete use in development are [15]:
- Insufficient guideline support
- Absence of ecological mindfulness by the business, political leaders, client, and feasible structure/development
- Absence of an all-around created squander reusing market
- Framework challenge for concrete industrial facility site area, nonattendance of site space and stuff for waste orchestrating, experience in waste reusing errands, arranged managers and delegates, data on helper materials markets, biologically

1st International Conference on Advances in Civil & Environmental Engineering, University of Engineering & Technology Taxila, Pakistan

Conference date 22 &23 Feb 2022

- Absence of government interests in supportable turn of events.
- Absence of impetuses
- Ill-advised garbage removal regions.
- Absence of interests from government offices.
- Intricacies in adjusting work practices of representatives
- Absence of authorization of development and waste administration strategies and plans
- Shortage of local environmental regulation.

The basic variables in improving the sustainable concrete hindrance are: 1) Legislation, 2) Project Control Guidelines, 3) Obtainment Systems, 4) Standardization, 5) Creation, 6) Knowledge and Skills [15].

3   CONCLUSION

Sustainable concrete has a 30% decrease in CO2 emissions in the concrete industry. Green concrete structures have a greater probability of hold out a catastrophic event like fire the concrete mix but with much less cement. The demand for inexperienced concrete is growing despite the fact that there are several hindrances. It also controls the environmental effect and energy.

- Sustainable concrete has a less environment effect than reference concrete. including shortened production time, decrease normal production cost, progressed quality, improved durability, higher architectural appearance, improved occupational fitness and safety.
- The usage of recycled aggregate has been researched for of accomplishing a more practical future. Cost-effective and ecologically beneficial alternatives to the environment More productive utilization of waste materials in advancement of low-energy, durable, adaptable structures and constructions.
- The review incorporates the absence of site space and gear for squander arranging, experience in squander reusing tasks, prepared bosses and representatives, information on auxiliary materials markets, ecologically. The significant hindrances for sustainable concrete use in development are fundamental lock-in, lower characteristics of locally accessible materials, expansion in development expenses.

Further research on using different methods of producing sustainable concrete should be possible to accomplish financial, ecological, and social concrete.

REFERENCES

1. P Kumar Mehta (2001). *Concrete international / OCTOBER 2001 61*. [online] Available at: http://ecosmartconcrete.com/docs/trmehta01.pdf.
2. Scrivener, K.L., John, V.M. and Gartner, E.M. (2018). Eco-efficient cements: Potential economically viable solutions for a low-CO2 cement-based materials industry. *Cement and Concrete Research*, 114, pp.2–26.

1st International Conference on Advances in Civil & Environmental Engineering, University of Engineering & Technology Taxila, Pakistan

Conference date 22 &23 Feb 2022

3. Anantha Lekshmi M L, 2015, Green Concrete-for the Future-A Review, INTERNATIONAL JOURNAL OF ENGINEERING RESEARCH & TECHNOLOGY (IJERT) RICESD – 2015

4. Hrabová, K., Teplý, B. and Hájek, P. (2019). Concrete, Sustainability and Limit States. *IOP Conference Series: Earth and Environmental Science*, 290, p.012049.

5. Czarnecki, L., 2013. Sustainable concrete; is nanotechnology the future of concrete polymer composites?. In *Advanced Materials Research* (Vol. 687, pp. 3-11). Trans Tech Publications Ltd.

6. Noël, M., Sanchez, L. and Fathifazl, G., 2016. Recent advances in sustainable concrete for structural applications. *Sustainable Construction Materials & Technologies*, *4*(10).

7. Karim, M.R., Zain, M.F.M., Jamil, M. and Lai, F.C., 2011. Significance of waste materials in sustainable concrete and sustainable development. *International Journal of Biotechnology and Environmental Management*, *18*, pp.43-47.

8. Sandanayake, M., Bouras, Y., Haigh, R. and Vrcelj, Z. (2020). Current Sustainable Trends of Using Waste Materials in Concrete—A Decade Review. *Sustainability*, 12(22), p.9622

9. Assi, L., Carter, K., Deaver, E. (Eddie), Anay, R. and Ziehl, P. (2018). Sustainable concrete: Building a greener future. *Journal of Cleaner Production*, [online] 198, pp.1641–1651. Available at: http://sciencedirect.com/science/article/pii/S0959652618321085.

10. Senaratne, S., Lambrousis, G., Mirza, O., Tam, V.W. and Kang, W.H., 2017. Recycled concrete in structural applications for sustainable construction practices in Australia. *Procedia engineering*, *180*, pp.751-758.

11. Gazipur, B., 2011. Necessity and opportunity of sustainable concrete from Malaysia's waste materials. *Australian Journal of Basic and Applied Sciences*, *5*(5), pp.998-1006.

12. Pramanik, P.K.D., Mukherjee, B., Pal, S., Pal, T. and Singh, S.P., 2021. Green smart building: Requisites, architecture, challenges, and use cases. In *Research Anthology on Environmental and Societal Well-Being Considerations in Buildings and Architecture* (pp. 25-72). IGI Global.

13. Mefalopulos, P., 2005. Communication for sustainable development: applications and challenges. *Media and glocal change. Rethinking communication for development*, pp.247-260.

14. Henry, M. and Kato, Y., 2009, August. The role of new material technologies for sustainable practice in the concrete industry. In *PICMET'09-2009 Portland International Conference on Management of Engineering & Technology* (pp. 1738-1744). IEEE.

15. Yunus, R. and Yang, J., 2016. Legislative challenge to sustainable application of industrialized building system (IBS). *Jurnal Teknologi*, *78*(5).

An overview on need for automatic structural detailing of line elements in BIM tools

Asad Iqbal and Majid Ali
Capital University of Science and Technology, Islamabad, Pakistan.
Asad8098@gmail.com; professor.drmajid@gmail.com

ABSTRACT

Structural detailing is done to provide adequate ductility to the structure and avoid failures due to different design parameters. Ductility is the ability of reinforced concrete members to undergo considerable deflection before failure. This characteristic of reinforced concrete is crucial as it indicates failure and prevents total collapse and damage of a structure. This is especially significant in seismic zones. Different design codes and detailing manuals are used for structural detailing. The main objective of this paper is to review the non-seismic and seismic detailing philosophy of RCC line elements and provide the need for automatic structural detailing of line elements in BIM tools. Therefore, a literature study was done to review and discuss the ability of BIM tools in the structural detailing of line elements. It was highlighted that BIM tools lack certain features that could automate the rebar selection in RCC line elements. The overview concludes with a detailed discussion of different aspects of non-seismic and seismic detailing of RCC line elements.
Keywords: Non-Seismic detailing; Seismic detailing; BIM; ETABS; AutoCAD.

1 INTRODUCTION

The main purpose of the detailing is to assure structure safety. Detailing of reinforcements in RCC members plays an important role in providing ductility, strength, and durability. The ductility of RCC members is ensured by seismic codes all around the world. In the conventional approach of detailing, the structural designer takes the area of steel, selecting rebars, and then detailing with the help of different software such as ETABs along with AutoCAD. During switching between software, human involvement is needed to make the reinforcement consistent, coherent and avoid variation in bar diameter. Building Information Modelling (BIM) consists of a variety of tools that have claimed the automation of many processes involved in the analysis. However certain tools are missing such as automated rebar selection.

The economy can be achieved by saving materials or by boosting the speed of construction. BIM tools speed up construction and reduce construction waste which ultimately helps in saving the economy and resources. Different optimization techniques are also used to achieve economy in the AEC industry. This study covers the critical review on the non-automation of the non-seismic and seismic detailing of RCC line from forces to rebars in BIM tools, economic aspect, and need for automation in BIM tools. Non-seismic and seismic detailing of beams.

1st International Conference on Advances in Civil & Environmental Engineering, University of Engineering & Technology Taxila, Pakistan

Conference date 22 &23 Feb 2022

2   NON-SEISMIC AND SEISMIC DETAILING OF LINE ELEMENTS

2.1   Non-Seismic and seismic detailing for beam

Beams are linear structural members used to transfer loads from slab to columns. Usually, Beams are subjected to slab loads but may also be subjected to other loads like wall loads, etc. In non-seismic detailing, there are three types of forces acting on a beam which are bending moment, shear force, and torsion. To resist bending moment top and bottom bars are provided in the beam. Similarly, transverse reinforcement is provided to resist shear and torsion and in some cases, mid-depth bars are provided for torsion. Detailing of reinforcements in beams plays an important role in providing ductility, strength, and durability [1]. It has been observed that many practical continuous beams that meet the usual deflection limits are also satisfactory regarding ductility. The deflection of beams was increased as the temperature increased and the tensile strength of concrete and steel decreases as temperature increased [2]. In rebar selection, the software does not incorporate an area of steel at other locations of the same span as well as at the location of other adjacent spans of beams.

In seismic detailing, lap location shifts to enhance the ductility of reinforced members. The requirements for designing and detailing monolithic reinforced concrete members is to give them adequate toughness and ductility to resist severe earthquake shocks without collapse. It is, therefore, important that structures should be more ductile for better performance during earthquakes. Seismic design purely based on strength criteria is neither practical nor financially beneficial. As a result, the fundamental approach should be focused on the structure's lateral strength, as well as its deformability and ductility capacity, with minimal damage but no collapse[3]. A comparison of moderate seismic and high seismic detailing of the beam is shown in Table 1.

Table 1 comparison of moderate seismic and high seismic zone detailing of beam

SR No	ITEM DESCRIPTION	MODERATE SEISMIC ZONE	HIGH SEISMIC ZONE
1	Beam Size	8" Min. width	10" Min. width with the width to depth ratio of 0.3
2	Lap location	A column/support	Min. twice the depth from column / support
3	Lap length for top bars	48 diameter of larger longitudinal bar	55 diameter of larger longitudinal bar
4	Positive Moment Strength at the joint face	1/3 of Negative Moment Strength at the joint face	1/2 of Negative Moment Strength at the joint face

Table 1 shows the difference between moderate and high seismic detailing of the beam. In a high seismic zone, the width of the beam increases, and the lap location of the beam shifts to improve the ductility and strength of the members.

2.2   Non-seismic and seismic detailing of columns

Columns are structural members designed to carry compressive loads, composed of concrete with steel rebars as reinforcement. Column transfer all the loads from the superstructure to the

1st International Conference on Advances in Civil & Environmental Engineering, University of Engineering & Technology Taxila, Pakistan

Conference date 22 &23 Feb 2022

substructure. The non-seismic detailing of the column involves the provision of adequate compression reinforcement to guarantee the stability of the structure. The major effects on the column are compressive axial force, bending moment, and shear force. Longitudinal reinforcement is provided to resist bending which is caused by transverse load, eccentric load, or moment. Similarly, transverse reinforcement or ties are provided to hold the longitudinal bars and prevent them from buckling. The use of ties exists a long history and is more likely to be accepted when incorporated into code for the design of the RCC column. Ties ensured the ductile behavior of RCC members by providing the following three roles: (1) providing restraint to main bars to resist bar buckling; (2) confining core concrete; (3) providing shear resistance [4].

In RCC column ductility is crucial for structure stability, especially in earthquake-resistant structures. Seismic codes around the world ensure the satisfactory ductility of RCC members. Steel reinforcement in the column is one of the key factors, which could influence the stability and integrality of the frame structure. Columns are classified into the following three categories based on the moments: (1) Axial column; (2) Uniaxial column; (3) Biaxial column. Reinforcement in the column is provided based on the type of column. In an axially loaded column the reinforcement can be provided in any pattern but in the uniaxial column it needs reinforcement in the two faces parallel to the axis of bending and in the biaxial column the reinforcement is provided in all four faces [5]. Non-seismic and seismic detailing of the column is shown in Figure 1.
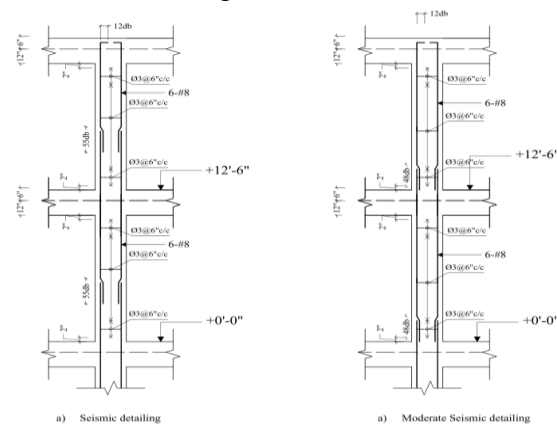
Figure 1 Moderate and high seismic detailing of column

Figure 1 shows the detailing of the column, in seismic detailing the lap location shifts to regions of less moments to enhance the ductility of the column.

3   ECONOMIC ASPECTS IN DETAILING OF LINE ELEMENTS

The paper shows how GA was used to optimize the structural frame. The hybrid GA (Genetic Algorithm) has been used to optimize different degrees of steel reinforcement: longitudinal tensile reinforcement, longitudinal compressive reinforcement, and shear reinforcement [6]. For the examination of the structure, the building codes BS8110 (British Standard) were employed. The optimization is carried out on two different examples: a multi-story frame building and an RCC beam. The GA optimization has shown efficient results as compared to calculated by other software like CSI ETABS, Autodesk RSA, and Manual Calculations. The greatest results using

1st International Conference on Advances in Civil & Environmental Engineering, University of Engineering & Technology Taxila, Pakistan

Conference date 22 &23 Feb 2022

hybrid GA for percentage difference between the minimum required steel and given steel reinforcement was just 0.004 percent, which was an incredible result when compared to other methodologies [7].

The cost optimization of RCC members has been carried out as per British standards. The cost objective function considers costs of various RCC elements, which includes concrete cost, steel fixer cost, formwork cost, and material cost. The equivalent frame method was used in the structural analysis, and optimization is done in three steps: column dimensions and slab thickness optimization, column layout optimization, and the sizes and number of reinforcements for reinforced concrete members. When compared to a conventional design, the results show that optimization reduces costs. The cost-saving was directly proportional to the number of structural elements, therefore the more RCC there, the more money saved [8].

MATLAB coding was used in the optimization of longitudinal reinforcement design. Different examples were compared by the author using ACI 318 to highlight the differences in the procedure for each building code. The authors discovered that MATLAB and computers have become fast computational tools for experts in a variety of fields. When compared to hand computations, the time spent on computing was found to be one-hundredth of a second [9].

4   NEED FOR AUTOMATION OF BIM TOOLS

BIM software is an effective and efficient tool to design cost-effective steel reinforcement for complex structures. BIM is an advanced technology, that provides a new vision to the architecture, engineering, and construction industry (AEC) and has many benefits[10]. Automated structure optimization using BIM models has gained vast popularity amongst researchers [11]. However certain tools are missing, one such problem is when the Revit-designed architectural model is exported into Autodesk Robot Structural Analysis Professional (ARSAP); certain elements get lost which have not been taken into consideration by the research community. During the detailing phase, after exporting analysis data from ARSAP to Revit; skilled human involvement for rebar selection must occur. So far research on this problem has not been contemplated.

5   CONCLUSION

Conventionally the structural detailing needs human involvement which is a time taking process and is prone to errors. The conclusion made from the above discussion is as follows:

- The structural detailing of line elements is provided to enhance the members' ductility and strength.
    - In beam detailing as per the codes, the rebars are calculated based on the area of steel at the particular governing locations, neglecting coherency and consistency at other locations.
    - In detailing of a column as per the codes, the rebars are selected based on the area of steel at the top or bottom of the column, while not incorporating the area of steel used throughout the column's height.
- In the AEC industry, BIM optimization can achieve economy by increasing the speed of construction or by saving materials.
- BIM is a powerful tool however certain tools are missing that need some advancement, which should be modified by the research community.

1st International Conference on Advances in Civil & Environmental Engineering, University of Engineering & Technology Taxila, Pakistan

Conference date 22 &23 Feb 2022

In structural detailing of line elements, the rebars are selected according to the codes based on the area of steel at a specific governing location without considering the area of steel at other locations which is a tedious and uneconomical task. An advancement in BIM tools can be done by automatic structural detailing of line elements to make the selected rebars consistent and coherent which will eventually save time and cost.

ACKNOWLEDGMENTS
The authors would like to thank everyone who helped them in their literature research.

REFERENCES

[1] R. Pierott, A. W. A. Hammad, A. Haddad, S. Garcia, and G. Falcón, "A mathematical optimisation model for the design and detailing of reinforced concrete beams," *Engineering Structures*, vol. 245, Oct. 2021, doi: 10.1016/j.engstruct.2021.112861.

[2] M. M. El-Hawary, A. M. Ragabs, A. Abd El-Azim, and S. Elibiarif, "Effect of fire on flexural behaviour of RC beams," 1996.

[3] J. Oho and B. Mander, "Beyond Ductility: The Quest Goes On," 2004.

[4] D. Wu, Y. Ding, J. Su, Z. X. Li, L. Zong, and K. Feng, "Effects of tie detailing configurations on reinforcement buckling and seismic performance of high-strength RC columns," *Soil Dynamics and Earthquake Engineering*, vol. 147, Aug. 2021, doi: 10.1016/j.soildyn.2021.106791.

[5] W. Xue, H. Bai, L. Dai, X. Hu, and M. Dubec, "Seismic behavior of precast concrete beam-column connections with bolt connectors in columns," *Structural Concrete*, vol. 22, no. 3, pp. 1297–1314, Jun. 2021, doi: 10.1002/suco.202000007.

[6] C. Xu *et al.*, "Using genetic algorithms method for the paramount design of reinforced concrete structures," *Structural Engineering and Mechanics*, vol. 71, no. 5, pp. 503–513, Sep. 2019, doi: 10.12989/SEM.2019.71.5.503.

[7] M. Mangal and J. C. P. Cheng, "Automated optimization of steel reinforcement in RC building frames using building information modeling and hybrid genetic algorithm," *Automation in Construction*, vol. 90, pp. 39–57, Jun. 2018, doi: 10.1016/j.autcon.2018.01.013.

[8] M. G. Sahab, A. F. Ashour, and V. v. Toropov, "Cost optimisation of reinforced concrete flat slab buildings," *Engineering Structures*, vol. 27, no. 3, pp. 313–322, Feb. 2005, doi: 10.1016/j.engstruct.2004.10.002.

[9] A. Tomás and A. Alarcón, "Automated design of optimum longitudinal reinforcement for flexural and axial loading," *Computers and Concrete*, vol. 10, no. 2, pp. 149–171, 2012, doi: 10.12989/cac.2012.10.2.149.

[10] E. N. Shaqour, "The role of implementing BIM applications in enhancing project management knowledge areas in Egypt," *Ain Shams Engineering Journal*, vol. 13, no. 1, p. 101509, Jan. 2022, doi: 10.1016/J.ASEJ.2021.05.023.

[11] A. Ejaz and M. Ali, "Limitations of Autodesk Robot Structural Analysis Professional for Structural Design Output: A Review of Frame Building." [Online]. Available: https://help.bricsys.com/hc/en_EU/articles/360007744834

1st International Conference on Advances in Civil & Environmental Engineering, University of Engineering & Technology Taxila, Pakistan

Conference date 22 &23 Feb 2022

The compressive strength of polypropylene fibres reinforced self compacting concrete

Muhammad Tariq, Mehwish Asad
University of Engineering & Technology Taxila, Pakistan
Muhammad.Tariq2@students.uettaxila.edu.pk;mehwish.asad@uettaxila.edu.pk

Mudassar Hassan
Mudassarhassan898@gmail.com

ABSTRACT

This research deals with the study of mechanical property of fibres reinforced self-compacting concrete in hardened state. The purpose of this investigation program is to find the effect of polypropylene fibres (PPF) proposed by the varying contents such as 0%, 0.5%, 1% &1.5% and to find the optimum polypropylene fibre (PPF) content which can be added safely. Moreover, the replacement of cement was done up to 10% with silica fume and fly ash which was constant for all the mixes. An experimental study program was intended to examine compressive strength at 7, 14, and 28 days of curing. Then a comparison was made between the mix containing polypropylene fibres with varying content and conventional concrete.

It was found that adding polypropylene fibres to the mix improved the compressive strength. The compressive strength is the maximum at 0.5% addition of polypropylene fibres. Furtherer addition of PPF which is 1% and 1.5% reduced the compressive strength of fibres reinforced SCC.

KEYWORDS: Polypropylene fibres (PPF), compressive strength, self compacting concrete (SSC)

1   INTRODUCTION

Self compacting concrete is actually known as self consolidating concrete. This type of concrete can be placed or adjusted in any place by its own weight. In case of congested reinforcement places, it can be placed easily. During the placing of SCC, no need of compaction by using mechanical vibrators.

In this experimental program four PPF containing mixes and one conventional mix were considered to find the compressive strength of SCC. The fixed replacement of content with fly ash and silica fume was done for all mixes. An increasing amount of 0.5 percent fibers were added to all mixes. The replacement percentages were 0%, 0.5%, 1%, 1.5%. For all of the mixes, a fixed water-cement (w/c) ratio of 0.32 was utilized and the workability of SCC was improved with help of super plasticizer without increasing the water content. This research program was

1st International Conference on Advances in Civil & Environmental Engineering, University of Engineering & Technology Taxila, Pakistan

Conference date 22 &23 Feb 2022

done to find the mechanical properties of concrete, for this purpose the compressive strength and the flexural strength were determined. A comparison was made for all the mixes with polypropylene fibers and conventional mix. It was found that, the inclusion of fiber to SCC enhanced the compressive strength of concrete. [1] The concrete mixes were prepared by the inclusion of four different polypropylene fibers quantities such as 0.1, 0.2, 0.3 and 0.4 percent by the weight of cement to determine the compressive strength. For this purpose four different mixes were prepared. The compressive strength was evaluated at 28 days. It was concluded that, the addition of polypropylene fibers considerably affect the compression performance of self-compacting concrete. [2] An experimental program was done to assess the characteristics of SCC in fresh and harden states. For this purpose polypropylene fibers volumes were added at 0%, 0.5%, 0.75% and 1% along with steel fibers. At the inclusion of 0.5% PPF, the maximum compression strength was obtained. [3]In this research program, polypropylene fibers were used in the quantities of 1, 2 and 3 kg/m^3. In this research, high performance PPF were added to the mixes. The mechanical properties included the tensile, compressive and the flexural strengths were studied at the temperatures of 25^0C, 100^0C, 200^0C and 300^0C. It was observed that, at the inclusion of 1 kg fibers to concrete, the compressive strength increased up to 14 percent, the tensile strength increased up to 17% and the flexural strength improved up 8.5%.[4] An experimental analysis was done for the damage evolution rule, the compressive strength and the damage performance of PPF concrete. A comparison for the results was done with the plain concrete. The outcomes showed that the inclusion of PPF enhanced the compression strength of concrete. [5]

2   Experimental program

2.1   Material characteristics

2.1.1   Polypropylene fibres

Polypropylene fibers are produced from the monomer C_3H_6. These are chemical resistant fibers. The white colour 12 mm diameter polypropylene fibres were used in the research for the experimental program are shown in figure1.

Figure 1: Polypropylene fibers

1st International Conference on Advances in Civil & Environmental Engineering, University of Engineering & Technology Taxila, Pakistan

Conference date 22 &23 Feb 2022

2.1.2 Fly ach

Fly ash is a material which is heterogeneous and manufactured as a by product during the process of combustion of coal which is used in power stations. It is a grey coloured fine powder material having glassy particles with spherical shape that rise with the flue gases. It is a fine that is low in lime content as shown in figure 2.
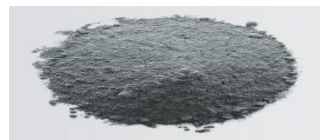
Figure 2: Fly ash

2.2 Mix proportion and procedure:

The ACI-211 standards were used for the mix design with mix ratio of (1:1.4:1.6). The w/c ratio of 0.32 was used in the mixes to determine the influence of PPF on concrete properties. PPF were used at 0, 0.5,1 and 1.5 percent. Designations and proportions of cement (C), sand (S),coarse aggregate (C.A), silica fume (S.F),fly ash (F.A),water reducing admixture (WRA) and polypropylene fibers (PPF) used in self compacting concrete mixes are shown in table 1.The missing of materials was done with the help of a drum type concrete mixer. First of all, the missing of all aggregates was carried out in a dry condition for the duration of almost one minute. After that, PPF were added and the missing is carried out in dry state for further one minute. At the initial stage 2/3 quantity of the water was used and mixing proceeded for a further one minute. The super plasticizer and the remaining 1/3 quantity of water were added at this stage. By using ASTM C143 standards, slump test for SSC was carried out. Then cylinders were casted by using the mould with dimensions 300 x 150mm. After 24 hours of casting, the concrete samples were removed from the moulds. Then these samples were placed in a water tank for curing of specimens.

Table 1 Mix proportions

Variations	PPF %	SF %	F.A %	PPF (Kg)	S.F (Kg)	C (kg)	F.A (kg)	S (kg)	C.A (kg)	W (kg)	WRA (gms)
M1	0	10	10	0	2.25	20.25	3.15	28.35	36	6.48	243
M2	0.5	10	10	0.1125	2.25	20.1375	3.15	28.35	36	6.444	241.65
M3	1	10	10	0.225	2.25	20.025	3.15	28.35	36	6.408	240.3
M4	1.5	10	10	0.3375	2.25	19.9125	3.15	28.35	36	6.372	238.95
CM						22.5		31.5	36	7.2	270

1st International Conference on Advances in Civil & Environmental Engineering, University of Engineering & Technology Taxila, Pakistan

Conference date 22 &23 Feb 2022

3. Results and discussions

3.1 Compressive strength test

To evaluate the effect of PPF on the performance of SCC in hardened state, the compressive strength was examined at 7, 14 and 28 days of curing. The compressive strength of SCC was determined according to ASTM C39 standards by applying compressive force to cylindrical specimens using a compression testing machine, and the compressive strength of SCC was measured using the average of results, as shown in table 2. And the graphical interpretation of the results shown by figure 3.

Table 2 Compressive strength at seven, fourteen and twenty eight days

Compressive strength in (N/mm²)	CM	M1	M2	M3	M4
7 Days(Average)	27	28	30	29	28
14 Days(Average)	28	33	35	33	31
28 Days(Average)	30	34	37	35	33
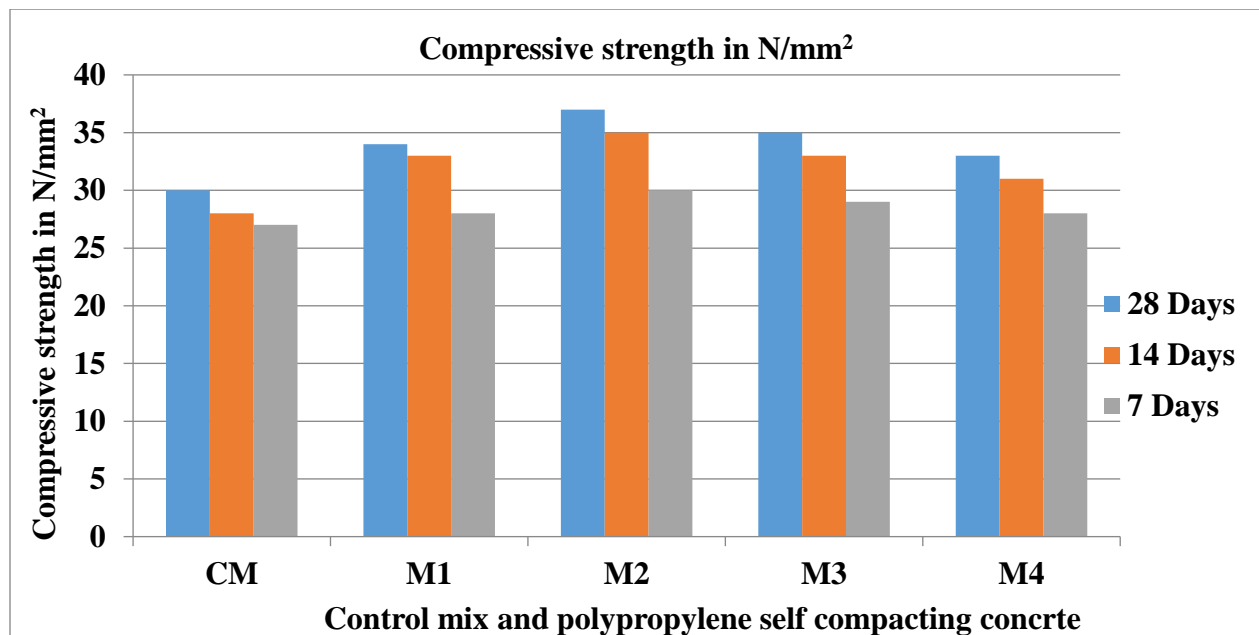
Figure 3: Compressive strength of control and PPF self compacting concrete

1st International Conference on Advances in Civil & Environmental Engineering, University of Engineering & Technology Taxila, Pakistan

Conference date 22 &23 Feb 2022

4. Conclusion

From the experimental investigation of results it has been revealed that the addition of polypropylene fibers to the self compacting concrete a positive affect on the compressive strength. At 0.5% addition of polypropylene fiber, the mix (M2) gains the maximum compressive strength of 37 N/mm^2 at 28 days. It has been concluded that, with the addition of 0 to 0.5% PPF, the compressive strength of SCC increases. Further addition of PPF i.e. 1 and 1.5% cause the reduction of strength.

REFERENCES

[1]   Rani, B.S. and N. Priyanka, *Self compacting concrete using polypropylene fibre* International Journal of Research Studies in Science, Engineering and Technology, 2017. **4(1)**: p. 16-19.

[2]   Kurian, S.V and A. Sarah, *Inflence of polyproplene fibbre in self compactng concrete*. International Research Journal of Engineering and Technology, 2017. **5(4)**: p. 1102-1104 .

[3]   Abaeian, R., et al., *Effects of high temperatures on mechanical behavior of high strength concrete reinforced with high performance synthetic macro polypropylene (HPP) fibres*. Construction and Building Materials, 2018. **165**: p. 631–638.

[4]   Liu, X, et al., *Properties of self-compacting lightweight concrete reinforced with steel and polypropylene fibers*, Construction and Building Materials, 2019. **226**:p. 388–398.

[5]   Qin, Y.,et al., *Experimental study of compressive behaviour of polypropylene-fibre-reinforced and polypropylene-fibre-fabric-reinforced concrete*, Construction and Building Materials, 2019. **194**: p. 216–25.

.

CFRP Partial Confinement Technique to Improve Mechanical Behaviour of Reinforced Concrete Damage Short Columns

Ali Raza, Pro. Dr. Muhammad Yaqub

University of Engineering & Technology Taxila, Pakistan

Ali.Raza5@students.uettaxila.edu.pk, muhammad.yaqub@uettaxila.edu.pk

ABSTRACT

An experimental study was performed to improve the confinement and to regain the axial capacity of damaged Reinforced Concrete (RC) circular shorts columns with partial confinement of Carbon Fiber Reinforced Polymer (CFRP) strips. Instead of wrapping the CFRP over the entire column, the partial confinement technique can be used as an alternative for restoring or upgrading the performance of concrete columns. CFRP strips has become increasingly attractive in the field of Civil Engineering for retrofitting and confinement of structural members due to high tensile strength and corrosion resistance. In this research, 6 damaged column specimens were repaired with high performance cementitious non-shrink grout and epoxy resin mortar. Repaired circular columns were retrofitted/strengthened with single layer of unidirectional CFRP, in the form of 2- and 9.5-inches wide strips, equally spaced. All columns were tested with monotonic axial compression load to determine the ultimate capacity and deformation in the direction of loading. It was concluded that CFRP retrofitted columns with 2-inch-wide strips increased the ultimate capacity by 24% and CFRP 9 inches wide strip increase the ultimate capacity by 34% as with respect to control specimens. Experimental results also indicated that the use of 9.5-inch-wide strip at top, centre, and bottom of circular columns was very efficient in terms of axial deformation and ultimate capacity as compared to control specimens.

KEYWORDS: CFRP; Axial capacity; Partial confinement; Damaged columns; Stiffness.

1 INTRODUCTION

Rapid deterioration and damaged of structure have major issues in the field of civil engineering, that need to be resolved by reliable, economical, and innovative material to increase the lifespan of structures. CFRP wrapping, on the other hand, has become an innovative and quick solution to the next generation of infrastructures for retrofitting and regaining the structural strength. Researchers find CFRP composite confinement is the most efficient technique for repair of circular columns due to uniform confinement and stress distribution in circular columns. In recent years, wrapping systems like CFRP have been widely used for repair and strengthening of RC columns [1-2]. Limited studies have done on partial retrofitting or confinement on damaged columns to increase the load bearing capacity. Different researchers have used full wrapping of CFRP sheet on whole column samples, to increase confinement, this causes a kind of wastage of material. CFRP is effective only where lateral deflection is more prominent and failure of structural member is more likely evident. This experimental study is performed to present an effective partial confinement technique, to examine the mechanical behaviour of already damaged RC shorts columns and to evaluate the availability of the partial confinement for future considerations.

1st International Conference on Advances in Civil & Environmental Engineering, University of Engineering & Technology Taxila, Pakistan

Conference date 22 &23 Feb 2022

2   EXPERIMENTAL PROGRAM:

2.1   Preparation of Specimens:

In this research 6 circular were taken, which were already damaged by compression testing machine. These reinforced columns were strengthened with CFRP (Wrap Hex-230 C) sheets strips as lateral reinforcement. For this 1st of all the physical inspection was done to check the conditions of columns, cracks width, damaged severeness. According to this inspection, mild cracks columns were repaired with Chemdur-31 Epoxy Repair and Bonding Mortar. While severe or crushed columns were repaired with Chemrite Grout NS which is high performance cementitious non-shrink grout. The previous condition of columns is shown in Figure1. left side and condition after Epoxy and Grout repaired is shown Figure 1. right side.

Figure 1.:Already damaged columns on left, on right epoxy and mortar repaired columns

2.2   Material Properties:

The circular columns used in this research was 1220 mm in longer and 200 mm in shorter dimension. The cross-sectional area of circular specimens was 31400mm^2. The reinforcement details of all specimens were 6 #12 mm main rebar and #10 mm rings with 150 mm c/c spacing. The Schmidt's Hammer and Ultrasonic Pulse Velocity (UPV) test were performed to check the in-place strength of concrete and the quality of concrete respectively. The average compressive strength of specimens was 32 Mpa. The UPV test shown the pulse velocity between 3 to 3.5 Km/sec, which indicated the concrete quality (Grading) medium. Moreover, the material properties of Chemrite Grout NS, Chemdur-31 Epoxy, CFRP Wrap Hex-230 C 0.12mm thickness and Chemdur 300 is shown in Table 1.[3]

Table 1. Material Properties

Material Type	Chemrite Grout NS	Chemdur-31 Epoxy Mortar	CFRP Wrap Hex-230C	Chemdur-300 Sheet Bonding
Tensile Strength (Mpa)	6-7	15-20	4100	18-22
Compressive Strength (Mpa)	60-62	60-70	-	65-75
Elastic Modulus (Mpa)	-	4300	231000	4800
Fiber/Density (g/cm^3)	2.2	1.65	1.78	1.8

2.3 Retrofitting of Specimens:

Circular Column's specimens were retrofitted with CFRP sheets strips by Chemdur-300 bonding. There was total 3 pairs of column specimens all were repaired with Epoxy and Grout as shown in Figure 1. One pair was taken as control specimens without any retrofitting, but it was properly grouted and repaired. 2nd pair of columns was retrofitted with 50mm/2inches wide single layer CFRP strip, by clear spacing of 150mm. 3rd pair of columns was retrofitted in 3 positions top, bottom, and centre with 240 mm / 9.5 inches single layer wide strip by providing 240 mm clear distance. The lap of CFRP sheets in all cases was taken as 150 mm. The specimen's id designated according to CFRP strip width shown in Table 2.

Table 2. Specimens Designations

Sr #	Specimens ID	Description of Specimens
1	CC-CS-1	Circular Columns Control Specimen 1
2	CC-CS-2	Circular Columns Control Specimen 2
3	CC-2WS-1	Circular Columns 2 inch Wide Strips Specimen 1
4	CC-2WS-2	Circular Columns 2 inch Wide Strips Specimen 2
5	CC-9.5WS-1	Circular Columns 9.5 inch Wide Strips Specimen 1
6	CC-9.5WS-2	Circular Columns 9.5 inch Wide Strips Specimen 2

2.4 Testing of Specimens:

The specimens were tested in 5000 KN Compression Testing Machine available in concrete Laboratory of UET Taxila, using two sets of Linear Variable Deflection Transducers (LVDT's). Firstly, the columns capping was done with high performance Plaster-of-Paris, after that 50 mm collars were attached at both ends of columns to beware from premature failure at the ends. Two LVDT's were connected at front and back side of columns sample at exactly the mid hight of 300 mm. Monotonic load was applied on column specimens and the axial deformation was recorded with respect to load variation. The rate of load was fixed as 0.02 MPa/sec & Peak sensitivity as 200 KN.

3 RESULTS & DISCUSSIONS:

All columns were tested under compression testing machine by monotonic loading condition. It was found from the testing that at the beginning of loading, in the elastic phase the columns exhibited the same mechanical behaviour. As the load increase the inelastic behaviour initiated and the concrete started cracking and CFRP sheets become active. The failure of all specimens is shown in Figure 3. It was noted that failure of control specimens 1 & 2 was due to crushing of concrete, due to end load concentration. Moreover, the mortar with which the columns were repaired possessed more stiffness than the concrete, also the weak bond between the mortar and concrete did not withstand the stress concentration at the top and bottom, so control specimens failed at the ends. Moreover, the failure of 2WS specimens 1 & 2 was with explosive sound of CFRP strips rupture at the top end. It indicated the full activation of CFRP strength at ultimate load, the 2 inches wide strip didn't withstand the full concentration of peak load and didn't provide confinement to concrete at top ends and

1st International Conference on Advances in Civil & Environmental Engineering, University of Engineering & Technology Taxila, Pakistan

Conference date 22 &23 Feb 2022

resulting the crushing of concrete. But still this takes the more axial load and deformation as compared to control specimens. On the other hand, the failure of 9.5WS specimens 1 & 2 were occurred due to crushing of concrete at the centre portion of middle and bottom strip shown in Figure 2. These pair of columns exhibited the higher ultimate load, deformation as compared to control and 2WS specimens shown in Figure 3 & 4. But secant stiffness of CFRP confinement columns was slightly less as compared to control specimens, shown in Figure 5, because CFRP confinement didn't enhance the stiffness. [4-5]
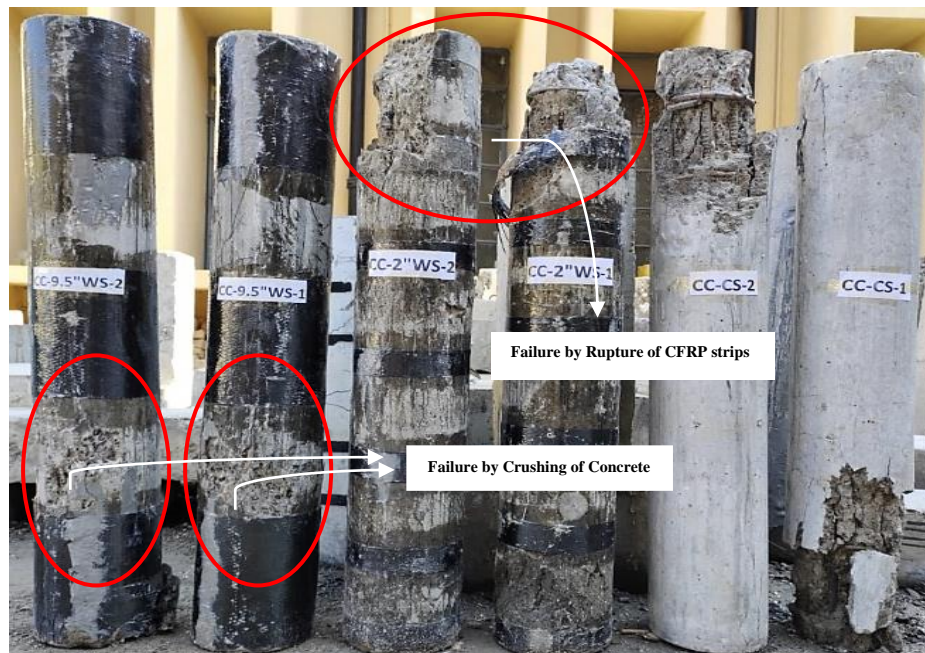
Figure 2. Failure of all control, 2- & 9.5-inches wide strip specimens from right to left
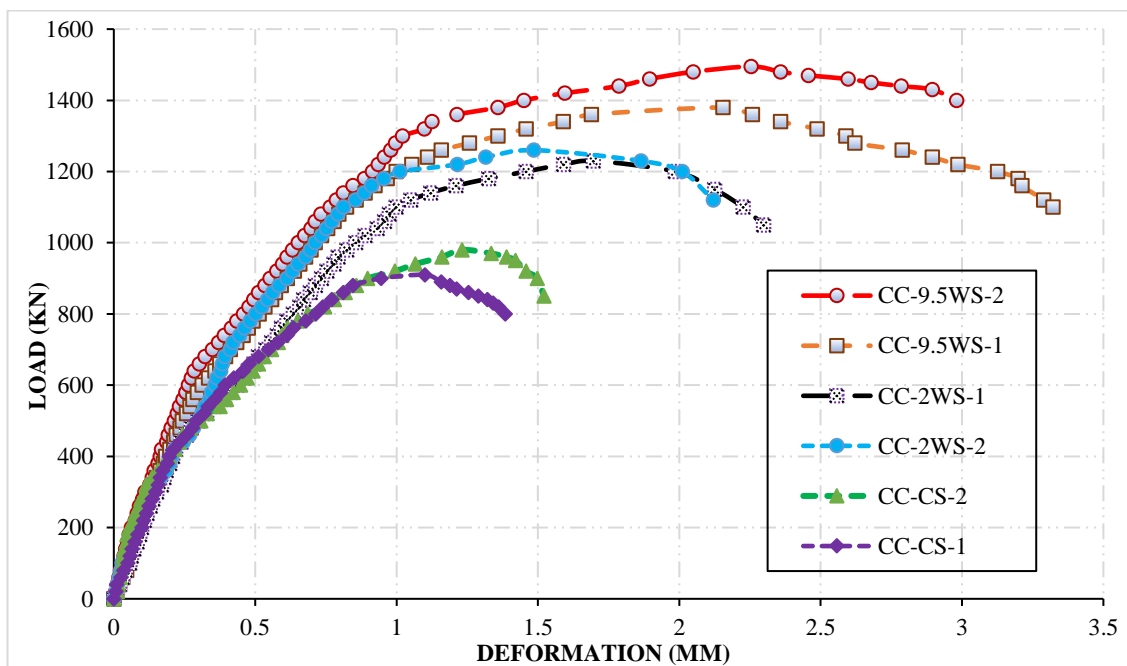
Figure 3. Load Deformation behavior of control, 2- & 9.5-inches wide strip specimens

1st International Conference on Advances in Civil & Environmental Engineering, University of Engineering & Technology Taxila, Pakistan

Conference date 22 &23 Feb 2022
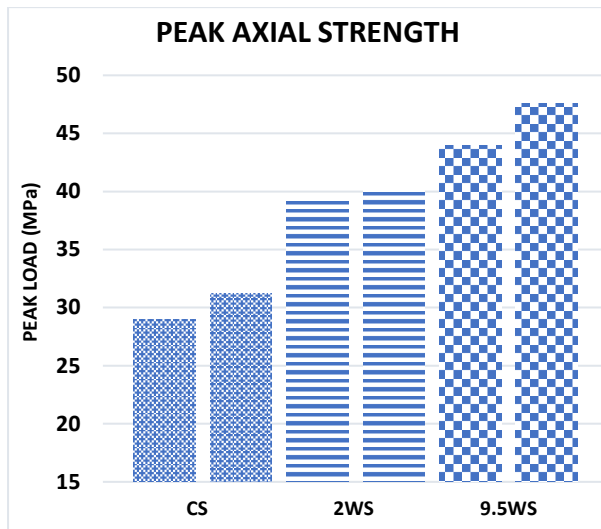
Figure 4. Peak Load Capacity of all specimens
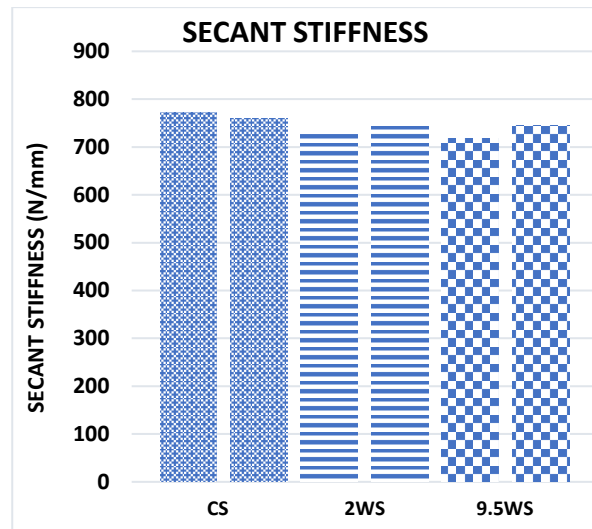
Figure 5. Secant Stiffness of all specimens

4 CONCLUSIONS:

This experimental study was taken to check the confinement and mechanical behavior of RC circular damaged columns by CFRP partial retrofitting technique. Results stated that CFRP 2- and 9.5-inches strips, increased the ultimate capacity of columns by 24% and 34% as compared to control specimens, respectively. The axial deformation was also enhanced by partial retrofitting techniques. But the secant stiffness of CFRP 2- and 9.5-inches confined columns was not restore due to crushing of concrete. So, it has concluded from this whole study that CFRP partial confinement techniques increase the axial capacity and lateral confinement but has less effect on the stiffness. Moreover, instead of wrapping the CFRP over the entire column, this partial confinement technique can be used as alternatives for restoring or upgrading the performance of concrete columns. Based on the experimental results, CFRP partial confinement on deteriorated parts of structural members can be done to save material, cost, and time-consumption.

REFERENCES

[1] C.G. Bailey, M. Yaqub "Seismic strengthening of shear critical post-heated circular concrete columns wrapped with FRP composite jackets" Composite Structures, Volume 94, Issue 3, 2012, Pages 851-864.

[2] Hua Wei, Zhimin Wu, Xia Guo, Fumin Yi, "Experimental study on partially deteriorated strength concrete columns confined with CFRP" Engineering Structures, Volume 31, Issue 10,2009, Pages 2495-2505.

[3] Material properties of Chemrite Grout NS, Chemdur-31 Epoxy, CFRP Wrap Hex-230 C and Chemdur 300. http://imporientgroup.com/portfolio-item/imporient-chemicals/

[4] M. Yaqub, C.G. Bailey "Repair of fire damaged circular reinforced concrete columns with FRP composites" Construction and Building Materials, Volume 25, Issue 1,2011, Pages 359-370.

[5] Yu Chen, Jun Wan, Kang He, "Experimental investigation on axial compressive strength of lateral impact damaged short steel columns repaired with CFRP sheets" Thin-Walled Structures, Volume 131, 2018, Pages 531-546.

A Review on Numerical Modelling of Dry-Stacked Masonry Wall against Blast Load

Imtiaz Ali[1], Ayesha Noreen[1], Zainab Akbar[1], Anass Khan[1], Azmat Ullah[2]

[1]BS students, Department of Civil Engineering,
University of Engineering & Technology Peshawar, Pakistan
[2]Ph.D scholar, Department of Civil Engineering,
University of Engineering & Technology Peshawar, Pakistan

imtiazanjum.pk@gmail.com; ayeshanoreen722@gmail.com; zain.mir195@gmail.com;
anasskhan143@gmail.com; Engr.azmat.mehsood@gmail.com

ABSTRACT

The increase in terrorist attacks during the last decades has led many researchers to pay special attention to evaluating the responses and failure mode of structures subjected to blast loads. In Pakistan, brick masonry is in common practice which fails badly under blast loading. Different research results have shown that Dry stacked masonry (DSM) gave sufficient resistance to the out-of-plane shear by using an interlocking mechanism. The response of DSM needs to be evaluated numerically as experimental research is costly. Understanding numerical modelling techniques and blast load analysis is needed for new researchers in this field. Hereby, this paper overviewed some basic terminologies, parameters of blast load, history of DSM, and different techniques for numerical modelling of blast and DSM as discussed by various researchers.
KEYWORDS: DSM, out of plan shear, interlocking mechanism, numerical modelling.

1   INTRODUCTION

The number of terrorist attacks has raised in the last decade. The death toll has risen sharply as a result of these strikes, which often have a global impact. Terrorism leads to financial losses due to structural damage, as well as loss of precious lives [1].

An explosion produces a wave of highly compressed air that spreads outwards from the point of explosion. Fire, sound, and high-pressure shock waves release energy in the form of heat. The gases created in the chemical reaction extend in the form of a high-velocity pressure wave. These high pressure shock waves transfer a pressure load to structural members upon collision with them. [2].

The structures in Pakistan are mostly constructed by using common masonry. Common masonry is a fast and economic way of construction, but it is very weak to withstand high lateral pressure. The mortar incorporated between two layers of masonry exposed the weakness of masonry which contributes to a predefined failure plane. DSM is another technique of masonry which is comprised of DSM units known as Hydraform, indicated in Figure 1. DSM (mortarless) uses an

1st International Conference on Advances in Civil & Environmental Engineering, University of Engineering & Technology Taxila, Pakistan

Conference date 22 &23 Feb 2022

interlocking mechanism as shown in Figure 2, and provides adequate resistance to the out-of-plane shear. The use of a Dry-Stacked system reduces the need for skilled labour, costly bonding material such as cement. Up to 27% of saving has been reported in DSM technique as compared to conventional masonry which includes savings in the cost of mortar, block unit, and construction time [3].

The history of DSM dates back to 15th Century from the ruins of Zimbabwe (the capital of Shona Kingdom at that time), whose construction has been said to be started in 400 AD. Currently, the contributing companies in the development and marketing of Dry-stacked construction include Azar and Spurlock of Canada, Haener of USA, and Hydraform of South Africa [4].

Figure 1): Hydraform block (DSM unit)

Figure 2): Confined DSM

2   BLAST WAVE PARAMETERS

Hopkinson-Cranz law classifies blast loading on basis of scaled distance (Z). Scaled distance, Z is defined by equation(1).

$$Z = \frac{R}{\sqrt[3]{W}} \qquad (1)$$

Where R(m) is the standoff distance of detonation point and W(Kg) is the equivalent weight of explosive charges [2].
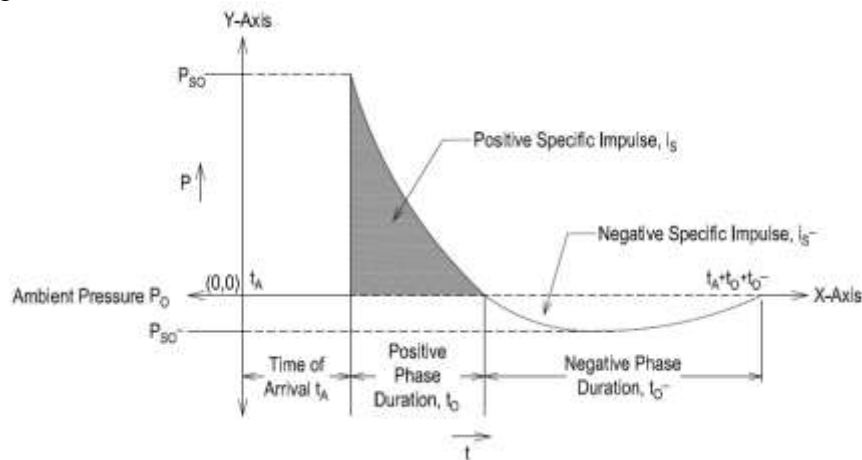
Figure 3:Incident and reflected pressure time histories[5]

1st International Conference on Advances in Civil & Environmental Engineering, University of Engineering & Technology Taxila, Pakistan

Conference date 22 &23 Feb 2022

Figure 3 is showing the typical incident and reflected pressure time histories of blast. Some of the parameters that can be used to characterise a blast wave are: Peak positive P_{so} and negative P_{so-} overpressures, positive I_s and negative I_{s-} impulses, time of arrival t_a, positive t_o and negative t_{o-} phase duration [6]. The Friedlander equation (eq.2) is used to approximate the decline of blast pressure values and blast wave pressure-time history.

$$P_s(t)=P_{so}(1-\frac{t}{t_o})exp(-b\frac{t}{t_o})\hspace{4cm}(2)$$

Where b is a decay coefficient of the waveform and t is the time elapsed, measured from the instant of blast arrival.

During explosion a blast wavefront is produced, where the air pressure rapidly increases to a value of pressure above the ambient atmospheric pressure (positive phase) indicated in Figure 3. The pressure may drop below the atmospheric pressure (negative phase), after a short duration of time from the explosion. The duration of the positive phase is shorter but the intensity is higher than the negative phase. Three key elements define the size of element load, i.e standoff distance, time of arrival, and the angle of incidence between the pressure wave and the element. When a blast wave hits a structure, the static overpressure and drag pressure both act at all sides of the structure. Thus the resultant pressure acting on a structure is a combination of static overpressure and dynamic pressure and is referred to as the peak reflected pressure (Pr). This reflected pressure can have a value up to ten times the peak overpressure in free air [2].

3   NUMERICAL MODELLING

3.1   Modelling Of Blast Load

The most common approaches used to model blast loads are the Compressed Balloon method, Mapping Algorithm, Pressure-Time function, and TNT equivalent. In the 1950s, Brode (1955) introduced the compressed balloon concept. The idea behind this technology is to use a compressed gas chamber (balloon). This produces a pressure-time function that fits exactly into the air-blast wave curve in numerical simulations or experiments. The Mapping Algorithm is a more general method that has been created to allow the calculation to be broken down into numerous steps. Bucket Surface and General Grid Interface are two well-known mapping methods (GGI). Commercial hydrocodes include mapping technologies in their programmes, such as AUTODYN and LS-DYNA. The pressure size can be determined using the Pressure-Time function approach based on the stand-off distance and the size of the explosive charge. The propagation of the blast wave in space may be calculated as a function of temporal pressure, which has two main phases: positive and negative. The modified Friedlander equation is used to describe the shape of this pressure-time curve. In the TNT equivalent method, pressure is estimated for the reduced distance of the targeted element from the point of explosion. [6].

3.2   Modelling of DSM

There are three most common methods of modelling. The first method is Detailed Micro Modelling in which plane stress elements are used to model units and mortar, and discrete

1st International Conference on Advances in Civil & Environmental Engineering, University of Engineering & Technology Taxila, Pakistan

Conference date 22 &23 Feb 2022

elements are used to describe the mortar contact between these two components. It takes into account the attributes of each structural component. Simplified Micro Modelling is the second method in which mortar joint qualities and interface behaviour are grouped into a discrete element with zero thickness, and the bricks are expanded in two directions with the joint thickness to maintain the model's dimensions. The third method of masonry modelling is the Macro modelling approach by using a cracking or plasticity material model, the properties of all components, including mortar, bricks, and the brick-mortar contact, are smeared out over a plane stress element [7].

Kapil Regmi et al. assessed a dry-stone masonry structure's seismic performance by modelling a conventional unreinforced dry-stone building in ANSYS workbench. The macro modelling approach of modelling masonry was utilized. Solid 65 element was used for modelling the masonry as this element is used in ANSYS for simulating brittle materials such as concrete, which can be crushed in compression and cracked under tension. This element consists of eight nodes, each node has three degrees of freedom that is translations in the nodal x, y, and z. The results suggested that DSM building is safe in all stresses under both gravity and earthquake loading but it is weak in tension and shear[7]. A micro modelling approach was used by Gelen et al. to run a 3D Finite Element Model. A masonry block was modelled to evaluate its mechanical properties and to predict the bearing capacity of the wall upon geometric imperfections. Masonry block was modelled using ANSYS 17 programme and a multi-linear elastic stress-strain relationship was utilized. ANSYS17's cubic element "SOLID65" was used for modelling and meshing the block. The results were compared with the experimental results and it suggested greater than 97% accuracy in predicting the failure modes and compressive strength [8].

M.Ishfaq et al. carried out a numerical study to assess the out-of-plane behaviour of confined DSM wall against blast load. In this study, ANSYS AUTODYNE hydrocode has been utilized for the non-linear numerical model of the wall. Dry stacked masonry wall, its footing and confining elements were defined using the hexahedral solid elements. The damage patterns and pressure time history obtained from numerical analysis were validated with experimental results which showed satisfactory agreement[9].

Macros et al. identified the behaviour of the dry-stacked masonry walls under out-of-plane loading which was validated with the experimental research [10]. Finite element models of dry-stacked masonry walls were developed in ANSYS v.15 to predict its behaviour in parallel with the experimental testing. K Lin et al. created a new infill masonry system by using dry-stacked interlocking brick, DIANA programme was used for its simulation. Bricks were modelled using an eight-node continuum planar stress element with Gauss integration, zero thickness (six nodes) line interface components were used to model joints between bricks. The friction exist between masonry units in a dry-stacked panel enclosed within a frame was discovered to contribute significantly (approximately 50%) to the assembly's in-plane strength [11].

1st International Conference on Advances in Civil & Environmental Engineering, University of Engineering & Technology Taxila, Pakistan

Conference date 22 &23 Feb 2022

4 CONCLUSION

The conclusions of this review paper are:
- Dry-stacked masonry can withstand high impact loadings such as blast load as compared to the common brick masonry.
- Different models can be assigned to model and simulate the blast as well as Dry stacked masonry, which shows significant and accurate results when compared to experimental results such as pressure during a blast, crack pattern and connection failure etc.
- Numerical analysis methods can be efficiently acquired to evaluate the response of DSM against blast loading under different standoff as well as charge weight.

5 REFERENCES

[1] P. A. Shirbhate and M. D. Goel, "A Critical Review of Blast Wave Parameters and Approaches for Blast Load Mitigation," *Arch Computat Methods Eng*, vol. 28, no. 3, pp. 1713–1730, May 2021, doi: 10.1007/s11831-020-09436-y.

[2] D. Kelliher and K. Sutton-Swaby, "Stochastic representation of blast load damage in a reinforced concrete building," *Structural Safety*, vol. 34, no. 1, pp. 407–417, Jan. 2012, doi: 10.1016/j.strusafe.2011.08.001.

[3] Azmatullah, 2020"Capacity Assessment of Confined Block Masonry Buildings Against Blast Loading.," UET, Peshawar.

[4] H C Uzoegbo1 and J V Ngowi, 2003, Structural Behaviour of Dry-stack Interlocking Block Walling Systems Subject to In-plane Loading," *Concrete Beton*, Volume 103, pp 9-13, May 2003.

[5] Eid Badshah, 2018" Performance Evaluation of Brick Masonry Building against Blast Loading" UET, Peshawar.

[6] European Commission. Joint Research Centre., *Analysis of blast parameters in the near-field for spherical free-air explosions.* LU: Publications Office, 2016. Accessed: Jan. 12, 2022. [Online]. Available: https://data.europa.eu/doi/10.2788/778898

[7] K. Regmi, "Seismic Performance of Dry Stone Masonry Building," p. 7.

[8] G. G. Chewe Ngapeya, D. Waldmann, and F. Scholzen, "Impact of the height imperfections of masonry blocks on the load bearing capacity of dry-stack masonry walls," *Construction and Building Materials*, vol. 165, pp. 898–913, Mar. 2018, doi: 10.1016/j.conbuildmat.2017.12.183.

[9] M. Ishfaq, Azmat Ullah,Awais Ahmed, Sarfraz Ali,Syed Muhmmad Ali,Marjan Uddin ,and Khan Shahzada , "Numerical Approximation of Blast Loads on Confined Dry-Stacked Masonry Wall," *Mathematical Problems in Engineering*, vol. 2021, pp. 1–13, Dec. 2021, doi: 10.1155/2021/2394931.

[10] M. Martínez and S. Atamturktur, "Experimental and numerical evaluation of reinforced dry-stacked concrete masonry walls," *Journal of Building Engineering*, vol. 22, pp. 181–191, Mar. 2019, doi: 10.1016/j.jobe.2018.12.007.

[11] K. Lin, Y. Z. Totoev, H. J. Liu, and A. W. Page, "Modeling of dry-stacked masonry panel confined by reinforced concrete frame," *Archives of Civil and Mechanical Engineering*, vol. 14, no. 3, pp. 497–509, May 2014, doi: 10.1016/j.acme.2013.12.006.

Modelling of Behaviour of Concrete Beam to Explore the Feasibility of Using Bamboo as Replacement of Steel Bars

Hasna Arshad, Sara Fatima Kazi, Hafiz Ahmed Waqas
Ghulam Ishaq Khan Institute of Engineering Sciences and Technology, Pakistan
u2018537@giki.edu.pk ; u2018536@giki.edu.pk; hafiz.waqas@giki.edu.pk

Muhammad Usman
University of Engineering and Technology, Lahore, Pakistan
m.usmaan@uet.edu.pk ;

ABSTRACT

The rapid advancement and development in the world, has escalated the demand for steel to be used as reinforcement bars in the construction industry. It will consequently add up to the wastes and gaseous emissions from steel production causing climatic change. On the other hand, bamboo being an abundantly available green material in Pakistan, is being encouraged to replace steel completely or partially as a standard reinforcement considering its sustainability, appropriate tensile strength, and cost-effectiveness. In this research, the concept of hybrid beams was introduced and a set of beams was modelled using ABAQUS to achieve comparable results in terms of the structural response. A total of 4 beams were created using conventional dimensions and material properties. All possible details were incorporated in the process of modelling, especially the bamboo knots were created to make it as realistic as possible.

The analysis revealed that all the beams would yield different results in terms of stress distribution and maximum displacements. It was concluded that bamboo can partially replace steel if used in combination with it. The stress distribution in the beam reinforced with bamboo and steel stirrups was found comparable to a typical concrete beam reinforced with steel only. Finally, recommendations of further investigation are suggested to gain in-depth interpretations of the phenomena.

KEYWORDS: Reinforcement, bamboo, green, hybrid

1 INTRODUCTION

Reinforced cement concrete (RCC) is the most common building material being used in developing countries, however only few of these are producing steel. While Pakistan might be one of those countries producing its own steel, it is the need of the era to invest in the sustainable options so as to avoid importing raw material in bulk to meet the increased demands of reinforcing steel by construction industry in the near future.

Bamboo being an eco-friendly and a locally available economic material, with a large tensile strength of up to 190 MPa [1], thus it can be considered a feasible option for the replacement of steel. Furthermore, it can also prove to be more sustainable as bamboo is an exceptionally green

1st International Conference on Advances in Civil & Environmental Engineering, University of Engineering & Technology Taxila, Pakistan

Conference date 22 &23 Feb 2022

material and leaves behind a less amount of carbon footprint. Hence, the use of bamboo as a replacement of reinforcing bars will be beneficial. This paper investigates the feasibility of adopting bamboo material as a concrete reinforcement in place of steel bars, and/or in combination with steel bars.

2 METHODOLOGY

To imitate the behaviour of the respective properties of concrete, steel, and bamboo, their mechanical and material properties were found from previous research as shown in Table 1.

Table 1 Mechanical Properties of a typical Bamboo

Properties	Value
Ultimate compressive strength	150 Mpa
Ultimate tensile strength	225 Mpa
Modulus of elasticity, E	1.72×10^4 Mpa
Poison ratio	0.15

Next, a set of following beam models was established to scrutinize the best out of them:
  i. Doubly reinforced beam with steel bars and stirrups as reinforcement
  ii. Doubly reinforced beam with bamboo bars only as main reinforcement
  iii. Doubly reinforced beam with bamboo as main reinforcement and stirrups
  iv. Doubly reinforced beam with bamboo bars as main reinforcement and steel stirrups

ABAQUS finite element modeling software was used as appropriate simulation tool to model the behaviour of these beams. The details of the modeling of different component is discussed in next sections.

2.1 Bamboo

For Bamboo standard sizes were used with outer diameter of 50 mm, for the knots the outer diameter was increased to 60 mm, while the inner was kept to a constant value of 40 mm [2]. The bamboo was created in Abaqus in parts of culm and nodal diaphragm, which were then assembled to form a bamboo of 4200 mm length with the total of 7 knots.

2.2 Concrete beam

The beam modelled in software was a 500x500 mm in cross-section and of 4300 mm length to ensure a clear cover of 50 mm on all sides when the bamboo is embedded inside the beam. The following properties were assigned to the concrete beam i.e. density = 2.3×10^{-6} Kg/mm^3, E = 33600 N/mm^2 and Poisson ratio = 0.15.

1st International Conference on Advances in Civil & Environmental Engineering, University of Engineering & Technology Taxila, Pakistan

Conference date 22 &23 Feb 2022

2.3   Steel

A typical steel bar of 13 mm diameter was used and given a Young's Modulus of 200 GPa and a Poisson ratio of 0.3. The density of the steel in the model was kept 7850 Kg/m^3.

2.4   Loads and Boundary Conditions

A total of 10 kN trial load was applied on the top surface area of the bamboo i.e., 2827 mm^2 as uniform pressure. A pressure value of 4 N/mm^2 was assigned at the top face of the simply supported beam.

2.5   Modelling the behaviour of Beams

The concrete beam was selected as host region and the bamboo bars, steel bars, bamboo stirrups and steel stirrups were considered as embedded region to create the bond between concrete, steel, and bamboo. 22 stirrups at 200 mm spacing with a standard diameter of 10mm were placed with 40 mm clear cover from all sides. These parts were meshed with Continuum, 3-Dimensional, 8 Node Elements with Reduced integration (C3D8R) and size of the mesh was kept as 30 mm for all components. Figure 1 show the meshed geometry of bamboo whereas Figure 2 presents the assembly of bamboo and stirrups. The general simulation framework is provided in Figure 3.
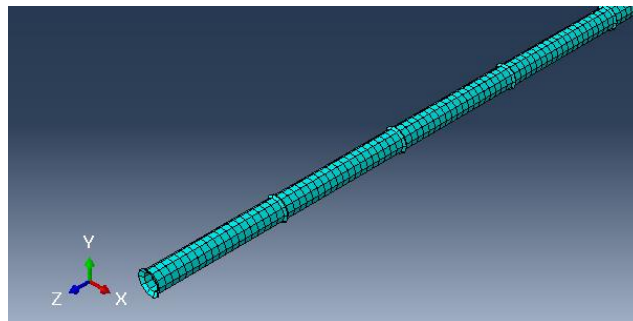
Figure 1 The meshed geometry of 4.2 m bamboo
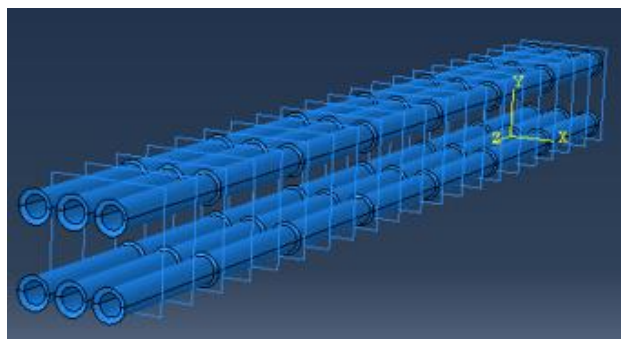
Figure 2 Bamboos and stirrups assembly

1st International Conference on Advances in Civil & Environmental Engineering, University of Engineering & Technology Taxila, Pakistan

Conference date 22 &23 Feb 2022
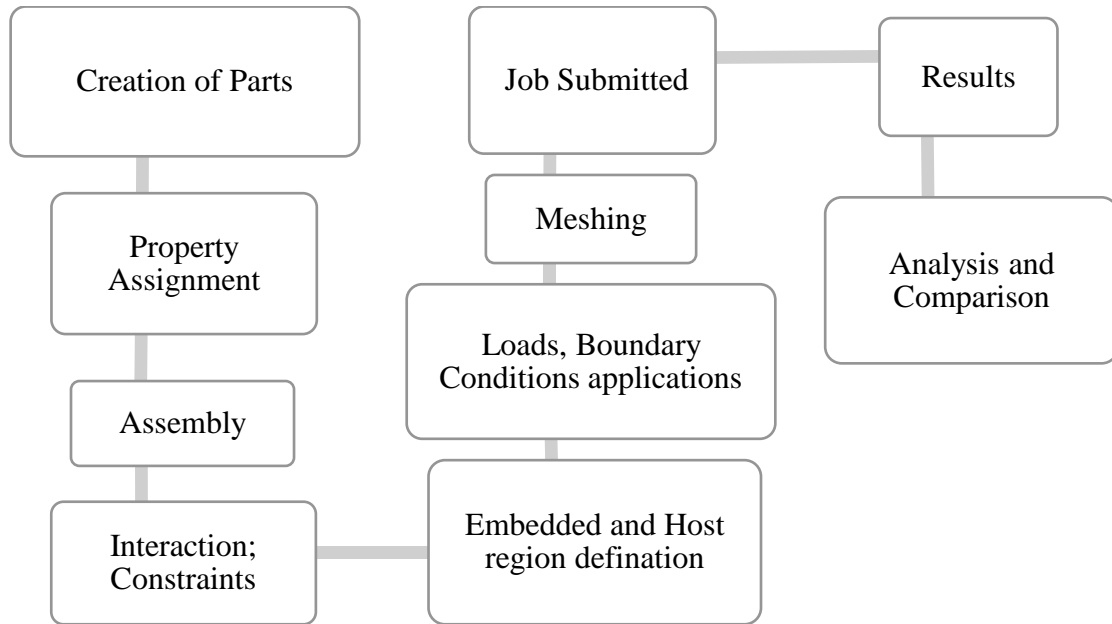
Figure 3 Flowchart representing the modeling framework adopted in ABAQUS

3   RESULTS

Following the analysis completion, the Von Mises stress (S) distribution was opted as a comparative indicator. The stress distribution for all the beams was noted to determine the extent and variation of stress in a given material. For the interest of readers, the stress distribution in bamboo reinforced beams with bamboo stirrups and steel stirrups are provided in Figure 4. The comparison of stress at the mid span location of the beam, for all the modelled cases, is summarized in Figure 5.
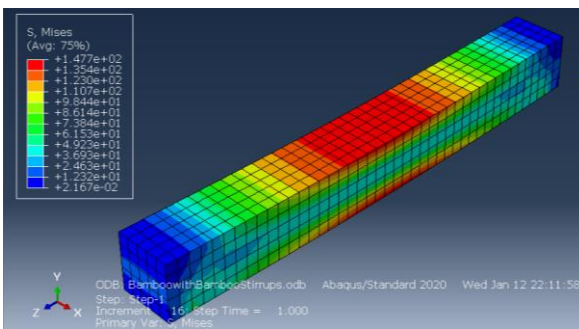
(a)
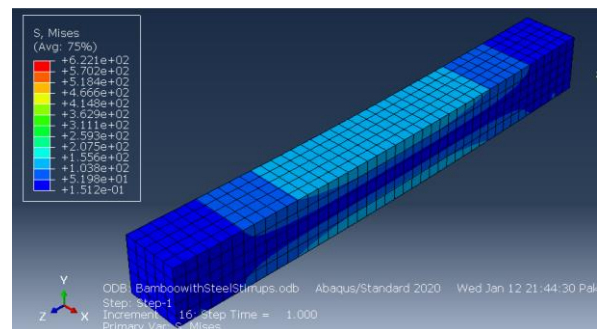
(b)

Figure 4 Stress distribution in Doubly reinforced beam (a) with bamboo bars and stirrups as reinforcement (b) with bamboo bars and steel stirrups as reinforcement

1st International Conference on Advances in Civil & Environmental Engineering, University of Engineering & Technology Taxila, Pakistan

Conference date 22 &23 Feb 2022
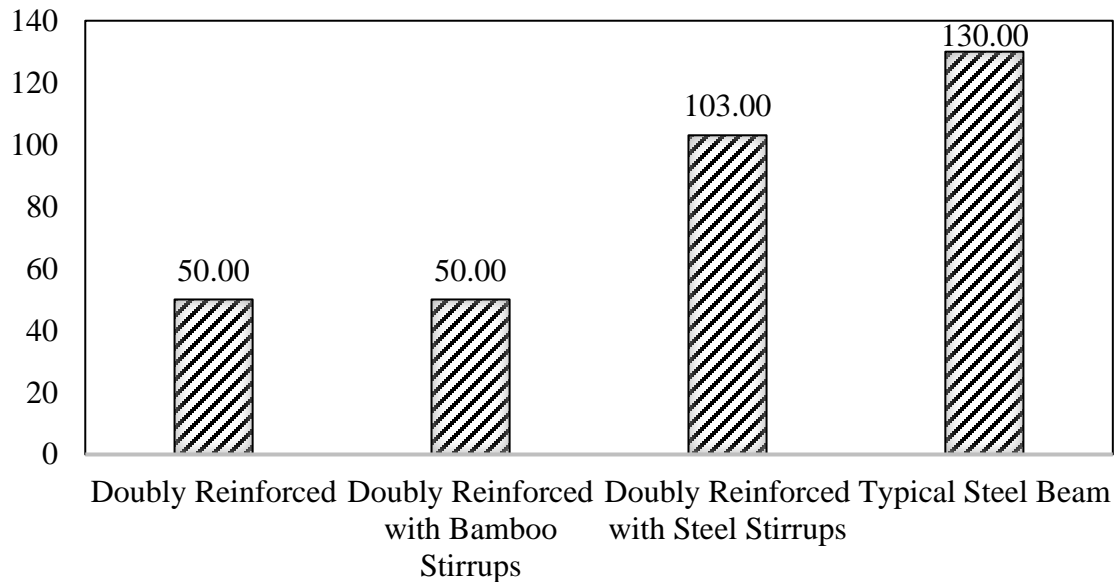
Figure 5 Comparison of Mises stress at the mid span location

4   CONCLUSION

From the comparative analysis it was revealed that bamboo alone might be insufficient to perform well in comparison to a standard steel reinforced beam, because of the difference in the overall strengths and low stiffness of bamboo. It could also be interpreted that the steel being a solid, when placed in the beam, can distribute loads well, but bamboo on the other hand, unlike steel, is a hollow material. Its hollowness along its entire length and uneven structure like knots at unequal distances can alter the stress distribution. The small bamboo wall thickness may also attribute insufficiency in resisting the loads. However, adding steel stirrups could significantly increase the stiffness and might make it comparable to the steel beam. It is also noted that the maximum displacement would not change for any of the beams since it depends on the moment of inertia of the beam which is kept constant. The aforementioned conclusions require further investigation to draw definite interpretations.

REFERENCES

1.   *Can Structural Bamboo Replace Steel in Construction Soon? SBC Magazine*. Retrieved February 5, 2022, from https://www.sbcmag.info/news/2020/jan/can-structural-bamboo-replace-steel-construction-soon

2.   Athauda A.M.B.B.S, Wijebandra M.M.A, *Feasibility of using Bamboo as a potential reinforcement in Concrete Beams*. 2010.

1st International Conference on Advances in Civil & Environmental Engineering, University of Engineering & Technology Taxila, Pakistan

Conference date 22 &23 Feb 2022

Flexural Capacity of Recycled Plastic Corrugated Sheet

Aaroon Joshua Das, Majid Ali
Department of Civil Engineering
Capital University of Science and Technology, Islamabad, Pakistan
ajodas@yahoo.com; professor.drmajid@gmail.com

ABSTRACT

The roofing sheets are usually rectangular that have different thicknesses and different geometries of corrugation. The thickness and corrugation impart strength and durability to the roofing sheet. The durability of the sheets comes from the material. The materials commercially available for the roof have a diverse set of thermal resistance, impermeability, corrosion resistance, noise conduction, and cost. Every material bears its pros and cons. Based on the use, galvanized steel sheets are renowned roofing material. The issue is that it is costly and vulnerable to rusting under certain climatic conditions. In consideration of this, environmentally friendly roofing materials shall provide a sustainable solution. Waste plastic, which produces landfill, marine, and other environmental damages, is a contender material that can be recycled for roofing and other construction items. In this study, sorted recycled waste plastic polypropylene was shredded in to small pieces for secondary recycling. A mould of 609 mm x 450 mm x 9.12 mm, was used to produce the waste plastic corrugated sheets from the extruded material. The testing for flexural strength, with the developed three-strip loads arrangement, was carried out on the sheet for comparison with the 28 gauge GI sheet. The GI sheet showed no resistance to load and deformed in a ductile pattern. The recycled waste plastic sheet, on the other hand, resisted the load significantly before deformation and showed ductility. Further studies are required to assess the properties of recycled waste plastic for the construction industry.

KEYWORDS: Corrugated sheet; Waste Plastic Recycling; Flexural Strength

1   INTRODUCTION

The corrugated sheets are intensely used for low-cost construction. In the 1820s, Henry Palmer developed the corrugated roof over the timber frame having footing of masonry [1]. The intention was to develop a less cost arrangement for construction. Over a period, due to the durability of the sheets preference for warehouses, parking, claddings were encouraged. In 1907, the Hatschek process was developed by Ludwig Hatschek to produce asbestos–cement-based roofs. The method is also called the wet process in literature. The method further developed the Magnani process to make sheets with corrugation. This method is semi-dry [2]. These methods were pioneers to develop the corrugated sheet. Studies further led to the production of the Portland cement-based corrugated sheets. These were brittle and damages occurred during shifting and stock piling[3].

1st International Conference on Advances in Civil & Environmental Engineering, University of Engineering & Technology Taxila, Pakistan

Conference date 22 &23 Feb 2022

The problem, which was recorded in literature, was that the cement-based had porosity issues. Many other materials exist for the corrugated sheet which has been developed over the years each has its own set of issues already available in the literature[4].

Around the globe, many concerns have risen on the alarming waste plastic. The unmanageability is being addressed by many countries by developing recycled packaging, reusing the original plastic, and putting it to incineration but still, a large quantum is going to waste. In recent studies, it has been substantiated that Polyethylene has the highest quantity of municipal solid waste because of its use. The second to place in the waste is polypropylene with 19%. These values are from different statistical studies done to assess the quantum of waste [5]. A concern was presented in the literature that with this rate of waste generation in 2050 alarming percentage of the landfill site and marine areas will be polluted. Already in 2015, 79% of the plastic is unmanaged polluting the land, air, and marine [6]. The construction industry has a low percentage of this waste plastic and being a huge industry it can provide a sustainable solution to utilize waste plastic in producing different products for construction [7]. Other attempts have been made to utilize waste plastic in construction, but that is limited to aggregate replacement[8].

This study focuses on the use of recycled waste plastic as a sustainable material for the construction industry. Plastic waste contains a high quantum of Polypropylene in plastic waste. The plastic waste can be synthesized to form mouldable shapes through the extrusion process. A setup has been established to recycle waste plastic with a mechanical extruder and a press-able mould has been prepared to develop corrugated sheets of sizes 609 mm x 450 mm x 9.12 mm. A comparison of flexural capacity was done with a steel sheet to determine the behaviour of the corrugated sheet. This study presents the prospective use of recycled waste plastic as a corrugated sheet. Further studies are required to assess other shapes, geometries, and structural properties of recycled waste plastic products.

2   EXPERIMENTAL PROCEDURE

2.1   Materials

2.1.1   Development of Recycled Waste Plastic Corrugated Sheet (RWPCS)

The raw waste plastic was collected from sources of automotive waste. The waste plastic was sorted for polypropylene. Usually, this material is used to produce bumpers for vehicles [9]. The raw material contains impurities, which are washed after shredding and before extrusion. A similar extrusion process was previously used for the development of recycled plastic rebars [7]. The material after extrusion is hot and is in semi-liquid form. To handle the material, a press arrangement made up of steel was prepared having a cycloidal shape [10]. The size of the specimen was kept at 609 mm x 450 mm x 9.12 mm considering the limitation of the testing facility.

2.1.2   Commercial steel corrugated sheet

The commercially available galvanized steel corrugated sheet was used having 28-gauge thickness and cut size equivalent to 609 mm x 450 mm. These are used for warehouses, stores, and parking have very low strength and structural properties.

1st International Conference on Advances in Civil & Environmental Engineering, University of Engineering & Technology Taxila, Pakistan

Conference date 22 &23 Feb 2022

2.2 Testing Procedure

The standard D790 exists for obtaining the flexural strength of the plastic and insulation material [11]. This standard limits the testing to a smaller specimen. The three-point flexural test has been used to evaluate the flexural strength of the metal roofing material [10]. The test setup was modified to obtain flexural behaviour of the recycled waste plastic corrugated sheet as shown in Figure 1. The supports were at 450 mm apart and the central load at mid-point. As a reference, the 28 gauge (about 0.4 mm) steel sheet was also tested. After the testing, the results were compiled.

| (a) | (b) |
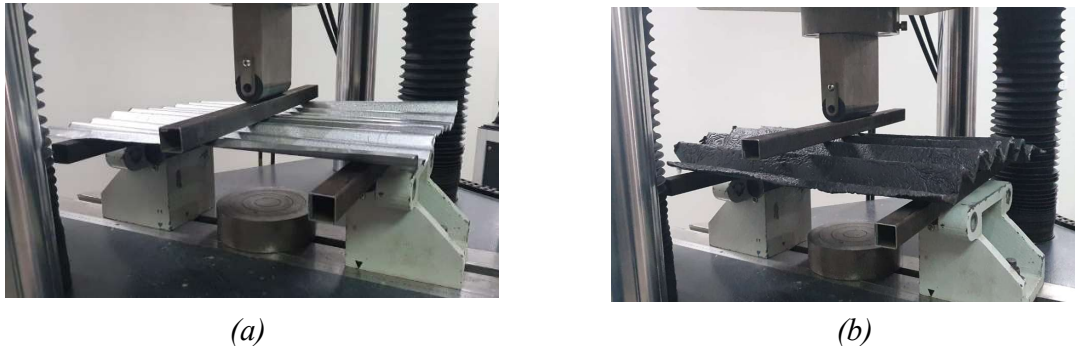
Figure 1: Three point flexural test setup (a) steel corrugated sheet (CS) (b) Recycled waste plastic corrugated sheet (RWP CS)

3 RESULTS AND ANALYSIS

Usually, the steel sheets are supported on a frame or truss, it was expected for the steel sheet to show a better behaviour under load, but actually, the steel sheet was thin and did not provide substantial resistance to load. Even with the minimum values of the load application, the setup was able to record low values. The behaviour was ductile and the steel sheet continued to deform under load with low values. The recycled waste plastic sheet comparatively showed the ability to bear the considerable loading. The load-to-deflection behaviour of the recycled waste plastic sheets is shown in Figure 2 c. The final deflected shapes of the corrugated sheets are shown in Figure 2 (a) and (b). Table 1 shows the details of the sheet and the obtained results of the testing.

Table 1 Flexural stress and corresponding deflection at mid-point for the test sample

Sheet	Thickness (mm) t	Weight (Kg)	Maximum Flexural Load (kN) L	Max Deflection Δ (mm)	Max stress (MPa) σ
Steel CS	0.4	0.66	0.5	75	1.2
RWP CS	9.12	2.65	3.64	16	5.75

1st International Conference on Advances in Civil & Environmental Engineering, University of Engineering & Technology Taxila, Pakistan

Conference date 22 &23 Feb 2022

(a)

(b)

(c)
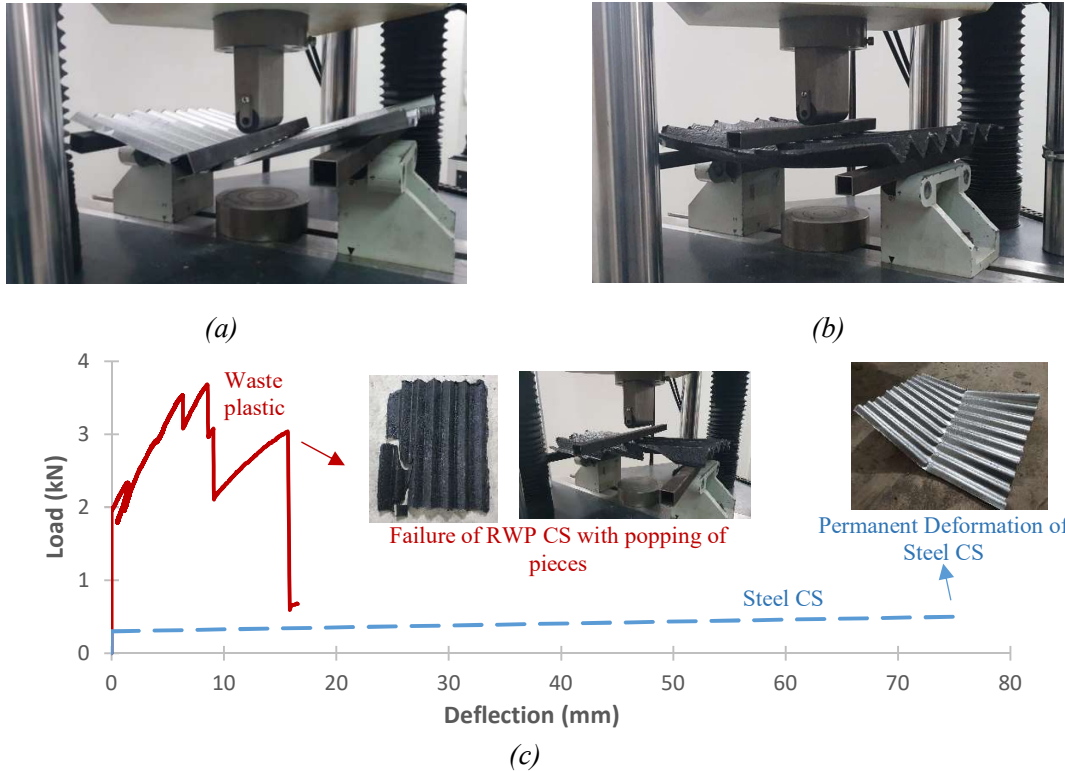
Figure 2: At peak load (a) steel CS (b) RWP CS (c) Load – Deflection behavior of recycled plastic corrugated sheet and failure profile

4   FLEXURAL CAPACITY OF RECYCLED PLASTIC CORRUGATED SHEET

The study showed that the recycled waste plastic corrugated sheet has performed under flexural loading. The behaviour was elastic initially and the sheet resisted a substantial load. The failure was brittle with cracking and popping up of pieces. With a deflection of about 16 mm at a peak load of 3.648 kN. The graph of Figure 2 (c) is jerky because on the application of load the corrugations aligned themselves under the strip and over the supports. The contact was significant in the dispersion of the load. The rise in the values has three peaks. The first is at the start at 2 kN with a marginal deflection of 1 – 3 mm the position where the strip settled on the corrugation. The second jerky peak at 3 – 3.5 kN where the sheet took maximum load and showed elastic behaviour with deformation of about 5 - 10 mm. The last part of the peak shows a clear elastic behaviour. At the final stage, the sheet cracked and the popping of the broken pieces was observed which was brittle. The crack pattern was at the midpoint and the broken piece was near the edge support Figure 2 (c). The steel CS showed permanent deformation with a deflection of 75 mm at the end.

5   CONCLUSION

Recycled waste plastic has its own set of material properties for corrugated sheets. Virgin plastic sheets are available in the market which has shown good aesthetics and durability properties but

1st International Conference on Advances in Civil & Environmental Engineering, University of Engineering & Technology Taxila, Pakistan

Conference date 22 &23 Feb 2022

are expensive [4]. Waste plastic recycling is required for reducing environmental and other concerns. Following conclusions can be drawn from the study:

i. The corrugated sheets developed from recycled waste plastic can bear the flexural load. The polypropylene waste recycled in this study showed efficient results to the low-cost steel variant.

ii. The behaviour of the corrugated sheet was elastic in initial loading, and the plastic deformation was less at the time of failure showing brittle behaviour.

The other mechanical properties of the waste plastic corrugated sheet need to be assessed in future studies. The behaviour of long-termed temperature also needs to be assessed. To improve the brittle behaviour of other waste plastics and use of additives needs to be considered in future studies.

6   ACKNOWLEDGEMENTS

REFERENCES

1. N. Thomson and P. Banfill, *Corrugated-Iron Buildings: An Endangered Resource within the Built Heritage*, *J. Archit. Conserv.*, vol. 11, no. 1, pp. **71**–**87**, 2005, doi: 10.1080/13556207.2005.10784936.
2. S. Delvasto, E. F. Toro, F. Perdomo, and R. M. de Gutiérrez, *An appropriate vacuum technology for manufacture of corrugated fique fiber reinforced cementitious sheets*, *Constr. Build. Mater.*, vol. 24, no. 2, pp. **187**–**192**, 2010, doi: 10.1016/j.conbuildmat.2009.01.010.
3. M. D. de Mello Innocentini, M. A. Vieira de Faria, M. Rosseto Crespi, and V. H. Batista Andrade, *Air permeability assessment of corrugated fiber-cement roofing sheets*, *Cem. Concr. Compos.*, vol. 97, no. October 2018, pp. **259**–**267**, 2019, doi: 10.1016/j.cemconcomp.2019.01.004.
4. A. J. Das and M. Ali, *An Overview on Different Corrugated Sheets from Manufacturing to Housing Element*, pp. **1**–**6**, 2021.
5. A. J. Das and M. Ali, *Recycling of waste plastic with least effect to environment : A review*, pp. **1**–**4**, 2021.
6. R. Geyer, J. R. Jambeck, and K. L. Law, *Production, use, and fate of all plastics ever made*, *Sci. Adv.*, vol. 3, no. 7, pp. **25**–**29**, 2017, doi: 10.1126/sciadv.1700782.
7. A. J. Das and M. Ali, *Energy absorption capabilities of recycled-plastic reinforcing bars for earthquake resistant housing construction*, in *Australian Earthquake Engineering Society, Virtual Conference 2021*, 2021, pp. **197**–**205**.
8. D. Li and S. Kaewunruen, *Mechanical properties of concrete with recycled composite and plastic aggregates*, *Int. J. GEOMATE*, vol. 17, no. 60, pp. **231**–**238**, 2019, doi: 10.21660/2019.60.8114.
9. M. P. Luda, V. Brunella, and D. Guaratto, *Characterisation of Used PP-Based Car Bumpers and Their Recycling Properties*, *ISRN Mater. Sci.*, vol. 2013, pp. **1**–**12**, 2013, doi: 10.1155/2013/531093.
10. H. L. Wakeland, *Flexural properties of corrugated metal roofing*, 1954.
11. ASTM INTERNATIONAL, *Standard Test Methods for Flexural Properties of Unreinforced and Reinforced Plastics and Electrical Insulating Materials. D790, Annu. B. ASTM Stand.*, pp. **1**–**12**, 2002, doi: 10.1520/D0790-10.

Use of Bio-Oil from Rice Straw to Improve the Rehological Performance of Asphalt Binder

Aziz ur Rahman[1], Syed Bilal Ahmed Zaidi[2]

[1] MSc. Scholar, Department of Civil Engineering, University of Engineering and Technology Taxila, Pakistan
engr.aziz007@gmail.com

[2] Associate Professor, Civil Engineering Department, University of Engineering and Technology Taxila, Pakistan
bilal.zaidi@uettaxila.edu.pk

ABSTRACT

The disposal of waste from industries and the agriculture sector is a major environmental concern across the globe. Recycling waste and reusing it in other sectors is an environmentally sustainable waste disposal method. In this paper, the agricultural waste from rice straw has been used after conversion to bio-oil employing a fast pyrolysis process. The bio-oil from the agriculture waste has been found beneficial if used as a partial replacement to conventional asphalt binder. Effective use of bio-oil from rice straw can help to reduce environmental problems due to agriculture waste and also decrease the use of petroleum asphalt binder. The bio-oil from the rice straw has been substituted 5% and 10% by weight into the conventional petroleum asphalt binder. The conventional and the rheological tests were performed to check the improvement in the properties of modified binder. Test results reveal that the Bio-oil produced from rice straw can be utilised to improve the low-temperature rheological properties of traditional petroleum asphalt binders. A comprehensive study considering other parameters has been recommended to get a deeper understating and practical field application.

KEYWORDS: Bio-oil, Rice straw, Agriculture waste, Asphalt binder, Fast pyrolysis

1   INTRODUCTION

Hot Mix Asphalt (HMA) is used globally for the roads network in a huge amount. The main constituent of the HMA is Aggregate particles and bonding material which is the by-products of the crude oil which is known as a conventional asphalt binder. With the rapid depletion, lack of availability and high demand of crude oil resources the asphalt binder industry is facing severe challenges in the form of a hike in the prices of conventional binder and its shorter supply. As a result, the cost of pavement construction and its maintenance is also increased. Therefore, there is a need to improve the performance of the conventional binder and to find its replacement.[1-3] The globe is now taking steps to establish a bio-based economy that relies on the renewable organic matter rather than natural fossil fuels as a source of energy. Bio-based energy is sustainable, efficient, cost-effective, and environmentally friendly, making it a valuable economic resource for any country. Generally, Organic waste, residues, and plant materials, such

1st International Conference on Advances in Civil & Environmental Engineering, University of Engineering & Technology Taxila, Pakistan

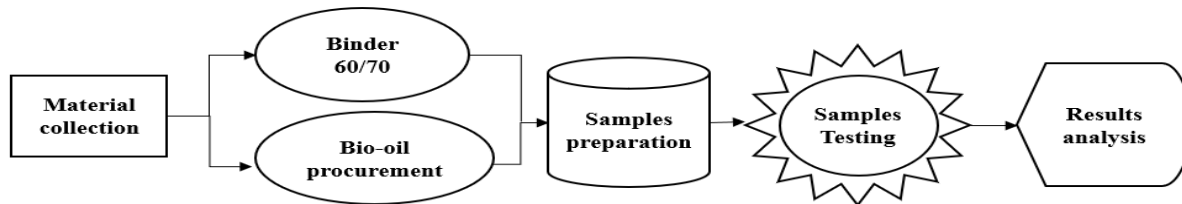*Conference date 22 &23 Feb 2022*

as agricultural and municipal waste, are used to make these. As a result, a new binding material generated from a more sustainable source is needed to replace the current fossil fuel-based traditional binder entirely or partially.[4, 5] Biomass is one of the abundant materials that include waste from animals, crops, forests, agriculture-based activities and so on. The materials from biomass are generally available in several forms like bio-oil, bio-ash and bio-char etc.[6] The bio-oil is the abundantly-available material, which is also regarded as an environmental friendly product[7, 8] The bio-oil from sugar cane bagasse (SCB) can produce a softer binder with better ductility properties. 10% SCB bio-oil content maximised the fatigue resistance of asphalt binder and mixture when compared with 0% and 5% content of SCB bio-oil.[9] The addition of a different percentage of wood oil of 5%, 10% and 15% increased penetration values with an increment of bio-oil while decreasing the softening point. From the chemical and rheological analysis, Bio binder may have the same or high ageing resistance, deformation and fatigue resistance as related to conventional binder with the same penetration values.[10] R. Zhang et al. concluded that some bio oil have low resistance to high temperature performance.[11]

The Pakistan agriculture sector is one of the best sectors which contribute 18.9% to the total GDP of the country and almost 42.3% labour employed here.[12]Pakistan agriculture sector produces Approximately 43437 thousand tonnes of Rice straw. The primary components of rice straw are cellulose, hemicellulose, and lignin.[13] Pakistan has difficulty with agricultural waste disposal, which can lead to environmental and health problems like the open burning of rice straw. Rice straw is one of the most significant farm leftovers in the country that is currently underutilised.[14]. S.-H. Jung et al. obtained the bio-oil from the rice straw by fast pyrolysis with optimum temperature ranges from 440-500℃ which produce the optimum yield of the bio-oil about 68 wt% with a fluidized bed reactor.[15] .

In this paper, the bio-oil was produced through fast pyrolysis process from rice straw waste. This bio-oil of rice straw (BORS) is replaced partially with traditional asphalt binder to reduce the use of petroleum asphalt binder and improved its properties. The Conventional and rheological tests were executed to analyse the outcome of BORS on conventional asphalt binder. The approach of this research is to recycle material of agriculture waste which is an environmentally friendly technique.

2   MATERIALS AND METHODS

The rice straw used in this study was taken from Khyber Pakhtunkhwa (KP) province of Pakistan and the bio-oil was extracted by fast pyrolysis method. The feedstock of the rice straw was sun-dried which have a moisture content of less than 10% and grind it with a mechanical grinder up to 10-20mm in size. Further, the feedstock of rice straw is put into the reactor at 200g per batch in which The bio-oil is made by heating rice straw and converting the vapours produced into a liquid state through the condensation process.

1st International Conference on Advances in Civil & Environmental Engineering, University of Engineering & Technology Taxila, Pakistan

Conference date 22 &23 Feb 2022

Fig. 1 Flow chart of the proposed methodology

The BORS was used to replace the traditional bitumen binder of 60/70 pen grade with 5% and 10% BORS by weight. First, the neat bitumen was heated to 120°C after that different dosage is prepared with 5% BORS and 10% BORS, for the uniform mixing of BORS in the conventional asphalt binder we used the automatic shear mixer machine at the speed of 1500 revolution per minute (RPM) for the 30 minutes and the temperature was maintained with help of hot plate at 120°C. Convention tests along with rheological testing was carriedout to study the rheological behaviour of the modified asphalt binder.

3   RESULTS AND DISCUSSION

3.1   CONVENTIONAL TEST

The conventional tests shown in Fig. 2 of penetration grade and softening point were performed on the neat and modified asphalt binder. In the modified asphalt binder, the BORS was added to the neat bitumen binder with 5% and 10% by weight. The results shown in Fig.1 the penetration of the needle increased by the addition of BORS. With the addition of 5% BORS, the penetration increased by 4.9% and the 10% BORS increased the penetration by 18%. The increase of the penetration shows the binder becomes softer the fluency increases and decrease the stiffness. On the other hand, the softening point of the neat bitumen decreases with the addition of the BORS. The addition of 5% and 10% BORS decrease the softening point by 2% and 3.9% respectively. The softening point of the bitumen shows the resistance to deformation of the binder at elevated temperatures.

1st International Conference on Advances in Civil & Environmental Engineering, University of Engineering & Technology Taxila, Pakistan

Conference date 22 &23 Feb 2022
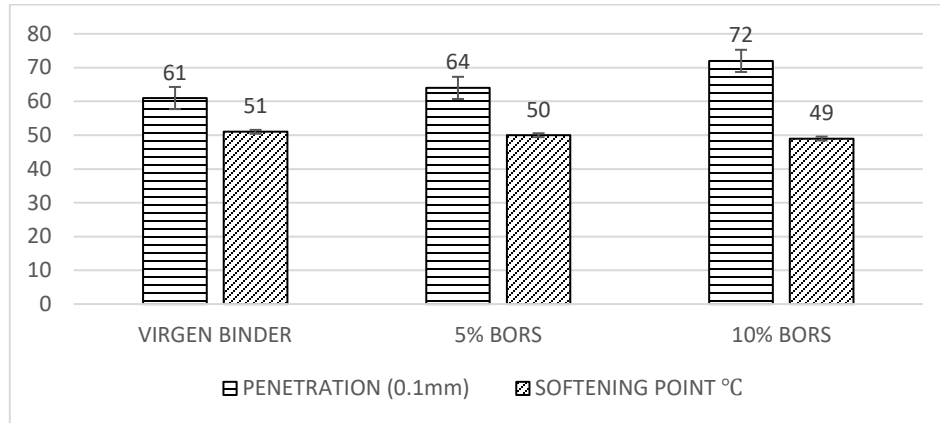
Fig. 2 the graphical representation of the conventional tests

3.2 Frequency Sweep test

The frequency sweep test was used to investigate the impact of time and temperature on all of the bitumen samples. The test was performed at a range of temperatures and frequencies. The test temperatures were 22, 34, 46, 58, 70, and 82 degrees Celsius. The range of frequencies was 1 to 10 hertz. The analysis was done through the sigmoidal function at a reference temperature of 58°C in the form of master curves.

$$\log|A| = \sigma + \frac{\alpha}{1+e^{\beta-\gamma\log(f_r)}} \tag{1}$$

Equation 1 shows the sigmoidal function where A denotes the complex modulus, δ denotes the reduced frequency at a reference temperature, α denotes the difference between the minimum and maximum complex modulus of asphalt binder, and β, γ indicate the curve shape parameters [16]. At a reference temperature of 58 ° C, the master curve in Fig. 3 was produced using a sigmoidal function. from the master curve between the complex modulus and reduced frequency, we concluded that the addition of BORS with control binder reduces the stiffness at high frequency and have no significant effect occur in the stiffness at low frequency.

1st International Conference on Advances in Civil & Environmental Engineering, University of Engineering & Technology Taxila, Pakistan

Conference date 22 &23 Feb 2022
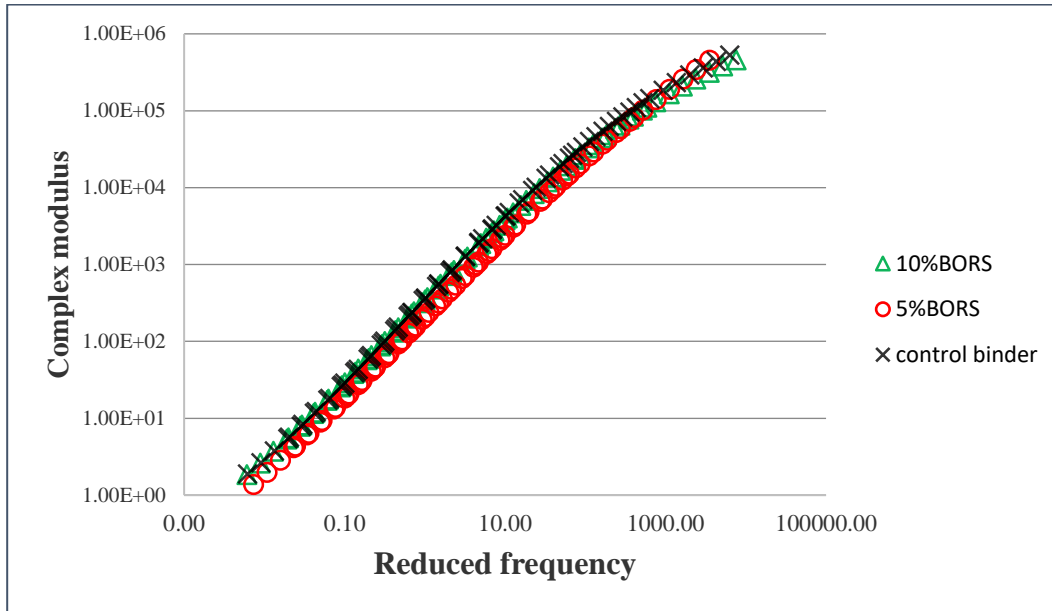
Fig. 3 Master curve of reduced frequency vs complex modulus

Rutting is a type of pavement depression caused by severe traffic loads in the wheel path at high temperatures. This is a significant problem with asphalt surfaces which can affect the roadway. From The master curve of G*/Sinδ agonist the reduced frequency at reference temperature 58°C shown in Fig. 4 shows the rut factor in the form of G*/Sinδ indicates high-temperature binder failure. in Fig. 4 shows the addition of BORS with control binder decrease rut factor in the high-frequency range i.e. the low-temperature range. This shows that BORS modified binder would give good anti-cracking efficiency when compared to control binder.

Fig. 4 G/Sin (δ) vs Red. Frequency*

1st International Conference on Advances in Civil & Environmental Engineering, University of Engineering & Technology Taxila, Pakistan

Conference date 22 &23 Feb 2022
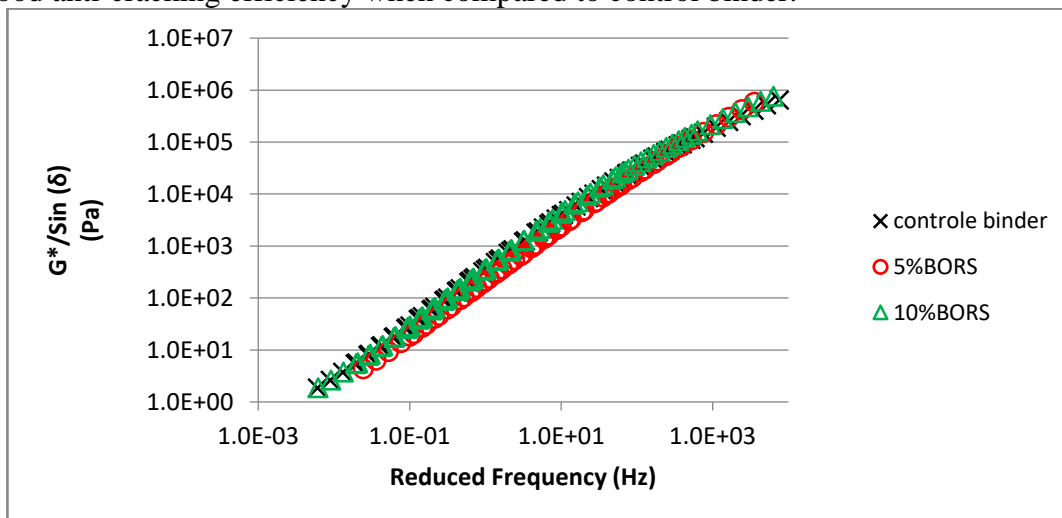
The failure occurs in the pavement due to cyclic loading, which is fatigue. In Fig. 5 The graph is drawn between fatigue factor G*Sin (δ) verses reduced frequency at a reference temperature of 58°C, the master curve of the fatigue factor shows the addition of the BORS with control binder has no significant effect at the low-frequency level and the fatigue performance have slightly improved at a high level which demonstrates the fatigue performance improved at the low-temperature level.
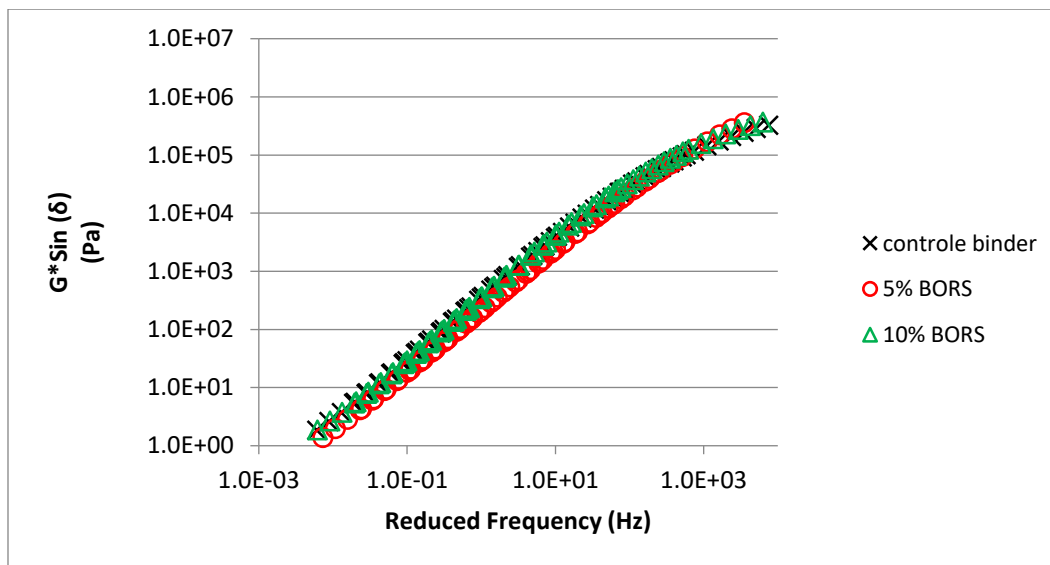
Fig. 5 Master curve of fatigue factor vs reduce frequency

CONCLUSION

- Conventional test results show that 5% and 10% BORS modified asphalt binder, increased the penetration and hence decreased softeness. These results makes the modified binder more suitable for low temperature zones of the region.
- From the frequency sweep test, it is revealed that the addition of BORS reduces the stiffness at low and high temperatures. The modified asphalt binder has no significant effect on rut depth at a low frequency however a decreasing trend in rut factor was observed at high-frequency i.e. in the low-temperature range. This shows that BORS modified binder would give good anti-cracking efficiency when compared to control binder. Furthermore, the fatigue performance of BORS modified binder has been founed improved at the low-temperature level.
- From the tests result it is concluded that the modified sample of 10% BORS have good resistance to rutting and fatigue in the low temperature as compared to 5% BORS and base binder.

1st International Conference on Advances in Civil & Environmental Engineering, University of Engineering & Technology Taxila, Pakistan

Conference date 22 &23 Feb 2022

- Finally, it is concluded that the modified asphalt of BORS has better performance at low temperatures hence it can be used in the low-temperature region.

4   ACKNOWLEDGEMENTS

I would like to thanks to the Civil Engineering Department, UET Taxila for their continue support and guidance.

REFERENCES

1.   Bostancioğlu, M., Ş.J.R.M. Oruç, and P. Design, *Effect of furfural-derived thermoset furan resin on the high-temperature performance of bitumen.* 2015. **16**(1): p. 227-237.
2.   Pereira, P., J.J.J.o.t. Pais, and t. engineering, *Main flexible pavement and mix design methods in Europe and challenges for the development of an European method.* 2017. **4**(4): p. 316-346.
3.   Cavaca, L.A. and C.A.J.E.J.o.O.C. Afonso, *Oleuropein: A Valuable Bio-Renewable Synthetic Building Block.* 2018. **2018**(5): p. 581-589.
4.   Al-Akhras, N.M., B.A.J.C. Abu-Alfoul, and C. Research, *Effect of wheat straw ash on mechanical properties of autoclaved mortar.* 2002. **32**(6): p. 859-863.
5.   Pan, X. and Y.J.B.T. Sano, *Fractionation of wheat straw by atmospheric acetic acid process.* 2005. **96**(11): p. 1256-1263.
6.   Zhang, X., et al., *Preparation of bio-oil and its application in asphalt modification and rejuvenation: A review of the properties, practical application and life cycle assessment.* 2020. **262**: p. 120528.
7.   Ji-Lu, Z.J.J.o.A. and A. Pyrolysis, *Bio-oil from fast pyrolysis of rice husk: Yields and related properties and improvement of the pyrolysis system.* 2007. **80**(1): p. 30-35.
8.   Seidel, J.C., *Rheological properties, moisture susceptibility and chemical functioning of soybean oil-based modified asphalt binders.* 2012, Purdue University.
9.   Ahmad, M.F., et al., *Assessment of sugar cane bagasse bio-oil as an environmental friendly alternative for pavement engineering applications.* 2021: p. 1-12.
10.   Ingrassia, L.P., et al., *Chemical and rheological investigation on the short-and long-term aging properties of bio-binders for road pavements.* 2019. **217**: p. 518-529.
11.   Zhang, R., et al., *The impact of bio-oil as rejuvenator for aged asphalt binder.* 2019. **196**: p. 134-143.
12.   Pakistan, F.D.G.o. *Pakistan Economic Survey 2017-2018*. Finance Division Government of Pakistan 2018; Available from: http://www.finance.gov.pk/survey/chapters_18/Economic_Survey_2017_18.pdf.
13.   Yasina, M., et al., *Efficient utilization of rice-wheat straw to produce value–added composite products.* 2010. **1**(2): p. 13-143.

1st International Conference on Advances in Civil & Environmental Engineering, University of Engineering & Technology Taxila, Pakistan

Conference date 22 &23 Feb 2022

14. Mahmood, A., S.H.J.J.o.S.E. Gheewala, and Environment, *A comparative assessment of rice straw management alternatives in Pakistan in a life cycle perspective.* 2020. **11**: p. 21-29.

15. Jung, S.-H., et al., *Production of bio-oil from rice straw and bamboo sawdust under various reaction conditions in a fast pyrolysis plant equipped with a fluidized bed and a char separation system.* 2008. **82**(2): p. 240-247.

16. Gao, J., et al., *Rheological behavior and sensitivity of wood-derived bio-oil modified asphalt binders.* 2018. **8**(6): p. 919.

1st International Conference on Advances in Civil & Environmental Engineering, University of Engineering & Technology Taxila, Pakistan

Conference date 22 &23 Feb 2022

Investigation of Self-Healing Concrete with Steel Slag Aggregates

Bilal Ahmad

Department of Civil Engineering, University of Engineering and Technology Taxila, 47050, Pakistan.

Faisal Shabbir

Department of Civil Engineering, University of Engineering and Technology Taxila, 47050, Pakistan.
E-mail: faisal.shabbir@uettaxila.edu.pk

ABSTRACT

In the present investigation, carbonated steel slag aggregates (SSA) are utilized to assess the concrete autogenous healing process by restraining the Bacillus subtilis bacteria. The regain of strength and the crack healing width after pre-cracking of the samples are assessed at different testing ages to examine the crack healing efficacy. The results showed that SSA is an efficient carrier media for bacterial growth portraying the crack healing widths of 0.56 mm. The direct incorporation of bacteria depicted the enhancement of 63% in the compressive strength.

KEYWORDS: Steel slag aggregates, Self-healing, Bacillus subtilis, Autogenous healing, Bio-mineralization

1   INTRODUCTION

Numerous research efforts have been done in the use of self-healing concrete in the previous decade. Though the bacteria and micro-capsules are deliberated as favourable self-healing specialists to enhance the durability of concrete, the significant expense of bacteria and micro-capsules are still huge challenges that limit the broad utilization of this innovation. Therefore, it is important to foster environmentally friendly and cost-effective materials such as self-healing in concrete. When aggressive chemicals infiltrate a reinforced concrete structure, they cause corrosion of the steel bars, reducing the axial strength capability of the system and decreasing its durability [1-3]. Steel slag is a result of the steel manufacturing system representing around 15 to 20% of the unrefined steel refining process. As per various kinds of steel refining processes, steel slag can be separated into various classes including open-hearth-furnace slag, electro-arc-furnace slag, and basic-oxygen-furnace slag where basic-oxygen-furnace slag represents the most available type [4]. To accelerate crack healing, healing agents such as polymers, admixtures, or bacteria are incorporated into concrete during the mixing process [5, 6].

The present investigation is dedicated to exploring the self-healing impacts of steel slag utilized as aggregates in an effort to produce steel slag aggregates (SSA) sustainable concrete. The main objective of the present study is to assess the concrete mechanical performance and autogenous healing process by restraining the bacteria via steel slag and fine aggregates. The regain of strength and the crack healing width after pre-cracking of the samples are assessed at different testing ages to examine the crack healing efficacy.

1st International Conference on Advances in Civil & Environmental Engineering, University of Engineering & Technology Taxila, Pakistan

Conference date 22 &23 Feb 2022

2   EXPERIMENTAL PROGRAM

2.1. Materials

Ordinary Portland cement (OPC) with a specific gravity of 3.15 was utilized, and its chemical properties met with ASTM C150 [7], chemical composition presented in Table 1 (Ref. [8]). The steel slag was taken from Pakistan Steel Mills Karachi with particles having angular form, sharp edges, and a permeable surface, as shown in Figure 1(a). Figure 1(b) shows the sieve analysis of the steel slag. The different mechanical property tests of steel slag are detailed in Table 1 as compared to natural aggregate take from Ref. [8]. XRF chemical analysis was utilized to identify the chemical composition of cement and steel slag, as shown in Table 2.
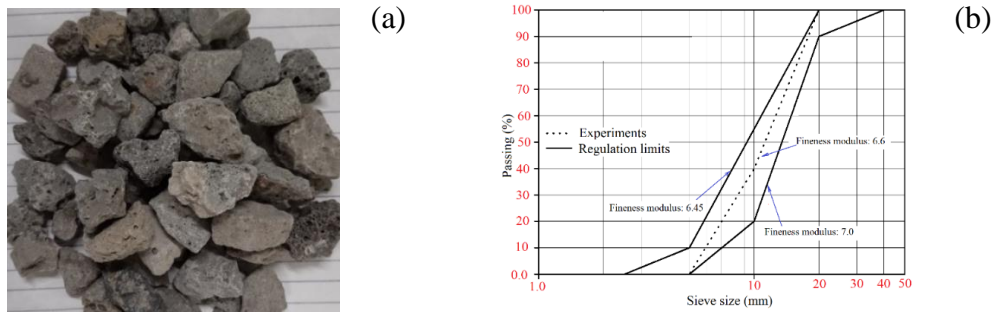
Figure 1. Steel slag used in the present study (a) SSA image (b) Sieve analysis results of SSA

Table 1. Physical properties of the steel slag

Type	Results	Normal aggregate
Density	1.48	1.547
Absorption ratio	1.67%	0.55%
Specific gravity	2.67	2.71
Maximum size	20 mm	12.5 mm
Minimum size	5 mm	4.75 mm

Table 2. Chemical composition of cement and steel slag (%)

Material	SiO_2	Al_2O_3	CaO	MgO	SO_3	Na_2O	Fe_2O_3	K_2O	P_2O_5	MnO	MnO	LOI
Cement	22.5	5	64.25	2.5	2.9	0.2	4.20	1	-	-	-	1.52
Steel slag	14.10	3.48	43.94	3.82	-	0.79	16.49	-	0.24	1.97	1.97	13.2

2.2. Selection of Bacteria and Immobilization Process

Bacillus subtilis (B. subtilis) bacteria were chosen for this study because they can generate endospores in an alkaline environment [9]. B. subtilis and calcium lactate are shown in Figure 2. This research work used B. subtilis from the ATCC number 11774. The liquid medium was inoculated in a laminar flow hood and incubated for 48 hours at 37°C under static incubation conditions.

1st International Conference on Advances in Civil & Environmental Engineering, University of Engineering & Technology Taxila, Pakistan

Conference date 22 &23 Feb 2022
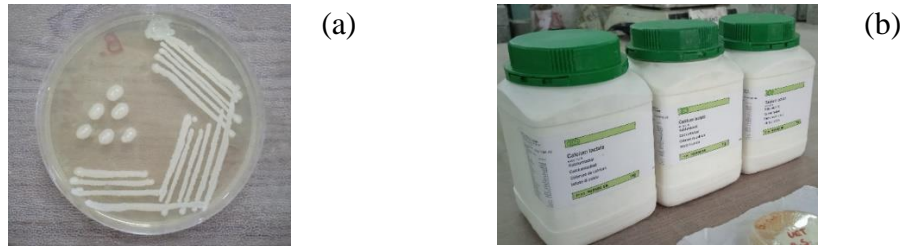
Figure 2. Bacteria grown on agar plate (a) Bacillus subtilis (b) Calcium lactate

2.3. Mix Proportions

Two distinct sorts of mixtures were examined in this experimental investigation. The reference mix (MIX-1) had no bacterial cells, but MIX-2 had bacterial cells by direction incorporation. The experimental program of the current study is presented in Table 3.

Table 3. Mix design

Constituent	Units	MIX-1	MIX-2
Cement	kg/m^3	420	420
SSA	kg/m^3	798	798
Fine aggregates	kg/m^3	893	893
Calcium lactate	kg/m^3	-	10.5
Super plasticizer	ltr/m^3	4.2	4.2
Bacterial suspension	ltr./m^3	-	87.7
Water	kg/m^3	210	210

3. DISCUSSION OF RESULTS

3.1. Recovery of Compressive Strength

The samples were pre-cracked under compression up to 85% of ultimate compressive strength to examine self-healing capacity. The compressive strength testing setup of the specimens is shown in Figure 3. All the analyzed mix composition compressive strengths are shown in Figure 4(a). The compressive strengths of original samples were 9.25 MPa and 22.5 MPa at three days while these were 12.45 MPa and 29.65 MPa at twenty-eight days for MIX-1 and MIX-2, respectively. The results from Figure 4(b) depict the recovery of strength returned after three and twenty-eight days for the two pre-cracked combinations while Figure 4(c) shows the percentages of strength recovered. According to the data, the recovered strength decreases with increasing pre-cracking duration. Reductions of 28.57% and 14.5% were observed when the testing age was increased from three to twenty-eight days. It might be credited to the gradual decrease in bacterial activity induced by increasing density and alkalinity of the matrix generated by hydration of remaining cement [10].

1st International Conference on Advances in Civil & Environmental Engineering, University of Engineering & Technology Taxila, Pakistan

Conference date 22 &23 Feb 2022

(a)   (b)
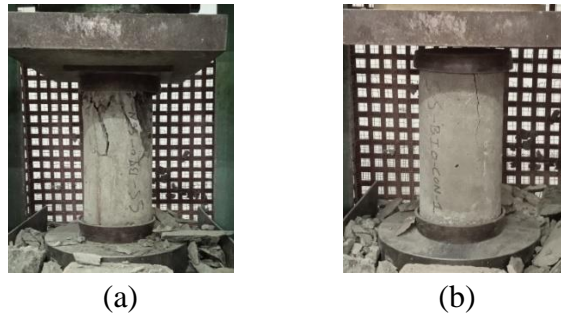
Figure 3. Testing of specimens (a) Compressive strength testing (b) Pre-cracking of specimens
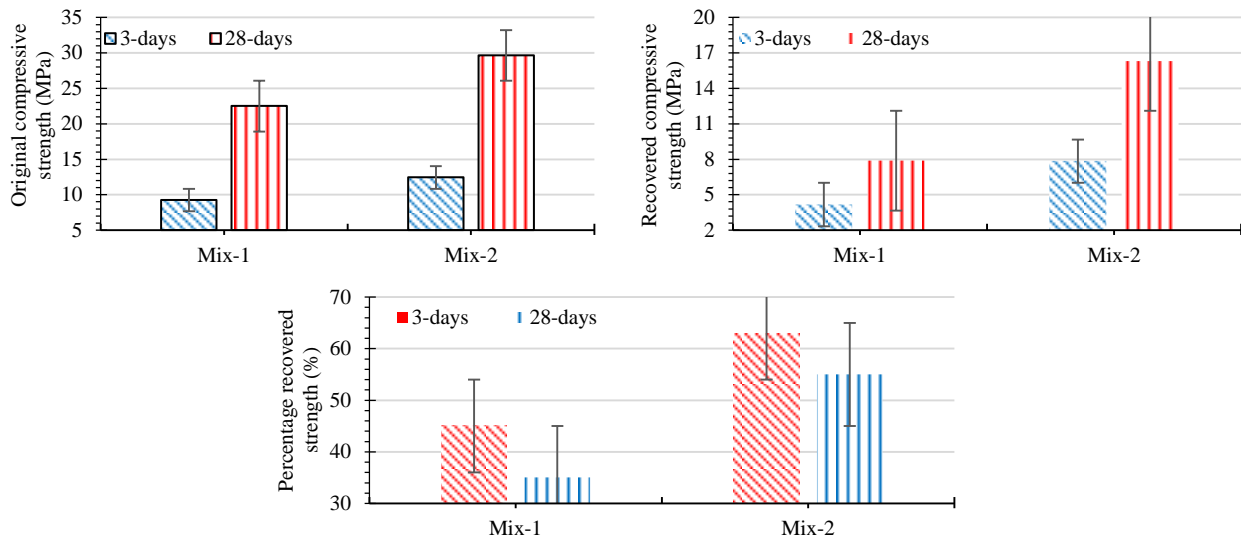
Figure 4. (a) Original compressive strength (b) Recovered strength of 85% pre-cracked samples (c) Percentage recovery of pre-cracked samples

3.2. Visual Examination and Crack Healing Measurement

Figure 5(a, b, c) depicts the healing of cracking widths for pre-cracked samples after twenty-eight days of cure. It shows bio-mineralization as infilled fissures with calcite precipitation generated by microbial metabolic activity at the healing duration of twenty-eight days. The largest recovered crack widths of evaluated pre-cracked mixes at curing durations of 28 days are depicted in Figure 5. MIX-1 had a crack healing width of only 0.098 mm. Crack healing widths of 0.563 mm were observed in MIX-2 being higher than the MIX-1. This may be due to the propagation of bacterial cells in the MIX-2 sample resulting in greater crack repair effectiveness.

4. CONCLUSIONS

The following main findings from the present study:

1st International Conference on Advances in Civil & Environmental Engineering, University of Engineering & Technology Taxila, Pakistan

Conference date 22 &23 Feb 2022
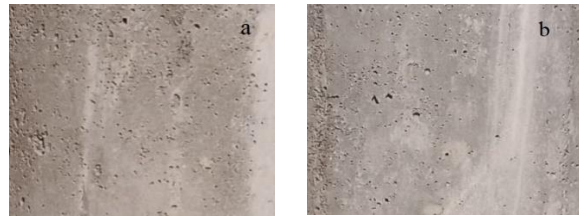
Figure 5. Crack healing (a) MIX-1, (b) MIX-2

1. Visual examination of the healing process of cracked samples portrayed the efficiency of healing compounds in the self-healing process and the recovery of the compressive strength of SSA concrete by a maximum value of 63%.

2. The addition of SSA to concrete has been reported as a suitable carrier for the growth of bacteria for the healing process of the crack widths. The control mix MIX-1 had a crack healing width of only 0.098 mm while the mixes MIX-2 (having bacterial cells) presented the crack healing widths of 0.563 mm depicting the efficiency of bacteria for the healing process of concrete.

ACKNOWLEDGEMENTS

REFERENCES

1. *Khaliq, W. and M.B. Ehsan, Crack healing in concrete using various bio influenced self-healing techniques. Construction and Building Materials, 2016.* **102**: *p. 349-357.*

2. *Portland Cement A. Types and Causes of Concrete Deterioration. PCA R&D Special N. 2617, pp. 1–16. 2002.*

3. *Zhang, J., et al., Immobilizing bacteria in expanded perlite for the crack self-healing in concrete. Construction and Building Materials, 2017.* **148**: *p. 610-617.*

4. *Yang, J., et al., Fluid permeability of ground steel slag-blended composites evaluated by pore structure. Advances in Materials Science and Engineering, 2020.* **2020**.

5. *Van Tittelboom, K., et al., Use of bacteria to repair cracks in concrete. Cement and concrete research, 2010.* **40**(1): *p. 157-166.*

6. *Wang, J.-Y., N. De Belie, and W. Verstraete, Diatomaceous earth as a protective vehicle for bacteria applied for self-healing concrete. Journal of Industrial Microbiology and Biotechnology, 2012.* **39**(4): *p. 567-577.*

7. *ASTM-C150/C150M-19a, Standard Specification for Portland Cement, ASTM International, West Conshohocken, PA. 2019.*

8. *Ali, B. and L.A. Qureshi, Influence of glass fibers on mechanical and durability performance of concrete with recycled aggregates. Construction and Building Materials, 2019.* **228**: *p. 116783.*

9. *Khushnood, R.A., et al., Bio-inspired self-healing cementitious mortar using Bacillus subtilis immobilized on nano-/micro-additives. Journal of Intelligent Material Systems and Structures, 2019.* **30**(1): *p. 3-15.*

10. *Jonkers, H.M., et al., Application of bacteria as self-healing agent for the development of sustainable concrete. Ecological engineering, 2010.* **36**(2): *p. 230-235.*

Axial Compressive Behaviour of Steel Confined Square Concrete Columns

Mustafeez Ur Rahman, Shahzad Saleem
Department of Civil Engineering, UET Taxila, Pakistan
engr.25783@yahoo.com; shahzad.saleem@uettaxila.edu.pk

ABSTRACT

The steel confinement has proved an effective and economical solution since 1990's for increasing the strength, stiffness and ductility of poorly detailed and deteriorated structures. The novelty of this research work is to investigate about the strength improvement of plain concrete square column specimens due to thin steel plates. The parameters considered were the plate thickness and corner shape of steel shell. Test results depicted a significant increase in both the peak and post peak strength of confined specimens. Moreover, the chamfered corner showed considerable effect on peak and ultimate strengths. In general, the confinement provided by thin shells of steel improved the compressive response of square concrete column specimens.

KEYWORDS: Retrofitting; Steel plates confinement; Steel jacketing; Chamfered corners; Corners shape.

1   INTRODUCTION

Earthquakes occurred in various parts of the world attracted researchers' attention towards the enhancement of RC columns capacity in stiffness, strength, and ductility. The steel confinement is used since early 1990's in the form of concrete-filled steel tubes (CFST) and external steel jacketing of existing columns [1]. It was evident from previous study that, the ultimate strength of steel jacketed rectangular RC columns was increased by 2.7 to 3.2 times to that of un-confined RC columns. Similarly, steel jacketed RC columns showed ductile behaviour and increase in deformation capacity. Steel confined RC columns failed due to the outward bulging of steel plate and crushing of inside concrete. In addition, the fill concrete strength was found to has negligible effect on the ultimate strength of jacketed RC columns [2]. In another study, the RC columns were confined with steel angles and strips, which resulted in an increase of 1.54 times in axial load capacity [3].

From previous studies, it is observed that the maximum stress concentration occurs at the sharp corners of rectangular columns which results in knife action causing rupture of confining material. Hence, the confining material fails before reaching its ultimate tensile strength. Contrarily, the circular columns have uniform surface which results in uniform utilization of confining pressure [4]. In most of the existing research, thick steel plates were used for confining purpose, and very limited work is available on confining action of thin steel plates [5]. Furthermore, the effect of corner shape of steel shell has not been paid much attention in previous literature. This paper reports an experimental investigation of steel confined plain concrete square specimens under the effect of thin steel plate and corner shape.

1st International Conference on Advances in Civil & Environmental Engineering, University of Engineering & Technology Taxila, Pakistan

Conference date 22 &23 Feb 2022

2   EXPERIMENTAL PROGRAM

All the specimens have cross-sectional dimension of 150×150mm and height of 300mm. The detailed summary of specimens is presented in Table 1.

Table 1 Specimens Details

Specimen Designation	Type of Specimen	Numbers of Specimens	Steel Plate Thickness Gauge (mm)	CornersShape
$R_1G_0C_0$	Un-confined	02	Nil	Sharp
$R_1G_{16}C_0$	Confined	02	16 (1.51)	Sharp
$R_1G_{20}C_0$	Confined	02	20 (0.91)	Sharp
$R_1G_{16}C_{21}$	Confined	02	16 (1.51)	Chamfered
$R_1G_{20}C_{21}$	Confined	02	20 (0.91)	Chamfered

In Table 1, the specimen designation is explained as follows: alphabet R means aspect ratio, G means gauge of steel plate, C means corner shape of the specimen. For example, in the notation "$R_1G_0C_0$" of unconfined specimen, 1 as subscript of R shows aspect ratio and 0 as subscript of G shows the absence of steel plate, while subscript 0 with C mean corners with sharp edges. Similarly, in "$R_1G_{20}C_{21}$", the subscript 20 of G shows the gauge of sheet and subscript 21 of C demonstrate the chamfered corners of 21mm.

2.1   Material Properties

All the specimens were casted from single batch of ready mixed concrete of 30 MPa target strength. Steel plates with different thicknesses (i.e., gauge 16 and 20) were used for the purpose of strengthening.

2.2   Specimens Preparation

In total, ten specimens including two control specimens were prepared for testing. Firstly, the moulds with required dimension and geometrical shape were prepared from plywood. Special arrangements were made inside the mould corners for required chamfered shape. The steel plate casings were welded around the concrete specimens with a 25mm overlap. The 25mm overlap was welded with electric arc welding on both the end. The 2mm gap between specimen and steel casing was filled with flowable and self-compacting grout. To avoid direct axial loading of steel plates, an offset of 10mm was provided at top and bottom ends of concrete specimens.

2.3   Testing Setup

All the specimens were tested after 15 days of grouting in a compression testing machine of 5000KN capacity. The specimens were tested under displacement-control manner at a rate of 1mm/min. The linear variable displacement transducer (LVDT) was used to measure the axial

1st International Conference on Advances in Civil & Environmental Engineering, University of Engineering & Technology Taxila, Pakistan

Conference date 22 &23 Feb 2022

deformation. The load was obtained from built-in load cell of compression machine. It is to be noted that, only the strength results are presented in this paper.

3   RESULTS AND DISCUSSION

The detailed summary of specimens' results is presented in Table 2.

Table 2 Summary of Test Results

Specimen Designation	Average Stress (MPa)		Normalized peak strength (f_{cc}/f_{co})	Normalized Ultimate Strength (f_{cu}/f_{co})
	Peak (f_{cc})	Ultimate (f_{cu}) (*When test stopped*)		
$R_1G_0C_0$	30.00	------	1	------
$R_1G_{16}C_0$	38.66	23	1.28	0.76
$R_1G_{20}C_0$	35.36	18	1.17	0.60
$R_1G_{16}C_{21}$	46.09	31.74	1.53	1.05
$R_1G_{20}C_{21}$	40.81	21.45	1.36	0.71

Overall, the peak strength of confined specimens was increased by 25% compared to that of control specimen. The G_{16} steel plates revealed 38.19% (17.8% to 28.8%) more increase in peak strength as compared to G_{20} steel plates.

3.1   Failure Modes

Typical failure modes of specimens are shown in Figure 1. In control specimen of Figure 1(a), shear failure was occurred at nearly 45° angle. Initially, very small surface cracks were shown on the top and bottom ends of the specimen. Furthermore, the diagonal cracks were appeared on the surface in the stress range 15-25MPa. Finally, the specimen was failed at average ultimate stress of 30MPa.
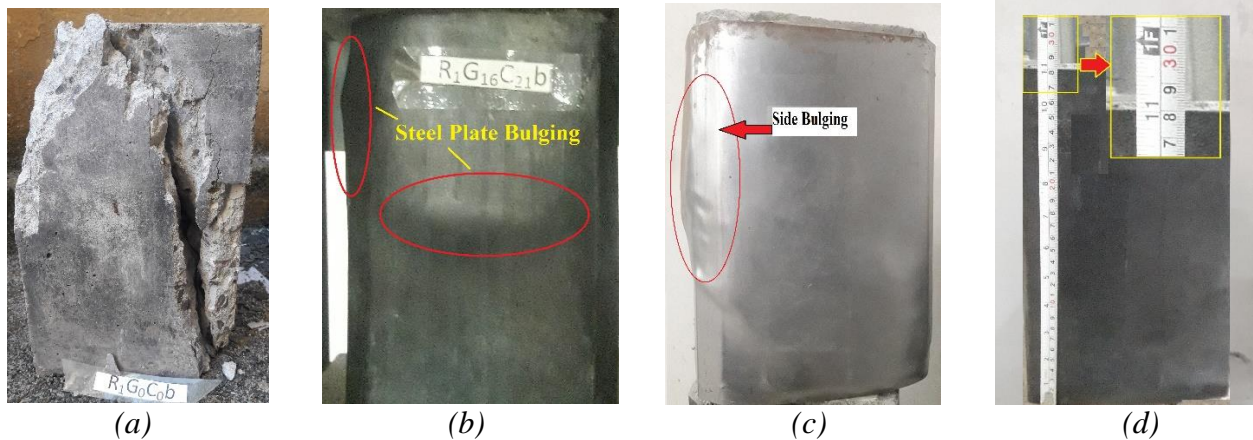
(a)   (b)   (c)   (d)
Figure 1: Failure modes of specimens (a). $R_1G_0C_0$ (b). $R_1G_{16}C_{21}$ (c). $R_1G_{20}C_0$ (d). $R_1G_{20}C_{21}$

1st International Conference on Advances in Civil & Environmental Engineering, University of Engineering & Technology Taxila, Pakistan

Conference date 22 &23 Feb 2022

Due to limited axial deformation measuring capacity of LVDT, confined specimens were strained up to 6% (19 mm deformation) capacity, see Figure 1(d). The axial load was applied directly over the 10mm offset region at the top and bottom ends of the specimen. Internal crushed concrete applied hoop pressure on the steel plates that produced excessive surface bulging and sharp corners were converted into rounded appearance, see figure 1(b) and Figure 1(c).

3.2   Comparison of Unconfined with Confined Specimens

The effect of steel plate thickness on peak and ultimate strength is summarized in Figure 2. For 16- and 20-gauge steel plates, the peak strength was increased by 28.8% (30 to 38.66 MPa) and 17.8% (30 to 35.36 MPa), respectively. The ultimate strength was sustained at 23 and 18MPa for 16- and 20-gauge steel plates, respectively, at the time of test stop.

From Figure 3, due to chamfered corners, an increase of 16.12% and 13.35% was recorded in peak strength for G_{16} and G_{20} thick steel plates, respectively. Moreover, the chamfered corners increased ultimate strength by 27.5% for G_{16} and 16% for G_{20} steel plate confinement.
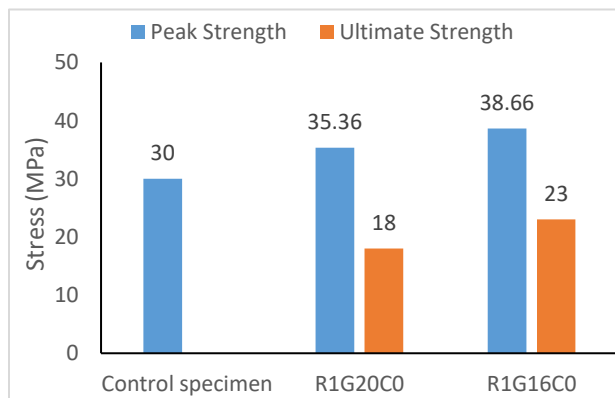
Figure 2: Specimens with sharp corner
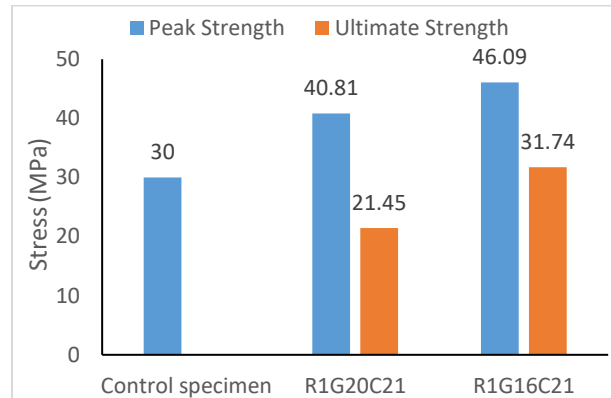
Figure 3: Specimens with chamfered corner

3.3   Effect of Corner Shape

Figure 4 and 5 presents a summary of chamfered corner effect on peak and ultimate strengths. In case of 20-gauge steel plates, the peak strength was increased by 13.35% (35.36 to 40.81 MPa), while in case of 16-gauge steel plate, the peak strength was increased by 16.12% (38.66 to 46.09 MPa). Furthermore, 27.5% (23 to 31.74 MPa) and 16% (18 to 21.45 MPa) increase in ultimate strength was also recorded for 16- and 20-gauge steel plates respectively.

1st International Conference on Advances in Civil & Environmental Engineering, University of Engineering & Technology Taxila, Pakistan

Conference date 22 &23 Feb 2022
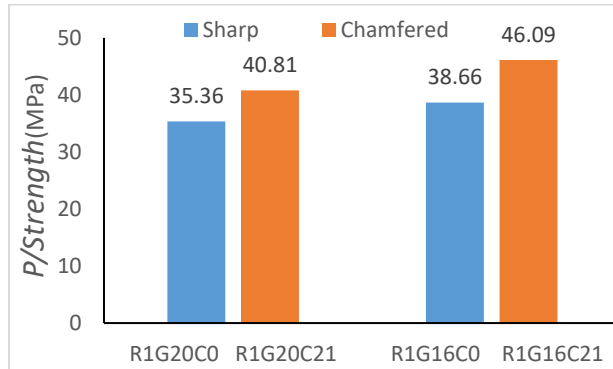
Figure 4: Effect of corner shape on P/strength
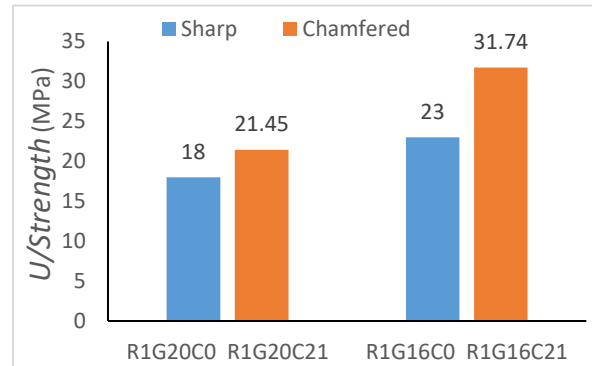
Figure 5: Effect of corner shape on U/strength

4   CONCLUSIONS

The aim of this research work was to investigate about the confinement effect of light gauge steel plates. Parameters of the study were plate thickness and corner shape. From above experimental results, the following conclusions are obtained.

- The overall peak strength of strengthened specimens were increased by 25% than that of control specimen.
- In chamfered corner specimens, remarkable strength improvement was manifested compared to specimens with sharp corners.
- The G_{16} steel demonstrated more strength improvement as compared to G_{20} steel plates.

REFERENCES

1. Di Sarno, L., Elnashai, A. S., and Nethercot, D. A. (2006). *Seismic retrofitting of framed structures with stainless steel*. Journal of Constructional Steel Research, 62(1-2), 93-104.
2. Landović, A., and Bešević, M. (2021). *Experimental Research on Reinforced Concrete Columns Strengthened with Steel Jacket and Concrete Infill*. Applied Sciences, 11(9), 4043.
3. Farooq, H., Usman, M., Mehmood, K., Malik, M. S., & Hanif, A. (2018, September). *Effect of steel confinement on axially loaded short concrete columns*. In IOP Conference Series: Materials Science and Engineering (Vol. 414, No. 1, p. 012026). IOP Publishing.
4. Saleem, S., Hussain, Q., & Pimanmas, A. (2017). *Compressive behavior of PET FRP–confined circular, square, and rectangular concrete columns.* Journal of composites for construction, 21(3), 04016097.
5.   Yan, Y., Xu, L., Li, B., Chi, Y., Yu, M., Zhou, K., & Song, Y. (2019). *Axial behavior of ultra-high performance concrete (UHPC) filled stocky steel tubes with square sections*. Journal of Constructional Steel Research, 158, 417-428.

1st International Conference on Advances in Civil & Environmental Engineering, University of Engineering & Technology Taxila, Pakistan

Conference date 22 &23 Feb 2022

Behaviour of RC Beam-Column-Slab Connection with CFRP Retrofitting Under Cyclic Loading

Babar Majeed, Muhammad Fahim, Mohammad Ashraf, Waqas Adil
University of Engineering & Technology Peshawar, Pakistan
engr_babar84@yahoo.com; drmfahim@uetpeshawar.edu.pk; mashraf@uetpeshawar.edu.pk; engrwaqasadil@uetpeshawar.edu.pk

ABSTRACT

Beam column is a critical element in seismic performance of RC frame structure, hence proper consideration is required in its design. However very limited research work has been carried out on behaviour of RC beam column joint that has been retrofitted with CFRP. This research aims to study the behaviour of retrofitted RC beam column connections. RC beam column joint specimen was tested for quasi static cyclic loading. After testing, damaged specimen was tested with CFRP and re-tested. The hysteresis of retrofitted specimen mostly restored its capacity from control specimen. The lateral capacity of retrofitted specimen also enhanced by 18% compared to control specimen. The retrofitting has significant effect on stiffness degradation of RC beam column joint.

KEYWORDS: beam-column joint, CFRP, RC frame, quasi static testing.

1 INTRODUCTION

Beam column joint is an essential part of building performance, especially in high seismic areas. Beam hinging is the most desirable mode of failure, whereas column hinging and joint shear failure should be avoided as per the capacity design philosophy of connections [1]. Several studies led to development of guidelines for beam column connections [2]. The displacement ductility (μD) factor for connections with no horizontal eccentricity (eh) ranges from 4 to 8, compared to 2.5 to 5 for eccentric specimens [3]. The confinement of the concentric connection is excellent compared to the eccentric connection; even at 4% drift, the concentric connection showed negligible diagonal compressive strain compared to the eccentric one [4]. This study compares the results of an eccentric beam-column-slab connection before and after CFRP retrofitting.

2 TEST SPECIMEN AND SETUP

For conducting the research, half scale model was selected, whereas the material strengths were kept same as prototype i.e., geometric similarity criteria were used in scaling of specimens. The specimen was designed conforming to ACI-352-02 and ACI-318-14. The cross sections and reinforcement details of the specimen are shown in Figure 1. The concrete constituents were proportioned as per ACI procedure. Water to cement ration was kept to 0.45. The average compressive strength was 4,200 psi. The steel used in this research has a yield and ultimate strength of 61,000 psi and 106,00 psi.

1st International Conference on Advances in Civil & Environmental Engineering, University of Engineering & Technology Taxila, Pakistan

Conference date 22 &23 Feb 2022
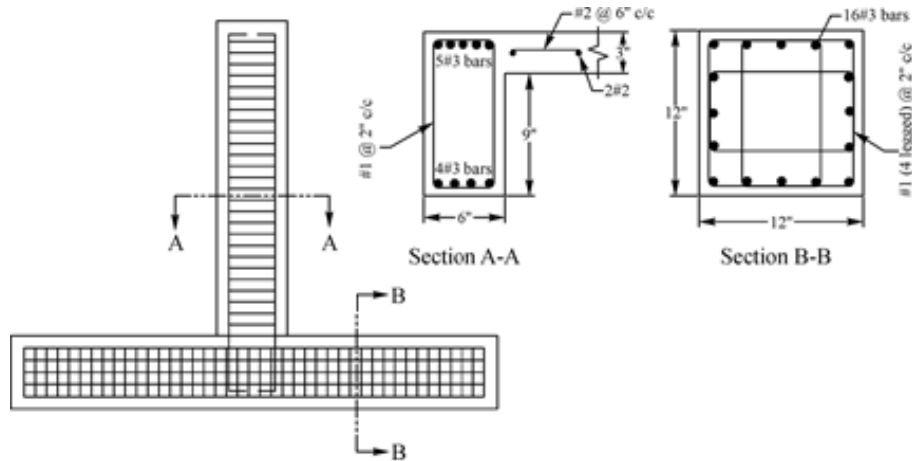
Figure 1. Reinforcement Details of Specimens

The control model was tested for quasi static cyclic loading. After testing of control specimen for ultimate load, the damaged specimen was retrofitted with CFRP sheets. To remove unevenness, the surface was smoothened by grinder first. Then FRP was applied on top and bottom of joint in L shape. Also U shaped sheets was applied for anchoring purposes. The final FRP layout is shown in and test setup are shown in Figure 22. A constant 32 tons load was applied on top of model through hydraulic actuator.
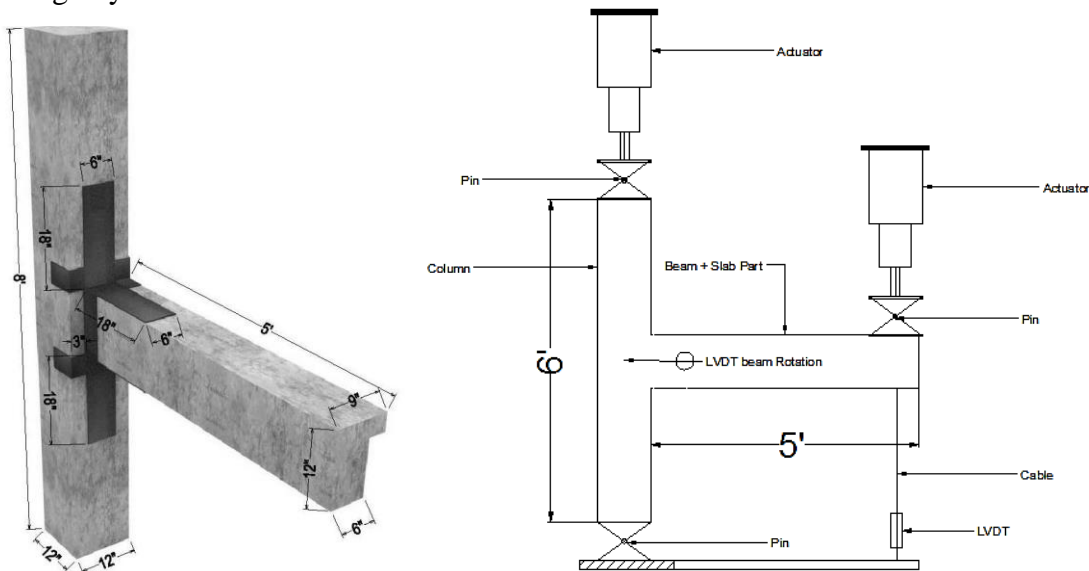
Figure 2. FRP layout installed on specimen and test setup

1st International Conference on Advances in Civil & Environmental Engineering, University of Engineering & Technology Taxila, Pakistan

Conference date 22 &23 Feb 2022

3   RESULTS

The results from experimental testing are discussed here in this section.

3.1   Hysteresis Loops

The hysteresis loops of the specimen show a linear behaviour in initial cycles. The linear elastic behaviour was observed until beam tip displacement of 8 mm, where maximum lateral load of 23 kN was observed. After 8 mm displacement, the lateral load kept on increasing, however, the specimen behaviour entered in non-linear stage. Further increasing the beam tip displacement, the load increased to a maximum value of 33 kN, afterward a drop in lateral load was observed. This drop was due to cracks formation in the beam adjacent to joint. Since specimen behave non-linear, a much lower slope compared to the initial slope was observed.

Further increasing the beam tip displacement enhanced width of already appeared cracks and decrease in load was observed. Finally, at displacement equal to 58 mm, the lateral load drops drastically. The maximum lateral load observed was 33 kN whereas maximum drift ratio observed was 3.8%.
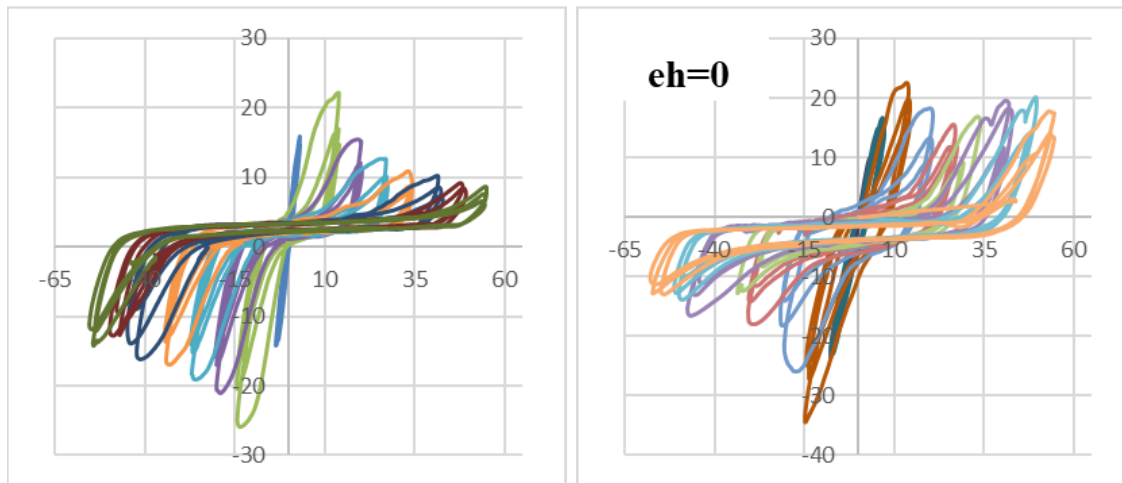
Figure 3. Hysteresis Loops of Control (left) and Retrofitted Specimen (right)

3.2   Backbone Curves

Backbone curves are developed by joining the maximum points in each cycle. Backbone curves of control and retrofitted specimens are compared as shown in Figure 44. In retrofitted specimen, lateral capacity was not only regained but also enhanced as shown in figure. The lateral capacity was enhanced by 18% compared to control specimen. Backbone curve for retrofitted specimen behave linearly up to 14 mm displacement with maximum load of 28 kN. Afterwards the load versus displacement curve drops and load kept on decreasing until 33 mm displacement, where the specimen regain increment in lateral load. Finally, the lateral load carrying capacity reduce at ultimate displacement of 53 mm.

1st International Conference on Advances in Civil & Environmental Engineering, University of Engineering & Technology Taxila, Pakistan

Conference date 22 &23 Feb 2022
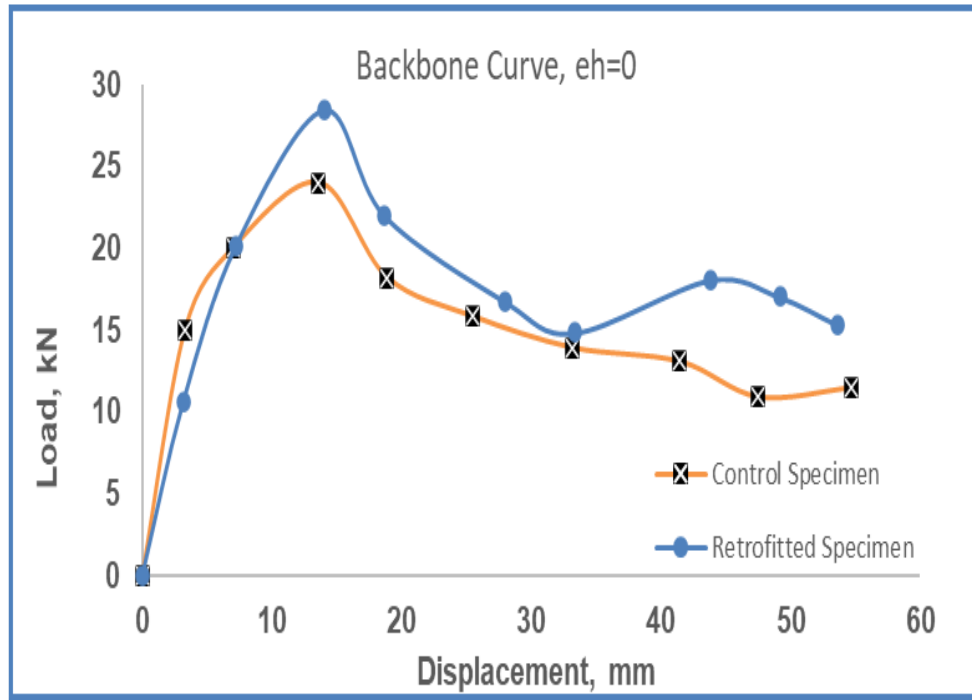
Figure 4. Backbone Curve of Control and Retrofitted Specimen

4   CONCLUSIONS

The following conclusions are derived from testing of retrofitted and control RC beam column joint.

- The retrofitting with FRP composites successfully regained the original strength of the specimen.

- Retrofitting with CFRP sheet enhanced the strength of the specimen by 18%.

- Anchorage of FRP sheet play a vital role in capacity enhancement since detachment of L-shaped effect the lateral strength.

5   REFERENCES

1. Shin M, LaFave J M. Seismic performance of reinforced concrete eccentric beam-column connections with floor slabs. ACI Structural Journal, 2004, 101(3): 403–412

1st International Conference on Advances in Civil & Environmental Engineering, University of Engineering & Technology Taxila, Pakistan

Conference date 22 &23 Feb 2022

2. Joint ACI-ASCE Committee 352. Recommendations for Design of Beam-Column Connections in Monolithic Reinforced Concrete Structures (ACI 352R-02). Farmington Hills, MI: American Concrete Institute, 2002

3. Joh O, Goto Y, Shibata T. Behavior of reinforced concrete beam column joints with eccentricity. ACI Special Publication, 1991, 123:317–357

4. Li B, Pan T C, Tran C T. Effects of axial compression load and eccentricity on seismic behavior of nonseismically detailed interior beam-wide column joints. Journal of Structural Engineering, 2009, 135(7): 774–784

Experimental Testing & Finite Element Modeling of RCC Columns Subjected to Fire

Muhammad Abrar Khan, Maaz Ahmad, Muhammad Noman
Department of Civil Engineering, Faculty of Engineering & Technology
International Islamic University, Islamabad, Pakistan
hafizabrar.137@gmail.com, Maaz4775@gmail.com, Muhammad.noman@iiu.edu.pk

Tauseef Ahmad, Syed Abid Ali Shah
Department of Civil Engineering, Faculty of Engineering & Technology
International Islamic University, Islamabad, Pakistan
Tauseefahmad012015@gmail.com, abid.shah@iiu.edu.pk

ABSTRACT

This paper presents an experimental and numerical investigation of fire-damaged reinforced concrete columns. A total number of six reduced-scale columns were cast and exposed to an elevated standard furnace temperature of 950°C. The columns were further tested for their axial compression residual capacity. The fire-damaged columns showed a 60 % loss in load-carrying capacity. The columns were modeled using Abaqus software using concrete damaged plasticity models for the non-linear behavior of the concrete. The obtained displacement and stress-strain data of the Finite Element Models (FEM) were compared with experimental results. A decent comparative outcome was seen between the experimental-tested data and FEM results.

KEYWORDS: Finite Element Modelling (FEM), Concrete Damage Plasticity (CDP), Furnace fire

1   INTRODUCTION

Fire is one of the most destructive loads that can accidentally occur in a structure during its lifetime, often when least expected. Concrete structures are seen to perform relatively better than timber and steel structures, the mechanical properties such as compressive strength, modulus of elasticity, stiffness decrease with the increase in elevated temperature [1–4]. The strength deterioration is primarily due to the differential thermal expansion between the concrete elements [5]. Columns are considered the main structural component of the building and thus require special attention in case of fires. Furthermore, experimental techniques for evaluating capacity are not always possible; proper validation of finite element techniques is required for quick analysis of structural components in the fire [6].

1st International Conference on Advances in Civil & Environmental Engineering, University of Engineering & Technology Taxila, Pakistan

Conference date 22 &23 Feb 2022

2   EXPERIMENTAL PROGRAM

A total of six (6) reinforced cement concrete (RCC) columns were cast. Three (3) columns were controlled samples, whereas three (3) columns were exposed to elevated temperatures. All the columns were subjected to axial compression loading. Each column was 3'-11" height, with a cross-section of 6"x6", reinforced with four longitudinal bars of 3/8" diameter. Ties/transverse bars were 2/8" in diameter placed at 6" center-to-center used. The clear cover for all columns was 0.75" from all sides.

2.1   Material Properties

Ordinary Portland Cement was used for the casting of columns. Local sand with fineness modulus (FM) of 2.6 and coarse aggregate with a maximum size of ½-inch was used. The 28 days compressive strength of concrete cylinders tested as per ASTM C-39 standard method gave the average value of 4493 psi. The average yield strength of reinforced bars was found to be 74,617 psi. The mix design (by weight) was 1:1.5:3 (cement:sand:aggregate) with 0.55 w/c ratio.

2.2   Fire Testing in Furnace

Ten thermocouples were fixed in the furnace at different localities to measure the temperature, directly coupled to a datalogger to convert & record the time-temperature history of the furnace. Thermocouples were also installed in the core of the columns to measure the core temperature of the column. The fire time-temperature followed the ASTM E119 [7] standard curve, as shown in Figure 1 (a). Propane gas burners were used to make high-intensity fire and ensure the heat was evenly spread through the furnace. Figure 1 (b) shows furnace dimensions and test setup for columns. The furnace was maintained at a maximum temperature of 950 °C; however, on rare occasions, the temperature rose to 975 °C, which was managed by closely monitoring and changing the gas pressure. Spalling in some portions of the column was detected. The average fire curve achieved inside the furnace compared to the standard ASTM E119 fire curve exhibited similarity. Overall, the columns did not fail, but a tiny portion spalled due to moisture content. However, the surface was porous the concrete surface color was changed.
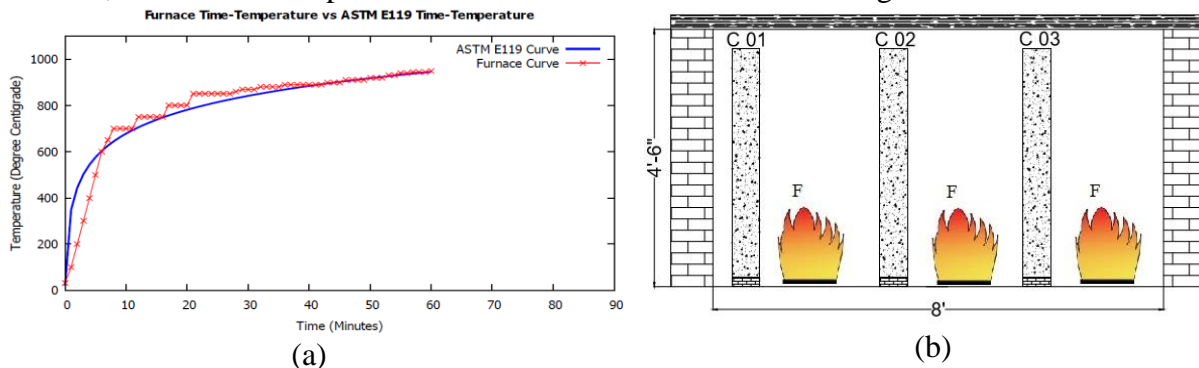
Figure 1: Fire testing of column specimen. (a) Time-temperature curve (b) Columns setup in the furnace

1st International Conference on Advances in Civil & Environmental Engineering, University of Engineering & Technology Taxila, Pakistan

Conference date 22 &23 Feb 2022

2.3 Compression Testing

A monotonic load control test was performed on undamaged columns. Two linear variable displacement transducers (LVDTs) were installed, having a length of 13" for displacement and strain measurement (see Figure 2 (b)) due to the applied load. A load was applied at a rate of. 0.2 kN/sec and data were recorded on the computer attached to the compression machine. The test setup is shown in Figure 2 (a). Tiny cracks appeared at 560 kN, increasing with the load. The ultimate load of the column was 715 kN (30.78 MPa stress was applied). In the case of fire-damaged columns, the ultimate load of the column was 504 kN (21.7 psi). All the columns failed in the middle section (see Figure 2 (c)).

| (a) | (b) | (c) |

Figure 2: Compression testing of the columns (a) Test setup (b) Arrangement of LVDTs (c) Failed column after ultimate load

3 FINITE ELEMENT MODELLING OF RCC COLUMN

Finite Element Modelling (FEM) Software ABAQUS 6.14 was used to perform the finite element analysis for the experimentally tested heated and un-heated columns using the concrete damaged plasticity model. Tensile cracking and compressive crushing of concrete are the two main damage failure mechanisms in this model. Concrete behavior under uniaxial tension is assumed to be linear until the initial microscopic cracks are formed at the peak stress. The linear proportional limit of concrete was assumed to equal 0.4 times the cylindrical compressive strength of concrete [8].

A solid 8-node linear brick reduced integration, hourglass control element C3D8R was used to model the concrete. The longitudinal and transverse reinforcements were modeled using a two-node linear truss element called T3D2. The concrete model was meshed into an 8 mm size in both the longitudinal & transverse directions to the whole model using the hex element shape option (Figure 3 (a)). The cubical mesh size of 3 mm was used in the model. The same mesh size was adopted for meshing the reinforcement type T3D2. The longitudinal & tie bars were embedded in the host solid element using the embedded option. The model was fixed at one end by applying the boundary conditions & the axially loaded column was simulated as simple support (pin support), as shown in Figure 3 (c & d). A uniform pressure load was applied on the top of the

1st International Conference on Advances in Civil & Environmental Engineering, University of Engineering & Technology Taxila, Pakistan

Conference date 22 &23 Feb 2022

column using static general analysis. The concrete column's thermal analysis was executed using the step heat transfer available in ABAQUS. A constant convective coefficient of 25 W/m2 K was considered for the fire-exposed surface. A concrete emissivity value of 0.7 was used to determine the radiative heat flux. [8]. The density of the column in the model was 2300 kg/m^3 for concrete dependence is included in the specific heat. Figure 3 depicts a comparison of the time-temperature curves derived from the FEA (Heat transfer) with the measured experimental data at the mid and core of columns. The time-temperature curves derived from the finite element (ABAQUS heat transfer) analytical model match the measured experimental data for the concrete columns pretty well.

(a)   (b)   (c)   (d)
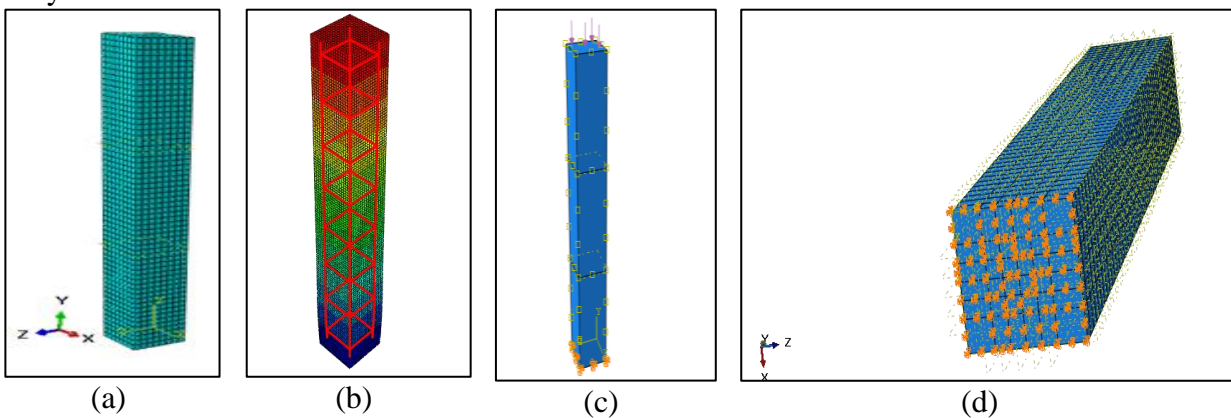
Figure 3: FEM models of the columns (a) meshed column (b) steel configuration (c & d) Load application and support conditions
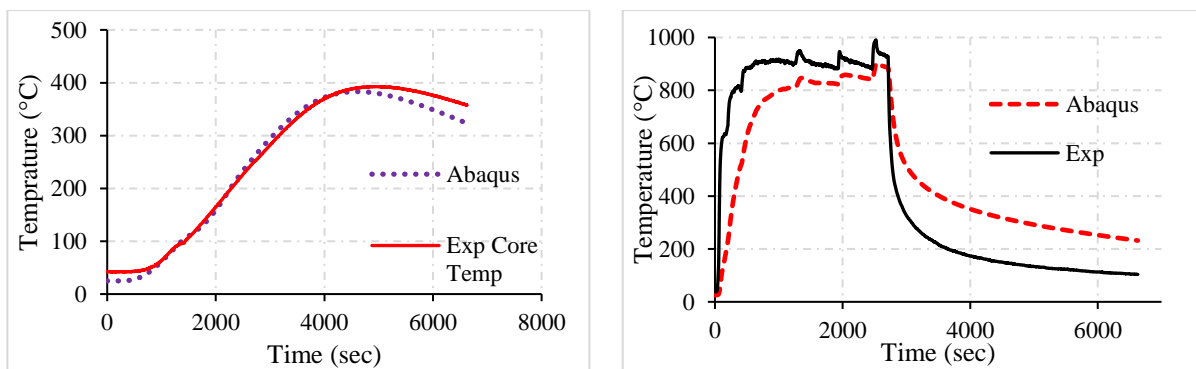
Figure 4: Comparison of time-temperature of furnace and core with FEM model

4   RESULTS & DISCUSSION

Evaluation of the stress-strain obtained from the finite element analysis using Abaqus software and the measured experimental data at the mid-height of reinforced un-heated concrete square columns are shown in Figure 5. The stress-strain plots from finite-element analysis and the

1st International Conference on Advances in Civil & Environmental Engineering, University of Engineering & Technology Taxila, Pakistan

Conference date 22 &23 Feb 2022

experimental results have a good agreement for the un-heated square column. The preheated and post-heated column strength was compared from the stress-strain graph and the concrete cylinders. The columns lose 60% of strength after being exposed to fire.
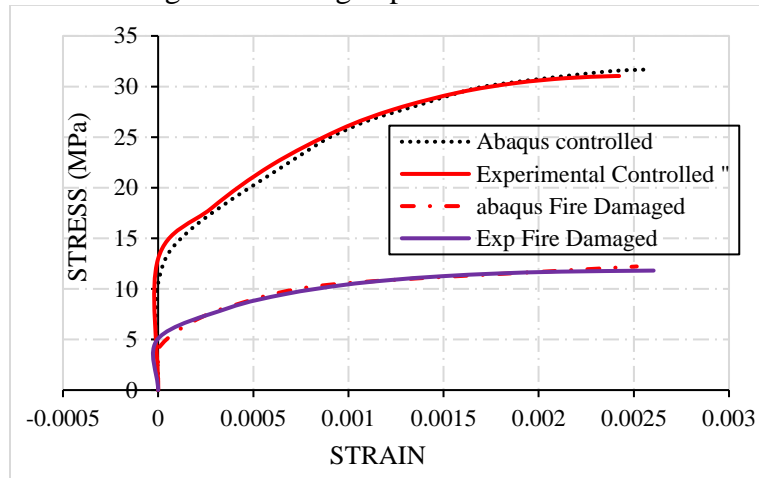
Figure 5: Stress-Strain curve for Experimental and FEM results for undamaged and fire damaged columns

5   CONCLUSION

Based on the experimental and numerical study of the columns, the following conclusions can be drawn:
  i.   The concrete columns lost their 60 % of compressive strength after being exposed to the elevated temperature of 950 ℃
 ii.   During the fire test, it was noted that severe spalling was occurred in the columns due to the moisture content present in the concrete, and also thermal strains were produced by the thermal stresses due to which the cracks generated in the concrete column, due to these cracks concrete loss its strength.
iii.   FEM is the best method to verify the results as in this work, the comparison of the results between experimental and FEM is shown. In this research, a concrete damage plasticity model is used to describe the best behavior of concrete in compression and tension.

REFERENCES

[1]   M. Tufail, K. Shahzada, B. Gencturk, J. Wei, Effect of Elevated Temperature on Mechanical Properties of Limestone, Quartzite and Granite Concrete, Int. J. Concr. Struct. Mater. 10 (2016) 1–6. https://doi.org/10.1007/s40069-016-0175-2.
[2]   M. Usman, M. Yaqub, M. Auzair, W. Khaliq, M. Noman, A. Afaq, Restorability of strength and stiffness of fire damaged concrete using various composite confinement techniques, Constr. Build. Mater. 272 (2021) 121984. https://doi.org/10.1016/j.conbuildmat.2020.121984.

1st International Conference on Advances in Civil & Environmental Engineering, University of Engineering & Technology Taxila, Pakistan

Conference date 22 &23 Feb 2022

[3]   M. Noman, M. Yaqub, M. Abid, M.A. Musarat, N.I. Vatin, M. Usman, Effects of Low-Cost Repair Techniques on Restoration of Mechanical Properties of Fire-Damaged Concrete, 8 (2022) 1–14. https://doi.org/10.3389/fmats.2021.801464.

[4]   M. Noman, M. Yaqub, Restoration of dynamic characteristics of RC T-beams exposed to fire using post fire curing technique, Eng. Struct. 249 (2021) 113339. https://doi.org/10.1016/j.engstruct.2021.113339.

[5]   M. Yaqub, Axial compressive and seismic shear performance of post-heated columns repaired with composite materials Doctor of Philosophy 2010, The University of Manchester, 2010. https://www.escholar.manchester.ac.uk/uk-ac-man-scw:101698.

[6]   L. Bisby, H. Mostafaei, P. Pimienta, State-of-the-Art on Fire Resistance of Concrete Structure s: Structure-Fire Model Validation, 2014.

[7]   ASTM-International, ASTM E119-20, Standard Test Methods for Fire Tests of Building Construction and Materials, in: Annu. B. ASTM Stand., West Conshohocken, PA, 2020. http://www.astm.org/cgi-bin/resolver.cgi?E119-20.

[8]   B.S. EN, 1-1. Eurocode 2: Design of concrete structures–Part 1-1: General rules and rules for buildings, Eur. Comm. Stand. (2004).

Enhancement of Self-Healing Tendency of Reclaimed Asphalt using Different Additives

Usama Zakir, Imran Hafeez

Department of Civil Engineering

University of Engineering & Technology Taxila, Pakistan

usamazakir172@gmail.com; imran.hafeez@uettaxila.edu.pk

ABSTRACT

Healing is an intrinsic property of bitumen. During long rest periods and hot summers, bituminous materials are supposed to heal themselves, extending the service life of asphalt pavement. Unfortunately, this property degrades due to ageing of bitumen. In this study, the effect of moisture sensitivity on the self-healing tendency of bituminous binders using different admixtures is observed by comparing the performance of four empirical test methods for loose asphalt mixtures: - static water immersion test (SWIT), boiling water test (BWT) total water immersion test (TWIT), and rolling bottle test (RBT). Two different types of modifiers based on polymer such as low-density polyethylene (LDPE) and high-density polyethylene (HDPE) are utilized. Three samples for each test are prepared for both LDPE and HDPE modified asphalt mixtures and heated at 40˚C for 5, 10 and 15 minutes in a controlled environment. The analysis of the test data showed that LDPE modified asphalt mixture offered better self-healing potential. Boiling water test is easy to perform and consume less time while rolling bottle test was found relatively more reliable as compared to other test on loose coated asphalt mixtures. Study reveals that samples of LDPE modified asphalt mixtures have percentage cover loss less than HDPE modified asphalt mixtures thus LDPE shows higher healing ratio.

KEYWORDS: Sustainability, Reclaimed Asphalt Pavement, Self-healing, LDPE, HDPE.

1   INTRODUCTION

Asphalt is a viscoelastic material made by refining petroleum that is commonly used in paving projects such as highways and airports [1]. But, after an in-service time of a few years, damages like fatigue cracks, surface roughness, degradation, pot holes, and ultimately structural problems on the surface of the pavement may occur [1]. In bituminous pavements, parts that are already damaged by stripping, fatigue cracking, ravelling and rutting are further damaged by moisture leading towards construction failure [2]. Long-life pavements are required to enhance pavement availability while minimising traffic hindrances caused by repair activities. Self-healing has been regarded as a significant method when constructing a sustainable infrastructure because of its potential to extend the service life of asphalt pavement[3].Waste plastic modifiers have a larger potential for extending the life of pavements. The increased degree of cohesion and adhesion is one of the most important qualities of polymer modified asphalt binder. Because waste plastic takes longer to biodegrade, it is harmful to the environment and ecological balance. In construction sector, it is rational to recycle the waste products in order to conserve resources and minimize the negative effects on the environment and nature[4, 5]. Different modifiers are utilized to enhance

1st International Conference on Advances in Civil & Environmental Engineering, University of Engineering & Technology Taxila, Pakistan

Conference date 22 &23 Feb 2022

the self-healing tendency of bituminous mixtures. González et al. studied the use of HDPE and LDPE in asphalt alteration [6, 7]. Chin and Damen also worked on an asphalt pavement project that included HDPE, LDPE, and PET. The use of plastics in asphalt could enhance moisture resistance, improve binding qualities, and facilitate performance at elevated temperature without any significant increase in costs or generating harmful gases, according to field test studies[8]. Also, addition of crumb rubber, HDPE and gilsonite in proper quantities could increase the self-healing property of asphalt. A higher HR of 102% was achieved using 8% HDPE-modified asphalt while analysing for self-healing tendency [9]. LDPE has more branching than HDPE (of approx. 2% of the carbon atoms), with lower tensile strength and higher resilience. This study uses 9% LDPE and 8.7% HDPE incorporating aggregate of size ranging from 6.3mm to 9.5mm by dry mixing process. For aggregate replacement or mixture modifiers, reused plastics are directly added into the mixture in dry process [10].The purpose of this research is to understand the moisture impact on self-healing process of bituminous materials and the outcome of material modifications, by means of qualitative assessment and testing.

2   RESEARCH OBJECTIVES

Main research objectives of this study are given below:
- To characterize the indigenous asphalt binders for self-healing capabilities of Reclaimed Asphalt Pavement (RAP) materials.
- To compare the self-healing tendency of different modifiers asphalt binder in RAP materials.
- To develop relationship among percentage modifier dose and the self-healing tendency of RAP materials.

3   RESEARCH MEHODOLOGY

The methodology designed to achieve the required research objective consisted of three phases. First phase comprised of material selection.
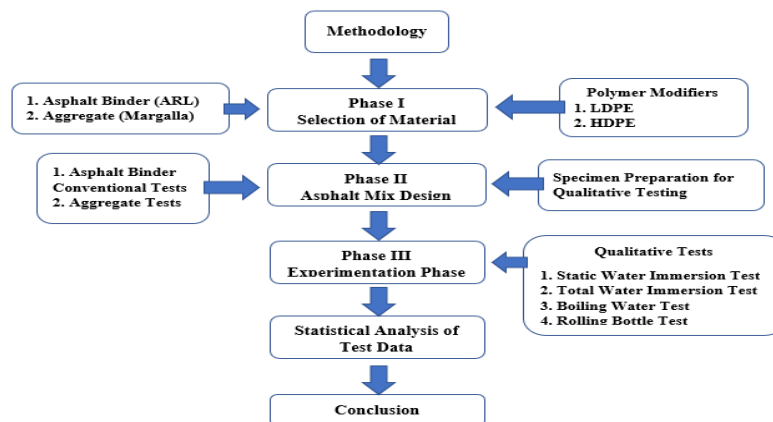
Figure 1: Scope of research work

1st International Conference on Advances in Civil & Environmental Engineering, University of Engineering & Technology Taxila, Pakistan

Conference date 22 &23 Feb 2022

For aggregate, Margalla stone quarry was selected, and material was brought from there. In qualitative testing, aggregate ranging from 6.3mm to 9.5mm in size were chosen to prepare the loose coated asphalt mixture. Asphalt binder which is 60/70 Pen Grade was acquired from Attock Oil Refinery (ARL). It is one of the most widely used binder in Pakistan Road Network. In second phase, samples were made i.e., asphalt mixture design. Dry method was used to add LDPE and HDPE modifiers in asphalt mixture. Modifiers were initially mixed with aggregate prior to adding the asphalt binder in the dry method. Samples were prepared for qualitative assessment. In the final step of the research, laboratory tests on loosely covered asphalt mixes were carried out. After that, results of all tests were analysed.

4 EXPERIMENTAL PROGRAM

The various tests on aggregate, bitumen, and asphalt concrete mixtures were performed. The Class B aggregate of the NHA Specification was chosen in this investigation since it is simple to compare test results in the case of fine classifications. Table 1 lists the physical parameters of the aggregate and bitumen used in this study. Using dry method, 9% LDPE and 8.7% HDPE is added to the pre-heated aggregate in accordance with ASTMD1559 standard. Density, ranging from 0.917-0.930 g/cm^3, is used to describe LDPE. LDPE has more branches than HDPE thus making its intermolecular forces weaker, its resilience greater and its tensile strength lower. HDPE has a density of more than 0.941 g/cm^3 and has few branches making its intermolecular forces and tensile strength greater as compared to LDPE. All qualitative tests on the loose coated asphalt mixture were carried out in the laboratory in accordance with standards. These tests' essential details have been summarised in Table 2.

Table 1: Physical properties of aggregate and bitumen

Test Nomenclature	Standards	Aggregate (Margalla)	Limita-tion	Test Nomenclature	Standards	Bitumen Binder (60/70)	Specifications
Elongation Index (%)	BS 812.109	6.4	15(max)	Softening Point (°C)	ASTM D36	47	46-54
Flakiness Index (%)	BS 812.108	4.75	10(max)	Penetration Test (0.1mm)	ASTM D5	63	60-70
Los Angeles Abrasion Test (%)	ASTM C 131	21	30(max)	Ductility (cm) (25 °C)	ASTM D70	119	100 (min)
Water Absorption Test (%)	ASTM C 127	0.95	2(max)	Flash and Fire Point (°C)	ASTM D92	247, 251	232-450

Table 2: Test conditions adopted in various asphalt mixture testing methods

Sr. No.	Test Nomenclature (Standards)	Testing Conditions	Pictorial Illustration
1.	Static Water Immersion Test (SWIT) (ASTM D1664)	Water temp = 25 ˚C, Sample immersion duration = 16 - 18 hr, Sample aggregate size = 6.3 - 9.5 mm	

1st International Conference on Advances in Civil & Environmental Engineering, University of Engineering & Technology Taxila, Pakistan

Conference date 22 &23 Feb 2022

2.	Total Water Immersion Test (TWIT) (ASTM D1664)	Water temp = 40 ˚C, Sample immersion duration = 3 hr, Sample aggregate size= 6.3 - 9.5 mm	
3.	Boiling Water Test (BWT) (ASTM D3625)	Water temp = 100 ˚C, Sample immersion duration= 10 min, Sample aggregate size= 6.3 - 9.5 mm	
4.	Rolling Bottle Test (RBT) (BS EN 12697)	Revolution per minute = 60, Rotation duration = 24 hr, 48 hr, 72 hr, Sample aggregate size= 6.3 - 9.5 mm	

5   RESULTS

The technique used for analysing results is the visual observation i.e., the qualitative determination (tests on loose coated asphalt mixtures). This technique conserves both time and cost. Four samples each for 8.7% HDPE and 9% LDPE were prepared including one control specimen while the rest of three samples are self-healed for 5 min, 10 min and 15 min at constant self-healing temperature i.e., 40 ˚C. Graphs indicating results of these tests are attached below (Fig. 2):

Figure 2: Moisture sensitivity test at different time intervals

1st International Conference on Advances in Civil & Environmental Engineering, University of Engineering & Technology Taxila, Pakistan

Conference date 22 &23 Feb 2022

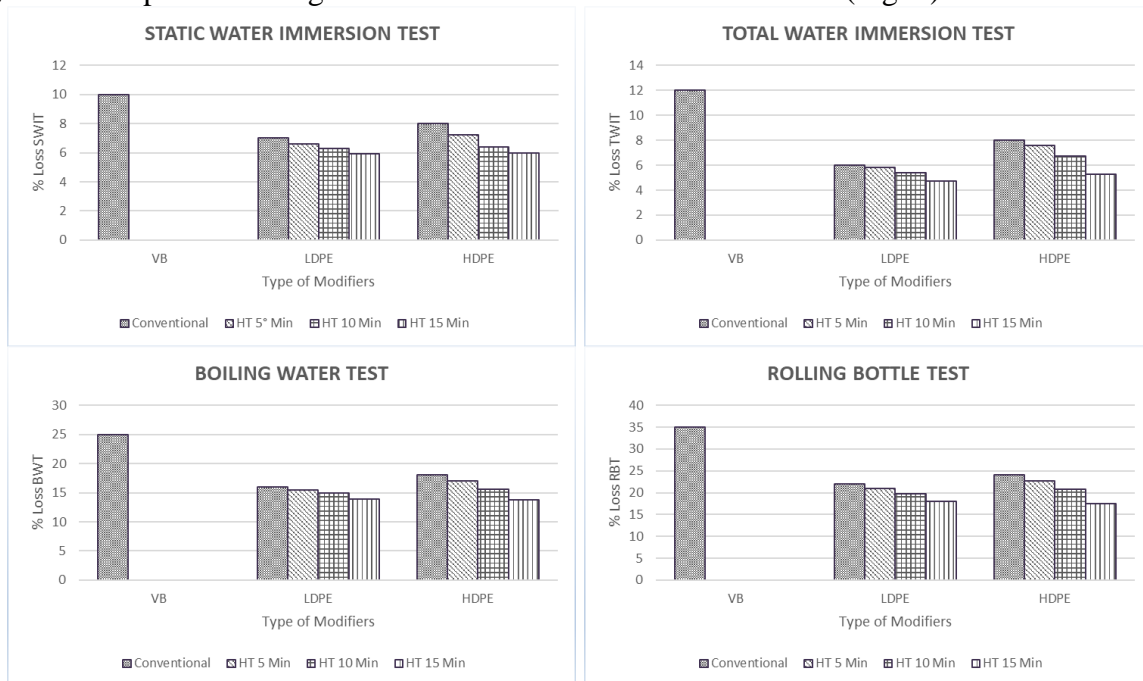In all qualitative tests, LDPE modified asphalt mixture offered better self-healing potential in comparison with HDPE modified asphalt mixture. LDPE modifier was found comparatively better in adhesion properties at higher self-healing temperature as compared to HDPE modifier.

6   CONCLUSION

The aim of this study was to analyse the beneficial effect of the LDPE and HDPE modified asphalt binder and the moisture impact on self-healing mechanism of bituminous materials. For qualitative analysis four different tests i.e., SWIT, TWIT, BWT and RBT, on loose coated asphalt mixtures were performed.

- 9% LDPE modified asphalt mixture shows better self-healing potential as compared to 8.7% HDPE modified asphalt mixture. Also, it was observed that moisture resistance of plastic modifiers is better than that of unmodified asphalt binder.
- Adhesion properties of LDPE modifier was better at higher self-healing time as compared to HDPE modifier.
- The boiling water test (BWT) conserves time as compared to other qualitative tests but rolling bottle test (RBT) gives better results.

REFERENCES

1. Agzenai, Y., et al., *Advanced self-healing asphalt composites in the pavement performance field: mechanisms at the nano level and new repairing methodologies.* Recent patents on nanotechnology, 2015. **9**(1): p. 43-50.
2. Liu, Y., et al., *Examination of moisture sensitivity of aggregate–bitumen bonding strength using loose asphalt mixture and physico-chemical surface energy property tests.* International Journal of Pavement Engineering, 2014. **15**(7): p. 657-670.
3. Sun, D., et al., *A comprehensive review on self-healing of asphalt materials: Mechanism, model, characterization and enhancement.* Advances in colloid and interface science, 2018. **256**: p. 65-93.
4. Bansal, S., A.K. Misra, and P. Bajpai, *Evaluation of modified bituminous concrete mix developed using rubber and plastic waste materials.* International Journal of Sustainable Built Environment, 2017. **6**(2): p. 442-448.
5. Gautam, P.K., et al., *Sustainable use of waste in flexible pavement: A review.* Construction and Building Materials, 2018. **180**: p. 239-253.
6. González,O., M. Munoz, and A. Santamaría, *Bitumen/polyethylene blends: using m-LLDPEs to improve stability and viscoelastic properties.* Rheologica acta, 2006. **45**(5): p. 603-610.
7. Ghuzlan, K.A., G.G. Al-Khateeb, and Y. Qasem, *Rheological properties of polyethylene-modified asphalt binder.* Athens Journal of Technology and Engineering, 2013. **10**: p. 1-14.
8. Chin, C. and P. Damen, *Viability of using recycled plastics in asphalt and sprayed sealing applications.* 2019.
9. Zhou, L., et al., *Evaluation of the adhesion and healing properties of modified asphalt binders.* Construction and Building Materials, 2020. **251**: p. 119026.
10. Movilla-Quesada, D., et al., *Use of plastic scrap in asphalt mixtures added by dry method as a partial substitute for bitumen.* Waste Management, 2019. **87**: p. 751-760.

1st International Conference on Advances in Civil & Environmental Engineering, University of Engineering & Technology Taxila, Pakistan

Conference date 22 &23 Feb 2022

Seasonal Variation of Sun Path and its Impacts on Energy Consumption Using BIM, A Case Study of Multi-Story Educational Building

Syed Shujaa Safdar Gardezi, Ahmad Shaheen
Department of Civil Engineering
Capital University of Science & Technology, Pakistan
dr.shujaasafdar@cust.edu.pk; ahmedhameedshaheen@gmail.com

Umair Sajjid
Capital University of Science & Technology, Pakistan
umairdurrani46@gmail.com

ABSTRACT

Energy is one of the major concerns for building sector. The sun path, at a particular location, plays a vital role in energy consumption patterns. The current work explores the impact of sun path on the energy levels for two different seasons, summer and winter. A four-story educational building with traditional construction has been adopted as a case study. The longest day in summer and shortest day in winter has been opted to run the sun path analysis for that particular location. Using Building Information Modelling (BIM), 3D virtual model was developed which was further transformed to building energy model (BEM) to conduct analysis. The results have shown a considerable difference in energy levels with a variation of 78%. However, the analysis only limited itself to roof constructions.

KEYWORDS: Sun Path, BIM, BEM, Energy Consumption

1   INTRODUCTION

Conventional energy sources are running our day by day and economies around the globe are confronting the difficulties of high energy interest to financial development and advancement uphold [1]. Building sector is one of the major consumers of energy throughout the world. The consumption of energy by building is not constant throughout the year and majorly depends upon the surrounding environment. Major portion of total energy consumed is to maintain specific environment inside the building. SUN is the prime contributor in the environmental temperature. The energy requirements of building can be managed by changing the properties such as Orientation, location on site, and landscaping [2]. To ensure the reduced energy consumption of building the sustainability principles are kept in mind while designing the building. Reduction in energy consumption is made possible by using the techniques such as site selection, passive solar design, using sustainable materials and replacement of incompetent systems [3]. The path of sun changes from summer to winter which in turn changes the temperature of the surrounding in different seasons. To reduce the energy consumption architects, engineers, public and private sector must have the understanding of building-climate interactions to address indoor and outdoor environment quality for humans. Sun path analysis would be key in maximizing the solar energy.

1st International Conference on Advances in Civil & Environmental Engineering, University of Engineering & Technology Taxila, Pakistan

Conference date 22 &23 Feb 2022

2   LITERATURE REVIEW

Energy consumption has drastically increased in buildings in the past few decades due to growth in population, excessive time spent indoors, increased building functionality demand, indoor environmental quality, and climate change. Building sector currently accounts for approximately 40% of total primary energy consumption. It is important to minimize energy consumption and reduce the rate of depletion of world energy reserves and environmental pollution due to the diverse effects of the energy consumption of buildings. Designing buildings that are more efficient in their use of energy for heating, lighting, cooling, ventilation, and hot water supply are one way of reducing building energy use [4]. The use of new energy efficient materials in existing building envelopes will help to reduce the demand for building energy. Various techniques might help to rescue the energy consumption. Yarramsetty, Rohullah, & Sivakumar, 2020 [5] and Ochedi & Taki, 2019 [6] suggested orientation of building. Fitriaty & Shen, 2018 [7] proposed PV panels. Sun breakers were being considered by Gadelhak, Aly, & Sabry, 2013 [8]. Luo, 2018 [9] suggested two options, Window to Wall ratio and Façade of the building.

3   METHODOLOGY

Simulation based parametric virtual modelling for energy analysis has been adopted.

3.1   Solar Analysis

During summer and winter season the position of sun changes and the energy consumption of building also changes. This change in energy consumption due to variation of sun path is of great importance in calculating the total energy consumption of building while considering different aspects of building construction, Figure 1. According to Khan, Ghadg (2019) [10], the cooling and thermal details, sun path details, wind details can be easily done by studying Environmental, Economic and social impacts in a virtual environment. By changing window area ratio, the energy performance increased up to 2.9 times on average.

Figure 1: Energy Gap Analysis

3.2   Parametric Modelling Using BIM

Building Information Modelling (BIM) helps to visualize the construction process and also support the actualization of energy consumption patterns. It is a smart 3D modelling process used to plan, design, construct, and manage buildings efficiently. A case study of an educational facility has been used in this research. It is located in Islamabad, Pakistan and designed on seismic zone 2B

1st International Conference on Advances in Civil & Environmental Engineering, University of Engineering & Technology Taxila, Pakistan

Conference date 22 &23 Feb 2022

standards. The facility is as a multipurpose building with ground plus three stories. The first two stories are allocated for administration purpose and the third story comprise of class rooms and lecture halls. The total covered area is approx. 6720 sq. ft. The selected case study was developed in a 3D virtual environment using BIM. Figure 2 presents the BIM model developed for case study.
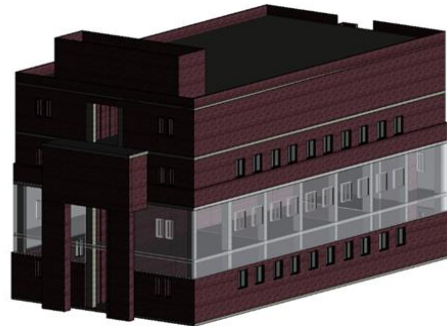
Figure 2: Energy Gap Analysis

3.3 Energy Modelling

The BIM model has been transformed to Energy model (BEM). It has very important significance in solar analysis as all the parameters required to run solar analysis are set using energy model. Energy model also differentiate between most prompt areas where energy may strike during a day.

4 ANALYSIS AND RESULTS

The energy analysis was performed on the developed using 3D model of the selected case study. Real time parameters were set according to the local conditions, table 1, which included Location and Weather, HVAC system, Air Information, Operation Schedule etc. Energy model of the building was made using energy optimization tool, Insight 360 in Revit, Figure 3.

Table 1 Parameters Adopted for Analysis

Building Type	Operating Schedule	HVAC System	Air Information	Area of Concern
Educational	12/5	NIL	3 m/h / 1007mb/h	Roof
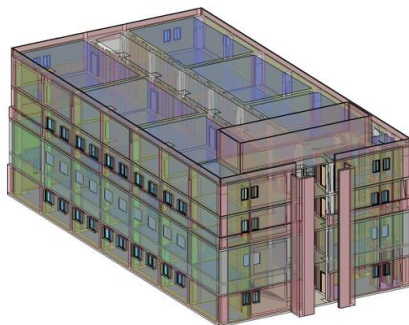
Figure 3: Energy model of case study

1st International Conference on Advances in Civil & Environmental Engineering, University of Engineering & Technology Taxila, Pakistan

Conference date 22 &23 Feb 2022

The energy analysis was based upon the local seasons observed for the local conditions at the location of building. Now, in case of buildings, both roof and building envelop contribute in energy performance analysis. However, in this particular work, only roof area has been considered. In other words, the building envelop remains outside the scope of this study. The roof is a conventional RCC slab with 6-inch thickness and no insulation on the top

.
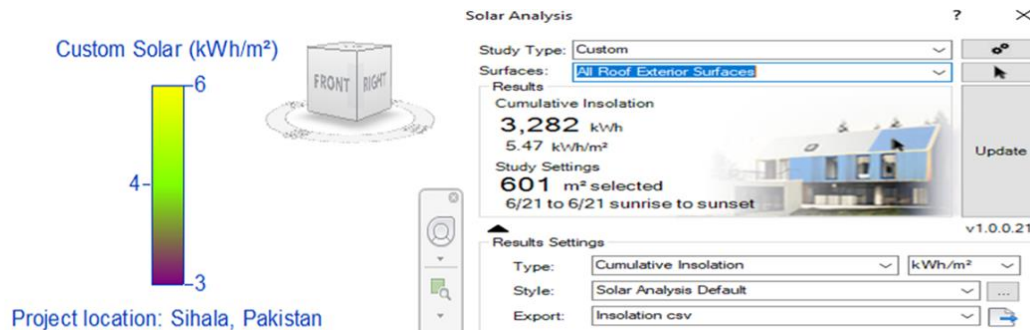
Figure 4: Energy consumption – summer
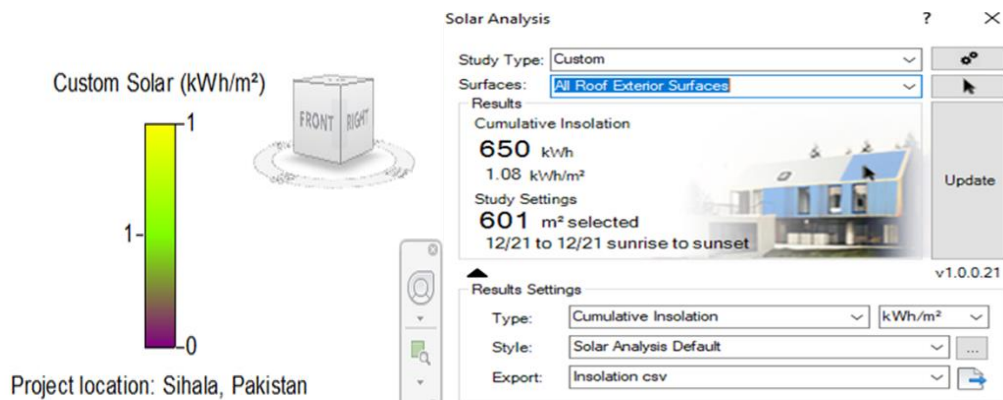
Figure 5: Energy consumption – winter

Table 2 details the summary of energy consumption.

Table 2 Parameters Adopted for Analysis

Season	Day	Average Consumption		Difference
		Kwh	Kwh/m^2	
Summer	21st July	3282	5.47	2667 kwh
Winter	21st December	605	1.08	4.39 Kwh/m^2

5   CONCLUSION

The current study has explored the energy level difference of a four-story conventional educational building for summer and winter season. The longest day and shortest day for summer and winter were opted respectively. Developed 3D model was analysed for energy using sun path analysis. The roof area was major concern of the study. The study observed a considerable difference in

1st International Conference on Advances in Civil & Environmental Engineering, University of Engineering & Technology Taxila, Pakistan

Conference date 22 &23 Feb 2022

energy levels. A 78% change in the energy pattern of building during summer and winter was observed. As more and more amount of energy strikes the roof during summer, thus, energy generation potential during the summer is very high. However, due to extreme hot weather during summer, the energy required to maintain the living environment in the building is also very high. In case of winter less energy strikes the roof and less amount of energy can be generated from the sun.

6   ACKNOWLEDGEMENTS

The study was carried to fulfil the requirement of Bachelor's Degree in Civil Engineering award at Capital University of Science and Technology (CUST). The authors acknowledge Civil Engineering Department and BIM Centre of Excellence, CUST for their valuable support.

REFERENCES

1.   Nawaz, W., M. Arif, and B. *Masood, Energy crises mitigation through available energy potential in Pakistan*. Superior University, 2014: p. 1-10.
2.   Su, X. and X. Zhang. *Environmental performance optimization of window–wall ratio for different window type in hot summer and cold winter zone in China based on life cycle assessment*. Energy and buildings, 2010. 42(2): p. 198-202.
3.   Kurian, C.P., S. Milhoutra, and V. George. *Sustainable building design based on building information modeling (BIM)*. IEEE Conference on Power System Technology 2016.
4.   Omer, A.M. *Energy use and environmental impacts: A general review*. Journal of Renewable and Sustainable Energy, 2009. 1(5): p. 053101.
5.   Yarramsetty, S., M.S. Rohullah, and M. Sivakumar. *An investigation on energy consumption in residential building with different orientation: A BIM approach*. Asian Journal of Civil Engineering, 2020. 21(2): p. 253-266.
6.   Ochedi, E. and A. Taki. *Energy Efficient Building Design in Nigeria: An Assessment of the Effect of the Sun on Energy Consumption in Residential Buildings*. 2019.
7.   Fitriaty, P. and Z. Shen. *Predicting energy generation from residential building attached Photovoltaic Cells in a tropical area using 3D modeling analysis*. Journal of cleaner production, 2018. 195: p. 1422-1436.
8.   Gadelhak, M., M. Aly, and H. Sabry. *High performance facades: the effect of sun breakers on daylighting performance and energy consumption in south oriented office spaces*. Building Solutions for Architectural Engineering. 2013. p. 776-784.
9.   Luo, K. (2018). *Multi-Domain Assessment of a Kinetic Facade Determining the Control Strategy of a Kinetic Façade Using Bim Based on Energy Performance, Daylighting, and Occupants' Preferences.*
10.   Khan, A. and A.N. Ghadg. *Building Information Modelling (BIM) based Sustainability analysis for a construction project*. Proceedings of Sustainable Infrastructure Development & Management (SIDM), 2019.

1st International Conference on Advances in Civil & Environmental Engineering, University of Engineering & Technology Taxila, Pakistan

Conference date 22 &23 Feb 2022

Estimation of Air Pollutants from vehicular emissions – A case study on Jinnah Avenue Road, Islamabad, Pakistan

Abaid Ullah, Mustafa Haidar
Department of Environmental Engineering
University of Engineering & Technology Taxila, Pakistan
abaid.ullah@uettaxila.edu.pk; 18-env-34@students.uettaxila.edu.pk
Qandeel Zahra, Mubashira Sitarish
University of Engineering & Technology Taxila, Pakistan
18-env-1@students.uettaxila.edu.pk; 18-env-25@students.uettaxila.edu.pk

ABSTRACT
Vehicular emissions are major cause of air quality deterioration. This research aims to assess the level of air pollution due to various types of vehicles moving on Jinnah Avenue Islamabad having a total length of 3km.Major pollutants include carbon dioxide (CO_2), hydrocarbons (HC), nitrogen oxides (NO_x) and carbon monoxide (CO). Results identified that CO_2 and CO are emitted in highest proportions compared to other pollutants, and the vehicles contributing more to these pollutants are cars and motorbikes. Moreover, these pollutants are also posing serious health impacts on nearby residents. Outcomes suggest that the reduction of air pollution up to permissible levels is necessary.

KEYWORDS: Air pollution levels, Health effects, Islamabad, Vehicular emissions.

1. INTRODUCTION

In mid-twentieth century, excessive deaths were reported in the United States and Europe due to high concentration of pollutants caused by a series of air pollution disasters [1]. Major pollutants to analyse in vehicular emissions usually include NO_x,SO_2, CO, CO_2, O_3 and hydrocarbons. A similar study on analysis of these major pollutants indicates that diurnal,weakly, and seasonal variations in the concentrations of these pollutants are strongly influenced by emission factors, photochemical process, weather and human habits[2].

The case study area Islamabad is the capital of Pakistan which is the second most beautiful capital in the world having a total population of 2 million [3]. In winters, continuous vehicular emissions cause haze pollution in Islamabad. The five major air contaminants emitting from vehicles include particulate matter (PM), nitrogen oxides (NOx), lead (Pb), sulphur oxides (SOx), and carbon monoxide (CO). The concentration of these contaminants depends on the proportional increase in vehicles [4].

Therefore, an attempt has been made to estimate the pollutant levels emitted due to vehicular emissions on Jinnah Avenue having a total length of 3km. So that air pollution control strategies could be recommended as per the significance of individual pollutant concentration levels.In this study, manual method was used to estimate the total emissions generated by various vehicle types during different hours of the day. For this purpose, vehicle passing data during different

1st International Conference on Advances in Civil & Environmental Engineering, University of Engineering & Technology Taxila, Pakistan

Conference date 22 &23 Feb 2022

times of the day was collected to estimate the total pollution load caused by each considered vehicle type.

2. LITERATURE AND STUDY

2.1. Air Pollution statistics and status

Abruption in global population has causedsignificant increase in numbers of road vehicles. This substantial increase in road vehicle usage is resulting into ever highest concentrations of pollutants being emitted.In 2019, 10.17 billion tons of just one pollutant (CO_2) were emitted only in china [5], similarly it was reported by [6] that year 2019 witnessed 6 million tons of NOx emissions by vehicles in china.

Major sources of air pollution in Islamabad include vehicular and industrial emissions, burning of solid waste, brick kilns, and natural dust. Recent study revealed that suspended particulate matter in the city is 6.5 times higher than world health organization (WHO) guidelines (i.e., $120\mu g/m^3$ for 24hrs) and 3.8 times higher than Japanese guidelines (i.e., $200\mu g/m^3$ for 1hr), identified that 30% of the data collected from the study area regarding NOx levels exceed WHO guideline (i.e., 40-60 ppb/d)**.**
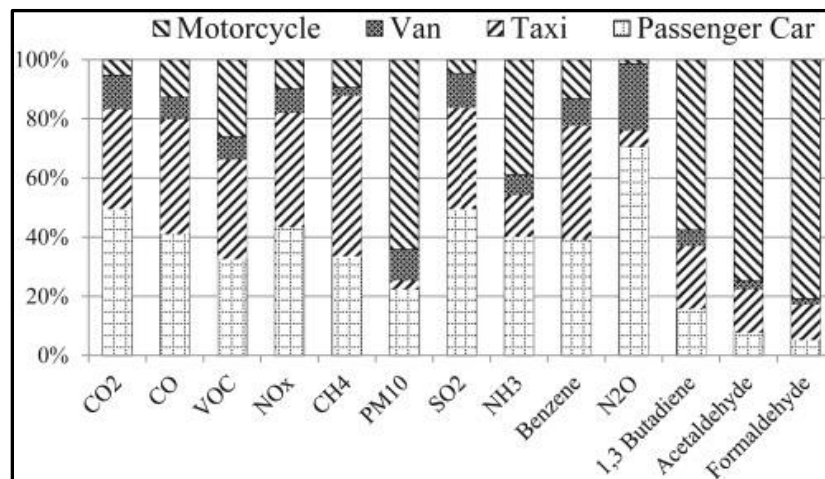
Figure 1: (Share of each vehicle type in pollutant emissions in Islamabad)[7]

CO is one of the emission gases from gasoline motor vehicles, passenger cars and taxis are the major type of vehicles contributing to CO pollution in Islamabad [7].

2.2. Effects of air pollution

High air pollution levels cause a range of health implications for young and elderly people including asthma, bronchitis, and conjunctivitis [8].

Pollutants of carbon adversely affect the health of victim in two ways, either directly through inhalation causing headache, breathlessness, and even delirium [9] or indirectly through climate change. NOx on the other hand produce secondary pollutants i.e. ozone which fundamentally causes respiratory health effects and cardio-metabolic risks [10].

High levels of particulate matter (PM) in the environment cause atmospheric turbidity which tend to reduce the visibility. Besides visibility, it also pose far reaching impacts on the health of

1st International Conference on Advances in Civil & Environmental Engineering, University of Engineering & Technology Taxila, Pakistan

Conference date 22 &23 Feb 2022

human beings thereby causing acute or chronic diseases.Toxicological literature links cardiovascular diseases, premature deaths and respiratory morbidity with long term exposures to PM [11].

Apart from health implications, rising air pollution levels are also the main contributors in drastic climate change, acid rain, damage to soil, and fresh water bodies [12].

3. METHODOLOGY AND PROCEDURE ADOPTED

The area of our concern is Jinnah Avenue Road located in Islamabad Pakistan. Its total length is almost 3km. Manual method was used to estimate the total emissions by different vehicles during different hours of the day in the case study area. One-month data regarding the total number of different vehicles passing through the Jinnah Avenue was collected. Various types of vehicles considered for this study include cars, motorbikes, vans, and buses/trucks. The emission factors for individual pollutants generated from these vehicle types were collected from comprehensive literature review.

The emission levels were calculated for peak and normal times, which varies with respect to the density of traffic at a specific time.
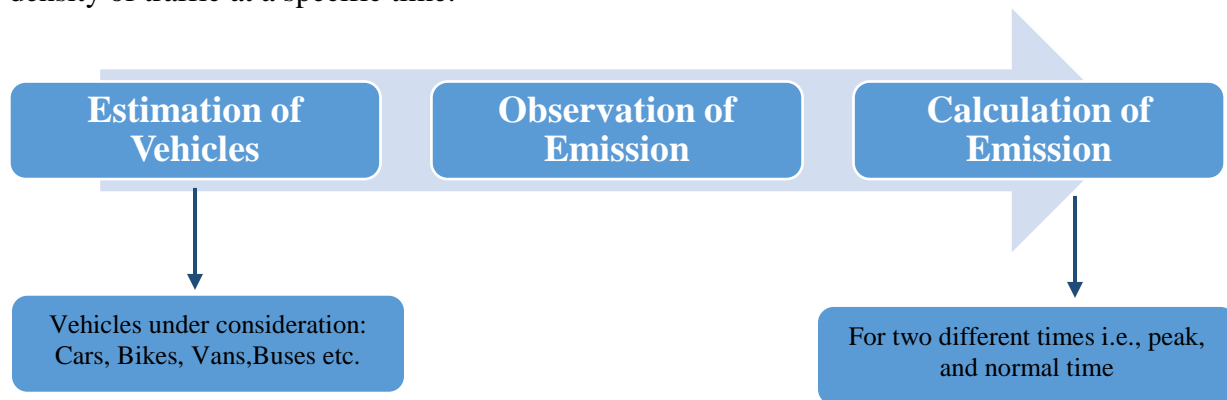
Figure 2: Methodology

4. RESULTS AND DISCUSSION

Pollutant levels emitted from different types of vehicles were calculated. Among different vehicle types, cars were found to be the major contributor of air pollution. These results are in coherence as identified in Europe by [13]. These results indicated that the number of cars were in greater proportion in the observed vehicle fleet, otherwise buses/trucks intrinsically cause more pollution due to comparatively high horse power and volumes [14-16]. This observation doesn't necessarily mean that cars have high pollution capacity than buses or vans but rather indicates that, the significantly large proportion of cars in the vehicular fleet make them the major sources of air pollutants in this case study. Table 1 shows the observed emission factors corresponding to each vehicle type.

Table 1: Emissions from different types of vehicles in g/km.

Vehicle type	CO_2	HC	NOx	CO
Car	690	5.25	2.61	39.18
Bike	63	2.4	0.45	6
Vans	525	0.18	1.5	1.92
Bus	303	10.8	0.0915	6.3

1st International Conference on Advances in Civil & Environmental Engineering, University of Engineering & Technology Taxila, Pakistan

Conference date 22 &23 Feb 2022

Table 2 shows the pollutant emissions during morning, noon and evening peak hours. It indicates that carbon dioxide emissions from transport sector exceed all other vehicular emissions as highlighted by USEPA. It is evident that the main contributors towards carbon dioxide emissions are cars and bikes, which constitute the major percentage of traffic in selected area of research. Furthermore it can be observed from the table that noon peak hour emissions for all the pollutants are the highest among other analysed peak hours. These results are in coherence with the traffic percentage compositions provided by the ministry of communication, Pakistan.

Table 2: Total average emission for morning, noon and evening peak hours in g/km.

Vehicle type	Morning peak hour emissions					Noon peak hour emissions					Evening peak hour emissions				
	Total No.	CO_2	HC	NOx	CO	Total No.	CO_2	HC	NOx	CO	Total No.	CO_2	HC	NOx	CO
Cars	1199.07	827356	6295.1	3129.6	46979	2426.2	1674055	12737.38	6332.3	95057.2	1573.8	1085922	8262.5	4107.6	61661.5
Bikes	369.9	23305.8	887.8	166.5	2219.6	614.1	38688.3	1473.8	276.3	3684.6	374.9	23616.6	899.7	168.7	2249.2
Vans	115.0	60392.5	20.7	172.5	220.9	197.7	103775	35.58	296.5	379.5	130.6	68565	23.5	195.9	250.7
Bus	22	6666	237.6	2.0	138.6	26.8	8130.5	289.8	2.6	169.1	12.9	3918.8	139.7	1.2	81.5
Total emissions		917720.3	7441.3	3470.6	49558.1		1824648.8	14536.6	6907.6	99290.3		1182022	9325.3	4473.4	64242.9

It is evident from Table 2 that maximum emissions are emitted during noon time. The maximum emission levels emitted by various considered vehicle types are shown in Figure 3.
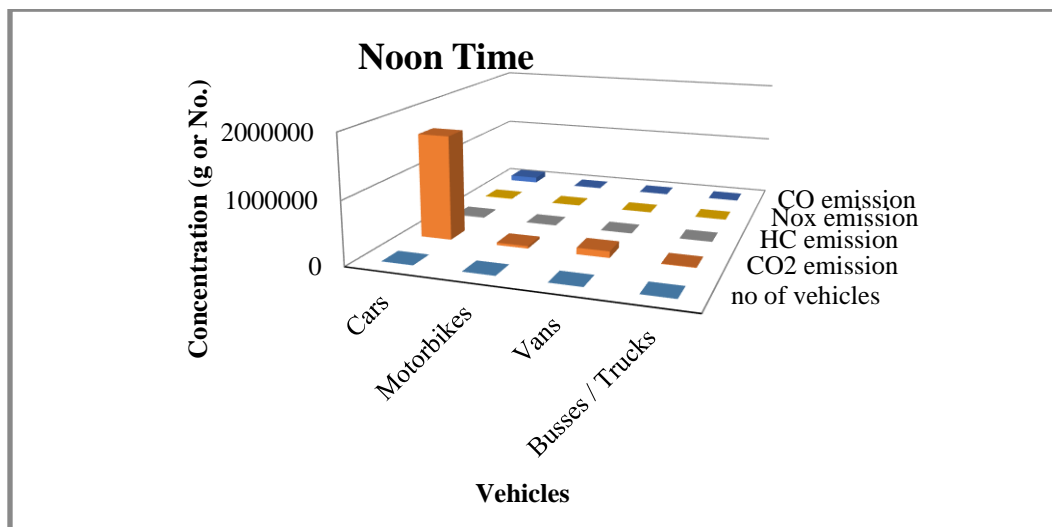
Figure 3: 3-D graph showing the maximum emission concentration of selected vehicles during noon time.

5. CONCLUSION

Concentrations of the understudy pollutants were successfully determined with respect to both diurnal and vehicular type variations. Outcomes revealed that among all the considered pollutants, carbon dioxide and carbon monoxide constitute a great proportion of vehicular pollutants. Of all the considered vehicles, private cars and bikes contribute the most towards air emissions. Islamabad experiences the maximum pollution load during noon peak hour. As per policy point of view, these emissions can be controlled by shifting towards the use of public transport (carpooling) and by using a fuel of high-octane number.In future, this study can be

1st International Conference on Advances in Civil & Environmental Engineering, University of Engineering & Technology Taxila, Pakistan

Conference date 22 &23 Feb 2022

extended further by investigating, comparatively broader area, using remote sensing and geographical information system (GIS).

6. REFERENCES

1. Thompson, C.a., *Health Effects of Air Pollution: A Statistical Review.* Logan and Glasg., 1961: p. 34.
2. Masiol, M., et al., *Analysis of major air pollutants and submicron particles in New York City and Long Island.* Atmospheric Environment, 2017. **148**: p. 203-214.
3. Abeer, N., et al., *Health risk assessment and provenance of arsenic and heavy metal in drinking water in Islamabad, Pakistan.* Environmental Technology & Innovation, 2020. **20**: p. 101171.
4. Ahmad, D.I., *Air Quality in Rawalpindi and Islamabad*. National Cleaner Production Center for Fuels: Islamabad. p. 38.
5. Wei, F., et al., *Energy and environmental efficiency of China's transportation sectors considering CO2 emission uncertainty.* Transportation Research Part D: Transport and Environment, 2021. **97**: p. 102955.
6. Sulaymon, I.D., et al., *COVID-19 pandemic in Wuhan: Ambient air quality and the relationships between criteria air pollutants and meteorological variables before, during, and after lockdown.* Atmospheric Research, 2021. **250**: p. 105362.
7. Shah, I.H. and M. Zeeshan, *Estimation of light duty vehicle emissions in Islamabad and climate co-benefits of improved emission standards implementation.* Atmospheric Environment, 2016. **127**: p. 236-243.
8. UNEP/WHO, *Mapping and Analysis of Air Pollution in Nairobi, Kenya.* 1992: p. 9.
9. Sechzer, P.H., et al., *Effect of CO2 inhalation on arterial pressure, ECG and plasma catecholamines and 17-OH corticosteroids in normal man.* Journal of Applied Physiology, 1960. **15**(3): p. 454-458.
10. Wang, C., et al., *Impact of ozone exposure on heart rate variability and stress hormones: A randomized-crossover study.* Journal of Hazardous Materials, 2022. **421**: p. 126750.
11. Vodonos, A., Y.A. Awad, and J. Schwartz, *The concentration-response between long-term PM2.5 exposure and mortality; A meta-regression approach.* Environmental Research, 2018. **166**: p. 677-689.
12. AcidRain/EPA, *EPA Acid rain Program*, EPA, Editor. 2000,2001: United States. p. 48.
13. Ehrnsperger, L. and O. Klemm, *Air pollution in an urban street canyon: Novel insights from highly resolved traffic information and meteorology.* Atmospheric Environment: X, 2022: p. 100151.
14. Sharmilaa, G. and T. Ilango, *A review on influence of age of vehicle and vehicle traffic on air pollution dispersion.* Materials Today: Proceedings, 2021.
15. Wikipedia. *European Emission Standards*. 2012; Available from: http://en.wikipedia.org/wiki/European_emission_standards.
16. ECF. *Carbon di Oxide*. 2013 [cited 2013; Available from: http://www.ecf.com/news/how-much-co2-does-cycling-really-save/.

1st International Conference on Advances in Civil & Environmental Engineering, University of Engineering & Technology Taxila, Pakistan

Conference date 22 &23 Feb 2022

Lateral Load Response of Full Scale Beam-Column Joints

Abdul Wadood, Muhammad Fahim, Muhammad Fahad
University of Engineering & Technology Peshawar, Pakistan
hmf.engr@gmail.com; drmfahim@uetpeshawar.edu.pk

ABSTRACT

Beam-column joints are the most critical regions in any reinforced concrete buildings as demonstrated in the past earthquakes. To understand the behaviour of code-compliant beam-column joints, two full scale specimens are tested under quasi static cyclic loading. The results are presented in the form of average back bone curves and its bilinear idealization which is used to determine various code defined performance levels. The average values of immediate occupancy, life safety, and collapse prevention levels are 26.3 mm, 89.6 mm, and 119.5 mm, respectively. The results obtained may be used to calculate response modification factor for reinforced concrete buildings in Pakistan.

KEYWORDS: Beam-Column Joints, Quasi-static, Performance Levels.

1 INTRODUCTION

Beam-column joint is one of the most critical region in any reinforced concrete buildings. Many buildings in the past earthquakes have experienced damages/collapse due to failure in the beam-column regions. The importance has long been recognised by researchers around the world and extensive research have been carried out to understand the behaviour of beam-column joints under lateral loading [1-3]. After Kashmir earthquake of 2005, Pakistan Building Code was developed, mainly based on UBC-97 [4]. However, indigenous research is required to understand the behaviour of reinforced construction connections to arrive at suitable values of response modification factor. This research is an attempt to understand the behaviour of RC connections under cyclic loading to help in the determination of response modification factor for RC buildings in Pakistan.

2 TEST SPECIMENS AND SETUP

Two full scale specimens were tested under quasi static loading. The cross sectionals and reinforcement details are shown in Figure 1. The average compressive strength of concrete for specimen 1 and 2 was 2.27 ksi and 3.20 ksi. To control the tensile failure in the model ASTM A615 Grade 60 steel was used as reinforcement in all specimens.

1st International Conference on Advances in Civil & Environmental Engineering, University of Engineering & Technology Taxila, Pakistan

Conference date 22 &23 Feb 2022
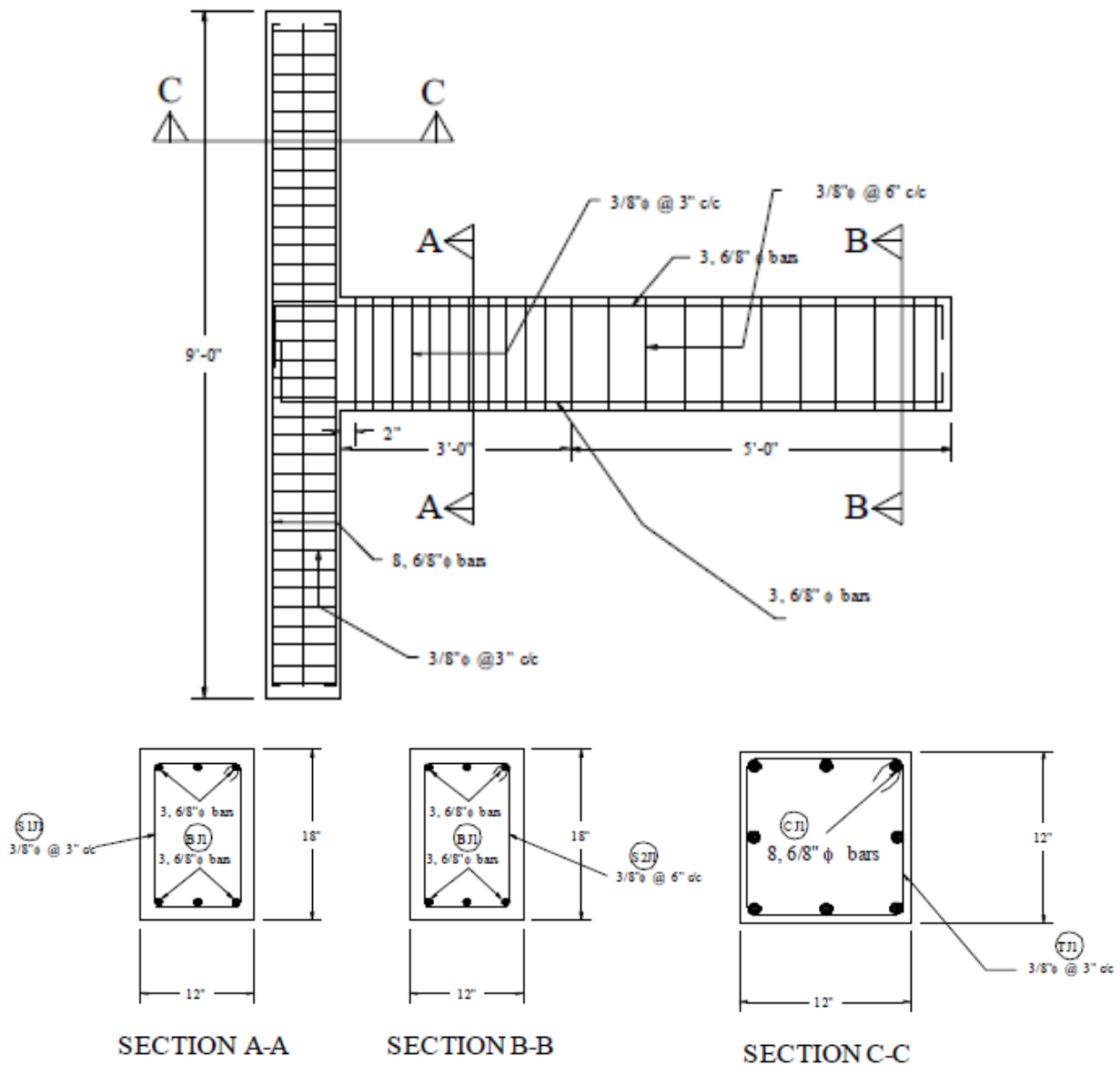
Figure 1. Cross section and reinforcement details of specimens

The test setup for beam column connection is shown in Figure 2. It is worth mentioning here that the column element is supposed to act as an elastic element, which shows that it is stiffer than beams in flexure.

1st International Conference on Advances in Civil & Environmental Engineering, University of Engineering & Technology Taxila, Pakistan

Conference date 22 &23 Feb 2022
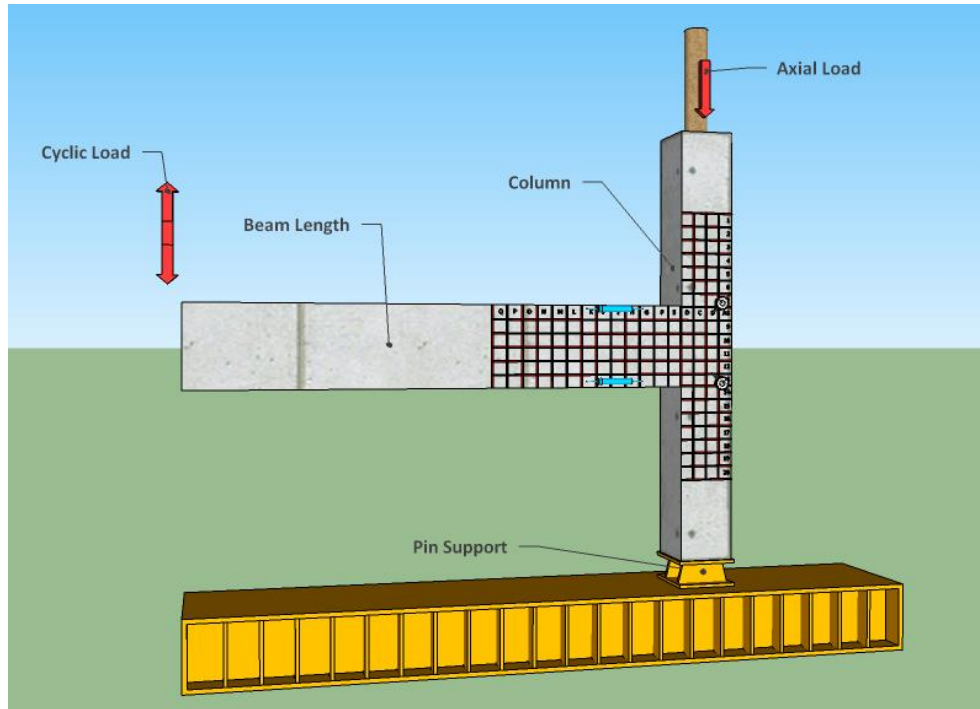
Figure 2. Schematic representation of beam-column connection

The column section was axially loaded with constant compressive load and was kept at 15% of the column axial capacity equals to 33 tons for the constructed model.

3   RESULTS AND DISCUSSIONS

The positive and negative backbone curve was developed by joining the peak ordinates of positive and negative hysteresis curves respectively. The positive and negative backbone curve were then interpolated and averaged to get an average backbone curve. Bilinear elasto-plastic curves were developed from average backbone curves using equal energy principle. By this principle, both the total and elastic energy under experimental and idealized curves were kept equal. The bilinear curve of both specimens are shown in Figure 3.

1st International Conference on Advances in Civil & Environmental Engineering, University of Engineering & Technology Taxila, Pakistan

Conference date 22 &23 Feb 2022
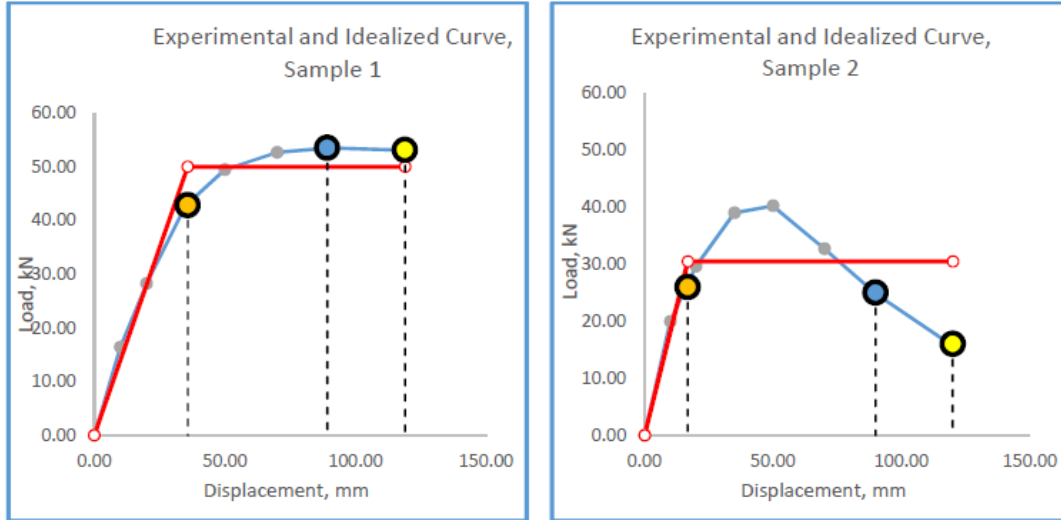
Figure 3. Bilinear Idealization of Both Specimen

Various strength parameters obtained from bilinear curve are summarized in Table 3-1. It can be noted that specimen 1 shows high yield load and displacement as compared to specimen 2, but shows less stiffness as compared to specimen 2.

Table 3-1 Various Parameters from Bilinear Curve

Property	Specimen 1	Specimen 2
Yield Displacement	35.8 mm	16.9 mm
Ultimate Displacement	119 mm	120 mm
Yield Load	50 kN	30.5 kN
Lateral Stiffness	1.4 kN/mm	1.8 kN/mm

ASCE/SEI 41-06 defines various performance levels for structure, which are summarized in Table 3-2. The immediate occupancy (IO) level correspond to first yield of system. The collapse prevention (CP) level is drift/displacement corresponding to ultimate level, where 20% reduction in lateral strength of test specimen has taken place. Life safety (LS) level is the drift/displacement corresponding to 75% of CP level. It can be noted that specimen 1 shows higher displacement at IO as compared to Specimen 2. Both specimens show similar displacement at LS and CP level.

Table 3-2 Displacement Corresponding to Performance Levels Specified by ASCE

Performance Levels	Specimen 1	Specimen 2
IO	35.8 mm	16.8 mm
LS	89.2 mm	90 mm
CP	119 mm	120 mm

1st International Conference on Advances in Civil & Environmental Engineering, University of Engineering & Technology Taxila, Pakistan

Conference date 22 &23 Feb 2022

4   CONCLUSIONS

This study was concluded on two code compliant RC beam column joint connections. Based on the test results and behaviour of specimens, the following conclusion can be derived from analysis.

- The peak loads of specimen 1 and 2 were 69.5 and 40.5 kN respectively.

- It can be noted that specimen 1 shows higher displacement at IO as compared to Specimen 2.

- Both specimens show similar displacement at LS and CP level.

5   REFERENCES

1.   Badrashi, Y.I., *response modification factors for reinforced concrete buildings in pakistan*, in *Civil Engineering Department*. 2016, University of Engineering and Technology, Peshawar.
2.   Khan, F.A., et al., *Evaluation of code compliant/non-compliant ECC-RC IMRF structures.* Structures, 2021. **32**: p. 1634-1645.
3.   Ullah, R., et al., *Effect of eccentricity in reinforced concrete beam-column-slab connection under cyclic loading.* Frontiers of Structural and Civil Engineering, 2021. **15**.
4.   BCP/SP-07, *Building Code of Pakistan (Seismic Provisions - 2007).* 2007, Government of Islamic Republic of Pakistan, Ministry of Housing & Works, Islamabad, Pakistan.

1st International Conference on Advances in Civil & Environmental Engineering, University of Engineering & Technology Taxila, Pakistan

Conference date 22 &23 Feb 2022

Design Optimization of Precast Reinforced Box Culvert with the Application of Finite Element Modeling and Analysis

Zia Uddin, Hafiz Ahmad Waqas,
M. Husnain, M. Ibrahim, Hammad Zaib, Muhammad Naveed
Ghulam Ishaq Khan Institute of Engineering Sciences and Technology, Pakistan
u2018524@giki.edu.pk; hafiz.waqas@giki.dedu.pk; u2018282@giki.edu.pk;
u2018558@giki.edu.pk; u2018553@giki.edu.pk; ; m.naveed@giki.edu.pk,

ABSTRACT

Culverts are small bridges that provides safe passage for crossing waterways over railroad and highways. The strong and economical culverts are certainly desirable and the availability of modern and convenient computational tools can offer great liberties to realize this goal. Among the different types, precast reinforced box culverts are known to be strong, safe, stiff, and economical alternative to others. These are easy to cast and have a larger water flowing capacity. This paper discusses the Finite Element Modeling (FEM) based design optimization approach to develop efficient and economical fabrication schemes for producing precast box culverts. A 3-D model of a typical box culvert was constructed in ABAQUS software to develop the capacity curves of the structure. Design improvements are suggested based on analysis outcome and visualization of stress distribution in the structure.

KEYWORDS: Pre-cast Box culvert, Finite element Analysis, Eigen value Analysis, Haunches

1   INTRODUCTION

Box culverts are crucial for crossing waterways beneath railroads, highways, and flyovers. Typically, these are provided to counter the poor bearing capacity of soil. There are two basic types, the rigid one (made of concrete) and the flexible one (made of steel). This classification is based upon the soil to structure interaction and how the structural loads are transferred to the soil by the underground structure. Rigid culverts are intended to resist the flexural loads whereas the flexible culverts don't. Selection of the shape of the box is based on the ease with which a box of reinforced concrete culvert is casted and the availability of flow capacity. These box-shaped culverts may also be made for more torsional resistant by adding internal web walls. Conventionally, the inner span length has been considered as 3.5 m [1]. For higher flows, this considered span becomes insufficient, and providing multiple sections become essential. Consequently, a larger span culvert might be a cost-effective alternative but its efficacy need to be explored. The effectiveness of a larger span culvert is evaluated in the present research using Finite Element Modelling (FEM) technique.

1st International Conference on Advances in Civil & Environmental Engineering, University of Engineering & Technology Taxila, Pakistan

Conference date 22 &23 Feb 2022

2   DESCRIPTION OF MODEL AND METHODOLOGY

2.1   Geometry

The box culvert geometry is composed of concrete and steel reinforcement. The assemblies of concrete box of outer size of 2.52 m × 4.8 m × 1.5 m and reinforcement cage were made in ABAQUS software as shown in Figure 1. The reinforcement cage included horizontal and vertical main and distribution bars having rebar dimeter of 16 mm. The inner span of the culvert is 4.0 m whereas slab and wall thickness is 0.4 m.
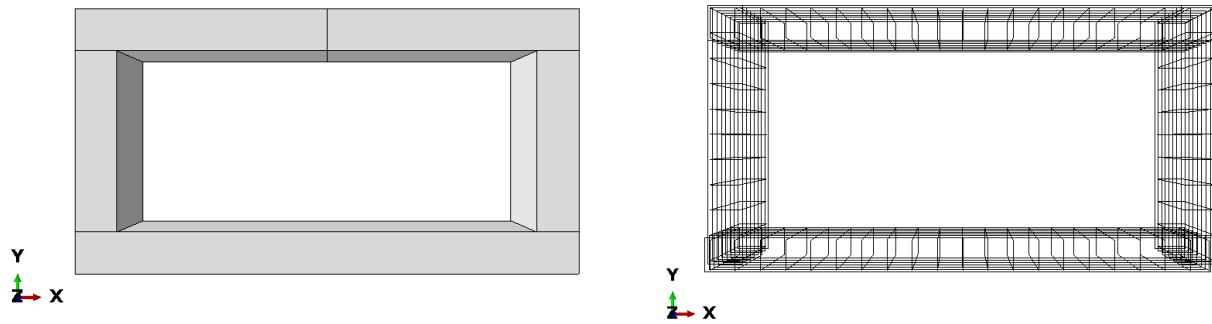
Figure 1 Assembly of concrete box and reinforcement cage

2.2   Materials and Meshing

Both linear and non-linear properties of the materials were retrieved from the literature to simulate the material behaviour [2]. Table 1 shows the properties of concrete and steel used in the modeling. The 3-D solid elements for concrete and 3-D wire elements for reinforcement were adopted for modeling. The concrete parts were meshed with Continuum, 3-Dimensional, 8 Node Elements with Reduced integration (C3D8R) and 3-Dimensional, 2 Node truss elements were used to mesh the steel reinforcement. The uniform mesh size of 100 mm was employed for all components.

Table 1 Properties of materials

Description	Concrete	Reinforcement
Modulus of elasticity, E (MPa)	32500	200000
Poisson's Ratio	0.2	0.2
Density (Kg/m^3)	2400	7850
Tensile strength (MPa)	2.39	400
Compressive strength (MPa)	26.8	400

1st International Conference on Advances in Civil & Environmental Engineering, University of Engineering & Technology Taxila, Pakistan

Conference date 22 &23 Feb 2022

2.3 Interactions, Constrains, Loading and Boundary Conditions

Embedded region algorithm was introduced to develop bond between concrete and steel. The bottom surface of culvert was modelled as fixed surface and appropriate loading was applied on different surfaces to properly constrain the model. The loads of asphalt layer of 75 mm and soil layer of 0.3 m was stacked over the top surface whereas lateral earth pressure and hydrostatic pressure were placed at the desired locations [3]. Figure 2 exhibits the loading and boundary conditions in the model.

To develop the capacity curve, the displacement controlled loading of 120 mm was applied at the reference point as shown in Figure 2. The reference point interacted with the associated surface through kinematic coupling procedure. Dynamic explicit analysis step was executed to obtain the load vs. displacement curve at the reference point.

Kinematic coupling of reference point and interacting surface
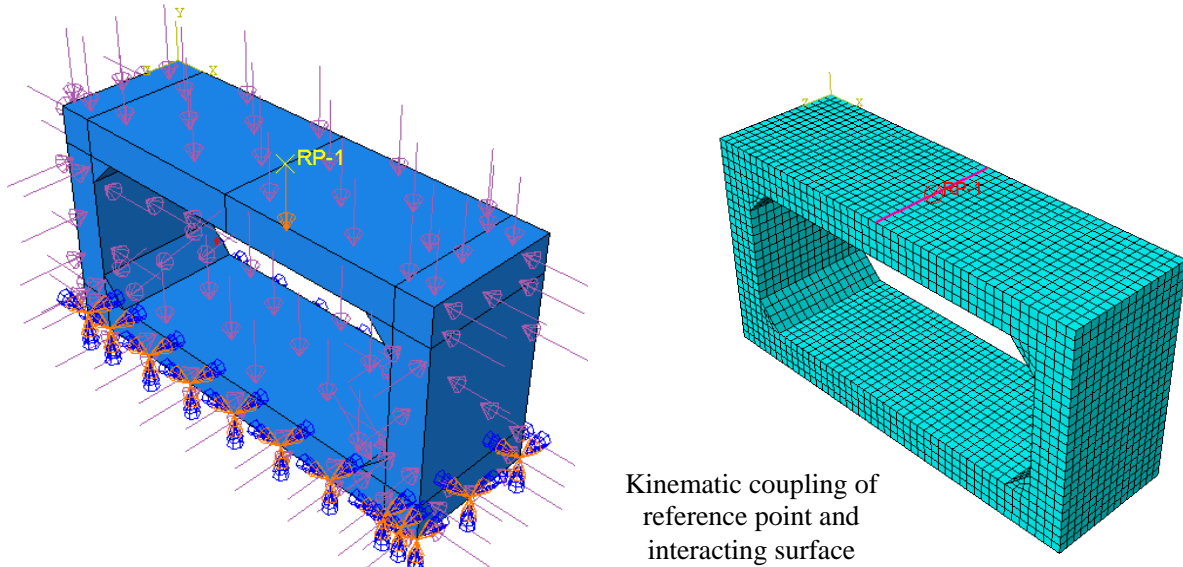
Figure 2 Description of loads and Boundary conditions

3 RESULTS AND DISCUSION

The completion of analysis yielded multiple outputs and stress distribution plot is exhibited here in the Figure 3. The load displacement curve at reference point, characterising the capacity of precast culvert, is further provided in the Figure 4. The maximum load carrying capacity of about 2000 kN is achieved. As shown in Figure 3, the stress is concentrated at the mid span and joint of slab and wall. The increase in capacity could be achieved with the provision of additional reinforcement at the optimum locations.

1st International Conference on Advances in Civil & Environmental Engineering, University of Engineering & Technology Taxila, Pakistan

Conference date 22 &23 Feb 2022
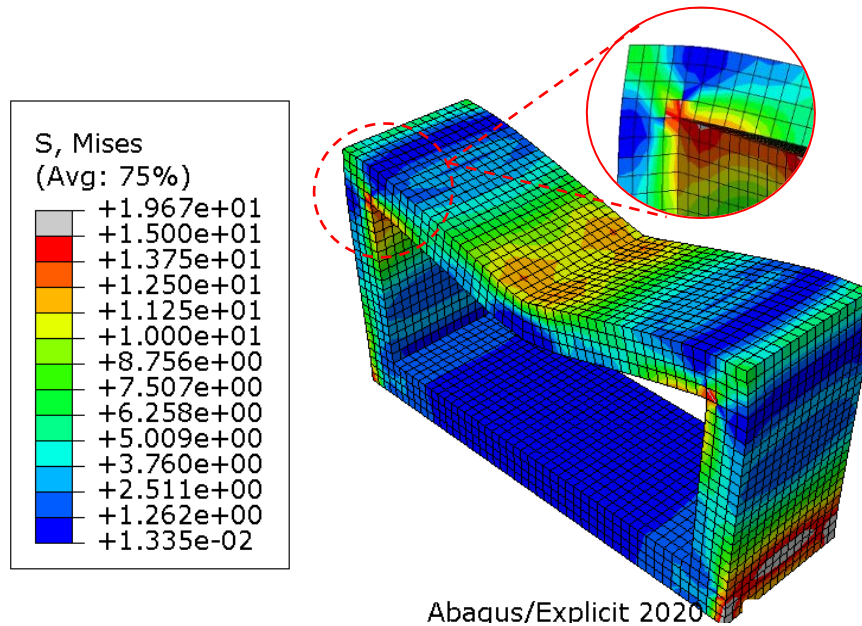
Figure 3 Stress distribution under displacement control loading
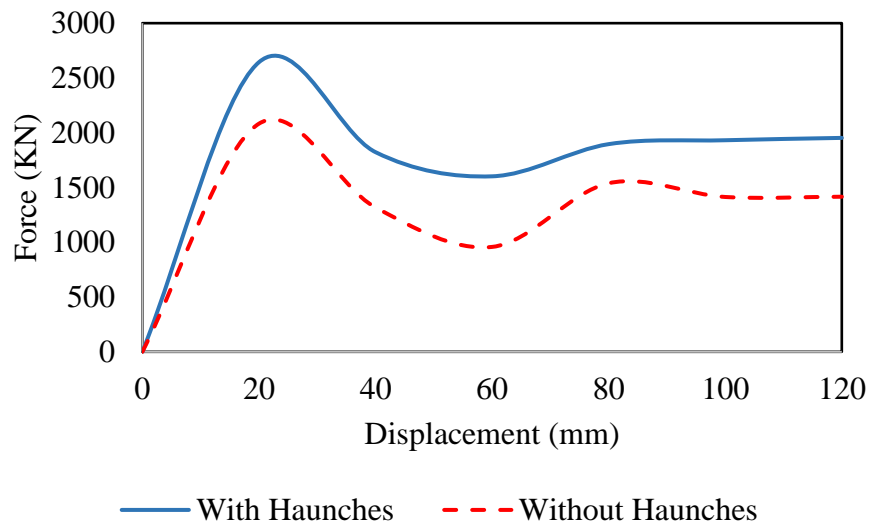
Figure 4 Load vs. displacement curves

3.1 Design optimization

A 0.3 m × 0.3 m haunch and additional steel reinforcement are provided at the location of stress concentration i.e. inner corners to systematically and promptly observe the improvements in

1st International Conference on Advances in Civil & Environmental Engineering, University of Engineering & Technology Taxila, Pakistan

Conference date 22 &23 Feb 2022

structural response and over all capacity. The quick changes in the model are presented in the Figure 5. The acquired capacity curve is also placed next to the curve of base model in Figure 4 which exhibits the gain in overall capacity by about 25%. Further optimization in the design process could be realized if additional iterations are carried out if deemed necessary.
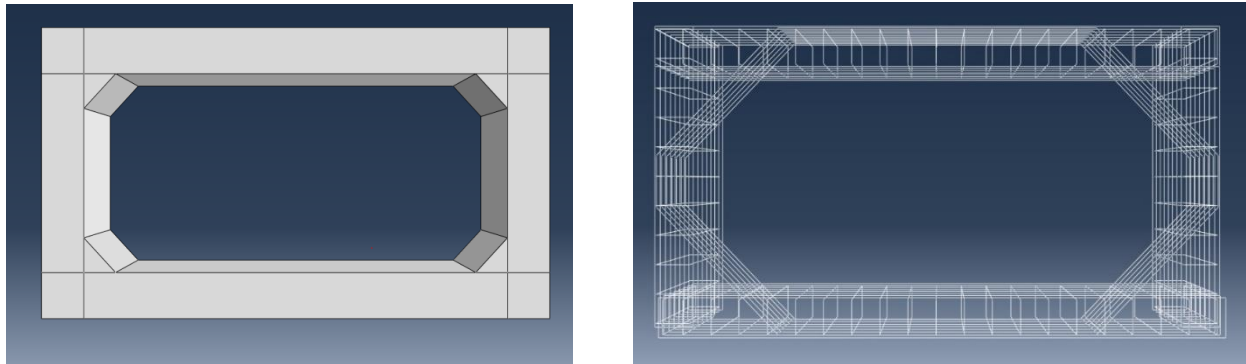
Figure 5 Introduction of haunches and additional reinforcement for design optimization

4   CONCLUSION

This paper demonstrated the effectiveness of FEM technique to swiftly incorporate the design changes and grasp the effects of introduced optimizations. The presented methodology authenticates the usefulness and appropriateness of FEM tools to conveniently and promptly execute the design optimization tasks. The FE modeling of precast reinforced box culvert revealed that joint of slab and wall is the location of stress concentration where improved results of retrofit/reinforcement could be gained. The comparison of capacity curves confirmed that haunches can increase the load carrying capacity by about 25%. However, the performance of box culvert with larger span under seismic actions is yet be investigated to comprehensively recognise the practicality of different design optimization methods for economical and safe design of infrastructure.

REFERENCES

1.   Zenagebriel Gebremedhn, Guofu Qiao, Jilong Li, *Finite Element Modeling and Analysis of Precast Reinforced Concrete U-Shaped Box Culvert Using ABAQUS*. American Journal of Civil Engineering, 2018. **6**(5): 162-166.
2.   Xiao, Y., et al., *Concrete plastic-damage factor for finite element analysis: Concept, simulation, and experiment*. Advances in Mechanical Engineering, 2017. **9**(9) 1–10.
3.   Ayaanle Maxamed Ali, *Manual RC Box Culvert Analysis and Designing*. International Journal of Innovative Science and Research Technology,2020. **5**.

1st International Conference on Advances in Civil & Environmental Engineering, University of Engineering & Technology Taxila, Pakistan

Conference date 22 &23 Feb 2022

Evaluation of GoogLenet, Mobilenetv2, and Inceptionv3, pre-trained convolutional neural networks for detection and classification of concrete crack images

Waqas Qayyum

Department of Civil Engineering, University of Engineering & Technology Taxila, Pakistan
waqas.qayyam@students.uettaxila.edu.pk

AIMAN ALJUHNI

Eng.aljuhni@gmail.com

Nida Chairman

Department of Civil and Architectural Engineering, University of Westminster, UK
N.chairman@westminster.ac.uk

Afaq Ahmad

Department of Civil Engineering, University of Engineering & Technology Taxila, Pakistan

Afaq.Ahmad@uettaxila.edu.pk

ABSTRACT

Crack detection and classification are critical tasks in inspecting civil engineering structures. Convolutional neural networks (CNNs), a subset of deep learning (DL), exhibit extraordinary potential for automatically classifying images. Different pre-trained CNNs are available for the classification of images. The current study evaluates three pre-trained neural networks, i.e., GoogLenet, Mobilenetv2, and Inceptionv3. For the classification of images between cracked (C) and un-cracked (UC) images, models are trained on 48000 images, while for the classification of images between diagonal crack (DC), horizontal crack (HC), and vertical crack (VC) images, models are trained on 24000 images. For C and UC classification, the accuracy of Googlenet, Mobilenetv2, and Inceptionv3 are 95.7 %, 96.3%, and 97.2%, respectively. While for the classification of DC, HC, and VC, the accuracy of Googlenet, Mobilenetv2, and Inceptionv3 is 84%, 91%, and 92% taking DC as a positive case. Similarly, HC's positive case accuracies are 92%, 96%, and 95%, and for VC, accuracies are 91%, 95%, and 96%, respectively. For the classification of C and UC, the training time for GoogLenet, Mobilenetv2, and Inceptionv3 are 3.76, 7.39, and 15.25 hours. While for DC, HC, and VC, training time is 2.17, 3.71, and 7.5 hours, respectively. The major drawback of Inceptionv3 is that its training time is greater compared to GoogLenet and Mobilenetv2.

KEYWORDS: Crack detection, Convolutional Neural Network (CNN), Pre trained Models

1st International Conference on Advances in Civil & Environmental Engineering, University of Engineering & Technology Taxila, Pakistan

Conference date 22 &23 Feb 2022

1   INTRODUCTION

Structural health monitoring is the process of developing a system for identifying degradation in aerospace, civil, and mechanical engineering infrastructure (SHM). This procedure entails monitoring a structure or mechanical system over time via periodically spaced measurements, extracting damage-sensitive features from these measurements, and statistically analysing these features to ascertain the current system health state [1]. Thousands of dollars are spent on purchasing various instruments and assets to detect defects in critical infrastructure such as roads, bridges, buildings, and bodies of water [2]. Roads, bridges, buildings, and pavements are frequently subjected to tremendous physical stress from natural catastrophes like earthquakes and bombings. These occurrences can cause structural collapse or physical damage in the form of cracks [2]. It also arises in structure due to load and, over time, drastically lowers the structure's performance and durability [3].

Owners have benefited from the adoption of digital technology to arrange monitoring and inspection activities effectively. Recent advances in computer vision have resulted in the development of deep convolutional neural networks (CNN) for picture categorization and object detection [4][5]. CNN is one of the most widely used deep learning networks. The CNN's fundamental architecture consists of three layers, i.e., convolutional layer (feature extraction), pooling layer (dimensionality reduction), and fully connected layer. Using the picture as input, the convolutional layer combines a limited number of filters (given by the kernel or filter size) to extract as many relevant characteristics as possible. The pooling layer downscales the resulting features, hence lowering the total processing cost of the network. To better understand the data, the convolution-pooling sequences can be repeated several times.

In the same way, high-dimensional features are extracted from the input by linking one or more fully connected layers for classification [6]. Zhang et al. presented CNN-based architecture (Cracknet) to detect cracks on the pavement [2,7]. Yang et al. employed a "fully convolutional network" (FCN) to segment fractures in photos of walls and pavements [8]. The FCN model is trained on various crack pictures [2,8].

 The present study focuses on the two classifications of images. The first classification (C-UC classification) is between cracked (C) and un-cracked (UC), second classification (DVH classification) among cracked category, i.e., Diagonal crack (DC), Horizontal crack (HC.), and Vertical crack (VC.). The pre-trained neural network used for classification is Googlenet [9], Inceptionv3 [10], and Mobilenetv2 [11]. The performance of these networks is analysed. Training of the models is done using open-source crack image datasets [13] online available, while for testing, a dataset containing concrete crack images from buildings and pavement in the U.E.T. Taxila campus is used.

2   METHODOLOGY

In the first steps, concrete crack images are collected from open sources and buildings and pavement around the campus. Then the second step is pre-processing, where irrelevant data is removed, noises and shadows are removed. The third step is the labelling of the data. For the C-UC classification, images are divided between cracked and un-cracked images, while for the DVH

1st International Conference on Advances in Civil & Environmental Engineering, University of Engineering & Technology Taxila, Pakistan

Conference date 22 &23 Feb 2022

classification, images are divided into diagonal, horizontal, and vertical crack images. The fourth step is the training of the models, which is done using labelled open-source datasets received from the previous step. The fifth step is testing the trained model, which is done using images taken from the campus building and pavement. The whole process is summarised in Figure 1.

| Data Collection | Preprocessing | Labelling | Training Model | Testing Model |
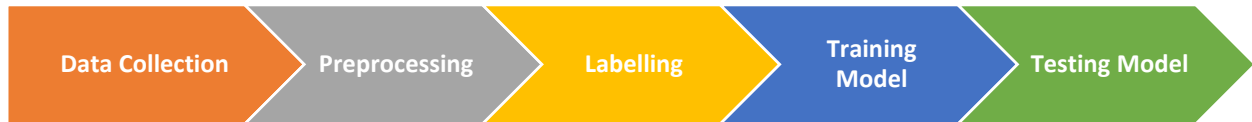
Figure 1: Schematic diagram of a methodology

2.1 Concrete crack Image database

For the training and validation, the percentage is set at 70% and 30%, respectively. The number of images for the C-UC classification in each category is set at 24000, while the DVH classification in each category is 8000. The number of test images taken for the C-UC classification is 300 images in each category, and for the DVH classification, it is 100 images in each category. Crack image databases are summarised in Figure 2 and 3.
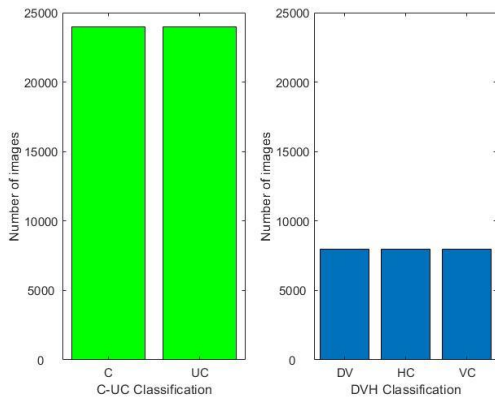
Figure 2: Number of Images for Training and Validation
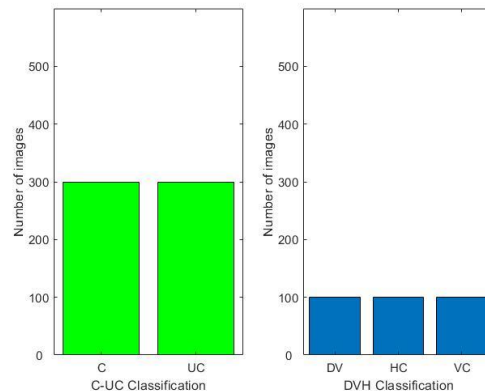
Figure 3: Number of images for testing

2.2 Pre-trained convolutional neural network

Several pre-trained convolutional neural networks are available for classification. A comparative plot between all the available architectures based on accuracy, prediction time, and sizes, as show in Figure 4.

1st International Conference on Advances in Civil & Environmental Engineering, University of Engineering & Technology Taxila, Pakistan

Conference date 22 &23 Feb 2022
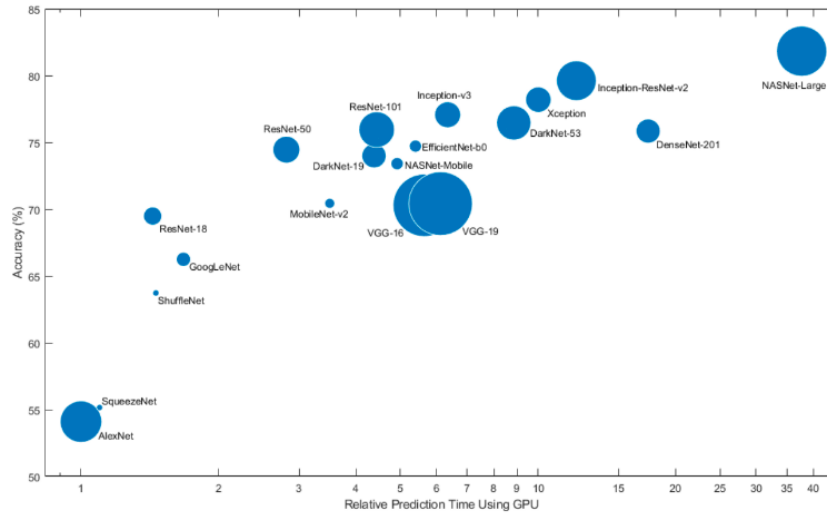
Figure 4: Accuracy vs. Prediction time plot [12]

Table 1: Characteristic of selected networks

Network	Size	Parameter (million)	Input size
Googlenet	27 MB	7.0	224-by-224
Mobilenetv2	13 MB	3.5	224-by-224
Inceptionv3	89 MB	23.9	299-by-299

Inceptionv3, Googlenet, and Mobilenetv2 are used. The selection is based on better accuracy and lesser size, referring to Figure 4. The summary of characteristics of these pre-trained models is mentioned in Table 1.

2.4 System specification

The system used in this research has specifications "Lenovo ThinkPad, Core i7, 4th Generation, 16 GB RAM, 2 GB NVIDIA Quadro Graphic card, 256GB SSD, 500GB HDD with 2.80GHz and 2.79GHz processor". Matlab 2020 (Student version) is used as a programming platform.

3 RESULTS AND DISCUSSION

Training time for the three models varies for both C-UC classification and the DVH classification set. Figure 5 shows a training time comparison between the three models. Inceptionv3 takes greater time, equal to 15.25 and 7.5 hours for C-UC and DVH classification, respectively. Training a model for C-UC classification takes much more time compared to DVH classification because, in the C-UC classification, the model is to be trained for 48 000 images, which are divided equally between C and UC images, while

1st International Conference on Advances in Civil & Environmental Engineering, University of Engineering & Technology Taxila, Pakistan

Conference date 22 &23 Feb 2022

in the DVH classification, the total images were equal to 24, 000, divided equally between DC, VC, and HC. Confusion matrixes for the C-UC and DVH classifications are shown in Figure 6 and 7 respectively. Based on these matrixes, accuracy, precision, recall, and f1-score are found using the formulas given in Table 2.
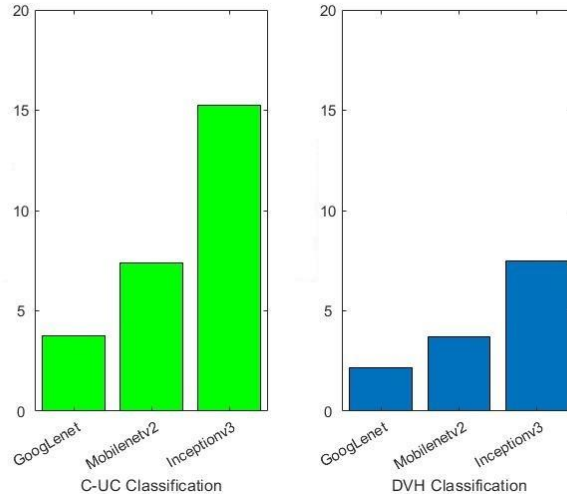
Figure 5: Training Time Comparison

Table 2: Accuracy, Precision, Recall, and F1-score formula

Parameter	Formula	Abbreviation
Accuracy	= TP+TN/TP+TN+FP+FN	TP = True Positive
Precision	= TP/TP+FP	TN= True Negative
Recall	= TP//TP+FN	FP = False Positive
F1-score	= (2xPrecision x Recall) / (Precision x Recall)	FN = False Negative

1st International Conference on Advances in Civil & Environmental Engineering, University of Engineering & Technology Taxila, Pakistan

Conference date 22 &23 Feb 2022

GoogLenet   Mobilenetv2   Inceptionv3

Figure 6: Confusion Matrix's (C-UC Classification)

GoogLenet   Mobilenetv2   Inceptionv3)
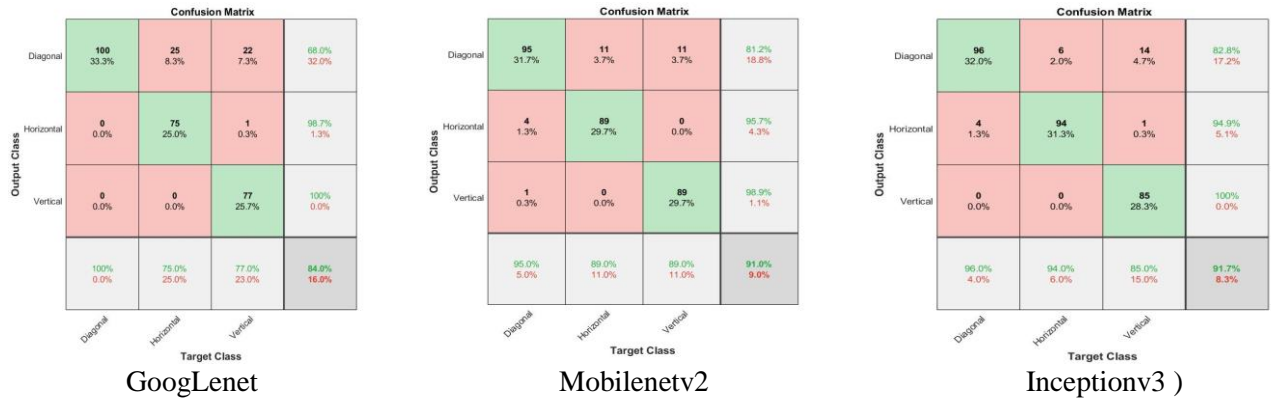
Figure 7: Confusion Matrix's (D.V.H. Classification)

Accuracy, precision, recall, and f1-scores value for all the three models on both types of classification are summarized in Table 3 and 4. DC, HC and VC are individually taken as positive cases, and the parameters are calculated which is summarized in Table 4.

Table 3: Results (C-UC Classification)

Parameters	GoogLenet	Mobilenetv2	Inceptionv3
Accuracy	0.957	0.963	0.972
Precision	1	0.99	1
recall	0.92	0.94	0.95
F1 score	0.958	0.964	0.972

1st International Conference on Advances in Civil & Environmental Engineering, University of Engineering & Technology Taxila, Pakistan

Conference date 22 &23 Feb 2022

Table 4: Results (DVH Classification)

Parameters	GoogLenet			Mobilenetv2			Inceptionv3		
	DC	HC	VC	DC	HC	VC	DC	HC	VC
Accuracy	0.84	0.92	0.91	0.91	0.96	0.95	0.92	0.95	0.96
Precision	1	0.77	0.75	0.95	0.89	0.89	0.96	0.85	0.94
Recall	0.68	1	0.986	0.812	0.99	0.96	0.83	1	0.95
F1 score	0.81	0.87	0.85	0.876	0.94	0.92	0.89	0.92	0.94

4   CONCLUSION

Based on the result in Table 3 and 4, it is observed that the performance of Inceptionv3 is better than the other two models in terms of accuracy, precision, recall and F1 score. Accuracy of Inceptionv3 is 97.2% C-UC classification which is greater than Googlenet and Mobilenetv2, having 95.7 % and 96.3%, respectively. While in DVH classification, taking DC as a positive case, the accuracy of GoogLenet, Mobilenetv2, and Inceptionv3 is 84 %, 91 %, and 92 %, respectively. Similarly, HC positive case accuracies are 92 %, 96 %, and 95 %, respectively, whereas VC as positive case accuracies are 91 %, 95 %, and 96 %. Size and Training time of Inceptionv3 is greater than GoogLenet and mobilenetv2. To reduce the training time, system with the better specification is recommended.

REFERENCES

[1]   C. R. Farrar and K. Worden, "An introduction to structural health monitoring," *Philos. Trans. R. Soc. A Math. Phys. Eng. Sci.*, vol. 365, no. 1851, pp. 303–315, 2007, doi: 10.1098/rsta.2006.1928.

[2]   H. S. Munawar, A. W. A. Hammad, A. Haddad, C. A. P. Soares, and S. T. Waller, "Image-based crack detection methods: A review," *Infrastructures*, vol. 6, no. 8, pp. 1–20, 2021, doi: 10.3390/infrastructures6080115.

[3]   N. Van Hung, V. V. Hung, and T. B. Viet, "The effect of crack width on the service life of reinforced concrete structures," *I.O.P. Conf. Ser. Earth Environ. Sci.*, vol. 143, no. 1, 2018, doi: 10.1088/1755-1315/143/1/012044.

[4]   C. V. Dung and L. D. Anh, "Autonomous concrete crack detection using deep fully convolutional neural network," *Autom. Constr.*, vol. 99, no. October 2018, pp. 52–58, 2019, doi: 10.1016/j.autcon.2018.11.028.

[5]   H. Salman, J. Grover, and T. Shankar, "Hierarchical Reinforcement Learning for Sequencing Behaviors," vol. 2733, no. March, pp. 2709–2733, 2018, doi: 10.1162/NECO.

[6]   S. Sony, K. Dunphy, A. Sadhu, and M. Capretz, "A systematic review of convolutional neural network-based structural condition assessment techniques," *Eng. Struct.*, vol. 226, no. September 2020, p. 111347, 2021, doi: 10.1016/j.engstruct.2020.111347.

[7]   L. Zhang, F. Yang, Y. D. Zhang, and Y. J. Zhu, "ROAD CRACK DETECTION USING DEEP CONVOLUTIONAL NEURAL NETWORK Lei Zhang , Fan Yang , Yimin Daniel Zhang , and Ying Julie Zhu," *IEEE Int. Conf. Image Process.*, pp. 3708–3712, 2016.

[8]   X. Yang, H. Li, Y. Yu, X. Luo, T. Huang, and X. Yang, "Automatic Pixel-Level Crack Detection and Measurement Using Fully Convolutional Network," *Comput. Civ. Infrastruct. Eng.*, vol. 33, no. 12, pp. 1090–1109, 2018, doi: 10.1111/mice.12412.

1st International Conference on Advances in Civil & Environmental Engineering, University of Engineering & Technology Taxila, Pakistan

Conference date 22 &23 Feb 2022

[9]   G. Zeng, Y. He, Z. Yu, X. Yang, R. Yang, and L. Zhang, "Preparation of novel high copper ions removal membranes by embedding organosilane-functionalized multi-walled carbon nanotube," *J. Chem. Technol. Biotechnol.*, vol. 91, no. 8, pp. 2322–2330, 2016, doi: 10.1002/jctb.4820.

[10]   C. Szegedy, V. Vanhoucke, S. Ioffe, J. Shlens, and Z. Wojna, "Rethinking the Inception Architecture for Computer Vision," *Proc. IEEE Comput. Soc. Conf. Comput. Vis. Pattern Recognit.*, vol. 2016-Decem, pp. 2818–2826, 2016, doi: 10.1109/CVPR.2016.308.

[11]   M.   Sandler,   A.   Howard,   M.   Zhu,   and   A.   Zhmoginov, "Sandler_MobileNetV2_Inverted_Residuals_CVPR_2018_paper.pdf," pp. 4510–4520, 2018.

[12]   *Pretrained Deep Neural Networks - MATLAB & Simulink.* (n.d.-c).
        https://www.mathworks.com/help/deeplearning/ug/pretrained-convolutional-neural-networks.html

[13]   SDNET2018: A concrete crack image dataset for machine learning applications
        https://digitalcommons.usu.edu/all_datasets/48/

PREDICTION OF STEEL FLUSH END PLATE CONNECTION THROUGH ARTIFICIAL NEURAL NETWORKS (ANN)

USAMA TARIQ, Afaq Ahmad
UET TAXILA
University of Engineering & Technology Taxila, Pakistan
Usama.Tariq@uettaxila.edu.pk, Afaq.Ahmad@uettaxila.edu.pk

Mohamed Suleiman, Mohamed Shaheen
Mohamed.Suleiman@uettaxila.edu.pk, Mohamed.Shaheen@uettaxila.edu.pk

ABSTRACT

Focus of this study is to develop a prediction model to predict the mode of failure of steel flush end plate (FEP) connection through the use of artificial neural networks (ANN's). A database of 148 sample point is developed for this purpose which includes geometric and material properties of column, beam, bolt and end plate. Variables such as height (h), breadth (b), thickness (t), length (l) etc are collected for all four members based on the available experimental studies. 5 different ANN models were trained by using customized mat lab code, depending on different combinations of input parameters. A variety of error metrics is also used to evaluate the performance of different ANN models. When values of ANN were compared with the experimental values then we find out a very close relation between both of them.

Keywords: Neural networks, ANN, FEP connections

1   INTRODUCTION

There are three types of connections rigid, semi rigid and pinned. Flush end plate connections are an example of semi rigid connections. Semi rigid type of connections is one of most commonly used connection. Reason for their wide use is that there rotational stiffness and ease of fabrication. Rigidity of semi rigid type of connections is between rigid and pinned connections. With all these advantages the major drawback with semi rigid type of connections is that there true behaviour is still not known and there rigidity is often considered to be equal to either pin or rigid connections. Some efforts were made to find their true behaviour but they were done on a very limited scale. For this purpose a database of 148 samples is prepared which comprehensively covers all variety of geometric and material properties and then a non

1st International Conference on Advances in Civil & Environmental Engineering, University of Engineering & Technology Taxila, Pakistan

Conference date 22 &23 Feb 2022

conventional approach of ANN is used to evaluate all these parameters. 5 different kinds of combinations were made out of this database and ANN models were trained on them using mat lab customized code and then these results were compared with the experimental results.

2 FEP CONNECTIONS DATABASE

A database which includes 148 sample points was prepared. This database covers all variety of geometric and material properties of column, beam, end plate and bolt. All critical parameters for all four of them were included in the database. These 148 sample points were categorized on the basis of failure mode. Figure 1 shows a plot of failure mode versus there number of occurrence for 5 most commonly occurring failures.
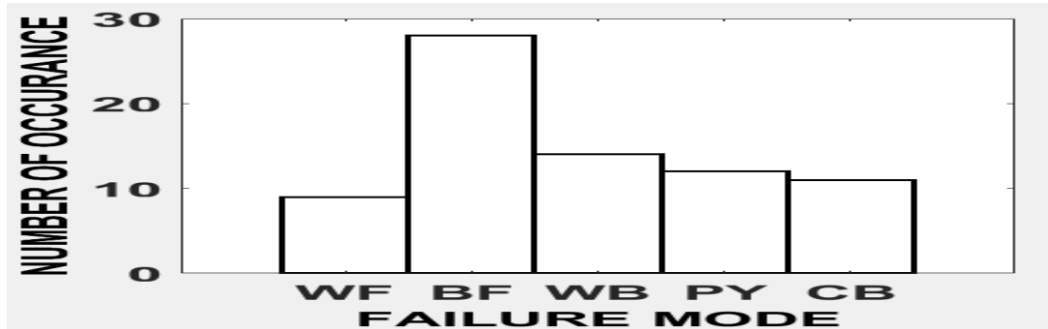

Figure 1: Failure mode plotted versus there number of occurrence in database

In figure 2 value of correlation value (R) of beam, column, end plate and bolt is shown with respect to the experimental values.
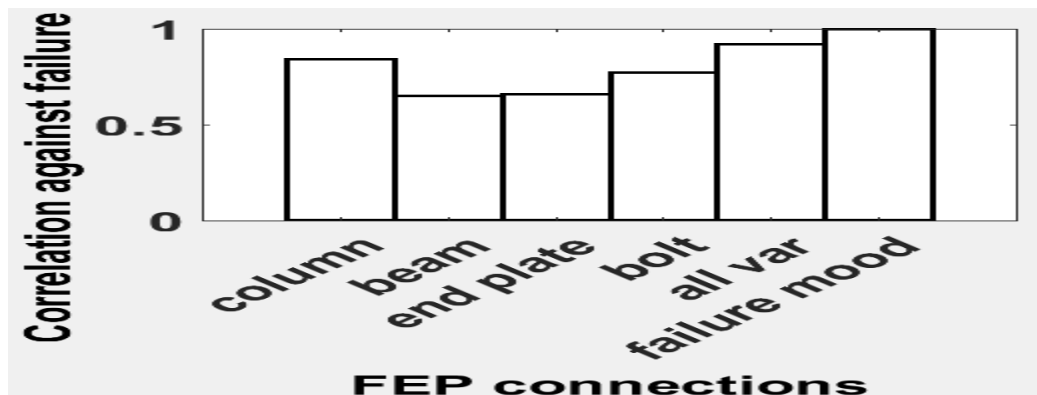

Figure 2: Values of R plotted against the experimental values

1st International Conference on Advances in Civil & Environmental Engineering, University of Engineering & Technology Taxila, Pakistan

Conference date 22 &23 Feb 2022

3   MODELLING OF ARTIFICIAL NEURAL NETWORKS (ANN)

Neural networks reproduce the human and other creature sensory systems and natural neural organizations in the mind. These networks are utilized to assess capacities in view of a huge number of information. ANNs can learn, characterize, sum up, and foresee the upsides of factors since they can keep the data introduced to them during the preparation cycle in their memory, and due to their versatility. They are made out of a few associated layers, every one of which contains a complex interconnected neuron framework. There is a connection between each two neurons in ceaseless layers, with a particular weight. Then, at that point, the forecast of the neuron is duplicated by these loads. In this last option process, the forecast of the neuron is gone through the connection and added to the predisposition. The Multilayer Feed forward ANN (MLFNN) is viewed as appropriate for taking care of these kinds of issues. MLFNN has an input layer, a result layer, and at least one secret layers. In this review, we explicitly use Back-Propagation Neural Networks (BPNNs). BPNN is a feed forward multi-facet organization with a standard construction. That is, neurons are not interconnected inside a layer, yet are associated with all neurons in the past and ensuing layers. For this kind of ANN, the result esteem is cross-approved with the objective reaction to get the mistake esteem. During many preparation Cycles to lessen blunder values; various methods are utilized, changing the heaviness of each connection. For this situation, one might say that the network has taken in the capacity of a specific objective. As the name of the calculation proposes, blunders are engendered back from the result hub to the input hub. The design of the ANN is characterized by the quantity of stowed away layers and the number of neurons in each layer.

The specific parameters used for the different ANN models are presented in Table 1.

Table 1: The five ANNs used and the sets of the input parameters used for every case

ANN NAME	SET OF INPUT PARAMETERS USED	OUTPUT
Column	h, b, tf, tw, l	Failure mode
beam	h, b, tf, tw, l, ix, zx	Failure mode
End plate	T, b, h, et, ec	Failure mode
Bolt	P, d, a, et, ec, p, g, pi, ntension, ntotal	Failure mode
All variables	All available parameters	Failure mode

ANNs functions admirably on standardized information/yield information. In the current review, every one of the parameters connected with FEP connections was normalized utilizing the outcome of Eq. (1). All parameters utilized are unit less.

$$X=(X/\Delta x)*x + (X_{max}-(\Delta X/\Delta x)*x_{max}) \qquad \textit{Equation 1}$$

1st International Conference on Advances in Civil & Environmental Engineering, University of Engineering & Technology Taxila, Pakistan

Conference date 22 &23 Feb 2022

In the above expressed formula, x is the genuine worth, X is the standardized worth, Δx is the contrast between the most extreme and the base x qualities, xmax is the greatest incentive for variable x, Xmax is the new required most extreme incentive for X, ΔX is the new required distinction between the most extreme and the base X qualities. In this review, we use Xmax=0.7 and ΔX=0.9 to acquire normalized values in the scope of [0.1, 0.9]. To concentrate on the accuracy of the created models, the proposed ANN models should be adjusted with experimental results.
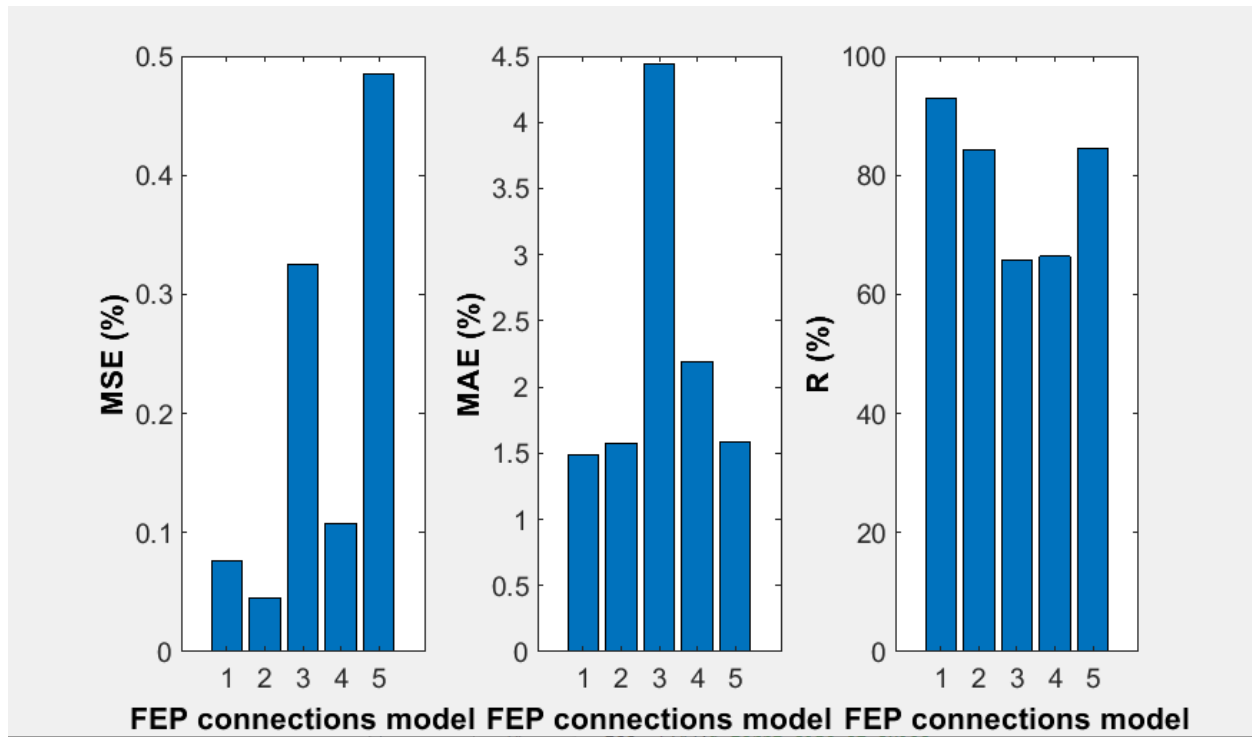
Figure 3: Performance of the various ANN models for the case of FEP connections

The values for MSE, MAE and R as gotten from various ANN models proposed for FEP connections are introduced in Figure 3. In this review, model in which all variables were used proved to be most noteworthy with values of R esteem (92%) and MSE (0.77%) and least MAE (1.48%), as displayed in Figure 3. Figure 4 shows the expectations of the different ANN models in contrast with the trial (target) values.

1st International Conference on Advances in Civil & Environmental Engineering, University of Engineering & Technology Taxila, Pakistan

Conference date 22 &23 Feb 2022
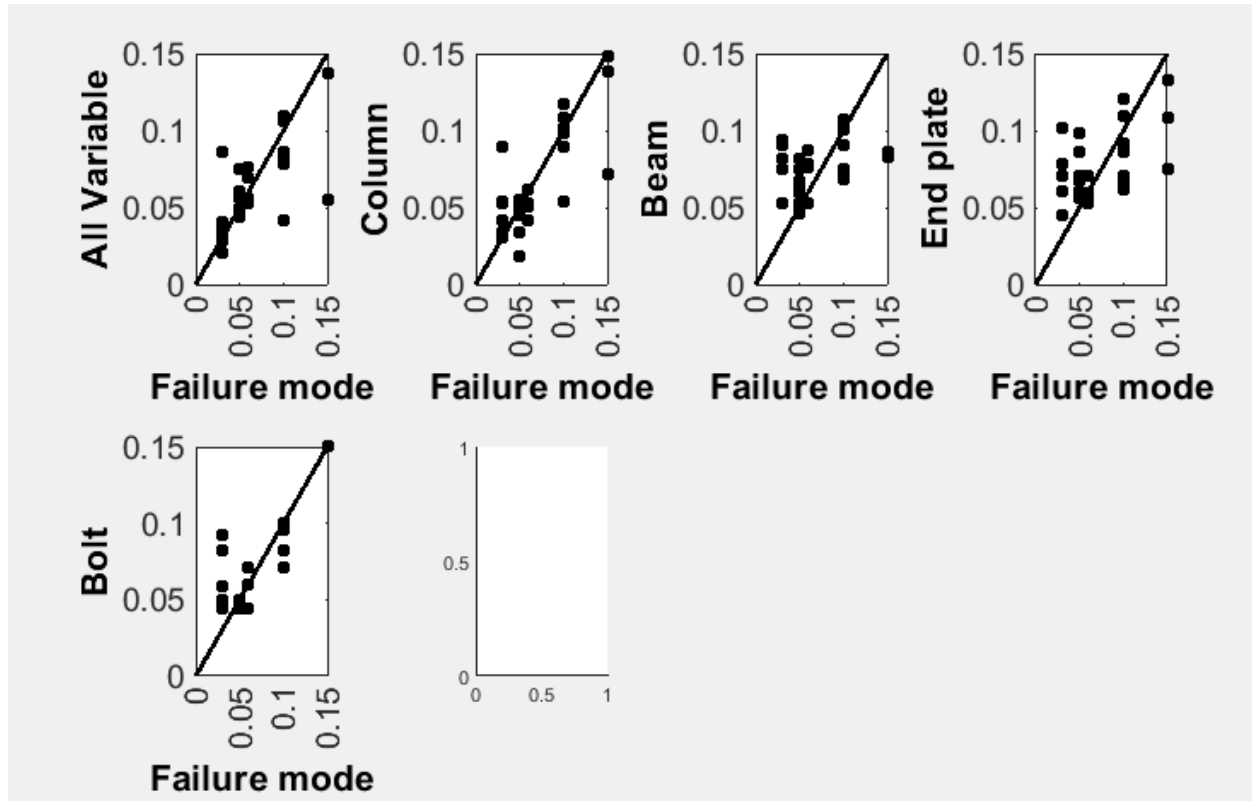
Figure 4: Predictions of the five examined ANN models for FEP connections

4   CONCLUSIONS

Research work had shown the capability of ANN modeling to predict the failure mode of fep connections. All the critical parameters of members like column, beam, end plate and bolt were examined one by one. Five ANN models were trained and parameters of column showed best performance after the performance of all variables in terms of the error metrics values (MSE, MAE and R values). Dissimilar to the traditional system, procedures like ANN models have the capacity to foresee the failure mode of the FEP connections with basic or complex geometry and also they can predict it under any type of load condition applied. When the ANNs are prepared on the given information base, they can give an exact forecast without relating to material conduct and the component fundamental primary reaction of FEP connections.

1st International Conference on Advances in Civil & Environmental Engineering, University of Engineering & Technology Taxila, Pakistan

Conference date 22 &23 Feb 2022

REFERENCES:

(Ahmad, A., et al. (2020). "Framework for the development of artificial neural networks for predicting the load carrying capacity of RC members." SN Applied Sciences **2**(4): 1-21.

Bahaz, A., et al. (2018). Analysis of the behaviour of semi rigid steel end plate connections. MATEC Web of Conferences, EDP Sciences.

Faridmehr, I., et al. (2016). "Classification system for semi-rigid beam-to-column connections." Latin American Journal of Solids and Structures **13**: 2152-2175.

Ferreira, F. P. V., et al. (2022). "Lateral–torsional buckling resistance prediction model for steel cellular beams generated by Artificial Neural Networks (ANN)." Thin-Walled Structures **170**: 108592.

Mak, L. and A. Elkady (2021). "Experimental Database for Steel Flush End-Plate Connections." Journal of Structural Engineering **147**(7): 04721006.

Ahmad, A., et al. (2021). "Knowledge-Based Prediction of Load-Carrying Capacity of RC Flat Slab through Neural Network and FEM." Mathematical Problems in Engineering **2021**.

Ahmad, A. and D. M. Cotsovos (2020). "Reliability analysis of models for predicting T-beam response at ultimate limit response." Proceedings of the Institution of Civil Engineers-Structures and Buildings: 1-23.

Ahmad, A. and A. Raza (2020). "Reliability analysis of strength models for CFRP-confined concrete cylinders." Composite Structures **244**: 112312.

Mapping Land Cover Dynamics in Chakwal District by using all Landsat Images in Google Earth Engine

Dr. Sarah Amir[1], Dr. Zafeer Saqib[1], Dr. Muhammad Irfan Khan[1], Dr. Syed Atif Bokhari[2],

Muhammad Zaman ul Haq[1]

[1]Department of Environmental Science, International Islamic University, Islamabad;
sarah.amirl@iiu.edu.pk; zafeer@iiu.edu.pk, drirfan@iiu.edu.pk; zaman@iiu.edu.pk
[2]Department of Geography, Government Postgraduate College, Rawalpindi; syedatifbokhari@gmail.com
*Correspondence: sarah.amir@iiu.edu.pk

ABSTRACT
Human activities, socio-economic, biophysical and environmental factors are mainly responsible for the land cover/land use conversions. The main focus of this study is to document the spatial-temporal changes in the LULC of the Chakwal District for the last 30 years. The study was designed to identify and map the prevalent land use/ land cover categories in the Chakwal District during 2018; to compile the spatial and temporal LULC changes in the study area and assess the magnitude and orientation of such changes for the last 30 years; and to evaluate the agricultural potential and productivity of the study area during the selected time period. The current study demonstrate that the LULC of Chakwal District significantly changed during the period from 2010 to 2017. A noticeable decline was observed in the cropland area during the time interval from 2000 to 2009. While, the significant decrease occur approximately in all the land cover classes during 1990-1999. While the tree cover, shrubland and cropland were the major victims. Whereas, a noticeable increase was also observed in the share of cropland during 1995 year. The findings of the study will help to construe about the dynamics that stimulate and influence the LULC changes in this region. The documentation of such trends will enable to design the frameworks for the socio-economic and environmental sustainability of this agrarian contextual setting of Pakistan.

KEYWORDS: Land use, Land cover change, Agriculture, Rain-fed, Climate change, Google Earth Engine

1. Introduction

The focus towards economic development is mandatory for poverty eradication and to fulfill the obligations associated with the United Nations (UN) Sustainable Development Goals (SDGs) by 2030**.** Resultantly, the reliance on technological gadgets for enhancing productivities is, also, gaining focus and impetus in the developing parts of the globe. On one hand, these initiatives supported by the technological advancements, are boon for the economic development. On the other hand, the effects of uncalculated advances may prove bane for the natural environment (Butt et al., 2015). Therefore, the resource exploitation needs careful assessments besides deploying the principles of integrated management practices during execution. These precautions are indispensable for the sustainability of natural resources and their productivity (Eniolorunda et al., 2017).

In the present times, the land resources are an easy prey and a major victim of regulated as well as unregulated attempts for natural resources exploitation (Huang et al., 2017; Atif et al., 2018). The manipulation with the land resources are carried out to accommodate the growing demand for food, shelter and to fulfill the demands for the raw material from the industrial sectors. The intrusions in the lithosphere are more pronounced in the developing

regions as compared to the developed regions. These actualities are exerting pressures on the land resources and posing challenges for the land management paradigms and practices in the less developed regions (Xiong et al., 2017).

The impacts of LULC changes are accentuating the ensuing phenomenon of global climate change (Eniolorunda et al., 2017; Yin et al., 2018). The findings based upon the empirical data corroborate such assertions that the spatial variations in the land surface temperature (LST) is suggestively influenced by the land cover type (Hereher, 2017). Besides this, the speed, scale and nature of influxes between the earth and atmosphere, in the form of mass and energy, are governed and modified by the alterations in the LULC. Herecher, (2017) elaborated that the LULC changes characteristically modified the geophysical processes such as evapotranspiration, hydrological cycle and energy budget of a geographical setting. The LULC changes also impact the social attitude in a geographical region and its proximity. Therefore, the initiatives for LULC changes should be taken after prior assessments and scrupulous decision making process (Mu et al., 2017). Besides this, the repercussions of such planned and unplanned LULC transformations are more detrimental for the agrarian settings as compared to urban areas (Dissanayake et al., 2017). As the majority of population in the developing countries such as Pakistan, are residing in the rural areas, therefore, the looming impacts will prove more devastating.

The situation is posing far reaching complications for those who are directly and indirectly dependent on the agricultural sector. The focus is more needed in the contextual settings where the economies are hooked on the primary economic activities such as mining, forestry and agricultural sectors (Dissanayake et al., 2017). However, the lack of awareness, compromises over policies and absence of a coherent mechanism to deal with such challenges are the noticeable hindrances in the developing regions. Besides this, the knowledge-gaps, limitations linked with the resources availability and capacity building are adversely impacting the situation. The scenario warrants for preventive and corrective measures for ensuring the resilience of natural environment, social uplift and sustainable economic progression.

The prevalent conventional methods relied upon for the land use mapping are labor intensive, time consuming and less amenable to statistical procedures. Besides this, these maps soon become outdated in a rapidly changing scenario (Eniolorunda et al., 2017; Mashame & Akinyemi, 2016). While, the recent advances in the domain of Remote Sensing (RS) and Geographic Information System (GIS) techniques have proved catalyst for making accurate LULC maps (Yin et al., 2018). The increased accessibility to Google Earth Engine (GEE) due to information technology have made this task much easier. The GEE is a cloud computing platform designed to store and process huge spatial-temporal data sets (at petabyte-scale) for analysis and decision making. The easily accessible and user-friendly front-end features of its environment provides a convenient space for interactive data management and algorithm development (Midekisa et al., 2017; Xiong et al., 2017).

The focus of this study is to document the spatial-temporal changes in the LULC of the Chakwal District for the last 30 years. The study was designed to achieve the following objectives (i) to identify and map the prevalent land use/ land cover categories in the Chakwal District during 2018; (ii) to compile the spatial and temporal LULC changes in the study area and assess the magnitude and orientation of such changes for the last 30 years; and (iii) to evaluate the agricultural potential and productivity of the study area during the selected time period. The findings of the study will help to construe about the dynamics that stimulate and influence the LULC changes in this region. The documentation of such trends will enable to design the frameworks for the socio-economic and environmental sustainability of this agrarian contextual setting of Pakistan.

2. MATERIALS AND METHODS

2.1 Study area

This study was carried out in the contextual settings of district Chakwal, one of the five rain-fed districts of northern Punjab in Pakistan known as Potohar Plateau; located in the land lying between river Indus and river Jhelum, called *Sind-Saghar doab* in local language. The field investigations were made in all five sub-district units *(tehsils)* of district Chakwal i.e. Chakwal, Choa Saiden Shah, Kallar Kahar, Lawa and Talagang. The study area approximately lies across 32°55'29.39" N and 72°51'11.99" E (Figure 1). The total area of Chakwal District is 6,687 km^2 inhabiting a population of 1.49 million out of it 81% are residing in rural areas (PBS, 2017). The terrain is mainly hilly, covered with forest in the southwest, and leveled plains interspaced with dry rocky patches in the north and northeast. The southern portion runs up into the Salt Range and includes the Chail peak; the highest point in the district is 1,128 meters above sea level (GoP, 2014).
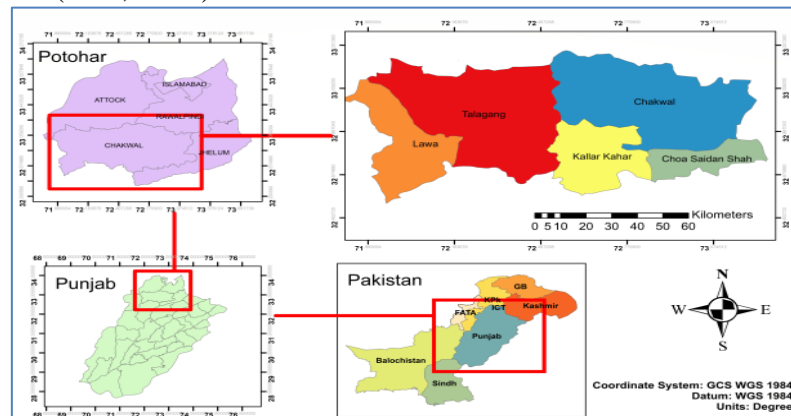
Figure 1: Location map of the study area

2.2 Data acquisition and source

The remotely sensed data were used. For the purpose, Landsat satellite imageries were relied. The study area, Chakwal District, is located at (Path 150/Row 37) according to the Landsat Worldwide Reference System (WRS). Landsat time-series data from 1989 to 2018 was obtained for extracting information regarding LULC changes through Google Erath Engine (GEE). The medium scaled Landsat TM and ETM satellite imageries were used. The trajectory-based change detection approach was deployed by developing algorithm to map the land cover changes in the GEE (Kennedy et al., 2018).

We use Landsat 5, 7 and Landsat 8 as inputs for image classification. The composite includes pixels with the lowest cloud cover, computed as per-band percentile values and scaled to 8 bits. We select the lowest possible range of cloud scores and compute per-band percentile values from the accepted pixels. The salient characteristics of the remotely sensed data have been condensed (Table 1). The values were scaled to 8 bits for ensuring precision and accuracy. Administrative map of Chakwal District was retrieved from Open street freely available data source.

Table 1: Satelllite data characteristics

Year	Satellite Sensor	Spatial Resolution	Bands Used	Worldwide Reference System (WRS)
1988-05	Landsat 5 TM	30 m × 30 m	1, 2, 3, 4, 5 & 7	WRS 2: 150/37
2006-13	Landsat 7 ETM+	30 m × 30 m	1, 2, 3, 4, 5 & 7	WRS 2: 150/37
2014-18	Landsat 8 TM+	30 m × 30 m	1, 2, 3, 4, 5 & 7	WRS 2: 150/37

Source: 'author

The figure 2 shows the procedures and measures used for LULC assessments. The flow chart explicitly portrays the methodological measures relied upon to quantify and analyze the orientation of such changes in the selected land cover classes of the study area.
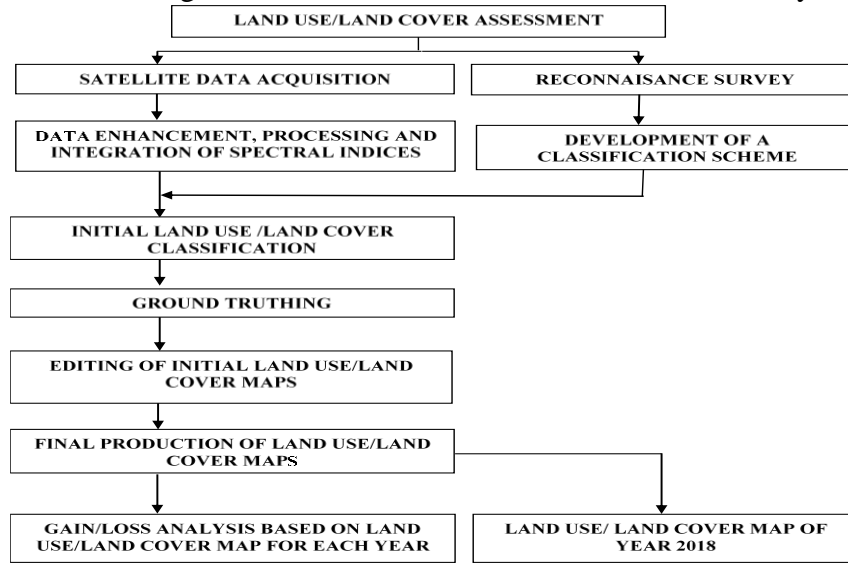
Figure 2. Flow diagram of methodology (*Source: 'author'*)

2.3 Spectral Indices
The spectral indices were calculated by using the following equations:

(I): *Normalized Difference Vegetation Index (NDVI):*
$$NDVI\left(\frac{B5 - B4}{B5 + B4}\right)$$

(II): *Normalized Difference Water Index (NDWI):*
$$NDWI\left(\frac{B3 - B5}{B3 + B5}\right)$$

(III): Modified Normalized Difference Water Index (MNDWI):
$$MNDWI\left(\frac{B5 - B4}{B5 + B4}\right), MNDWI\left(\frac{B3 - B7}{B3 + B7}\right)$$

(IV): *Normalized Difference Built Index (NDBI):* This model is used in conjunction with the traditional NDVI for the detection of urban areas, for a single Landsat scene.
$$NDBI\left(\frac{B7 - B4}{B7 + B4}\right)$$

2.4 Software used
The following softwares were used for measurements, assessments and portraying findings of the investigation. These are:
- **(a) Google Earth Engine**: This online spatial data sources was relied upon for data acquisition and subsequent processing. The GEE, a cloud computing platform, was used to develop LULC classes and change detection analysis in the study.
- **(b) ArcGIS 10.3** – was also used for assessments and to portray the final data products.

(c) R (Version 3.4.3) – The change detection (Gain/Loss) analysis were performed through R machine learning scripts.
(d) Microsoft word – was used to present the research.
(e) Microsoft Excel was used to display the findings.

2.5 Development of a classification scheme

Based on the priori knowledge about the contextual settings of the study area and based upon the information from previous research, a classification scheme was conceived for the current study. The classification scheme is developed to identify a particular LULC class by a single digit. For the purpose, the field observation from 600 sites were made with the help of Geographic Positioning System (GPS). In addition, a total of 1835 sample plots, were manually observed from 1989 to 2018 through higher resolution images in GEE. Both the training and validation samples of each year were separately uploaded to the GEE via the Google Fusion Tables (GFT). The primary objective of this technique was to classify the land cover of a respective year. The classes and their interpretations were carried out to display the contextual settings to ensure the accuracies of the findings (Table 2).

Table 2. Interpretation of LULC Classification

Sr. No.	Classes	Description
1.	Cropland	Mostly rain-fed cropping areas
2.	Grasses	The land areas dominated by natural grass cover
3.	Shrub land	The areas covered by the shrubs and tall herbs
4.	Trees/Forest	The forest covers in the study area
5.	Water	The natural and man-made water cover and hydrological systems in the study area
6.	Built-up	The rural and urban settlements and infrastructures
7.	Bare soil/rocks	Barren land with extremely low vegetative cover and rocky land surfaces

Source: 'author'

2.6 Classification of the images

To classify the land cover of the study area, complex pixels of satellite image containing multiple spectral bands and colors were classified into definite number of classes. Classification and Regression Tree classifier (CART) package proposed by Breiman in 1984 (Hu et al., 2018) was deployed to generate land cover maps.

The CART enables to classify images and collect required data for the selected land cover classes. The method does not require parameters. Besides this, it is easier to manipulate and quicker to operate. Therefore, the CART is gaining rapid acceptance as a reliable tool for classification with the remotely sensed images (Hu et al., 2018). The CART algorithm are embedded in dichotomous recursive segmentation technique that refer to the Gini coefficient as the criterion for optimal test variances and segmentation. It, ultimately, generates a binary tree-based decision tree for classification. The Gini coefficient is defined as follows:

$$\text{Gini Index} = 1 - \sum_{j}^{h} p^2 (j|h)$$

$$p(j|h) = \frac{n_{j(h)}}{n(h)}$$

$$\sum_{j=1}^{J} p\ (j|h) = 1$$

"Where $p(j|h)p(j|h)$ is a sample that is randomly selected from a training set $n_j(h)$. $n_j(h)$ is the number of samples that belong to category j when the test variable value is h in the training set. $n(h)$ is the number of samples with the test variable value of h in the training set, and j represents the category number".

2.7 Methods of Data Analysis
    (i) In the first step, the classified images were downloaded and processed in the ArcGIS 10.3 for further processing and analysis.
    (ii) In the next stage, the calculation pertaining to the selected LULC types were made in km^2 for the subsequent comparison.
    (iii) In the last step, R Packages were used to compute, calculate and plot the gains/losses for each of the selected LULC class. The information were cartographically portrayed to illustrate the spatial-temporal fluctuations in the land cover of study area.

3 RESULTS
3.1 Quantitative assessment of LULC classes of study area (2018)

The land use land cover map of the study area was prepared to quantify the share of each selected class (Fig 3). The assessments were also made to decipher the orientation of spatial changes in order to illustrate the gains and losses in the categories of the land cover classes (Figs 6 & 7). Figure 4 shows that the largest share of the total land area is occupied by the croplands. The share of this category was observed approximately 3633.928 km^2 (54.32%). It is followed by the shrub land (22.08%), grassy surfaces (8.83%), trees covers (5.53%), bare land (5.34%), built-up areas (2.8%) and water surfaces (1.28%). The percentage share and total area of each land cover class have been condensed in Table 3. While, *tehsil-wise* break-up of each land cover was also made (Table 4) and percentage distribution of these land cover class in respective tehsils of the district Chakwal were portrayed in Fig. 5.

The findings rendered that the tehsil Chakwal, the largest administrative sub-division in terms of area, occupies the largest share in the categories of agricultural area (1377.384 km^2), shrub land (419.6982 km^2) and in the built-up areas (68.923632 km^2) as compared to the other sub-divisions of the district. While, the least share of cropland was found in the sub-division of Choa Saiden Shah i.e. 123.4409 km^2. However, the sub-divisions Choa Saiden Shah (109.5564 $km^{2)}$ and Kallar Kahar (103.2416 km^2) hold the largest share of trees/forest resources of the district. The share of Lawa tehsil was alarmingly found very low in this regard i.e. 13.94495 km^2. The largest share in the category of water bodies is occupied by the Talagang tehsil i.e. 40.9817 km^2 followed by the Chakwal sub-division i.e. 19.71269 km^2. The Lawa (166.5283 km^2) and Talagang (160.7216 km^2) have the largest cover of grasses surfaces in the study area.
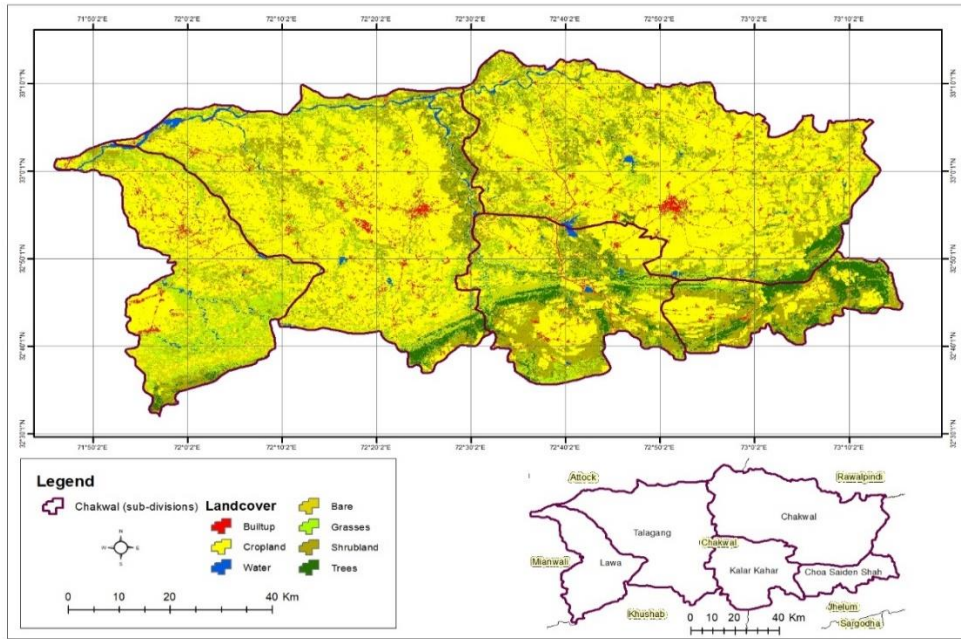
Figure 3. Land use Land cover map of Chakwal District (2018)
Source: 'author'

Table 3. Land use/land cover (LULC) classes of Chakwal District (2018)

Sr. No.	LULC Classes	Area (km²)	%age
1.	Built-up	189.5201	2.83
2.	Cropland	3633.928	54.32
3.	Water	85.48074	1.28
4.	Bare	356.9638	5.34
5.	Grasses	590.7543	8.83
6.	Shrubland	1476.849	22.08
7.	Trees	356.5041	5.33

Source: 'author'
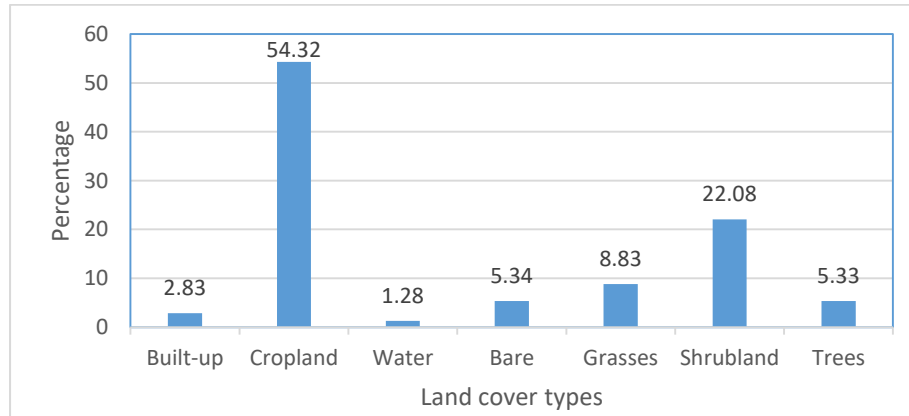
Figure 4: Bar graph showing the percentage of LULC classes of Chakwal District
Source: 'author'

Table 4. Land use/land cover classes of Chakwal (sub-divisions) of year 2018 (km²)

Zone	Built-up	Cropland	Water	Barren	Grasses	Shrub land	Trees
Chakwal	68.923632	1377.384	19.71269	79.80031	149.8709	419.6982	71.58484
Choa Saiden Shah	7.8168235	123.4409	0.456032	10.51017	24.95017	178.3439	109.5564
Kallar Kahar	21.962244	348.4883	8.216234	45.8917	88.46646	322.0599	103.2416
Lawa	31.682008	530.7612	16.04683	125.9843	166.5283	152.7724	13.94495
Talagang	59.431119	1254.206	40.9817	94.87845	160.7216	403.3813	58.30022

Source: 'author'

7
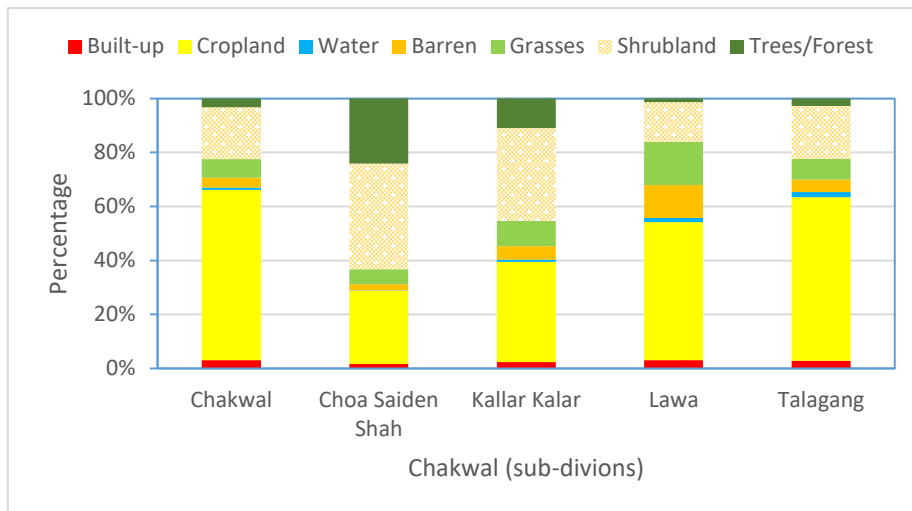
Figure 5: Percentage area of LULC classes of Chakwal (sub-divisions)
Source: 'author'
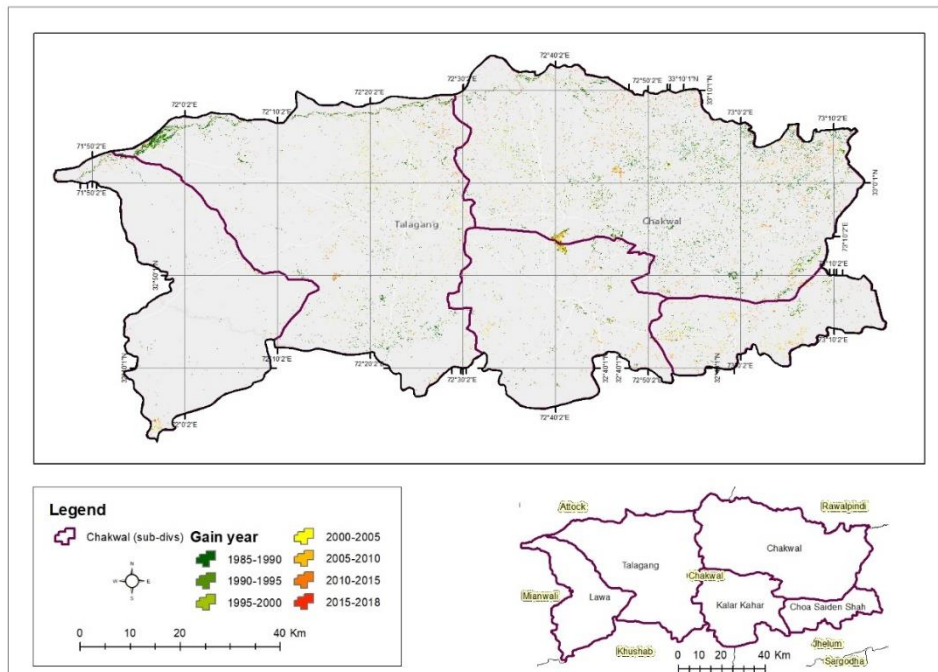
Figure 6: Year-wise gain magnitude of land covers of Chakwal District (1985-2018)
Source: 'author'
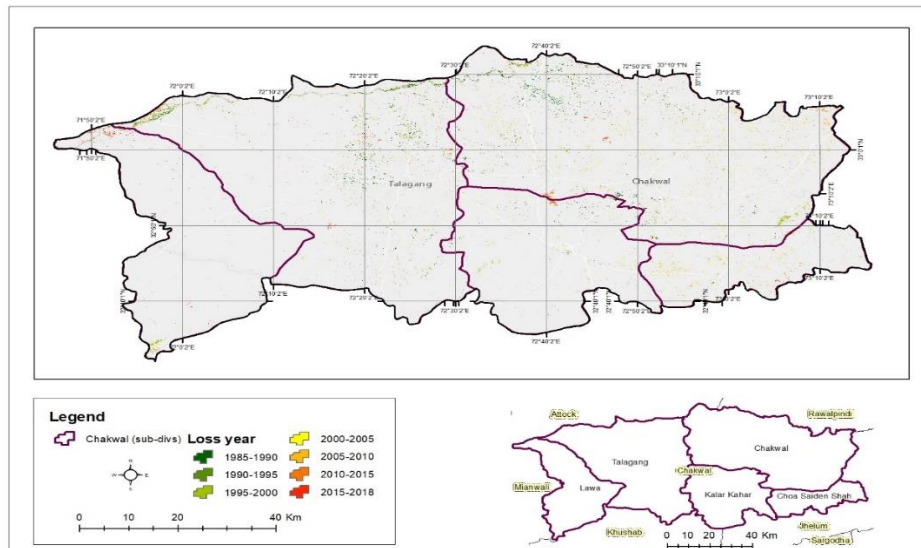
Figure 7: Year-wise loss magnitude of land covers of Chakwal District (1985-2018)
Source: 'author'

3.2   Gain and loss magnitude of land cover classes (1985-2018)

The cartographic illustrations (Fig 8 a & b) reveal the gains and losses that have occurred in each of the selected land cover type during the last 30 years (1985-2018). The green colour reflect the highest gain in the area of a specific land cover class, while, the red colour in portray the lowest transformation in a particular category of the land cover during this time period. The yellow colour depicts the moderate changes in the area of a specific land cover class. The schematic map (Fig 8) describes the quantum of such modifications in the entire study area and its constituting units i.e. the administrative sub-divisions of the Chakwal district.

(a) Gain

(b) Loss
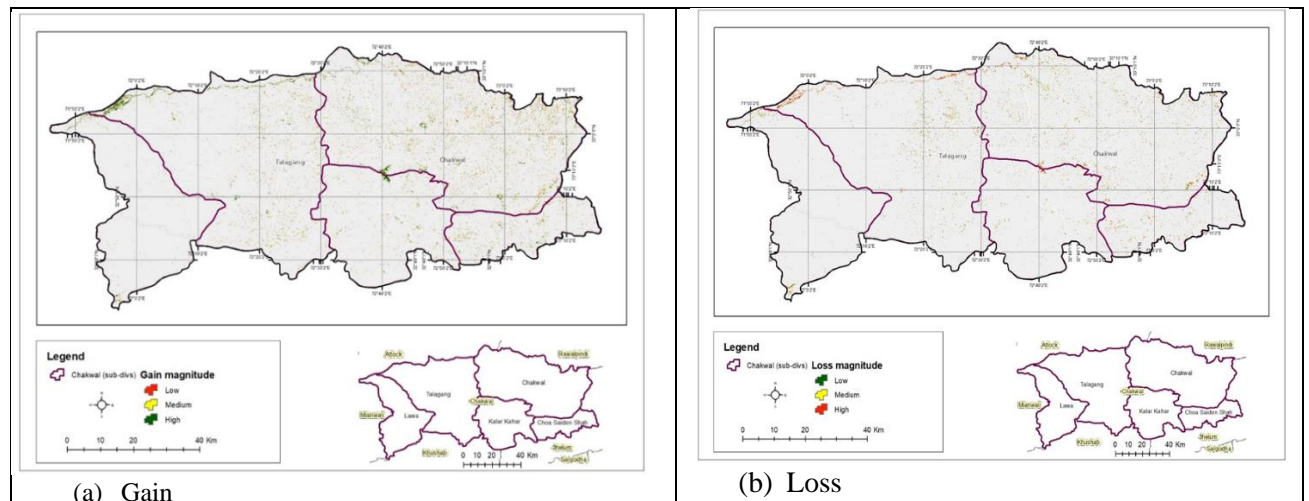
Figure 8 (a&b). Overall magnitude of gain and loss in land covers of Chakwal District (1985-2018)
Source: 'author'

3.3   Gain and loss of LULC classes during (2010 - 2017)

Figure 9 shows that the area for cropland and water surfaces significantly increased during the early years of the selected time period (2010-2017). During the similar time-interval, the noticeable increases in the share of tree cover, shrubland and grass land were also observed (Fig. 9). However, a visible decline in the proportion of tree cover, shrubland and grassy surfaces is noticeable during the years 2016 and 2017 (Fig.9). It has been found that the share

of built up area is constantly inreasing in the study area. The oscillations in the proportion of the remaining land cover classes have been summarized in Fig.9.

3.4   Gain and loss of LULC classes during (2000-2009)

The share of the tree cover increased during the early years from 2000 to 2009. Similarly, the significant increases in the share of shrubland were observed in the years 2002 and 2007. However, the noticeable reduction in the proportion and area of cropland surfaces was also observed (Fig 10).

3.5   Gain and loss of LULC classes durning (1990-1999)

The significant declines in the shares of tree cover, shrubland and croplands areas have been found. The tendencies became more noticeable in the last year of this decade (1990-1999). However, a conspicuous oscillation in the case of cropland was also observed. The share of this category stretched in the year 1995 but inverted to the previous pattern in the suceeding years of this time-interval (Fig. 11).
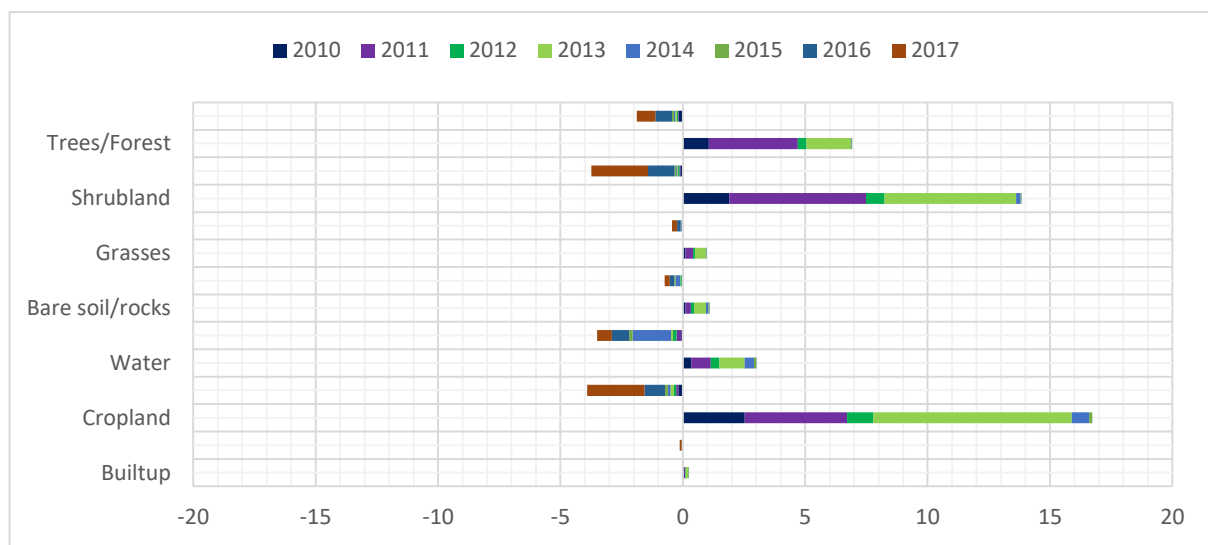
Figure 9: LULC gain and loss during 2010 to 2017
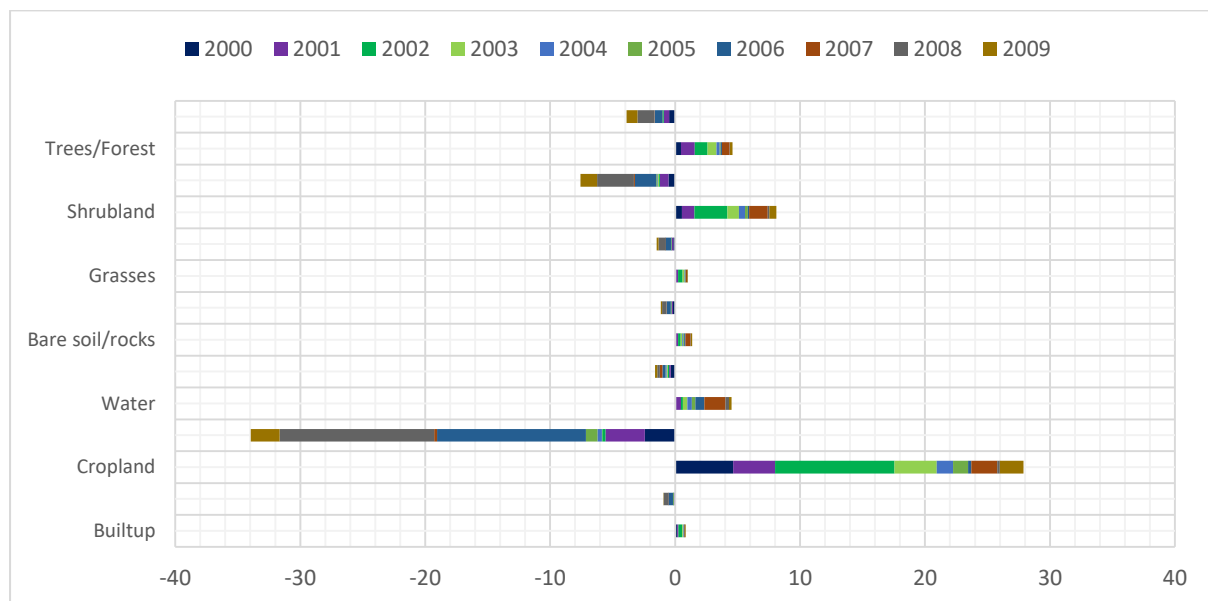
Figure 10: LULC gain and loss during 2000 to 2009
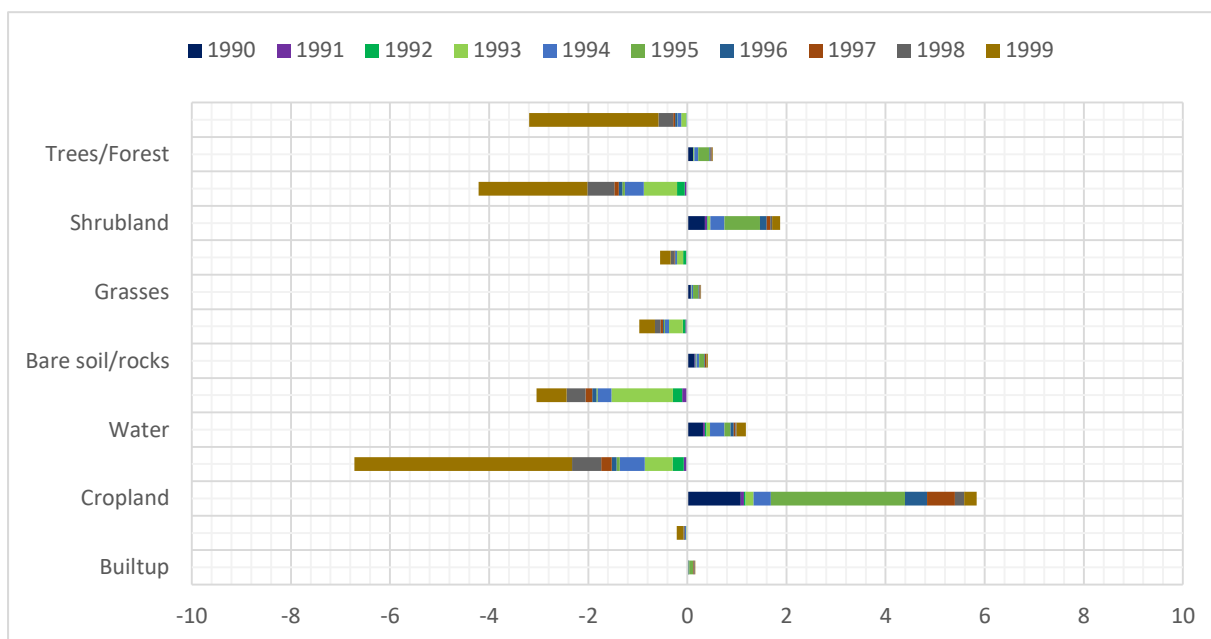
Figure 11: LULC gain and loss during 2000 to 2009

3.6 Agricultural productivity of *Kharif* crops

Table 5 shows that the total area of the district is 669,000 ha (GOP, 2017). The area for cropping is fluctuating between 239,000 ha to 270,000 ha from 2003 to 2017 (GOP, 2017). The assessments were made to assess the agricultural productivity of the study area. The data obtained from Pakistan Bureau of Statistics (Fig 12) reveal that the agricultural productivity for the *kharif* crops significantly reduced during the three decades. The major *kharif* crops in this region are groundnuts, *bajra* (millet), jowar (sorghum), lentils (*mash, moong*), maize, guar seed etc. show a substantial reduction in the yield. While, the signs of improvements are visible in the case of sun hemp production.

3.7 Agricultural productivity of *Rabi* crops

The data was also obtained from the Pakistan Bureau of Statistics (Fig 13) to evaluate the agricultural productivity of *rabi* crops. The most prominent *rabi* crops in this region are wheat, gram, barley and lentils. The significant reductions in the yields of these crops were observed during the similar time period of the last 30 years. These assessments portray a dismal about the agricultural productivity for the *rabi* crops as well.

Table 5. Agricultural land statistics of Chakwal District

| Years | Reported area | Cultivated area '000' hectares | | | Cropped area |
		Total	Net sown	Current fallow	
2003	720	326	237	89	239
2004	720	327	235	92	259
2005	720	327	245	82	276
2007	669	318	261	57	260
2008	669	319	248	71	270
2009	669	319	253	66	250
2010	669	319	226	93	257
2011	669	319	244	75	176
2012	669	319	175	144	180
2013	668	318	242	76	245
2014	668	319	242	77	243
2015	668	318	270	48	262
2016	669	319	272	47	259
2017	669	319	247	72	270

Source: Punjab Development Statistics, 2017
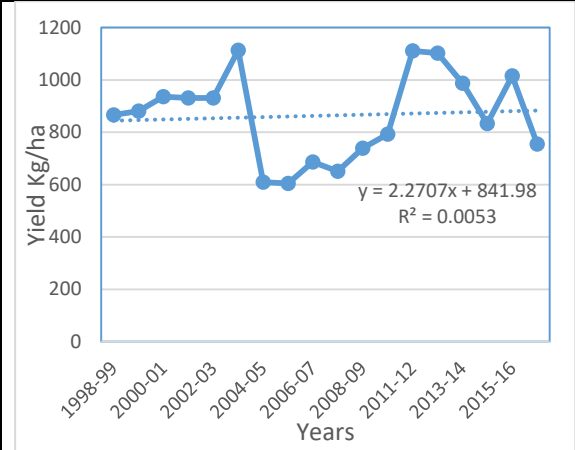
A. **Groundnut**
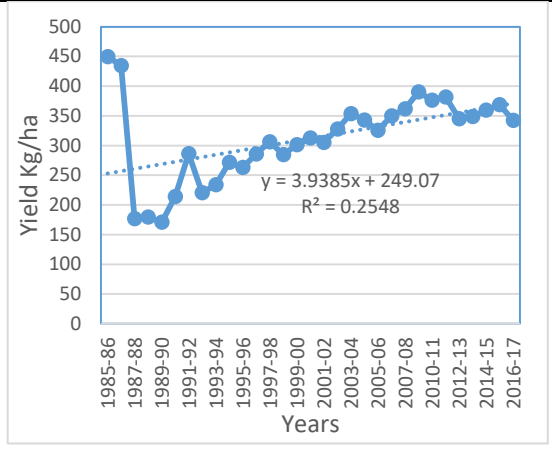
B. **Bajra (Millet)**
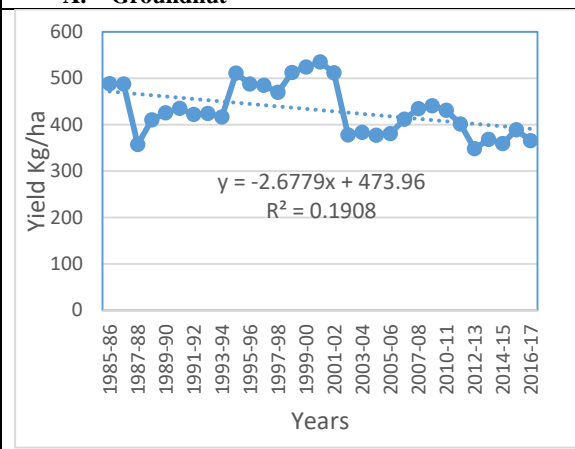
C. **Jowar (Sorghum)**
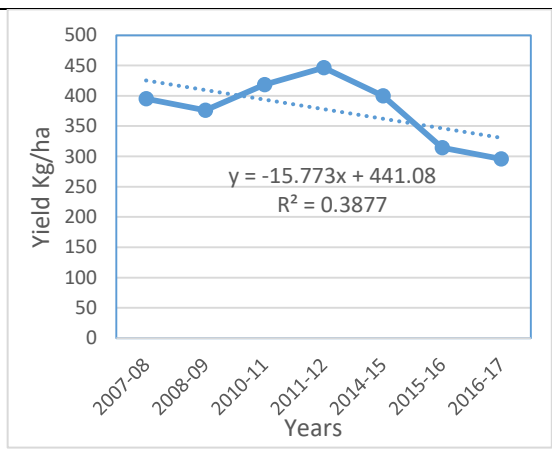
D. **Mash**
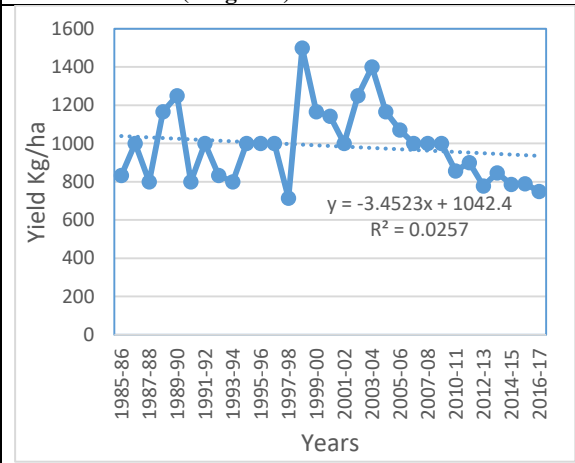
E. **Maize**
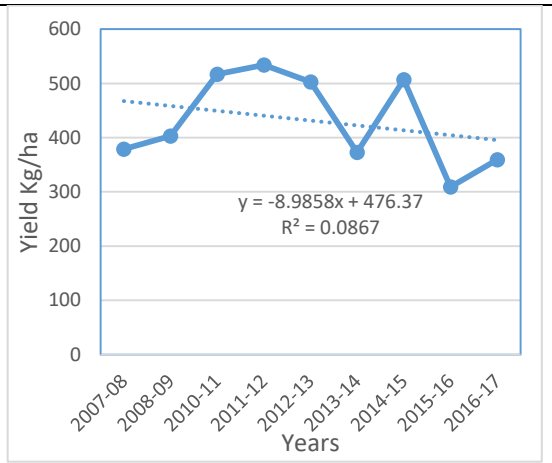
F. **Moong**
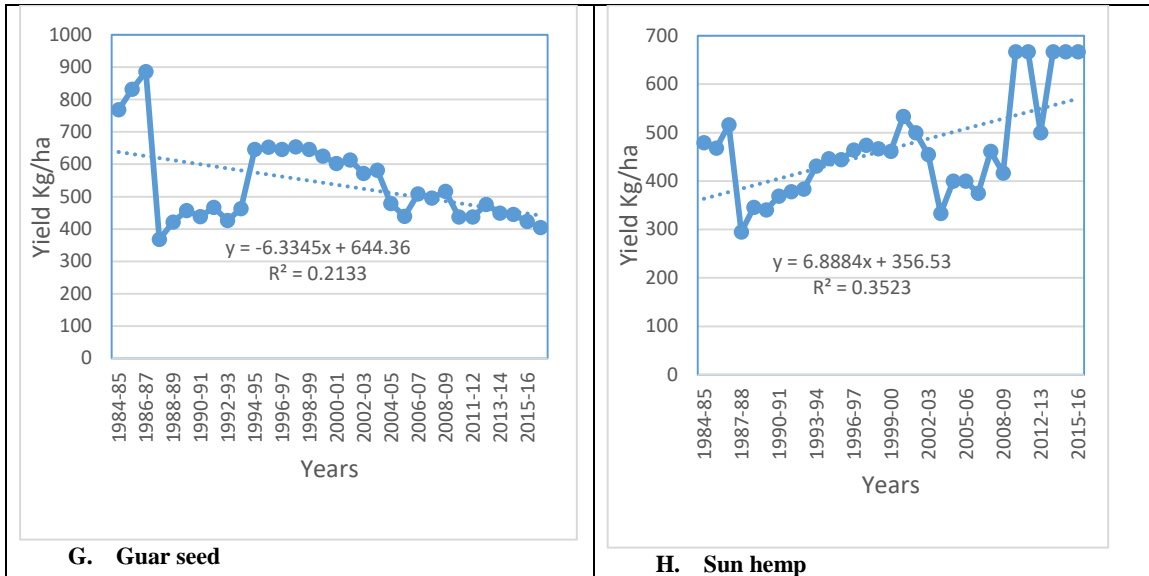
Figure 12. Yield of major *Kharif* crops during the last 30 years in the study area

Figure 13: Yield of major *Rabi* crops in the study area.
Source: Pakistan Bureau of Statistics (www.pbs.gov.pk)

4   Discussion

The socio-economic resilience of Potohar plateau is dependent on rain-fed agriculture. The water is scanty and associated weather and climatic anomalies also have marked imprints on the agricultural practices in this dissected and undulating geographical region. Despite, these unfavorable and non-conducive topographical and environmental conditions for the cropping, the agricultural sector is substantially contributing towards the livelihood and socio-economic resilience (Qasim et al., 2016). In this connection, the contributions of groundnut is widely referred. The groundnut is an important cash crop of this rain-fed region (Qasim et al., 2016). The official statistics and study conducted by Qasim et al. (2016) reveals that the per unit area yield of the groundnut is very discouraging, though having significant productivity potentials, which may significantly contribute in the rural economies of Potohar plateau.

However, the findings based upon the empirical studies infer that the agricultural production in such contextual settings are more exposed to weather climatic abnormalities as compared to the developed nations. In this connection, the scholars such as Dissanayake et al. (2017), Deressa et al. (2009) and Derbile et al. (2016) deliberated to assess the ensuing threats for the agro-based economies of the South Asian region. They conjectured about a substantial decline in the crop yields by the 2050s. In this connection, Bandara & Cai (2014) and Cai et al. (2016) focused to construe about the climate-induced impacts on the food prices in this region. They feared that a surge in the climatic abnormalities will cause a rise in the food prices. Thus, the present study was designed to assess the use of land resources in the study area and to evaluate the trajectory of LULC changes for selected time interval. The findings of the study will provide the base line information about the land resources of the study area. The absence of such data is a missing link and needed for conclusive assessments, planning and for coordinated management of land resources.

The findings of the present study indicate that the croplands (54.32%) are the predominant land cover type of the study area. The findings also construe that the share of this category in the land cover of the study area remained stable during the last decade. The findings of similar nature were reported by the Punjab Development Statistics in 2017 (GOP, 2017). The stability in the share of cropping land is credited to the efforts initiated by the ICARDA-Paksitan (International Centre for Agricultural research in Dry Area and USDA (United States Development Agency) (Oweis & Ashraf, 2014). These interventions were focus to shield the rain-fed agriculture from the impacts of climate related anomalies. The adaptation of these strategies indicate that the rural population is willing and ready to accept the innovation for the socio-ecological resilience. Tran et al. (2015) reported that the absence of a coherent mechanism accentuate the gravity of the situation and causes incalculable stresses on the land resources. Therefore, the stakeholder responsible to ensure the integrity of the land resources should include the component of awareness in their frame of actions. It also implies that the participatory mode of action yield better dividends as compared to the decision making based upon the top-down approach.

The critical finding portray that during the year (2016-17), seven mini-dams and 20 small dams were constructed in Chakwal District to overcome is water scarcity (GOP, 2017). However, due to lack of awereness, planning and coherence in the implementation, the imprints of these initiatives are, still, far from the desired level. The majority of the population, still, forced to rely on the rain water for the agriculture. The findings transpire that the initiation of new project for water conservation is needed in the study area. Besides this, the awarness and training of the farmers is more important to ensure the efficient and effective use of the available water. It also require an enhance focus towards the prospects of water scarce crops through bio-technological innovation as a measure to ensure agricultural productivity in the face of looming water scarcity.

The decline in the forest cover is a global phenomenon (Keenan et al., 2015). The findings of the study also portrayed that the share of forested cover significantly dropped from 63658 ha in 2011 to 60961 ha in 2017 (GOP, 2017). Ahmad (2001) postulated that there is a correlation between the decline in the semi-natural forest cover and roads. The researcher estimated that the degradation is more acute near the road networks but decreases as the distance increases. The development of infrastructure stimulate for development activities and forested cover are the prime victims of such intrusions in the agrarian settings as the farmer try to save the agricultural land. Resultantly, the forests situated closer to roads and developed sites are likely to be highly disturbed and fragmented. The findings based upon the present study substantiate these observations. The similar nature of situation was observed during field survey and detected through remote sensing results that the areas closer to M-2 motorway were significantly cleared from tree cover during the construction of the project and after the start of the venture. The progress without infrastructural development is impossible, therefore, the dichotomy of the interests, demands that focus efforts should be made for the protection of agriculture, conservation of vegetation cover and environmental resilience. The situation demand the integration of efforts to stimulate public attention towards forestation and afforestation activities in the study area. However, the recent empirical formulate that the land-based mitigation are a cost-effective portfolio of mitigation strategies to ensure the long-term climate stabilization (Hu et al., 2018). The innovation in the technologies is also required to cope with the emerging pressures on the land resources.

The assessments based upon the findings of this study construe that the agricultural sector is under-performing as compared to its potential. The land productivity during the *rabi* and *kharif* seasons is very low. It helped to infer that the human factor is also responsible for the situation. In this regard, the researcher such as Oweis & Ashraf (2014) and Qasim et al. (2016) extensively probed/ assessed and enlisted the causes and factors impeding the contributions of the agricultural sectors in alike situations. However, there is a concurrence of opinion that through research, informed decision making and improved governance the situation can be reversed. It requires the change of perspective about the environment, land resources and the role of people for the protection of natural resources and socio-economic resilience.

5 Conclusions

The current study demonstrate that the LULC of Chakwal District significantly changed during the period from 2010 to 2017. The investigation is the first detailed LULC analysis of the study area. The findings portrayed that LULC changes were observed in the selected categories. A noticeable decline was observed in the cropland area during the time interval from 2000 to 2009. While, the significant decrease occur approximately in all the land cover classes during 1990-1999. While the tree cover, shrubland and cropland were the major victims. Whereas, a noticeable increase was also observed in the share of cropland during 1995 year. The study transpire the usefulness of RS and GIS resources in such type of investigation. The findings of the study establish that an understanding about the drivers of land use change is a prerequisite for informed decision making.

References

Ahmad, G. (2001). Mapping a Dry Shrub Forest for Biodiversity Mapping a Dry Shrub Forest for Biodiversity. *Distribution*.

Atif, S. B., Saqib, Z., Ali, A., & Zaman, M. H. (2018). The impacts of socio-economic factors on the perception of residents about urban vegetation: A comparative study of planned versus semi-planned cities of Islamabad and Rawalpindi, Pakistan. *Applied Ecology and Environmental Research*, *16*(4), 4265–4287. https://doi.org/10.15666/aeer/1604_42654287

Bandara, J. S., & Cai, Y. (2014). The impact of climate change on food crop productivity, food prices and food security in South Asia. *Economic Analysis and Policy*, *44*(4), 451–465. https://doi.org/10.1016/j.eap.2014.09.005

Butt, A., Shabbir, R., Ahmad, S. S., & Aziz, N. (2015). Land use change mapping and analysis using Remote Sensing and GIS: A case study of Simly watershed, Islamabad, Pakistan. *Egyptian Journal of Remote Sensing and Space Science*, *18*(2), 251–259. https://doi.org/10.1016/j.ejrs.2015.07.003

Cai, Y., Bandara, J. S., Newth, D., & Asia, S. (2016). Environmental Modelling & Software A framework for integrated assessment of food production economics in South Asia under climate change. *Environmental Modelling and Software*, *75*, 459–497. https://doi.org/10.1016/j.envsoft.2015.10.024

Derbile, E. K., File, D. J. M., & Dongzagla, A. (2016). The double tragedy of agriculture vulnerability to climate variability in Africa: How vulnerable is smallholder agriculture to rainfall variability in Ghana? *Jàmbá: Journal of Disaster Risk Studies*, *8*(3), 1–9. https://doi.org/10.4102/jamba.v8i3.249

Deressa, T. T., Hassan, R. M., Ringler, C., Alemu, T., & Yesuf, M. (2009). Determinants of farmers' choice of adaptation methods to climate change in the Nile Basin of Ethiopia. *Global Environmental Change*, *19*(2), 248–255. https://doi.org/10.1016/j.gloenvcha.2009.01.002

Dissanayake, S., Asafu-Adjaye, J., & Mahadeva, R. (2017). Addressing climate change cause and effect on land cover and land use in South Asia. *Land Use Policy*, *67*(June), 352–366. https://doi.org/10.1016/j.landusepol.2017.06.003

Eniolorunda, N. B., Mashi, S. A., & Nsofor, G. N. (2017). Toward achieving a sustainable management: characterization of land use/land cover in Sokoto Rima floodplain, Nigeria. *Environment, Development and Sustainability*, *19*(5), 1855–1878. https://doi.org/10.1007/s10668-016-9831-6

GoP. (2014). Land Cover Atlas of Pakistan: The Punjab Province. FAO, SUPARCO.

Hereher, M. E. (2017). Effect of land use/cover change on land surface temperatures - The Nile Delta, Egypt. *Journal of African Earth Sciences*, *126*, 75–83. https://doi.org/10.1016/j.jafrearsci.2016.11.027

Hu, Y., Dong, Y., & Batunacun. (2018). An automatic approach for land-change detection and land updates based on integrated NDVI timing analysis and the CVAPS method with GEE support. *ISPRS Journal of Photogrammetry and Remote Sensing*, *146*, 347–359. https://doi.org/10.1016/j.isprsjprs.2018.10.008

Huang, H., Chen, Y., Clinton, N., Wang, J., Wang, X., Liu, C., … Zhu, Z. (2017). Mapping major land cover dynamics in Beijing using all Landsat images in Google Earth Engine. *Remote Sensing of Environment*, *202*, 166–176. https://doi.org/10.1016/j.rse.2017.02.021

Keenan, R. J., Reams, G. A., Achard, F., de Freitas, J. V., Grainger, A., & Lindquist, E. (2015). Dynamics of global forest area: Results from the FAO Global Forest Resources Assessment 2015. *Forest Ecology and Management*, *352*, 9–20. https://doi.org/10.1016/j.foreco.2015.06.014

Kennedy, R. E., Yang, Z., Gorelick, N., Braaten, J., Cavalcante, L., Cohen, W. B., & Healey, S. (2018). Implementation of the LandTrendr algorithm on Google Earth Engine. *Remote Sensing*, *10*(5), 1–10. https://doi.org/10.3390/rs10050691

Mashame, G., & Akinyemi, F. (2016). Towards a remote sensing based assessment of land susceptibility to degradation: examining seasonal variation in land use-land cover for modelling

land degradation in a semi-arid context. *ISPRS Annals of the Photogrammetry, Remote Sensing and Spatial Information Sciences*, *3*(July), 137–144. https://doi.org/10.5194/isprs-annals-III-**8**-137-2016

Midekisa, A., Holl, F., Savory, D. J., Andrade-Pacheco, R., Gething, P. W., Bennett, A., & Sturrock, H. J. W. (2017). Mapping land cover change over continental Africa using Landsat and Google Earth Engine cloud computing. *PLoS ONE*, *12*(9), 1–15. https://doi.org/10.1371/journal.pone.0184926

Mu, J. E., Sleeter, B. M., Abatzoglou, J. T., & Antle, J. M. (2017). Climate impacts on agricultural land use in the USA: the role of socio-economic scenarios. *Climatic Change*, *144*(2), 329–345. https://doi.org/10.1007/s10584-017-2033-x

Oweis, T., & Ashraf, M. (2014). *Assessment and Options for Improved Productivity and Sustainability of Natural Resources in Dhrabi Watershed Pakistan*.

PBS. (2017). Pakistan Bureau of Statistics. Population census. Government of Pakistan, Islamabad.

Qasim, M., Bakhsh, K., Tariq, S. A., Nasir, M., Saeed, R., & Mahmood, M. A. (2016). Factors Affecting Groundnut Yield in Pothwar Region of, *29*(1).

Tran, H., Tran, T., & Kervyn, M. (2015). Dynamics of land cover/land use changes in the Mekong Delta, 1973-2011: A Remote sensing analysis of the Tran Van Thoi District, Ca Mau Province, Vietnam. *Remote Sensing*, *7*(3), 2899–2925. https://doi.org/10.3390/rs70302899

Xiong, J., Thenkabail, P. S., Gumma, M. K., Teluguntla, P., Poehnelt, J., Congalton, R. G., … Thau, D. (2017). Automated cropland mapping of continental Africa using Google Earth Engine cloud computing. *ISPRS Journal of Photogrammetry and Remote Sensing*, *126***,** 225–244. https://doi.org/10.1016/j.isprsjprs.2017.01.019

Yin, H., Pflugmacher, D., Li, A., Li, Z., & Hostert, P. (2018). Land use and land cover change in Inner Mongolia - understanding the effects of China's re-vegetation programs. *Remote Sensing of Environment*, *204*, 918–930. https://doi.org/10.1016/j.rse.2017.08.030

1st International Conference on Advances in Civil & Environmental Engineering, University of Engineering & Technology Taxila, Pakistan

Conference date 22 &23 Feb 2022

Evaluation of Pre-trained ResNet and MobileNetV2 CNN models for the Concrete Crack Detection and Crack Orientation Classification

Ehtisham Rana

Department of Civil Engineering, University of Engineering & Technology Taxila, Pakistan
rana.ehtisham@students.uettaxila.edu.pk

Charles V. Camp

Department of Civil Engineering, The University of Memphis, Tennessee
charles.camp@memphis.edu

Junaid Mir

Department of Electrical Engineering, University of Engineering and Technology, Taxila
junaid.mir@uettaxila.edu.pk

Nida Chairman

Department of Civil and Architectural Engineering, University of Westminster, UK
n.chairman@westminster.ac.uk

Afaq Ahmad

Department of Civil Engineering, University of Engineering & Technology Taxila, Pakistan
afaq.ahmad@uettaxila.edu.pk

ABSTRACT

In this research, four different convolutional neural network (CNN) models are used to predict the orientation of cracks. Towards ameliorating this, a dataset of 32,000 images is collected from available online sources, with 75% of the images showing cracks and 25% without cracks. The 24,000 crack images are divided equally into three categories based on the orientation of cracks named vertical, horizontal, and diagonal. The remaining 8,000 images are categorized as un-crack. Pre-trained CNN models: ResNet18, ResNet50, ResNet101, and MobileNetV2, are trained on this dataset to find out the accuracy, precision, recall and F1 score. The computational complexity of each model is also assessed by noting the time model takes to train, keeping the dataset and laptop specifications the same. The confusion matrices are also given to check the overall performance of the utilized pre-trained models. ResNet50 model gives the maximum classification accuracy of 86.2% with an average training time of 8,208 sec.

KEYWORDS: Cracks detection, image classification, CNN, pre-trained models.

1   INTRODUCTION

Infrastructures, such as dams, roads, bridges, and buildings, have experienced accelerating deterioration due to the loading and environmental effect, which results in cracking the structures [1]. Cracks in concrete are omnipresent phenomena that occur in every concrete structure. In reinforced cement concrete structures, such cracks cause rusting reinforcement and spall developments in structures. So, the mitigation and precise monitoring of structural cracks are very important. Among the oldest non-destructive evaluation (NDE) methods, human visual inspection

1st International Conference on Advances in Civil & Environmental Engineering, University of Engineering & Technology Taxila, Pakistan

Conference date 22 &23 Feb 2022
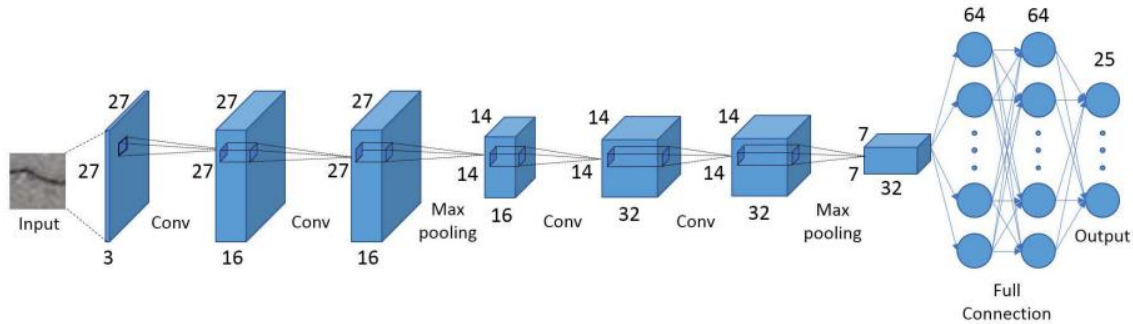
Figure 1: General architecture of Deep CNN [4].

is reliable and often serves as a baseline to confirm observation from other NDE methods [2]. There are many other NDE methods like infrared, laser, thermal, radiographic, and thermal testing techniques that have been used in the past [3]. But these methods have many limitations, like being time-consuming and expensive. Moreover, they can pose a risk to human safety because of the critical points of cracks where humans cannot perform such tests easily. Thus, there is a need to develop an automatic cracks assessment system that can be efficiently applied to the unreachable and critical points in a structure.

Deep convolutional neural networks (CNN) have been developed recently for image processing and applications in computer vision [1]. After its inspiring achievements, several recent studies are developing the algorithms of CNN for automated object detection. CNN are the most well-organized tool in handling the multiple arrays with high correlations with the neighbouring pieces. Deep CNN layer is developed by assembling the different layers such as input layers, convolution, pooling, fully connected (also known as hidden layers), and output layers, as shown in Figure 1. More layers in CNN's model minimize the error during the object detection and identification. Different pre-trained CNN models have been proposed in the literature based on their application and accuracy.

In this paper, images are collected from the internet for the training and testing of pre-trained models of CNN for crack orientation detection. The classification and detection performance of the utilized pre-trained models is given in terms of performance measures such as accuracy, precision, recall and F1 score. The rest of the paper is organized as follows: Section 2 details the related literature, the proposed methodology is presented in Section 3, Results and discussion are given in Section 4, and the paper is concluded in Section 5.

2   LITERATURE REVIEW

A CNN architecture was utilized in [2] using Google street view images to detect cracks and un-cracks patches of pavement. They trained their model to detect cracks and their types. Many automated image crack detection techniques are based on the extracted hand-crafted features. Abdel-Qader et al. used the four different techniques to identify cracked images. In their study, they used fast Haar transform (FHT), fast Fourier transform, Canny, and the Sobel images filters and

1st International Conference on Advances in Civil & Environmental Engineering, University of Engineering & Technology Taxila, Pakistan

Conference date 22 &23 Feb 2022

found the FHT as the best crack detector filter from the images [5]. Pashaie-Rad et al. used the principal component analysis for the crack detection from the bridge deck image and found that application of the local processing in the algorithm increased overall detection accuracy to 73%, decreased false negative to 12.5%, and increased false positive to 15% [6]. Krizhevsky et al. used the AlexNet for the image classification with 26 hidden layers [7]. They used 15 million high-resolution images, categorized in 22,000 different labels with a resolution of 250×250 pixels. Wang et al. developed a CNN model for the image-based cracks identification using the Sobel and Canny edge detection filters [8].

Cha et al. used the faster Region-based CNN model with 2366 images, categorized in five different damages types with 500×375 pixels [9]. A classification technique was proposed through modifying the ratio of positive to negative samples [4]. They developed a CNN model for the classification of multi-labeled categories. Choi et al. developed a CNN model having eight hidden layers including convolution, pooling, ReLU, and softmax in their architecture [10]. They have divided 40,000 images for training and validation to detect the different cracks features. He et al. presented in their paper a residual learning framework to ease the training of different models such as ImageNet, VGGNet, ResNet50, ResNet101, ResNet152, etc. and relate their error [11]. Gopalakrishnan et al. trained an ImageNet model to detect the cracks in hot mix asphalt and portland cement concrete. They found that a single-layer neural network trained on ImageNet showed the best performance but failed to distinguish the cracks from joints [12].

3   PROPOSED METHODOLOGY

The adopted methodology in this research is based on three stages. The dataset is acquired and categorized into different crack orientation classes in the first stage. Then, the pre-trained CNN models are acquired and finally, the training and testing of the CNN models is performed.

3.1   Acquisition of Dataset

In the data acquisition stage, 32,000 images are collected from the internet [14] and have a resolution of 256×256×3. This dataset of images is divided into four equal classes depending upon its cracks orientation. The sample images from the four classes, namely vertical crack, horizontal crack, diagonal crack, and un-crack images, are shown in Figure 2. Each class contains a total of 8000 images of the same resolution.
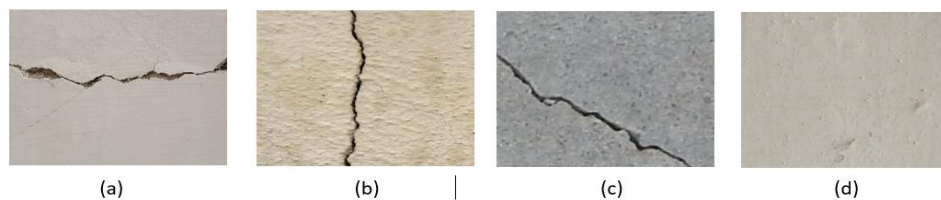
Figure 2: (a) Horizontal Crack, (b)Vertical Crack, (c) Diagonal Crack, (d) Un-crack.

1st International Conference on Advances in Civil & Environmental Engineering, University of Engineering & Technology Taxila, Pakistan

Conference date 22 &23 Feb 2022

Table 1: Specifications of Pre-Trained Models.

Model	No. of Layers	Parameters	Size(Mb)	Input Image size
ResNet18	18	11.7 M	44	224 x 224 x 3
ResNet50	50	25.6 M	98	224 x 224 x 3
ResNet101	101	44.6 M	171	224 x 224 x 3
MobileNetV2	53	3.50 M	13	224 x 224 x 3

3.2 CNN Architectures

CNN architectures consist of many affixed layers and convolutional blocks, which are composed of convolutions, batch normalization, activation, ReLU, pooling, Max pooling, average pooling, fully connected, etc. [1]. Many models are trained and tested in the recent literature, but four different pre-trained models are used in our work with the stochastic gradient descent moment algorithm. These models include ResNet18, ResNet50, ResNet101 and MobileNetV2. Specifications of all these models are given in Table 1. The concept of residual learning is introduced in ResNet models [11]. The name ResNet followed by the number implies the number of layers in that architecture. MobileNetV2 [13] is a low-complexity CNN model designed while keeping in view the strict resources of on-device or embedded applications. This is evident from the number of training parameters in MobileNetV2, which are considerably low compared to the ResNet models.

3.3 Training and Testing

For the training of models, 60% of the images from each class are selected at random. The remaining 40% of the images are used for testing purposes. While testing the pre-trained models, parameters such as accuracy, precision, recall, F1 score and processing time will be calculated to evaluate them.

4 RESULTS AND DISCUSSIONS

The evaluation of the pre-trained models is conducted based on the performance measures. The same dataset and laptop specifications are used to train and test the pre-trained models with the same ratio of data division. The accuracy, precision, recall, and F1 score parameters are calculated from the Equations 1-4, where, TP is true positive, TN is true negative, FP is false positive, and FN is false negative.

$$Accuracy = \frac{TP + TN}{TP + TN + FP + FN} \tag{1}$$

1st International Conference on Advances in Civil & Environmental Engineering, University of Engineering & Technology Taxila, Pakistan

Conference date 22 &23 Feb 2022
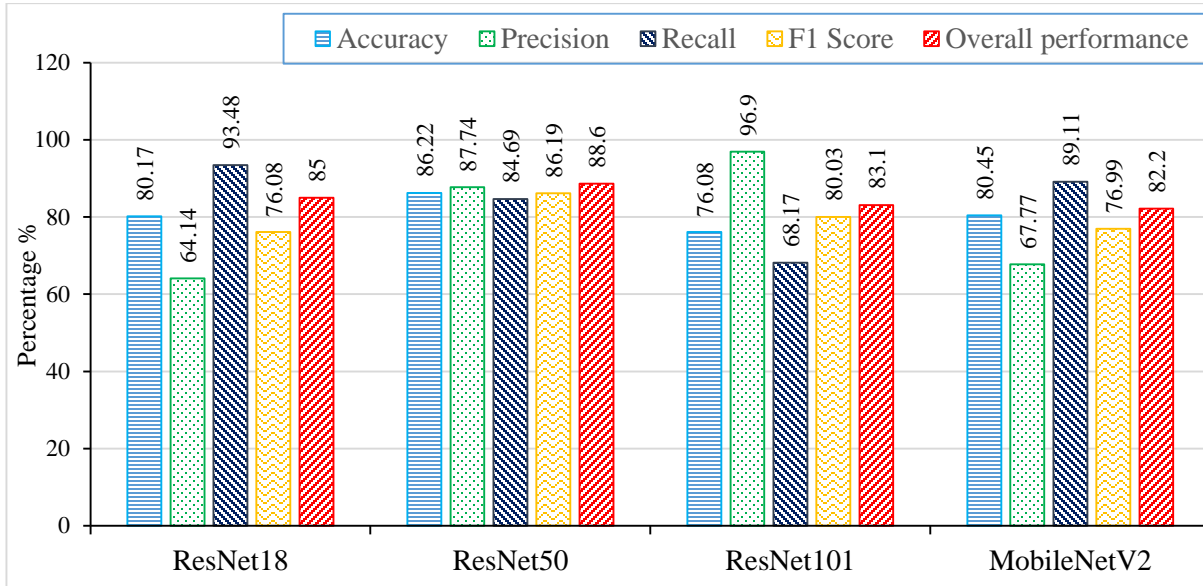
Figure 3: Results of Pre-trained Models.

$$Precision = \frac{TP}{TP + FP} \tag{2}$$

$$Recall = \frac{TP}{TP + FN} \tag{3}$$

$$F1\ score = \frac{Precision + Recall}{2} \tag{4}$$

Accuracy is the rate of all true predicted values to the total number of predictions, and the ResNet50 model offers a good balance of accuracy and F1 score compared to other models. As shown in Figure 3, the classification accuracy and F1 score of 86.22% and 86.19%, respectively, is achieved by the ResNet50 model. In terms of precision which is the accuracy of all positive prediction values, ResNet 101 offers the highest precision of 96.90%, whereas the ResNet18 model shows the highest recall of 93.14%. The recall parameter is the true positive rate of predictions and Resnet18 offers 93.14%. The F1 score is the harmonic mean of precision and recall, so the model with good precision and recall values will also have a good F1 score.

1st International Conference on Advances in Civil & Environmental Engineering, University of Engineering & Technology Taxila, Pakistan

Conference date 22 &23 Feb 2022
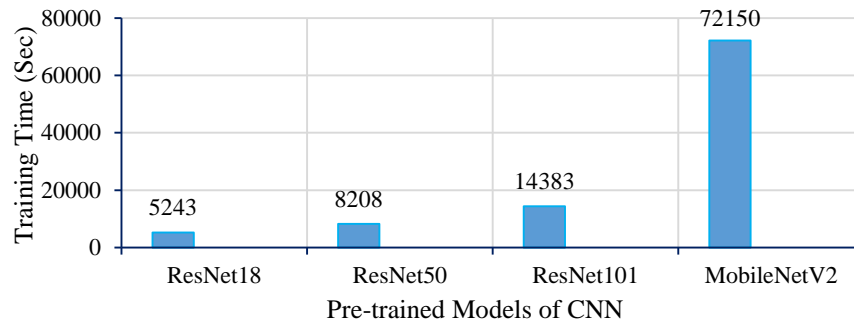
Figure 4: Processing Time of Pre-trained Models of CNN.

Figure 4 depicts the time it takes the used CNN model to train our data on the laptop with specifications of "Dell Latitude E5450, Core i5, 5th Generation, 16 GB RAM, 256GB SSD and 2x2.30GHz processor". It can be seen that MobileNetV2 takes the maximum time in terms of training. In contrast, ResNet18 takes the minimum time of 5243 seconds for training.

The confusion matrices are shown in Figure 5, which summarizes the predictions done by the pre-trained models and is given between the output class and target class. The green boxes show the number of truly identified images and percentages, and the pink boxes show the number of wrongly identified images and percentages.

5   CONCLUSIONS

Four CNN pre-models are trained and tested on a comprehensive image dataset to detect cracks and then classify them into three orientations. ResNet50 CNN model gives the best overall performance in terms of both accuracy and F1 score. The values of confusion matrix parameters depend upon the ratio of training and testing and a good division of the dataset into categories. In this research, 60% of the data was used for training and 40% for testing. If we change these percentages to 80% and 20%, the parameter values will be more effective. So, it is concluded that more deep layers in models will give an effective result and consume more time during training and testing. The processing time depends on the layers and the size of the dataset, machine specifications, and other changeable hidden parameters.

1st International Conference on Advances in Civil & Environmental Engineering, University of Engineering & Technology Taxila, Pakistan

Conference date 22 &23 Feb 2022
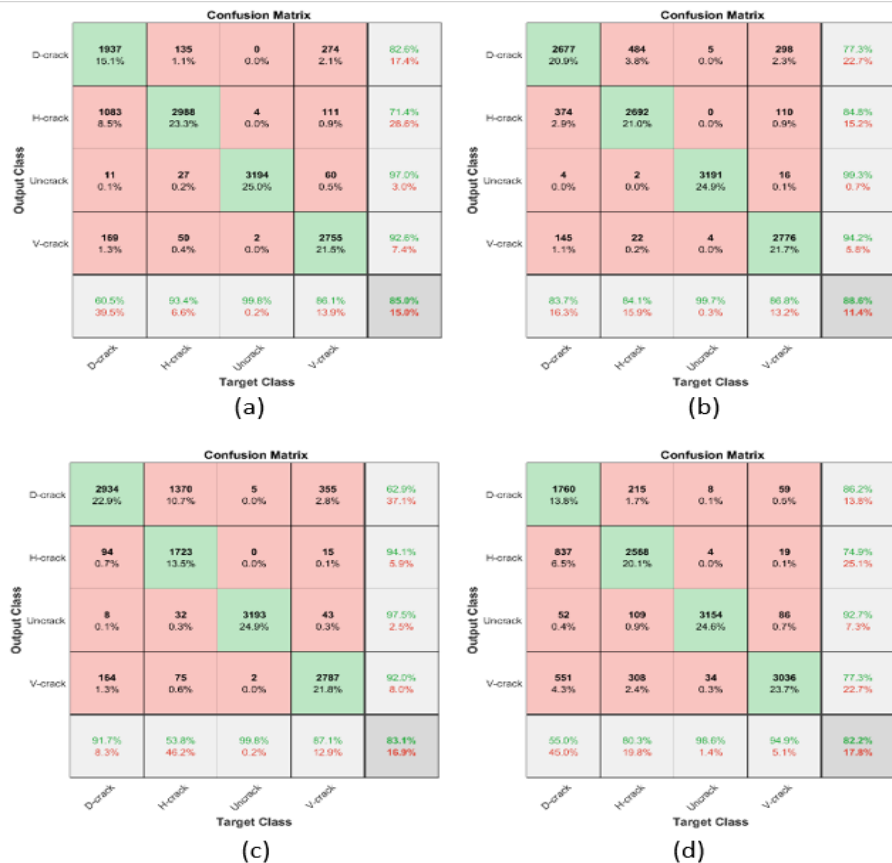
Figure 5: Confusion Matrix (a) ResNet18, (b) ResNet50, (c) ResNet101, (d) MobileNetV2.

6   REFERENCES

[1]   C. V. Dung and L. D. Anh, "Autonomous concrete crack detection using deep fully convolutional neural network," *Autom. Constr.*, vol. 99, no. December 2018, pp. 52–58, 2019, doi: 10.1016/j.autcon.2018.11.028.

[2]   M. Maniat, C. V. Camp, and A. R. Kashani, "Deep learning-based visual crack detection using Google Street View images," *Neural Comput. Appl.*, vol. 33, no. 21, pp. 14565–14582, 2021, doi: 10.1007/s00521-021-06098-0.

[3]   H. S. Munawar, A. W. A. Hammad, A. Haddad, C. A. P. Soares, and S. T. Waller, "Image-based crack detection methods: A review," *Infrastructures*, vol. 6, no. 8, pp. 1–20, 2021, doi: 10.3390/infrastructures6080115.

[4]   Z. Fan, Y. Wu, J. Lu, and W. Li, "Automatic Pavement Crack Detection Based on Structured Prediction with the Convolutional Neural Network," no. May, 2018, [Online]. Available: http://arxiv.org/abs/1802.02208.

[5]   I. Abdel-Qader, O. Abudayyeh, and M. E. Kelly, "Analysis of Edge-Detection Techniques for Crack Identification in Bridges," *J. Comput. Civ. Eng.*, vol. 17, no. 4, pp. 255–263, 2003, doi: 10.1061/(asce)0887-3801(2003)17:4(255).

[6]   I. Abdel-Qader, S. Pashaie-Rad, O. Abudayyeh, and S. Yehia, "PCA-Based algorithm for

1st International Conference on Advances in Civil & Environmental Engineering, University of Engineering & Technology Taxila, Pakistan

Conference date 22 &23 Feb 2022

unsupervised bridge crack detection," *Adv. Eng. Softw.*, vol. 37, no. 12, pp. 771–778, 2006, doi: 10.1016/j.advengsoft.2006.06.002.

[7]   B. A. Krizhevsky, I. Sutskever, and G. E. Hinton, "Cnn实际训练的," *Commun. ACM*, vol. 60, no. 6, pp. 84–90, 2012.

[8]   Z. Wang, G. Xu, Y. Ding, B. Wu, and G. Lu, "A vision-based active learning convolutional neural network model for concrete surface crack detection," *Adv. Struct. Eng.*, vol. 23, no. 13, pp. 2952–2964, 2020, doi: 10.1177/1369433220924792.

[9]   Y. J. Cha, W. Choi, G. Suh, S. Mahmoudkhani, and O. Büyüköztürk, "Autonomous Structural Visual Inspection Using Region-Based Deep Learning for Detecting Multiple Damage Types," *Comput. Civ. Infrastruct. Eng.*, vol. 33, no. 9, pp. 731–747, 2018, doi: 10.1111/mice.12334.

[10] Y. J. Cha and W. Choi, "Vision-based concrete crack detection using a convolutional neural network," *Conf. Proc. Soc. Exp. Mech. Ser.*, vol. 2 Part F2, pp. 71–73, 2017, doi: 10.1007/978-3-319-54777-0_9.

[11] K. He, X. Zhang, S. Ren, and J. Sun, "Deep residual learning for image recognition," *Proc. IEEE Comput. Soc. Conf. Comput. Vis. Pattern Recognit.*, vol. 2016-Decem, pp. 770–778, 2016, doi: 10.1109/CVPR.2016.90.

[12] K. Gopalakrishnan, S. K. Khaitan, A. Choudhary, and A. Agrawal, "Deep Convolutional Neural Networks with transfer learning for computer vision-based data-driven pavement distress detection," *Constr. Build. Mater.*, vol. 157, pp. 322–330, 2017, doi: 10.1016/j.conbuildmat.2017.09.110.

[13] M. Sandler, A. Howard, M. Zhu, A. Zhmoginov, and L. C. Chen, "MobileNetV2: Inverted Residuals and Linear Bottlenecks," *Proc. IEEE Comput. Soc. Conf. Comput. Vis. Pattern Recognit.*, pp. 4510–4520, 2018, doi: 10.1109/CVPR.2018.00474.

[14] https://digitalcommons.usu.edu/all_datasets/48/

Effect of Temperature on Self-Healing of Asphalt Material

Moazam Sattar, Imran Hafeez,

University of Engineering and Technology Taxila, Punjab, Pakistan

Moazam.Sattar@students.uettaxila.edu.pk; imranhafeez@yahoo.com

ABSTRACT

Micro cracks develop in asphalt pavement during the service life of a pavement mainly due to climatic and loading conditions. These cracks reduce the pavement fatigue life. Cracks that once appear in asphalt mixture can heal with an increase in temperature. This paper aims to find the impact of temperature on self-healing of asphalt pavement material by microwave induction method. The four-point beam fatigue test apparatus was used to find bending strength of asphalt material. A set of conditioning time and temperature were selected for this study. The test was performed on specimen before and after conditioning. Study reveals a huge drop in bending strength after the first healing cycle, whereas there was no huge drop from second bending strength to third bending strength. Moreover, self-healing capabilities of asphalt material increased with temperature. It was concluded that temperature is the principal factor in self-healing of asphalt material. Healing index was maximum at temperature between 37-40 °C.

Keywords: Self-Healing, Microwave oven heating, Four-point beam test,

1   INTRODUCTION

Asphalt pavement is extensively employed in highway building because of its pleasant operating experience and low cost. However, owing to traffic volumes, bitumen aging, and environmental characteristics such as moisture damage, temperature influence, and sun radiation, degradation begins quickly after the road is put into operation. Meanwhile, minute fractures appear in asphalt pavement, which eventually become deeper and cause more serious issues, such as traveling, potholes, and fracturing [1]. These kinds of deteriorations jeopardize road safety while necessitating pricey upkeep. Originally, fractures in asphalt mixtures are micrometric in width, but owing to traffic circulation and environmental stressors, they can expand quite quickly.

As a result, to extend the life of asphalt pavements, preventive maintenance program procedures must always be employed. Furthermore, fissures in asphalt mixtures can self-heal without the need for human involvement. Additionally, if asphalt roads are not subjected to traffic stresses that might widen fractures, they can self-heal. Consequently, total healing may take several months, which is unachievable in practice owing to the continuous flow of traffic.

Asphalt is a self-healing substance, according to Bazin and Saunier [2]. It has been observed that fractures in the asphalt pavement that are visible in the winter vanish in the summertime, but it is required to heat asphalt concrete intentionally to optimize temperature-related healing

performance [3]. Microwave heating produces a temperature that is difficult to manage; it may be greater than asphalt's flash temperature limit, destroying the chemical structure of the adhesive. As a result, the heating duration should really be carefully monitored [4]. Lou et al. investigated microwave absorbers based on element composition, morphology, and electromagnetic characteristics, and calculated the influence of fer-rite on the rheological performance of asphalt adhesive by supplementing a specific quantity of limestone filler. They looked at the possibilities of using ferrite as a substantial limestone filler in steel slag asphalt mixes to increase self-healing characteristics and microwave heating uniformity [5].

Among three types of metallic garbage, Baowen et al. discovered that hot braised steel slag (HBSS) had the best microwave absorption performance [6]. Liu et al. offered a novel investigation in which they demonstrated that SiC-Fe3O4 increased the microwave heating capability of asphalt concrete while solar radiation had no further heating impact [7]. Microwave preprocessed grounded Tyre rubber enhanced binders obtained a decrease inclination in compound viscosity, as well as rutting resistance potential after being exposed to microwave radiation, according to Xu et al. [8]. Gallego et al. investigated the efficacy of a new thermomechanical therapy in facilitating the mending of scorching asphalt mixes. [9]. Yalcin looked at the effects of induction heating and microwaves on the self-healing of an asphalt mixture utilizing waste materials [10].

2   METHODOLOGY

In this Experimental study, we used 60/70 penetration bitumen of Attock Oil Refinery. Aggregates of Margalla used for Asphalt mixture. In this study, first we prepared asphalt material slabs by mixing aggregates and bitumen and then we divided this slab into four beams of asphalt mixture. The length, width and depth of Beam was 12 inches, 2 inches and 2 inches, respectively. Total 20 asphalt material beams were made. Four-point Beam test apparatus was used to check bending strength of asphalt material beam. Frequency range of apparatus was 0.1 to 30 Hz. Tests were performed at different temperatures and frequencies. The load at which cracks start to develop was noted as a bending strength value F1. Cracked beams were put in a microwave oven. Beams were heated at different temperatures between 25 °C to 40 °C and a set of conditioning times were selected. After heating and Conditioning, the healed beam was tested again by four-point fatigue apparatus and bending strength was measured as F2. Healing Index was calculated by using equation (1).

$$S = F2/F1 \qquad\qquad\qquad (1)$$

After finding second bending strength, cracked beam was healed again and tested again by four-point fatigue test apparatus. Healing index was calculated again by using equation (1).
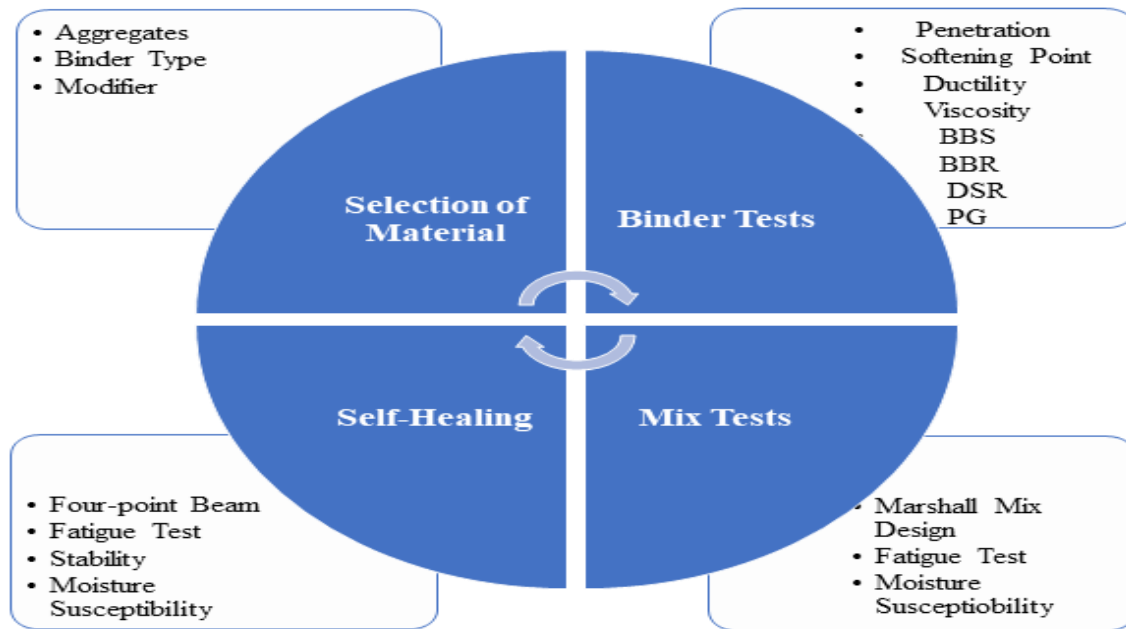
Figure 1: Flowchart of Methodology and Testing

3   RESULTS AND DISCUSSION

It was revealed that there is much difference between first and second bending strength but there is no huge drop from second to third bending strength. It is due to the fact, during the first four-point fatigue test a few aggregate grains were damaged, and they could not completely get better at their strength when they were carried out microwave healing. Results showed that with the increase of microwave oven temperature, first, second and third bending strengths increased as shown in figure (2).

The discovered decrease within the third bending strength as compared to the second one bending strength might be ascribed to the change in the inner shape of asphalt material.
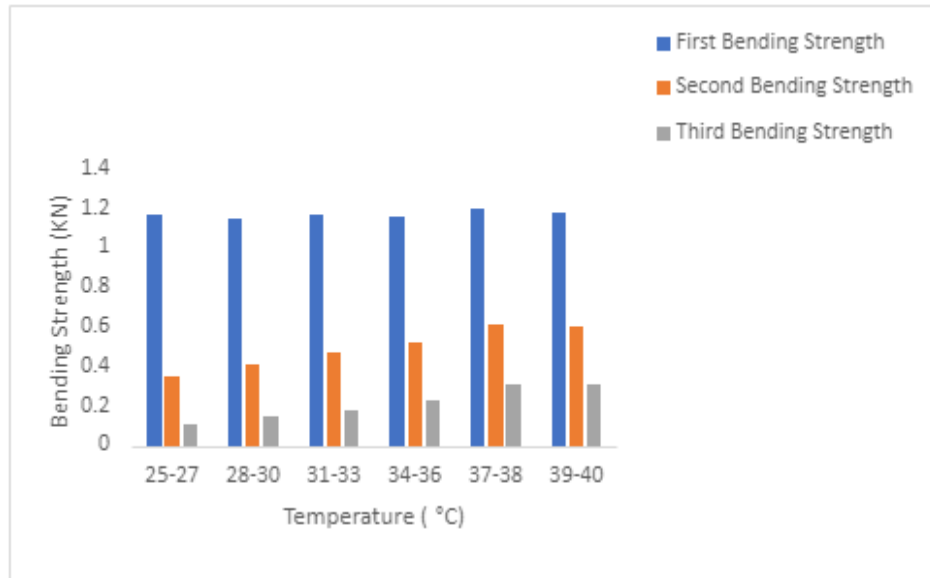
Figure 2: Bending strength of specimen

The study revealed that there is a co-relation between temperature and healing level of Asphalt material. Healing Performance increased by increasing temperature. Highest healing performance was noted at temperature between 37-40 °C as shown in figure (3).
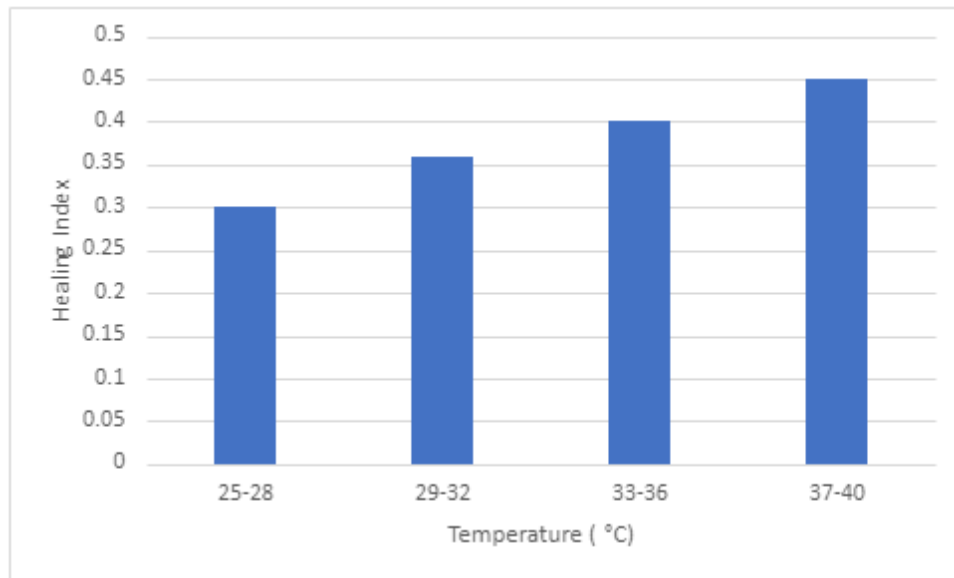
Figure 3: Effect of temperature on healing level

4   CONCLUSION

- Self-healing capabilities of asphalt material can enhance by increasing temperature.
- It has been proven that heating temperature is the primary element for the self-recovery of asphalt material. Healing index was maximum at temperature 37-40 °C.
- Pavement fatigue life can be extended by increasing temperature because cracks in asphalt material heal at high temperatures.

5   REFERNECE

[1] S. Xu, A. García, J. Su, Q. Liu, A. Tabakovic´, E. Schlangen, Self-Healing Asphalt Review: From Idea to Practice, Adv. Mater. Interfaces, 2018. 1–21 p. ISBN 10-1002-201800536.

[2] A. Menozzi, A. Garcia, M.N. Partl, G. Tebaldi, P. Schuetz, Induction healing of fatigue damage in asphalt test samples, Constr. Build. Mater, 2015. 162–168 p. ISBN 10.1016-10-034.

[3] Q. Liu, S. Wu, E. Schlangen, Induction heating of mastic asphalt for crack control, Constr. Build. Mater, 2013. 345–351 p, ISBN 10-1016-2012-11-075.

[4] E. Lizasoain-Arteaga, I. Indacoechea-Vega, P. Pascual-Muñoz, D. Castro-Fresno, Environmental impact assessment of induction-healed asphalt mixtures, J. Cleaner Prod, 2018.1546–1556 p. ISBN 10-1016-2018-10-223.

[5] B. Lou, A. Sha, D.M. Barbieri, Z. Liu, F. Zhang, W. Jiang, Improved microwave heating uniformity and self-healing properties of steel slag asphalt containing ferrite filler, Mater. Struct. Materiaux et Construct, 2021. 1–14 p.

[6] L. Baowen, S. Aimin, L. Yupeng, W. Wentong, L. Zhuangzhuang, J. Wei, C. Xin, Effect of metallic-waste aggregates on microwave self-healing performances of asphalt mixtures, Constr. Build. Mater, 2020. 246 p. ISBN 118510.

[7] X. Liu, Y. Zhao, Z. Wei, D. Zhang, Microwave absorption enhancement of asphalt concrete with SiC-Fe3O4 mixtures modifier, Constr. Build. Mater, 2020. 254 p. ISBN 119209.

[8] O. Xu, M. Li, D. Hou, Y. Tian, Z. Wang, X. Wang, Engineering and rheological properties of asphalt binders modified with microwave preprocessed GTR, Constr. Build. Mater, 2020. 256 p. ISBN 119440.

[9] J. Gallego, F. Gulisano, V. Contreras, A. Pa´ez, the crucial effect of re-compaction energy on the healing response of hot asphalt mortars heated by microwaves, Constr. Build. Mater, 2021. 285 p. ISBN 122861.

[10] E. Yalcin, Effects of microwave and induction heating on the mechanical and self-healing characteristics of the asphalt mixtures containing waste metal, Constr. Build. Mater, 2021. 286 p. ISBN 122965.

1st International Conference on Advances in Civil & Environmental Engineering, University of Engineering & Technology Taxila, Pakistan

Conference date 22 &23 Feb 2022

Application of Machine Learning to Predict the Flexural Moment Capacity of Near Surface Mounted Beam

Jahanzaib Mehmood[1], Afaq Ahmad[1]
[1]Civil Engineering Department
University of Engineering & Technology Taxila, Pakistan
jahanzaib.mehmood@students.uettaxila.edu.pk; afaq.ahmad@uettaxila.edu.pk

Jose Sena Cruz[2]
[2]Department of Civil Engineering, University of Minho, Guimarães, Portugal
jsena@civil.uminho.pt

ABSTRACT

The present study focuses on the use of Artificial Neural Networks (ANNs) to predict the flexural moment capacity of near surface mounted (NSM) RC beams. For doing this, a database of 52 samples containing 40 different parameters is collected from previous literature. Out these 40 parameters, critical parameters such as area of steel reinforcement (A_{sl}), stress in steel (f_s), effective depth (d), ratio of depth of equivalent rectangular stress block to depth of the neutral axis (β_1), the distance between neutral axis and extreme fiber (c), area of FRP (A_f), effective depth of FRP (d_f) and tensile modulus of FRP (E_f) are identified and further used as input value in ANNs. These input parameters are arranged in 4 different ways and ANNs model is trained using these 4 combinations. Equations are used to remove errors such as MSE and MAE during prediction. The results obtained after prediction have shown that the model B-4 gave highest value of correlation factor R (96%) with minimum value of MSE (0.34%) and MAE (2.8%) which clearly depicts the predictions of ANNs model are much closer to experimental values. Furthermore, results from ANNs model are also compared with ACI code to authenticate the performance of ANNs models.

KEYWORDS: ANN, NSM, MSE, MAE, ACI

1   INTRODUCTION

The idea of near surface mount (NSM) is not new. Indeed, during the 1940s it began to be utilized in Europe to improve the strength of reinforced concrete constructions. This innovative method comprised on setting rebar into grooves present at the concrete cover. These groove cuts are then filled with concrete mortar[1]. It took more than 10 years of research studies until this method of strengthening the concrete was more commonly used in practice and when it was compared with Externally Bonded Reinforcement (EBR), it showed benefits such as the preparation of surface was reduced in case of NSM, removal of weak layer was not needed in NSM, it was less prone to debonding and damage occurred to reinforcement as it was placed inside concrete cover[2]. Now a days this technique is becoming popular in its practical application for both shear and flexural

1st International Conference on Advances in Civil & Environmental Engineering, University of Engineering & Technology Taxila, Pakistan

Conference date 22 &23 Feb 2022

strengthening of beams. It offers more resistance to different environmental factors such as corrosion and fire because the reinforcement is placed inside the concrete cover. Commonly, adopted cross-section of the reinforcement for NSM is a bar or a strip. The efficiency of the reinforcement is influenced by the cross-section. Due to this fact, the efficiency of rounded FRP is less as compared to Squared FRP[3]. Figure 1 (a) and (b) shows the cross-section of FRP.

(a)   (b)

Figure 1 Cross-section of NSM-FRP

Flexural strengthening of RC beams with FRP had been an area of interest for many researchers in recent time. This study aims to predict the flexural moment capacity of NSM RC beams using artificial neural network (ANNs) approach. For prediction, a database containing different parameters is prepared. Four different ANNs models are used for predicting the results. In the end, the predicted results are compared with their experimental values and ACI code.

2   RC BEAM DATABASE

A database of 52 samples of RC beams strengthened with NSM-FRP is prepared by collecting data from literature. Each sample contains 40 different parameters related to different characteristics of RC beam. From these 40 parameters, 8 critical parameters which have the highest influence on the result are separated. These parameters are shown in the Table 1 with their correlation factor R[4] in Figure 2.

Table 1 Critical Parameters of Database

Parameter	Unit	Max	Min	Mean	St. Dev
A_{sl}	mm^2	794	39.27	304.21	208.29
f_s	MPa	788	426	518.50	80.66
D	mm	352	145.53	238.76	57.82
β_1	-	0.85	0.742	0.812	0.038
C	Mm	38	14	28.35	8.46
A_f	mm^2	126.68	13.44	65.56	28.15
d_f	Mm	395	164	274	64.22
E_f	GPa	172	109	142.69	18.30
$Mu\text{-}Exp$	KNm	190.1	11.985	63.56	44.14

1st International Conference on Advances in Civil & Environmental Engineering, University of Engineering & Technology Taxila, Pakistan

Conference date 22 &23 Feb 2022
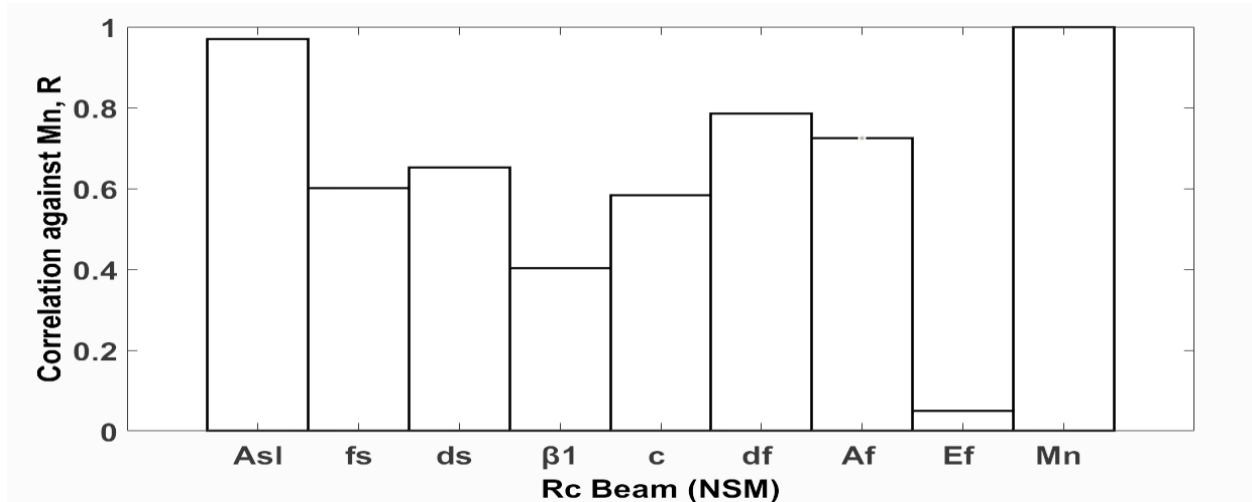
Figure 2 Correlation Factor R with respect critical parameters

3   ARTIFICIAL NEURAL NETWORKS

Artificial Neural Networks (ANNs) are like genetic algorithms and fuzzy logics. They are similar to human neural network[5]. They have the ability to calculate solution for a wide range of problems without demanding high level computational resources or lengthy analysis[6]. ANNs are capable of learning, categorizing and predicting the values based on the earlier learning process because they have the ability to remember information introduced to them in training. Different number of layers are used in ANNs depending on the accuracy of the work. The ANNs used in the present work consists of 4 layers as input layer, output layer and 2 hidden layers. All these layers are connected by neurons. Feed forward and back propagation of ANNs is shown in Figure 3.
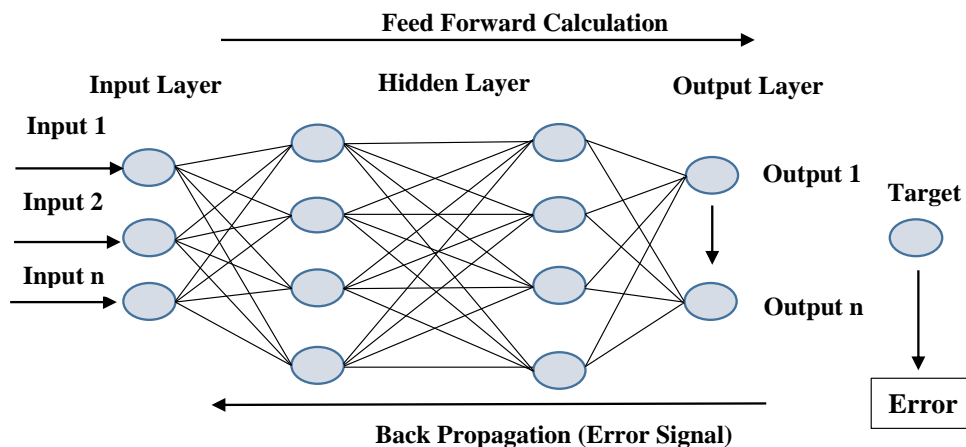
Figure 3 Layout of Artificial neural networks

1st International Conference on Advances in Civil & Environmental Engineering, University of Engineering & Technology Taxila, Pakistan

Conference date 22 &23 Feb 2022

In forward pass neuron apply calculations on input value and predict the output value. This predicted value is compared with the target result. The difference between the predicted and target value is sent back to input layer by back propagation[7]. The input layer takes this error value and forward it to neuron which predict the result again. This cycle goes on until target value is reached. In the present work the data was normalized because low learning rates is a problem with raw data[8]. Normalization range was kept [0.1-0.9] by using Equation (1)[9].

$$X = \frac{\Delta X}{\Delta x} x + (X_{max} - \frac{\Delta X}{\Delta x} x_{max}) \tag{1}$$

In the above-mentioned equation X is the normalized value, x is the given value, ΔX is the difference between range 0.9-0.1, Δx is the difference between maximum and minimum value of x, X_{max}=0.9 and x_{max} is the maximum value of x.

After normalization four different combinations of input parameters were used[10]. Details of these parameters is mentioned in Table 2.

Table 2 Combinations of input parameters

Name	Input Parameters	Output Parameter
B-1	$A_{sl}, f_s, d, \beta_1, c, A_f, d_f, E_f$	M_{exp}
B-2	$Asl/Af, f_s, d/d_f, \beta_1, c, E_f$	M_{exp}
B-3	$A_{sl}, f_s, d, \beta_1, c/d_f, A_f, E_f$	M_{exp}
B-4	$A_{sl}, f_s, d, \beta1/c, A_f, d_f, E_f$	M_{exp}

4   COMPARATIVE STUDY

Depending on the combinations of input parameter 4 different ANNs models were prepared on MATLAB software through coding[11]. These models predicted the output value for each combination. In this work, model named B-4 gave the highest value of correlation factor R (96%) and minimum value of MSE (0.34%) and MAE (2.8%). The predicted values are plotted against experimental results in Figure 4. Both MSE and MAE are plotted in Figure 5.
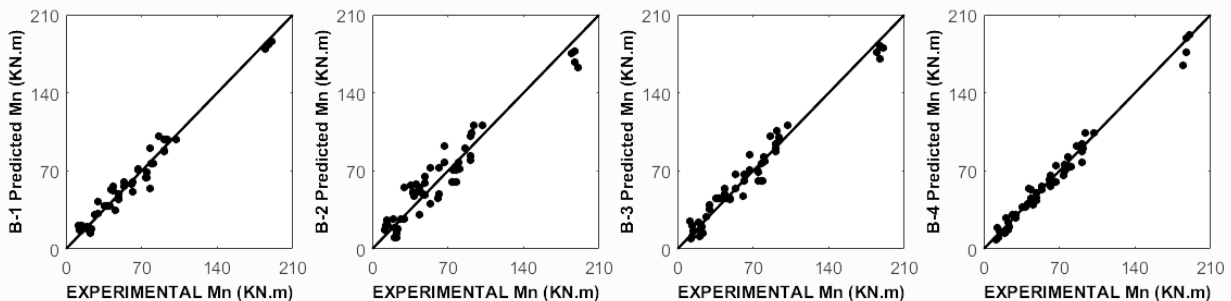
Figure 4 ANNs model's predictions

1st International Conference on Advances in Civil & Environmental Engineering, University of Engineering & Technology Taxila, Pakistan

Conference date 22 &23 Feb 2022
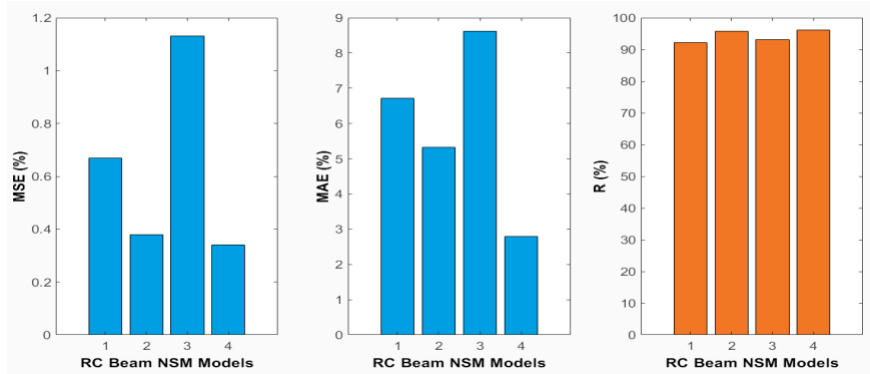
Figure 5 Correlation factor R, MSE and MAE

In the last phase comparison of predicted result and experimental results are made with ACI code[12]. The results are plotted against ACI code and it shows the values obtained by prediction are closer to experimental results as compared to ACI code.
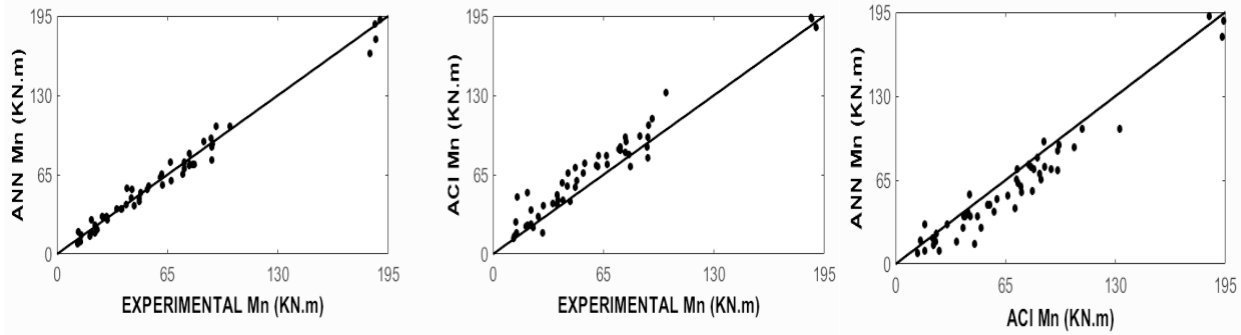
Figure 6 Comparison of ANNs predictions

5   CONCLUSIONS

In this study, the potential of Artificial Neural Networks to predict the behaviour of RC beam strengthened with near surface mount FRP has been discussed. Different parameters from a well-prepared database are selected for prediction. Results obtained has revealed that the model named B-4 has better efficiency with highest value of R (96%) which means the predictions made with ANNs are much closer to the experimental value. It has not only predicted accurate results but also the errors MSE and MAE are minimum. This clearly shows the potential of ANNs a non-conventional technique to be used in the industry to predict the behaviour of different structural members with different cross-sections and geometry as an alternative to conventional methods. The structural performance can be studied from predictions by training the algorithms of ANNs with an accurate database. If ANNs are used in industry, it would not only make accurate predictions without length analysis but also save a lot time.

1st International Conference on Advances in Civil & Environmental Engineering, University of Engineering & Technology Taxila, Pakistan

Conference date 22 &23 Feb 2022

REFERENCES

1. Asplund, S. *Strengthening bridge slabs with grouted reinforcement*. in *Journal Proceedings*. 1949.
2. De Lorenzis, L. and J.-G. Teng, *Near-surface mounted FRP reinforcement: An emerging technique for strengthening structures*. Composites Part B: Engineering, 2007. **38**(2): p. 119-143.
3. Sena-Cruz, J., et al., *NSM systems*, in *Design Procedures for the Use of Composites in Strengthening of Reinforced Concrete Structures*. 2016, Springer. p. 303-348.
4. Giordano, F., M.L. Rocca, and C. Perna, *Input variable selection in neural network models*. Communications in Statistics-Theory and Methods, 2014. **43**(4): p. 735-750.
5. Basheer, I.A. and M. Hajmeer, *Artificial neural networks: fundamentals, computing, design, and application*. Journal of microbiological methods, 2000. **43**(1): p. 3-31.
6. Ahmad, A., D.M. Cotsovos, and N.D. Lagaros, *Framework for the development of artificial neural networks for predicting the load carrying capacity of RC members*. SN Applied Sciences, 2020. **2**(4): p. 1-21.
7. Rojas, R., *The backpropagation algorithm*, in *Neural networks*. 1996, Springer. p. 149-182.
8. Ahmad, A., et al., *Knowledge-Based Prediction of Load-Carrying Capacity of RC Flat Slab through Neural Network and FEM*. Mathematical Problems in Engineering, 2021. **2021**.
9. Sharib, S., et al., *PREDICTION MODELS FOR LOAD CARRYING CAPACITY OF RC WALL THROUGH NEURAL NETWORK*. 2021.
10. Ahmad, A. and A. Raza, *Reliability analysis of strength models for CFRP-confined concrete cylinders*. Composite Structures, 2020. **244**: p. 112312.
11. Alam, M., *Codes in MATLAB for training artificial neural network using particle swarm optimization*. Research Gate, 2016: p. 1-16.
12. Al-Obaidi, S., Y.M. Saeed, and F.N. Rad, *Flexural strengthening of reinforced concrete beams with NSM-CFRP bars using mechanical interlocking*. Journal of Building Engineering, 2020. **31**: p. 101422.
13. Dias, S.J., J.A. Barros, and W. Janwaen, *Behavior of RC beams flexurally strengthened with NSM CFRP laminates*. Composite Structures, 2018. **201**: p. 363-376.
14. Fernandes, P., et al., *Durability of bond in NSM CFRP-concrete systems under different environmental conditions*. Composites Part B: Engineering, 2018. **138**: p. 19-34.
15. Jung, W.-t., et al., *Flexural behavior of concrete beam strengthened by near-surface mounted CFRP reinforcement using equivalent section model*. Advances in Materials Science and Engineering, 2017. **2017**.

1st International Conference on Advances in Civil & Environmental Engineering, University of Engineering & Technology Taxila, Pakistan

Conference date 22 &23 Feb 2022

EFFECT OF NON-PLASTIC FINES ON HYDRAULIC CONDUCTIVITY OF LAWRENCEPUR SAND

Hammad Haider1, Naveed Ahmad2, Shaheera Sharib3
[1,2,3]Civil Engineering Department
University of Engineering & Technology Taxila, Pakistan
Corresponding Author: hammad.haider1@uettaxila.edu.pk

ABSTRACT

Presence of fines alter the engineering properties and behavior of sandy soils. For sites located near water bodies or having shallow water table, hydraulic conductivity becomes an important engineering property to be determined. In this study, Lawrencepur sand has been used and non-plastic were produced by grinding the same sand to avoid any possible change in mineral composition. It was observed that presence of fines decreased the hydraulic conductivity of sand significantly and rate of decrease was higher at smaller percentages of fines and kept decreasing at higher percentages.

KEYWORDS: Lawrencepur sand, non-plastic fines, hydraulic conductivity

1   INTRODUCTION

For the analysis of seepage, settlement of soil, understanding of soil permeability plays a key role [1,2]. The soil moisture interaction greatly affects its structural stability [3,4]. For earth structures like levees, embankments and dams, hydraulic conductivity is required to see seepage quantity through them. To plan dewatering for any underground structure, soil permeability needs to be known [5]. In the past, many failures of dam have happened because of lack of geological and geotechnical investigations. As far as number of seepage failures are concerned through foundation or body of dam, almost 30% of them happened due to lack of geotechnical investigation [6].

The research of the hydraulic conductivity of sand with gradation and shape has been presented by researchers [7] and also on the soil grain size [8]. According to the data by researchers, equations do not give fair results in case of clayey soils with grain size distribution and for soils with effective grain sizes ($D_{10} > 3$ mm) [9]. There is difficulty in the prediction of hydraulic conductivity of well graded soils due to the presence of different size particles [10]. Furthermore, there are weaknesses and limitations on types of fields and lab tests [11].

To enhance the clay quality as liner, silica fume is used that increases compressive strength, whereas permeability, swelling pressure and plasticity index are reduced [12]. By adding upto 10% bentonite to dune sand, the permeability of sample is reduced from 10^{-4} cm/s to 10^{-8} cm/s [13]. The laboratory test of permeability and shear strength are expensive and time consuming. Therefore, researchers are working on prediction models for soil permeability based on soil index properties. There are co-relations between important parameters with soil index properties, e.g. plasticity characteristics and grain size distribution [5].

1st International Conference on Advances in Civil & Environmental Engineering, University of Engineering & Technology Taxila, Pakistan

Conference date 22 &23 Feb 2022

Reduction in aggregate base course was observed with increase in fines [14]. A sharp decline in permeability was reported with initial increase of fines, followed by less rapid drop [15]. By increasing silt content from 0 to 30%, permeability decreased slowly initially, followed by rapid drop of permeability when silt content increased beyond 30% [16]. The peak of undrained shear strength can be corelated with saturated hydraulic conductivity with fines content upto 50 percent, as it reduces linearly as the saturated hydraulic conductivity [log (k_{sat})] decreases and the fines content (F_c) increase [17]. Decreasing trend in curves was observed in the hydraulic conductivity of sand-fine mixtures with the addition of fines [18]. Hydraulic conductivity of sand-fine mixtures was decreased with addition of fines [19].

In Pakistan, there are a number of sources for sand collection, both bed-run and from quarries. These sands are used for different purposes, both as foundation support and as construction material. Permeability of sand plays an important role to control stability of earthen structure constructed near water bodies. Sometimes, clean sand deposits are not located and it becomes unavoidable to use sands containing certain amount of fines into it. In our study, effect of fines has been studied on permeability of locally available Lawancepur sand.

2   MATERIALS AND METHODS

Locally available source of lawrencepur sand was selected for sample collection. Sand was collected in bulk and transported to the Soil Mechanics and Foundation Engineering Laboratory, UET Taxila for detailed testing. Sand collected from site was washed and fines were separated by wash sieving. Fines were prepared by grinding the sand using Los angeles Abrasion machine.

Sand had uniformity coefficient 2.89 and curvature coefficient 1.11. Samples with different percentage of fine content were prepared in the laboratory. The mineral composition of fines and sand was same as fines were prepared from the same sand.

3   EXPERIMENTATION

Particle size distribution of dried sand samples was done by using a set of sieves. Other index properties tests conducted were specific gravity and hydrometer test for fines used in the study. Hydraulic conductivity tests were done by using different percentages of fines produced by grinding the sand.

4   EXPERIMENTAL RESULTS

Results of different type of tests conducted are presented in subsequent sections.

4.1   Grain size distribution curve for sand

Grain size distribution curve for sand is presented Figure 1. Co-efficient of curvature and Co-efficient of uniformity are presented Table 1.

1st International Conference on Advances in Civil & Environmental Engineering, University of Engineering & Technology Taxila, Pakistan

Conference date 22 &23 Feb 2022
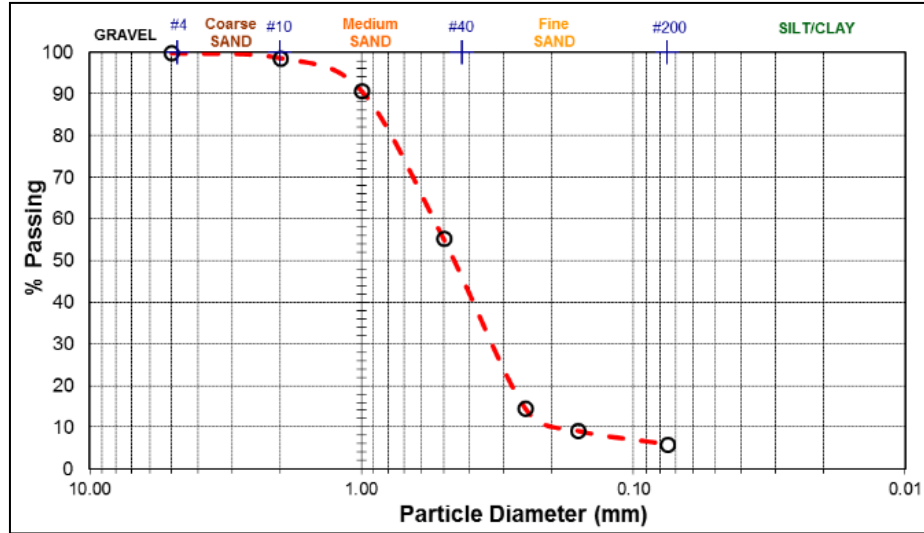
Figure 1: Grain Size Distribution Curve

Table 1: Gradation characteristics of clean sand

Parameters	Value
D_{10}	0.19 mm
D_{30}	0.34 mm
D_{50}	0.45 mm
D_{60}	0.55 mm
Cc	1.11
Cu	2.89

4.2 Soil Classification

As per American association of state Highways and Transportation Officials (AASHTO) soil classification system, the sand was fine sand, categorized as A3 with group index value of zero. Whereas, sand was classified as poorly graded sand (SP) as per Unified Soil Classification system (USCS).

4.3 Hydraulic Conductivity

Variation of hydraulic conductivity of sand with different percentage of fines is presented in Table 2 and Figure 2 below.

1st International Conference on Advances in Civil & Environmental Engineering, University of Engineering & Technology Taxila, Pakistan

Conference date 22 &23 Feb 2022

Table 2:Hydraulic Conductivity of Sand-Silt mixtures

Percentage of Fines	Permeability (cm/s)
0	2.003E-02
10	6.900E-03
20	4.538E-04
30	2.994E-04
50	1.372E-04
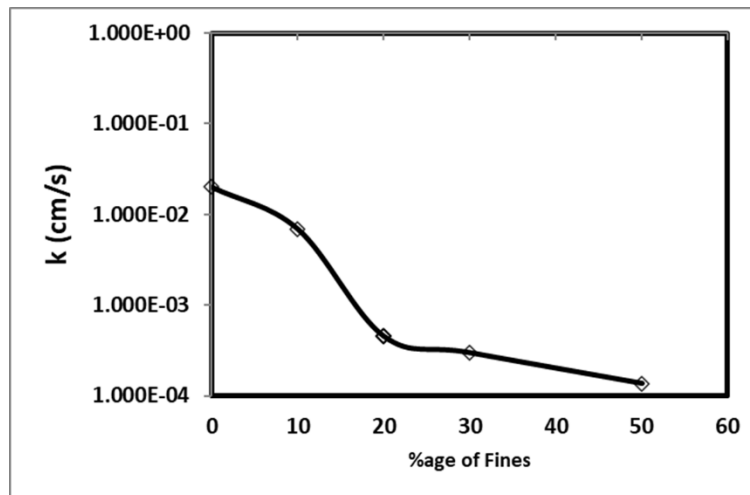
Figure 2: Variation of Hydraulic Conductivity with fines

5   CONCLUSION AND RECOMMENDATIONS

5.1   Conclusion

1. By adding small percentages of fines, the gap between sand particles were decreased and rapid decrease in permeability was observed i.e. upto 20%. Whereas, with further addition of fines, control of sand-silt mixture was transferred to fines and decrease in void sizes was not so significant, resulting in less decrease in permeability of the mixture.

5.2   Recommendations

1. Sand collected from sources having different sizes and mineralogy can be used to develop a general correlation.
2. Fines in our case were non-plastic. Plastic fines can be added to study behavior of same sand.

1st International Conference on Advances in Civil & Environmental Engineering, University of Engineering & Technology Taxila, Pakistan

Conference date 22 &23 Feb 2022

REFERENCES

1. Sivapullaiah, P. V., A. Sridharan, and V. K. Stalin. "Hydraulic conductivity of bentonite-sand mixtures." *Canadian geotechnical journal* 37, no. 2 (2000): 406-413.
2. Tizpa, Parichehr, Reza Jamshidi Chenari, Mehran Karimpour Fard, and Sandro Lemos Machado. "ANN prediction of some geotechnical properties of soil from their index parameters." *Arabian Journal of Geosciences* 8, no. 5 (2015): 2911-2920.
3. Alhassan, Musa. "Permeability of lateritic soil treated with lime and rice husk ash." (2008).
4. Roy, Surendra, and Sanjeev Kumar Bhalla. "Role of geotechnical properties of soil on civil engineering structures." *Resources and Environment* 7, no. 4 (2017): 103-109.
5. Elhakim, Amr F. "Estimation of soil permeability." *Alexandria Engineering Journal* 55, no. 3 (2016): 2631-2638.
6. Barzegari, Ghodrat. "Geotechnical evaluation of dam foundation with special reference to in situ permeability: A case study." *Geotechnical and Geological Engineering* 35, no. 3 (2017): 991-1011.
7. Cabalar, Ali Firat, and Nurullah Akbulut. "Evaluation of actual and estimated hydraulic conductivity of sands with different gradation and shape." *SpringerPlus* 5, no. 1 (2016): 1-16.
8. van Ginkel, Marloes, and Theo N. Olsthoorn. "Distribution of grain size and resulting hydraulic conductivity in land reclamations constructed by bottom dumping, rainbowing and pipeline discharge." *Water Resources Management* 33, no. 3 (2019): 993-1012.
9. Carrier III, W. David. "Goodbye, hazen; hello, kozeny-carman." *Journal of geotechnical and geoenvironmental engineering* 129, no. 11 (2003): 1054-1056.
10. Göktepe, Ahmet Burak, and Alper Sezer. "Effect of particle shape on density and permeability of sands." *Proceedings of the Institution of Civil Engineers-Geotechnical Engineering* 163, no. 6 (2010): 307-320.
11. Jabro, J. D. "Estimation of saturated hydraulic conductivity of soils from particle size distribution and bulk density data." *Transactions of the ASAE* 35, no. 2 (1992): 557-560.
12. Kalkan, Ekrem, and Suat Akbulut. "The positive effects of silica fume on the permeability, swelling pressure and compressive strength of natural clay liners." *Engineering geology* 73, no. 1-2 (2004): 145-156.
13. Ameta, N. K., and Abhay Shivaji Wayal. "Effect of bentonite on permeability of dune sand." *Ejge* 13 (2008): 1-7.
14. Siswosoebrotho, Bambang Ismanto, Pamudji Widodo, and Erwandy Augusta. "The influence of fines content and plasticity on the strength and permeability of aggregate for base course material." In *Proceedings of the Eastern Asia society for transportation studies*, vol. 5, pp. 845-856. 2005.
15. Aldaood, Abdulrahman. "Impact of fine materials on the saturated and unsaturated behavior of silty sand soil." *Ain Shams Engineering Journal* 11, no. 3 (2020): 717-725.
16. Hsiao, Darn-Horng, Vu To-Anh Phan, Yi-Ting Hsieh, and Hsin-Yi Kuo. "Engineering behavior and correlated parameters from obtained results of sand–silt mixtures." Soil Dynamics and Earthquake Engineering 77 (2015): 137-151.
17. Belkhatir, Mostefa, Tom Schanz, and Ahmed Arab. "Effect of fines content and void ratio on the saturated hydraulic conductivity and undrained shear strength of sand–silt mixtures." Environmental earth sciences 70, no. 6 (2013): 2469-2479.
18. Khan, Tanveer Ahmed, Khalid Farooq, Mirza Muhammad, Mudasser Muneer Khan, Syyed Adnan Raheel Shah, Muhammad Shoaib, Muhammad Asif Aslam, and Syed Safdar Raza. "The Effect of Fines on Hydraulic Conductivity of Lawrencepur, Chenab and Ravi Sand." Processes 7, no. 11 (2019): 796.
19. Karim, Mohammad Emdadul, and Md Jahangir Alam. "Effect of nonplastic silt content on undrained shear strength of sand–silt mixtures." International Journal of Geo-Engineering 8, no. 1 (2017): 1-26.

1st International Conference on Advances in Civil & Environmental Engineering, University of Engineering & Technology Taxila, Pakistan

Conference date 22 &23 Feb 2022

Structural Strength Evaluation and Investigating Cracking Behaviour of Newly Constructed Building

Muhammad Usman Rashid, Qaiser Uz Zaman Khan
University of Engineering & Technology Taxila, Pakistan

m.usman@uettaxila.edu.pk, dr.qaiser@uettaxila.edu.pk
Rameez Sohail
University of Engineering & Technology Taxila, Pakistan
Rameez.sohail@uettaxila.edu.pk

ABSTRACT

The objective of this research is to investigate the cracking behavior of slab and reinforced concrete columns of four story under construction building situated in Bahria Town Rawalpindi. Although, construction industry is emerging with its full resources of manpower and machinery but there exist certain reasons behind these, surface and through surface cracks in under construction buildings. It is fact that utilization of resources may improve its efficiency many folds. In this research, work has done to investigate the technical flaws in utilization of resources that the construction industry is futile to tackle cracking behavior in under construction building. For investigation of cracks nondestructive testing techniques were used to assess the possible causes and there affects in structural integrity. For nondestructive testing, Schmidt hammer test, ultrasonic pulse velocity test and concrete core cutter test was applied directly on structural concrete members. Nondestructive testing helps to assess compressive strength, uniformity of concrete and cavities in concrete of existing structure. The cracks were produced due to the poor quality of concrete and lacking experience of shuttering party especially in roof slabs. Extraction of concrete cores also showed low concrete cover in slabs and through cracks that penetrated through the whole section of roof slab.

KEYWORDS: cracking behavior, strength evaluation, concrete's uniformity, nondestructive testing, roof slab, concrete cover, through cracks

1   INTRODUCTION

The primary purpose of a building is to keep the occupants safe and if the cracks appear during a construction process, then it is a threatening situation. For long survival of building it should be structurally safe, and normal imposed loads must be resisted by slabs and floors [1]. In concrete construction, quality control was based primarily on concrete's compressive strength. Only that concrete was considered acceptable which satisfies the minimum criteria of concrete strength. Several buildings deteriorate early during its service life which raises the concern about quality of concrete. It was mostly observed that cracks and failures mostly occur due to the use of poor quality of construction material [2]. In reinforced concrete structures, most of problems faced nowadays are associated to inadequate constructional practices [3]. Most of the reinforced concrete (RC)

1st International Conference on Advances in Civil & Environmental Engineering, University of Engineering & Technology Taxila, Pakistan

Conference date 22 &23 Feb 2022

structures that were placed in seismic zones are planned by taking into consideration only the gravity loads without providing any ductile detailing [4].

A strength evaluation is used for determination of inner irregularities such as cracks, inner voids, or areas of inferior concrete quality which lessens structural capability [5]. In strength evaluation, stability, safety, serviceability and strength of individual component or entire structure is seen [6]. Nondestructive techniques are a challenging task used for assessment of mechanical properties of concrete. There are several techniques which are used nowadays that are sounding, pulse velocity, impact-echo method, impulse-response method, ground-penetrating radar, infrared thermography, radiography, schmidt hammer test and concrete core cutter test.

Aoyama [7] evaluated the structural performance of new RC structures. They proposed constructional guidelines and structural design. These guidelines were primarily for earthquake resistance. Trtnik et al. [8] predicted concrete strength by ultrasonic pulse velocity. Akkaya et al. [9] measured concrete strength by a non-destructive technique which is ultrasonic wave reflection method. Shimizu et al. [10] estimated the concrete strength of existing RC structures in Japan. In order to retrofit the existing structure and for seismic resistance inspection, it becomes essential to evaluate strength of concrete.1130 existing buildings were taken into consideration and 10788 cores were taken from them. Kheder [11] developed mathematical relationships using multiple linear regressions in order to evaluate concrete's compressive strength by using rebound hammer and ultrasonic pulse velocity method. Schueremans and Gemert [12] assessed safety of existing structures and also evaluated their bearing capacity. Qasrawi [13] estimated concrete strength by combined methods of nondestructive testing; ultrasonic pulse velocity and rebound hammer tests were used. The results obtained were compared to prior ones from literature and with actual results also attained from samples taken from existing structures. Imbsen et al. [14] worked on the strength evaluation of existing bridges including slab bridges, T-beams, girder and box beams. Bartlett and MacGregor [15] determined an equivalent concrete strength using concrete core tests. Several related aspects are also quantified which affects the concrete compressive strength.

Most of strength evaluation methods are done on the existing structures to assess the structural stability. Therefore, in this paper strength of under construction building is evaluated. Schmidt rebound hammer test, concrete core cutter test and ultrasonic pulse velocity test was applied directly on structural concrete members.

2   EXPERIMENTAL PROGRAM

Non-destructive testing techniques were applied in order to evaluate the strength of under construction four story building. The details and methodology of tests applied on structural concrete members are also given below. Following tests were applied

- Concrete core cutter test (ASTM C-42/42M) [16]
- Schmidt rebound hammer test (ASTM C-805) [17]
- Ultrasonic pulse velocity test (ASTM C-597) [18]

2.1   Concrete core cutter test (ASTM C-42/42M)

Total 19 No of cores were extracted from site from random locations for determining of compressive strength of slab and raft. Total 18 No of cores were extracted from slab of first floor

1st International Conference on Advances in Civil & Environmental Engineering, University of Engineering & Technology Taxila, Pakistan

Conference date 22 &23 Feb 2022

and second floor; due to poor access to raft foundation for core extraction we were able to extract only one core from raft foundation.

2.2   Schmidt rebound hammer test (ASTM C-805-16)

Schmidt hammer test was performed on random locations of slab and columns on under construction four story building. Complete results of all test locations were tabulated in result section of this report.

2.3   Ultrasonic pulse velocity test (ASTM C-597-16)

Concrete's uniformity, presence of crack and quality can be assessed by using this method. Zero time adjustment was made to confirm that instrument is functioning appropriately. If zero adjustments could not be achieved for reference bar then instrument must be repaired or changed for accurate measurements. The transducers (emitter and receiver) having coupling agent (e.g. mouldable rubber, water, grease, oil, or any other viscous material) was pressed with concrete surface until unless a stable transit time was displayed. The straight-line distance from centre of transducers faces was also measured to calculate velocity of waves. Strength of concrete was assessed using graph shown in Figure 1.
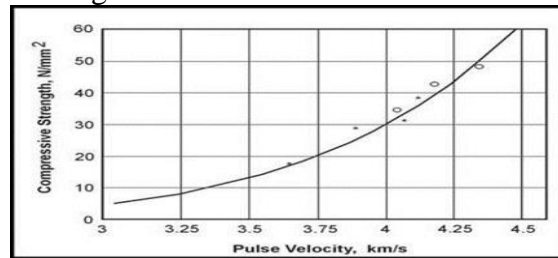
Figure 1: Relative compressive strength measurement graph [19].

3   RESULTS AND DISCUSSIONS

3.1   Results of concrete core testing

Cores extracted form site were examined and tested in Concrete Technology Laboratory of UET Taxila. Results of concrete cores are shown in Figure 2.
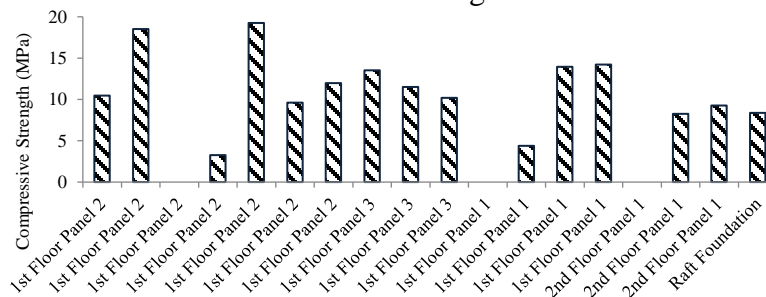
Figure 2: Test results of concrete cores.

4 out of 19 cores were damaged during extraction process due to poor quality concrete. It was worth mentioning that the slab thickness wasn't uniform in all panels. It was seen that there

1st International Conference on Advances in Civil & Environmental Engineering, University of Engineering & Technology Taxila, Pakistan

Conference date 22 &23 Feb 2022

was about 5-8% sag in slab panels that could be viewed by naked eye as well. This is the indication of poor shuttering work during casting operation. It was observed that cores extracted from center of the panel has lower strength than that of extracted near supports. The density of cracks was also less near supports. There was another factor of less compressive strength of concrete as the workability of concrete was very high as compared to standard requirements.

3.2   Results of Schmidt rebound hammer test

The estimated cylinder strength is shown in Figures 3-6. It was observed that compressive strength values for schmidth hammer test results were satisfactory. There is uniformity in rebound values of all reinforced concrete columns. The test results for compressive strength values are in close relation with required compressive strength of 28MPa for columns. The column S-1-3 C-3 and P-10, C-1 showed minimum compressive strength as there was honeycombing in these columns. Although during testing the areas exhibiting honeycombing were avoided but in these columns honey combing was existed throughout the length. The columns at ground floor were good in strength and in geometry as well (Figure 3).
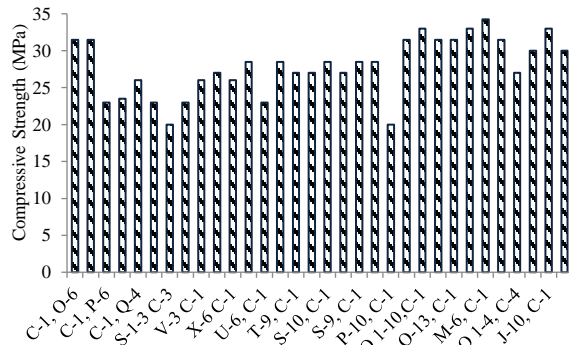
Figure 3: Results of ground floor columns.
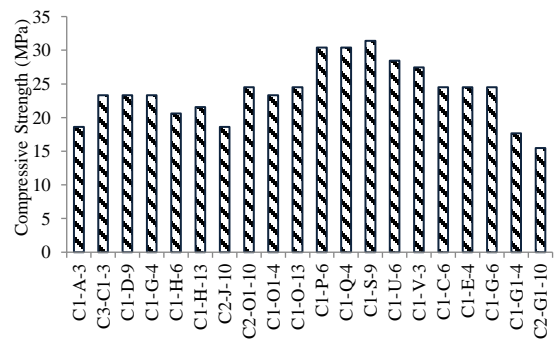
Figure 4: Results of first floor Column.
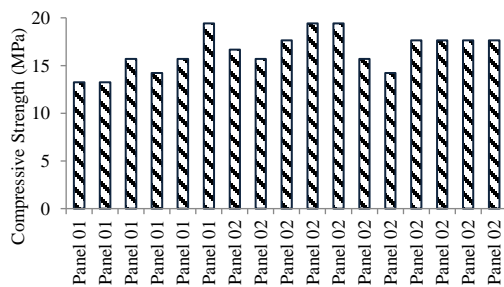
Figure 5: Test results of first floor Slabs.
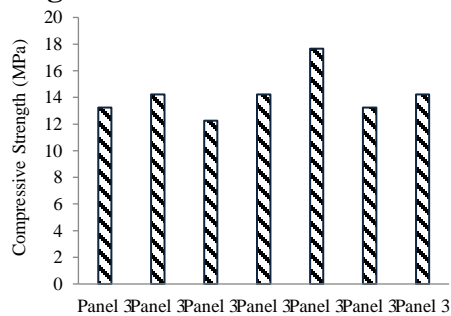
Figure 6: Test results of second floor slab.

Schmidth hammer test results of first floor columns are shown in Figure 4. The test results of columns of first floor weren't satisfactory. Only two columns achieved the required strength of 28MPa. Most of the columns have compressive strength in the range of 70 to 80% of the required strength. In comparison to ground floor columns the concrete quality at first floor columns was very poor both in strength and physical appearance as well.

1st International Conference on Advances in Civil & Environmental Engineering, University of Engineering & Technology Taxila, Pakistan

Conference date 22 &23 Feb 2022

The concrete quality of first floor and second floor roof slab was very poor. The average rebound values showed the irregular results for all panels. There wasn't any uniformity in test results for all roof slab panels as shown in Figure 5 & 6, even the panels were cast in one go of concreting operation. Some of the locations on roof slab showed 60% of required strength. The average strength varies from 60 to 70% of the required strength. However, the major problems of slabs were micro and macro cracks. The crack detection could not be examined by using schmidht hammer test results. To check cracks ultrasonic pulse velocity test was applied.

3.3   Results of Ultrasonic pulse velocity test of slab

Ultrasonic Pulse Velocity test was performed on random locations of first floor slab on under construction four storey building. As discussed in previous section of schmidth hammer test results that cracks in concrete can be examined by using ultrasonic pulse velocity test. Due to presence of cracks none of the UPV test location exhibit high value of velocity. The lower values of UPV indicated the poor-quality concrete. This also indicates that the crack density in roof slab panels was too much high. Complete results of all test locations are shown in Figure 7. Locations of UPV tests are designated as first floor panel 1,2 and 3 and abbreviated as "FF P1,2, and 3" etc.
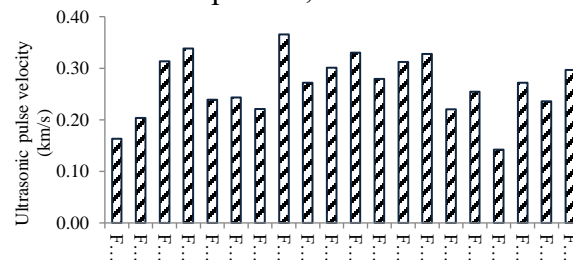
Figure 7: UPV results of first floor slab.

4   CONCLUSIONS

Based on experimental investigations following conclusions were drawn by this research:

1. There was considerable sagging in slab panels due to poor workmanship during casting of slabs and shuttering quality was very poor.
2. The cracks in slabs of all panel were not only in vertical direction but also in horizontal direction as well.
3. Crack density was higher at mid span of slab panels as compared to areas near to supports.
4. The columns of the building showed higher rebound values and of good quality concrete.

5   ACKNOWLEDGMENTS

1st International Conference on Advances in Civil & Environmental Engineering, University of Engineering & Technology Taxila, Pakistan

Conference date 22 &23 Feb 2022

6   REFERENCES

[1]   Michael S.Poles. What are Construction Defect. Retrieved at 15 Sept 2008, from http://www.mmgroup.com.

[2]   Ahzahar N, Karim NA, Hassan SH, Eman J. A study of contribution factors to building failures and defects in construction industry. Procedia Engineering. 2011 Jan 1;20:249-55.

[3]   Naser Alenezi. Strength Evaluation of Existing Reinforced Concrete Structure. International Conference on Artificial Intelligence, Energy and Manufacturing Engineering (ICAEME'2015) Jan, 2005, 7-8.

[4]   Masi A, Vona M. Estimation of the in-situ concrete strength: provisions of the European and Italian seismic codes and possible improvements. InEurocode 2009 (Vol. 8, pp. 67-77).

[5]   ACI Committee. 437R-03: Strength Evaluation of Existing Concrete Buildings. Committee Report. 2003;437:1-28.

[6]   ACI Committee. 437R-91: Strength Evaluation of Existing Concrete Buildings. 1991;437:1-24.

[7]   Aoyama H. Development of new reinforced concrete structures. Sistema Nacional de Protección Civil, Centro Nacional de Prevención de Desastres; 1995.

[8]   Trtnik G, Kavčič F, Turk G. Prediction of concrete strength using ultrasonic pulse velocity and artificial neural networks. Ultrasonics. 2009 Jan 1;49(1):53-60.

[9]   Akkaya Y, Voigt T, Subramaniam KV, Shah SP. Nondestructive measurement of concrete strength gain by an ultrasonic wave reflection method. Materials and Structures. 2003 Oct 1;36(8):507-14.

[10] Yasushi SHIMIZU, Masaya HIROSAWA and Jiandong ZHOU. Statistical Analysis of Concrete Strength in Existing Reinforced Concrete Buildings in Japan.

[11] G. F. Kheder. A two stage procedure for assessment of in situ concrete strength using combined non-destructive testing. Materials and Structures, Vol. 32, July 1999, pp 410-417

[12] Luc Schueremans & Dionys Van Gemert (2004) Assessing the safety of existing structures: Reliability based assessment framework, examples and application, Journal of Civil Engineering and Management, 10:2, 131-141

[13] Hisham Y. Qasrawi Concrete strength by combined nondestructive methods Simply and reliably predicted. Cement and Concrete Research 30 (2000) 739-746

[14] R. A. IMBSEN, W. D. LIU, R. A. SCHAMBER and R. V. Nutt. STRENGTH EVALUATION OF EXISTING REINFORCED CONCRETE BRIDGES.

[15] F. Michael Bartlett and James G. MacGregor. Statistical Analysis of the Compressive Strength of Concrete in Structures AC1 Materials Journal, V. 93, No. 2, March-April 1996.

[16] ASTM C42/42M-16, Standard test method for obtaining and testing drilled cores and sawed beams of concrete., ASTM International, West Conshohocken, PA, 2016, www.astm.org

[17] ASTM C805 -16, Standard test method for rebound number of hardened concrete., ASTM International, West Conshohocken, PA, 2016, www.astm.org

[18] ASTM C497 -16, Standard test method for pulse velocity through concrete., ASTM International, West Conshohocken, PA, 2016, www.astm.org

[19] Neville AM. Properties of concrete. London: Longman; 1995 Jan.

1st International Conference on Advances in Civil & Environmental Engineering, University of Engineering & Technology Taxila, Pakistan

Conference date 22 &23 Feb 2022

Finite Element Modelling and Analysis of Typical Industrial Precast Tray Slab Using ABAQUS

Ijaz Ali, Fayiz Amin, Muhammad Usman, Muhammad Naveed, Hafiz Ahmad Waqas

Ghulam Ishaq Khan Institute of Engineering Sciences and Technology, Pakistan

u2018544@giki.edu.pk; u2018117@giki.edu.pk; u2018559@giki.edu.pk; m.naveed@giki.edu.pk, hafiz.waqas@giki.edu.pk.

ABSTRACT

Precast concrete slabs are a helpful addition to any construction project. They are used in small homes to large industrial buildings. These slabs are strong and durable than in-situ ones owing to the quality and controlled environment. They are available in variety of shapes, sizes and design which make them more versatile and easily applicable in most of the construction projects. This paper discusses the Finite Element Modelling (FEM) based design optimization approach using different mesh sizes to plot and develop more accurate capacity curve of the typical industrial precast tray slabs and to design more efficient and economical precast slab. A 3D model of the typical tray slab was created in the ABAQUS FEM software and the suggestions for the design improvements are recommended based on analysis and visualization of results considering stress distributions in the structure.

KEYWORDS: Finite Element Modelling (FEM), Precast Concrete Tray Slab, Design optimization

1   INTRODUCTION

Precast concrete slabs are made by pouring standard concrete into a specific mould and cured under controlled supervision. The concrete and steel materials are used conform to ACI code and ASTM standards. This prevents environmental or human errors and enhances the strength of member. Design improvements are always deemed necessary aiming to offer a sustainable, environmentally friendly and affordable construction approach. Conventionally experimental methods are employed and less attention is given to use of FE modelling in precast structures to execute design improvements [1]. This research effectively opts the FEM tools for analysing the structural behaviour of target member.

2   DESCRIPTION OF MODEL AND METHODOLOGY

2.1   Geometry

The tray slab is comprised of concrete and steel with dimensions of 457.2 mm $\times$ 2133.6 mm and thickness at centre as 25.4 mm. The size of steel reinforcement and clear cover was kept as 10 mm. Figure 1 shows the assembly of model in FE software.

1st International Conference on Advances in Civil & Environmental Engineering, University of Engineering & Technology Taxila, Pakistan

Conference date 22 &23 Feb 2022
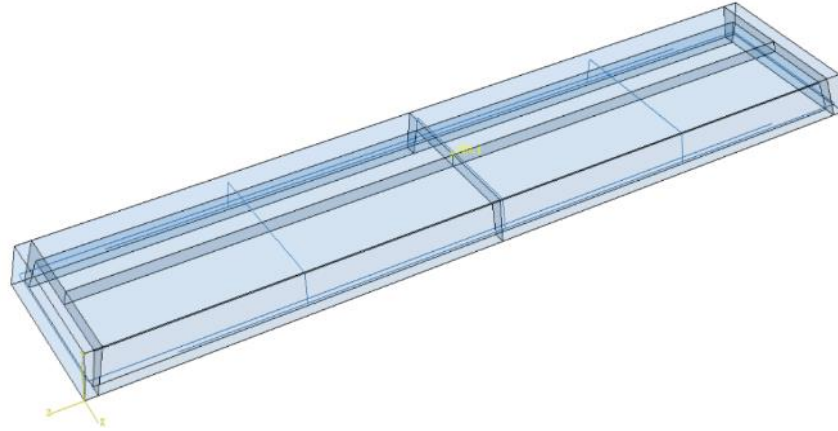
Figure 1 Assembly of try slab with concrete geometry and steel reinforcement cage

2.2   Materials and damage model

Both elastic and plastic properties for the steel and concrete were used from the literature to simulate the realistic material behaviour. For concrete, the concrete damage plasticity model was used and for steel the values from tensile test were considered [2]. Table 1 and Table 2 provides the typical details of materials used in modeling process.

Table 1 Properties of steel reinforcement

Modulus of elasticity, E (GPa)	200	Yield strength (MPa)	275
Poisson's Ratio	0.32	Density (kg/mm^3)	8.0e-9

Table 2 Properties of concrete material

E (GPa)	21	Poisson's Ratio	0.21	Density (Kg/mm^3)	2.00E-09

2.3   Interactions, Boundary Conditions and Loading

The embedded region interaction type was employed to simulate the bond between concrete and steel rebar. The ends of the slab were modelled with pinned supports where rotation about x-axis was only permitted [3]. The displacement controlled loading was considered to effectively induce the cracking behaviour and complete structural failure of the slab. A displacement of 25 mm was imposed at the reference point, constrained with the target surface of the slab. The kinematic coupling of reference point and median surface of slab enabled the desired application of displacement and aided in constructing load displacement curve. Figure 2 exhibits the boundary conditions and location of reference point. Next, the damage

1st International Conference on Advances in Civil & Environmental Engineering, University of Engineering & Technology Taxila, Pakistan

Conference date 22 &23 Feb 2022

mechanism was simulated through Dynamic explicit analysis step and overall capacity of the precast slab was determined after gaining the appropriate size of the mesh.
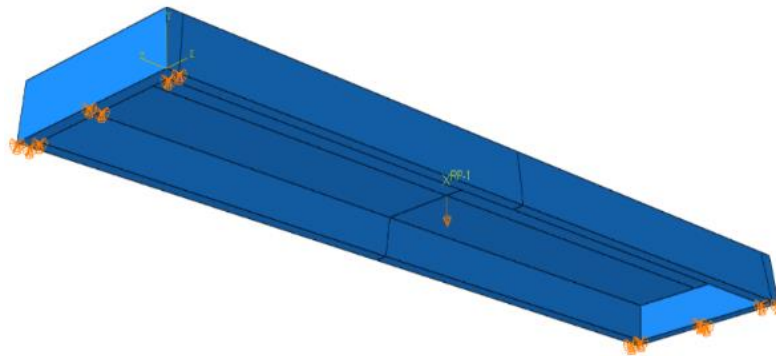
Figure 2 Boundary condition and location of reference point

2.4   Element types and Mesh size

The 3-Dimensional elements for concrete and reinforcement were considered where the concrete parts were assigned Continuum, 3-Dimensional, 8 Node Elements with Reduced integration (C3D8R) and on the other hand, the steel reinforcement was assigned with, 3-D, 2 Node truss elements (T3D2) for improved accuracy and lesser computational cost [4]. The behaviour of the modelled member was found sensitive to the mesh size and it was deemed necessary to carryout sensitivity analysis for selection of the optimum mesh size. The load carrying capacity of slab was obtained from FE analysis using different mesh size and it was compared with the known capacity of industrial precast slab. A mesh size of 100 mm was initially selected and was revised after every subsequent analysis until the desired results were achieved. Figure 3 presents the meshed geometry of try slab.
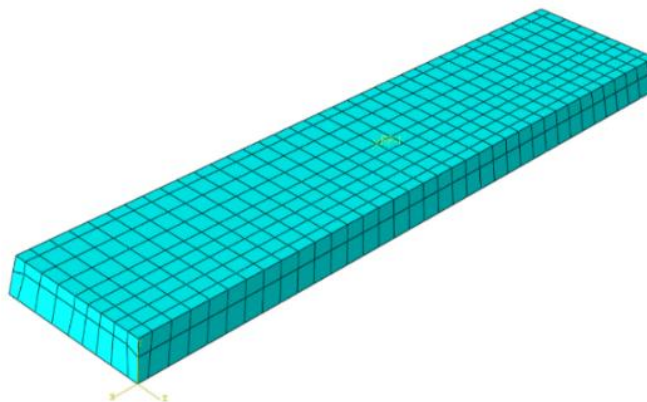
Figure 3 Meshed geometry of the model

1st International Conference on Advances in Civil & Environmental Engineering, University of Engineering & Technology Taxila, Pakistan

Conference date 22 &23 Feb 2022

3   RESULTS AND DISCUSION

The analysis was carried out for mesh sizes of 100, 60, 40 and 20 mm and corresponding load vs. displacement curves were drawn. The load displacement curves, reflecting the capacity of the typical industrial slab, are provided in the Figure 4. The results indicate that the capacity is decreased with the reduction in the mesh size and the maximum force appears at smaller displacements. With larger mesh size the slab appears to be stiffer and exhibit larger load carrying capacity. With the decrease in mesh size, the results converged towards the actual reported capacity of the precast slab i.e. 5600 N however, larger computational time was involved. The mesh size of 20 mm was found adequate to get improved results with suitable computational time. The selected mesh size gave the capacity of about 4930 N which was found nearer to the actual load carrying capacity of typical industrial slab.
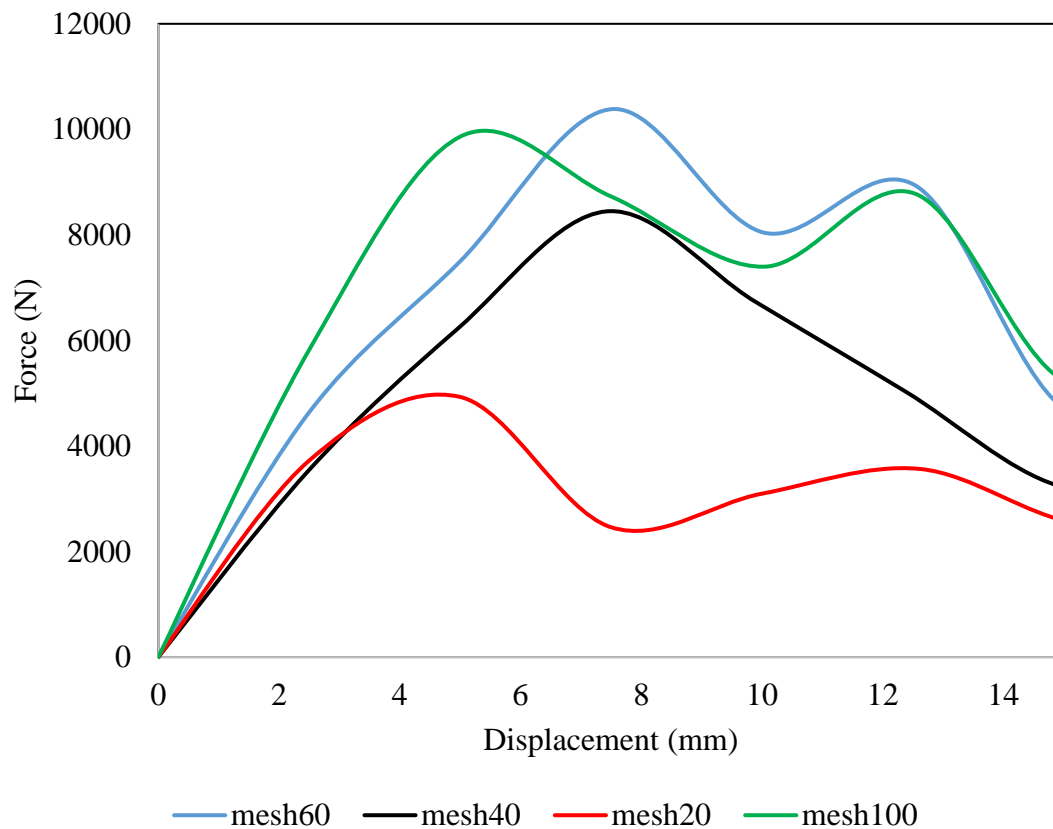
Figure 4 Force vs. displacement curves of different mesh size

3.1   Design optimization

Multiple limitations are associated with the typical precast slabs presently being used in the industry. These limitations include short width of slabs which results in greater number of joints, more material consumption, plethora of time for erection and all this with a lesser load capacity. Therefore, the adopted technique of modelling and analysis with viable mesh size can be further utilized to analyse the similar sort

1st International Conference on Advances in Civil & Environmental Engineering, University of Engineering & Technology Taxila, Pakistan

Conference date 22 &23 Feb 2022

of slabs with a variation in its geometry and material parameters to reach at an optimized design solution for the precast slabs. This optimized design then can be proposed to industry for its commercial implementation.

4   CONCLUSION

This paper illustrates the impact on the accuracy of analysis results due to variation in the mesh size of a FE model using ABAQUS. It was demonstrated that how the change in mesh size can affect the accuracy of results as well as the time required for the completion of analysis. From the analysis results, it was observed that with the smaller mesh size, the solution is more accurate and convergent towards the desired target however it costs more computational time. Based on these results, it is concluded that choice of improper mesh size can diverge the results significantly therefore, selection of a felicitous mesh size to get a better solution with a lesser computational time is very necessary and of profound importance. The optimum parameters of the modeling and mesh size are believed to vibrant contributing factors to consider during the refinement process of design to achieve economy and productivity in the construction process.

REFERENCES

1. Precast Concrete Slabs | Commercial Engineering. Retrieved February 9, 2022, from https://florida-engineer.com/commercial-engineering/precast-concrete/precast-concrete-slabs/
2. Abed, F., Oucif, C., Awera, Y., Mhanna, H. H., & Alkhraisha, H., *FE modeling of concrete beams and columns reinforced with FRP composites*. Defence Technology, 2021. **17**(1), p. 1–14.
3. Kankeri, P., & Suriya Prakash, S., *Efficient hybrid strengthening for precast hollow core slabs at low and high shear span to depth ratios*. Composite Structures, 2017. **170**: p. 202–214.
4. Masching, H., & Bletzinger, K. U., *Parameter free structural optimization applied to the shape optimization of smart structures*. Finite Elements in Analysis and Design, 2016. **111**: p. 33–45.

Detection of Pavement cracks of UET Taxila using pre-trained model Resnet50 of CNN

Chaudhary Fazeel Ahmed, Abdullah Cheema
Department of Civil Engineering, University of Engineering and Technology Taxila
18-CE-61@students.uettaxila.edu.pk; 18-CE-49@ students.uettaxila.edu.pk

Waqas Qayyum

Department of Civil Engineering, University of Engineering & Technology Taxila, Pakistan

waqas.qayyam@students.uettaxila.edu.pk

Ehtisham Rana
Department of Civil Engineering, University of Engineering and Technology Taxila
Rana.Ehtisham@students.uettaxila.edu.pk

Afaq Ahmad
Department of Civil Engineering, University of Engineering & Technology Taxila, Pakistan
Afaq.Ahmad@uettaxila.edu.pk

ABSTRACT

Image processing through MATLAB using a pre-trained model of CNN Resnet50 is utilized in this research. The objective of this research is to focus on the crack types, their bad effect on the structure, and to identify these cracks using image processing. Resnet50 is used for crack detection and the dataset of 48,000 images is collected. This dataset is further divided into two categories crack and normal (un-crack), 24000 images (50%) are placed in the crack category and the rest of the 50% images are placed in the normal class, and Resnet50 is trained on this dataset. A dataset of some cracks and normal images is collected from the different parts of the institutional buildings for testing of the pre-trained model. A confusion matrix is also plotted to check the accuracy, precision, recall, f1 score, and overall performance of resnet50. The accuracy achieved by testing was 99.8% and a precision of 1.

KEYWORDS: Pavement Cracks, Cracks Detection, Resnet50, Convolutional Neural Network.

1   INTRODUCTION

Cracks are the major problem in every structure. They need to be identified and find out through various methods. For long pavements, it is almost impossible to go to every location and analyze the pavement structure. The necessary parts for evaluating road pavement maintenance activities

1st International Conference on Advances in Civil & Environmental Engineering, University of Engineering & Technology Taxila, Pakistan

Conference date 22 &23 Feb 2022

are measuring, monitoring, and evaluating the condition of pavements. One of the most common problems in the road is cracking [1]. It is a very important issue to identify the cracks which allow to efficiently plan the interventions for preventive maintenance. Recent advancement in technology and research has a significant influence on the field related to distress evaluation of pavements which makes it possible to analyze the damage reliably and quickly than using consolidated methods [2].

The system of identification of cracks is now based on processing through digital imaging which is already being used for the detection of infrastructures related to transport such as bridges, tunnels, and highways [3]. The images from the road surface are collected typically by surveyor robots or road detection vehicles which are multi-functional.

Convolutional Neural Network (CNN) is related to the algorithm of Deep Learning which takes data from an input image, it assigns important variables to the different aspects which help in differentiating one aspect from others [4], as shown in Figure 1. CNN requires less pre-processing data, due to which it is considered as one of the most efficient image processing functions as compared to other algorithms used for classification [3]. While previously used methods need to be hand-engineered, CNN can learn relevant characteristics.
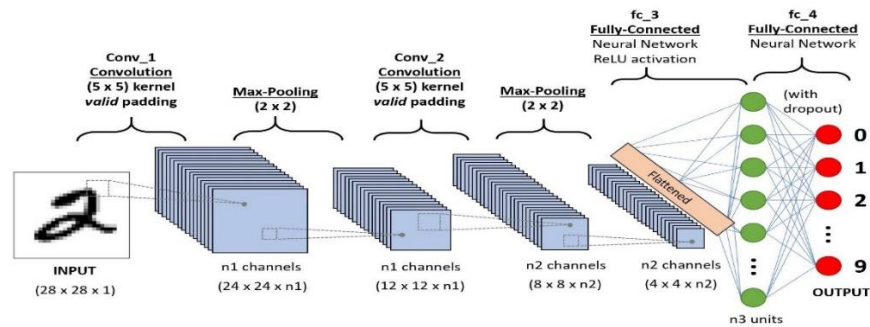
Figure 1: Convolutional Neural Network [8]

The focus of this research will be on evaluating crack detection using image processing methods. For this purpose, a pre-trained model is used, which an automated tool for crack detection is named Resnet50. Its other parameters like accuracy, precision, recall, and f1 score are also measured to check its performance.

2   LITERATURE REVIEW

Research related to the detection of autonomous crack detection is done by [5]. Which, the main focus was on the classification of images and approaches related to the bounding box that has been

1st International Conference on Advances in Civil & Environmental Engineering, University of Engineering & Technology Taxila, Pakistan

Conference date 22 &23 Feb 2022

proposed on existing detection methods for concrete cracks by using deep convolutional neural networks. The study has focused on the method of crack detection by focusing on the Fully Convolutional Network (FCN) related to semantic segmentation in images of concrete cracks. An average of 90% precision is achieved by FCN [5]. It was found that the cracks are detected reasonably and their density is also evaluated accurately. The comparative study related to the assessment of pavement quality was conducted between images from the sophisticated commercial company for visual inspection and classified images from CNN that were obtained from GSV [6]. This study has demonstrated that the classification of the images of pavements in different categories of defined categories can be achieved using CNN. Sandeep et al. studied the systematic review of the CNN-based assessment methods. The review is related to the categorization of different classes based on a specific application of CNN applied to the data which is obtained through a range of structures [7].

3   ADOPTED METHODOLOGY

In this research, the adopted methodology consists of five steps, as shown in Figure 2. Images dataset is collected for training from an online source and divided into two categories named crack and un-crack. Resnet50 is trained on this dataset and the testing dataset is collected from the pavements of UET Taxila. A confusion matrix is plotted to check the performances of resnet50.

Collection of dataset → Distribution of Images → CNN Model → Training and Testing → Results

Figure 2: Adopted Methodology

3.1   Acquisition of Images:

A dataset of 48000 images is collected and is equally divided into two categories [10], 24000 images (50%) are placed in the 1st category named crack and the rest of the 24000 images (50%) are placed in an un-crack category. Another dataset of 400 images is also collected for the testing of the pre-trained model of CNN from the pavements of UET Taxila and is equally divided into two crack and un-crack categories, as shown in Figure 3.

1st International Conference on Advances in Civil & Environmental Engineering, University of Engineering & Technology Taxila, Pakistan

Conference date 22 &23 Feb 2022

Figure 3: Pavement Cracks of UET Taxila

3.2   Resnet50 Specifications

Resnet50 also stands for Residual Networks is a well-known neural network used for many projects and serves as the foundation for many CNN tasks [1]. Resnet50 has 50 Deep layers and 157 DAG network layers used in it, as shown in Table 1. Resnet50 can classify the 1000 categories and can get training on more than a million images with 224 x 224 x 3 image features, as shown in Table 1.

Table 1: Specifications of Resnet50

Pre-Trained Models	Deep Layers	DAG network layers	Parameters	Size (MB)	Input Image size
Resnet50	50	177	25.6 M	98	224 x 224 x 3

4   RESULTS

In this research pavement cracks of UET Taxila are predicted by using the pre-trained model of CNN. Data set of 200 cracks images and 200 un-cracks images are tested. The accuracy, precision, recall, and f1 score are calculated from the equations 1, 2, 3, and 4. Resnet50 results in the accuracy rate of 99.75%, precision 100%, recall 99.50%, and F1 score 99.75%, as shown in Table 2. The overall performance of resnet50 is found to be very efficient with 99.8%, are shown in Figure 3. A confusion matrix is also plotted for the calculations of these parameters.

$$\text{Accuracy} = (TP+TN) / (TP+TN+FP+FN) \tag{1}$$

$$\text{Precision} = (TP) / (TP+FP) \tag{2}$$

$$\text{Recall} = (TP) / (TP+FN) \tag{3}$$

1st International Conference on Advances in Civil & Environmental Engineering, University of Engineering & Technology Taxila, Pakistan

Conference date 22 &23 Feb 2022

F1 Score = (Precision + Recall) / 2 $\hspace{4cm}$ (4)

Resnet50 is a pre-trained model which has 50 deep layers and 157 DAG network layers, utilizes the processing time of 464 sec for training and testing, as shown in Table 2. The PC used for training and testing of the Pre-trained model has specifications Intel(R) Corei3, 9th Generation, 16GB RAM, 2x3.60GHz processor, and NVIDIA GeForce GTX 1650 SUPER graphic card.

Table 2: Results of Resnet50

Pre-trained Model	Accuracy (%)	Precision (%)	Recall (%)	F1 Score (%)	Processing Time (sec)
Resnet50	99.75	100	99.50	99.75	464
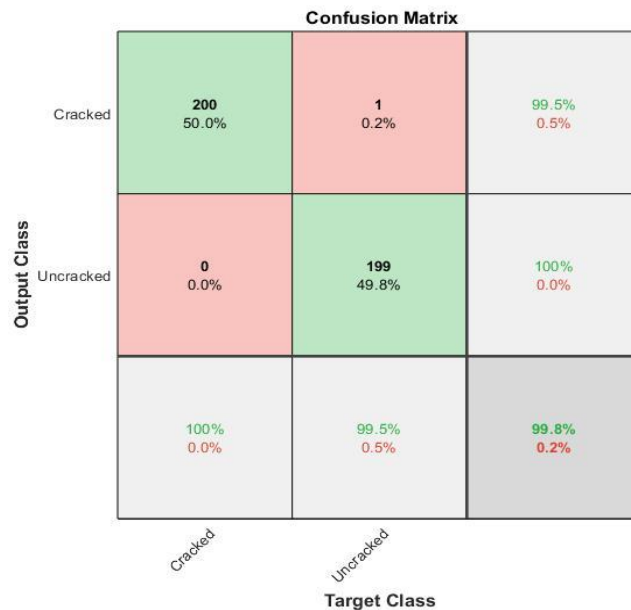
Figure 3: Confusion Matrix of test images

5   CONCLUSIONS

The results were really precise and the system can analyze all the cracks with good precision. Although hairline crack was not identified it is due to the image quality. High pixel images should be used for this program for accurate results and good performance. The accuracy of the model is found 99.8 % and precision is 100%, and overall performance is 99.8%. This is due to the number of images used for the training. In this research, many attempts have been made to rightly classify

1st International Conference on Advances in Civil & Environmental Engineering, University of Engineering & Technology Taxila, Pakistan

Conference date 22 &23 Feb 2022

cracks using resnet50 but all the same, results are found same. Due to the use of good PC specifications resnet50 having 50 deep layers take very lass time for training and testing. In the future Google net will be used for image classification and unmanned aerial vehicles will be used for the acquisition of images.

6 REFERENCES

[1] C. N. E. M.-M. L. a. S. L. Zhang, "Pavement distress detection using convolutional neural network (CNN): A case study in Montreal, Canada," International Journal of Transportation Science and Technology, 2021.

[2] S. M. M. a. X. Q. Dorafshan, "Automatic surface crack detection in concrete structures using Otsu thresholding and morphological operations.," 2016.

[3] T. S. N. R. S. a. S. H. Yamaguchi, "Image-based crack detection for real concrete surfaces," TRANSACTIONS ON ELECTRICAL AND ELECTRONIC ENGINEERING, p. 128–135, 2007.

[4] B. W. K. Z. A. Y. E. a. W. G. Li, "Automatic classification of pavement crack using deep convolutional neural network," International Journal of Pavement Engineering, vol. 21, no. 4, pp. 457-463, 2020.

[5] C. Dung, " Autonomous concrete crack detection using deep fully convolutional neural network," Automation in Construction, vol. 99, pp. 52-58, 2019.

[6] M. C. C. a. K. A. Maniac, "Deep learning-based visual crack detection using Google Street View images," Neural Computing and Applications, vol. 33, no. 21, pp. 14565-14582, 2021.

[7] S. D. K. S. A. a. C. M. Sony, " A systematic review of convolutional neural network-based structural condition assessment techniques," Engineering Structures, vol. 226, p. 111347, 2021.

[8] S. Saha, "A Comprehensive Guide to Convolutional Neural Networks — the ELI5 way," TDS, 2 2018. [Online]. Available: https://towardsdatascience.com/a-comprehensive-guide-to-convolutional-neural-networks-the-eli5-way-3bd2b1164a53. [Accessed 2022].

[9] P. Dwivedi, "Understanding and Coding a ResNet in Keras," Doing cool things with data, 4 January 2019.

[10] https://digitalcommons.usu.edu/all_datasets/48/

1st International Conference on Advances in Civil & Environmental Engineering, University of Engineering & Technology Taxila, Pakistan

Conference date 22 &23 Feb 2022

Review of Forensic Structural Investigations to South Champlain Tower Florida, Collapse

Muhammad Hazib Hafiz, Mirza Ahmad
Department of Civil Engineering, University of Engineering & Technology Taxila, Pakistan
18-CE-106@students.uettaxila.edu.pk; 18-CE-114@students.uettaxila.edu.pk

Ehtisham Rana
Department of Civil Engineering, University of Engineering & Technology Taxila, Pakistan
Rana.Ehtisham@students.uettaxila.edu.pk

Nida Chairman
Department of Civil and Architectural Engineering, University of Westminster, UK
N.chairman@westminster.ac.uk

Afaq Ahmad
Department of Civil Engineering, University of Engineering & Technology Taxila, Pakistan
Afaq.Ahmad@uettaxila.edu.pk

ABSTRACT

Forensic analysis of collapse structures to investigate the mitigating source of the possible collapse is a fast-growing engineering field. The investigation methodologies are still in evolving stages but fundamental practices practice involves engineering investigations using finite element-based simulations, destructive and non-destructive testing, and analysis of the as-built structure. Failure investigation in forensic structural engineering involves the finite element simulations of as-built structures to investigate the possible failure modes and comparison of the existing design with published codes and standards to quantify any lapse in design. Similar approaches have been adopted in different researches published in investigating the possible collapse cause of South Champlain Tower. The possible reasons for the collapse include several deviations from design code standards, poor design choices such as fewer support beams and large column spaces to support pool deck slab resulting in punching shear failure, inadequate shear walls, and application of loads not part of the original design.

KEYWORDS: Forensic Structural Analysis, Causes/Predictions of Failure, Reviews

1   INTRODUCTION

A 12 stories residential condominium complex of Champlain Towers South, East, and North formed an L-shaped structure located in surfside town, north of Miami Beach, Florida. The Champlain Tower South containing residential units and rooftop penthouse was a reinforced

1st International Conference on Advances in Civil & Environmental Engineering, University of Engineering & Technology Taxila, Pakistan

Conference date 22 &23 Feb 2022

concrete flat plate structure completed in 1981. On June 24, 2021, at approximately 0630 hrs Coordinated Universal Time (UTC), the high-rise beachfront condominium building experienced a partial collapse resulting in a dead tool of 98 people to date [1].

Figure 1:Aerial Photograph of Partially Collapsed South Champlain Tower [2]

Structures are essentially designed to ensure safety and economy by considering the anticipated natural and man-made loads. In spite of extensive design improvements, to date, catastrophic failure of the structure still embarks a question mark on their safety. Researchers in the past and recently have made significant efforts in studying the failure mechanism of civil structures. Recently, forensic studies of civil structures have utilized the benefits of numerical simulations to study the collapse mechanism of failed structures. Numerical simulations methods provide significant insight into the forensic studies of structural failure but given the constraints of non-linear properties of the material, convergences issues of computational algorithms, and simplifications required to analyze the structure, significant research is still required in the area of forensic analysis of the collapsed structure using numerical simulations.

2   REVIEWS OF RESEARCHERS

The root cause of the sudden collapse of Champlain Towers South Condominium is still under investigation with several researchers presenting their studies into the likely causes of this event. Some of the most highly likely causes under investigation include the long-term waterproofing problem identified during preliminary investigations, differential settlement of the foundation, and punching shear failure of the pool deck. Numerical simulation studies and forensic investigations carried out by different researchers to deduce the cause of failure are presented, as shown in Table 1.

1st International Conference on Advances in Civil & Environmental Engineering, University of Engineering & Technology Taxila, Pakistan

Conference date 22 &23 Feb 2022

Table 1: Summary of Causes of Failure/Predictions by Researchers

Sr. No	Name of Researcher	Designation	Causes of Failure/Predictions	Summary
1.	Xinzheng LU et al.	Professor, Department of Civil Engineering, Tsinghua University.	i. Lower demand to capacity ratio of columns. ii. Inadequate inter-story drift iii. Weak reinforcement detailing of slab-column joint. iv. Inadequate number of shear walls	The axially compressive force ratios of columns within the collapsed zone, as well as the punching shear of crucial joints, failed to meet Chinese code standards [3]. Inter-story drift calculations subjected to design wind loads surpassed the Chinese code design threshold value of 1/800. The weak reinforcement detailing of the slab-column joint was designed via ACI-318 [4] code prior to 1981 as compared to current Chinese code requirements. There were fewer shear walls along the Y-axis (the Eastern part of the building that collapsed) as compared to the X-axis.
2.	Randall W. Parkinson	Research Associate Professor, Florida International University	i. Seawater intrusion	The structural integrity of the building might have been compromised due to seawater intrusion caused by several events of sea level rising above the building's basement floor.
3.	Jon Swaine	Investigative Reporter, The Washington Post	i. Structural damage of pool deck slab due to water ii. Violation of ACI 318 design code in detailing of slab-column joint.	Major structural damage of the pool deck slab and the adjacent area was caused by the water damage which resulted in the separation of the slab into different layers and weakened it. The failure of the pool deck increased the demand on columns causing excessive stresses that resulted in the column's buckling. Severe violation of ACI 318 code in detailing of rebar in the column-slab area as well as non-compliance of construction as per structural drawings was observed.
4.	Anjali Singhvi	Reporter, The New York's Time	i. Foundation damage due to seawater intrusion. ii. Failure of the waterproof layer of pool deck slab. iii. Inadequate beam and column layout and design.	The water intrusion from underground due to past storm surges resulted in damaging foundation piles. Similarly, the concrete structural slab was severely damaged due to the failure of waterproofing below the ground level deck. There was inadequate design of support beams below the ground level deck with fewer than required numbers to support the load with large column-span resulting in overstressing of the ground-level slab. Finally, inappropriate design of column-slab overlap reinforcement caused poor bonding and contributed towards punching shear failure.

1st International Conference on Advances in Civil & Environmental Engineering, University of Engineering & Technology Taxila, Pakistan

Conference date 22 &23 Feb 2022

3   METHODS AND MATERIAL

The methodology used in the investigation of progressive collapse of Champlain Towers South Condominium involved the review of recent research work carried out in quantitative assessment of key structural components, punching shear behavior, and modeling of post punching shear failure along with hybrid simulation of collapse process using finite element method and physics engine by Xinzheng LU et al [5], historic study of seawater level rise and its effect on Champlain Towers South [6], extensive 3D-modelling study, review of structural drawings, video evidence and published reports [7][8]. The Finite element-based computer model was established using the existing drawings without involving any time-based structural degradation, checking the punching strength of a typical slab-column joint, and axial strength check of typical. The finite element analysis carried out in LS-DYNA involved the development of two full-scale numerical 3D slab-column models of the typical story (9th story) joint using the designed reinforcement details and updated details based on Chinese code, as shown in Figure 2.
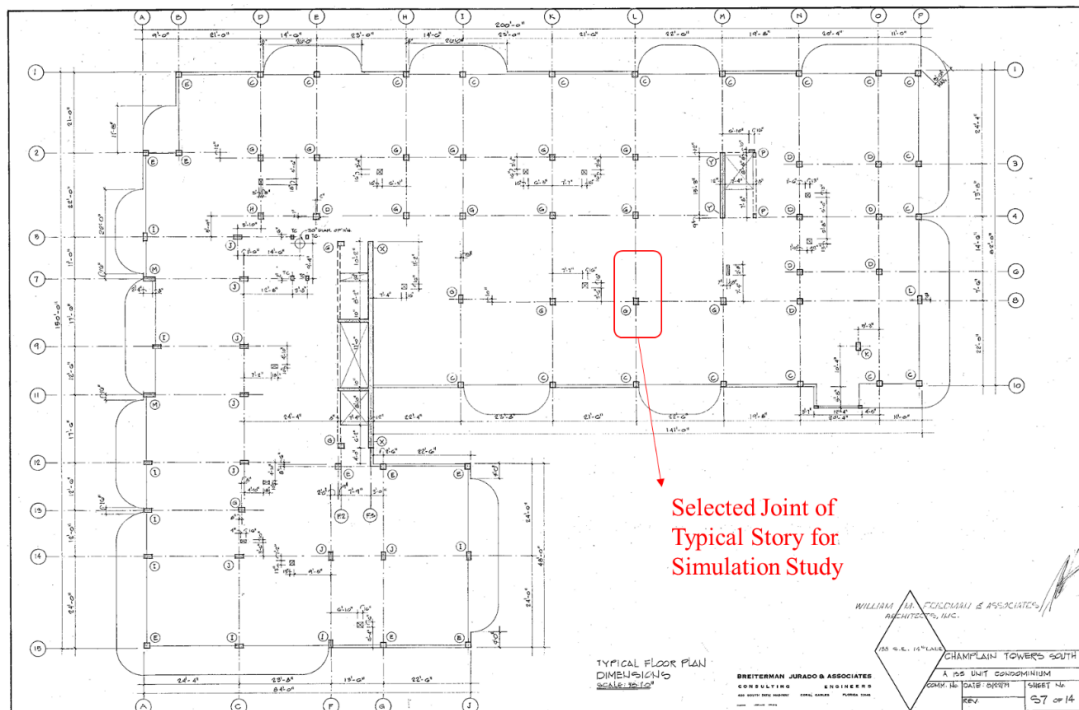
Figure 2: Selected Joint of Typical Floor Plan for Simulation Study [6]

The finite element models used eight-node 3D solid elements of concrete with explicitly modeled reinforcing bars using two-node Hughes-Liu beam elements with a 2×2 Gauss quadrature integration scheme. The behavior of concrete was modeled using continuous surface cap modeling with an adaptation of erosion function in the simulation of the concrete spalling. Slab edge surfaces were modeled using the simple supports whereas the horizontal restraints to the slab boundaries were modeled as spring elements. High fidelity simulation of the building collapse was performed

1st International Conference on Advances in Civil & Environmental Engineering, University of Engineering & Technology Taxila, Pakistan

Conference date 22 &23 Feb 2022

using Fiber2RBD developed by Zheng et al. [9]. The code is used for the conversion of the developed finite element model into a geometric model in the physics engine. After the coupling of the finite element model into the geometric model, the physics model was established and columns (I-2, 4,8,10, K-2, 4, 8, and K-10), as shown in Figure 1, were removed to simulate the building collapse under gravity. Historic study of seawater level rise involved the study of mean daily water-level elevations records (1981-2020), hourly water-level tides, and groundwater events reaching the elevation of the Champlain Tower South basement floor to speculate on the building's structural integrity being jeopardized as a result of climate change-induced sea-level rise. The 3D model of Champlain Tower South was developed to study the different possible causes of collapse using evidence collected from videos, structural drawings, site investigations after the collapse, and past evaluation reports.

4 RESULTS AND DISCUSSIONS

Extensive analysis using computer-based simulation showed that the calculated axial strength of columns within the collapse zone exceeded the design strength. Similarly, the results of the lateral stability in the analysis of the whole structure showed that the 1/800 barrier established in the Chinese Code was likewise exceeded by inter-story drift ratios subjected to the design wind load.. The simulated failure mode of the building showed that the shear walls ability to resist the propagation of collapse to the west side was greater as compared to the east part due to shorter length with no flanges in the failure propagation direction as compared to the west side having sufficiently long flanges to resist lateral loads. Numerical results in investigating of punching shear using LS-DYNA showed that punching shear capacity obtained using Chinese code was about 6% greater as compared to the ACI code slab-column junctions have poor construction details which lead to the poor resistance in decreased post punching stage resistance. Investigations of the possible compromise to structural integrity due to the saltwater intrusion revealed that there have been a number of times when sea level rises above the ground floor level from 244 a year between 1994 and 2006 to 636 from 2007 to 2020 due to a threefold increase in sea level rise after -2006. Furthermore, investigations on pool deck failure gathered multiple causes of failure that include the faulty design of a waterproof layer with an inadequate slope for drainage, a limited number of shallower support beams, and insufficiently large column spans.

5 CONCLUSIONS

Forensic investigations for root cause analysis of structural collapse require a significant amount of data for finite element modeling of the as-built structure and its integrity analysis. A review of different research work published in determining the possible root cause of the structural collapse of the South Champlain Tower showed that the main joints' punched shear strengths and the axial compressive strengths of the collapsed structure's columns were both low, and the collapsed structure was essentially unable to fulfill the criteria of contemporary Chinese design rules. The collapsed construction used a gravity column-shear wall arrangement, and the number of shear walls was inadequate. The sheer walls created in the X and Y axes have vastly different ratios. Due to insufficient reinforcement details, the critical slab-column junction had restricted strength

1st International Conference on Advances in Civil & Environmental Engineering, University of Engineering & Technology Taxila, Pakistan

Conference date 22 &23 Feb 2022

at the big deformation stage, according to an analysis. The pool deck slab was also poorly designed with an inadequate number of supports beams followed by large column spacings and poor waterproof slop. Similarly, the rising sea level due to climate change as a prime cause of increasing soil saturation might be one of the possible reasons for the structural collapse and forensic investigation must be expanded to analyze the damage resulting from seawater intrusion.

REFERENCES

[1] S. BLASKE et al., "House of Cards, How decades of problems converged the night Champlain Towers fell", *www.miamiherald.com*, 2021. [Online]. Available: https://www.miamiherald.com/news/special-reports/surfside-investigation/article256633336.html. [Accessed: 13- Feb- 2022].

[2] T. STAFF, "1 killed, dozens missing as building collapses in heavily Jewish Florida town", *Timesofisrael.com*, 2021. [Online]. Available: https://www.timesofisrael.com/1-killed-dozens-missing-as-building-partly-collapses-in-florida-town/. [Accessed: 13- Feb- 2022].

[3] GB 50010. Code for design of concrete structure. Beijing: China Architecture & Building Press, 2010

[4] ACI-318. Building code requirements for structural concrete. Farmington Hills: American Concrete Institute, 2019

[5] X. Lu et al., "A preliminary analysis and discussion of the condominium building collapse in surfside, Florida, US, June 24, 2021", Frontiers of Structural and Civil Engineering, vol. 15, no. 5, pp. 1097-1110, 2021. Available: 10.1007/s11709-021-0766-0 [Accessed 13 February 2022].

[6] R. Parkinson, "Speculation on the role of sea-level rise in the tragic collapse of the Surfside condominium (Miami Beach, Florida U.S.A.) was a bellwether moment for coastal zone management practitioners", Ocean & Coastal Management, vol. 215, p. 105968, 2021. Available: 10.1016/j.ocecoaman.2021.105968 [Accessed 14 February 2022].

[7] A. Singhvi, M. Baker, W. Cai, M. Gröndahl and K. Patanjali, "The Surfside Condo Was Flawed and Failing. Here's a Look Inside.", Nytimes.com, 2021. [Online]. Available: https://www.nytimes.com/interactive/2021/09/01/us/miami-building-collapse.html. [Accessed: 13- Feb- 2022].

[8] J. Swaine, E. Brown, J. Sohyun Lee, A. Mirza and M. Kelly, "How a collapsed pool deck could have caused a Florida condo building to fall", washingtonpost.com, 2021. [Online]. Available: https://www.washingtonpost.com/investigations/interactive/2021/pool-deck-condo-collapse/. [Accessed: 13- Feb- 2022].

[9] Zheng Z, Tian Y, Yang Z B, Lu X Z. Hybrid framework for simulating building collapse and ruin scenarios using finite element method and physics engine. Applied Sciences, 2020, 10(12): 4408

A Brief Introduction to Blockchain Technology and its Applications in Civil Engineering and Construction

Vagelis Plevris
Department of Civil and Architectural Engineering
College of Engineering, Qatar University, Doha, Qatar
vplevris@qu.edu.qa

ABSTRACT

Blockchain is a novel technology which permits the recording of data in a way that it is extremely difficult to change, hack or cheat. It is a promising technology that is considered as a general-purpose technology (GPT), by many. GPTs are technologies that have the power to influence and change an entire economy, affecting economic growth and the way people behave in their everyday lives and do business. We present some technical details about blockchain, how it began and its possible applications today, with focus on civil engineering and the construction industry. We also examine future applications of the technology, the challenges and opportunities it brings and its potential to reshape the construction industry to the better.

KEYWORDS: blockchain, general purpose technology, civil engineering, construction, engineering

1   INTRODUCTION

The Architecture, Engineering, and Construction industry has entered a period of major change caused by a host of new digital technologies that have been proven helpful due to the benefits and the potential they offer. These technologies include Virtual Reality, Artificial Intelligence, Geographic Information Systems, Building Information Modelling (BIM), Augmented Reality, the Internet of Things (IoT), Big Data, Sensors, among others [1]. Lately, a new digital technology has appeared, Blockchain, which promises to change the way people do transactions, keep their records, validate their data, and more. For many, blockchain is a general-purpose technology (GPT) that can change both our everyday lives and the way we do business.

By looking at the most recent scientific literature, one can realize how important blockchain technology has become lately. The word "blockchain" returns 27,959 results in the Scopus database (www.scopus.com) when searching within "Article title, Abstract and Keywords" (query made on Feb. 20, 2022). 27,715 of these results (99.1%) have a publication year of 2017 or later, as only 244 papers were published in the topic between 1990-2016. The trend is similar if we limit the search within the "Engineering" field, where we similarly receive 11,641 results (documents) in total. Figure 1 shows these search results, per year. It should be noted that for the most recent year 2021 the process of indexing and adding papers is still in progress in Scopus.
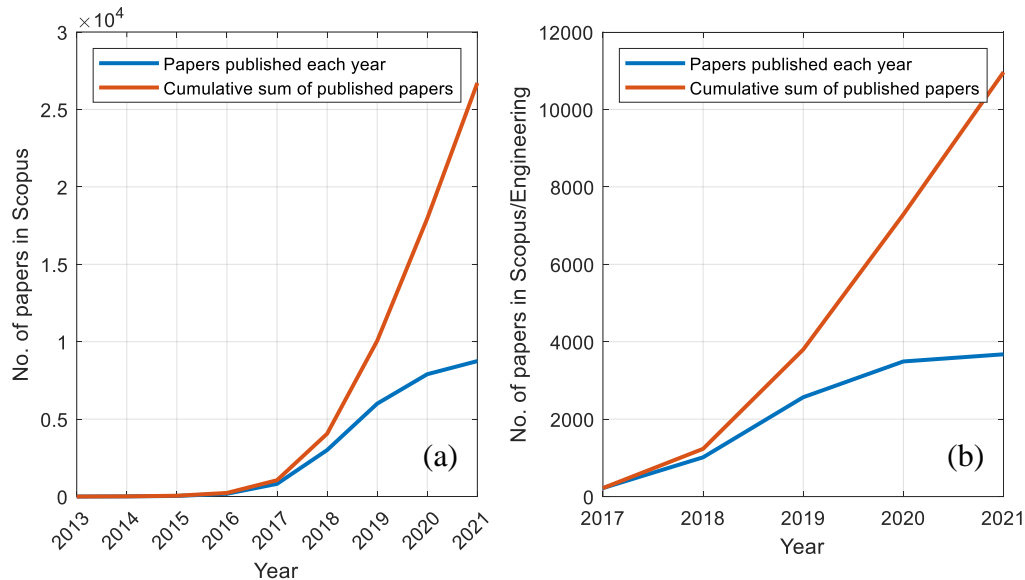
1st International Conference on Advances in Civil & Environmental Engineering, University of Engineering & Technology Taxila, Pakistan

Conference date 22 &23 Feb 2022

Figure 1: Papers in "blockchain" in Scopus database: (a) All fields, (b) Engineering field.

2   BITCOIN: THE FIRST IMPLEMENTATION OF BLOCKCHAIN

In the long past, there were no monetary mediums. People would exchange goods using barter agreements. Then came money, in the form of a metal coin, a piece of paper or another object that people could use as a medium of exchange. The 21st century and the evolution of computers and digital technology gave rise to "digital money", allowing electronic, mobile payments between different parties. Such digital payments offer the advantage that the parties involved need not be in the same physical location. Unlike cash payments which are "peer-to-peer", mobile payments are made through an institution (usually a bank) which acts as an intermediary. This can cause problems, such as high transaction fees, censorship of transactions, while not all people can have access to a bank account due to bank restrictions or other reasons.

In 2008, Satoshi Nakamoto introduced Bitcoin. In his novel work [2] the brilliant idea of a system for electronic transactions which does not rely on a "trusted third party" is explained. It was the first implementation of blockchain technology. Blockchain allowed Bitcoin to transfer value in a decentralized network without any central authority, for the first time, offering an elegant solution to the "double spending" problem in digital currency, and opening horizons for other important applications in the future. Bitcoin is a peer-to-peer digital cash system which uses cryptography and the concept of "proof-of-work" (PoW) to record transactions.

In Bitcoin there is no bank or any other intermediary playing a special role. It is a fully decentralized network where all parties are "equal", having the same rights. It uses a decentralized approach, based on the creation of blocks linked together, forming a chain of blocks (blockchain). In the blockchain, every transaction and every block have a timestamp and blocks are linked together with their hash values and PoW. The record of a transaction is distributed among many nodes in the system, making it impossible for a bad actor to manipulate the ledger to their advantage. Using PoW, the amount of computational power needed to reverse

1st International Conference on Advances in Civil & Environmental Engineering, University of Engineering & Technology Taxila, Pakistan

Conference date 22 &23 Feb 2022

or change a transaction is enormous. This technology allows bitcoin to transfer value in a decentralized way without the need for any trusted third.

3   TECHNICAL DETAILS

3.1   Asymmetric cryptography

Asymmetric cryptography uses a pair of keys (Public and Private key) to encrypt/decrypt a message. The private key is private, while the public key can be shared with anyone. A message which is encrypted with the private key can only be decrypted with the public key, and vice-versa. There are two main uses: (i) Sender authentication, and (ii) Receiver authentication. The first is used to ensure that a message came from the stated sender, while the second is used to ensure that a message can only be read by the intended recipient. In Bitcoin and similar blockchain-based networks, the two keys are used to ensure the integrity of transactions.

3.2   Cryptographic hash functions

A hash function is a one-way function that maps data of an arbitrary size to fix-sized values [3]. Its return is called the hash value or digest. A hash function is deterministic and designed to be irreversible, i.e. it is not possible to generate the input from the hash. Additional properties of a cryptographic hash function are: (i) Quick computation, (ii) impossibility to generate a message that will give a given hash, (iii) impossibility to find two messages giving the same hash, (iv) a slight change in a message results to a drastic change in the hash. Bitcoin uses the SHA-256 algorithm which was designed by the US National Security Agency and first published in 2001 [4]. The value set of SHA-256 contains $2^{256} = 16^{64} \approx 10^{77}$ different message digests.

3.3   Proof of Work and Proof of Stake

Calculating the hash function of a block is a computationally easy operation. The bitcoin protocol and other blockchain networks make it harder by introducing a level of difficulty. A miner has to add a special integer number into the header of a block, to achieve a hash that has a value lower than a predefined threshold (i.e. the hash has a number of leading zeros). Since hash values cannot be predicted and the outcome is "random", a miner has to try many times with different numbers until it finds the right hash. This concept, called "Proof of work" (PoW) is used in Bitcoin as a consensus mechanism requiring members in a decentralized network to do some computational work to prevent bad actors from harming the system. An alternative approach is Proof of Stake (PoS), which extends the voting power to the stakeholders of the system. In PoS, participants owning crypto coins can stake them, which gives them the right to check new blocks, validate them and add them to the blockchain. PoS, which is used in some other blockchains, is newer and it is tremendously more energy efficient than PoW.

4   BLOCKCHAIN

Distributed Ledger Technology (DLT) or blockchain is a technology able to simplify and secure transactions among parties. It has to do with a growing number of blocks containing records such as transaction data or any other data that can be recorded. The blocks are linked together using hash values created with a cryptographic hash function. Each new block of data is connected with the previous, using the cryptographic hash. The hash value of a given block is part of the information stored in the next block. As a result, any small change in a block would lead to a

1st International Conference on Advances in Civil & Environmental Engineering, University of Engineering & Technology Taxila, Pakistan

Conference date 22 &23 Feb 2022

new hash value for the block, which would automatically invalidate all subsequent blocks. Additionally, the ledger is distributed in thousands of copies among the nodes of the network, which are also asked to validate the blocks containing the transactions [5].

General Purpose Technologies (GPTs) can affect an entire economy. They can impact economic growth and transform both our everyday lives and the ways we do business [6]. Examples of GPTs include electricity, the electric motor, the computer and the internet. Given its unique characteristics, such as immutability, transparency, and distribution [7], blockchain is recognized by many as a form of GPT. Although blockchain is still at the infrastructure building stage, it is expected to unleash several applications across different verticals within the next 5-15 years. Like the internet in its first years, blockchain is difficult to predict or even understand well, but in the future, it could become ubiquitous in the exchange of physical and digital goods.

4.1 Blockchain in Civil Engineering and Construction

Construction is one of the largest industries in the world. Blockchain has the potential to play a significant role in construction industry in the future and reshape it to the better. Shojaei [8] explored the applications of blockchain in improving information management systems in the construction industry concluding that blockchain has the potential of addressing various problems. Nawari and Ravindran [9] reviewed blockchain, how it is related to the built environment and its potential applications in the AEC industry, focusing mainly on BIM. Blockchain can be used to provide live and trustworthy information for BIM, by information sharing among present and future information owners. Furthermore, it can help enhance the benefits of BIM by allowing architects and engineers to design on the same BIM model with clear ownership, while design and construction decisions can be recorded on the blockchain for future analysis and liability.

Smart contracts, working on an "if/then" principle can identify accountabilities and trigger payments based on milestones [10]. They are executed automatically reducing the necessity of intermediaries and saving time and money. They can be used to automate agreements, thus revolutionizing construction contracts and payments which usually rely on traditional methods. Construction project management (CPM) can potentially benefit from an agile and more decentralized approach based on blockchain, with high transparency, and the parties being compensated for outcomes and work performed. The construction industry has been historically reported as one of the slowest sectors in the adaptation of information technology. Given that, the question of whether blockchain is hype or real in the construction industry was addressed by Perera et al. [11]. Their work aimed at analysing the potential of blockchain applications in construction. According to the study, blockchain has a credible potential in the construction industry, due to its exponential general use, the investments involved, and a number of start-up businesses contributing to Industry 4.0.

As urbanization is increasing rapidly, offering improved liveability and a higher standard of living, the concept of "smart cities" is one of the main focus areas of many governments attempting to establish special strategies for transforming their cities. Smart cities enable operational efficiency, maximize environmental sustainability efforts and create new citizen services. Blockchain innovation can be utilized to make cities smarter, enhancing them and

1st International Conference on Advances in Civil & Environmental Engineering, University of Engineering & Technology Taxila, Pakistan

Conference date 22 &23 Feb 2022

providing for better economic development and liveability [12]. Another major problem in construction and supply chain management is the disconnect between construction and design, due to the lack of trustworthy and open information across the supply chain. Blockchain can adverse these issues using open and transparent transactions [13].

5 CONCLUSION

New opportunities arise as we are moving to a digital economy where financial and physical assets will have digital representations. Although nobody can predict the degree to which Blockchain will affect the economy and our lives in the long run, most experts agree that it has the potential to play a significant role in the future, in a wide range of fields. The present study briefly examined the technical details and main concepts of blockchain technology and aimed at formulating a brief picture of the current state and practice of its use in civil engineering and construction. The study also summarized application areas related to the AEC industry where blockchain has the potential to provide new solutions. The general conclusion of the study is that although blockchain technology is new and there are certainly several early challenges to tackle, it has great potential to become an extremely positive force of change in the construction industry, in the near future.

REFERENCES

1. Wang, M., et al., *A Systematic Review of Digital Technology Adoption in Off-Site Construction: Current Status and Future Direction towards Industry 4.0.* Buildings, 2020. **10**(11): p. 204.
2. Nakamoto, S., *Bitcoin: A peer-to-peer electronic cash system.* 2008.
3. Estébanez, C., et al., *Performance of the most common non-cryptographic hash functions.* Software: Practice and Experience, 2014. **44**(6): p. 681-698.
4. Penard, W. and T. van Werkhoven, *On the Secure Hash Algorithm family*, in *Cryptography in Context*, G. Tel, Editor. 2008: Utrecht. p. 1-18.
5. Xu, J., H. Liu, and Q. Han, *Blockchain technology and smart contract for civil structural health monitoring system.* Computer-Aided Civil and Infrastructure Engineering, 2021. **36**(10): p. 1288-1305.
6. Bresnahan, T.F. and M. Trajtenberg, *General purpose technologies 'Engines of growth'?* Journal of Econometrics, 1995. **65**(1): p. 83-108.
7. Sandner, P. and P.M. Schulden, *Speciality Grand Challenges: Blockchain.* Frontiers in Blockchain, 2019. **2**(1).
8. Shojaei, A. *Exploring applications of blockchain technology in the construction industry*. in *ISEC 2019 - 10th International Structural Engineering and Construction Conference*. 2019.
9. Nawari, N.O. and S. Ravindran, *Blockchain and the built environment: Potentials and limitations.* Journal of Building Engineering, 2019. **25**: p. 100832.
10. Vigliotti, M.G., *What Do We Mean by Smart Contracts? Open Challenges in Smart Contracts.* Frontiers in Blockchain, 2021. **3**(45).
11. Perera, S., et al., *Blockchain technology: Is it hype or real in the construction industry?* Journal of Industrial Information Integration, 2020. **17**: p. 100125.
12. Valtanen, K. *Design challenges of developing a blockchain-enabled smart home*. in *2021 Conference on Information Communications Technology and Society, ICTAS 2021 - Proceedings*. 2021.
13. Tezel, A., et al., *Insights into Blockchain Implementation in Construction: Models for Supply Chain Management.* Journal of Management in Engineering, 2021. **37**(4): p. 04021038.

A STUDY ON THE PROPERTIES OF CONCRETE AGGREGATE REPLACEMENT IN RUBBER CEMENT COMPOSITE

Muhammad Ali

School of Civil Engineering and Surveying, University of Portsmouth, UK

Muhammad.ali@port.ac.uk

ABSTRACT

The automobiles industry has grown rapidly in the last three decades throughout the world and the increasing use of cars as the main mode of transport has brought a huge boom in car tyre production. This means that an enormous number of waste car tyres are left at the end of its life. Apart from domestic cars, a large number of tyres wastes are also generated from commercial and heavy goods vehicles. Producing rubberised concrete by utilising waste tyre rubber as an aggregate can prove to be an effective approach to massively reduce tyre waste.

In this study, the performance of concrete mixtures containing rubber as fine and coarse aggregate was investigated. Scanning electron microscopy (SEM), water absorption, density, compressive strength and non-destructive tests were performed using test specimen (w/c = 0.43) containing two types of rubber. Two mix designs were designed containing 10% of as-received rubber or cement paste treated rubber. The results of two mixtures have been compared with the control mix which is used as a reference. It was found that using 10% v/v of crumb rubber into concrete reduced 12% of compressive strength while only 2% reduction was observed when 5% crumb rubber with 5% chipped rubber coated with cement paste was utilised. Overall the results showed that the use of cement coated rubber in concrete gave favourable results when compared to the control.

The SEM observation for interfacial transition between cement, aggregate and rubber was also studied. It was observed that a strong interface bonding occurs between cement paste and aggregate, but a weak interface bonding is formed rubber, cement paste and aggregate.

Keywords: Waste tyre, crumb rubber, chipped rubber, Cement paste, Rubberised concrete.

1   INTRODUCTION

It is estimated that about 1.5 billion rubber tyres are manufactured in the world and more than 50% of waste tyres are discarded without any treatment [1]. According to the Environment Agency, UK, every year the United Kingdom produces more than 55 million waste tyres. This is now becoming one of the major waste management problems in the UK and this number is set to increase by more than 60% in 2021, in line with the growth in road traffic and car ownership [2]. At present, it is thought that 11% of post-consumer tyres are exported, 62% are reused, recycled or sent for energy recovery and 27% are sent to landfills (shredded tire), stockpiled or dumped illegally.

1st International Conference on Advances in Civil & Environmental Engineering, University of Engineering & Technology Taxila, Pakistan

Conference date 22 &23 Feb 2022

It is reported [3] that about 32 million tyres are produced annually in Brazil, and it is estimated that 10-15 million units are discarded each year. Similarly, in China, the production of waste tyres is increasing with an annualised rate of 15%. The production of waste tyres was 0.2 billion (6 million tonnes in weight) in 2009, about 65% of the waste tyres were not recycled or received any treatment [4].

The major issue lies within the fact that rubber tyres are not biodegradable and these waste tyres can last many years. There is no doubt that if they are to be landfilled then they are a serious threat to the environment. Rubber tyres compound contain large quantities of oxygen within their particles, which aids burning, hence they are classed as a major fire hazard. Furthermore, the toxic smoke of burning tyres can cause serious damage to human health and the environment [5. Additionally, rubber tyres accumulation into landfills and dumps provides a breeding ground for mosquitoes causing a further problem to human health [6]. These are the major reasons that the European Union (EU) has adopted laws to prevent the disposal of tyres to landfill sites. The European landfill directive [7] means that this type of waste disposal would be illegal in Europe and from 2006 EU legislations have banned the disposal of tyres in landfills, leaving about 480,000 tonnes of recyclable shredded rubber every year [8]. The legislation forces the UK and other EU member countries, that they must be recovered, recycled and reused tyres. This, however [9] not only calls for environmental concern but also represent a waste of useful resources, considering the enormous number of £1.8 billion that is spent annually only in the United Kingdom on concrete products, it is easily understandable that this is a very potential market for this material.

Rubber from vehicles tyres, after being shredded into smaller pieces, can be used in various Civil Engineering applications, mainly as aggregates and sand substituents in concrete. The two methods used to grind tyres to the required size: the first method is related to ambient size reduction using mechanical processes at or above room temperature while the second method is related to cryogenic size reduction by the use of liquid nitrogen or commercial agents to reduce the tyre to the desired size. The first process produces rubber chips with a rough surface, while cryogenic grinding is generally used for the production of rubber in the form of powder or crumbs. By reducing the particle size of worn tyres, separation of steel wires and textile fibres can also be achieved as well as a further treatment of the worn tyres so that commercial particle sizes are created. Scrap tyres are shredded into sizes ranging from >300 mm to <500 μm, depending upon the intended use.There is no doubt that the number of waste tyres is increasing every year, about 112 million scrap tyres remained in the stockpiles, only in the UK. These statistics bring out the importance of the more widespread and durable application program for the reuse of scrap tyres. Tyre rubber mainly consists of a complex mixture of elastomers including poly-isoprene, polybutadiene, styrene-butadiene, some stearic acid (1.2%), zinc oxide (1.9%), extender oil (1.9%), and carbon black (31%) [12]. As a flammable material, stockpiling of waste tyres is dangerous not only due to potential negative impact but it presents a fire hazard.

In this research, the scrap tyre rubber aggregates are used to substitute the natural aggregates in the concrete to improve the flexibility and durability of the concrete. Rubber aggregates were also coated with cement paste to enhance their bonding properties. The mechanical properties, the morphology of hydration productions and the microstructure of the interfacial transition zone (ITZ) were observed using Scanning Electron Microscopy (SEM).

1st International Conference on Advances in Civil & Environmental Engineering, University of Engineering & Technology Taxila, Pakistan

Conference date 22 &23 Feb 2022

2   MATERIALS AND METHODS

Previous work conducted on rubber substitution in concrete [12, 13, 14, 15] recommended incorporating lower percentages as replacements. Therefore, this study assesses the behaviour of rubberised concrete with a maximum of 10% replacement of aggregates (See Table 1). This work also evaluates the results from SEM to understand the ITZ between rubber and natural aggregates. Table 1 shows the concrete mixtures produced during this study.

Table 1 Concrete mixtures

MIX NO	DESCRIPTION
1	The control according to mix design, without any replacement of rubber aggregates.
2	Crumb rubber replaces fine aggregate by 10% (v/v).
3	Crumb rubber replaces fine aggregate by 5% (v/v) and chipped rubber coated with cement paste replaces coarse aggregate by 5% (v/v).

2.1   Aggregates

The traditional limestone aggregates and the rubber aggregates were used in this project. Traditional limes stone aggregates included, coarse aggregates (10mm and 20mm) and fine aggregates (sand, 0.2-0.3mm). All-natural aggregates were held at room temperature (20-25°C). Figure 1 shows rubber aggregates utilised as replacements, this included, chipped rubber (10-14 mm), chipped rubber pre-coated with cement paste (10-14 mm) and crumb rubber (0.6 mm). All substitutions were made according to weight taking into account the ratio between the specific weight of rubber and natural aggregates. The rubber aggregates were supplied by Crumb Rubber Ltd, Plymouth, UK. For Mix 3 (see Table 1), cement paste was prepared blending 800g cement with 400g of tap water. Chipped rubber was added to the cement paste and was mixed thoroughly for about 5 minutes. After which, the chipped rubber was spread on a clean dry surface and left for drying at room temperature for 24 hours.

Figure 1 Chipped rubber, Cement coated chipped rubber and crumb rubber

1st International Conference on Advances in Civil & Environmental Engineering, University of Engineering & Technology Taxila, Pakistan

Conference date 22 &23 Feb 2022

2.2 Concrete mix design

The purpose of this study was to investigate the general procedure for the production of fresh and hardened concrete and to evaluate differences between control and waste tyre rubber modified concrete. Three separate concrete mixes were produced (Table 2) for this study.

Table 2 Concrete mix design proportions (kg m^{-3})

MIX	CEMENT	WATER	FINE AGGREGATE	COARSE AGGREGATE		CRUMB RUBBER	CHIPPED RUBBER	UNIT WEIGHT
				(20mm)	(10mm)			
1	390	195	582	394	789	0	0	2350
2	390	195	523.8	394	789	25.3	0	2317.1
3	390	195	552.9	374.3	549.5	12.6	25.4	2299.8

3   RESULTS AND DISCUSSION

Recent research into rubberised concrete [11, 15, 22] suggested that replacing greater than 10% rubber with natural aggregate adversely affects the mechanical and durability properties of concrete. Therefore, in this investigation, we have evaluated the performance of rubberised concrete by incorporating crumb and chipped rubber as 10% replacement (see Table 1).

3.1 Compressive strength test

It is widely accepted [12, 14, 26, 27] that the substitution of rubber mainly affects the density, compressive strength, and split tensile strength of concrete. These studies indicated that in rubberised concrete approximately 85% reduction in compressive strength, whereas the splitting tensile strength is reduced by about 50% when the coarse aggregate was fully replaced with chipped tyre rubber. Results in Fig. 2 shows that for 10% of crumb rubber into concrete (MIX 2) there is a reduction of 12% strength, while MIX 3 showed only 2% reduction when compared to the control. In comparison four rubber contents (5%, 10%, 15% and 20%, v/v) were studied [12]. We observed only 2% reduction when coated chipped rubber (5%) and crumb rubber (5%) was used. This shows that by coating the chipped rubber, a significant improvement in compressive strength can be achieved. Furthermore, It is suggested that the maximum of 10% rubber, with coated chipper rubber, can be used in structural concrete while up to 40% could be utilised for non-structural works [14].

3.2 Beam flexural and elastic young's modulus tests

Figure 3 shows the beam flexural strength for the three mixes. It can be seen that for both rubberised mixes there is no significant difference in flexural strength compared to the control, Mix 2 and 3 showed a reduction of only 3%. In contrast a recent study on beam flexural test
The results for elasticity young's modulus is shown in Figure 4. It can be seen that the 10% crumb rubber replacement presents a 21% reduction in elastic young's modulus. However, using MIX 3 elastic modulus value (34.76 GPa) was almost similar to the control (34.04 GPa). During this study, it was noticed from the cracks after the failure of the test specimens that the rubberised

1st International Conference on Advances in Civil & Environmental Engineering, University of Engineering & Technology Taxila, Pakistan

Conference date 22 &23 Feb 2022

concrete appears to be less brittle than the control mix, especially the samples containing chipped rubber. Thus, it is believed that the rubberised concrete could serve as an energy-absorbing material. The results of UPV tests showed that the average pulse velocities for MIX 1, MIX 2 and MIX 3 were 4.26 km/s, 4.61 km/s and 4.73 km/s respectively. All three mixes recorded pulse velocity >4 km/s which are classed as very good quality.
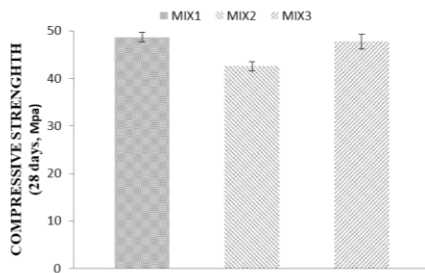

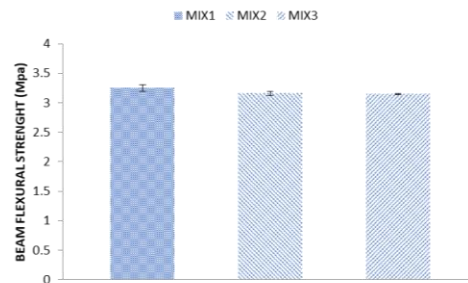Figure 2 Compressive strength after *28* days (value represent means ± standard deviation, n=3)

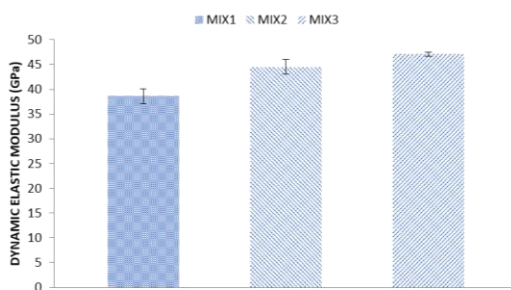Figure 3 Flexural strength in beams (value represent means ± standard deviation, n=3)

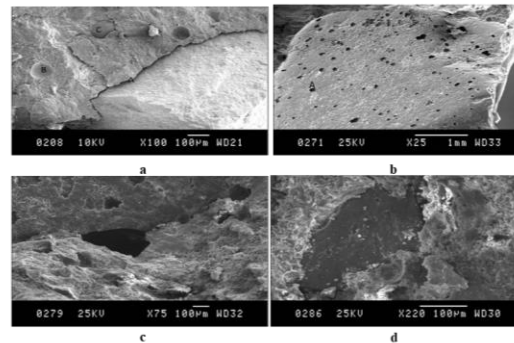Figure 4 Dynamic elastic modulus (value represent means ± standard deviation, n=3)

Figure 5 a) SEM image of fractured surface of control specimen A (Cracks), B (Air bubbles) and C (limestone aggregate), MIX1 b) ITZ between crumb rubber and cement paste, MIX2 c) ITZ between crumb rubber, aggregate and cement paste, MIX3 d) Image showing bond between cement coated chipper rubber and aggregate.

3.3 SEM analysis

It was observed that a strong interface bonding occurs between cement paste and natural aggregates (Figure 5a), while in the rubberised concrete there is no obvious interface bonding between cement paste and crumb rubber hence, a poor adhesion was observed (see Figure 5b). SEM images (Figure 5c and d) show that the cement paste coated rubber surface appears similar to natural aggregates and presents signs of a strong interface bonding between cement coated rubber and mineral aggregates.

4   CONCLUDING REMARKS

Based on this study it is recommended that high strength cement should be utilised for manufacturing rubberised concrete, to address compressive strength reductions. The flexural strength of beams containing cement coated chipped rubber did not crack completely and appeared less brittle compared to the other samples tested. It is believed that this was due to rubbers' ability to absorb energy. Overall, based on the results achieved, it is proposed that 5% crumb rubber and 5% cemented coated chipped rubber should be utilised in a wide range of structural applications including structures that require concrete to absorb energy.

1st International Conference on Advances in Civil & Environmental Engineering, University of Engineering & Technology Taxila, Pakistan

Conference date 22 &23 Feb 2022

REFRENCES

1. SIDDIQUE R AND NAIK R T, *Properties of concrete containing scrap-tire rubber-an overview, Waste Management,* 2004, Vol. 24, pp 563–569.

2. Cairns R A, Kew H Y and Kenny M J, *The use of recycled rubber tyres in concrete construction,* In: Sustainable Waste Management and Recycling, 2004, Thomas Telford Ltd, London, pp 135-142.

3. SERGE N AND JOEKES I, *Use of tire rubber particles as addition to cement paste, Cement and Concrete Research,* 2000, Vol. 30, pp 1421-1425.

4. ALAMO-NOLE L A, PERALES-PEREZ O AND ROMAN-VELAZQUEZ F R, *Sorption study of toluene and xylene in aqueous solutions by recycled tires crumb rubber,* Journal of hazardous materials, 2011, Vol. 185, pp 107–111.

5. OIKONOMOU N AND MAVRIDOU S*, The use of waste tyre rubber in civil engineering works, Sustainability of Construction Materials,* 2009, Vol. 9, pp 213-238.

6. NEHDI M AND KHAN A, *Cementitious Composites Containing Recycled Tire Rubber: An Overview of Engineering Properties and Potential Applications,* 2001, Vol. 23, No. 1, pp 3-9.

7. THE ECONOMIST, *Quieter traffic, When the rubber hits the road, Turning old tyres into new roads can help cut noise pollution,* June 30th 2012.

8. BENAZZOUK A, DOUZANE O, LANGLET T, MEZREB K, ROUCOULT J M AND QUE´NEUDEC M, *Physico-mechanical properties and water absorption of cement composite containing shredded rubber wastes,* Cement and Concrete Research, 2007, Vol. 30, pp 732 - 740.

9. THE ENVIRONMENT AGENCY, UK, disposing of tyres, 27th March 2015.

10. AMARI T, THEMELIS N J AND WERNICK I K, *Resource recovery from used rubber tires,* Resource Policy, 1999, Vol. 25, pp 170–188.

11. SHEN W, SHAN L, ZHANG T, MA H, CAI Z AND SHI, H *Investigation on polymer–rubber aggregate modified porous concrete* Construction and Building Materials. 2013, 38, pp 667 - 674.

12. EMIROGLU M AND YILDIZ S, *An investigation on its microstructure of the concrete containing waste vehicle tire,* Computers and Concrete, 2008, Vol. 5, No. 5 , pp 503 - 508.

13. GANJIAN E, KHORAMI M AND MAGHSOUDI A A, *Scrap-tyre-rubber replacement for aggregate and filler in concrete.* Construction and Building Materials, 2009, Vol. 23, No. 5, pp 1828- 1836.

14. *LING T C, Prediction* of density and compressive strength for rubberized concrete blocks, Construction and Building Materials, 2011, Vol. 25, pp 4303–4306.

1st International Conference on Advances in Civil & Environmental Engineering, University of Engineering & Technology Taxila, Pakistan

Conference date 22 &23 Feb 2022

15. ISSA C A AND SALEM G, *Utilization of recycled crumb rubber as fine aggregates in concrete mix design,* Construction and Building Materials, 2013, Vol. 42, pp 48 - 52.

16. GADKAR, S, *Freeze-Thaw Durability of Portland cement Concrete Due To Addition of Crumb Rubber Aggregates,* PhD Thesis, 2013, Clemson University.

17. GUNEYISI E, *Fresh Properties of Self-compacting Rubberized Concrete incorporated with Fly ash,* Materials and Structures, 2010, Vol. 43, pp1037–1048.

18. GESOGLU M AND GUNEYISI E, *Strength Development and Chloride Penetration in Rubberized Concretes with and without Silica fume*, Materials and Structures, 2007, Vol. 40, pp 953– 964.

19. GUNEYISI E, GESOGLU M AND OZTURAN T, *Properties of Rubberized Concretes Containing Silica Fume,* Cement and Concrete Research, 2004, Vol. 34, pp 2309–2317.

20. ELDIN N N AND SENOUCI A B, *Rubber-tire particles as concrete aggregate.* Journal of Materials in Civil Engineering, 1993, Vol. 5, No. 4, pp 478-496.

21. TOPCU I B, *The Properties of Rubberized Concretes,* Cement and Concrete Research, 1995, Vol. 25, No. 2, pp 304-310.

22. KHATIB Z K AND BAYOMY F M*, Rubberized Portland cement Concrete,* Journal of Materials in Civil Engineering, 1999, Vol. 11, No. 3, pp 0206-0213.

23. SHAH S N, JADHAO P D AND DUMNE S M, *Effect of Chipped Rubber Aggregates on Performance of Concrete,* American Journal of Engineering Research, Vol. 3, No. 12, pp 93-101.

24. GOULIAS D G AND ALI A H, *Evaluation of Rubber-Filled Concrete and between Destructive and Nondestructive Testing Results.* Cement, Concrete, and Aggregates, 1998, Vol. 20, No. 1, pp140–144.

25. TOUTANJI H A, *The Use of Rubber Tire Particles in Concrete to Replace Mineral Aggregates.* Cement and Concrete Composites, 1996, Vol. 18, pp 135-139.

26. SALAM, A, *Ultrasonic Pulse Velocity versus Strength for Concrete in Qatar*, Engineering Journal of Qatar University, Vol.5, pp 87-93.

27. BLIGHT G E AND ALEXANDER M G, *Alkali-Aggregate Reaction and Structural Damage to Concrete: Engineering Assessment, Repair and Management,* 2011, pp 59-60.